

ADVERTIMENT. L'accés als continguts d'aquesta tesi doctoral i la seva utilització ha de respectar els drets de la persona autora. Pot ser utilitzada per a consulta o estudi personal, així com en activitats o materials d'investigació i docència en els termes establerts a l'art. 32 del Text Refós de la Llei de Propietat Intel·lectual (RDL 1/1996). Per altres utilitzacions es requereix l'autorització prèvia i expressa de la persona autora. En qualsevol cas, en la utilització dels seus continguts caldrà indicar de forma clara el nom i cognoms de la persona autora i el títol de la tesi doctoral. No s'autoritza la seva reproducció o altres formes d'explotació efectuades amb finalitats de lucre ni la seva comunicació pública des d'un lloc aliè al servei TDX. Tampoc s'autoritza la presentació del seu contingut en una finestra o marc aliè a TDX (framing). Aquesta reserva de drets afecta tant als continguts de la tesi com als seus resums i índexs.

ADVERTENCIA. El acceso a los contenidos de esta tesis doctoral y su utilización debe respetar los derechos de la persona autora. Puede ser utilizada para consulta o estudio personal, así como en actividades o materiales de investigación y docencia en los términos establecidos en el art. 32 del Texto Refundido de la Ley de Propiedad Intelectual (RDL 1/1996). Para otros usos se requiere la autorización previa y expresa de la persona autora. En cualquier caso, en la utilización de sus contenidos se deberá indicar de forma clara el nombre y apellidos de la persona autora y el título de la tesis doctoral. No se autoriza su reproducción u otras formas de explotación efectuadas con fines lucrativos ni su comunicación pública desde un sitio ajeno al servicio TDR. Tampoco se autoriza la presentación de su contenido en una ventana o marco ajeno a TDR (framing). Esta reserva de derechos afecta tanto al contenido de la tesis como a sus resúmenes e índices.

WARNING. The access to the contents of this doctoral thesis and its use must respect the rights of the author. It can be used for reference or private study, as well as research and learning activities or materials in the terms established by the 32nd article of the Spanish Consolidated Copyright Act (RDL 1/1996). Express and previous authorization of the author is required for any other uses. In any case, when using its content, full name of the author and title of the thesis must be clearly indicated. Reproduction or other forms of for profit use or public communication from outside TDX service is not allowed. Presentation of its content in a window or frame external to TDX (framing) is not authorized either. These rights affect both the content of the thesis and its abstracts and indexes.



Universitat Autònoma de Barcelona

Synthesis and characterization of fluorinated polymers

Doctoral Thesis

Miriam Laiz Treceño

Supervised by: Joan Carles Bayón Rueda

Chemistry Doctorate Program- Chemistry Department

Universitat Autònoma de Barcelona

2021

Report submitted for the achievement of the Doctor's Degree in Chemistry by:

Miriam Laiz Treceño

Checked and accepted

Dr. Joan Carles Bayón Rueda

Bellaterra, 21 de desembre del 2021

Agradecimientos

Hace ya unos años, empecé el manuscrito de mi TFG con una cita de Félicité Robert Lamennais "*La science ne sert guère qu'à nous donner une idée de l'étendue de notre ignorance*", y ahora que estoy a punto de acabar esta etapa, no puedo dejar de pensar en como cierta era esa frase en aquel momento, y cuanto más lo es ahora. De las muchas cosas que he podido aprender durante estos últimos años, hay una que sobresale por encima de todas, y es que todavía me falta por aprender muchísimo más.

En este recorrido de aprendizaje, quiero agradecer a mis directores de tesis. Dr. Joan Carles Bayón ha sido un ejemplo durante toda esta aventura, del que he aprendido no sólo química, sino también esfuerzo, dedicación y pasión por la ciencia. La puerta de su despacho siempre ha estado abierta para cualquier duda, reflexión o discusión filosófica. Gracias.

A Dr. Juli Real, a pesar de habernos dejado, quiero agradecerle por acoger una persona extraña en su grupo de investigación y demostrarle que todavía hay mucho más por descubrir. Su confianza me permitió empezar esta etapa, y su exigencia a mejorar como científica. Gracias otra vez.

Como ya es normal ahora toca agradecer a todos aquellos compañeros, y sobre todo amigos, que han estado durante este tiempo. Por todos es conocidos mi facilidad de llorar, y como os podéis imaginar, intentar escribir estas líneas está siendo un desafío de contención. Perdonar que no os nombre uno a uno, pero somos unos cuantos. De todos vosotros me llevo, grandes momentos que ya estoy echando de menos. Cafés químicos y no tan químicos, comidas, celebraciones de cumpleaños, cenas improvisadas, despedidas infinitas, tardes de confinamiento, viajes y visitas. Cada laboratorio, y cada integrante de él ha aportado detalles indispensables para esta tesis. En uno he tenido mi remanso de paz, mi zen particular. Otro de ellos ha sido diversión y locura, junto con un realismo difícil de encontrar. Y finalmente, el proveedor oficial de comida de la planta, y nuestra pequeña escapada particular de las tardes. No tengo suficientes páginas para agradecer a todos y cada uno de vosotros la ayuda, los buenos momentos, las risas y

lloros. La experiencia de la tesis ha sido única por muchas cosas, pero todos vosotros habéis sido una parte fundamental. A pesar de todo, sí que quiero agradecer de forma especial a Dani, por su paciencia incansable, sus discusiones químicas y por el aguante que ha tenido conmigo. En el fondo, muy en el fondo, algo me echaras de menos. Gracias a todos.

A todos los compañeros y profesores de la planta de inorgánica, ha sido un placer compartir todo este tiempo con vosotros.

Fuera de mi pequeña burbuja de UAB, quiero agradecer a las personas que siempre han estado y que han tenido una paciencia infinita, aunque yo no haya podido estar todo lo presente que hubiera querido. Gemma, Mónica i Laia, gracias porque siempre estabais a una llamada de distancia.

Finalmente quiero agradecer a mis padres, mis abuelos y a mi hermano, de los que no puedo estar más orgullosa. Sus palabras de ánimo en todo momento han sido la base de que hoy pueda estar cerrando esta etapa.

Abbreviations

General abbreviations

AI	Acidity index	HS	Hard segment
ATR-FTIR	Attenuated Total Reflection Fourier Transform Infrared	I	Nuclear spin
B_{eff}	Net Magnetic field	ICP-MS	Inductively Coupled Plasma-Mass Spectrometry
B_{ind}	Induce Magnetic field	IR	Infrared
B_o	External magnetic field	MFI	Melt Flow Index
BSE	Backscattered electrons	MMD	Molar Mass distribution
CA	Contact Angle	M_n	Number Average Molecular Weight
COF	Coefficient of friction	MS	Mass spectrometer
DGT	Derivative thermogravimetric curve	M_w	Molecular weight
DoE	Design of Experiments	NMR	Nuclear Magnetic Resonance
DSA	Drop shape analysis	OCS	Optical Control System
DSC	Differential Scanning Calorimetry	OHI	Hydroxyl index
EDS	Energy-dispersive X-ray spectroscopy	PCL	Polycaprolactone
FID	Flame-ionization detector	PE	Polyethylene
FWHM	Full width at half maximum	ppm	part per million
GC	Gas Chromatography	ppt	part per trillion
GPC	Gel permeation chromatography	PU	Polyurethane
		ROP	Ring Opening Polymerization

R_t	Retention time	T_{cc}	Cold-crystallization temperature
SAXS	Small-angle X-ray Scattering	TGA	Thermogravimetric analysis
SE	Secondary electrons	T_m	Melting temperature
SEC	Size Exclusion Chromatography	TPU	Thermoplastic polyurethane
SEM	Scanning Electron Microscopy	UV	Ultraviolet
SFE	Surface Free Energy	WCA	Water Contact Angle
S_N2	Nucleophilic substitution	XPS	X-ray photoelectron spectroscopy
SS	Soft Segment	YI	Yellow index
T_c	Crystallization temperature		

NMR abbreviations

δ	Chemical shift	m	multiplet
d	Doublet	q	quadruplet
dd	doublet of doublet	s	singlet
Hz	Hertz	t	triplet
J	Coupling constant		

Compounds abbreviations

ADP	Adipic acid	DMAc	N,N-dimethylacetamide
ADPCI	Adipoyl chloride	DMAP	4-dimethylaminopyridine
BDO	1,4-butanediol	DMF	N,N-dimethylformamide
DAST	Diethylaminosulfur trifluoride	DMSO	Dimethylsulfoxide
Deoxo-fluor	<i>Bis</i> (2-methoxyethyl)aminosulfur trifluoride	ECL	ϵ -caprolactone
DIPA	N,N'-diisopropylamine	H₁₂MDI	4,4'-dicyclohexylmethane diisocyanate

HDI	1,6-hexamethylene diisocyanate	PPG	Polypropylene
HDO	1,6-hexanediol	PPHF	Pyridinium polyhydrogen fluoride
MDI	4,4'-methylene diphenyl diisocyanate	PTFE	Polytetrafluoroethylene
MeCN	Acetonitrile	SelectFluor	N-Fluoro-N'-(chloromethyl)triethylenediamine bis(tetrafluoroborate)
NaTFE	Sodium trifluoroethoxide	TBAC	Tetrabutylammonium chloride
NMP	N-methyl-2-pyrrolidone	TDI	Toluene diisocyanate
NPG	1,3-neopentyl glycol	TFE	2,2,2-trifluoroethanol
PMe₂Ph	Dimethylphenylphosphine	THF	Tetrahydrofuran
PMePh₂	Methyldiphenylphosphine		

INDEX

1. INTRODUCTION	3
1.1. THERMOPLASTIC POLYURETHANES	3
1.1.1. RAW MATERIALS	5
1.2. TPU STRUCTURE-PROPERTIES RELATIONSHIP	17
1.2.1. HS CONTENT	17
1.2.2. HS INTERACTIONS	18
1.2.3. EFFECT OF THE SS	19
1.2.4. TPU PRODUCTION	20
1.2.5. POST-PROCESS TREATMENTS: ANNEALING	22
1.3. FLUORINATED POLYMERS	23
1.3.1. FLUORINATED TPUS	26
1.4. LUBRIZOL CORPORATION	29
LITERATURE	31
2. TECHNIQUES	39
2.1. NUCLEAR MAGNETIC RESONANCE SPECTROSCOPY	39
2.2. ELEMENTAL ANALYSIS	42
2.3. INDUCTIVELY COUPLED PLASMA-MASS SPECTROMETRY	42
2.4. GAS CHROMATOGRAPHY	42
2.5. INFRARED SPECTROSCOPY	43
2.6. MELT FLOW INDEX	44
2.7. KOFLER	45
2.8. DIFFERENTIAL SCANNING CALORIMETRY	46
2.9. THERMOGRAVIMETRIC ANALYSIS	47
2.10. HARDNESS	49
2.11. DENSITY	50
2.12. FRICTION	50
2.13. ABRASION RESISTANCE	51
2.14. YELLOWNESS INDEX	53
2.15. TRANSMITTANCE AND HAZE	53
2.16. GLOSS	55
2.17. CONTACT ANGLE ANALYSIS	56
2.18. SURFACE FREE ENERGY	58

2.18.	SURFACE FREE ENERGY	58
2.19.	SIZE EXCLUSION CHROMATOGRAPHY	59
2.20.	SCANNING ELECTRON MICROSCOPY AND ENERGY-DISPERSIVE X-RAY SPECTROSCOPY.....	60
2.21.	X-RAY PHOTOELECTRON SPECTROSCOPY.....	62
2.22.	SMALL-ANGLE X-RAY SCATTERING	64
	LITERATURE	68
3.	OBJECTIVES	73
4	FLUORINATED MONOMERS.....	77
4.1	PRECEDENTS.....	79
4.1.1	FISHER ESTERIFICATION	79
4.1.2	ALKYLATION OF MALONIC ESTERS.	80
4.2	SYNTHESIS OF FLUORINATED MONOMERS.....	81
4.2.1	CLICK REACTION: THIO-ENE MICHAEL ADDITION	81
4.2.2	TRIFLUOROETHYL FRAGMENT AS A NON-ESTER COMPOUND	85
4.3	SUMMARY AND CONCLUDING REMARKS.....	106
	LITERATURE	108
5.	FLUORINATED POLYESTERS	113
5.1.	SYNTHESIS OF ADP:HDO-8F BY ACYL CHLORIDE APPROACH.....	114
5.1.1.	CHARACTERIZATION OF ADP:HDO-8F AND ADP:HDO.....	116
5.2.	SYNTHESIS OF ADP:DIOLF	121
5.2.1.	SYNTHESIS OF ADP:DIOLF BY ACYL CHLORIDE APPROACH (1)	121
5.3.	SYNTHESIS OF PCL-DIOLF BY RING OPENING POLYMERIZATION APPROACH	139
5.3.1.	CHARACTERIZATION OF PCL-DIOLF AND PCL-BDO.....	141
5.4.	SUMMARY AND CONCLUSIVE REMARKS.....	146
	LITERATURE	148
6.	FLUORINATED TPUS.....	151
6.1.	GENERAL INFORMATION	152
6.1.1.	SYNTHESIS.....	153
6.1.2.	CHARACTERIZATION	154
6.2.	SINGLE-COMPONENT PCL-BASED TPU FAMILY.....	156
6.2.1.	INFRARED ANALYSIS	157
6.2.2.	VISUAL BEHAVIOR	160
6.2.3.	THERMAL BEHAVIOR	162

6.2.4.	TRIBOLOGICAL BEHAVIOR.....	166
6.2.5.	SURFACE BEHAVIOR: WETTABILITY.....	168
6.3.	BLENDED PCL-BASED TPU FAMILY	172
6.3.1.	INFRARED ANALYSIS	173
6.3.2.	VISUAL PROPERTIES	175
6.3.3.	THERMAL BEHAVIOR	177
6.3.4.	TRIBOLOGICAL BEHAVIOR.....	181
6.3.5.	SURFACE BEHAVIOR: WETTABILITY.....	183
6.4.	PC-BASED FAMILY	186
6.4.1.	INFRARED ANALYSIS	188
6.4.2.	VISUAL PROPERTIES	190
6.4.3.	THERMAL BEHAVIOR	192
6.4.4.	TRIBOLOGICAL BEHAVIOR.....	196
6.4.5.	SURFACE BEHAVIOR: WETTABILITY.....	198
6.5.	AGING AND ANNEALING EFFECT ON TPU PROPERTIES	202
6.5.1.	VISUAL PROPERTIES	203
6.5.2.	SURFACE BEHAVIOR: WETTABILITY.....	207
6.6.	SUMMARY AND CONCLUDING REMARKS.....	209
6.7.	FINAL CONCLUSIONS ABOUT FLUORINATED TPUS	210
	LITERATURE	211

7. OBJECTIVES II 215

8. PROCESS CONTROL..... 219

8.1.	SYSTEM DESCRIPTION	222
8.2.	RAW MATERIAL ANALYSIS.....	229
8.2.1.	E-CAPROLACTONE MONOMER.....	229
8.2.2.	4,4'-DICYCLOHEXYLMETHANE DIISOCYANATE.....	238
8.3.	PCL ANALYSIS.....	245
8.3.1.	PCL-NPG ANALYSIS.....	245
8.3.2.	POLYOL ANALYSIS	254
8.4.	TPU ANALYSIS	256
8.4.1.	COMPARISON BATCHWISE VS. CONTINUOUS PRODUCTION	256
8.4.2.	ANALYSIS OF THE TPU PELLETS.....	260
8.5.	EFFECT OF ANTIOXIDANTS.....	262
8.5.1.	PHENYL DIISODECYL PHOSPHITE (PDDP).....	262
8.5.2.	IRGAFOS 126.....	267

8.6.	FILMS ANALYSIS.....	271
8.6.1.	ICP-MS MEASUREMENTS	271
8.6.2.	X-RAY PHOTOELECTRON SPECTROSCOPY	271
8.6.3.	SCANNING ELECTRON MICROSCOPY	272
8.6.4.	SMALL-ANGLE X-RAY SCATTERING	279
8.6.5.	SUMMARY AND CONCLUDING REMARKS.....	281
	LITERATURE	283

9. MEASURING PROCEDURES287

9.1.	FLUORINE QUANTIFICATION	287
9.2.	ACIDITY INDEX.....	288
9.3.	HYDROXYL INDEX.....	288
9.4.	POLYESTER M_N DETERMINATION BY TITRATION	289
9.5.	POLYOL M_N DETERMINATION BY 1H NMR SPECTROSCOPY	289
9.5.1.	DETERMINATION OF THE M_N OF LINEAR ALIPHATIC POLYESTERS	290
9.5.2.	DETERMINATION OF THE M_N OF ADP:DIOLF.....	291
9.5.3.	DETERMINATION OF M_N OF PCL	292
9.6.	MELT FLOW INDEX.....	293
9.7.	KOFLER	294
9.8.	DIFFERENTIAL SCANNING CALORIMETRY.....	294
9.9.	HARDNESS TESTS.....	295
9.10.	DENSITY.....	295
9.11.	FRICTION.....	296
9.12.	ABRASION RESISTANCE.....	297
9.13.	YELLOWNESS INDEX.....	298
9.14.	TRANSMITTANCE AND HAZE	298
9.15.	GLOSS	298
9.16.	CONTACT ANGLE	299
9.17.	SURFACE FREE ENERGY	299
9.18.	INDUCTIVELY COUPLED PLASMA MASS SPECTROMETRY	301
9.19.	ANALYSIS ECL SAMPLES BY GAS CHROMATOGRAPHY	301
9.20.	DETERMINATION OF ECL MONOMER AND DIMER IN A PCL BY GAS CHROMATOGRAPHY	301
9.21.	DETERMINATION OF ECL MONOMER IN A PCL BY 1H NMR SPECTROSCOPY	302
9.22.	ISOMER DISTRIBUTION IN H_{12} MDI SAMPLES	303
9.22.1.	DISTRIBUTION DETERMINATION BY 1H NMR SPECTROSCOPY	303
9.22.2.	DISTRIBUTION DETERMINATION BY GAS CHROMATOGRAPHY	304
9.23.	PCL-NPG ANALYSIS	305

9.24. POLYOL MIXTURE	306
9.25. SPECIATION OF THE ANTIOXIDANTS IN POLYMERIC SAMPLES	307
9.25.1. PDDP CONTENT	307
9.25.2. IRGAFOS CONTENT.....	308
9.26. SCANNING ELECTRON MICROSCOPY AND ENERGY-DISPERSIVE X-RAY SPECTROSCOPY.....	308
9.27. SMALL-ANGLE X-RAY SCATTERING	308
LITERATURE	310

10. EXPERIMENTAL PART.....313

10.1. CHEMICALS	313
10.2. INSTRUMENTATION.....	314
10.3. DETAILED PROCEDURES. PART I. FLUORINATED POLYURETHANES	317
10.3.1. MONOMER SYNTHESIS.....	317
10.3.2. POLYOL SYNTHESIS.....	325
10.3.3. TPU SYNTHESIS	330
10.4. DETAILED PROCEDURES. PART II. PROCESS CONTROL.....	331
10.4.1. PCL REACTIVITY.....	331
LITERATURE	332

Chapter 1

Introduction

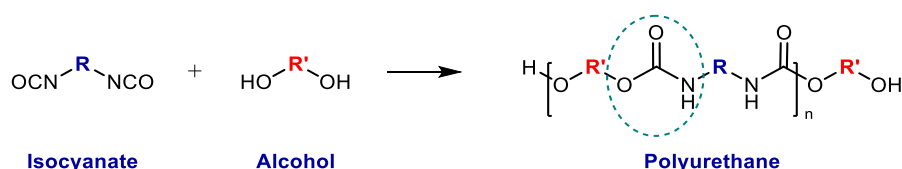
Chapter 1 introduces the fundamental ideas of polyurethanes, paying special attention to the chemistry of the partaking reagents, and their effect on the final properties of the materials.

1. Introduction

1.1. Thermoplastic polyurethanes

Polyurethanes (PUs) are a class of specialty block copolymers with high versatility in structure and properties, resulting in materials used in such different areas as furniture, construction, automotive, packaging, or electronics. Traditionally, PUs are synthesized by the polycondensation of isocyanate groups with alcohol moieties.^[1] Therefore, chemically speaking, they are a class of polymer containing carbamate esters in their structure. However, although its nomenclature is related to the generated urethane bond, other linkages are abundant in the backbone owing to their diverse building blocks, like ethers, esters, ureas, or amides, among others that can be introduced in the structure.

A specific subclass of PUs is the so-called thermoplastic polyurethanes (TPUs). These compounds are obtained from the reaction of difunctional isocyanate and dihydroxylated compounds (Scheme 1.1), leading to the generation of thermoplastic linear polymers. In particular, TPUs are produced with two different types of hydroxyls, the chain extenders, typically low molecular weight (M_w) hydroxyl-terminated compounds, and the polyols, already synthesized hydroxylated-terminated polymers with longer chains. The combination of diisocyanates and two types of compounds containing alcohols, the chain extender, and the polyol, results in an infinite number of products.^[2]



Scheme 1.1. General polycondensation reaction to form PUs starting from difunctional monomers. The green dashed circle indicates the carbamate bond.

TPUs have a humongous number of properties, enabling the generation of such different materials as stiff sealants or extremely light and flexible coatings. The reason behind the

diverse and outstanding properties is the formation of two distinct regions within the material. Areas enriched in alternated segments of chain extender and diisocyanates are known as the hard segment (HS), and contain an elevated number of polar carbamate moieties, whereas regions comprising polyols bounded by isocyanates are referred to as soft segments (SS). Both segments are thermodynamically incompatible owing to their difference in polarity, but as they are chemically bonded, their macrophase separation is prevented by the formed covalent links. Moreover, the carbamate moieties act as both hydrogen donor and acceptor, generating strong hydrogen-bonding interactions amongst them, which fosters the phase segregation process and enhances the crystallinity of the domain.^[3]

The HS domain provides stiffness and hardness to the material owing to its high ordering and strong supramolecular interactions, while the SS increases the flexibility of the system by acting as an amorphous matrix with weaker intermolecular interactions.^[4] Ideally, the system can be understood as an ordered and structured HS with equal chain length dispersed within an elastomeric matrix of SS, as shown in Figure 1.1. However, the reality is far from the ideality. The HS is not completely immiscible with the SS, resulting in areas that do not interact with other HS chains, but that are mixed in the SS. Moreover, a certain degree the phase segregation process can be inhibited by the restriction in the chain mobility, increasing the mixing between both compounds. Therefore, the polymer not only consists of pure HS and SS, but it also includes some dissolved HS chains into the matrix.^[5]

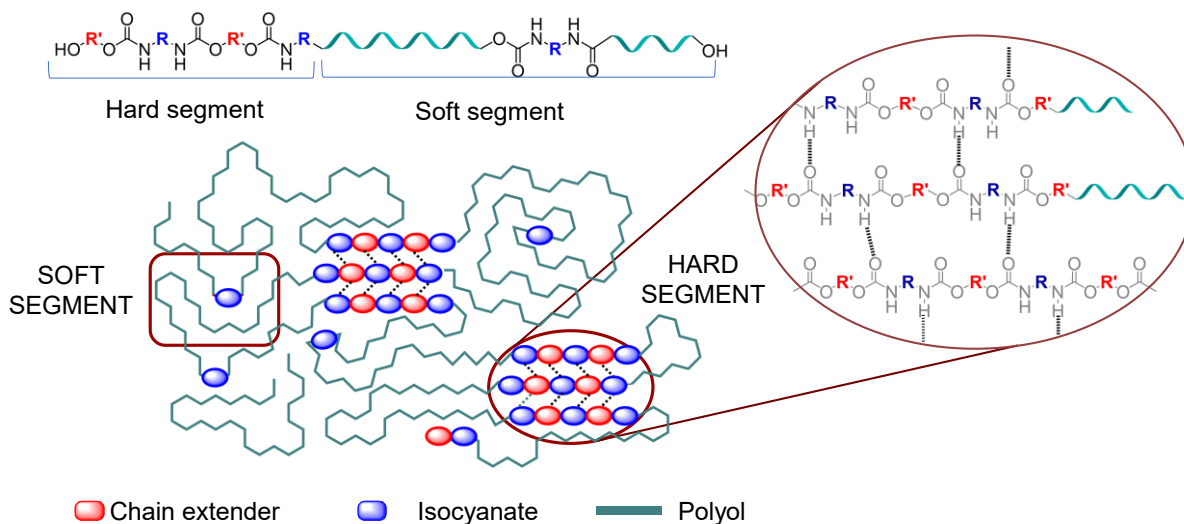


Figure 1.1. Schematic representation of the microphase separation of a TPU.

The HS remains packed through a highly strong secondary network of hydrogen bonds that are destroyed at high temperatures or under stress but are reformed after cooling down or

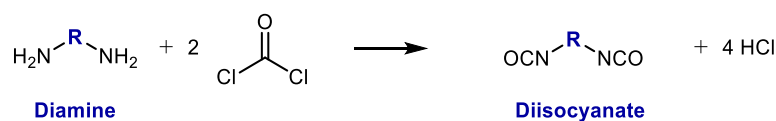
stopping the strain. This behavior provides thermoplasticity to the materials, allowing the reprocessing of the polymer several times without losing the mechanical or thermal properties.^[4]

The TPU phase segregation and consequently the tailoring of the material properties depend on different parameters as the raw materials, the backbone variability, the molecular weight, the ratio among the segments, or the synthetic process, among others.^{[6][5][7][8]} The effect over the TPU of some of the mentioned concepts is detailed hereafter.

1.1.1. Raw materials

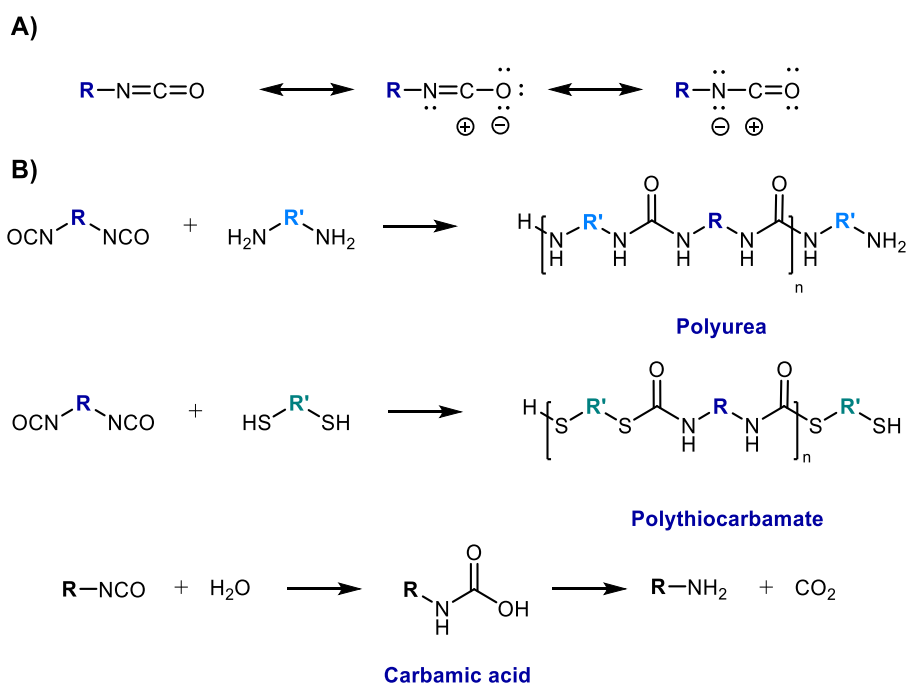
1.1.1.1. Isocyanates

Conventionally, isocyanates are obtained from the phosgenation of primary amines in an excess of phosgene (Scheme 1.2).^{[9][10]} However, this synthesis presents some environmental issues as it involves two highly toxic compounds, the phosgene and isocyanate itself. For this reason, other alternatives to generate carbamate bonds avoiding these two reagents are currently being researched.^{[11][12][13]}



Scheme 1.2. Industrial synthesis of isocyanates.

The high reactivity of isocyanates arises from their unsaturated -N=C=O group, in which the high electronegativity of both heteronuclei generates an electrophilic carbon vastly prone to nucleophilic attacks (Scheme 1.3.A). The isocyanate group reacts rapidly with several reagents containing active hydrogens like amines, thiols, or glycols, forming different products (Scheme 1.3.B).^[14] Despite their excellent reactivity, to improve the reaction rates and the selectivity of the process some Brønsted bases and Lewis acid, like tertiary amines, metal acetylacetonates, or alkylmetals salts of fatty acids are often employed as catalysts.^{[15][16]}



Scheme 1.3. A) Electron density of the isocyanate group. B) Addition reactions of isocyanates with diverse nucleophiles.

The final TPU properties are strongly influenced by the employed isocyanate, especially in its electronic and steric hindrance.^{[17][18][19]} Their main role, other than increasing the polymer's M_n , is to induce rigidity and enhance the tensile strength of the materials by generating physical crosslinks in the form of hydrogen-bonding interactions. Generally, diisocyanates are classified into aliphatic and aromatic. As a rule of thumb, aromatic diisocyanates are more reactive than aliphatics due to aromatic conjugation which stabilizes the positive charge on the central carbon.^{[17][20]} Moreover, owing to their ability to form π - π stacking interactions and their rigidity, they produce TPUs more crystalline, harder, and stiffer than their aliphatic counterpart.^[21] However, the latter exhibits higher UV resistance, flexibility, weatherability, and optical clarity as a consequence of the fewer and smaller HS crystallites generated owing to their poorer chain packing.^[2]

The most employed isocyanates in the TPU industry are the aromatic 4,4'-methylene diphenyl diisocyanate (**MDI**) and toluene diisocyanate (**TDI**), and the aliphatic 1,6-hexamethylene diisocyanate (**HDI**) and hydrogenated MDI, 4,4'-dicyclohexylmethane diisocyanate, (**H₁₂MDI**) (Figure 1.2).

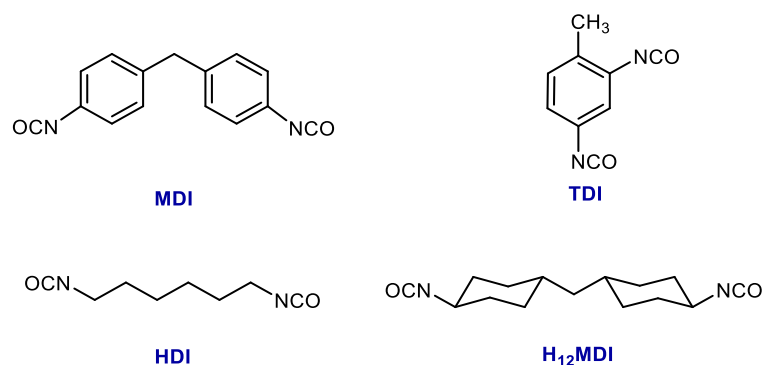


Figure 1.2. Structures of the most employed diisocyanates.

1.1.1.2. Chain Extenders

Chain extenders are low M_w compounds (40-300 g/mol) with, at least a functionality of 2, such as glycols, diamines, or hydroxylamines.^[22] If crosslinked polymers are aimed, reagents with higher functionality had to be employed, *e.g.* glycerine or triethanolamine, but the elastomeric properties will be decreased.

Their reaction rate depends to a great extent on the nature of the nucleophile. The reactivity order is reported as primary aliphatic amines > primary aromatic amines > primary alcohols > secondary hydroxyls > tertiary alcohols > phenols > thiophenols.^[17]

However, the most conventional alcohol chain extenders to form TPUs are ethylene glycol, 1,4-butanediol (**BDO**), and 1,6-hexanediol (**HDO**) (Figure 1.3). Nonetheless, the large library of accessible glycols allows the fine-tuning of the properties arising from the HS for their use in each application.

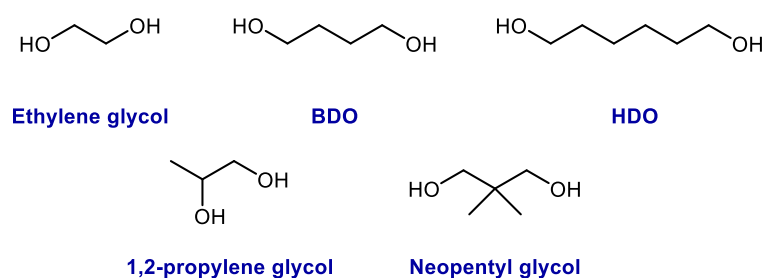


Figure 1.3. Common linear diols.

The use of branched diols, disrupts the chain packing of the HS domains, leading to less crystalline TPUs, which produces worse mechanical properties, but better optical characteristics.^[23]

1.1.1.3. Polyols

The third basic constituent of TPUs is the polyol, which comprises compounds with M_n between 1000 and 3000 g/mol,^[2] although some specific applications would require even larger polymers. Commonly, polyols are polyethers, polyesters, or polycarbonates, possessing low glass transition temperatures (T_g) values in the range of -70 to 30 °C, and not extremely high melting temperatures. The produced TPU display different properties according to the employed polyol and its structure, but some of the most used are shown in Figure 1.4.^[24]

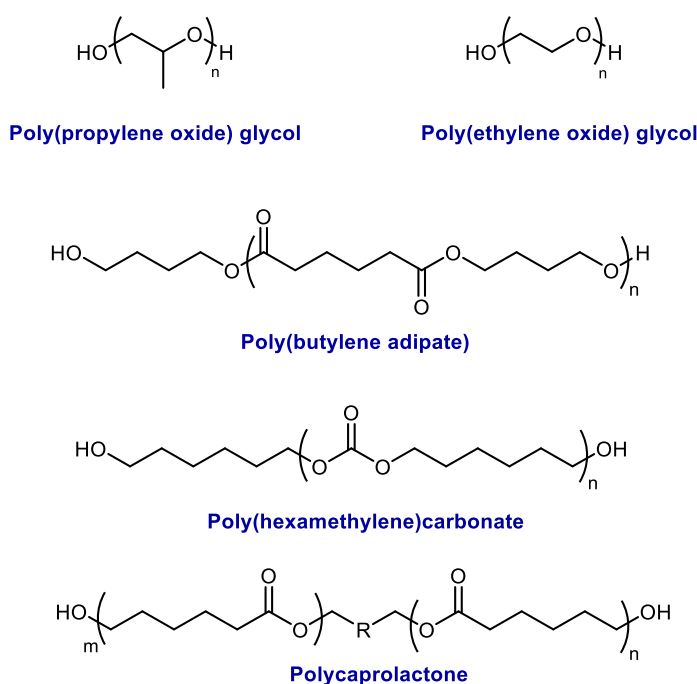


Figure 1.4. Most common polyols employed in the TPU market.

Polyethers are usually the cheaper class of polyol and are formed by cationic or anionic Ring-Opening polymerization (ROP) of epoxides, usually initiated by acid or bases, and terminated with active hydrogen compounds, like diols or water (Figure 1.5).^{[25][26]}

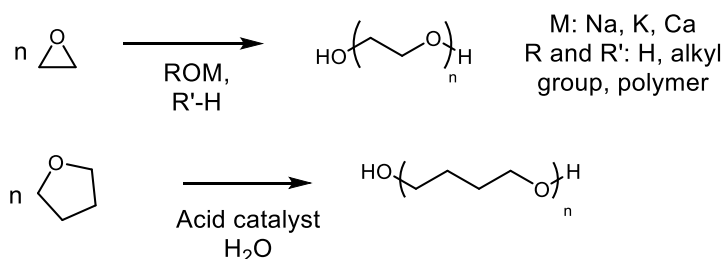
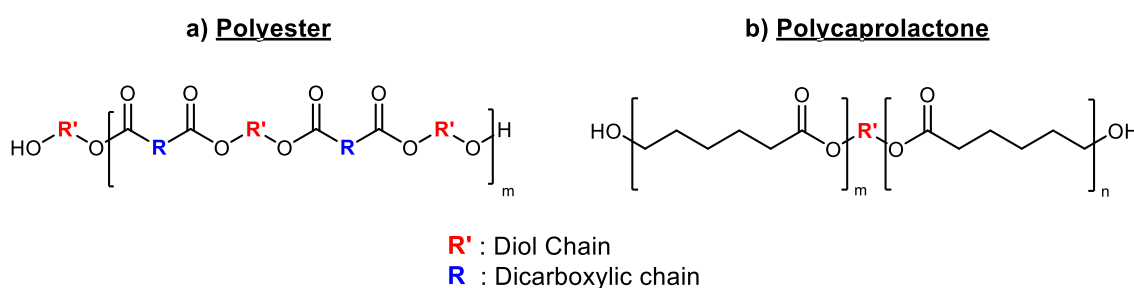


Figure 1.5. Schematic synthesis of polyether from epoxides and THF.

Owing to their ether linkage, polyethers display a low polarity. This lack of strong dipole moments leads to weak cohesion interactions among the polymeric chains. Therefore, polyether-based SS are highly amorphous structures, which imparts high flexibility to the TPUs, even at low temperatures, but reduces their ultimate tensile strength and abrasion resistance.^[27] Moreover, the high stability of the ether linkage grants them a high hydrolytic resistance.^[28]

Polyester polyols can be classified as classical polyesters or polycaprolactones (PCLs).^{[29][30][31]} Although they all are based on the same fundamental linkage, the subtle differences between them lead to singular properties. Classical polyesters are block copolymers that alternate hydroxyl-terminated and carboxylic acid monomers (Scheme 1.4. Left). However, PCLs consist of a repetitive sequence of opened lactones (Scheme 1.4. Right). To distinguish between them, from now on, ABAB block copolymers will be referred to as polyesters while the product of lactones polymerization will be denoted as PCL.



Scheme 1.4. General representation of the studied polyols.

Contrarily to polyethers, polyesters present stronger cohesive forces owing to the higher polarity of the ester moiety with respect to ethers, resulting in materials with higher T_g and melting temperature (T_m). Moreover, the increase in cohesive interactions produces materials with better tensile and abrasive properties, but less flexible than polyethers.^{[27][30]}

Predominantly, polyesters present a good resistance to oils, as their strong attractive intermolecular forces difficult their solvation. Moreover, they exhibit good thermal stability and low water absorption.^[32] However, their major drawback is their susceptibility to hydrolysis in conditions of high temperature and humidity, as a consequence of the repetitive ester bonds in their structure.^[33]

Overall, all the properties of polyesters, both their advantages and drawbacks, are increased as their number of ester linkages increase. For this reason, the selection of the monomers that constitute the polyester fulfills a crucial role in the final properties of the produced material.

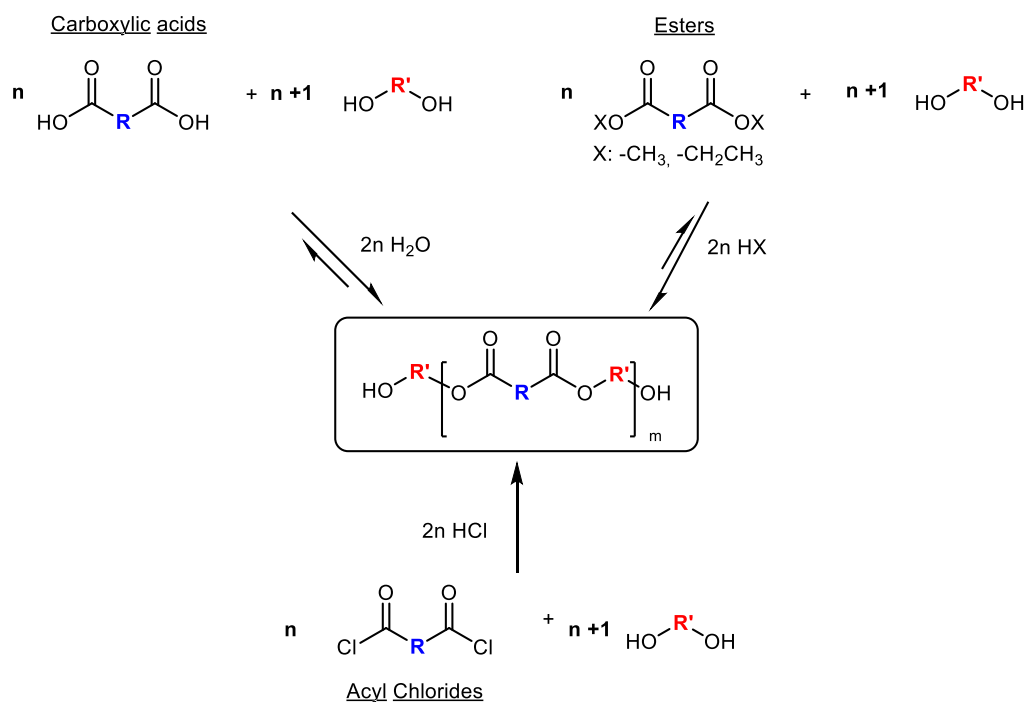
For example, a lower degree of hydrolysis is achieved in samples with a low concentration of ester bonds, high steric hindrance around the mentioned moiety, or with hydrophobic diols.^{[34][35]}

Although most of the properties are shared between polyester and PCLs, as they share the same defining moiety, there are some differences amongst them PCLs are known as biocompatible and relatively inexpensive compounds. Furthermore, multiple structures can be produced only by modifying the initiator species. Their physicochemical properties are tuned by their M_n , polydispersity, and degree of crystallinity of the polymer, which in part is defined to said compound. They are semicrystalline polymers with melting temperatures (T_m) between 59-64 °C and glass transition temperatures (T_g) around -60 °C, which makes them susceptible to aging at room temperature.^{[36][37]} They blend successfully with multiple classes of polymers, opening a window of opportunities to develop and improve new materials.^[38] PCLs are claimed to be promising macromolecules in the pharmaceutical and medical fields, with applications such as drug delivery systems.^{[39][40][41]}

Commonly, the primary route to synthesize polyesters is the polycondensation of carboxylic acids and glycols, while other minority methods are the polymerization of hydroxy acids or the transesterification of diesters or acyl chlorides. In the case PCLs, they are generally synthesized by Ring-Opening polymerization (ROP) of lactones.

1.1.1.3.1. Polycondensation of classical polyesters

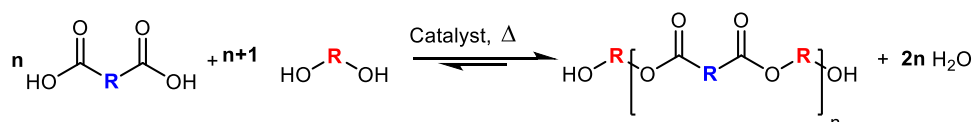
A standard polycondensation is a step-growth polymerization process that involves the coupling of two monomers and the elimination of a small by-product by each formed linkage (Scheme 1.5). Wallace H. Carothers and Paul J. Flory were the firsts to lay the foundations for the study of polycondensation, being their major contribution the premise that the reactivity of the active groups is independent of the molecular weight of the polymer.^[42-44]



Scheme 1.5. General polycondensation reactions to form polyesters.

Polycondensation can be applied to numerous monomers, both aliphatic and aromatic, to generate polyesters. But, to obtain telechelic hydroxylated-terminated polyesters an excess of diol must be incorporated into the mixture. Precisely, the glycol must be $n+1$, being n the number of dicarboxylic units on the polymer. Moreover, high M_n polymers could be obtained by this methodology, but for that purpose is extremely important the nature of the employed catalyst and the monomer purity. Even a few monofunctionalized building blocks will result in a premature completion of the polymerization, preventing the target M_n .

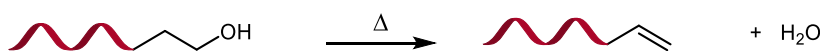
The conventional synthesis of polyesters is carried out at elevated temperatures at which the polyester is melted, thus removing the need for industrially unfriendly solvents. These reaction conditions allow the polymerization of high-melting monomers and the increase of the diffusion rate of the participating compounds by decreasing the viscosity. This synthesis consists of a two-step process: esterification between carboxylic groups with hydroxyls and the subsequent transesterification of the chains (Scheme 1.6).^{[35][31]}



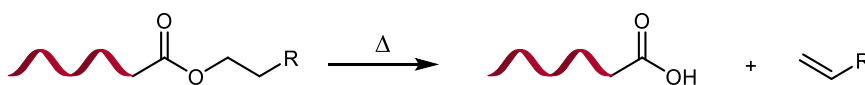
Scheme 1.6. Conventional melt-polycondensation reaction.

Esterification is an equilibrium process in which the excess of water must be eliminated to displace the reaction toward the polymeric product. The distillation at the initial stages is usually very fast, but as the reaction advances, reduced pressure is employed to facilitate the evaporation of water from the viscous mixture. Diols could be relatively volatile and be distilled during the synthetic process by the inert gas stream or the reduced pressure. This fact, especially in the early stages of the reaction, will disrupt the balance between the reagents and severely hamper the production of the target polymer. For this reason, once the *prepolymers* are formed, more diol is introduced into the system. The transesterification of the already formed esters with an excess of hydroxyls takes place to modulate the molecular weight of the polyester. This step must be carried out under an inert atmosphere to avoid thermo-oxidative degradation in form of dehydration of diols or β -scission of polyesters (Scheme 1.7).^{[45][46]} These degradation phenomena are observed by the darkening of the crude, signposting materials with poor quality.

a) Dehydration of alcohol groups



b) β -scission of ester groups



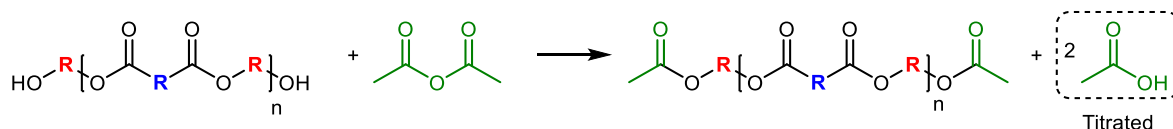
Scheme 1.7. Main side reaction on the polyester synthesis.

The presence of carboxylic acids autocatalyzed the reaction, but as their concentration decreases, other catalysts like scandium (III) trifluoromethanesulfonate ($\text{Sc}(\text{OTf})_3$)^{[47][48]}, bismuth (III) trifluoromethanesulfonate ($\text{Bi}(\text{OTf})_3$)^[49], titanium isopropoxide^[50] or tin chloride^[51] are commonly employed. Strong protic acids, like the ones used on Fisher esterification, could cause undesired byproducts, generate salts after the neutralization or corrode the reactor. Therefore, they are typically averted at an industrial scale.

Different parameters monitor the polyester synthesis, both during the reaction and after the production. Those continuously executed during the reaction are the acidity index (AI) and the hydroxyl index (OHI), whereas the ones usually carried out after the synthesis are the color determination or the infrared and NMR spectroscopy structural confirmation.

AI (mg KOH/ g polymer) quantifies the amount of base demanded to neutralize the acid contained in 1 g of polymer, which is used as a tool to analyze the carboxylic acid conversion in the polycondensation reaction. It consists of a direct titration of the sample with KOH, in

which only the carboxylic acid groups of the polyester are determined. The lower the AI, the smaller the concentration of COOH moiety and the higher the condensation of the mixture. OHI (mg KOH /g polymer) determines the number of alcohol groups that contain 1 g of polymer and allows the quantification of the polymer's M_n . It consists of the acetylation of the hydroxyl-ended groups, releasing an equimolar amount of acetic acid which then, is titrated (Scheme 1.8). A more elaborate explanation about the analysis and the quantification is described in *Measuring procedures* (See Section 9.3).

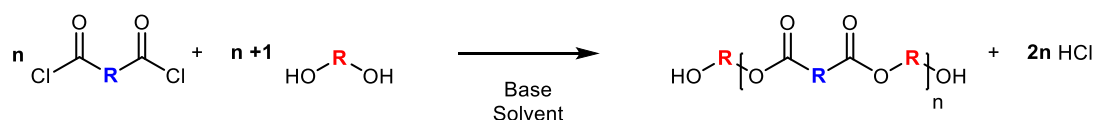


Scheme 1.8. Acetylating reaction employed to determine OHI.

The M_n of the generated polyesters can be determined by the end-group analysis, among others, with either the AI and OHI determination, or ^1H NMR spectroscopy. This latter analysis is carried out if the samples are soluble enough in a deuterated solvent and the chemical environment of the terminal and internal fragments are sufficiently different. The exact procedure will depend on the structure of the polymer and should be assessed for each new product.

Although successful results in polyester synthesis are generally obtained by the traditional polycondensation methodology, the long reaction times under harsh conditions restrict its use for unreactive or unstable monomers. Furthermore, melt-polycondensation is a variable process that requires continuous monitoring of the system. The loss of matter to conduct the analyses and the need to incorporate an extra quantity of diol in the transesterification step are additional drawbacks. These facts might be significant disadvantages when developing materials at a laboratory scale, although negligible in an industrial process.

As an alternative, polyesters can be also obtained at low temperature by the reaction of diols with highly reactive monomers, like activated carboxylic acid derivatives. Generally, this process achieves polymers in less time and milder conditions than conventional polycondensation of carboxylic acids, avoiding the transesterification step. The standard methodology entails the reaction of acyl chlorides and diols in chlorinated solvents in the presence of stoichiometric amounts of base (Scheme 1.9).^[52] Usually, nitrogen-based compounds, like pyridine or NEt_3 are employed as both, catalyst and HCl acceptor to neutralize *in-situ* the released acid, resulting in an irreversible reaction.

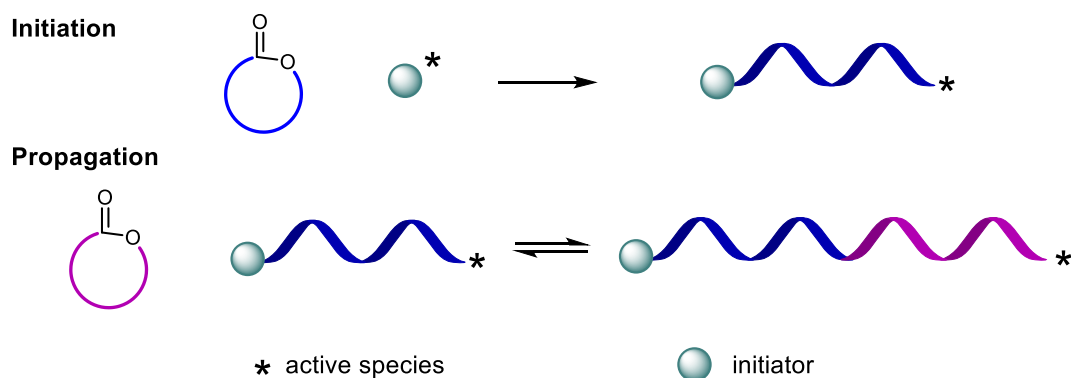


Scheme 1.9. General polycondensation of acyl chlorides.

This methodology sidesteps multiple AI and OHI titrations during the synthesis and the subsequent corrections. Therefore, no additional hydroxyl-terminated compound was required to tailor the polymer M_n . However, the generated nitrogen-based salt must be separated from the polymer employing filtration or extraction, somehow difficult to achieve at mass-production. Thereby, this process is not industrially friendly as large amounts of solvents are required for the neutralization and purification steps.

1.1.1.3.2. Ring-opening polymerization of lactones

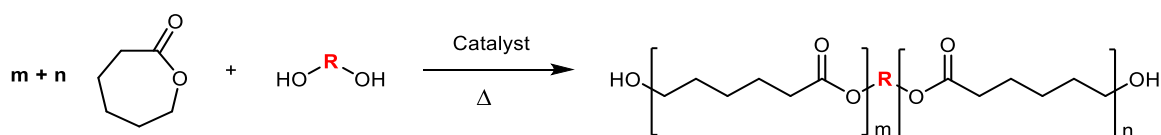
Although PCLs could be synthesized from the polycondensation reaction of **6-hydroxyhexanoic acid**, ROP of cyclic lactones is usually preferred. It consists of a chain-growth polymerization, in which the initiator ring-opens a cyclic monomer which then continues incorporating lactones to increase the polymer's length (Scheme 1.10). PCLs are obtained in solution, emulsion, or dispersion, but typically they are industrially produced at melt-phase with the presence of a catalyst. The main advantages of this methodology are its relatively mild conditions and the absence of small by-products as water.^[53]



Scheme 1.10. Fundamental steps in ROP.

Many cyclic compounds could be employed as monomers, but only a set of esters is thermodynamically favored to be polymerized by this methodology. ROP has a great dependence on the ring size and the substituents of the monomers.^{[54][55]} Owing to its seven-member ring and its strain, ϵ -caprolactone (**ECL**) is one of the most employed cyclic ester monomers. If the nucleophile to initiate the polymerization is a diol, linear growth of the

polymer is achieved by the two terminations of the initiator (Scheme 1.11). Increasing the functionality of the initiator modifies the final structure of the product, being possible to obtain hyperbranched molecules.



Scheme 1.11. ROP of ECL.

The main advantages of this class of polymers compared to others is the stoichiometric control of the terminal groups, the large diversities of structures that could be achieved by changing the initiator, the absence of water, and the low values of AI. The last two parameters are the reason behind the increase in hydrolytic stability.

1.1.1.4. Additives in TPUs

Although TPUs exhibit good chemical resistance, they are, like most polymers, susceptible to a loss of their mechanical properties by the slow degradation of their structure by temperature, oxygen, light, or humidity. To reduce to the maximum extent the disruption of their backbone and increase the service lifetime of the materials, some additives are incorporated into formulations in small percentages with specific targets.^{[56][57]}

One of the main causes of degradation is the oxidation of the polymer during the synthesis or the molding process. The mixture of atmospheric oxygen and elevated temperature may result in carbonyl or peroxide groups, which foster photo-degradation. It consists of a chain reaction with a fast self-propagating step. Usually, polymers suffering from this deterioration process exhibit an increase in color and a decrease in the mechanical properties as a consequence of the chain scission. To reduce it to the minimum possible, the injecting profile temperatures should be optimized, and some antioxidants and UV stabilizers may be incorporated into the formulation (Figure 1.6).

The habitual thermal antioxidant molecules are hindered phenols that avoid the degradation process by oxidizing themselves to colored quinones, phosphite esters, and secondary aromatic amines.^[58] Some synergetic effects might be obtained by employing two types of antioxidants as they partake in different action mechanisms.

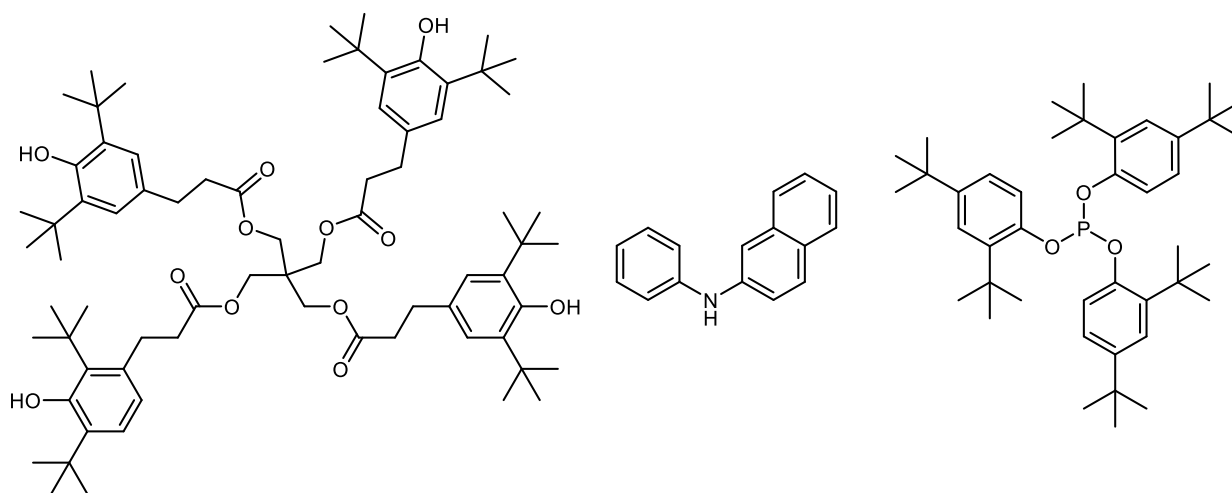


Figure 1.6. Chemical structure of some of the most used antioxidants.

When high-energetic ultraviolet (UV) radiation is involved in the cleavage of bonds, some UV stabilizers with strong absorption in this region of light and stable aromatic excited states might be used. Some well-known stabilizers are based on hydroxybenzophenone or hindered amines as piperidine, among others (Figure 1.7).^[56]

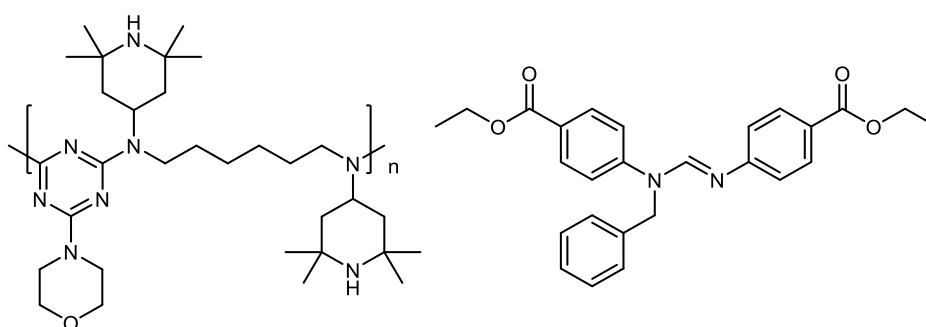


Figure 1.7. Chemical structure of examples of UV-stabilizers and antioxidants.

Because of the multiple ester groups in a polyol, they are easily cleaved in the presence of water, shortening the M_n of the polymer and producing carboxylic acid moieties. Moreover, they autocatalyze further reactions leading to the additional loss in properties. To prevent further hydrolysis of the polyester chain, carbodiimides are used as acid scavengers (**Figure 1.8**).^[59]

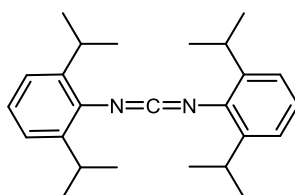


Figure 1.8. Example of a hydrolysis stabilizer.

Therefore, the use of stabilizers is often vital to obtain products with the appropriate lifespan and enhance the material's properties.^[60]

1.2. TPU structure-properties relationship

The combination of isocyanates with short and long hydroxylated-terminated compounds (chain extender and polyols) generates the segmented structure formed by HS and SS. As previously discussed, each domain plays a specific role in the properties of the final material. The latter confers flexibility to compound, especially at low temperatures, owing to the disordered nature of the long polyols, which lead to low T_g values. Conversely, the HS consists of chain extenders and isocyanate groups, resulting in areas with a high concentration of carbamate moieties, which create strong hydrogen-bonding interactions and favor their packing and crystallinity. Hence, HS is the rigid and hard domain that acts as a physical cross-link or reinforcement filler, being responsible for the mechanical properties of the material.^[24]

When isocyanates are condensed exclusively with polyols, omitting chain extenders in the formulation, no phase segregation is formed in the PUs and poor physical properties are observed.^[61] This clearly marks the need for phase segregation systems to obtain materials with the desired properties, as the higher the material's phase segregation, the higher its strength, hardness, and thermal and chemical stability will be.^[62] However, understanding the different factors that regulate the degree of phase segregation of TPU systems is an arduous job as there is a large number of variables, some synergistic, others antagonistic, to take into account. These factors include the miscibility of the segments, given by the HS content, the intermolecular interactions of the HS, the type and M_n of the polyols of the SS, and the employed reagents, among others. Therefore, without the aim of detailing the properties of each TPU, some general trends are discussed hereafter.

1.2.1. HS content

The HS content corresponds to the percentage of HS, in weight, with respect to the total weight of TPU. It can be calculated according to several manners, but in this manuscript it will be understood as it is depicted in **Equation 1.1**, in which $W_{(NCO)_r}$, $W_{(CE)_r}$ and $W_{(total)}$ are the weight in grams of diisocyanate bounded to any chain extender, the chain extender in the mixture and the total weight of the TPU, respectively. This is an equal number of mols of chain extender

than diisocyanate. The employed estimation only ponders those isocyanates that contribute to the HS and differs from other expressions that overestimate the amount of HS in the sample.

$$HS \text{ content}[\% HS] = \frac{w_{(CE)} + w_{(NCO)}}{w_{(total)}} \quad \text{Equation 1.1}$$

An increase in the HS content in the polymer (remaining constant the overall molar ratio of $[NCO]/[OH]$) leads to more crystalline samples, consequently with higher strength, and thermal and abrasion resistance.^[63] Conversely, as a general trend, the greater the percentage of SS in a TPU, the higher is their flexibility and the elongation to break, and the lower the temperature in which the material remains elastomeric. However, the hardness decreases as well as the elastic modulus.^[64]

Koberstein, Stein, and Leung studied the effect of the HS in the TPUs, concluding that extremely low HS contents led to no phase segregation as the isocyanate-chain extender segments dissolved in the SS. They proposed that a critical length of the HS chains fragment was required to cause two morphologies. Moreover, the more and longer the HS regions, the better the folding and coiling of the chains to form these ordered polar regions is (Figure 1.9).^{[65][66][67]} As the HS content increases, the average length of the segment also rises, favoring the aggregation between the chains and increasing the strength of the material.^[68]

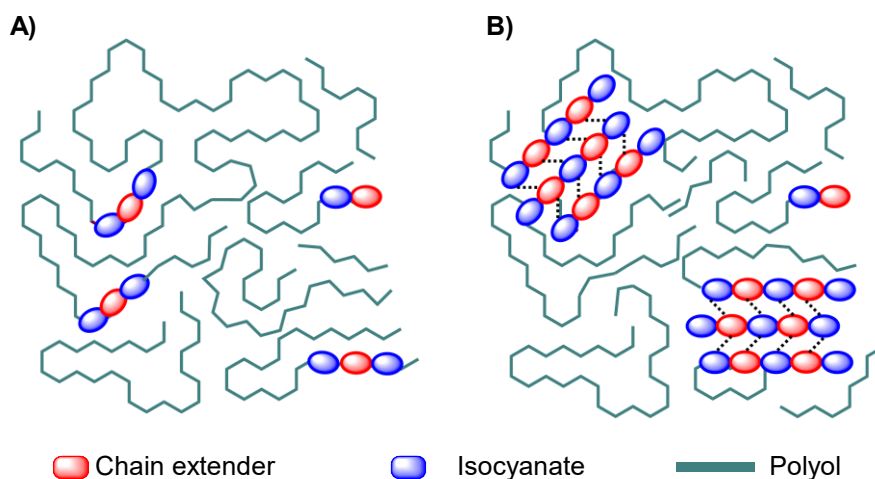


Figure 1.9. Schematic representation of Koberstein-Stein model. A) Dispersion of the HS in the SS. B) Phase segregation consequence of ordered HS.

1.2.2. HS interactions

In addition to increasing the content of HS and obtaining the optimal properties of the materials, the HS must be ordered. This increase in crystallinity is achieved through the formation of stronger interactions among the HS chains. Hence the selection of both the

isocyanate and the chain extender plays a relevant part in the final properties of the TPU. An increase in the molecular packing could be obtained by employing short diols which would increase the urethane concentration and the corresponding hydrogen bond density. Moreover, while linear backbones will promote to different extends the interaction between the chains, branched compounds will disrupt the packing owing to their higher molar volume, as few interactions will be formed (Figure 1.10). Moreover, backbones with an even number of carbons promote to a greater extent the symmetry of the HS which allows a better packing efficiency of the chains and therefore, a higher crystallinity.^{[69][70][71]}

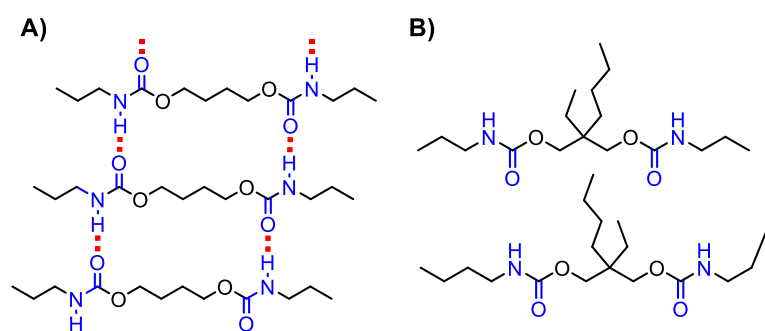


Figure 1.10. Schematic representation of the HS interactions as a function of A) linear chain extenders and B) branched-chain extenders.

Just as with the chain extenders, the isocyanate's symmetry increases the chain packing of the samples, facilitating the formation of supramolecular interactions and the corresponding ordered domains.^[72]

1.2.3. Effect of the SS

It has been extensively reported that the type of polyol, either polyether, polyester, or polycarbonate has a huge impact on the phase segregation of the material, owing to the interaction with the carbamate moieties in the HS. As was mentioned before, polyethers are compounds with poor polarity and incapable of acting as strong hydrogen-bond acceptors. Their lack of attraction forces and the corresponding difference in polarity with the HS, causes a high degree of phase segregation, which is translated into a high crystallinity of the material.^{[73][74]} However, owing to the poor cohesion forces of the SS, this is not observed as materials with high tensile strength, but rather as polymers with good rebound resilience and elastic recovery.^{[75][76][77]}

Contrarily, the carbonyls of polyester and polycarbonates can act as hydrogen bond acceptors of the HS carbamate moieties and trigger the mixing of both phases. As consequence,

polyester-based TPUs have less phase segregation and less ordered HS regions than polyether-based TPUs. Overall, the highest phase segregation will be achieved with polyethers > polyesters > polycarbonates when linear aliphatic systems are compared.^{[78][79]} If aromatic and branched structures are considered, the order might vary owing to the additional π - π stacking or by the steric hindrance of the dangling chains. The effect of this modification has to be studied for each system, as different behavior can be observed, from a high decrease in the crystallinity to foster a better packing by their segregation of the dangling chains away from the main backbone. Ultimate, it should be reminded that especially polyester might also exhibit chain packing in the form of crystallites that might modify the properties of the TPU. Another factor that affects the microphase structure of TPUs is the M_n of the involved compounds. In the case of the polyols, an increase in the M_n leads to less compatible segments, and better phase segregation was achieved.^[80] Finally, by the same token as the chain extender, those polyols that are formed by even monomers, have better chain packing, resulting in ordered structures that would not mix with the HS.^[81]

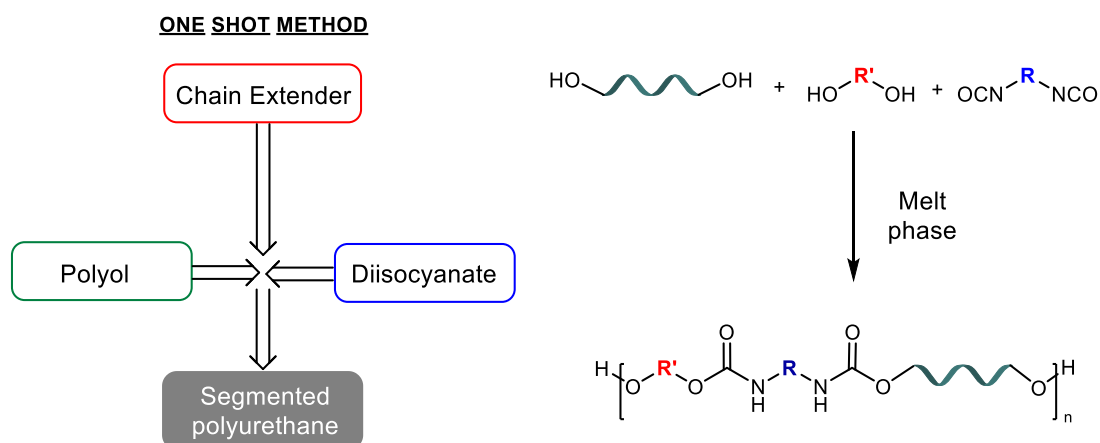
As was remarked, multiple parameters affect the microphase morphology, and thus, the properties of a TPU, all of which need to be considered to understand and try to predict the material behavior. This difficult to a great extent the parametrization of the behavior of this class of polymers.

1.2.4. TPU production

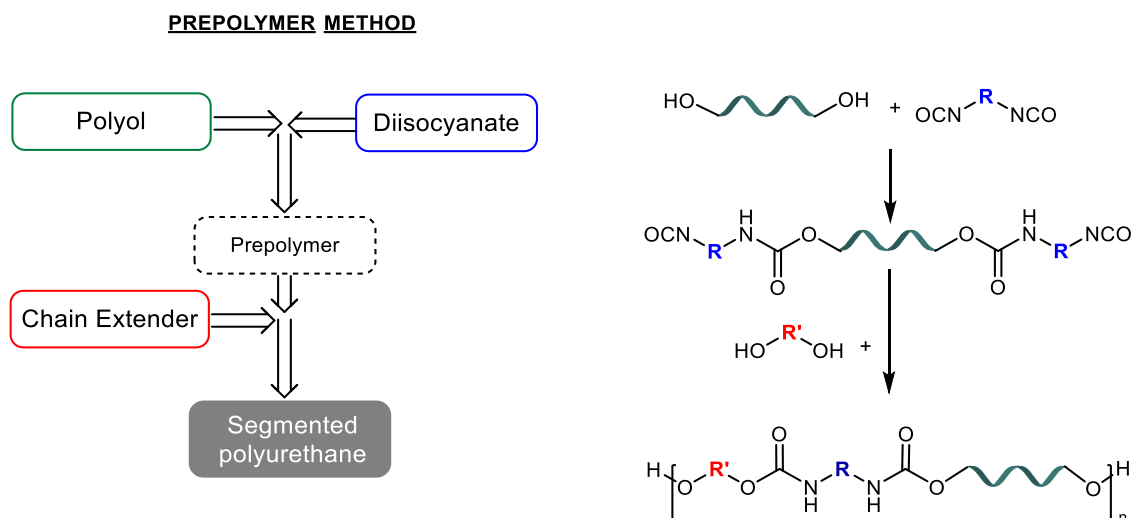
Moreover, the final properties of a material do not only depend on the partaking constituents and the ratio among the reagents, but also its synthetic method. In the TPU field, there are two common approaches to obtain the target products: the *one-shot* method and the *prepolymer* method.^{[1][82][83]} Both methods use moisture-sensitive compounds; therefore, reagents and solvents must be carefully dried previously to their use.

One-shot method can be considered as the fastest and easiest approach to manufacture TPUs. It involves the simultaneous addition of the three components with the appropriate stoichiometry along with the required additives and catalyst. (Scheme 1.12).^[84] Once all the reagents are mixed in the melt phase, the reaction begins immediately, generating an exothermic transformation. Commonly, the produced material requires a curing time of a few hours after the reaction. This method has the advantage of avoiding the use of solvents and the small reaction time (usually less than 5 minutes), which results extremely practical at an industrial scale. The polymer produced by this method has a completely random structure

arising from the reactivity of the embroiled groups. However, as the reaction depends on the diffusion of the reagents, the higher mobility of the chain extender and the diisocyanate in comparison with the long chains of the polyol lead to relatively large, polydispersed HS chains domains. Moreover, a very low proportion of HS fragments containing a single diisocyanate unit are obtained. This leads to products with a high degree of phase segregation as the large HS fragments have an increased capacity for crystallization.^{[80][85][86]}



Conversely, the *Prepolymer method* consists of a two-step process (Scheme 1.13). First, a low M_n isocyanate-terminated prepolymer is formed by the reaction between an excess of isocyanate and the polyol. The temperature must be controlled to avoid secondary reactions between the unreacted isocyanate moieties. Then, a suitable amount of chain extender is added to complete the polymerization. Owing to the high viscosity of the mixture, non-protic polar solvents like *N,N*-dimethylformamide (DMF), and *N,N*-dimethylacetamide (DMAc) are usually employed to produce a more homogeneous mixture and promote the formation of high M_n TPUs. In some cases, mainly in academic researches, the quantity of free isocyanate in the prepolymer is quantified by titration.^[87]



Products obtained by this methodology are considered multiblock copolymers. Although the chains possess a higher symmetry,^[88] lower phase segregation is usually obtained employing this procedure. During the synthesis, a large amount of HS fragments containing a single diisocyanate unit are obtained as the concentration of free diisocyanate units is extremely low once the addition of chain extender is effectuated. This hampers the phase segregation of the system and leads to products with a low number of HS crystallites.^{[80][85]}

1.2.5. Post-process treatments: Annealing

Although the phase segregation process is thermodynamically favorable, sometimes it can be restricted due to a low chain movement of the material, resulting in materials with short HS chains dissolved in the SS domains. To obtain all the potential of the synthesized TPUs, sometimes the produced material must be subjected to thermal treatment for a certain period of time, which is known as annealing. Subjecting the material to a high temperature might foster the development of well-organized HS domains and to higher phase segregations, which might modify the microphase morphology and consequently, the properties of the treated TPU.^[89] In this way, increasing the mobility of the chains might aid in the rearrangement of the two segments and form more stable systems with a higher number of supramolecular interactions. Heating at temperatures below the T_m of the HS, fosters the SS chains mobility and the rearrangement of the domains. This might result in the formation of new crystallites

within the matrix of the polymer that will act as cross-linking points increasing the mechanical properties of the material.^[90]

However, heating at a temperature over the T_m of the HS, results in even higher mobility of the HS and the disruption of the ordered regions of the HS. The outcome of the so high temperature is a complete phase mixing and the corresponding loss of the mechanical and physical properties of the material. The increasing temperature might have the disadvantage of the "leaching/disentangling" of the HS. Therefore, the annealing temperature has to be carefully selected.

1.3. Fluorinated polymers

Since the serendipitous discovery in 1938 of polytetrafluoroethane or Teflon®(PTFE, Figure 1.11) by Roy J. Plunkett,^[91] the research about macromolecules containing fluorine has not stopped. Teflon® is possibly one of the most known fluorinated compounds, but it exhibits complex processability owing to its highly viscous melt stage.^[92] Moreover, its monomer, tetrafluoroethylene, is synthesized by an energy-consuming process (>10 000 kWh/ ton of monomer), is difficult to handle, and is highly explosive to air.^{[93][94][95]} However, PTFE displays unique properties, like lubricity, reduced Surface Free Energy (SFE = 20 mN/m), low friction (static coefficient of friction $\mu_s=0.05-0.08$), antiadhesion, and chemical inertness to moisture, acids, bases, and organic solvents. The reason behind these remarkable properties is fluorine.^{[96][97][98]}

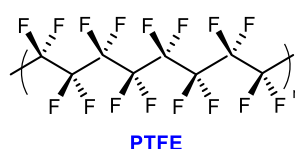


Figure 1.11. Chemical structure of PTFE.

Fluorine has an electronic configuration of 9 closely packed electrons, in contraposition with the single electron of hydrogen. Thus, the electronic density of fluorine is considerably larger, which justifies its values of ionization energy (17.42 eV), electron affinity (328 kJ/mol), and electronegativity. This halogen is by far the most electronegative element, with a value of 4.0 on Pauling scale, while other conventional elements like oxygen or chloride exhibit smaller values (Table 1.1). Owing to its electron-withdrawing behavior, the bonds formed by fluorine are highly polar (*e.g.* C-F dipole moment = 1.51). This increase in the polarity of the system results in the formation of the strongest single bond with carbon (Table 1.1).^[96] Its polarity, as

well as its high electronic density, changes the behavior of perfluorocarbons compared to common hydrocarbons. The inductive effect of fluorine atoms does not only modify the bounded element, but also the common reactivity of other neighboring functional groups, like decreasing the basicity of fluorinated amines or increasing the acidity of alcohols.^{[99][100]} Moreover, it also causes an increase in the energy required to dissociate the neighboring bonds, and thereby, molecules comprising the halogen exhibit higher thermal stability (*e.g.* the C-C bond energy is 413 kJ/mol in $\text{CF}_3\text{-CF}_3$ whereas in $\text{CH}_3\text{-CH}_3$ is 376 kJ/mol).^[101] The non-bonding electrons pull the electronic density toward the halogen nuclei in a C-F bond, shielding the central carbon, and decreasing its susceptibility to being attacked, thus forming compounds with higher chemical resistance.

Table 1.1. Properties overview of selected elements. Adapted from ^{[102][101][103]}.

	H	O	F	Cl
Electronic configuration	$1s^1$	[He] $2s^2 2p^4$	[He] $2s^2 2p^5$	[Ne] $3s^2 3p^5$
Electronegativity (Pauling scale)	2.1	3.5	4	3.0
Van der Waals radius (Å)	1.20	1.52	1.47	1.75
Bond dissociation C-X (kJ/mol)	414	352	485	331
Bond length of C-X	1.09	1.43	1.32	1.78

Fluorine possesses a relatively small size but differs from hydrogen radius (Table 1.1). Although the substitution of hydrogen by fluorine atoms does not radically change the structure of the molecules that contain the halogen, both elements cannot be considered isosteric. Fluorine's radius is closer to that of hydroxyl, and regarding hydrocarbons, the $-\text{CF}_3$ van der Waals volume resembles more to an ethyl group than to the methyl (Figure 1.12).^[104] Therefore, the trifluoromethyl group is bulkier than its hydrogen analog.^[105]

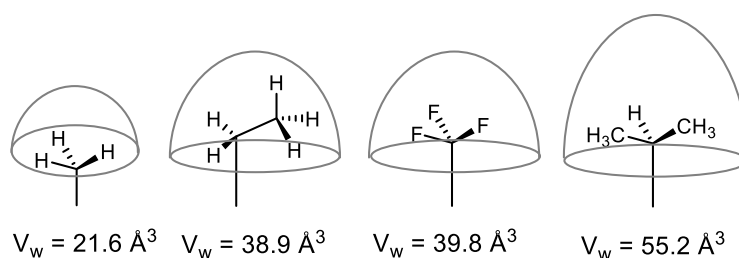


Figure 1.12. Representation of the van der Waals hemisphere.

The slight size variation between fluorine and hydrogen, the significant polarity of the C-F bonds, and the corresponding low polarizability cause a decrease in London forces between fully perfluorinated linear chains. The weak cohesive forces of fluorinated compounds are

manifested in properties like higher vapor pressures and lower, or quite similar boiling points than their hydrogen-containing analogs, although the formers have much higher M_w .^[106]

As a general trend, the replacement of hydrogen by fluorine improves the thermal stability, the electrical and optical properties. Despite the low intermolecular forces between the perfluorinated species, their melting temperature (T_m) and the T_g are higher than their corresponding hydrogenated counterparts, owing to the difference in structural packing resulting in more crystalline materials.^[98] At the same time, the low cohesive energy of this type of polymer triggers low values of coefficient of friction and dielectric constant.^[107] Most of these improvements arise from the repulsion among the non-bonding electrons of fluorine, the low polarizability of the C-F bond, and the shielding of the carbon backbone which provides a robust structure with few intermolecular forces, resulting in materials in which the chains slide over each other.^[105] However, the lack of attractive forces between the polymer worsens the mechanical properties as fluorine content increases.^[108]

When water or other liquids are deposited onto the surface of a perfluorinated compound, the internal adhesion interactions of the liquid molecules are greater than those formed with the moieties on the outermost region of the material. Therefore, as the material has a low SFE, the drop does not spread and remains a circular entity. Moreover, owing to the poor capability of fluorine to act as hydrogen bond acceptor (2-3 kcal/mol),^{[109][110]} perfluorinated molecules display fewer interactions with water, generating hydrophobic interfaces. The mentioned tendency is exemplified in Table 1.2 where the surface tension of perfluorocarbons is compared with their hydrocarbon analogs, displaying in all cases the lowest values.

Table 1.2. Surface tension values of fluorocarbons and hydrocarbons analogs.^[111]

Substance	Surface tension (mN/m)	
	Perfluorocarbon	Hydrocarbon
<i>n</i> -pentane	9.4	15.2
<i>n</i> -hexane	11.4	17.9
<i>n</i> -octane	13.6	21.1
benzene	22.6	28.5

SFE is inversely proportional to contact angle (CA); therefore, weak interactions between liquids and solids are obtained in systems in which the CA is high and the SFE value is low. Among all fluorinated chains, some totally and other partially fluorinated, Zisman *et al.* analyzed the effect of the atomic composition of the surface with monolayers containing different fluorinated moieties.^[112] They concluded that the most substantial reduction of the SFE was accomplished

with the higher density of the $-\text{CF}_3$ groups, followed by $-\text{CHF}_2$ and $-\text{CF}_2-$. The reported SFE values for surfaces closed-packed enriched in those moieties are 6 mN/m, 15 mN/m, and 18 mN/m, respectively.^[113]

Fluoropolymers are synthesized by fluorination of a hydrocarbon, addition polymerization, or free-radical polymerization, usually in water-based processes.^{[92][114][115][116]} Temperature, initiators, pressure, emulsifiers, and catalyst are carefully controlled for each specific reaction to obtain the desired compound. Their challenging synthesis and their limited availability are some of the reasons behind the high price of these polymers in comparison with their hydrogenated analogs. Furthermore, one of their most important drawbacks is their processability. Owing to their high tendency to crystallize, they are difficult to solubilize in organic solvents and require to be sintered to be processed. To avoid these drawbacks and broaden their potential applications, copolymerization of fluorinated monomers with bulky moieties that decrease the efficiency of the chain packing or copolymerize with other functional groups is extensively researched (Figure 1.13).^{[117][118]}

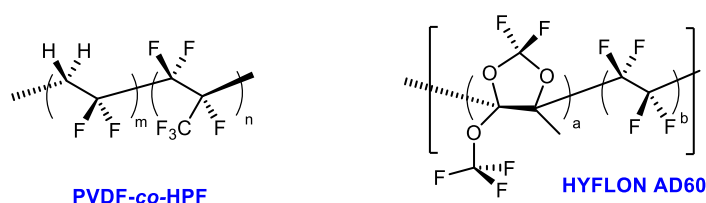


Figure 1.13. Examples of fluorinated copolymers.

1.3.1. Fluorinated TPUs

PUs are notoriously materials employed in every branch of industry, but among the infinity number of applications, their use in wearable products or the support for them is sought in this current thesis. The essential characteristic that a wearable must exhibit is flexibility, lightweight, mechanical and thermal resistance, and compatibility with other systems.^[119] However, PUs display SFE values up to 40 mN/m owing to the high concentration of polar groups on the material,^{[120][121]} which facilitates the appearance of discolored areas or stains in the material or even the degradation of it by its hydrolytic instability in contact with water. Overall, this behavior could be translated into fair-quality products, or at least with short service life.

Therefore, an enhancement of the surface properties is sought to prevent this type of shortcomings and produce added-value materials.

As has been previously mentioned, fluorine-containing molecules are known to decrease the interfacial energy of the system, achieving in some cases SFE values of 12 and 15 mN/m, which produces materials with low friction, hydrophobicity, and oleophobicity, properties that are lacking in most TPUs. Therefore, blending of fluorinated and fluorine-free compounds with enough SFE difference is proposed to reach an enhancement of the properties. The reorganization and the segregation of the halogenated chains toward the outmost part of the product, derived from their poor cohesion interactions, would minimize the interfacial free energy of the material.^{[122][123]} As a result, TPUs bearing fluorinated compounds could combine properties of both systems, and promote the segregation of the fluorine to the surface while maintaining its outstanding properties, leading to materials with low SFE, hydrophobicity, thermal resistance, oxygen permeability, flexibility, and weatherability. Hence, the use of fluorinated structures in TPUs is industrially appealing.

The SFE of fluorinated macromolecules depends on two factors: the efficiency of the fluorinated chain packing and the amount of fluorine on the surface. Optimal results in terms of wettability are found when perfluorinated chains ended in trifluoromethyl groups are closely packed and with an elevated concentration of the halogen, ideally saturating the outmost layer of the solid. Regarding the surface properties, small percentages of fluorine do affect the SFE and contact angle of the polymer.^[124] However, changes in the morphology of the phases or the mechanical properties might require higher quantities of fluorine.

Since most of the mass production of TPUs is carried out by polycondensation of diisocyanates with alcohols, both chain extender or polyols, the main strategies are focused on polymerizing molecules containing the halogen, instead of modifying the already formed polymer.^{[125][126][127]}

Fluorinated diisocyanates are the least employed, owing to their difficulty generation and their thermal and hydrolytic instability of the generated PU. However, a few examples are reported in the literature (Figure 1.14).^{[125][126]}

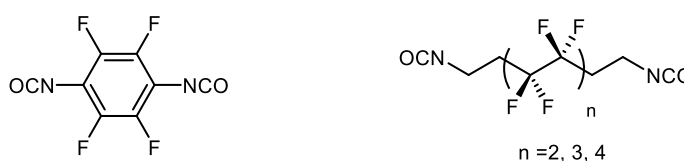


Figure 1.14. Examples of fluorinated structures used for the PU synthesis.

Fluorinated chain extenders are frequently employed owing to their broad range of structures, from aliphatic to aromatic, and from linear to branched, as can be seen in Figure 1.15. Nevertheless, all of them share the same feature, the fluorinated fragment is spaced from the hydroxyl moiety by at least one methylene group. This spacing is introduced to reduce the inductive effect of the halogen and increase the reactivity of the termination.^[128] When lineal fluorinated diols are employed as components of the HS, the crystallinity of this segment increased, as well as the enrichment of the segment concentration in the outermost part of the studied material. It results in materials with higher tensile strength and low elongation to break.^[129] One of the most employed is the 2,2,3,3,4,4,5,5-octafluorohexanediol (**HDO-8F**), likely by its symmetry.^[130]

The second class of chain extenders contains the fluorinated entity as a side chain. This generates higher mobility of the branched group than their linear counterpart and allows the rearrangement of the tails with a superior packing efficiency on the surface. Moreover, those chains terminated with a fluorinated group, especially a trifluoromethyl moiety are more prone to migrate. Tan *et al.* reported that an increase in the phase segregation was detected when the concentration of fluorinated tangling chains rises as the inductive effect of fluorine surprisingly promotes the formation of stronger hydrogen bonds between the carbamates groups in the HS.^[131]

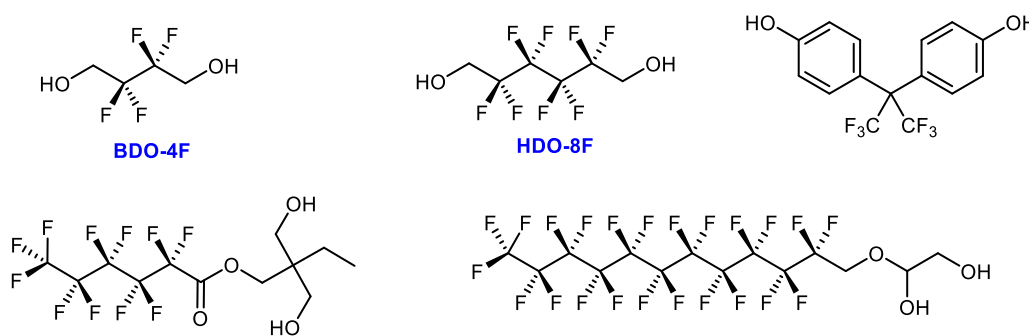


Figure 1.15. Examples of fluorinated chain extenders.

Finally, the last strategy involves the use of fluorinated polyol. The most usual class of polymers used are polyethers, as the ether bond provides flexibility to the macromolecule and form weak interactions with other chains. Similarly to the fluorinated chain extenders, multiple architectures with different halogen content and M_n can be employed. Their structure can be a central hydrocarbon backbone with fluorinated side groups or be alternate short fragments with and without fluorine (Figure 1.16).

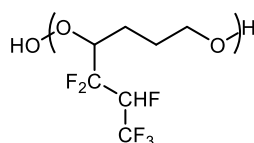


Figure 1.16. A few examples of commonly employed fluorinated polyethers.

The introduction of fluorinated macromolecules increases phase segregation, mainly when using perfluoropolyethers. However, it depends on the M_n of the polyol. Delucchi *et al*/ studied the effect of the polyether length in TPUs, concluding that higher M_n resulted in better surface and mechanical properties. Conversely, when shorter chains were employed ($M_n \approx 500$ g/mol) the material presented a single phase in which the polyol was mixed with the HS. ^[132]

Relatively good properties are obtained with perfluoroether polyols when the HS content is moderately high. However, when this parameter decreases, worse mechanical properties are obtained. To prevent this decline, some authors report the blending of two different polyols in a SS, like a second non-fluorinated polyether or a polyester. ^{[124][133]}

To summarize, TPUs produced with fluorinated chain extenders and polyols with an elevated number of CF_2 and CF_3 groups, exhibited higher thermal stability than the fluorine-free analogs, both in terms of transition temperatures and degradation onsets, owing to the shielding of the carbon backbone by the halogen. ^[130] Moreover, excellent surface properties are reached if fluorine can migrate to the outermost region of the material and arrange in relative order, especially pointing the CF_3 to the air-solid interface. However, most of the explored compounds display an elevated price in the market, which hampers their industrial application.

1.4. Lubrizol Corporation

Lubrizol Corporation is a multinational company founded in 1928 focused on the development of new materials for a sustainable future. It is segmented into three main markets: *Lubrizol Additives*, *Lubrizol Corporate Ventures*, and *Lubrizol Advanced Materials*. The former is dedicated to the generation of fluids for the automobile field to increase energy efficiency, reduce emissions and improve the durability of engines, either combustion or electric. *Lubrizol Corporate Ventures* is the newest incorporation and has the aim of solving the challenges of energy and thermal management. Finally, *Lubrizol Advanced Materials* is focused on the generation of wellness-related products. ^[134]

The multinational company, headquartered in Wickliff, Ohio (USA), has around 8800 employed in more than 100 countries and 100 different facilities. One of them is located in Montmelò, Lubrizol Engineered Polymers, and it is focused on the production of specialty TPUs for footwear, electronics, automotive, adhesives, or protection films, among other applications.

The following thesis has been developed in collaboration with Lubrizol Engineered Polymers in two different projects: the generation of new fluorinated TPUs with improved surface properties (Part 1) and the study of an industrial process to generate TPU films (Part 2).

Literature

- [1] M. Szycher, *Szycher's Handbook of Polyurethanes*, Taylor & Francis, Boca Raton, United States, **n.d.**
- [2] J. Datta, P. Kasprzyk, *Polym. Eng. Sci.* **2018**, *58*, E14–E35.
- [3] R. Bonart, E. H. Müller, *J. Macromol. Sci. Part B Phys.* **1974**, *10*, 177–189.
- [4] M. Szycher, in *Szycher's Handb. Polyurethanes* (Ed.: M. Szycher), Taylor & Francis Group, Boca Raton, **2013**, pp. 37–86.
- [5] S. Velankar, S. L. Cooper, *Macromolecules* **2000**, *33*, 382–394.
- [6] S. Velankar, S. L. Cooper, *Macromolecules* **1998**, *31*, 9181–9192.
- [7] P. J. Yoon, C. D. Han, *Macromolecules* **2000**, *33*, 2171–2183.
- [8] M. F. Sonnenschein, in *Polyurethanes. Sci. Technol. Mark. Trends*, John Wiley & Sons Inc., Hoboken, New Jersey, **2015**, pp. 20–114.
- [9] L. Cotarca, H. Eckert, in *Phosgenations - A Handb.* (Eds.: L. Cotarca, H. Eckert), Wiley-VCH Verlag GmbH&Co. KGaA, Weinheim, **2003**, pp. 44–148.
- [10] J. Disteldorf, W. Hubel, J. Reiffer, *Process for Continuous Hot Phosgenation of Amines*, **1985**, 4,549,991.
- [11] M. S. Kathalewar, P. B. Joshi, A. S. Sabnis, V. C. Malshe, *RSC Adv.* **2013**, *3*, 4110–4130.
- [12] P. Dannecker, M. A. R. Meier, *Sci. Rep.* **2019**, 1–6.
- [13] P. Stachak, I. Łukaszewska, E. Hebda, K. Pielichowski, **2021**.
- [14] C. Six, F. Richter, in *Ullmann's Encycl. Ind. Chem.*, **2003**, pp. 63–82.
- [15] H. Sardon, A. Pascual, D. Mecerreyes, D. Taton, H. Cramail, J. L. Hedrick, *Macromolecules* **2015**, *48*, 3153–3165.
- [16] A. L. Silva, J. C. Bordado, *Catal. Rev. - Sci. Eng.* **2004**, *46*, 31–51.
- [17] F. Parodi, in *Compr. Polym. Sci. Suppl.* (Eds.: G. Allen, J.C. Bevington), Elsevier Ltd., **1989**, pp. 387–412.
- [18] M. Kaplan, *J. Chem. Eng. Data* **1961**, *6*, 272–275.
- [19] M. Szycher, in *Szycher's Handb. Polyurethanes* (Ed.: M. Szycher), Taylor & Francis Group, LLC, **2013**, pp. 87–133.
- [20] K. . Saunders, in *Org. Polym. Chem.* (Ed.: K.J. Saunders), Chapman And Hall, New York, **1988**, pp. 358–387.
- [21] M. V. Pandya, D. D. Deshpande, D. G. Hundiwale, *J. Appl. Polym. Sci.* **1986**, *32*, 4959–4969.
- [22] M. Szycher, in *Szychers Handb. Polyurethanes, Second Ed.* (Ed.: M. Szycher), Taylor & Francis Group, LLC, **2013**, pp. 155–180.
- [23] C. Lee, C. Chen, S. Rwei, F.-S. Chuan, *Appl. Sci.* **2021**, *11*, 1–18.
- [24] T. J. Touchet, in *Adv. Polyurethane Biomater.* (Eds.: S.L. Cooper, J. Guan), Elsevier Ltd, Duxord, England, **2016**, pp. 3–22.
- [25] G. Pruckmayr, P. Dreyfuss, M. P. Dreyfuss, *Kirk-Othmer Encycl. Chem. Technol.* **2000**, 1–24.

- [26] A.-L. Brocas, C. Mantzaridis, D. Tunc, S. Carlotti, *Prog. Polym. Sci.* **2013**, *38*, 845–873.
- [27] C. Hepburn, in *Polyurethane Elastomers* (Ed.: C. Hepburn), Springer Science + Business Media, Dordrecht, The Netherlands, **1992**, pp. 51–106.
- [28] G. Sacchetti, S. Mussini, B. Maccari, *J. Cell. Plast.* **1993**, *29*, 13–28.
- [29] E. Saldívar-Guerra, E. Vivaldo-Lima, Eds., *Handbook of Polymer Synthesis, Characterization and Processing*, John Wiley & Sons Inc., Hoboken, United States, **2013**.
- [30] H. R. Kricheldorf, O. Nuyken, G. Swift, Eds., *Handbook of Polymer Synthesis*, Marcel Dekker, New York, United States, **2005**.
- [31] H. R. Kricheldorf, *Polycondensation. History and New Results*, Springer-Verlag Berlin Heidelberg GmbH, Heidelberg, Germany, **2014**.
- [32] Q. Zhang, M. Song, Y. Xu, W. Wang, *Prog. Polym. Sci.* **2021**, *120*, 101430.
- [33] L. Xi-lan, G. Xiu-fen, S. Jia-long, S. Guag-yan, *J. Phys. Conf. Ser.* **2020**, *1635*, 1–8.
- [34] L. N. Woodard, M. A. Grunlan, *ACS Macro Lett.* **2018**, *7*, 976–982.
- [35] M. Ionescu, *Chemistry and Technology of Polyols for Polyurethanes*, Rapra Technology, Shropshire, United Kingdom, **2005**.
- [36] M. Hakkarainen, *Adv. Polym. Sci.* **2002**, *157*, 113–138.
- [37] A. C. Albertsson, I. K. Varma, R. K. Srivastava, in *Handb. Ring-Opening Polym.* (Eds.: P. Dubois, O. Coulembier, J.-M. Raquez), Wiley-VCH Verlag GmbH&Co. KGaA, **2009**, pp. 287–306.
- [38] L. S. Nair, C. T. Laurencin, *Prog. Polym. Sci.* **2007**, *32*, 762–798.
- [39] S. M. Kamath, K. Sridhar, D. Jaison, V. Gopinath, B. K. M. Ibrahim, *Sci. Rep.* **2020**, *10*, 1–13.
- [40] A. Mun, H. S. Yameen, G. Edelbaum, D. Seliktar, *Sci. Rep.* **2021**, *11*, 1–12.
- [41] A. G. A. Coombes, S. C. Rizzi, M. Williamson, J. E. Barralet, **2004**, *25*, 315–325.
- [42] P. J. Flory, *Chem. Rev.* **1946**, *39*, 137–197.
- [43] P. J. Flory, *Principles of Polymer Chemistry*, **1953**.
- [44] W. H. Carothers, *Collected Papers of Wallance Hume Carothers on High Polymeric Substances*, **1940**.
- [45] I. J. Goldfarb, R. McGuchan, *THERMAL DEGRADATION OF POLYESTERS I. Aliphatic Polymers*, **1968**.
- [46] F. D. Trischler, J. Hollander, *J. Polym. Sci. Part A-1 Polym. Chem.* **1969**, *7*, 971–975.
- [47] Y. Shibata, A. Takasu, *J. Polym. Sci. Part A Polym. Chem.* **2009**, *47*, 5747–5759.
- [48] A. Takasu, Y. Oishi, Y. Iio, Y. Inai, T. Hirabayashi, *Macromolecules* **2003**, *36*, 1772–1774.
- [49] P. Buzin, M. Lahcini, J. Schellenberg, G. Schwarz, H. R. Kricheldorf, *Macromolecules* **2008**, *41*, 8491–8495.
- [50] B. D. Ahn, S. H. Kim, Y. H. Kim, J. S. Yang, *J. Appl. Polym. Sci.* **2001**, *82*, 2808–2826.
- [51] T. Kajiyama, H. Kobayashi, T. Taguchi, K. Kataoka, J. Tanaka, *Biomacromolecules* **2004**, *5*, 169–174.
- [52] R. J. Ouellette, in *Org. Chem.*, Elsevier, London, England, **2018**, pp. 625–663.
- [53] M. Labet, W. Thielemans, *Chem. Soc. Rev.* **2009**, *38*, 3484–3504.
- [54] A.-C. Albertsson, S. Boileau, M. R. Buchmeiser, O. Coulembier, O. Dechy-Cabaret, P. J. Dijkstra, A. P. Dove, P. Dubois, A. Duda, C. J. Duxbury, et al., *Handbook of Ring-Opening Polymerization*, Wiley-VCH Verlag GmbH&Co. KGaA, Weinheim, Germany, **2009**.
- [55] X. Zhang, M. Fevre, G. O. Jones, R. M. Waymouth, *Chem. Rev.* **2018**, *118*, 839–885.
- [56] V. Marturano, P. Cerruti, V. Ambrogi, *Phys. Sci. Rev.* **2017**, *2*, 1–20.
- [57] H. Zweifel, *Stabilization of Polymeric Materials*, Springer, Heidelberg, Germany, **1998**.
- [58] R. F. Grossman, in *Polym. Modif.* (Eds.: R.F. Grossman, J.T. Lutz Jr.), Mar, New York, **2000**, pp. 1–34.

- [59] C. S. Schollenberger, F. D. Stewart, *Die Angew. Makromol. Chemie* **1973**, *29*, 413–430.
- [60] R. F. Grossman, J. T. Lutz Jr., in *Polym. Modif. Addit.* (Eds.: R.F. Grossman, J.T. Lutz Jr.), Marcel Dekker, New York, **2000**, pp. i–xvi.
- [61] J. Barbedo De Oliveira, L. Gustavo dos Reis, F. Silva Semaan, in *Polyurethane Prop. Struct. Appl.* (Eds.: L.I. Cavaco, J. Almeida Melo), Nova Science Publishers, Inc, New York, **2012**, pp. 1–23.
- [62] Y. He, D. Xie, X. Zhang, *J. Mater. Sci.* **2014**, *49*, 7339–7352.
- [63] R. J. Zdrahala, R. M. Gerkin, S. . Hager, F. E. Critchfield, *Journa Appl. Polym. Sci.* **1979**, *24*, 2041–2050.
- [64] K. Nakamae, T. Nishino, S. Asaoka, *Int. J. Adhes. Adhes.* **1996**, *16*, 233–239.
- [65] J. T. Koberstein, R. S. Stein, *J. Polym. Sci. Polym. Phys. Ed.* **1983**, *21*, 1439–1472.
- [66] L. M. Leung, J. T. Koberstein, *Macromolecules* **1986**, *19*, 706–713.
- [67] J. T. Koberstein, L. M. Leung, *Macromolecules* **1992**, *25*, 6205–6213.
- [68] X. Jin, N. Guo, Z. You, Y. Tan, *Materials (Basel)*. **2020**, *13*, 1–26.
- [69] J. Blackwell, M. R. Nagaran, T. B. Hoitink, *Polymer (Guildf)*. **1981**, *23*, 950–956.
- [70] L. Hojabri, X. Kong, S. S. Narine, *Biomacromolecules* **2010**, *11*, 911–918.
- [71] C. Prisacariu, E. Scortanu, *High Performance Polym.* **2011**, *23*, 308–313.
- [72] S. Das, D. F. Cox, G. L. Wilkes, D. B. Klinedinst, I. Yilgor, E. Yilgor, F. L. Beyer, *J. Macromol. Sci. Part B Phys.* **2007**, *46*, 853–875.
- [73] N. S. Schneider, C. S. Paik Sung, *Polym. Eng. Sci.* **1977**, *17*, 73–80.
- [74] C. B. Wang, S. L. Cooper, *Macromolecules* **1983**, *16*, 775–786.
- [75] C. Prisacariu, *Polyurethane Elastomers. From Morphology to Mechanical Aspects*, Springer Science + Business Media, Vienna, Austria, **2011**.
- [76] K. Ragaert, L. Delva, N. Van Damme, M. Kuzmanovic, S. Hubo, L. Cardon, *J. Appl. Polym. Sci.* **2016**, *133*, 1–12.
- [77] A. Voda, K. Beck, T. Schaubert, M. Adler, T. Dabisch, M. Bescher, M. Viol, D. E. Demco, B. Blümich, *Polym. Test.* **2006**, *25*, 203–213.
- [78] S. Petrovic, Zoran, J. Ferguson, *Prog. Polym. Sci.* **1992**, *16*, 695–836.
- [79] S. B. Clough, N. S. Schneider, A. O. King, *J. Macromol. Sci. Part B* **1968**, *2*, 641–648.
- [80] D. B. Klinedinst, I. Yilgör, E. Yilgör, M. Zhang, G. L. Wilkes, *Polymer (Guildf)*. **2012**, *53*, 5358–5366.
- [81] C. C. Chang, K. S. Chen, T. L. Yu, Y. S. Chen, C. L. Tsai, Y. H. Tseng, *Polym. J.* **1999**, *31*, 1205–1210.
- [82] M. F. Sonnenschein, in *Polyurethanes. Sci. Technol. Mark. Trends*, John Wiley & Sons Inc., Hoboken, United States, **2015**, pp. 294–335.
- [83] C. Pattamaprom, C. Wu, P. Chen, Y. Huang, P. Ranganathan, S. Rwei, F. Chuan, *ACS Omega* **2020**, *5*, 4058–4066.
- [84] S. L. Axelrood, C. W. Hamilton, K. C. Frisch, *Ind. Eng. Chem.* **1961**, *53*, 889–894.
- [85] J. A. Miller, S. B. Lin, K. K. S. Hwang, K. S. Wu, P. E. Gibson, S. L. Cooper, *Macromolecules* **1985**, *18*, 32–44.
- [86] M. Xu, W. J. MacKnight, C. H. Y. Chen, E. L. Thomas, *Polymer1* **1983**, *24*, 1327–1332.
- [87] A. C. Society, *ASTM D2572-19. Standard Test Method for Isocyanate Groups in Urethane Materials or Prepolymers*, West Conshohocken, PA, **2019**.
- [88] C. Tan, T. Tirri, C.-E. Wilen, *Polymers (Basel)*. **2017**, *9*, 1–19.
- [89] R. J. G. Dominguez, *Polym. Eng. Sci.* **1981**, *21*, 1210–1217.
- [90] M. Amirkhosravi, L. Yue, T. Ju, I. Manas-Zloczower, *Polymer (Guildf)*. **2021**, *214*, 1–8.
- [91] U. States, *US 2,230,654. Tetrafluoroethylene Polymers*, **1941**, *2 230 654*.
- [92] S. Ebnesajjad, P. R. Khaladkar, in *Fluoropolymer Appl. Chem. Process. Ind.* (Ed.: S. Ebnesajjad), William Andrew Publishing, Norwich, US, **2018**, pp. 279–319.
- [93] T. Okazoe, *Proc. Japan Acad. Ser. B Phys. Biol. Sci.* **2009**, *85*, 276–289.

- [94] G. J. Puts, P. Crouse, B. M. Ameduri, *Chem. Rev.* **2019**, *119*, 1763–1805.
- [95] R. Dams, K. Hintzer, in *Fluorinated Polym. Vol. 2 Appl.* (Eds.: B. Ameduri, H. Sawada), The Royal Society Of Chemistry, **2017**, pp. 1–31.
- [96] B. Ameduri, *Chem. Eur. J.* **2018**, 18830–18841.
- [97] R. Dams, K. Hintzer, in *Fluorinated Polym. Vol. 2 Appl.* (Eds.: B. Ameduri, H. Sawada), Royal Society Of Chemistry, **2017**, pp. 1–14.
- [98] W. McKeen, Laurance, in *Eff. Temp. Other Factors Plast. Elastomers* (Ed.: W. McKeen, Laurance), William Andrew Publishing, Norwich, US, **2008**, pp. 447–502.
- [99] E. P. Gillis, K. J. Eastman, M. D. Hill, D. J. Donnelly, N. A. Meanwell, *J. Med. Chem.* **2015**, *58*, 8315–8359.
- [100] M. Tredwell, V. Gouverneur, in *Compr. Chirality* (Eds.: E.M. Carreira, H. Yamamoto), Elsevier Ltd., Amsterdam, The Netherlands, **2012**, pp. 70–85.
- [101] V. P. Reddy, in *Organofluor. Compd. Biol. Med.* (Ed.: V.P. Reddy), Elsevier B.V., Amsterdam, The Netherlands, **2015**, pp. 1–27.
- [102] R. D. Chambers, in *Fluor. Org. Chem.*, Blackwell, Oxford, England, **2009**, pp. 91–121.
- [103] A. Bondi, *J. Phys. Chem.* **1964**, *68*, 441–451.
- [104] F. Leroux, *ChemBioChem* **2004**, *5*, 644–649.
- [105] M. P. Krafft, J. G. Riess, *Chem. Rev.* **2009**, *109*, 1714–1792.
- [106] D. O. Hagan, *Chem. Sci.* **2008**, *37*, 308–319.
- [107] B. Ameduri, B. Boutevin, in *Well-Architected Fluoropolymers Synth. Prop. Appl.*, Elsevier Ltd., **2004**, pp. 1–99.
- [108] S. Ebnesajjad, in *Fluoroplastics, Vol. 1. Non-Melt Process. Fluoropolymers- Defin. User's Guid. Data B.*, **2015**, pp. 24–37.
- [109] J. A. K. Howard, V. J. Hoy, D. O'Hagan, G. T. Smith, *Tetrahedron* **1996**, *52*, 12613–12622.
- [110] J. D. Dunitz, R. Taylor, *Chem. - A Eur. J.* **1997**, *3*, 89–98.
- [111] D. W. Grainger, C. W. Stewart, in *Fluorinated Surfaces, Coatings, Film.* (Eds.: D.W. Grainger, C.W. Stewart), American Chemical Society, Washington, D.C., **2001**, pp. 1–14.
- [112] H. W. Fox, B. A. H. Ellison, H. W. Fox, *J. Chem. Educ.* **1953**, *57*, 622–627.
- [113] W. A. Zisman, in *Contact Angle, Wettability Adhes.* (Ed.: F.M. Fowkes), American Chemical Society, Washington, D.C., **1964**, pp. 1–51.
- [114] R. D. Fowler, W. R. Burford, J. M. J. Hamilton, R. G. Sweet, C. . Weber, J. S. Kasper, I. Litant, *Ind. Eng. Chem.* **1947**, *39*, 292–298.
- [115] T. Nakajo, T. Arai, T. Ohi, *US 5 675 046. Process for Producing Perfluorocarbon*, **1997**, 5675046.
- [116] P. Wang, D. Lu, H. Wang, R. Bai, *Polymers (Basel)*. **2019**, *11*, 1–13.
- [117] B. Ameduri, *Macromol. Chem. Physics*, **2020**, *221*, 1900573–1900598.
- [118] J. Gardiner, *Aust. J. Chem.* **2015**, *68*, 13–22.
- [119] J. Wood, in *High-Performance Appar. Mater. Dev. Appl.* (Eds.: J. McLoughlin, T. Sabir), Elsevier Ltd., Duxord, England, **2017**, pp. 325–339.
- [120] P. Król, B. Król, *Colloid Polym. Sci.* **2012**, *290*, 879–893.
- [121] H. Tan, X. Xie, J. Li, Y. Zhong, Q. Fu, *Polymer (Guildf)*. **2004**, *45*, 1495–1502.
- [122] H. Yabu, M. Shimomura, *Chem. Mater.* **2005**, *17*, 5231–5234.
- [123] M. Hernández-Guerrero, M. H. Stenzel, *Polym. Chem.* **2012**, *3*, 563–577.
- [124] C. Tonelli, G. Ajroldi, *J. Polym. Sci.* **2003**, *87*, 2279–2294.
- [125] A. A. Malik, D. Tzeng, P. Cheng, K. Baum, *J. Org. Chem.* **1991**, *56*, 3043–3044.
- [126] T. Lammers, M. E. Mertens, P. Schuster, K. Rahimi, Y. Shi, V. Schulz, A. J. C. Kuehne, S. Jockenhoevel, F. Kiessling, *Chem. Mater.* **2017**, *29*, 2669–2671.
- [127] Z. Gu, J. Cheng, M. Zhang, J. He, P. Ni, *Chinese J. Polym. Sci.* **2017**, *35*, 1061–1072.
- [128] L. Mashlyakovskiy, V. Zaiyiy, G. Simeone, C. Tonelli, *J. Polym. Sci. Part A Polym. Chem.*

- 1999**, *37*, 557–570.
- [129] L. Yang, Y. Wang, X. Peng, *J. Macromol. Sci. Part A* **2017**, *54*, 516–523.
- [130] C. Wu, S. Chiu, H. Lee, M.-C. Suen, *Polym. Adv. Technol.* **2016**, *27*, 665–676.
- [131] H. Tan, M. Guo, R. Du, X. Xie, J. Li, Y. Zhong, Q. Fu, *Polymer (Guildf)*. **2004**, *45*, 1647–1657.
- [132] M. Delucchi, S. Turri, A. Barbucci, M. Bassi, S. Novelli, G. Cerisola, *J. Polym. Sci. Part B Polym. Phys.* **2002**, *40*, 52–64.
- [133] T. Liu, L. Ye, *J. Fluor. Chem.* **2010**, *131*, 36–41.
- [134] Lubrizol, *Move, Create, Live. Lubrizol, Company Report*, **2021**.

Chapter 2

Characterization techniques

The following section summarizes the theoretical fundamentals of the techniques employed to study and characterize monomers, polyols and TPUs. A dual academic and industrial purpose is sought in this thesis. Thus, some properties have been analyzed from an industrial perspective applying ASTM and ISO methodologies, while others have been evaluated with conventional research procedures.

2. Techniques

2.1. Nuclear Magnetic Resonance Spectroscopy

Nuclear Magnetic Resonance (NMR) spectroscopy is a widely employed non-destructive analytical technique to explore the content, the molecular structure or the purity of a sample, both in solution and solid-state. It is based on the polarization of nuclei with nonzero nuclear spin (I). These active nuclei are positively charged particles and act as randomly oriented magnets with degenerated energetic states. However, when an external magnetic field (B_0) is applied, they arrange in the same direction as the field, aligning in diverse states depending on I (number of states = $2I + 1$) (Figure 2.1). The energy difference between these states (ΔE) is the energy required to resonate the nucleus.

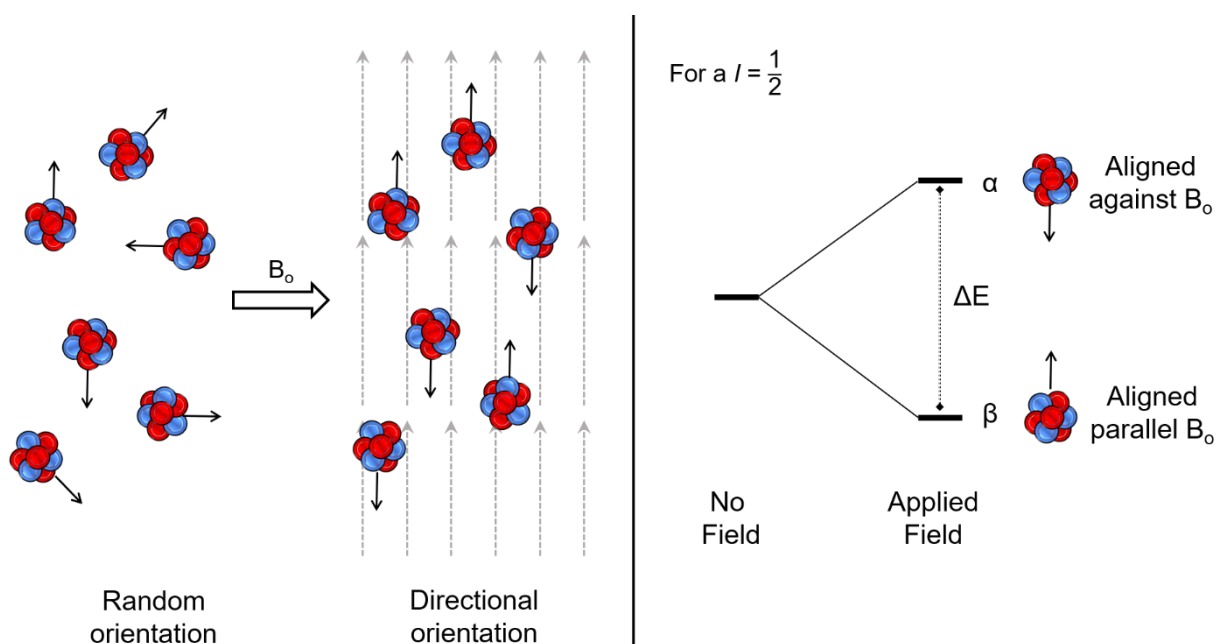
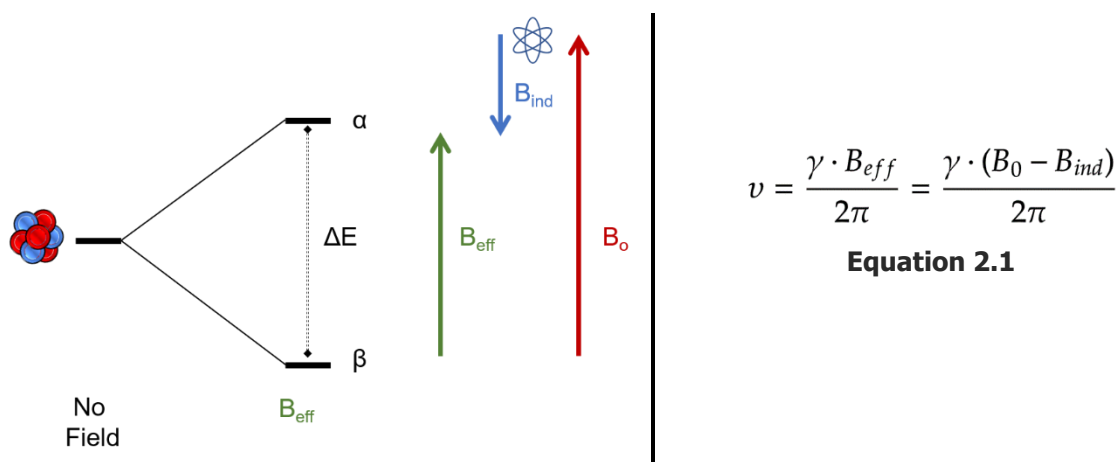


Figure 2.1. Schematic representation of the alignment of the nuclei and the number of generated states.

However, electrons are negatively charged particles that also induce magnetic fields (B_{ind}) opposite to B_0 . Consequently, the electronic cloud shields the active nucleus from the B_0 , which

inevitably results in a different net magnetic field (B_{eff}) (Figure 2.2). The measured resonance frequency of the nucleus (ν) depends on the gyromagnetic ratio (γ) and the chemical environment, as described by **Equation 2.1**.



$$\nu = \frac{\gamma \cdot B_{\text{eff}}}{2\pi} = \frac{\gamma \cdot (B_0 - B_{\text{ind}})}{2\pi}$$

Equation 2.1

Figure 2.2. Graphic representation of the effective magnetic field caused by the applied field, the nucleus, and the surrounding electrons (Left). **Equation 2.1** displays the relation between the resonance frequency and the magnetic field (Right).

NMR experiments apply specific radio frequencies to excite the active nuclei to the highest energetic state. Subsequently, the relaxation is detected and converted by means of Fourier transformation in a spectrum. NMR spectra display on the X-axis the frequencies (in ppm) in which the nuclei resonate against the intensity (a.u.) on the Y-axis. Usually, spectra are analyzed based on the chemical shifts, the multiplicity, and the intensity of each peak. The former corresponds to the frequency in which each active nucleus appears on the spectrum and is directly related to the chemical environment of the compound. Chemical shifts are usually tabulated and are used to tentatively identify groups similar to the analyzed specimen. Multiplicity is the splitting of the peaks in certain patterns, consequence of the interaction of the nuclei under consideration with other neighboring within the molecule. Lastly, the intensity provides information about the number of equivalent nuclei per signal.^[1]

Traditionally, the most studied atoms are ^1H and ^{13}C . The former presents an enhanced sensitivity consequence of the high gyromagnetic ratio of the nuclei. Contrary, carbon exhibits a small natural abundance (1.11%) but, the information extracted from it is tremendously valuable owing to the simplification of the spectra by the decoupling with hydrogen and the low probability of carbon-carbon coupling between adjacent ^{13}C atoms. Furthermore, it displays

a broader working range than protons, which results in signals with larger dispersion of chemical shifts.

Nevertheless, other nuclei with a spin other than zero may be employed (**Table 2.1**). Elements with large natural abundance typically provide the highest sensitivity and thus, they are the most suitable for NMR analysis. Consequently, ^{19}F and ^{31}P nuclei might add relevant information about the sample structure and its composition.

Table 2.1. Selection of nuclear spin features of NMR active nuclei.^[2]

Nucleus	Abundance (%)	Sensitivity ^[a]	Spin (I)	Common Working range (ppm)
^1H	99.98	5680	1/2	-1 to 12
^2H , D	0.02	0.000821	1	-1 to 12
^{13}C	1.11	1.00	1/2	0 to 220
^{15}N	0.37	0.0219	1/2	0 to 900
^{19}F	100	4730	1/2	-250 to 50
^{31}P	100	377	1/2	-180 to 250

^[a] Sensitivity relative to carbon.

In particular, ^{19}F NMR spectroscopy benefits from the $1/2$ spin and 100% natural abundance. The wide working range (from -250 to 50 ppm) and the large coupling constants (J) are some potential advantages of carrying out experiments with this nucleus. Fluorine couples with hydrogen and carbon, reaching coupling constants up to 50 Hz for $^2J_{\text{C-F}}$ and 370 Hz in $^1J_{\text{C-F}}$.^[3] Furthermore, ^{19}F NMR can be gathered decoupled from ^1H , simplifying the spectra and providing further data from the sample. Obviously, the carbon-fluorine coupling constants can only be observed in the ^{13}C NMR spectra owing to the low natural abundance of ^{13}C atoms.

In this thesis, NMR spectroscopy has been widely used. In addition to its standard use for characterizing the resulting structures, it has been also implemented to analyze the reaction's evolution, the chemical composition of mixtures, and the molecular weight of the produced polymers.

Some considerations must be bear in mind when working with polymers. The elevated chain length and the mobility restriction cause broader signals than in small molecules. Therefore, to obtain quantitative spectra, the spin-spin relaxation times must be considered and modified according to the sample.

2.2. Elemental analysis

Elemental analysis precisely identifies and quantifies the elements in the sample and according to the accuracy and the target chemical elements, various techniques can be selected.

2.3. Inductively Coupled Plasma-Mass Spectrometry

Inductively Coupled Plasma-Mass Spectrometry (ICP-MS) quantifies the element's concentration contained in a sample. As the name indicates, this technique comprises two coupled modules: an ICP and the mass spectrometer. In the former, the sample is nebulized and atomized into ions in excited states by a plasma, and then, it is transferred to the spectrometer where fragments are separated according to their mass-to-charge (m/z) ratio and quantified. Depending on the sensitivity, resolution, or number of simultaneously detected elements, different mass spectrometers can be selected.^[4]

The technique can semi-quantitatively estimate the concentration of several elements without the need to calibrate one by one with its own corresponding calibration curve. Moreover, it can provide information about the isotope composition or their unnatural abundances in a sample.

The detection limit of ICP-MS reaches up to parts per trillion (ppt) in some cases.^[5] Therefore, it is frequently utilized to determine high diluted analytes. In these cases, a fully quantitative analysis is carried out with an appropriate calibration standard plot with samples of known concentration.

2.4. Gas Chromatography

Gas Chromatography (GC) is an analytical technique that allows the separation, detection, and quantification of volatile components of a mixture without thermal decomposition. As with most chromatographic techniques, GC depends on a mobile and a stationary phase. The former is an inert carrier gas, usually helium or nitrogen. On the contrary, the stationary phase is a substance adsorbed onto an inert support placed inside the chromatographic column.^[6]

The sample is vaporized and transported by the carrier gas through a thin column located inside an oven. The distinct vapor pressures and affinities between the analytes and the stationary phase lead to the separation of the chemicals. Small analytes with a low affinity to the stationary phase will move swiftly through the column, whereas relatively polar substances will adsorb and elute slower. The interval in which a substance remains in the column is called

retention or elution time (R_t). For specific chromatographic conditions, R_t is characteristic for each compound.^[7]

After exiting the column, vaporized and separated substances proceed to a detector. There are several types, such as Flame-ionization detector (FID) or Mass-spectrometer (MS), among others. GC-FID burns the analytes in a hydrogen-air flame and measures the number of formed ions. On the other side, GC-MS ionizes the compounds too, but it identifies and quantifies the created charged fragments. In this latter case, besides the common chromatogram, a mass spectrum of each peak is produced. This supplemental information might enable the elucidation of the substance's chemical composition.^[8]

Regardless of the detection used, the concentration of the analytes is calculated by comparing the area under the considered peak with the areas of the known concentrations of the standard with a calibration curve.

2.5. Infrared Spectroscopy

Infrared (IR) spectroscopy is a qualitative and, in some cases quantitative, technique extensively used to characterize samples. It relies on the interaction of IR radiation with the studied molecules.

IR spectrophotometers measure the variation in absorbance when atoms vibrate and generate spectra that represent the percentage of IR radiation transmitted (Transmittance, Y-axis) at a given wavenumber (X-axis). The vibration mode of each bond is associated with an energy, thereby possessing a characteristic wavenumber range.^[9] However, only vibration modes that change the dipole moment of the molecule are declared as active on the IR. Comparing experimental results with tabulated values and patterns allows the characterization of the most important functional groups present in a sample. Moreover, the intensity of the band depends on the bond and its concentration in the sample. The intensity increases with the number of functional groups within the molecule.

Currently, most IR analyses are carried out in Attenuated Total Reflection Fourier Transform Infrared (ATR-FTIR) in the mid-IR region (4000 and 400 cm^{-1}).^[10] This instrument relies on the variation in the IR beam when a crystal is in contact with a sample. Crystals have a high refractive index to promote the internal total reflection of the beam. However, the inflection point of propagation occurs a few microns within the contacting sample. The fraction of

radiation that enters the studied material is known as the evanescent wave and contains chemical information of the sample (Figure 2.3).

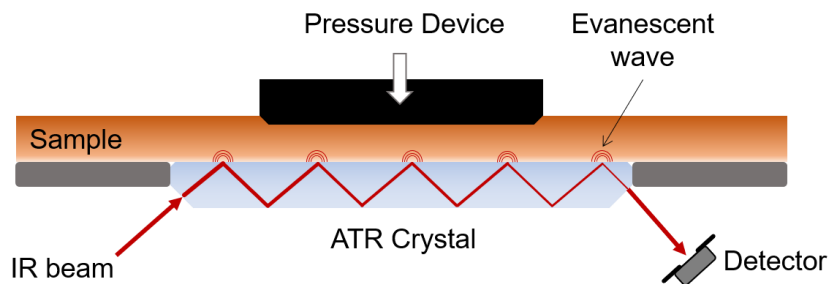


Figure 2.3. Schematic representation of an ATR-FTIR technique.

The primary advantage of ATR-FTIR in comparison with other methods is the direct analysis of solids and liquids without almost any preparation.

2.6. Melt Flow Index

Melt Flow Index (MFI) is one of the most frequently used routine tests to control the processability and quality of polymers. It measures the flowability of melted thermoplastic polymers, concretely the weight that is extruded through a die in 10 minutes. MFI measurements do not indicate any fundamental property of the sample, but some parameters can be indirectly related to it.^[11]

The standard procedure consists in heating the material above the softening or melting temperature and then forcing it to pass through a capillary of specific dimensions by applying a deadweight (Figure 2.4). Depending on the required standard (usually ASTM D1238),^[12] different temperatures and weights can be used.

The average molecular mass cannot be obtained directly from this measurement, but a high MFI typically entails low viscosity and thereby, short-chain length. Hence, it is to be expected variations in the properties when comparing samples with significantly different MFI. Furthermore, for routine analysis, and working with the same type of polymer, a calibration plot MFI vs. M_w can be built. Then, the MFI analysis provides a fast control on the average M_w of a sample. Customarily, moderate values of MFI would be preferred for materials designed for extrusion as they provide better control of the process. Conversely, materials aimed for injection prefer high MFI and consequently, low viscosity, to completely occupy all the nooks of the mold.^[13]

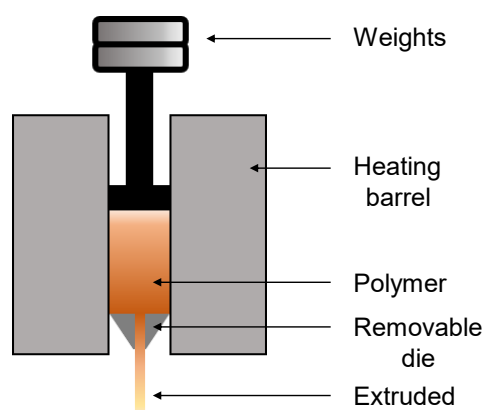


Figure 2.4. Schematic representation of a Melt Flow Indexer.

2.7. Kofler

Kofler or Kofler Hot Bench is an instrument that determines the softening and melting point of polymers in a simple and swift manner. In addition, it is widely employed in the fine chemicals industry as it provides information about the purity and polymorphisms of the studied samples.

Kofler consists of a stainless-steel strip with a linear temperature gradient in which samples are heated when they are placed over it. The softening point refers to the temperature at which the material loses its rigid structure and begins to transform into a viscous liquid with adhesive properties. It approximates somehow the heat deflection temperature of a polymer.^[a] The melting point corresponds to the temperature at which the crystallites and rigid parts of the material disappear. At that point, the studied substance becomes completely liquid and does not possess any stiffness.

In the polymer industry, Kofler is widely employed to assess the temperature profile of a material prior to injection molding. The melting point gives an idea of the temperature required to obtain the necessary viscosity to flow the polymer through the screw and promptly fill the mold. On the contrary, the softening provides information about the temperature at which the material could be extracted from the mold with little deformation. Ideally, the smaller the difference between the melting and the softening temperature, the faster the molding process and the higher the production efficiency.

^[a] Temperature at which a polymer deforms a specific distance under a given load. Generally, the reported value is the temperature at which thick test bar with specific dimensions distorts 0.25 mm under 0.455 MPa or 1.82 MPa.^[43]

Despite being the Kofler technique a cost-effective analysis, some differences might arise between the acquired values and those obtained with other measurement techniques.

2.8. Differential Scanning Calorimetry

Differential Scanning Calorimetry (DSC) is an analytical technique widely utilized to explore the thermal behavior of a material. It estimates the changes in the heat capacity when a sample is subjected to temperature. The basic procedure consists of heating and cooling two crucibles at a fixed rate, one containing the sample and another usually empty. The difference in the amount of energy or heat flow needed to maintain both pans at the same temperature is precisely measured (Figure 2.5).

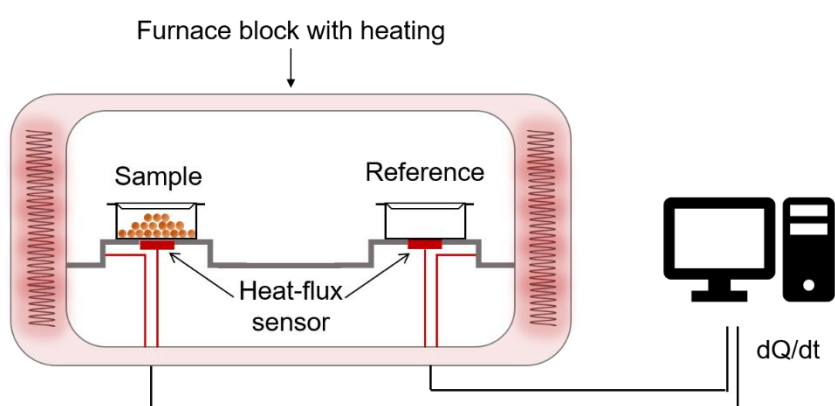


Figure 2.5. Schematic representation of a DSC cell.

DSC's data is represented in a thermogram, depicting the changes of the heat flow (dQ/dt) as function of time or temperature (Figure 2.6). The direction of the exothermic process is arbitrary, and it must be indicated in all diagrams. From these plots, the thermal transitions that a sample undergoes are extracted.

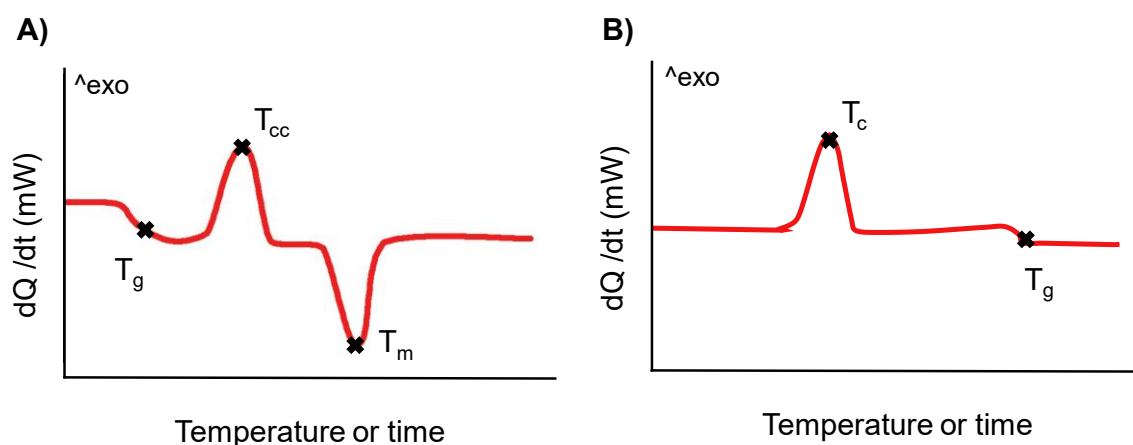


Figure 2.6. Basic DSC thermogram with the conventional thermal transition of a semi-crystalline material. A) Heating scan and B) Cooling scan.

These transitions are classified as first or second-order, being the presence of enthalpy the fundamental difference among them. First-order are those state changes that involve enthalpy, *i.e.* that release or absorb heat during the phase transition. Ideally, these transitions are represented as gaussian peaks on the thermogram. The enthalpy of the transition (ΔH) is calculated from **Equation 2.2**, which considers the area under the peak (A), the weight of the sample (m), the heating rate (q), and a calibration factor specific for each instrument (K_{DSC}).

$$\Delta H = \frac{K_{DSC} \cdot A}{m \cdot q} \quad \text{Equation 2.2}$$

The most recurrent first-order transitions are cold crystallization, melting, and crystallization. The former is an exothermic process observed in the heating process (Figure 2.6.A), attributed to the ordination of the chains upon heating. The maximum of the exotherm is denoted as the cold-crystallization temperature (T_{cc}). The following transition is an endothermic process, in which the characteristic value is the melting temperature (T_m). It is obtained at the highest height of the melting peak on the thermogram. Conversely, crystallization is an exothermic process and is defined by the crystallization temperature (T_c). It is determined as the temperature at the highest point of the crystallization exotherm (Figure 2.6.B).

The glass transition temperature (T_g) is a second-order transition, which only presents a change in the heat capacity, but not in the enthalpy. Therefore, no associated peak is observed. T_g is depicted as a smooth step in the baseline and its value is determined at the inflection of the slope.

Totally amorphous materials may not display T_c , while highly crystalline polymer lack T_g . However, most polymers possess some of both regions and all three transitions are typically observed on these semi-crystalline compounds. The amorphous part of these systems will undergo a transition from the glassy to the rubbery state, while the crystalline regions will melt when heated and crystallize at cooling, exhibiting the three transitions on the DSC thermogram.

2.9. Thermogravimetric analysis

Thermogravimetric analysis (TGA) is a quantitative analytical technique that detects the thermal processes that a sample may undergo when heated.^[14] Contrary to DSC, it is based on the quantification of the mass loss of the sample (%) caused by physical and chemical processes, such as evaporation, decomposition, or oxidation.

Analyses are carried out in a thermobalance that monitors the sample weight while it is simultaneously heated. The tested substance is situated on a holder suspended from a precision balance placed within a furnace (Figure 2.7).

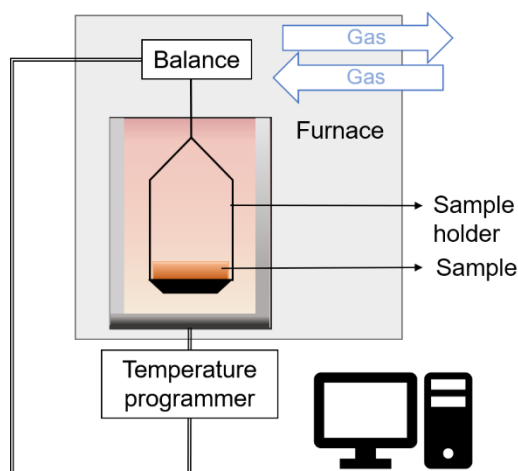


Figure 2.7 Schematic representation of a thermogravimetric analyzer.

The thermal behavior can be studied under inert and reactive environments (*e.g.* argon, nitrogen, or air). Moreover, different temperature programs can be employed, like isotherms, constant or variable heating rates.

Measuring the mass along the programmed range produces a thermogravimetric curve (TG) that displays the mass variation as a function of time or temperature (Figure 2.8). Supplemental information can be achieved from the first derivative of the previous curve, which corresponds to the derivative curve (DTG). Each peak of DGT represents a distinct process. It determines the temperature or time in which the mass loss or the overlapping processes takes place.

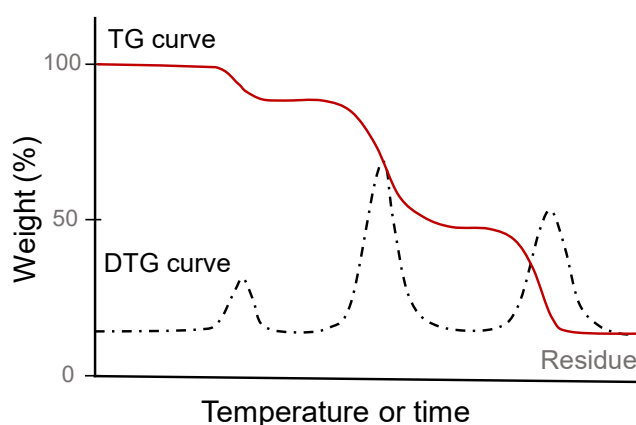


Figure 2.8. TGA thermal curve. TG and DTG curves are represented as a red line and a black dotted line, respectively.

Although TGA precisely quantifies the changes in a sample, it does not recognize which constituents are progressively lost. Compounds released between room temperature and 300 °C are considered volatile components. Conventionally, the first substances to be lost are solvents and absorbed water, followed by low M_w compounds, like unreacted monomers. Traditionally, products released above 300 °C arise from polymer chain scission. At elevated temperatures (> 600 °C) and under oxidizing conditions, organic polymers carbonize leaving the weight of the degraded sample, called residue. In addition to the formed carbon black, inorganic additives or fillers (*e.g.* silica particles or CaCO_3) typically remain in this residue.

2.10. Hardness

Hardness is an intrinsic parameter of materials closely related to the mechanical properties. It assesses the resistance of metals, polymers, and ceramics to plastic deformation. Hardness tests are usually implemented as a simple, quick, and non-destructive control.

Among the different hardness tests, Shore Hardness estimates the impediment of the studied material to be permanently indented with a truncated cone. When the indenter presses against the polymer, a force is applied to the surface. Simultaneously, the material exhibits an opposite resistance until both forces reach equilibrium. At this point, the depth of the needle penetration stipulates the hardness of the material (Figure 2.9). Values can vary from zero (full penetration of the indenter) to 100 (no penetration).

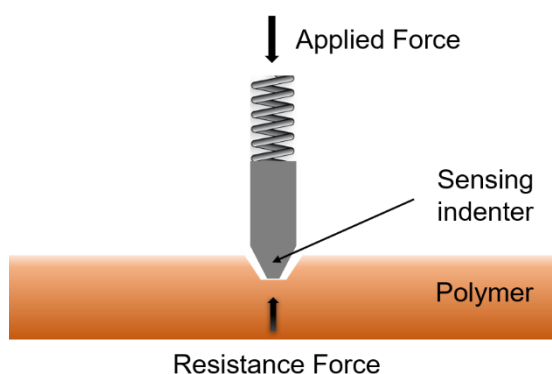


Figure 2.9. Graphical representation of a Shore Hardness test.

There are diverse scales to determine the hardness of different types of polymers. The primary distinction between them is the form of the indenter and thus, the force applied over the material.^[15] Often, elastomers are tested using Shore A scale, while rigid thermoplastics and thermosets are assessed with Shore D scale. Finally, Shore 00 scale is employed for highly soft rubbers or gels. However, for each of them, the greater the number on the scale, the higher the resistance to indentation, and the harder the resin. Generally, high values imply better

mechanical properties and enhanced chemical and abrasion resistance than those materials with lower hardness.

2.11. Density

Density (ρ) is a scalar magnitude defined as the mass per unit of volume. Apart from a characterization parameter, ρ is a quality control test for a given polymer as different additives or processing conditions might modify its value.

There are several techniques to quantify it, but most of them exploit Archimedes' principle.^[b] Specifically in this thesis, ρ is measured by the immersion method, which relies on determining accurately the weight difference between the specimen weighed in the air and immersed in a liquid of known density.^[16] The most employed liquid is paraffin as it is non-hygroscopic and inert toward the tested specimen and exhibits a density similar to the polymer.

2.12. Friction

Friction is conventionally defined as the resistance to motion when two surfaces in direct contact are forced to slide against each other (Figure 2.10).^[17] One of the essential features of this physical phenomenon is that no material is lost during the studied process.

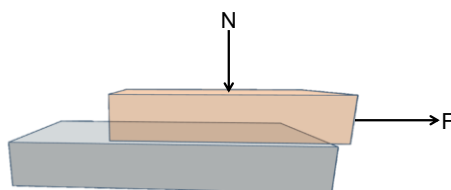


Figure 2.10. Graphical illustration of friction between a polymer (orange block) and a counterface (grey plane).

The fundamental parameter that traditionally defines friction is the coefficient of friction (COF, μ), a dimensionless value obtained by Equation 2.3. F represents the resisting force to move the studied sample over a counterbody while N is the normal load force, which is perpendicular to the sliding surface.

$$\mu = \frac{F}{N} \quad \text{Equation 2.3}$$

^[b] Any body, totally or partially submerged in a fluid at rest, exerts an upward buoyant force equal to the weight of the fluid displaced by the body.

The maximum force required to initiate the motion determines the static coefficient of friction (μ_s). In contrast, the dynamic coefficient of friction (μ_d), also described as kinetic, arises from the force required to sustain the movement between both contacting bodies. Usually, the second parameter is smaller than the first one, as starting the movement presents higher resistance than sliding. The higher the obtained values, the greater the resistance of the tested material to slide on this specific counterface.

Coefficients of friction might vary according to the normal force applied, the counterfaces over which the samples are moved, the sliding speed, the temperature, and the roughness of the studied surface. The latter parameter presents a high relevance because the microscopic protuberances or asperities of the surface are the real contact area between both materials. They support the applied load and are responsible for the resistance. To obtain comparable data, all experiments should be conducted under the same load, humidity, temperature, and similar topographical sheets. Moreover, the coefficient of friction is not an intrinsic property of a material, but of the system involving the two bodies in the motion.

The friction can include several mechanisms, but in the case of metal to polymer motion, the most common are adhesion and plowing. The former is instigated by the adhesion forces produced between the partaking surfaces. Conversely, plowing is caused by the plastic deformation of the studied material against a harder counterface. These processes might lead to the formation of transfer films, which could behave as a lubricant.

Several methods and instruments can be used to explore the friction of a material. However, in this thesis, the coefficients of friction are measured in a motorized tribometer according to ASTM D1894.^[18] The experiment involves sliding a polymer sheet over a stationary metallic plane at a uniform speed and measuring the force required to start the motion and sustain it.

2.13. Abrasion resistance

Wear is described as the progressive loss of solid fragments from the material's surface as consequence of its motion against a contacting counterface (Figure 2.11). Like friction, the wear is not an intrinsic property of the material, but the result of the contact of at least two specimens under certain conditions. It might determine the lifetime of a product; and therefore, the viability of a material for a specific application.

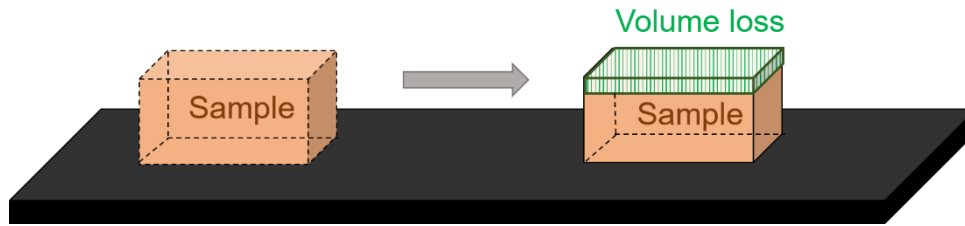


Figure 2.11. Graphical representation of wear.

Several mechanisms can cause the fracture of the material, but according to Budinski, they are classified as adhesion, erosion, abrasion, or fatigue.^[19] However, in this manuscript, the evaluation of the wear is only focused on the abrasion mechanism, which corresponds to the loss of matter when the sample is forced to move against the hard asperities of a counterbody. These damages occur on the surface of the softer material, which almost always is the polymer.

Several techniques quantify the wear of a material, but here the abrasion resistance is considered by a two-body abrasive method, in which the polymer is abraded by hard solid particles fixed onto a surface. Concretely, it is determined by "pin on drum", measuring the volume loss (ΔV) of a sample against a rotating abrasive sheet. The greater the volume loss, the poorer the abrasion resistance of the material.

The test is based on moving a specimen along an abrasive sheet in a drum (Figure 2.12). The sample under study rotates on its axis while following a sinusoidal path along the rolling abrasant, thereby continuously reaching fresh abrasive sheet during the displacement.^[20]

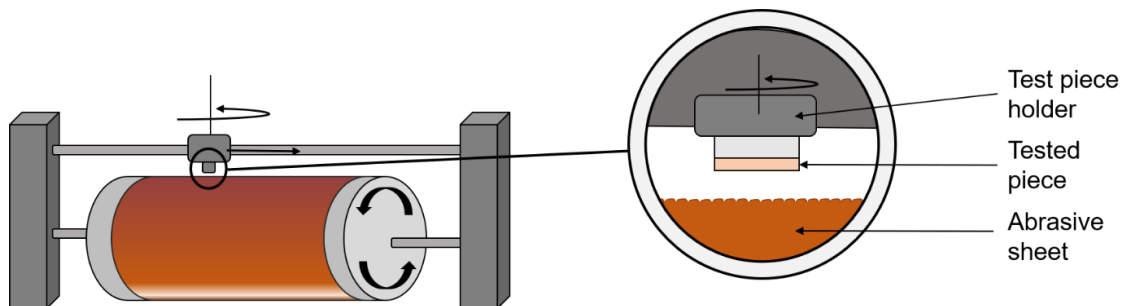


Figure 2.12. Graphical representation of "Pin on drum" method.

Although the employed procedure starts with a two-body wear, it could easily evolve to a three-body system when the polymer debris remains between the tested sample and the counterface. The impact of these particles on the wear is uncertain as they can form a transfer film onto the asperities and reduce the abrasion, or may cause higher damage on the tested piece.

2.14. Yellowness index

The yellowness index (YI) is a quality control parameter related to the color of the sample. It measures the degree of yellowness relative to colorless or whiteness after exposing plastics to day light radiation.^{[21][22]}

Usually, the yellowing of a sample is caused by thermal and oxidative degradation of the material. Therefore, significant deviations typically indicate low-quality products if no colorants are added. In some cases, it could be reduced by synthesizing and processing the polymer under an inert atmosphere or decreasing the processability temperature.

YI is calculated from Equation 2.4, where C_x and C_z are tabulated values that depend on the type of illuminant and the angle of the observer.^[22] X , Y , and Z are the tristimulus values provided by the instrument after the measurements and are related to the three parameters of the CIELAB color space (L^* , a^* , and b^*).^[21]

$$YI = \frac{C_x \cdot X - C_z \cdot Z}{Y} \cdot 100 \quad \text{Equation 2.4}$$

Measurements are usually carried out in a tristimulus colorimeter which produces X , Y , and Z , and the final YI value. Results are interpreted according to the symbol and the value. The higher the value, the greater the departing from whiteness. A negative YI number implies a bias toward bluish tones, while a positive value is toward yellow.

YI analysis is restricted to nearly white translucent plastic (Transmittance superior to 25%) or practically colorless transparent plastic. This parameter depends on the thickness of the sample. Hence, polymers must have similar dimensions and appearance to be comparable.

2.15. Transmittance and Haze

Light interacts in different manners with materials. The difference in the refraction indices from the crystalline and the amorphous domains causes the scattering of the light, decreasing the transparency and producing turbidity. Transparent materials lack crystallites or heterogeneities with dimensions that match or exceed the wavelength of visible light (400 nm-700 nm). Therefore, highly amorphous systems are usually transparent while, semi-crystalline are translucent and crystalline are opaque.

Although transparency is not exclusively reported as Transmittance, this parameter plays a significant role in describing the appearance of the material and it is used as a characterization and control property. Moreover, Haze contributes to the clarity to see an object through the

polymer. Transmittance is defined as the percentage of transmitted light ($T_{transmitted}$) through a specimen respect the incident transmittance ($T_{incident}$) (Equation 2.5). Usually in colorless compounds, the higher the transmittance percentage, the greater the level of transparency of the material. However, 100 % is commonly unreached owing to the absorbance and reflectance of the two surfaces of the material.

$$T_{total} = \frac{T_{transmitted}}{T_{incident}} \cdot 100 \quad \text{Equation 2.5}$$

Another phenomenon caused by the interaction between a material and light is the haze. It is defined as the percentage of light that deviates from the incident beam with an angle greater than 2.5° (Figure 2.13).^[23] In particular, in transparent or nearly translucent materials, it is only considered the transmission haze which measures just the light scattered in the same direction as the incident beam and omits the backscattered radiation.

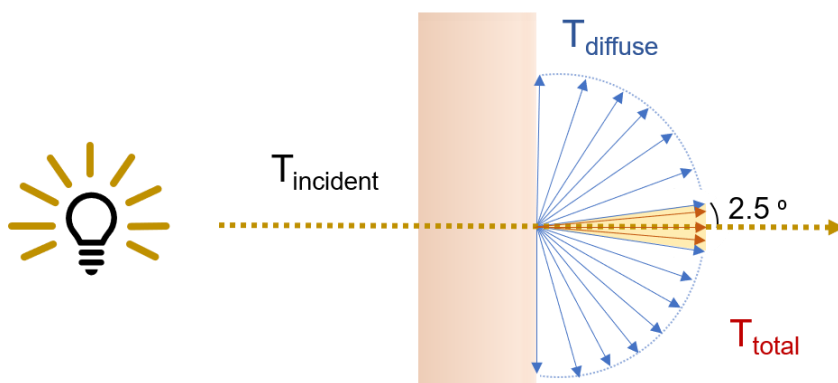


Figure 2.13. Graphical representation of Haze.

Transmission haze is quantified by the following expression (Equation 2.6) in which $T_{diffuse}$ is the diffuse transmittance (light diffusively scattered with an angle higher than 2.5°) and T_{total} is the total light transmitted.

$$Haze = \frac{T_{diffused}}{T_{total}} \cdot 100 \quad \text{Equation 2.6}$$

The Haze is an appearance attribute that is generally noted as the cloudiness of a material and thus, is responsible for the decrease of contrast of an object observed through the polymer sample. Light scattering is affected by defects of the sample (*e.g.* particles, pigments, or fillers) or heterogeneity of the surface. Moreover, its variation might indicate the material's weathering. In view of the foregoing, the estimation of the Haze is frequently used to characterize and control the production and evolution along time of some polymers.

2.16. Gloss

Gloss is the property responsible for the lustrous or metallic appearance of a material. Specular gloss is the ratio of the reflected light respect the incident beam at the specular angle (same angle as the incoming beam). A glossy surface entails a focused and intense outgoing beam in the specular direction. For that purpose, the surface of the material should be even and smooth. Conversely, matte surfaces are characterized by low values of gloss, in which the major intensity of the light is in all the diffused directions, probably caused by the surface roughness (Figure 2.14).

The importance of gloss relies on its effect on the color of objects. Samples with modest values of gloss are perceived as matte products with lower intensity on the color, whereas high gloss surfaces appear as darker and more saturated. Samples with high gloss are aesthetically preferred for application in automobiles or wearables.^[24]



Figure 2.14. Schematic representation of glossy and matte surfaces according to the specular gloss.

Gloss is measured in a glossmeter, which consists of an incandescent light source placed at a specific angle and a photodetector that receives the beam at the corresponding specular directions. (Figure 2.15). Glossmeters are calibrated with a highly lustrous black surface with a refractive index of $n=1.567$, and the obtained value is attributed to 100 gloss units (GUs). To obtain comparable results, the glossmeter incorporates a built-in mask that measures the same area for all the tested samples.

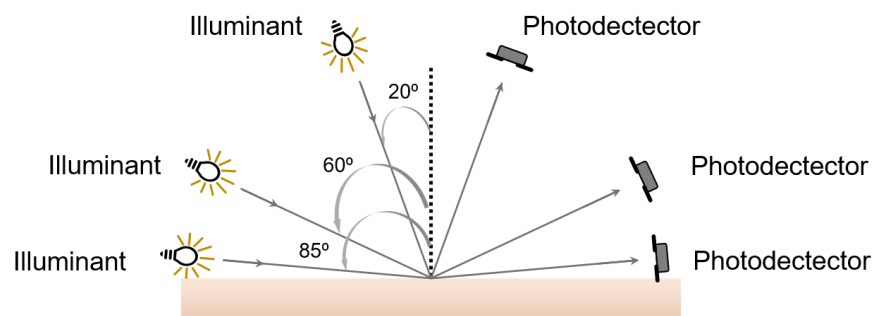


Figure 2.15. Schematic representation of a glossmeter.

Gloss depends on the angle of the illuminant, especially in the fields of paints and plastics. For samples with a matte appearance, measurements at high angles are employed, while for significant glossy materials, angles near the perpendicular are used. Preferentially, three different geometries are measured relative to the surface normal: 20°, 60°, and 85°. Generally, the routine procedure relies on measuring 60° geometry, and if the obtained value is greater than 70 GUs, the 20° measurement is covered. Contrarily, if the value obtained at 60° is less than 10 GUs, then 85° is re-measured.^[25]

In addition to the angle of the incident beam, gloss is altered by the surface texture and the refractive index of the polymer. The former might produce unusual reflected angles preventing the proper measurement by the detector and the latter may cause internal reflections of the material.

2.17. Contact Angle Analysis

Contact Angle (CA) measurement is a popular tool to unravel the behavior of numerous fluids on surfaces and examine the liquid-solid interaction. Therefore, it allows characterizing and exploring the wettability of materials and enables the assessment of formulations for applications like printing, cleaning, or coatings.

The CA (θ) is the angle between the tangent line formed by the surface of the liquid and the solid at a given temperature and pressure. It reflects the balance between the three forces arising from the liquid, the solid, and the gas phase.^[26] Young at the beginning of the century explored the water CA and its correlation with the phases involved in the formation of a drop over a chemically homogeneous and even surface. Prominently, he reported Young's equation (Equation 2.7), which relates the CA and the three surface tensions involved in the equilibrium state of a drop.^[27]

$$\gamma_{SA} = \gamma_{SL} + \gamma_{LA} \cdot \cos \theta \quad \text{Equation 2.7}$$

where γ_{SA} , γ_{SL} and γ_{LA} represent the solid surface free energy (SFE), the solid-liquid interfacial free energy, and the liquid free energy or surface liquid tension, respectively. Accordingly, spontaneous wetting is considered when θ is near 0°. Low interactions result in rounded drops with a small contact area between the solid and liquid phase, which is translated into high CA

values (Figure 2.16.A). Contrarily, high interactions lead to flattened drops, which possess low CA values (Figure 2.16.B).

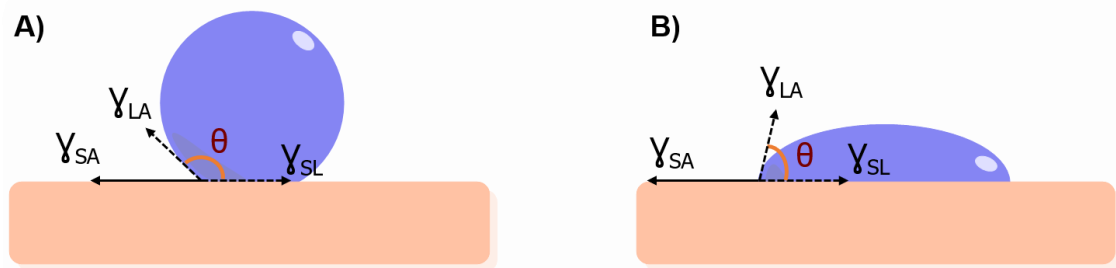


Figure 2.16. Graphical interpretation of the CA for a drop of water in A) a smooth hydrophobic surface and B) a smooth hydrophilic surface.

There are different types of CA according to the conditions in which they are measured. However, in this thesis, only the static CA is studied. It relies on obtaining the CA value of a drop at the equilibrium. Although there are several methods for determining the static CA, hereafter, it is only detailed the Drop shape analysis (DSA), also called the Sessile drop technique. This measurement is carried out by a CA goniometer, in which the liquid is dispensed onto an even surface, and an image of the sessile drop is captured. Most instruments possess a curve-fitting software that recognizes the contour of the liquid and fits it to the appropriate function (Young Laplace equation, circle, polynomial...). Ultimately, CA is measured by determining the height (H) and the radius (R) of the drop (Equation 2.8).

$$\theta = 2 \cdot \tan^{-1} \left(\frac{H}{R} \right) \quad \text{Equation 2.8}$$

To obtain reproducible results, some considerations must be bear in mind. Static CA measurements are usually carried out at an open lab atmosphere; hence, a controlled temperature and pressure are recommended. The drop's volume is usually fixed by the system and must be the same for all the measurements. Finally, to achieve static CA, a few seconds must be waited to accomplish the real equilibrium state in which the drop is stabilized.

CA measurements depend on the employed solvent, and different behaviors can be observed for the same material when changing the liquid used for producing the drop. However, among the different liquids that can be used to determine the CA, water generates which is called Water Contact angle (WCA, θ_w). Particularly, it enables the surface categorization according to its behavior exclusively with this fluid. Superhydrophilic surfaces are those with $\theta_w < 10^\circ$. Hydrophilic or wettable surfaces possess a $10^\circ < \theta_w < 90^\circ$. Conversely, hydrophobic or

non-wettable surfaces have $\theta_w > 90^\circ$ and superhydrophobic surfaces must fulfill two conditions, $\theta_w > 150^\circ$ and CA hysteresis ^[c] $< 10^\circ$.

Analogously to WCA results, the CA measured with liquids such as alcohols or some other organic solvents might indicate the analog surfaces: oleophobic, oleophilic, and superoleophilic. Finally, compounds that present low interaction with both types of fluid (water and organic solvents) are superhydrophobic and superoleophobic, which is called superomniphobic.

2.18. Surface Free Energy

Surface Free Energy (SFE, γ_{SA}) is defined as the energy excess of the atoms at the surface of a solid in comparison with the energy of the atoms at the bulk part. It quantifies the intermolecular interactions between a solid and a liquid, independently of the employed fluid. This property is characteristic for a solid, likewise the surface tension is distinctive for a liquid. This parameter provides an idea of the adhesion between the two involved phases, and thus, the wettability. Low SFE values are associated with materials with a WCA between 90° and 180° , and thereby not wettable. Contrary, metals, and glass are materials with high SFE values. Usually, the latter exhibit greater adhesion and reactivity than the former owing to the higher spread of the liquid on their surface.

SFE cannot be directly calculated, and different approximations have been developed to obtain it. Fowkes deemed the free energy of a solid and a liquid is constituted by two components, the dispersive (γ^d) and the polar (γ^p) (Equation 2.9).^[28]

$$\gamma = \gamma^d + \gamma^p \quad \text{Equation 2.9}$$

Owens, Wendt, Rabel, and Kaelble (OWRK) method extended the previous concept considering the interfacial free energy (γ_{SL}) as described in Equation 2.10.^[29,30] The dispersive component includes the van der Waals forces whereas, the hydrogen bonding and dipole-dipole interactions are encompassed on the polar part. Generally, the former is stronger in comparison with the latter.

$$\gamma_{SL} = \gamma_{SA} + \gamma_{LA} - 2 \cdot (\gamma_{SA}^d \cdot \gamma_{LA}^d)^{1/2} - 2 \cdot (\gamma_{SA}^p \cdot \gamma_{LA}^p)^{1/2} \quad \text{Equation 2.10}$$

^[c] CA hysteresis correspond to the difference between the advancing and receding angle in a dynamic CA measurement.^[26]

where γ_{SL} , γ_{SA} and γ_{LA} correspond to the previously described parameters and the superscripts p and d correspond to the dispersive and polar components of each energy.

The combination of Equation 2.10 with Young's equation (Equation 2.7), followed by a mathematical rearrangement generates a linear expression of the type $y = mx + b$ (Equation 2.11).

$$\frac{\gamma_{LA}(1 + \cos \theta)}{2 \cdot (\gamma_{LA}^d)^{1/2}} = (\gamma_{SA}^p)^{1/2} \cdot \left(\frac{\gamma_{LA}^p}{\gamma_{LA}^d} \right)^{1/2} + (\gamma_{SA}^d)^{1/2} \quad \text{Equation 2.11}$$

where the polar and dispersive components of the solid SFE correspond to m^2 and b^2 of the regression.

2.19. Size Exclusion Chromatography

Size Exclusion Chromatography (SEC) or also called Gel Permeation Chromatography (GPC) is a chromatography technique that separates dissolved macromolecules according to their size. It is widely employed in the polymeric field as it allows the assessment of the molar mass distribution (MMD) and the polydispersity.^[31]

It comprises the analysis of polymeric samples dissolved in organic solvents. The selected solvent has great relevance in the analysis, as the polymer must be dissolved and swell but not form aggregates.^[32] The analytes are separated in a porous column depending on their "effective size in solution" (Figure 2.17). During elution, polymer coils may permeate into the pores, being the small ones those with more prominent withholding with the column particles. Contrarily, large molecules are excluded from these pores and elute in shorter retention volumes. Hence, the order of elution is related to a gradual decrease in the MMD of the sample.

As the molecules exit the column, they are detected, and chromatograms are generated. They represent the detector response in the Y-Axis and the elution volume in the X-axis. However, to determine the MMDs, a calibration curve must exist to transform the elution volume to the elution time and then, to the MMD. Routinely, it is accomplished with standards of polystyrene, ideally monodisperse, or with narrow polydispersity, and well-known MMD. Analysis of several standards generates the required calibration curve. This correlation allows the assignment of the MMDs to each peak, and the corresponding M_n , M_w ,... Furthermore, the polydispersity is estimated by the width of the peaks. The broader the peak, the larger the chain length distribution.^[33]

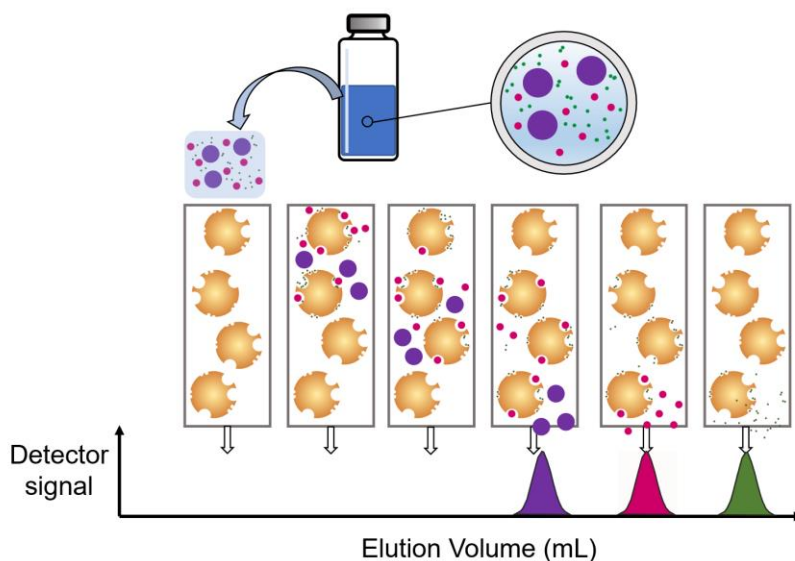


Figure 2.17. Schematic representation of the component separation in a SEC.

2.20. Scanning Electron Microscopy and Energy-dispersive X-ray spectroscopy

Scanning Electron Microscopy (SEM) is a widely used analytical technique to explore materials at micro- and nano-scale and produce magnified images. The topography and chemical composition of the studied samples are achieved by scanning the area with a high-energy, fine, and focused electron beam.

Electrons of the beam, which are also called primary electrons, interact with the surface of the material leading to the emission of multiple signals. (Figure 2.18.A). Secondary electrons (SE) or backscattered electrons (BSE) are used to produce images, while Auger electrons or characteristic X-ray emission generate analytical data. Concretely, SE are electrons ejected from the outer shell of the atom by the incident beam (Figure 2.18.B). These electrons are emitted with low kinetic energy (0-50 eV) and thereby, only those very close to the surface are detected. BSE are electrons coming from the beam that after interacting with the specimen, modify their trajectory and escape from the material (Scheme 2.18.C). Owing to its higher energy ($\gg 50$ eV), BSE interacts with atoms deeper on the sample.^[34] Therefore, valuable information of a few nanometers in depth can typically be obtained in these analyses.

The angle between the studied surface and the beam determines the number of detected SE. The higher the intensity of those, the brighter the spot. Scanning multiple spots with the SE mode will produce a 3D image of the sample, representing the topography of the analyzed area. Conversely, BSE's detection provides additional compositional information of the sample.

In this case, BSE depends on the atomic number (Z) of the elements. Obscured regions indicate that the number of detected BSE is reduced, and thereby, analyzed areas are formed by elements with low Z .

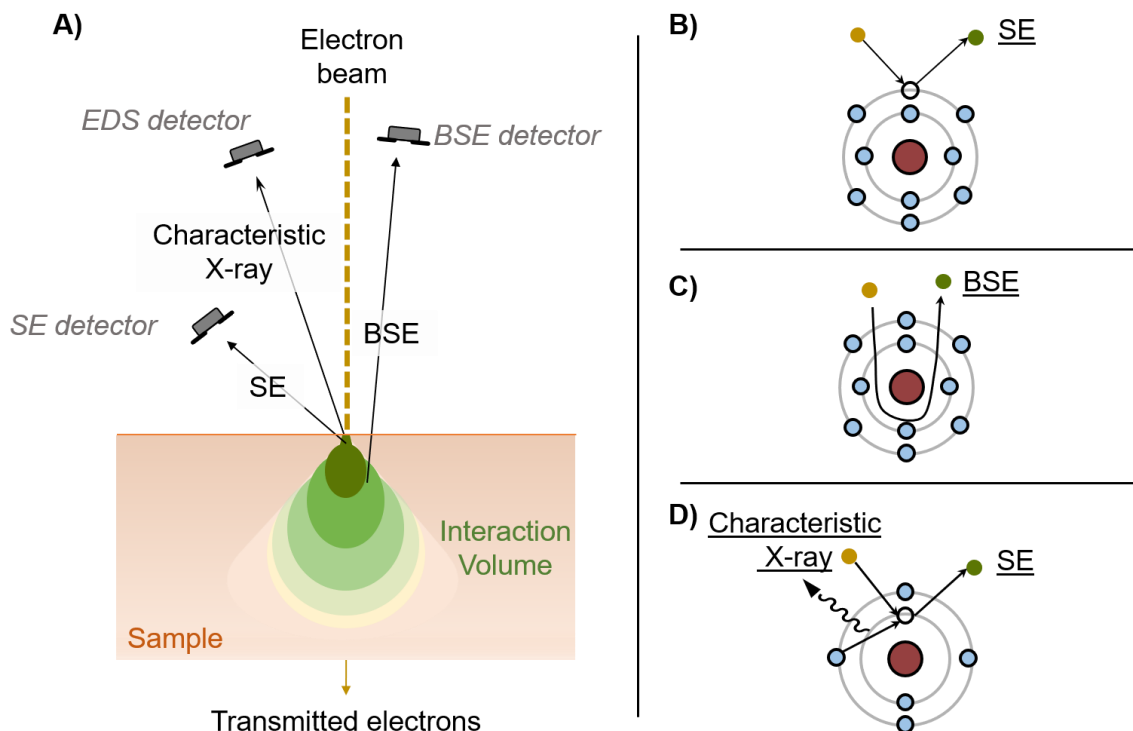


Figure 2.18. Schematic representation of A) the interaction of the electron beam with the material through the formation of B) SE, C) BSE, and D) characteristic X-ray emissions.

Energy-dispersive X-ray spectroscopy (EDS), also known as EDX or EDAX, is a qualitative and quantitative X-ray microanalysis of a material. BSE provides an idea about which regions contain atoms with higher Z than others, and EDX is the technique used to positively identify them. It is based on the detection of the characteristic X-ray produced by the electron beam. Primary electrons create vacancies in the inner shell of the atom, and when the generated hole is occupied with another electron from a higher shell, X-ray radiation is emitted (Figure 2.18.D). Owing to their characteristic X-ray spectrum lines, elements with Z greater than four can be ascertained by this spectroscopic technique.

Usually, data is displayed in a spectrum where the Y-axis represents the number of counts while the X-axis shows the X-ray energy (KeV; elements from beryllium to uranium are detected in the 0.1 to 20 KeV range) (Figure 2.19). Properly knowing the energy associated with each

element enables the determination of the sample composition, and in some cases even the concentration.

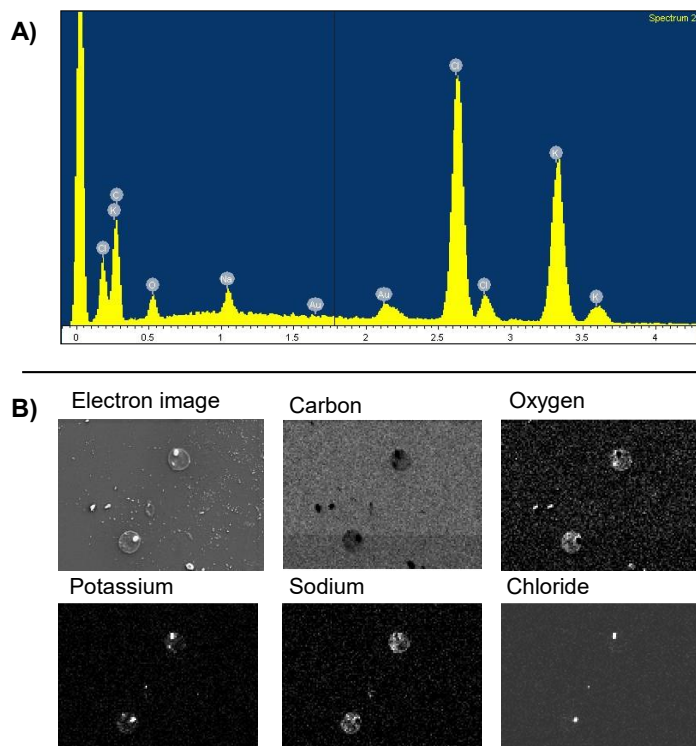


Figure 2.19. A) EDS spectrum of a single spot by its characteristic X-Ray and B) mapping an area, in which the brighter regions are richer in the corresponding element.

There are multiple modes for obtaining data from the EDS, like mapping specific areas on the surface, detecting the composition of a spot, or evaluating changes in one element along the sample, among others. Analysis of samples can be carried out in short times, even with low-energy beams. However, some element's transitions may be misidentified because of the overlapping of the energy of the emitted photons. For instance, the *L* line of bromine overlaps with the *K* line of aluminum, while the *M* line of lead is confused with the *K* of sulfur, etc.^[35] The detection limit of the analysis is commonly in the range of 1000 and 3000 ppm.^[36]

2.21. X-ray photoelectron spectroscopy

X-ray photoelectron spectroscopy (XPS) or Electron Spectroscopy for Chemical Analysis (ESCA) is a quantitative technique employed for the study of surface composition, the speciation of the detected elements, and the nature of their bonds. The main advantage is the possibility to explore the top layers of the studied materials, conversely to the bulk, as in other techniques.

It is based on the photoelectric effects, in which electromagnetic radiation is absorbed by a material, causing the emission of an electron, referred to as photoelectron. It is explained by

the wave-particle duality, in which the incident radiation is not considered as a wave, but as a discrete energy packet, called photon. Therefore, only when the incident photon has enough energy to compensate for the attraction between the negative particle and the positively charged nucleus and provide enough kinetic energy to displace it to the vacuum, a photoelectron is emitted (Figure 2.20). If the energy is too low, the photoelectron will not be ejected from the Fermi level.

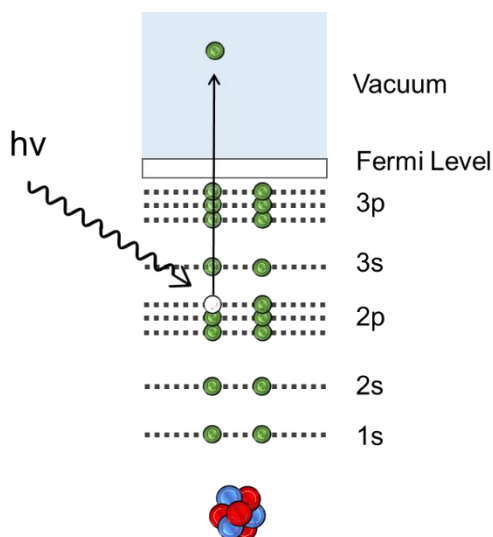


Figure 2.20. Schematic representation of the photoelectric effect.

XPS measures the kinetic energy of the emitted photoelectron when X-ray radiation is directed to the surface in an ultra-high vacuum atmosphere. The ejected photoelectrons are then collected in an analyzer which counts the number of particles with a specific energy. Each instrument related the measured parameter with the binding energy according to the following expression (Equation 2.12)

$$E_{binding} = E_{photon} - (E_{kinetic} + \phi) \quad \text{Equation 2.12}$$

where $E_{binding}$ corresponds to the energy required to ionize an electron, E_{photon} represents the energy of incoming radiation, $E_{kinetic}$ is the kinetic energy of the ejected electron measured in the analyzer and finally, ϕ is a work-function parameter that corrects the deviation of the instrument.

Each element generates characteristic XPS peaks attributed to the different orbitals in the atom (1s, 2s, 2p...), varying the number from 1 to 20, according to the element. Moreover, the technique displays slight variations according to the oxidation state of the element and the chemical environment of each atom.

It is a quantitative technique, so the concentration of each of the detected elements can be determined through the area of their peaks and corrected by the electrons in the studied orbitals. In contrast, the position of the peak ($E_{binding}$) is commonly tabulated and allows the identification of the element and its surrounding environment. However, other parameters as the full width at half maximum (FWHM), the presence of the spin orbitals peaks, or their relative intensity of the peaks had to be considered for an appropriate interpretation of an XPS plot.

2.22. Small-angle X-ray Scattering

Small-angle X-ray Scattering (SAXS) is a non-destructive analytical technique capable of studying the morphology and composition of materials. In the polymer field, it uses the different interactions of the ordered regions of semi-crystalline materials and their matrix with X-ray radiation to explore the shape, size, and spacing of crystalline and semi-crystalline domains.

The monochromatic and collimated X-ray radiation employed in the analysis causes, among other types of interactions with the electrons of the sample, an elastic scattering. During the process, the X-ray radiation is absorbed by the electrons and re-emitted in all directions, with the same energy. The combination of the reemitted waves in the space causes interferences that could be constructive when they superpose and result in a wave with higher amplitude or be destructive and cancel each other (Figure 2.21.A). The detection of the coherent waves leads to bright areas, while the destructive are observed as dark regions in the 2D pattern (Figure 2.21.B). The detection of the fringe pattern of the scattered waves contains information of the size, shape, dispersity, internal structure, pore size, among others.^[37]

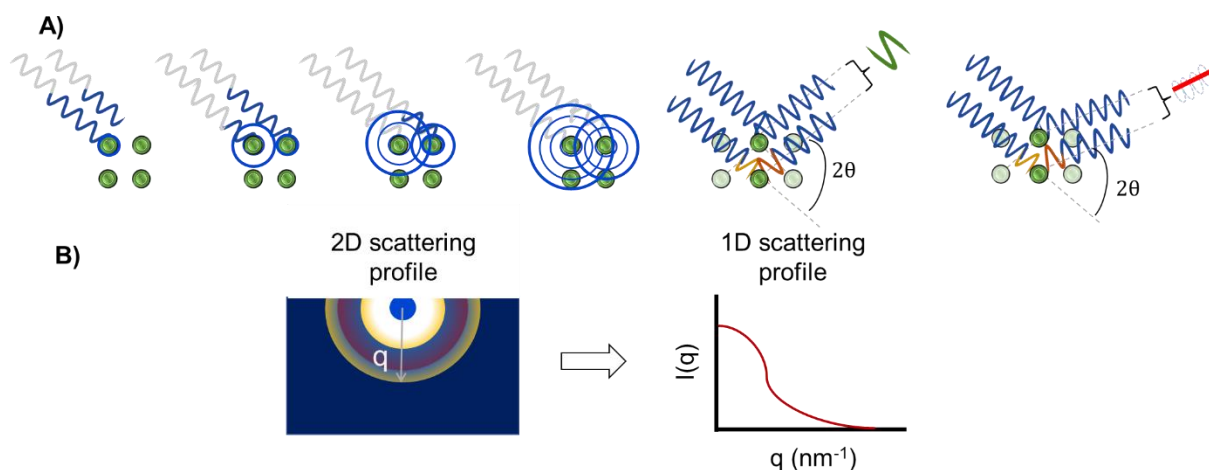


Figure 2.21. A) Representation of the inelastic scattering from neighboring atoms and the resulting constructive waves (green line) and destructive waves (red lines). B) 2D scattering profile from interferences and 1D scattering profile, representing the scattering intensity as function of the scattering vector, q .

When all the scattering particles are randomly oriented, the obtained 2D pattern consists of concentric circular bands. However, as the anisotropy appears on the systems the circular pattern is disrupted, morphing into a star-like pattern or even in the extreme cases only discrete points. In the measured 2D scattering profile or pattern, the intensity of each band (brightness of the signals) depends on the scattered angle (θ) and on the azimuthal angle (φ) at which the detector is located (Figure 2.22). From the 2D scattering profiles, data is reduced to a 1D profile by integrating angularly the intensity in all the directions and normalizing by the number of pixels. Both plots represent the intensity (I) as a function of scattering vector, q , in the reciprocal space, which is defined as Equation 2.13.^[38]

$$q = k_s - k_i = \frac{4\pi}{\lambda} \cdot \sin \theta \quad \text{Equation 2.13}$$

where k_s and k_i are the scattered and incident wave vectors (see scheme in Figure 2.22), λ is the wavelength of the incident radiation and θ is the scattered angle.

The total scattered intensity of a sample depends on the measured intensity I_o , a form factor, $P(q)$, which contains information from the shape and size, and a structure factor ($S(q)$), which comprises the interactions between the scattering particles (Equation 2.14).

$$I(q) = I_o \cdot P(q) \cdot S(q) = I_{in} \cdot (\Delta\rho)^2 \cdot V^2 \cdot P(q) \cdot S(q) \quad \text{Equation 2.14}$$

where I_o and I_{in} are the intensity measured in the detector and of the incident radiation, respectively, $\Delta\rho$ is known as the electronic contrast and refers to the difference in the electronic density of the scattering particles and the rest of the matrix or solvent. Finally, the parameter expressed as V is the irradiation volume.

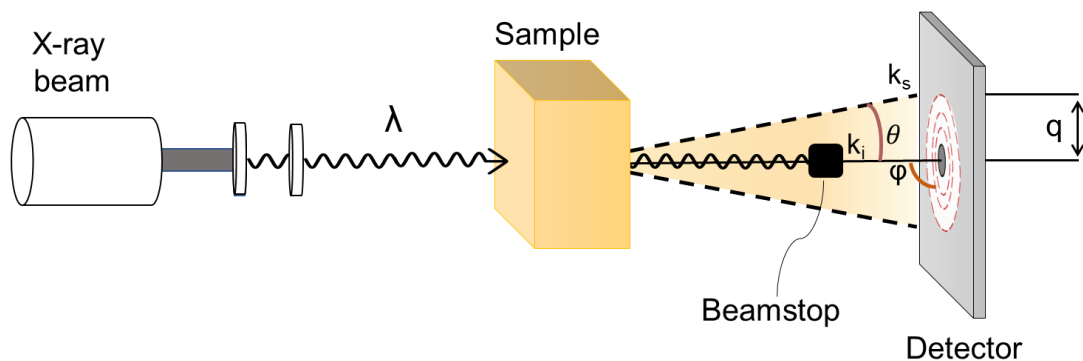


Figure 2.22. Schematic representation of a SAXS measurement.

From the previous expression, several mathematical models with different equations have been developed to explore different systems. Focusing on the analysis of solid polyurethanes, the

bands observed on the 2D profile arise from the difference in electron density of the ordered HS in a less ordered SS matrix. Depending on the HS content and phase segregation, models considering the HS as spheres, rods, gyroids, or lamellae can be employed.^[39]

In our case, we will treat the data considering that the HS comprises polydisperse spheres, as our samples contain a small HS content and relatively elevated miscibility. Therefore, the form factor selected will be that of spherical particles (Equation 2.15).^[40]

$$P(q) = 9 \cdot (\Delta\rho)^2 \cdot V^2 \cdot \left[\frac{\sin(q \cdot R) - q \cdot R \cdot \cos(q \cdot R)}{q \cdot R^3} \right]^2 \quad \text{Equation 2.15}$$

Regarding the structure factor, following the bibliography, Percus-Yevick^[41] and Zernike-Prins^{[42][38]} hard-sphere models have been selected (Figure 2.23). The former treats the system as a HS gradient with a solid core of radius R and a diffuse area of radius R_h around the particle, similar to a dissolved particle and its hydrodynamic radius (Equation 2.16). The Zernike-Prins considers that particles are not equally dispersed, but there are inhomogeneous interparticle distances. Hence, the Zernike-Prins model describes the system with an interparticle distance d and its standard deviation σ (Equation 2.17). Multiple other variables can be studied through this technique, but they are beyond the scope of this study.

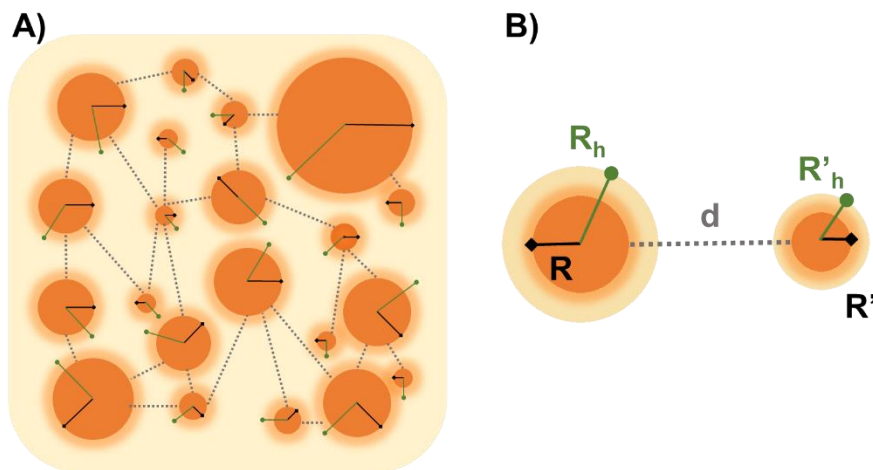


Figure 2.23. A) Schematic representation of a polydisperse dispersion with hard-sphere particles. B) Main features of the dispersion.

Percus-Yevick model:

$$S(q) = \left[1 + \frac{24 \cdot \phi}{x} \cdot G(x) \right]^{-1} \quad \text{Equation 2.16}$$

$$x = 2 \cdot q \cdot R_h$$

$$G(x) = \frac{\alpha}{x^2} (\sin x - x \cos x) + \frac{\beta}{x^3} [2x \sin x + (2 - x^2) \cos x - 2] + \frac{\alpha \cdot \phi}{2x^5} [24 - x^4 \cos x + (12x^2 - 24) \cos x + (4x^3 - 24x) \sin x]$$

$$\alpha = \frac{(1 + 2\phi)^2}{(1 - \phi)^4}; \quad \beta = \frac{-6\phi (1 + \frac{\phi}{2})^2}{(1 - \phi)^4}$$

Zernike-Prins model:

$$S(q) = \frac{1 - A^2}{1 - 2 \cdot A \cdot \cos(q \cdot d) + A^2} \quad \text{Equation 2.17}$$

$$A = e^{-\frac{q^2 \cdot \sigma^2}{2}}$$

Literature

- [1] J. Keeler, *Understanding NMR Spectroscopy*, John Wiley & Sons Inc., Chichester, **2011**.
- [2] M. Weller, in *Inorg. Chemistry* (Eds.: P.M. Atkinson, T. Overton, J. Rourke, M. Weller, F. Armstrong), Oxford University Press, Oxford, GB, **2014**, pp. 234–270.
- [3] W. R. Dolbier, *Guide to Fluorine NMR for Organic Chemists*, John Wiley & Sons Inc., Honoken, New Jersey, **2009**.
- [4] S. Richter, *Encycl. Anal. Chem.* **2019**, 1–25.
- [5] G. Tyler, *ICP-OES, ICP-MS and AAS Techniques Compared*, **2003**.
- [6] H. M. McNair, J. M. Miller, in *Basic Gas Chromatography* (Eds.: H.M. McNair, J.M. Miller), John Wiley & Sons Inc., Honoken, New Jersey, **2018**, pp. 14–28.
- [7] H. M. McNair, J. M. Miller, in *Basic Gas Chromatography* (Eds.: H.M. McNair, J.M. Miller), John Wiley & Sons Inc., Honoken, New Jersey, **2008**, pp. 29–52.
- [8] H. M. McNair, J. M. Miller, in *Basic Gas Chromatography* (Eds.: H.M. McNair, J.M. Miller), **2008**, pp. 104–128.
- [9] J. Coates, *Encycl. Anal. Chem.* **2006**, 1–23.
- [10] G. Ramer, B. Lendl, *Encycl. Anal. Chem.* **2013**, 1–27.
- [11] A. V Shenoy, *Adv. Polym. Technol.* **1986**, 6, 125–145.
- [12] *ASTM D1238-13. Standard Test Method for Melt Flow Rates of Thermoplastics by Extrusion Plastometer*, West Conshohocken, PA, **2013**.
- [13] D. W. Van Krevelen, K. Te Nijenhuis, in *Prop. Polym.* (Eds.: D.W. Van Krevelen, K. Te Nijenhuis), Elsevier Science, Amsterdam, The Netherlands, **2009**, pp. 799–818.
- [14] R. B. Prime, H. E. Bair, S. Vyazovkin, P. K. Gallagher, A. Riga, in *Therm. Anal. Polym. Fundam. Appl.* (Eds.: J.D. Menczel, R.B. Prime), John Wiley & Sons Inc., Hoboken, **2009**, pp. 241–317.
- [15] *ASTM D2240-15. Standard Test Method for Rubber Property — Durometer Hardness*, **2017**.
- [16] *ASTM D792-07. Standard Test Methods for Density and Specific Gravity (Relative Density) of Plastics*, **n.d.**
- [17] A. Shrivastava, in *Introd. to Plast. Eng.* (Ed.: A. Shrivastava), William Andrew Publishing, Cambridge, **2018**, pp. 49–110.
- [18] *ASTM D1894-00. Standard Test Method for Static and Kinetic Coefficients of Friction of Plastic Film and Sheeting*, West Conshohocken, PA, **2011**.
- [19] K. G. Budinski, *Guide to Friction, Wear, and Erosion Testing*, ASTM International, West Conshohocken, PA, **2009**.
- [20] U. Nirmal, J. Hashim, S. T. W. Lau, *Int. J. Mech. Mater. Eng.* **2011**, 6, 367–373.
- [21] R. S. Berns, in *Billmeyer Saltzman's Princ. Color Technol.*, John Wiley & Sons Inc., **2019**, pp. 51–84.
- [22] *ASTM E313-05. Standard Practice for Calculating Yellowness and Whiteness Indices from Instrumentally Measured Color Coordinates*, West Conshohocken, PA, **2005**.
- [23] *ASTM D1003-00. Standard Test Method for Haze and Luminous Transmittance of Transparent Plastics*, West Conshohocken, PA, **2000**.

- [24] R. Silvennoinen, K.-E. Peiponen, K. Muller, Eds. , in *Specular Gloss*, Elsevier, **2008**, pp. 79–101.
- [25] *ASTM D523-08. Standard Test Method for Specular Gloss*, West Conshohocken, PA, **2008**.
- [26] K.-Y. Lao, H. Zhao, in *Surf. Wetting. Charact. Contact Angle Fundam.*, Springer International Publishing Switzerland, **2016**, pp. 7–35.
- [27] T. Young, *Philos. Trans. R. Soc. London* **1805**, *95*, 65–87.
- [28] F. M. Fowkes, *Ind. Eng. Chem.* **1964**, *56*, 40–52.
- [29] D. . Owens, R. . Wendt, *J. Appl. Polym. Sci.* **1969**, *13*, 1741–1747.
- [30] D. H. Kaelble, *J. Adhes.* **1970**, *2*, 66–81.
- [31] B. Trathnigg, *Encycl. Anal. Chem.* **2006**, 1–26.
- [32] D. Held, P. Kilz, *Chem. Teach. Int.* **2021**, *3*, 77–103.
- [33] S. Podzimek, in *Light Scatt. Size Exclusion Chromatogr. Asymmetric Flow F. Flow Fractionation*, John Wiley & Sons Inc., Hoboken, New Jersey, **2011**, pp. 99–206.
- [34] J. I. Goldstein, D. E. Newbury, P. Echlin, D. C. Joy, C. E. Lyman, E. Lifshin, L. Sawyer, J. R. Michael, in *Scanning Electron Microsc. X-Ray Microanal.*, Springer Science + Business, New York, **2003**, pp. 61–78.
- [35] D. E. Newbury, in *Characterization Mater.* (Ed.: N. Kaufmann, Elton), John Wiley & Sons Inc., **2012**, pp. 1854–1879.
- [36] D. E. Newbury, N. W. M. Ritchie, *Scanning* **2012**, *00*, 141–168.
- [37] H. Schnablegger, Y. Singh, *SAXS Analysis*, Anton Paar GmbH, Graz, **2013**.
- [38] O. Glatter, O. Kratky, *Small Angle X-Ray Scattering*, Academic Press INC., London, England, **1982**.
- [39] L. Leiblert, *Macromolecules* **1980**, *13*, 1602–1617.
- [40] P. R. Laity, J. E. Taylor, S. S. Wong, P. Khunkamchoo, K. Norris, M. Cable, G. T. Andrews, A. F. Johnson, R. E. Cameron, *Polymer (Guildf)*. **2004**, *45*, 7273–7291.
- [41] K. Percus, Jerome, J. Yevick, George, *Phys. Rewiew* **1958**, *110*, 1–13.
- [42] F. Zernike, J. A. Prins, *Zeitschrift für Phys. A Hadron. Nucl.* **1927**, *141*, 184–194.
- [43] *D 648: Standard Test Method for Deflection Temperature of Plastics Under Flexural Load in the Edgewise Position*, **2007**.

Chapter 3

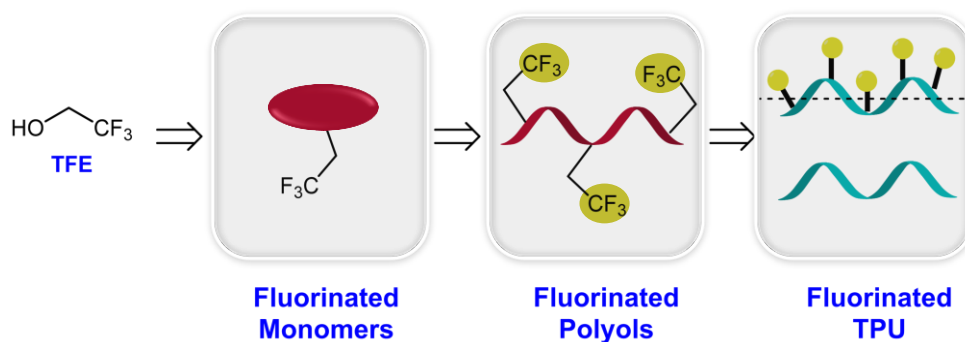
Objectives and Scope.

Chapter 3 describes the general objectives of the first developed project and the scope of this work. The main aim of each chapter will be detailed at the end.

3. Objectives

The main objective of this thesis project is to develop new fluorinated thermoplastic polyurethanes (TPUs) with hydrophobic and oleophobic properties, this is with low surface free energy, conferring an anti-staining behavior to the material that last over time. The enhancement of the mentioned properties is closely related to the presence of fluorine on the surface. Therefore, it was attempted to produce a system in which fluorine is mainly located in the surface of the material.

To fulfill the aim, diverse approaches were explored to incorporate fluorine in different monomers, starting from a low-priced reagent, 2,2,2-trifluoroethanol (**TFE**). This reagent will generate difunctional molecules with trifluoroethyl fragments as side chains. Subsequently, the obtained compounds will be incorporated in polyols and tested as soft segments in TPUs. The general approach followed in this project is outlined in Scheme 3.1.



Scheme 3.1. Planned strategy to generate materials with enhanced properties.

Although monomers with fluorinated pendant chains could promote the migration of the halogen from the bulk to the surface of the material, they could also disrupt the packaging of the polymer. To test this hypothesis, a complete characterization of the final materials and their properties would be necessary, devoting special attention to the surface free energy and water contact angle. Since this thesis seeks the possibility to produce novel materials from an industrial approach, all the involved synthetic processes must be adapted to be industrially manufactured at reduced cost and large scale.

This doctoral thesis has been developed in collaboration with Lubrizol Advanced materials S.A. Therefore, the overarching objective of producing fluorinated TPUs must be hand in hand with synthetic routes and purification processes scalable to industrial productions. Consequently, common separation procedures in organic synthesis as column chromatography and repetitive crystallizations will be intentionally avoided in most of this manuscript. All the syntheses are planned to be easily scaled up, highly selective, and including few simple steps and inexpensive reagents.

This manuscript has been structured following the previous scheme. **Chapter 4** will describe the monomer proposals and their problematic syntheses and purifications. Taking advantage of these synthesized compounds, **Chapter 5** will assess the feasibility of the polymerization reactions to obtain fluorinated diacid-diol polyesters as well as polycaprolactones. Further studies of their structural and thermal behavior will be discussed in this section. The final incorporation of the previously produced oligomers into TPUs as soft segment will be disclosed in **Chapter 6**. Moreover, their properties will be examined in the same chapter. Experimental procedures and spectral data of these developed substances will be recounted in **Chapter 9** and **Chapter 10**.

Chapter 4

Synthesis of monomers

Chapter 4 focuses on the development of various fluorinated monomers with industrially friendly approaches. The first part summarizes the precedents and the acquired knowledge of our research group. In view of that, new synthetic routes were explored employing trifluoroethanol as the main building block.

4 Fluorinated Monomers

Fluorine can be incorporated in several structures on polyurethanes like chain extenders^{[1][2][3][4][5][6][7][8]}, additives,^{[9][10]} or isocyanates,^{[11][12][13][14]} other authors also incorporate fluorinated moieties on hydroxyl-terminated macromolecules such as polyethers^{[15][16][17][18]} or aromatic polyesters.^{[19][20]}

Several methodologies to introduce fluorine into organic molecules and build monomers are detailed in the literature.^{[21][22]} Direct fluorination has proved to be successful but requires the use of F_2 ,^[23] neat HF,^[24] or HF-amine complexes like pyridinium polyhydrogen fluoride (PPHF)^[25] (Figure 4.1). Regrettably, specialized equipment is entailed to carry out these reactions, as the reagents are highly exothermic and can ignite the surrounding organic matter. Alternatively, commercial fluorinated agents such as diethylaminosulfur trifluoride (DAST),^{[26][27]} *bis*(2-methoxyethyl)aminosulfur trifluoride (Deoxo-fluor[®]),^[28] or *N*-Fluoro-*N*-(chloromethyl)triethylenediamine *bis*(tetrafluoroborate) (SelectFluor[®])^{[29][30]} are suitable agents to selectively introduce a single fluorine atom into organic molecules.

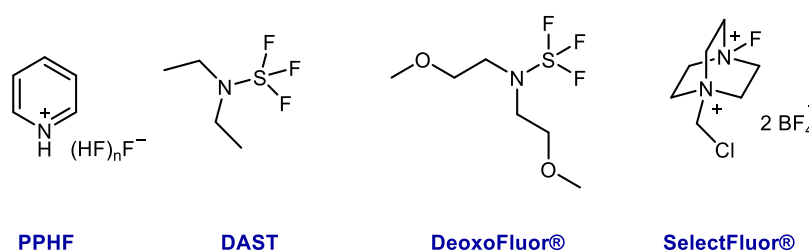


Figure 4.1. Commercially available fluorinating agents.

Regarding the introduction of more than one fluorine atom, Ruppert-Prakash, Umemoto, or Togni reagents are some of the most common trifluoromethylation agents (Figure 4.2)^{[31][32][33][34][35]}. These types of fluorinated reagents are widely employed in pharmaceutical companies in which the final drug possesses a high added value. However, for

a multikilogram scale synthesis of polyesters or TPUs, their price (over €100/g) is considered excessive.

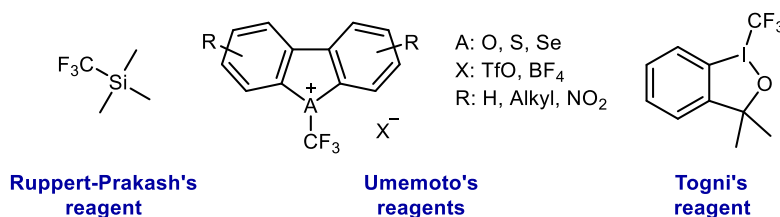


Figure 4.2. Commercially available trifluoromethylating agents.

An alternative approach is the use of already synthesized fluorinated monomers, which usually are long perfluorinated oligomers.^{[16][36]} Nevertheless, their high content of fluorine increases their cost in comparison with their non-fluorinated analogs. Hence, achieving cheap fluorinated monomers is a genuine challenge for the current polymer industry which desires a significant enhancement of the thermal and surface properties of new materials at a low cost. In light of the previous approaches, synthesizing new low-priced monomers is of high relevance from an industrial standpoint.

Our proposal consists in synthesizing fluorinated monomers containing a trifluoroethyl fragment as a side chain with a -CF₃ group to reduce the surface free energy (SFE) of TPUs. Among the different tested approaches, special attention has been paid in this project to the use of trifluoroethanol (**TFE**) as starting building block, as it is one of the most affordable fluorinated reagents on the market (€60/Kg) and possesses unique properties (Table 4.1).

Table 4.1. Properties of **TFE** and ethanol at 300 K and 1 atm.^{[37][38]}

Property	Water	Ethanol	TFE
Molar mass, M (g/mol)	18.02	46.07	100.04
Density, ρ (g/cm ³)	0.997	0.789	1.383
Heat of vaporization, ΔH _{vap} (kJ/mol)	43.99	42.31	43.97
pK _a	14.0	15.9	12.4
Dielectric constant, ε	78	24	27
Boiling point (°C)	100.0	78.0	73.8
Melting point (°C)	0.0	-114.1	-43.5

The three fluorine atoms generate an inductive effect that increases the acidic character of the hydroxyl in comparison with its non-fluorinated analog, ethanol, and produce a superior capacity to form hydrogen bonds by the hydroxyl groups.^[39] Hence, **TFE** has proved to be a

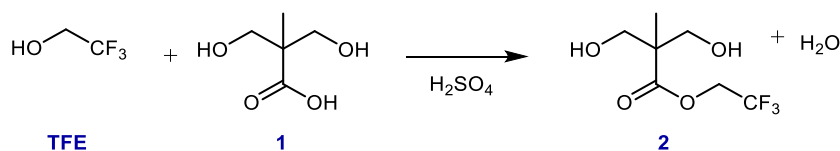
highly interesting reagent and solvent, which might alter the electrostatic and hydrophobic interactions of the medium. Furthermore, **TFE** is well-known in biochemistry owing to its singular effect with proteins, as it promotes preferentially their secondary structures opposite to other solvents.^[40]

Hereinafter, a brief overview of the precedents of our group regarding fluorinated compounds will be discussed and then, the synthetic procedures attempted during this thesis will be thoroughly described. Moreover, a concise summary of the proposed compounds in the literature will be also examined in each part. During the development of the monomer syntheses, some of the essayed procedures resulted in negative outcomes owing to their purification processes or their lack of stability. However, these reactions provide valuable data about the behavior of the involved chemicals and have been included in this manuscript.

4.1 Precedents

4.1.1 Fisher Esterification

Fisher esterification of **TFE** and 2,2-*bis*(hydroxymethyl)propionic acid (**1**) (Scheme 4.1) was previously studied in our research group to synthesize compound **2**. This transformation is industrially interesting owing to its simplicity, absence of solvent, and the generation of water as a non-toxic byproduct.



Scheme 4.1. Proposed Fisher esterification.

Although H_2SO_4 was employed as a dehydrating agent and as a catalyst to polarize the carbonyl bond, no significant amounts of the target product were obtained after heating the mixture to reflux. Instead, an intermolecular polymerization process took place between the hydroxyl groups and the carboxylic moiety, leading to the formation of polyesters.

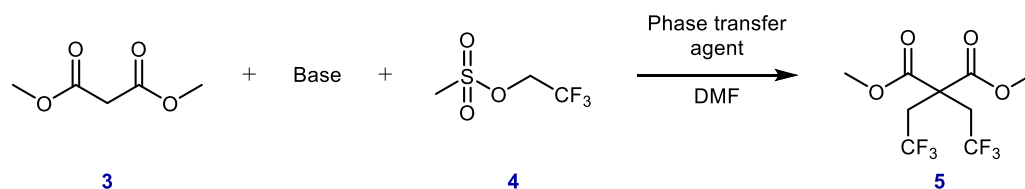
Different concentrations of **TFE** and H_2SO_4 combined with different temperatures were explored; but as **TFE** is more acidic than the primary hydroxyls of **1**, the esterification was hampered. In addition, **TFE** is a good leaving group and in the specific case of generating the ester, it could facilitate the polymerization process and its posterior release. If the esterification between **1** and **TFE** competes with the reaction between the carboxylic acid and the hydroxyls

of **1**, or if by the contrary, the initial esterification with **TFE** helps the transesterification, has been unassessed.

4.1.2 Alkylation of malonic esters.

Malonic esters are common starting materials in organic synthesis. In these compounds, the hydrogen atoms of the methylene are easily removed by a strong base, generating a carbanion that could attack a halide or sulfonate derivative and achieve an alkylated product. The higher acidity of the α -hydrogens compared to methylenes of other alkyl chains make malonic esters remarkable building blocks.

Preceding this thesis, diverse conditions to alkylate dimethyl malonate (**3**) were tested in our group (Scheme 4.2). Bases as potassium carbonate, sodium methoxide, or potassium *tert*-butoxide were essayed with different phase transfer agents as crown-ethers or potassium iodide. Nevertheless, none of those previous experiments were successful for the synthesis of 2,2-*bis*(trifluoroethyl) dimethyl ester malonate (**5**). In the best scenario, only 2% of the monoalkylated product was detected, but no evidence of the dialkylation was noticed. All attempts to improve the yield were unsuccessful. Probably, the sulfonate derivative **4** is not reactive enough to alkylate the starting reagent. Plus, elevated temperatures could cause the degradation of the malonic ester, leading to complex mixtures.



Scheme 4.2. Previously tested alkylation of **3**.

To summarize, both Fisher esterification and alkylation of malonic ester were tested with unproductive results previously to the start of this thesis. Despite its exploratory nature, these precedents offer some insight into the behavior of **TFE**. The common reactivity of hydroxyl groups should be cautiously considered owing **TFE**'s peculiar chemistry. Its higher acidity modifies the usual alcohol reactivity, becoming a better leaving group. Hence, a simple reaction such as esterification led to intricate mixtures and the release of the fluorinated moiety into the crude in the presence of better nucleophiles. The reactivity of its sulfonates derivatives also is reduced compared to its non-fluorinated analogs; therefore, higher electrophilicity could be needed to carry out similar transformations.

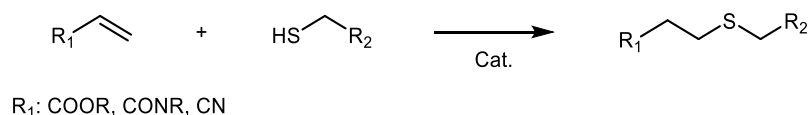
4.2 Synthesis of fluorinated monomers

Hereunder there will be the work developed in this thesis.

4.2.1 Click reaction: Thio-ene Michael addition

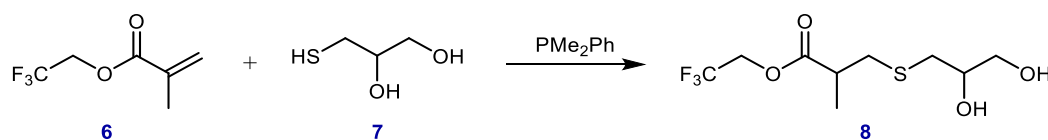
In 2001, K. B. Sharpless defined the term "Click Chemistry" as a type of reactions easy to carry out, stereospecific, with high yields, available to a wide versatility of reagents, and with no or little by-products, which were simply removed without the use of chromatographic techniques.^[41] In addition, regarding solvents, they should be easily removable or considered green. Hence, this type of reaction generates considerable interest, especially at industrial level.

Lubrizol scientists at the R+D department proposed the generation of a monomer by means of Thio-ene Michael addition. The reaction consists of the nucleophile attack of a thiol onto an unsaturated carbon bond activated by electron-withdrawing groups like esters, amides, or nitrile (Scheme 4.3).^[42] Generally, this reaction takes place under mild conditions, with high selectivity, and presents a wide tolerance toward different functional groups. This hydrothiolation is reported to use simple catalysts such as hexylamine,^[43] triphenylphosphine,^[44] or dimethylphenylphosphine (**PMe₂Ph**)^[45] to form specific products with high conversions in short times. In all cases, the driving force of the reaction is the low pK_a of the thiol, which allows an easy deprotonation and the generation of a good nucleophile.



Scheme 4.3. General Thio-ene Michael Addition.

Our proposal is based on the nucleophilic attack of α -thioglycerol (**7**) to 2,2,2-trifluoroethyl methacrylate (**6**) to generate 2,2,2-trifluoroethyl 3-((2,3-dihydroxypropyl)thio)-2-methylpropanoate (**8**) with **PMe₂Ph** as catalyst (Scheme 4.4). The reaction between the selected unsaturated compound and the thiol enables the synthesis of a dihydroxylated molecule containing the target fluorinated moiety bounded by an ester linkage. Even though **TFE** was not directly employed, the studied fragment was already incorporated in the starting reagent. Precedents of our research group already pointed to the lability of the trifluoroethyl ester bond, but a last attempt was tried with a reaction carried out at mild conditions and short times.



Scheme 4.4. Proposed thiol-ene Michael Addition.

Although thiol-ene reactions with methacrylates have been widely used in the literature, only one publication reports a synthesis starting from **6**.^[46] However, their experiments were carried out with *N,N'*-diisopropylamine (DIPA) as catalyst instead of phosphines. Amines are odorous compounds and at industrial scale present difficulties to be separated, reused, or deactivated. Therefore, their use as catalyst was discarded for these trials and replaced by phosphorus-based compounds.

Initially, all the experiments were conducted at the NMR tube scale following the procedure described by Li *et al.* which test the synthesis with α -thioglycerol.^[45] The authors reported a ratio between acrylate **6** and thiol **7** of 1.0:1.5 equivalents to achieve the desired product. Compound **8** was obtained in an hour with a catalyst loading of 5 mol%, both in acetone-*d*₆ and dimethyl sulfoxide (DMSO-*d*₆). The methodology proved to be reproducible, although **TFE** traces were observed at advanced reaction times. The role of water on the solvents was also explored at NMR tube scale, and no significant differences were observed among dried or undried conditions. Thus, among the tested solvents, acetone was selected to be used, owing to its easy removal.

PMe₂Ph was compared with methyldiphenylphosphine (**PMePh₂**) as catalyst. However, only the former exhibited catalytic activity towards the Thio-ene Michael addition and generated the aimed product **8**. Employing **PMePh₂** led to the transesterification of **6** with the alcohols of the thiol in the media, and the release of **TFE** without altering significantly the olefinic peak signals (Figure 4.3.A). Conversely, **PMe₂Ph** completed the addition of the thiol onto double bond as can be observed by the absence of the olefinic peaks in Figure 4.3.B. However, as the mixture contained hydroxyl groups some degree of transesterification occurred, and small oligomers were generated. This side-reaction led to **TFE** release and the increase of its concentration over time.

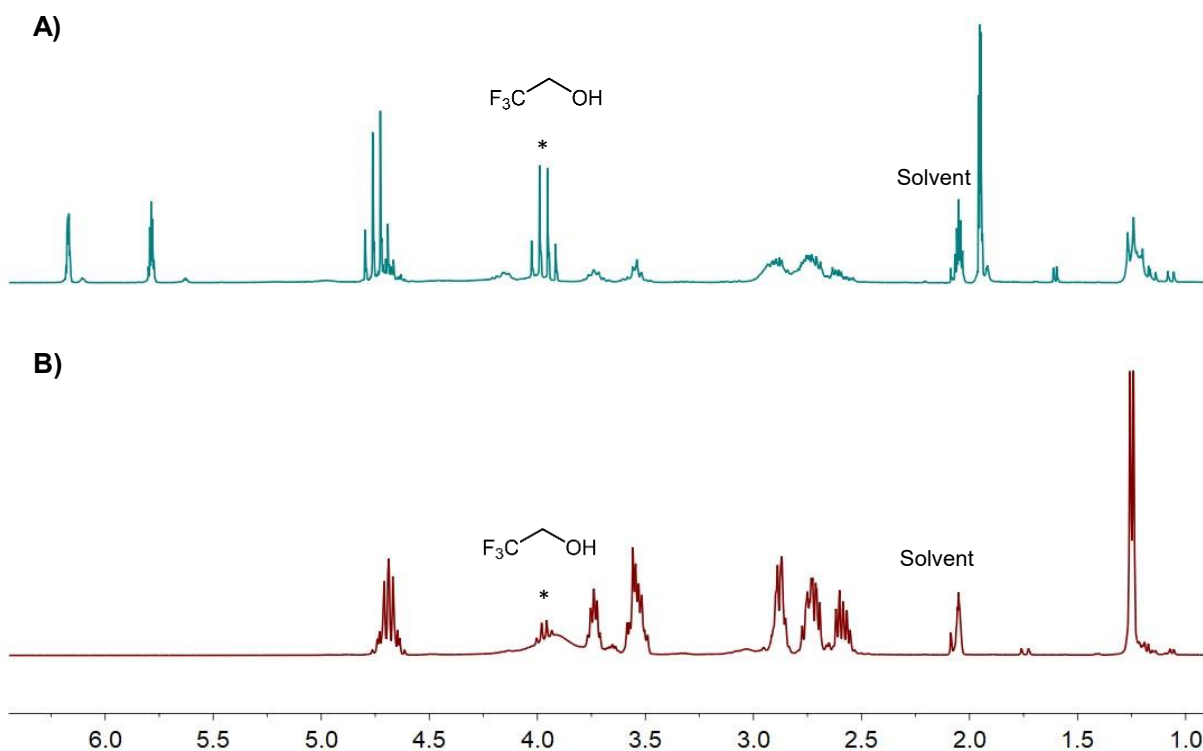
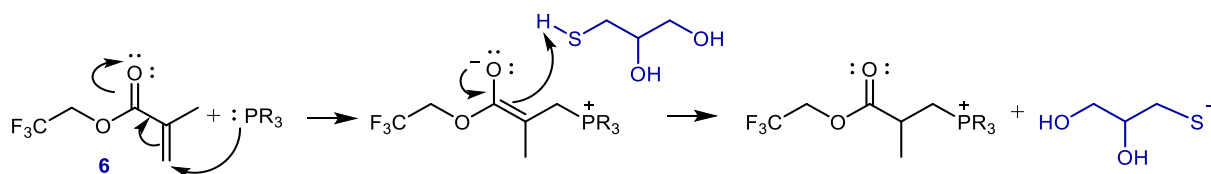


Figure 4.3. A) ^1H NMR (250 MHz) spectrum of **PMePh₂**-catalyzed reaction crude after 200 minutes. B) ^1H NMR (400 MHz) spectrum of **PMe₂Ph**-catalyzed reaction crude after 60 minutes. Signal marked with * in the spectra correspond to **TFE**. Solvent: Acetone-*d*₆.

The possible reason behind the different reactivity of both compounds could be the substitution of a methyl by a phenyl group in the phosphine. This change decreases the nucleophilicity of the phosphine and consequently, the activity of the catalyst. **PMePh₂** triggered, to a less extent than **PMe₂Ph**, the double bond activation causing a reduction on the successive deprotonation and attack of the thiol (Scheme 4.5). Accordingly, with **PMePh₂**, the transesterification reaction is faster than the 1,4-addition, leading to the generation of the undesired product.



Scheme 4.5. Adaptation of the proposed mechanism for the phosphine-catalyzed thiol-ene Michael addition.^[47]

The reaction was optimized to a laboratory scale, testing different catalyst loadings and ratios of α -thioglycerol **7** (Table 4.2). First attempts were scaled up to 2 grams, working under inert conditions to avoid the oxidation of **PMe₂Ph**. When the already tested 1.0:1.5 ratio between the fluorinated methacrylate **6** and α -thioglycerol **7** was employed, the target compound was

obtained with the presence of other sub-products. However, using the stoichiometric ratio (1.0:1.0) yielded the breakage of the ester group and the release of **TFE** (Entry 2, Table 4.2).

Table 4.2. Evaluation of reaction conditions.^[a]

Entry	Scale (g)	Ratio 6:7	PMe ₂ Ph loading (mol%)	Yield (%) ^[b]
1	2	1.0 : 1.5	5	50
2	2	1.0 : 1.0	5	Transesterification
3	2	1.0 : 1.5	1	80
4	10	1.0 : 1.5	1	87
5	10	1.0 : 1.0	1	Transesterification
6 ^[c]	10	1.0 : 1.0	1	Transesterification

^[a] Reaction conditions: 30 minutes at 0 °C and then, 1 hour at room temperature. Solvent: Acetone.

^[b] Yield is quantified by ¹³C{¹H} NMR spectroscopy.

^[c] Dropwise addition of **6**.

To improve the moderate yield and reduce the generation of impurities, a decrease in the catalyst loading from 5 mol% to 1 mol% was attempted. Considering that the phosphine activates the acrylate not only for the desired thiol-ene addition but also for the transesterification reaction, a drop of the catalyst concentration might increase the selectivity. This hypothesis was evaluated with successful results, as is seen in Entry 3 (Table 4.2), in which the decrease of phosphine loading generated higher yields than in Entry 1 (Table 4.2).

Carrying out the reaction at bigger quantities with a reagent ratio of a 1.0:1.5, reproduced smaller scale values (Entry 4, Table 4.2), while transesterification was the predominant process when the ratio between the starting materials was 1.0 (Entry 5, Table 4.2).

Maintaining the stoichiometric proportion, the addition rate of acrylate **6** was also evaluated. As the methacrylate was added over the thiol, the progressive addition would promote a continuous excess of thiol **7** in the reaction crude. Despite that, a dropwise incorporation of **6** resulted in the transesterification of the methacrylate (Entry 6, Table 4.2). These negative results demonstrate that an excess of **7** is mandatory to prevent side reactions and obtain the target product.

Although yields higher than 80% of product **8** were obtained in our best conditions, significant amounts of α -thioglycerol remained on the mixture. The reported work-up typically consisted of the separation of the synthesized product from the mixture by precipitation in distilled water. However, a single-phase was observed, and no separation was possible upon this treatment. Moreover, **7** possesses a high boiling point (118 °C/ 5 mmHg, according to the supplier), so

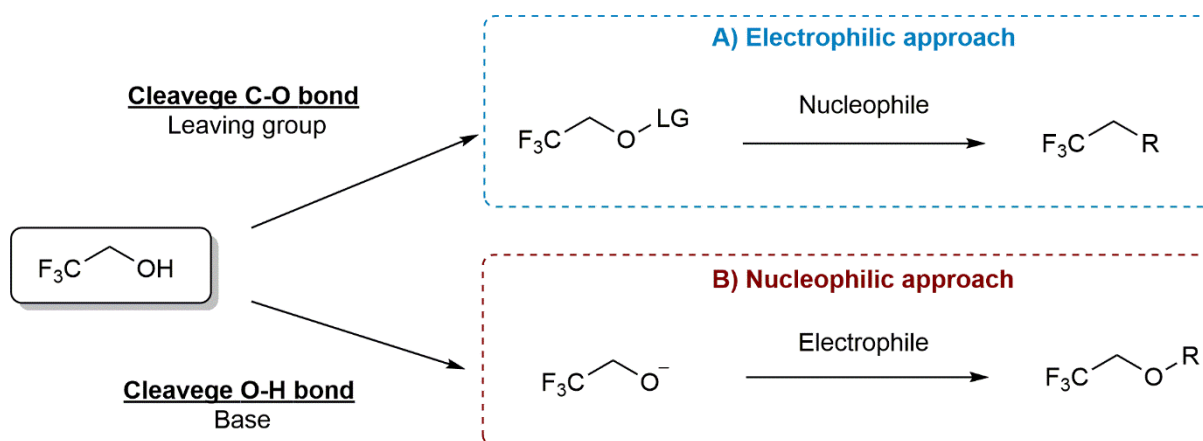
evaporating it could promote condensation or side reactions leading to polymerization. Because of that, alternative purification procedures were studied.

After quenching the reaction with distilled water, filtrations with different materials (silica, and alumina) and extractions with several organic solvents were evaluated. Neither of them proved to be successful and sub-products arising from the hydrolysis of the ester were observed. It seems that transesterification reactions are prone to happen in the presence of nucleophiles as water or alcohols owing to the electron-withdrawing nature of the trifluoromethyl group. Alternatives as chromatographic separation or distillation were discarded as they cannot be industrially implemented or could degrade the sample.

Hence, compound **8** was synthesized with high yields, but no appropriate purification processes were devised. Transesterification side products were observed in all the tested work-ups owing to the lability of the ester bond, which in polymerization conditions could generate undesired and uncontrolled macromolecules. This lack of success resulted in dismissing the incorporation of trifluoroethyl moieties in organic molecules by means of esters and other approaches for synthesizing low-priced monomers were evaluated.

4.2.2 Trifluoroethyl fragment as a non-ester compound

Two different routes were proposed to introduce a trifluoroethyl moiety once the fluorinated ester was rejected. Owing to the acidic character of **TFE**, it can act as an electrophile if it is converted into a compound with a good leaving group (Scheme 4.6.A); or it can play the role of a nucleophile if the corresponding alkoxide is formed (Scheme 4.6.B). Both synthetic approaches enforce disparate reactivities, giving rise to different compounds. In the electrophilic approach, reagents with good leaving groups could produce a myriad of compounds where the fluorinated fragment ($-\text{CH}_2\text{CF}_3$) and the non-fluorinated are bounded by a C-C bond, among other possibilities. Alternatively, trifluoroethoxide in the presence of an electrophile could generate ethers by Williamson reaction.



Scheme 4.6. Synthetic routes to convert **TFE** into monomers. A) Electrophilic approach (in the blue rectangle) and B) nucleophilic approach (in the red square rectangle).

4.3.1.1. *TFE as an electrophile*

4.3.1.1.1. *Leaving groups with TFE*

TFE is frequently considered a poor electrophile, but it can be converted into one if leaving groups are introduced. The best leaving groups are those which produce stable fragments after reacting, which usually correspond to conjugated bases of strong acids, such as halides and sulfonate derivatives.

In the developed thesis, trifluoroethyl *p*-toluenesulfonate (tosylate, **9**), trifluoroethyl methanesulfonate (mesylate, **4**), and trifluoroethyl trifluoromethanesulfonate (triflate, **10**) were assessed as fluorinated compounds with good leaving groups (Figure 4.4).

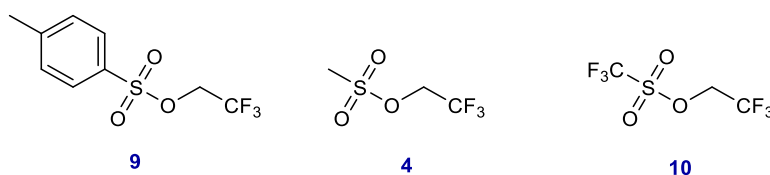


Figure 4.4. Leaving groups containing the trifluoroethyl moiety.

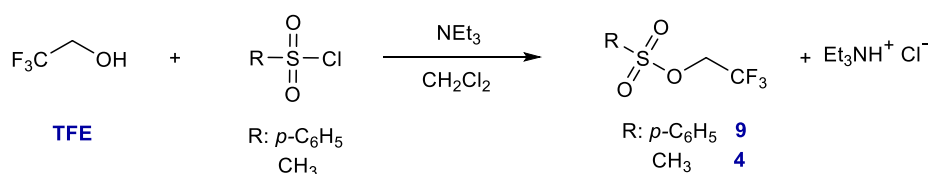
The general trend for sulfonate reactivity follows tosylate < mesylate < triflate, being the latter the most reactive but, as well, the most expensive, especially compared with the price of the sulfonyl starting reagents (Table 4.3). Considering an industrial perspective, the use of triflate **10** to synthesize building blocks should be extremely justified as it will increase to a great extent the monomer prices.

Table 4.3. Sulfonyl compounds and trifluoroethyl sulfonates prices by Sigma Aldrich.^[a]

Retail price starting materials (€/g)		Retail price TFE derivative (€/g)	
<i>p</i> -CH ₃ (C ₆ H ₄)SO ₂ Cl	0.09	9	1.7
CH ₃ SO ₂ Cl	0.07	4	9.0
(CF ₃ SO ₂) ₂ O	4.96	10	28.0
CF ₃ SO ₂ Cl	13.46		

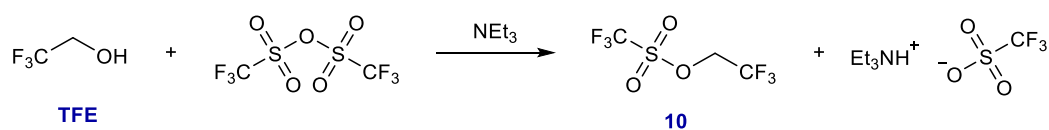
^[a] Purities above 98%.

Tosylate **9** and mesylate **4** were initially synthesized according to the literature by coupling **TFE** and the corresponding sulfonyl chloride in basic media for three hours (Scheme 4.7).^{[48][49]} Reactions were carried out in CH₂Cl₂ at a temperature lower than 40 °C and required an excess of NEt₃ to neutralize the generated HCl.



Compound **9** was obtained as a solid after neutralizing the reaction crude to neutral pH, carrying out a liquid-liquid extraction, and removing the solvent. It was successfully synthesized in a 50 g scale reaction with a yield of 80%. For mesylate **4**, the same work-up process was required, followed by a distillation to complete the purification. It was achieved with a yield of 78% as a colorless liquid.

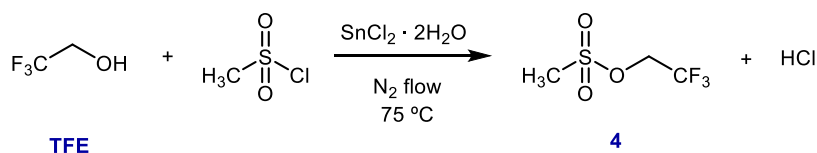
In the case of triflate **10**, it was also synthesized in the presence of one equivalent of NEt₃, but in the absence of solvent as reported in the literature (Scheme 4.18).^[50] The starting reagent was trifluoromethanesulfonic anhydride instead of the corresponding chloride as it has a higher boiling point and is more cost-effective. After the addition of **TFE** at a low temperature (-20 °C), the mixture reacted for 4 hours at room temperature. Then, the sulfonate product was directly distilled from the reaction mixture without a liquid-liquid extraction. Triflate **10** was obtained as a liquid with a high yield (~90%) and high purity in a more straightforward synthesis than the previous sulfonate derivatives.



Overall, the traditional synthesis of these compounds is not an industrially friendly route even at a small scale, requiring large amounts of solvents or bases, and additional reagents to carry out the purification processes. Furthermore, *p*-toluenesulfonic chloride and methanesulfonic chloride are moisture-sensitive products, so reagents and solvents involved in the reaction had to be carefully dried beforehand, entailing extra steps.

As the project evolved, it was essential to increase the amount of product generated in each batch. Because of that, mesylate **4**'s synthesis was scaled up and some modifications of the previous procedure were performed to improve the efficiency.

An industrial alternative was reported by Vastra and Saint-Jalmes,^[51] in which they replace solvents and base with a Lewis acid catalyst. Their best results achieved a 98% of **TFE** conversion and 91% yield with a catalyst loading of 5 mol% of SbCl₅. Direct distillation of the reaction crude allowed obtaining **4** with high purity and the recycling of the catalyst. However, SbCl₅ is highly hygroscopic which could cause its deactivation. Built on this premise, our approach is based on a solvent-free reaction where NEt₃ is replaced by a N₂ stream (Scheme 4.9). A specific setup was used to promote the displacement of the reaction toward the products. It consists in connecting the round bottom flask to the inert gas stream to drag the generated acid to an external NaOH_(sat, aq.) solution. In addition, a soft Lewis acid, SnCl₂·2H₂O (2.5 mol%), was employed as an ease-to-use catalyst. This catalyst is less moisture-sensitive than SbCl₅, so deactivation by hydrolysis should not be an issue under the tested conditions.



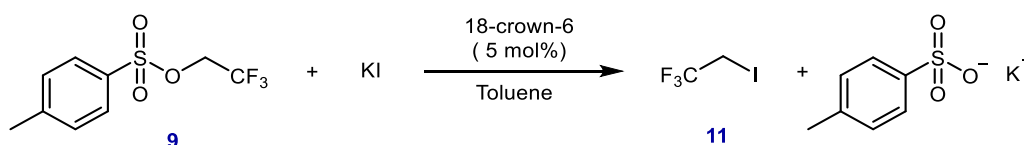
Scheme 4.9. Alternative synthesis of **4**.

The addition of the sulfonyl chloride is an exothermic process; hence, the mixture of alcohol and catalyst must be cooled down on an ice bath before the dropwise incorporation of the methanesulfonyl chloride. Exploiting the presence of fluorine, the reaction was monitored by ¹⁹F{¹H} NMR spectroscopy, determining the end when completed conversion was reached. At that moment, product **4** was fractionally distilled from the reaction crude with high purity. In a 35 g scale, yields up to 81% were reached with this methodology after 5 days at reflux temperature.

Carrying out a solvent-free reaction and replacing stoichiometric quantities of bases for gas streams prevents liquid-liquid extractions and fosters the scale-up of the process. Moreover, from an industrial viewpoint, the external $\text{NaOH}_{(\text{sat, aq})}$ solution could be replaced by HCl absorption columns if the scale enforced it.

In addition to the sulfonate leaving groups, halogenated derivatives were considered. Bromide and chloride compounds possess low boiling points (6.1 °C and 26.0 °C, respectively), which hampered their synthesis and their posterior use.^[52] Alternatively, the synthesis of 2-iodide-1,1,1-trifluoroethyl (**11**) was attempted benefiting from its higher boiling point than the previous halogenated compounds (boiling point 54-55 °C).^[53] However, to the best of our knowledge, synthetic methods to directly iodinate primary alcohols were unreported.

Therefore, our alternative was to start from an already synthesized derivative of **TFE**, tosylate **9**, and then, substitute the sulfonate group with iodide to produce **11**. The replacement of this sulfonate leaving group by an iodide in the presence of an excess of an iodide salt is an already reported methodology.^{[54],[55]} The described substitution was carried in toluene at 50 °C. The immiscibility of the KI in the employed solvent required 5 mol% of 18-crown-6 ether to increase the solubility of the involved ions (Scheme 4.10).



Scheme 4.10. Proposed synthesis for **11**.

The reaction was monitored by $^{19}\text{F}\{^1\text{H}\}$ NMR spectroscopy and reached a conversion of the tosylate **9** of 53%. Although product **11** was possible to be synthesized, the major problem was the purification process. Liquid-liquid extractions of the product were avoided and distillation proved to be unsatisfactory, both at reduced pressure and atmospheric pressure. Observing the difficulty to produce fluorinated electrophiles containing halides as leaving groups, it was decided to move forwards on the synthesis of monomers only using sulfonate derivatives.

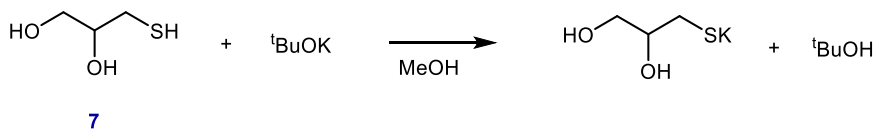
4.3.1.2. Synthesis of 3-[(2,2,2-trifluoroethyl)thio]-1,2-propanediol (**12**)

The first monomer attempted in this thesis by the electrophilic approach is 3-[2,2,2-trifluoroethyl)thio]-1,2-propanediol (**DiolsF**, **12**). The presence of $-\text{CF}_3$ moiety in an organic molecule influences the nucleophilicity of the neighboring groups, as was described by the

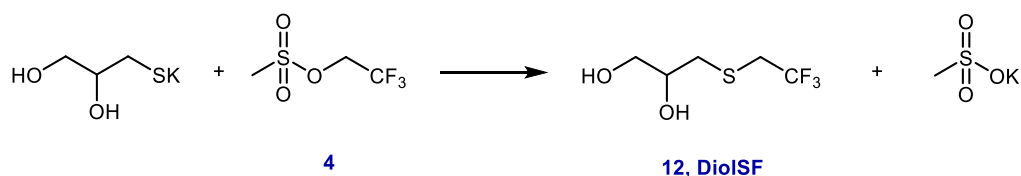
alcohol in **TFE**. However, in the target compound **12**, this effect is overcome by separating the halogens atoms from the other alcohols through methylene groups.^[56] To the best of our knowledge, the synthesis of compound **12** is not reported in common databases, although it is commercialized by some suppliers by request at high price (€785/g).

The proposed approach to obtain **12** consists of a two-step synthesis: the generation of the thiolate salt of compound **7**, and then, the nucleophilic substitution on mesylate **4** to form a diol with a trifluoethyl moiety (Scheme 4.11). This specific proposal takes advantage of thiol's chemistry. Usually, these compounds possess lower pK_a values than hydroxyls, which make them more prone to deprotonate and generate better nucleophiles than standard alcohols. The acid-base reaction was carried out with $t\text{BuOK}$ because of its affordable cost, its high steric hindrance, and its non-nucleophilic basic behavior. Previous experiences with **TFE** sulfonate derivatives revealed that tosylate **9** was not a strong enough electrophile; therefore, the reaction was evaluated with mesylate **4**.

A) Thiolate generation



B) Nucleophilic substitution

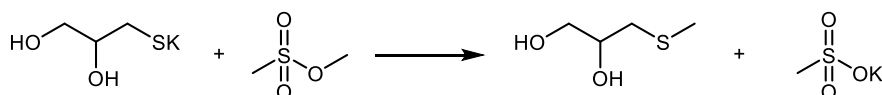
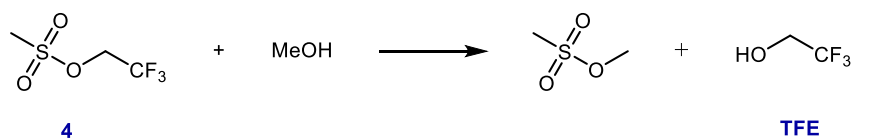


Scheme 4.11. Proposed synthesis of **12**.

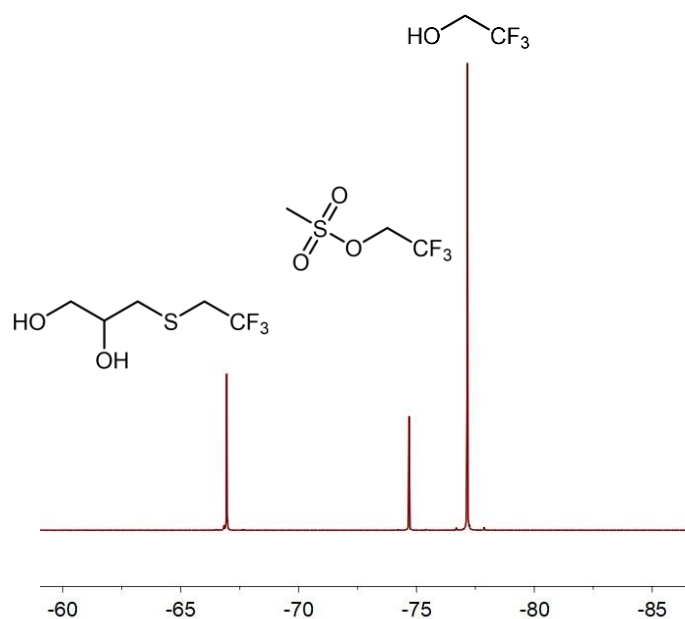
Initial experiments successfully generated the potassium thiolate by the reaction between compound **7** and $t\text{BuOK}$ in MeOH. After the reaction, the mixture of alcohols ($t\text{BuOH}$ and MeOH) was evaporated to obtain a white salt. However, if some traces of MeOH remained when mesylate **4** was incorporated, the methyl mesylate was generated and consequentially the methyl thioether was obtained as by-product (Scheme 4.12.A). **TFE** is a more acidic alcohol than MeOH and thereby, it behaves as a better leaving group fostering the nucleophilic attack of MeOH over mesylate **4** and the corresponding sulfonate transesterification. The mixture of three compounds on the $^{19}\text{F}\{^1\text{H}\}$ NMR spectrum confirmed this inconvenient reaction (Scheme 4.12.B). To avoid the mentioned side products, the thiolate salt must be totally dry.

In addition to the evaporation of the generated t BuOH under reduced pressure, an azeotropic distillation with toluene was carried out to ensure this result

A)



B)



Scheme 4.12. A) Side reaction consisting of the nucleophilic attack of MeOH over mesylate **4** and the subsequent alkylation of the thiol. B) $^{19}\text{F}\{^1\text{H}\}$ NMR spectrum (235.39 MHz) of the crude mixture. Solvent: D_2O .

Even though sub-products were generated in the first tests, target diol **12** was also achieved. Therefore, an optimization of the synthetic procedure was required to improve the moderate yields of the nucleophilic substitution (Table 4.4). Generally, to favor bimolecular nucleophilic displacements ($\text{S}_{\text{N}}2$) type reactions, high concentration of reagents and the use of polar aprotic solvents are recommended. In this case, both anhydrous DMF and MeCN were assessed with two different volumes. Moreover, two ratios between the thiolate salt and the mesylate **4** were evaluated.

Table 4.4. Optimization conditions for the synthesis of **DiolSF**.^[a]

Entry	Solvent	Solvent volume (mL)	Ratio Thiolate: Mesylate 4	Yield (%) ^[b]
1	Anhydrous DMF	15	1.0:1.0	56
2 ^[c]		15	1.0:1.0	61
3		30	1.0:1.0	67
4		15	1.5:1.0	86
5		30	1.5:1.0	86
6	Anhydrous MeCN	15	1.0:1.0	69
7		30	1.0:1.0	65
8		15	1.5:1.0	61
9		30	1.5:1.0	80

^[a] Reaction conditions: 7.9 mmol of **4**, 80 °C, 48 hours.

^[b] Determined by ¹⁹F{¹H} NMR spectroscopy with a delay time of 10 seconds to ensure quantification.

^[c] TBAC (5 mol%).

All the tested reaction conditions resulted in moderate yields of **12** at 48 hours without reaching complete conversion of the mesylate **4**. This suggests that better results than the ones displayed in **Table 4.4** could be achieved at longer times as a fraction of the limiting reagents remained in the mixture.

The explored ratio between the potassium salt of the diol **7** and the mesylate **4**, were 1.5:1.0 and 1.0:1.0. When the stoichiometric ratio was assessed, the lowest yields were obtained (Entry 1 or Entry 2, Table 4.4). Conversely, an excess of the salt yielded in higher quantities of the diol **12**, agreeing with common S_N2 reactions. Although both solvents exhibited similar solubility with the reagents, the reaction mixture tended to form a gel after a few hours hampering the homogenization, likely by the low solubility of the formed salt in the tested conditions. This fact could explain the lower results achieved with MeCN than with DMF when high ratios of **7** and low solvent volumes are employed (Entry 4 and 8, **Table 4.4**). As the reaction progressed, the formation of **DiolSF** and the corresponding potassium methanesulfonate solid decreased the reaction rate by trapping the reagents and impeding the appropriate homogenization. The higher solubility of the salts in DMF compared to MeCN generates higher yields than the former solvent. 15 mL of MeCN (Entry 8, Table 4.4) was insufficient volume to disperse all the salts and therefore, displayed a notable lower yield than the reaction tested with 30 mL. Although DMF seems to have a better capability to disperse the produced compounds in the mixture, an increase in the reaction volume of MeCN compensates for the reduced solvating capacity.

Trying to improve the solubility of the crude, a phase transfer compound, tetrabutylammonium chloride (TBAC), was examined with a stoichiometric relation between the potassium thiolate and the fluorinated mesylate **4** (Entry 2, Table 4.4). Although it slightly increased the yield of the reaction, it also decreased the efficiency of the extraction process. Thereby, its use was dismissed for the subsequent reactions. The improvement was not enough to justify the posterior drawbacks in the purification.

Common purification processes were employed in the first attempts, but liquid-liquid extraction required the use of considerable amounts of Et₂O or CH₂Cl₂, and several washings of the aqueous phase to obtain the product owing to its high polarity (Figure 4.5). Although the highest yields were obtained with DMF, the posterior liquid-liquid extraction was less efficient with this solvent. It behaved as a phase transfer agent, distributing the target product in both phases and hampering its extraction. Moreover, it displays more health and legislative concerns than MeCN.^[a] As a result of these drawbacks, MeCN was selected as the reaction solvent. Furthermore, to reduce the volume of solvents in the purification step, a new methodology was tested. Instead of dissolving all the reaction crude in water and then, proceed with the extraction, the reaction solvent was evaporated to obtain a dough followed by a solid-liquid extraction with Et₂O. The product was finally purified by reduced pressure distillation.

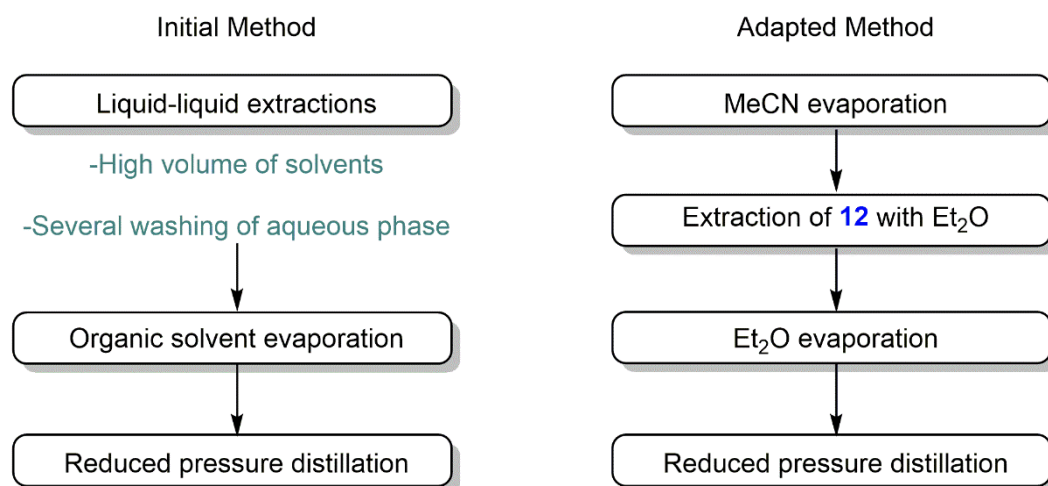


Figure 4.5. Tested procedures to purify product **12**.

Finally, the reaction with an excess of the thiolate salt of **7** in non-anhydrous MeCN was tested at different scales. The temperature was increased to reflux and the reaction was monitored by NMR spectroscopy until the complete disappearance of mesylate **4**. The gathered results are

^[a] DMF has been identified as a Substance of Very High Concern (SVHC) according to Article 57 (c) as toxic for reproduction and it slowly been replaced by other solvents, specially at industrial scale.

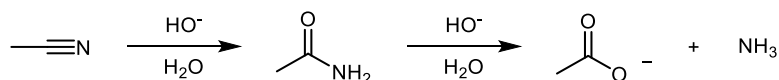
summarized in Table 4.5, displaying positive results toward the formation of diol **12** even in the presence of traces of water from the solvent. The synthesis was successfully attempted to 25 grams of mesylate **4** with moderate yields.

Table 4.5. Scalable synthesis of **DiolSF**.^[a]

Entry	Mesylate 4 (g)	Time (h)	Ratio Thiolate: Mesylate 4	Isolated Yield (%)
1	10	24	1.5:1	56
2	10	39	1.5:1	71
3	15	35	1.5:1	73
4	25	20	1.5:1	62

^[a] Reflux temperature. Purification following the adapted method.

However, the distillation required for the purification of the product led to a mixture of two substances: **DiolSF** and potassium acetate. Although the latter is a salt, we postulated that the diol could somehow solubilize it and drag it along the distillation. Potassium acetate is the product of the alkaline hydrolysis of MeCN (Scheme 4.13), in which the excess of thiolate salt acting as a base, water, and long reaction times at elevated temperatures could promote the transformation from a nitrile to a carboxylate.^{[57][58]} However, product **12** was successfully separated from potassium acetate by a further liquid-liquid extraction with Et₂O. Filtration over silica was also attempted to avoid the use of solvents but no differences were observed in the amount of salt.



Scheme 4.13. Alkaline hydrolysis of MeCN.

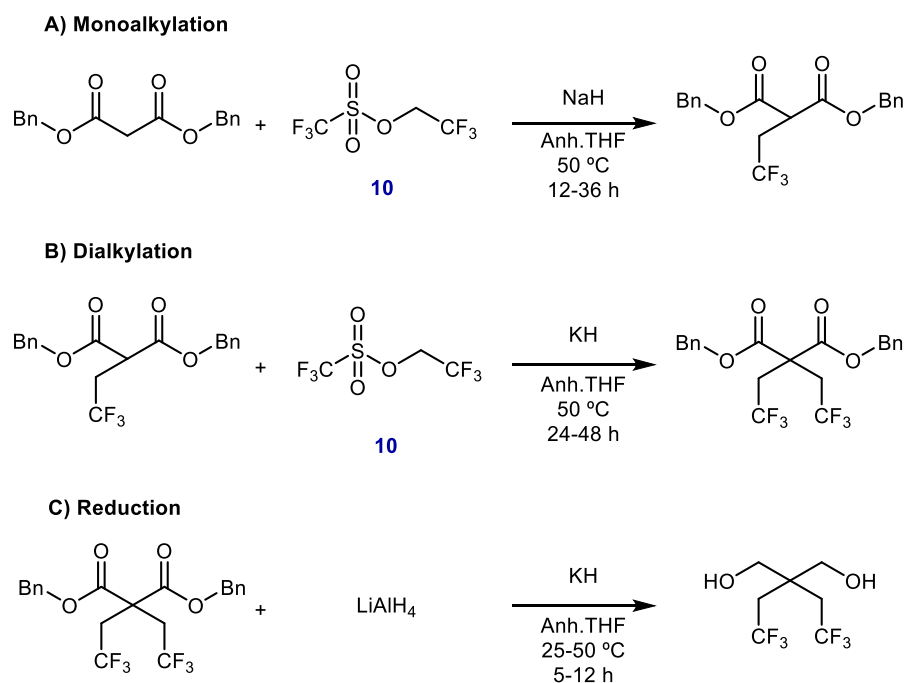
In conclusion, the desired fluorinated diol **12** was successfully synthesized by a two-step process in a multigram scale. However, a solid-liquid extraction followed by distillation at reduced pressure and an additional liquid-liquid extraction were required to obtain a highly pure product with a final yield of 73% in the best cases.

In light of the aforementioned, the synthesis of the fluorinated monomer was not suitable to be carried out at industrial scale and still requires further improvements owing to the multistep purification process and/or the large quantities of solvents employed.

4.3.1.3. Synthesis of trifluoroethyl derivative malonic acid

Thus far, the previous proposals were based on the synthesis of fluorinated dihydroxylated monomers. However, to generate polyesters it is equally valid to produce fluorinated dicarboxylic molecules, especially if the halogenated moiety is not in the main backbone. Malonate esters are known as diacid precursors which can be modified by the incorporation of different groups in the central methylene. Commonly, the synthesis of these derivatives is based on S_N^2 reactions, in which the alkylating compound plays a crucial role.

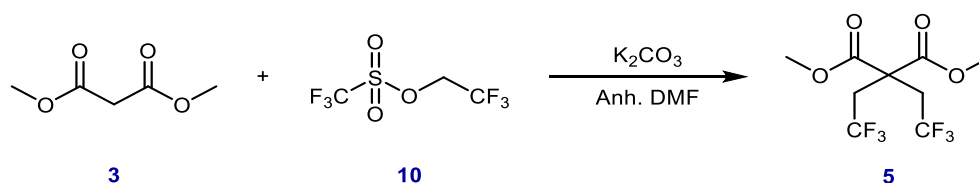
When dimethyl 2,2-*bis*(2,2,2-trifluoroethyl)malonate (**5**) was sought in the literature, no reports were found in common databases. However, a similar compound was described starting from a more robust ester: dibenzyl malonate. Concretely, its synthesis was only outlined in a Chinese patent in which 2,2-*bis*(trifluoroethyl)propanol was the target product.^[59] The complete procedure consists of 5 reactions, but only the first three steps, in which a diester or a diol are synthesized (Scheme 4.14), would be relevant for our synthesis. If this route was also successful with dimethyl malonate, it could provide monomers of both types, diacids, and diols. However, the patented procedure requires long reaction times and the use of an excess of strong bases, such as NaH and KH.



Scheme 4.14. Reported synthesis of the *bis*-alkylated product.^[59]

Previous tests in our group with trifluoroethyl mesylate **4** and dimethyl malonate **3** were unsatisfactory, possibly because the mesylate was not electrophilic enough to carry out the

reaction. Thus, said fluorinated compound **4** was replaced by triflate **10** to increase the electrophilicity of the sulfonate derivative and improve the reactivity. With this information in hand, a new one-pot synthesis was tested. Dialkylation of dimethyl malonate **3** with an excess of triflate **10** was undertaken to obtain **5** (Scheme 4.15). The reaction was essayed in an anhydrous system of K_2CO_3 in DMF to provide the strong basic media required to deprotonate the malonate while avoiding possible hydrolysis of the carboxylate ester.^[60]

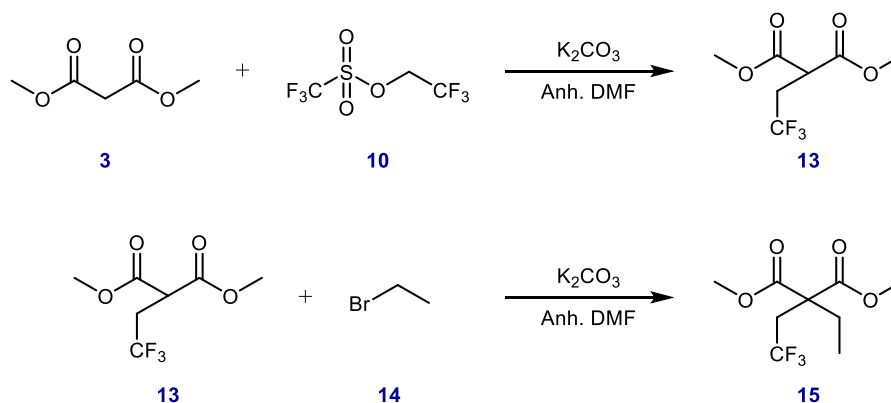


Scheme 4.15. Proposed dialkylation reaction of dimethyl malonate **3**.

The reaction was initially essayed at room temperature and monitored by gas chromatography (GC). At short reaction times, the crude became a mixture of monoalkylated and dialkylated malonate. After four days, the ratio between the mono and the dialkylated product was 66:32. This relation progressed to a 21:79 mono:di relation after 12 days. It seems that the monoalkylation was reached relatively easily, but the subsequent addition was much slower. Monoalkylated derivative is less acidic than the malonic diester and in addition, the trifluoroethyl moiety will stabilize the formed carboanion, both by steric hindrance and its electron withdrawing nature.^[61] Therefore, the second S_N^2 reaction is not favored enough even with the triflate. This fact is in agreement with the literature that reports that malonic diesters tend to typically generate the monoalkylated compounds with higher selectivity than the dialkylated product.^{[60][62][63]} When the temperature was raised to increase the reaction rate, sub-products appeared on the crude, possible consequence of the degradation of the esters. Hence, synthesis of **5** required long reaction times in soft conditions, even at a very small scale (1.9 mmol dimethyl malonate **3**). Attempts to scale up the reaction under the softest conditions entailed longer times to convert the starting reagent **3** into the dialkylated ester.

As far as we know, the synthesis of the malonate monoalkylated diol or its corresponding diacid has not been extensively researched. The only synthetic procedure of (2,2,2-trifluoroethyl) malonic acid is published in a 1985-paper and it was based on the electrolysis of trifluoroacetic and acrylic acid.^[64] However, the author reported that this compound undergoes decarboxylation to a greater extent than malonic acid. This fact, along with its complex separation from **5**, detracts from its possible use as a monomer in polyester condensation.

Considering that the reaction must be carried out at room temperature to avoid hydrolysis of the esters and the decarboxylation of the corresponding acid, another dialkylation of dimethyl malonate was pursued. This time it was assessed the introduction of two alkyl chains, but only one of them fluorinated (Scheme 4.16).



Scheme 4.16. Proposed dialkylation reaction of the dimethyl malonate **3**.

This proposal was based on a two-step reaction, in which firstly malonate **3** reacted with a single equivalent of the triflate to form the monoalkylated product **13**. Then, an equivalent of ethyl bromide (**14**), a compound with a similar structure and higher susceptibility to being attacked by the carboanion, was added to the mixture to obtain dimethyl 2-ethyl-2-(2,2,2-trifluoroethyl) malonate (**15**). Both steps were carried out one-pot under anhydrous basic conditions. Reactions were monitored by GC and $^{19}\text{F}\{^1\text{H}\}$ NMR spectroscopy.

Although the amount of triflate **10** was reduced to one equivalent, a complex mixture of products was observed on the crude of the first step: residues of the starting material **3**, the target compound **13**, and small amounts of the *bis*(2,2,2-trifluoroethyl) malonate **5**. Consequently, on the second step one equivalent of ethyl bromide seemed to be insufficient to complete the reaction and a second smaller addition (reaching a total of 1.2 equivalents) was required. However, this extra amount of reagent reacted also with the starting dimethyl malonate (**3**) left in the reaction mixture and alkylated it.

The proposed synthesis led to a final crude of **5**, the **15**, and dimethyl 2-ethyl malonate, **16**, with a ratio among them of 1.0:7.8:1.2, respectively (Figure 4.6). These three components have similar structures and properties, which hamper their separation using simple industrial processes. Therefore, no further steps of purification or optimization were aimed, and this second approach to dialkylated dimethyl malonate was also dismissed.

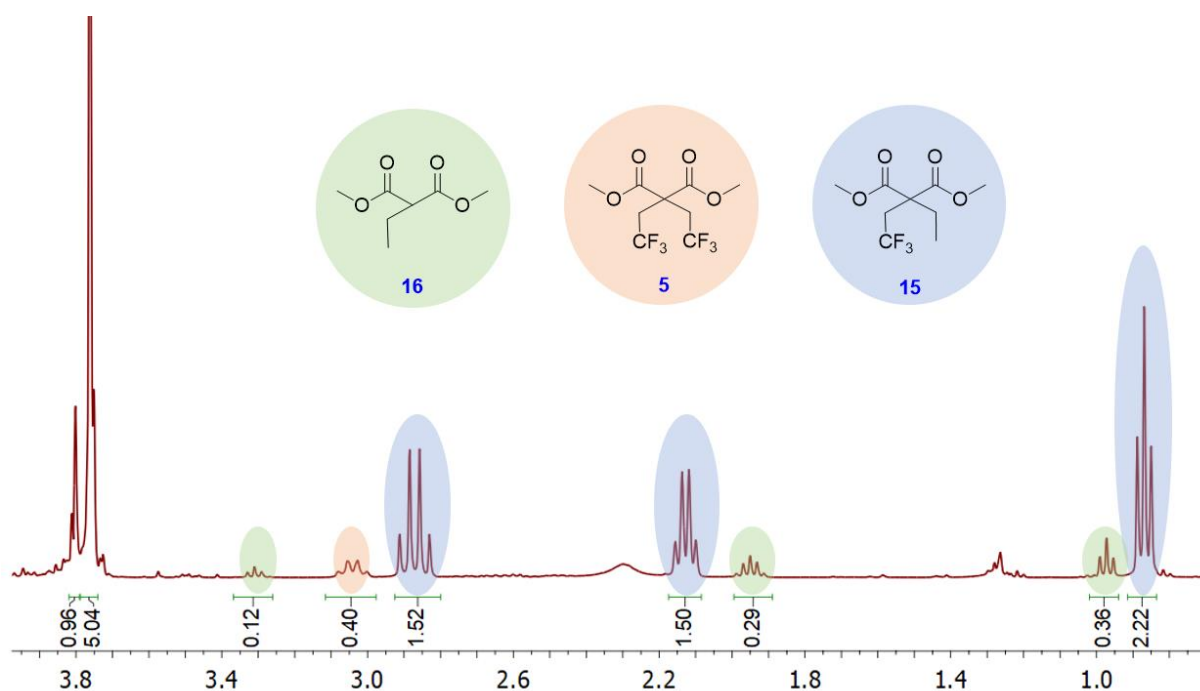


Figure 4.6. ^1H NMR spectrum (400.13 MHz) of the reaction crude after extraction. Solvent: CDCl_3 .

The proposed synthetic route could have been an excellent opportunity for the synthesis of fluorinated monomers, both diacid, and diols. Nevertheless, it inevitably required an expensive reagent, trifluoroethyl trifluorosulfonate **10**, a non-desirable solvent. Moreover, reaction crudes were difficult to separate. It could have been employed for further reactions even in the event of generating a mixture of bis(trifluoroethyl) malonate **5** and the monoalkylated analog **13**, provided the ratio between them was quantified. However, the possibility of diacid decarboxylation hinders its use in conventional polyester synthesis. In addition, the dialkylation reaction to form **15** was not sufficiently favored, so it was decided to forsake this type of monomers and their synthesis.

4.3.1.4. *TFE as a nucleophile.*

The second general strategy was to directly employ **TFE** as a nucleophile. The relatively acidic behavior of this alcohol decreases its efficiency compared to other alcohols. However, a synthetic route was tested by increasing its nucleophilicity through the generation the alkoxide.

4.3.1.4.1. *Synthesis of 3-(2,2,2-trifluoroethoxy)-1,2-propanediol (18)*

3-(2,2,2-trifluoroethoxy)-1,2-propanediol (**18**, **DiOLF**) is a 1,2-dihydroxylated product with a structure similar to compound **12**, but instead of a thioether linkage, we propose the synthesis of an ether (Figure 4.7). Sulfur-containing compounds are known to be odorous and provide

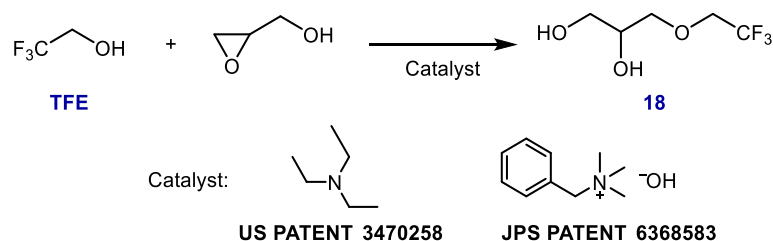
some yellowing on polymeric matrixes, whereas ethers, although being equally chemically resistant, mainly are not-scented and colorless.



Figure 4.7. Chemical structure of the proposed compounds **12** and **18**.

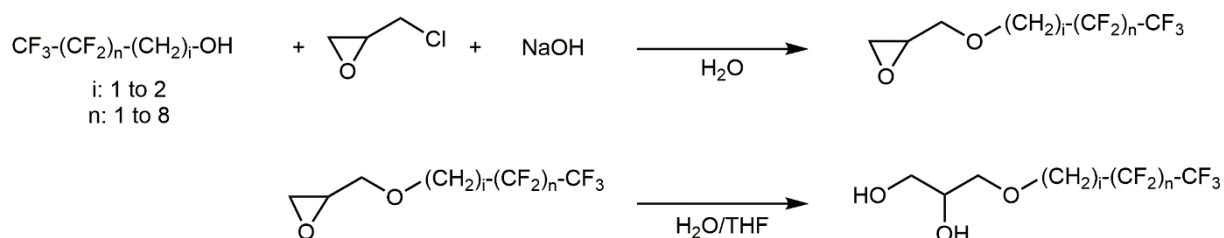
The formation of ethers has been extensively reported. Etherification could be accomplished by several synthetic routes, for instance, Mitsunobu reaction,^{[65][66][67][68]} bimolecular dehydration,^{[69][70][71]} or Ullman couplings.^{[72][73]} However, most of these reactions involved specific apparatus, reagents, or expensive metal catalysts. Although being expensive processes, they are frequently used in fine chemistry because of the high-added value of the synthesized compounds.

At the beginning of this thesis, reported data only showed four different references about product **18**. Two patents were based on the reaction between **TFE** and 2,3-epoxy-1-propanol with different tertiary and quaternary amines as catalysts (Scheme 4.17).^{[74][75]}



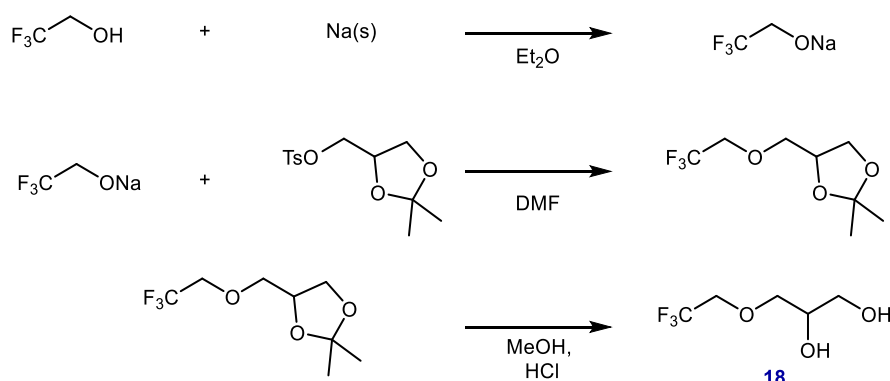
Scheme 4.17. Patented reaction for the synthesis of **18**.^{[74][75]}

Alternatively, the third patent consists of the coupling of a fluorinated alcohol and epichlorohydrin to obtain 1,2-diols with a fluorinated side chain (Scheme 4.18).^[76] Its main advantage is that could be applied to the synthesis of several monomers with different contents of fluorine. Although diol **18** was included in the patent as a potential product, it did not fulfill some of the requirements described in the text. Therefore, even though the compound is mentioned, this methodology is not completely reliable for the synthesis of **18**.



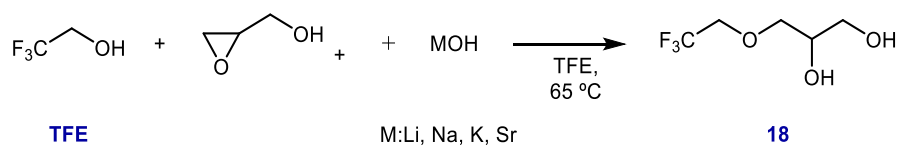
Scheme 4.18. Additional patented proposal for the synthesis of **18**.^[76]

Ultimately, Kvicala *et al.* reported in 1997 a multistep synthesis relying on the formation of the fluorinated alkoxide with sodium followed by the nucleophilic attack over a tosylate, and afterwards, the cycle cleavage to form the target product (Scheme 4.19).^[77] The yield of the completed synthesis was 26% with several purification processes in between the intermediates.



Scheme 4.19. Reported synthesis of **18**.^[77]

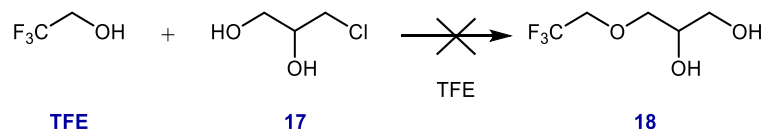
However, a new publication arose during the course of this thesis, obtaining compound **18** in a straightforward procedure.^[78] The authors reported the synthesis of different monoethers starting from glycidol and several alcohols, and employing metal hydroxides as catalysts (Scheme 4.20). This information was unknown at the moment in which the monomer was being developed by us.



Scheme 4.20. Reported synthesis of **18**.^[78]

Considering the industrial perspective of this work, new synthetic routes to produce this compound were aimed without employing neither of the previous publication as-described. In this thesis, different conditions were evaluated to obtain the target compound **18** by means of coupling **TFE** and 1-chloropropanediol (**17**), both low-priced reagents. As expected, an excess of **TFE** did not directly react with the chloride derivative, even at reflux temperature

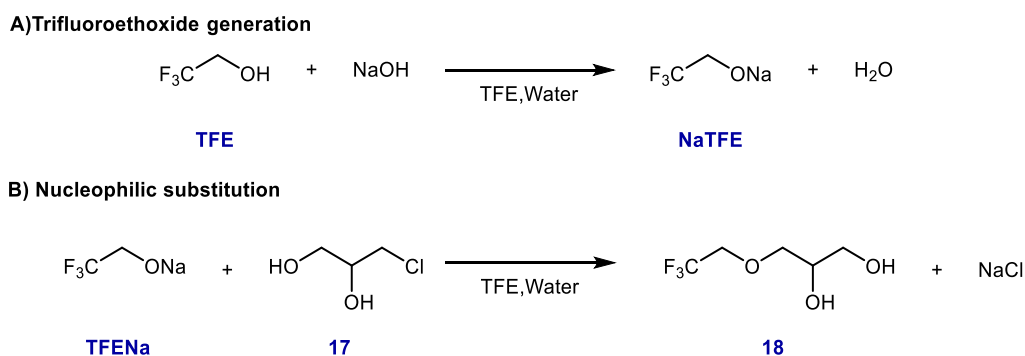
(Scheme 4.21), confirming again that **TFE** is a poor nucleophile unable to attack the electrophilic carbon of **17**.



Scheme 4.21. Direct synthesis of **18**.

Our proposal is a one-pot synthesis based on a two-step Williamson's reaction. This class of transformation involves the displacement of the leaving group from an alkyl halide by an alkoxide ion.^[79] This substitution can only be applied to compounds with leaving groups attached to primary and secondary positions; otherwise, some side reactions like eliminations might happen.

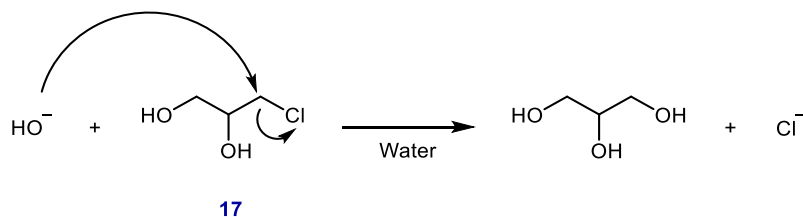
The intended synthetic route consists of the generation of sodium trifluoroethoxide (**NaTFE**), to generate a good nucleophile, and then proceed to the substitution reaction on **17** (Scheme 4.22). This reaction is carried out in a mixture of **TFE** and water without the need to heat the solution.



Scheme 4.22. Proposed synthesis of **18**.

NaTFE was generated by the gradual addition of 50 % NaOH_(aq) solution over **TFE**. This acid-base reaction is highly exothermic, and the mixture temperature must be kept under 45 °C. This careful vigilance avoids alcohol evaporation which would lead to a reagent unbalance. After the generation of the salt, the most critical step of the reaction takes place: the addition of **17** over the already obtained reaction crude. Initial experiments led to a complete conversion of **17**, but low yields of fluorinated diol **18**. These results are explained by an excess of NaOH in the reaction crude. The extra hydroxyl groups from the base attack the electrophilic methylene, displacing the chloride and producing glycerin (Scheme 4.23). This compound was observed by ¹³C{¹H} NMR spectroscopy, and its appearance caused a decrease in the synthesis

selectivity. To avoid this side reaction, the alkyl halide must be added dropwise to foster the swift attack of the **NaTFE** over the chloro-derivative.



Scheme 4.23. Hydrolysis of the starting reagent **17**.

Another factor to consider is that S_N^2 reactions are promoted at high concentrations of the nucleophile. Moreover, increasing **NaTFE**'s concentration will also decrease the probability of the hydroxyl attack. To test these assumptions, several ratios between the reagents were evaluated (Table 4.6). **NaTFE** was tried from nearly stoichiometric up to 4.0 equivalent respect **17**, reaching a 70% yield with the highest excess of the salt.

Table 4.6. Optimization conditions for the synthesis of **18**.^[a]

Entry	Theoretical yield (g)	Ratio H ₂ O : NaTFE : DiolF			Isolated Yield (%)
1 ^[b]	100	9.5	1.1	1.0	33 ^[c]
2	100	9.5	2.0	1.0	35 ^[d]
3 ^[e]	150	9.5	2.0	1.0+0.5	60 ^[f]
4	150	15.5	4.0	1.0	70 ^[f]
5 ^[g]	300	14.4	4.0	1.0	61 ^[f]

^[a] Reaction conditions: T < 45 °C. Dropwise addition of a 50 wt.% solution of NaOH_(aq) over **TFE**. Slow incorporation of **17**. Reaction time: 2 hours.

^[b] 35% of excess of NaOH_(aq) solution.

^[c] Purification process: Liquid-liquid extraction Et₂O/H₂O, and subsequent distillation.

^[d] Purification process: Evaporation of the solvent, extraction with Et₂O, and subsequent distillation.

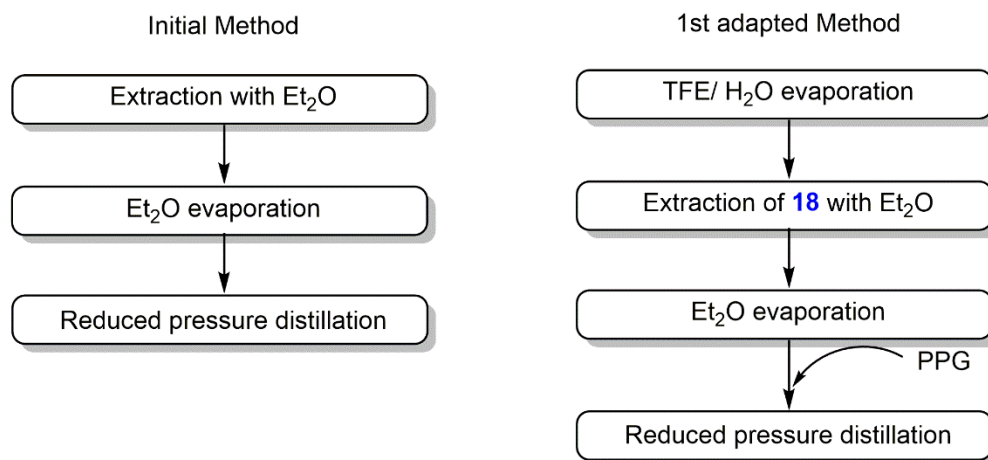
^[e] **17** was added dropwise in two batches. Initially 1 equivalent and reacted by one hour and then, the remaining 0.5 equivalents. The mixture was left to react for 1 additional hour.

^[f] Purification process: acidification of the solution, addition of PPG, and distillation.

^[g] **TFE** recycled from a previous reaction.

Although product **18** was achieved with high selectivity, the purification process hampered obtaining even higher yields. The initial work-up consisted of a liquid-liquid extraction, but the high polarity of the mixture led to poor isolation yields. As an alternative, the reaction solvents were evaporated until acquiring a dough and then, the product was extracted with Et₂O. Subsequently, the alcohol was mixed with polypropylene glycol (PPG, M_n≈400) to avoid overheating and was purified by distillation at reduced pressure (Scheme 4.24). However, it was estimated that between 3-40% of the target product **18** remained in the solid depending on the extraction volume. Overall, the quantitative extraction of the product entailed large

volumes of organic solvents, long times, and led to the loss of the fluorinated moieties, **TFE** and **NaTFE**.



Scheme 4.24. Extraction processes tested at early stages of the optimization.

When the volumes required for the reaction increased, reactors were used to carry out the coupling, as they allow better control on the temperature and homogenization of the mixture. Moreover, the employed jacketed reactor allowed the refrigeration of the mixture during the additions and reduced the addition time.

Unexcitingly, when high amounts of the product were aimed (superior weights than 300 g of product), two phases were formed after the neutralization of **NaTFE** (Figure 4.8). Both phases were saturated by the produced NaCl, and the excess of salt precipitated at the bottom of the reactor. Most likely, the three-component system (water/ **TFE**/ **18**) overcomes the miscibility point and separates in two phases, helped to a great extent by the high ionic force of the solution.

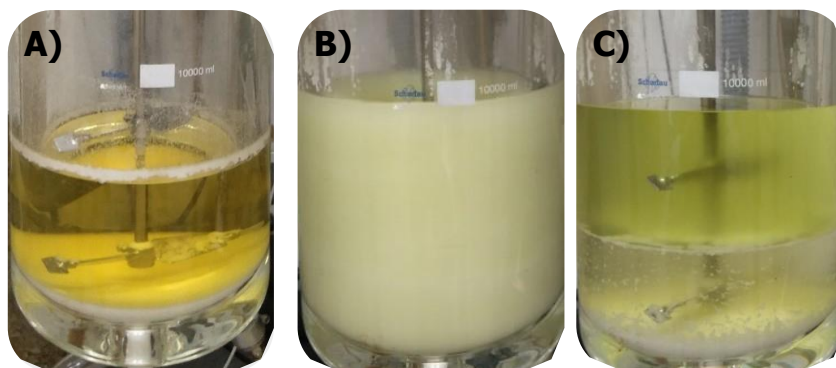


Figure 4.8. Reaction crude A) at the end of the reaction without stirring, B) after the neutralization (pH 3) with stirring and C) after the neutralization without stirring.

Both phases were studied to determine their composition in terms of fluorinated compound distribution. The percentage of **TFE** and **18** in each phase was accurately determined by $^{19}\text{F}\{^1\text{H}\}$ NMR spectroscopy using KPF_6 as standard. All the spectra were recorded with a delay time of 10 seconds to ensure the complete relaxation of the involved nuclei. Interestingly, both phases exhibited different proportions of each component. The bottom phase is enriched in the fluorinated compounds **TFE** and **18**, possessing a percentage of 30 wt.% of the latter. Contrarily, the upper one was mainly composed of water and NaCl and only around 2 wt.% corresponded to **18**. **TFE** has the tendency to self-aggregate in $\text{H}_2\text{O}/\text{TFE}$ mixture through $\text{F}\cdots\text{F}$ interaction to reduce the contact between the hydrophobic trifluoromethyl moiety and the highly polar molecules of water.^{[40][39]} These interactions might promote fluorophilicity and possibly cause the enrichment of one of the phases.^[80]

Owing to the fluorine enrichment fraction, an alternative purification process was developed to recover the valuable **TFE** and diol **18** (Figure 4.9).

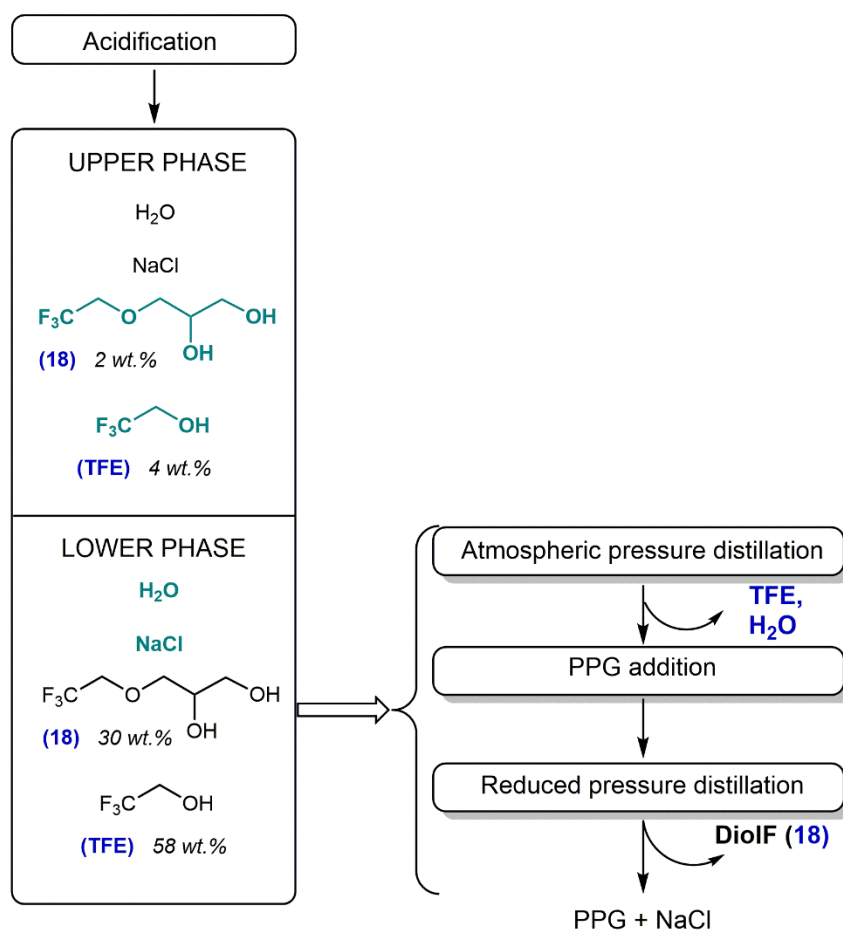


Figure 4.9. Overview of the purification process. Molecules in green are the minority components. Reported percentages indicate the quantity of fluorinated components in each phase.

Once the reaction was completed, the solution was acidified until pH 3 with concentrated $\text{HCl}_{(\text{aq})}$ to neutralize the excess of **NaTFE**. The acid-base reaction regenerated **TFE** and produced the corresponding salt, NaCl , which at a large scale caused the separation of the phases. Collecting the enriched phase, an atmospheric pressure distillation was carried out to recover the starting fluorinated reagent and afterward, water. At the final stages, PPG ($M_n \approx 400$ g/mol) was incorporated into the mixture and **DiolF** was distilled at reduced pressure. The addition of this short polymer improves the efficiency of the distillation and prevents degradation processes caused by overheating the sample. At industrial level, the recovery of small quantities of **18** from the upper phase, in which the fluorinated diol is one of the minority components, is discouraged by the required high-energy consumption.

Results of the synthesis of the fluorinated diol **18** at different scales and purified by the detailed method are summarized in Table 4.7. The target compound was generated in moderate yields, especially considering that only the inferior phase was distilled. Moreover, it was tested if the **TFE** distilled from a previous reaction could be reused. Entry 3 displays the yield of this experiment in which a decrease was measured.

Table 4.7. Results of **DiolF** synthesis with the new purification process.^[a]

Entry ^{a)}	Theoretical yield (g)	Diol 17 (mols)	Isolated yield (%)
1	150	0.86	86
2	300	1.72	75
3 ^[b]	300	1.72	64
4 ^[c]	1200 g	6.89	59
5	1500 g	8.61	65

^[a] Reaction conditions: 4.0 equivalents of **NaTFE**. Temperature below 45 °C. Slow addition of a 50 wt.% solution of $\text{NaOH}_{(\text{aq})}$ over **TFE**. Slow addition of **17**. Reaction time: 2 hours.

^[b] **TFE** recycled from a previous reaction.

^[c] Reaction temperature was regulated with ice.

Therefore, the synthetic procedure was gradually increased from a 50 g scale to 1500 g, without significant variations on the methodology. The final scale-up of the reaction required the use of the 10 L reactor at Lubrizol facilities. There, the maximum reached scale was 1500 g of product with a final yield of 65% as a transparent liquid. Only the inferior phase was employed to isolate the diol, but in the same process, it was possible to recover the excess of **TFE**.

4.3 Summary and concluding remarks

This chapter was devoted to the synthesis of six fluorinated monomers containing a trifluoroethyl moiety as a side chain (Figure 4.10). Although all of them were obtained, some with relatively good yields, only a few of the monomers were able to be scaled up and purified using industrial approaches.

The incorporation of the trifluoroethyl fragment in the form of an ester bond was attempted in compound **8**, but in the presence of slightly acidic conditions or other nucleophiles, such as thiolate or hydroxyl groups, the linkage is quite labile. Processes of hydrolysis and transesterification were observed on the crude mixture because of the acidic character of **TFE**, making them unsuitable for the posterior polymerization.

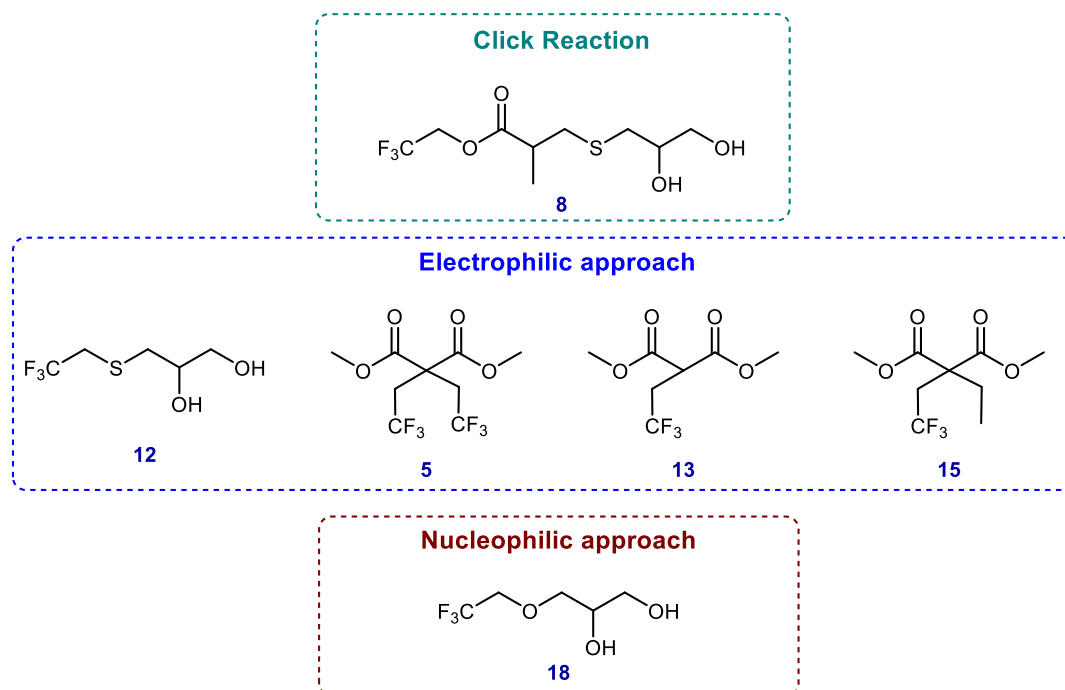


Figure 4.10. Monomers tried to synthesize.

Two further routes were tested for the synthesis of the target monomers. First, an electrophilic approach resulted in two distinctive types of compounds: alkylated malonic esters (compounds **5**, **13**, and **15**) and a diol with the fluorinated moiety anchor by a thioether bond (**DiolSF**, **12**). Alkylation of malonic esters was sought using compounds with excellent leaving groups as triflate and bromide. Monoalkylation of the starting material seems to be the most favorable process; however, product **13** exhibits a reactive position, and some authors reported their susceptibility to decarboxylation. The second alkylation was complex to achieve, especially the introduction of the second fluorinated chain to form **5**. The proposed alternative, the

synthesis of the dialkylated compound **15** containing only one fluorinated chain, led to a mixture difficult to purify with industrial processes.

Compound **12** was successfully generated in a two-step process with a final yield of 75%. However, the basic media of the reaction led to the hydrolysis of the solvent and the formation of acetate on the mixture. The purification process required an extended use of solvents and a final step of distillation.

Alternatively, the nucleophilic approach afforded the synthesis of a diol containing an ether linkage. The generation of compound **18** by means of Williamson reaction was successful. A one-pot synthesis obtained the target product easily and the reaction scaled up to 1.5 kg maintaining a moderate yield (*ca.* 65%). In addition, the separation and purification methodology developed in this thesis allowed achieving the compound and recovering the excess of **TFE**.

Literature

- [1] S. Su, J. Gu, H. Lee, C. Wu, Y. Su, M. Suen, *J. Polym. Res.* **2018**, *25*, 1–17.
- [2] C.-L. Wu, S.-H. Chiu, H.-T. Lee, M.-C. Suen, *Polym. Adv. Technol.* **2016**, *27*, 665–676.
- [3] Y. Li, L. Yuan, H. Ming, X. Li, L. Tang, J. Zhang, R. Wang, G. Wang, Y. Jiang, Z. Li, et al., *Biomacromolecules* **2020**, *21*, 1460–1470.
- [4] J. Datta, P. Kasprzyk, *Polym. Eng. Sci.* **2018**, *58*, E14–E35.
- [5] J. Li, Y. Cheng, H. Lee, C. Wang, C. Chiu, M. Suen, *J. Appl. Polym. Sci.* **2020**, *137*, 1–15.
- [6] Z. Qiao, D. Xu, Y. Yao, S. Song, M. Yin, J. Luo, *Polym. Int.* **2019**, *68*, 1361–1366.
- [7] A.-C. Albertsson, S. Boileau, M. R. Buchmeiser, O. Coulembier, O. Dechy-Cabaret, P. J. Dijkstra, A. P. Dove, P. Dubois, A. Duda, C. J. Duxbury, et al., *Handbook of Ring-Opening Polymerization*, Wiley-VCH Verlag GmbH&Co. KGaA, Weinheim, Germany, **2009**.
- [8] S. C. Yoon, B. D. Ratner, *Macromolecules* **1986**, *19*, 1068–1079.
- [9] S. Ebnesajjad, R. A. Morgan, in *Fluoropolymer Addit.* (Ed.: S. Ebnesajjad), William Andrew Publishing, Oxford, England, **2012**, pp. 157–174.
- [10] DuPont, *DuPont Fluoroguard Polymer Additive*, **2001**.
- [11] T. Lammers, M. E. Mertens, P. Schuster, K. Rahimi, Y. Shi, V. Schulz, A. J. C. Kuehne, S. Jockenhoevel, F. Kiessling, *Chem. Mater.* **2017**, *29*, 2669–2671.
- [12] A. A. Malik, D. Tzeng, P. Cheng, K. Baum, *J. Org. Chem.* **1991**, *56*, 3043–3044.
- [13] Z. Ge, X. Yuan, J. Bing, W. Hu, Y. Jun, *Chinese Chem. Lett.* **2008**, *19*, 1293–1296.
- [14] J. Hollander, F. D. Trischler, *J. Polym. Sci. Part A-1* **1967**, *5*, 2757–2767.
- [15] T. Liu, L. Ye, *J. Fluor. Chem.* **2010**, *131*, 36–41.
- [16] C. Tonelli, G. Ajroldi, *J. Appl. Polym. Sci.* **2003**, *87*, 2279–2294.
- [17] T. Ho, A. A. Malik, K. J. Wynne, T. J. McCarthy, K. H. Z. Zhuang, K. Baum, R. V. Honeychuck, in *Step-Growth Polym. High-Performance* (Eds.: J.L. Hedrick, J.W. Labadie), **1996**, pp. 362–376.
- [18] B. Zhao, R. Jia, *Prog. Org. Coatings* **2019**, *135*, 440–448.
- [19] Z. Huang, X. Pei, T. Wu, S. Sheng, S. Lin, C. Song, *J. applie* **2011**, *119*, 702–708.
- [20] D. Pospiech, D. Jehnichen, A. Gottwald, L. Häussler, W. Kollig, K. Grundke, A. Janke, S. Schmidt, C. Werner, *Surf. Coatings Int. Part B Coat. tTansactions* **2003**, *86*, 43–52.
- [21] G. K. Surya Prakash, F. Wang, in *Org. Chem. Break. Perspect.* (Eds.: K. Ding, L.-X. Dai), Wiley-VCH Verlag GmbH&Co. KGaA, Weinheim, Germany, **2012**, pp. 413–476.
- [22] P. A. Champagne, J. Desroches, J.-D. Hamel, M. Vandamme, J. F. Paquin, *Chem. Rev.* **2015**, *115*, 9073–9174.
- [23] G. Sandford, *J. Fluor. Chem.* **2007**, *128*, 90–104.
- [24] A. V Grosse, C. B. Linn, *J. Org. Chem.* **1938**, *03*, 26–32.
- [25] G. A. Olah, J. T. Welch, Y. D. Vankar, M. Nojima, I. Kerekes, J. A. Olah, *J. Org. Chem.* **1979**, *44*, 3872–3881.
- [26] W. J. Middleton, *J. Org. Chem.* **1975**, *40*, 574–578.
- [27] R. P. Singh, J. M. Shreeve, *Synthesis (Stuttg).* **2002**, *17*, 2561–2578.

- [28] G. S. Lal, G. P. Fez, R. J. Pesaresi, F. M. Prozonic, *J. Org. Chem.* **1999**, *64*, 7048–7054.
- [29] R. E. Banks, S. N. Mohialdin-Khaffaf, G. S. LaI, I. Sharif, R. G. Syvret, *J. Chem. Soc. Chem. Commun.* **1992**, 595–596.
- [30] R. E. Banks, *J. Fluor. Chem.* **1998**, *87*, 1–17.
- [31] G. K. S. Prakash, A. K. Yudin, *Chem. Rev.* **1997**, *97*, 757–786.
- [32] X. Liu, C. Xu, M. Wang, Q. Liu, *Chem. Rev.* **2015**, *115*, 683–730.
- [33] T. Umemoto, K. Adachi, S. Ishihara, *J. Org. Chem.* **2007**, *72*, 6905–6917.
- [34] P. Eisenberger, S. Gischig, A. Togni, *Chem. - A Eur. J.* **2006**, *12*, 2579–2586.
- [35] J. Charpentier, N. Früh, A. Togni, *Chem. Rev.* **2015**, *115*, 650–682.
- [36] W. Wu, Q. Zhu, F. Qing, C. C. Han, *Langmuir* **2009**, *25*, 17–20.
- [37] R. Chitra, P. E. Smith, *J. Chem. Phys.* **2001**, *114*, 426–435.
- [38] C. H. Rochester, in *Chem. Hydroxyl Gr. Part 1* (Ed.: S. Patai), John Wiley & Sons, Ltd., **1971**, pp. 327–392.
- [39] B. Biswas, P. C. Singh, *J. Fluor. Chem.* **2020**, *235*, 109414–109425.
- [40] R. M. Culik, R. M. Abaskharon, I. M. Pazos, F. Gai, *J. Phys. Chem. B* **2014**, *118*, 11455–11461.
- [41] H. C. Kolb, M. G. Finn, K. B. Sharpless, *Angew. Chemie - Int. Ed.* **2001**, *40*, 2004–2021.
- [42] B. D. Mather, K. Viswanathan, K. M. Miller, T. E. Long, *Prog. Polym. Sci.* **2006**, *31*, 487–531.
- [43] J. W. Chan, C. E. Hoyle, A. B. Lowe, M. Bowman, *Macromolecules* **2010**, *43*, 6381–6388.
- [44] S. Chatani, R. J. Sheridan, M. Podgo, C. N. Bowman, *Chem. Mater.* **2013**, *25*, 3897–3901.
- [45] G. Z. Li, R. K. Randev, A. H. Soeriyadi, G. Rees, C. Boyer, Z. Tong, T. P. Davis, C. R. Becer, D. M. Haddleton, *Polym. Chem.* **2010**, *1*, 1196–1204.
- [46] K. Takami, R. Matsuno, K. Ishihara, *Polymer (Guildf)*. **2011**, *52*, 5445–5451.
- [47] A. B. Lowe, *Polym. Chem.* **2010**, 17–36.
- [48] N. N. Su, Y. Li, S. J. Yu, X. Zhang, X. H. Liu, W. G. Zhao, *Res. Chem. Intermed.* **2013**, *39*, 759–766.
- [49] D. Prescher, T. Thiele, R. Ruhmann, *J. Fluor. Chem.* **1996**, *79*, 145–148.
- [50] T. B. Nguyen, A. Martel, R. Dhal, G. Dujardin, *Synlett* **2009**, 2492–2496.
- [51] J. Vastra, L. Saint-Jalmes, *Org. Process Res. Dev.* **2006**, *10*, 194–197.
- [52] E. T. McBee, D. H. Campbell, C. W. Roberts, *J. Am. Chem. Soc.* **1955**, *77*, 3149–3151.
- [53] H. Gilman, R. G. Jones, *J. Am. Chem. Soc.* **1943**, *65*, 2037.
- [54] H. Tamiaki, K. Nomura, T. Mizoguchi, *Bioorganic Med. Chem.* **2017**, *25*, 6361–6370.
- [55] S. Laulhé, J. M. Blackburn, J. L. Roizen, *Chem. Commun.* **2017**, *53*, 7270–7273.
- [56] R. C. Reis-Nunes, E. Riande, N. C. Chavez, J. Guzmán, *Macromolecules* **1996**, *29*, 7989–7994.
- [57] S. Rabinovitch, B., A. Winkler, C., *Can. J. Res.* **1942**, *20b*, 185–188.
- [58] Z. Wang, S. M. Richter, M. J. Rozema, A. Schellinger, K. Smith, J. G. Napolitano, *Org. Process Res. Dev.* **2017**, *21*, 1501–1508.
- [59] *CN Patent 102942449A*, **2012**.
- [60] D. A. White, *Synth. Commun.* **1977**, *7*, 559–568.
- [61] R. D. Chambers, in *Fluor. Org. Chem.* (Ed.: R.D. Chambers), Blackwell, Oxford, England, **2004**, pp. 1–22.
- [62] A. C. Cope, H. L. Holmes, O. H. Herbert, in *Org. React.*, **1957**, pp. 107–163.
- [63] M. Fedoryński, K. W. Z. munt Matacz, M. Mąkosza, *J. Org. Chem.* **1978**, *43*, 4682–4684.
- [64] N. Muller, *J. Org. Chem* **1986**, 263–265.

- [65] K. C. K. Swamy, N. N. B. Kumar, E. Balaraman, K. V. P. P. Kumar, *Chem. Rev.* **2009**, *109*, 2551–2651.
- [66] A. R. Tunoori, D. Dutta, G. I. Georg, *Tetrahedron Lett.* **1998**, *39*, 8751–8754.
- [67] D. Szabó, A.-M. Bonto, I. Kövesdi, A. Gömöry, J. Rábai, *J. Fluor. Chem.* **2005**, *126*, 641–652.
- [68] C. Do, F. Wang, T. Mathew, G. A. Olah, *Synthesis (Stuttg.)* **2010**, *11*, 1891–1898.
- [69] F. Figueras, A. Nohl, L. Mourges, Y. Trambouze, *Trans. Faraday Soc.* **1971**, *67*, 1155–1163.
- [70] E. Catizzone, A. Aloise, M. Miglorio, G. Giordano, *Appl. Catal. A General* **2015**, *502*, 215–220.
- [71] M. A. Armenta, R. Valdez, R. Silva-Rodrigo, A. Olivas, *Fuel* **2019**, *236*, 934–941.
- [72] J. S. Sawyer, *Tetrahedron* **2000**, *56*, 5045–5065.
- [73] A. B. Naidu, E. A. Jaseer, G. Sekar, *J. Org. Chem.* **2009**, *74*, 3675–3679.
- [74] G. C. Tesoro, D. Ferry, *United States Patent US. 3470258 A*, **1969**.
- [75] K. Masaoka, H. Shimizu, N. Nakayama, F. Nemoto, *FLUORINE-CONTAINING CYCLIC CARBONATE JPS6368583A*, **1988**.
- [76] I. Kojiro, H. Song, *CN101812805A. Aqueous Fluorine-Containing Finishing Agent and Preparation Method Thereof*, **2010**, CN200910117921A.
- [77] J. Kvíčala, B. Dolenský, O. Paleta, *J. Fluor. Chem.* **1997**, *85*, 117–125.
- [78] A. Leal-Duaso, M. Caballero, A. Urriolabeitia, J. A. Mayoral, J. I. García, E. Pires, *Green Chem.* **2017**, *19*, 4176–4185.
- [79] A. Williamson, *Justus Liebigs Ann. der Chemie* **1851**, *77*, 37–49.
- [80] K. Matsumoto, H. Mazaki, H. Matsuoka, *Macromolecules* **2004**, *37*, 2256–2267.

Chapter 5

Synthesis of polyesters

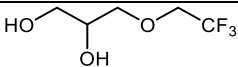
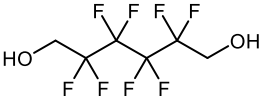
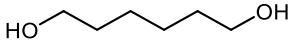
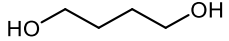
Chapter 5 focuses on the synthesis of fluorinated polyols, with special attention to **DiOLF**-based structures. Various approaches have been assessed to produce novel polyesters with dispaired results. Furthermore, the structural and thermal characterization of each produced macromolecule is discussed hereafter.

5. Fluorinated Polyesters

The introduction of fluorinated moieties into polyesters fulfills a beneficial role as they share most of the characteristics of conventional polyesters, but in addition, they also exhibit low surface energy, exceptional dielectric behavior, thermal stability, and weatherability.^{[1][2]} However, fluorinated polyesters are relatively hydrolytically unstable when fluorinated diacids are employed in their synthesis.^{[3][4]} In view of this fact, the already prepared fluorinated diol **18** have been polymerized with standard diacids as monomers. Among them, aromatic dicarboxylic compounds generate rigid polyesters which exhibit several drawbacks like difficult processability, high T_g , and low solubility in organic solvents.^{[5][6]} Therefore, only aliphatic polyesters have been prepared in this thesis.

The chemical structure of the utilized diols in addition to their M_w and fluorine content is shown in Table 5.1. In this section, the reactivity of fluorinated product **DiolF (18)** and a commercial diol, 2,2,3,3,4,4,5,5-octafluoro-1,6-hexanediol (**HDO-8F, 19**) are evaluated. This last monomer is the fluorinated analog of one of the most employed compounds in polyester synthesis, 1,6-hexanediol (**HDO**), which is used as its non-fluorinated benchmark. Ultimately, the most common diol employed at industrial scale was 1,4-butanediol (**BDO**), which is also included in some tests.

Table 5.1. Hydroxylated compounds tested as monomers.

Compound	Structure	M_w (g/mol)	Fluorine content (wt.%)
DiolF, 18		174.12	33
HDO-8F, 19		262.10	53
HDO		118.18	-
BDO		90.12	-

In the previous chapter, it was already mentioned that the proximity of fluorine atoms to an alcohol causes an inductive effect that decreases the nucleophilicity and increases the acidity

of the hydroxyl group. However, this problem has been overcome by the presence of methylene groups between the $-(CF_n)-$ moiety and the hydroxyl.^[7] This is a common feature of the employed diols, in which at least a $-CH_2-$ group is attached to the alcohol.^[a]

Although all the monomers are difunctional glycols, **DioIF** is a 1,2-diol. In particular, one of the alcohols is a secondary hydroxyl, which generally exhibits lower reactivity than a primary hydroxyl group. Oppositely, commercially available **HDO-8F** is a perfluorinated linear compound in which the hydroxyl groups have the same reactivity, being both primary. This structural disparity between the employed monomers may promote dissimilar reactivity, leading to mixed outcomes.

In the following lines, the synthesis of linear polyols is detailed. Each synthesized polyester has been characterized by NMR and FTIR spectroscopy to confirm its structure, and by DSC to identify its thermal features.

5.1. Synthesis of ADP:HDO-8F by acyl chloride approach

One of the preferred routes for the synthesis of fluorinated polyesters is the transesterification of acyl chlorides with fluorinated diols.^{[8][9][10]} Employing those chloride derivatives instead of carboxylic acids compensates for the lower reactivity of fluorinated hydroxylated compounds in comparison with the corresponding hydrogenated ones, and prevents degradation processes typically caused by elevated reaction temperatures used in standard polycondensations. Furthermore, the use of the acyl chloride methodology is straightforward to obtain the target average number molecular weight (M_n), and neither continuous monitoring by titration nor correction with additional monomer is required.

To achieve a greener approach, instead of the conventional methodology discussed in the Introduction's (see section 1.1.1.3.1), the reaction was carried out neat. The reaction relies on the slow addition of the acyl chloride over the melt-phase diol, and the use of a N_2 stream to instantly remove the generated HCl. Then, this gas is neutralized in an external trap filled with a highly concentrated basic solution, displacing the reaction toward the polymeric compound (Figure 5.1). This adaptation of the common methodology sidesteps the use of catalysts, bases, and solvents. Moreover, this assembly could be adapted at an industrial scale with the use of base anion exchange resin.

^[a] Compounds containing a primary or secondary alcohol group attached to a C-F bond are unstable owing to the release of HF and the formation of a carbonyl moiety. ^[22]

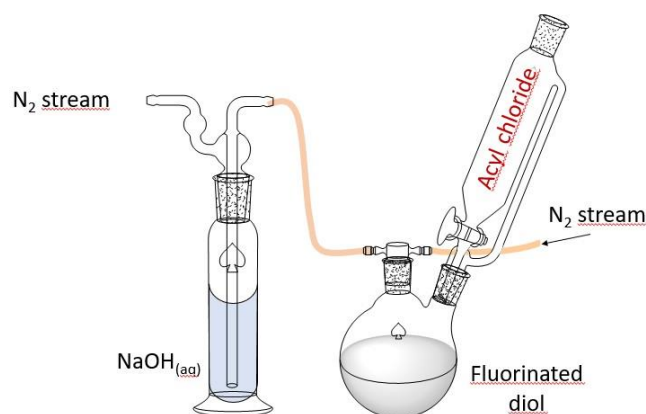
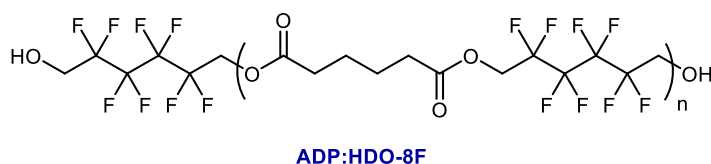


Figure 5.1. Schematic representation of reaction system.

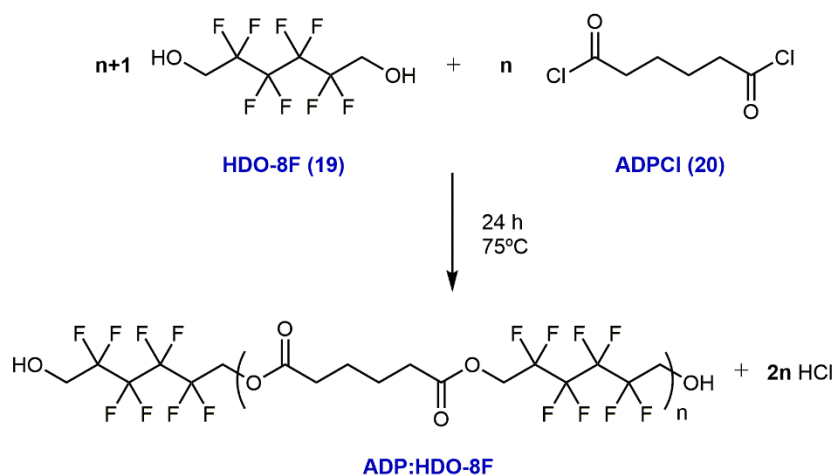
ADP:HDO-8F was the first generated polyester (Scheme 5.1) and its synthesis had comparison purposes with the subsequent reactions. This polymer is intentionally designed to evaluate the behavior of a high spatial concentration of fluorine in the main chain of the polyester. However, **HDO-8F** is not an industrially profitable monomer owing to its elevated price (according to Sigma-Aldrich catalog: €15 920/kg, 98 % purity) and it was merely used as an academic test.



Scheme 5.1. **ADP:HDO-8F** structure.

To explore the performance of fluorine in polyesters and subsequently in TPUs, two polyols were compared: the fluorinated **ADP:HDO-8F** and the reference **ADP:HDO** (provided by Lubrizol). To evaluate exclusively the effect of fluorine, isosteric polyols were aimed. Both polyols exhibit an equivalent number of diacid (n) and diol units ($n+1$) on the structure and thereby, the same molar fraction of ester groups in their backbone. Nevertheless, their M_n differ owing to the replacement of eight hydrogens of **HDO** by eight fluorine atoms in **HDO-8F**. Thereby, a 2000 g/mol **ADP:HDO** (n displaying a theoretical value of 8.24) corresponds to an M_n of 3300 g/mol in the fluorinated polyester.

ADP:HDO-8F with a target M_n of 3300 g/mol was successfully synthesized through the polycondensation of **HDO-8F** and adipoyl chloride (**ADPCI**, **20**) (Scheme 5.2.). Mild conditions of 75 °C and 24 hours of reaction were enough to obtain the desired product on a scale of 300 g without further purification.



Scheme 5.2. Synthesis of **ADP:HDO-8F** from **ADPCI** and **HDO-8F**.

ADP:HDO and **ADP:HDO-8F** resemble in their appearance, being both white opaque solids at room temperature.

5.1.1. Characterization of **ADP:HDO-8F** and **ADP:HDO**

5.1.1.1. Structural analysis

Both polyesters were analyzed in solution by NMR spectroscopy and their structures were confirmed by ^1H NMR and $^{13}\text{C}\{^1\text{H}\}$ NMR experiments (Figure 5.2 and Figure 5.3). Spectra exhibit significant differences mainly owing to the constituent diols. Furthermore, the analysis of the obtained solid was carried out by FTIR spectroscopy (Figure 5.4).

5.1.1.1.1. ^1H NMR analysis

The replacement of hydrogens by fluorine atoms is observed in the number of peaks and their chemical shifts in the recorded ^1H NMR spectra of both compounds (Figure 5.2.). **ADP:HDO**'s spectrum (Figure 5.2. top) depicts a lower number of peaks than the amount of non-chemically equivalent hydrogens due to the overlap of the methylene groups of the adipate and the **HDO** (δ_{H} 1.60 ppm). However, in the **ADP:HDO-8F** spectrum (Figure 5.2. bottom) due to the inductive effect of the perfluorinated fragment, it is observed a deshielding and displacement toward lower fields of the remaining proton signals is observed.

The chemical environment of the methylene group attached to the terminal hydroxyl ($-\text{CH}_2\text{OH}$, **a**) differs from the $-\text{CH}_2$ linked to an ester moiety ($-\text{CH}_2\text{OCO}-$, **b**), being typically the latter more deshielded. Exploiting this fact, the M_n of the polymer can be determined by end-group analysis (See Measuring Section 9.51). According to the analyses and considering

the AI of both crudes, the M_n values of **ADP:HDO** and **ADP:HDO-8F** employed in the posterior Section 6.4 were 2015 g/mol ($n_{RMN} = 8.31$) and 3270 g/mol ($n_{RMN} = 8.24$), respectively. The obtained results were close to the theoretical values. The number of repeated units of alcohol in the final polymer ($n+1$) was used to estimate the fluorine content of the polyester, which was 43 wt.% for **ADP:HDO-8F**.

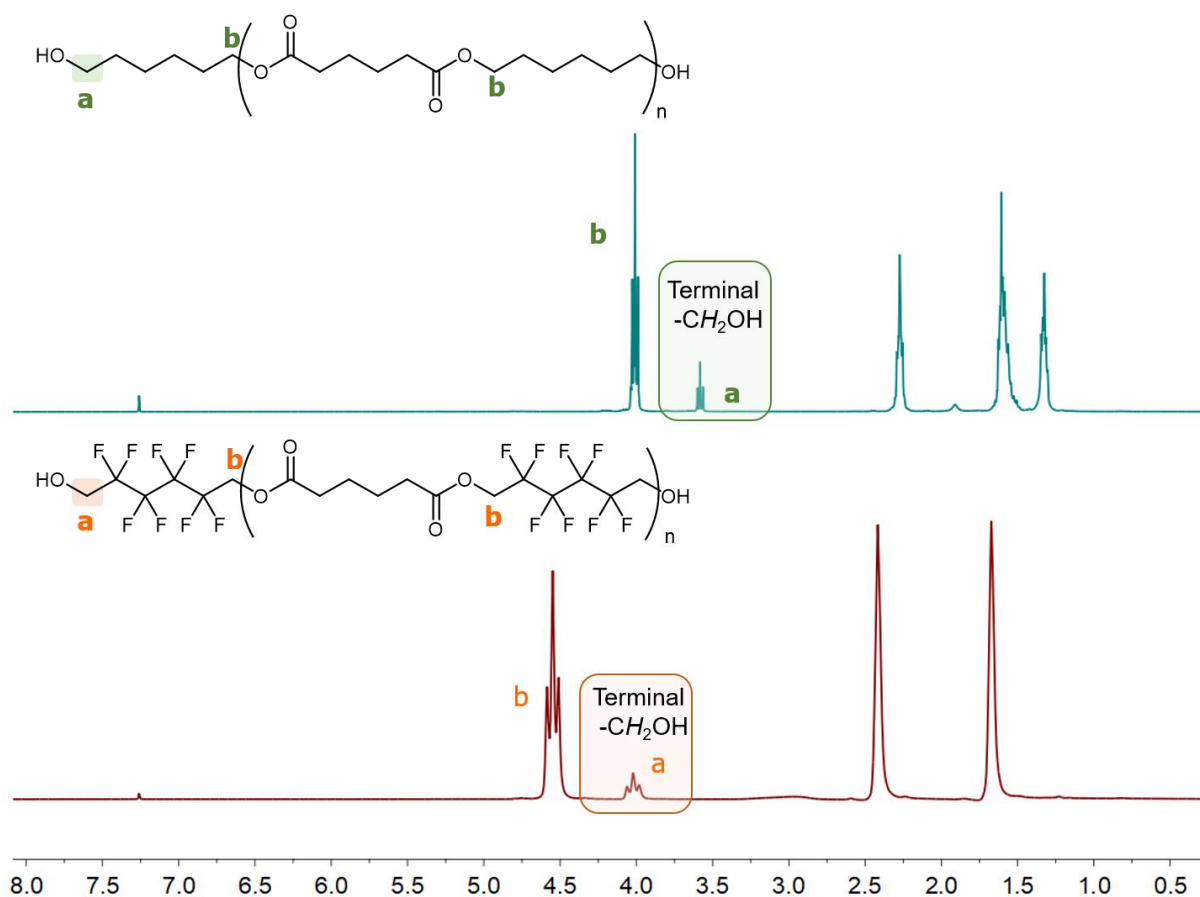


Figure 5.2. ^1H NMR (360 MHz) spectra of **ADP:HDO** (top) and **ADP:HDO-8F** (bottom) with a delay time of 10 seconds to ensure quantification. Solvent: CDCl_3 .^[11]

5.1.1.1.1. $^{13}\text{C}\{^1\text{H}\}$ NMR analysis

Figure 5.3 shows both $^{13}\text{C}\{^1\text{H}\}$ NMR spectra of the studied polymers with the most relevant areas enlarged. As a rule of thumb, fluorinated polymers present peaks at higher chemical shifts than their hydrogenated analogs owing to the higher electronegativity of fluorine.^[12] Both ^{13}C and ^{19}F , have a nuclear spin of $\frac{1}{2}$, leading to the coupling between the two nuclei and the signal multiplicity on NMR spectroscopy. The splitting of these peaks causes smaller intensities, even when there are several repetitive units in the chain.

The fragments arising from **HDO-8F** are observed as two multiplets attributed to two non-equivalent $-CF_2-$ groups (δ_c 114.65 and 111.15 ppm). Coupling constants between the bonded C-F ($^1J_{C-F}$, 258.4 Hz, and 266.1 Hz, respectively), are within the typical range of linear CF_2 groups.^[11] In contrast, the non-fluorinated monomer displays the two analogous carbons as singlets at higher fields (δ_c 28.27 and 25.33 ppm).

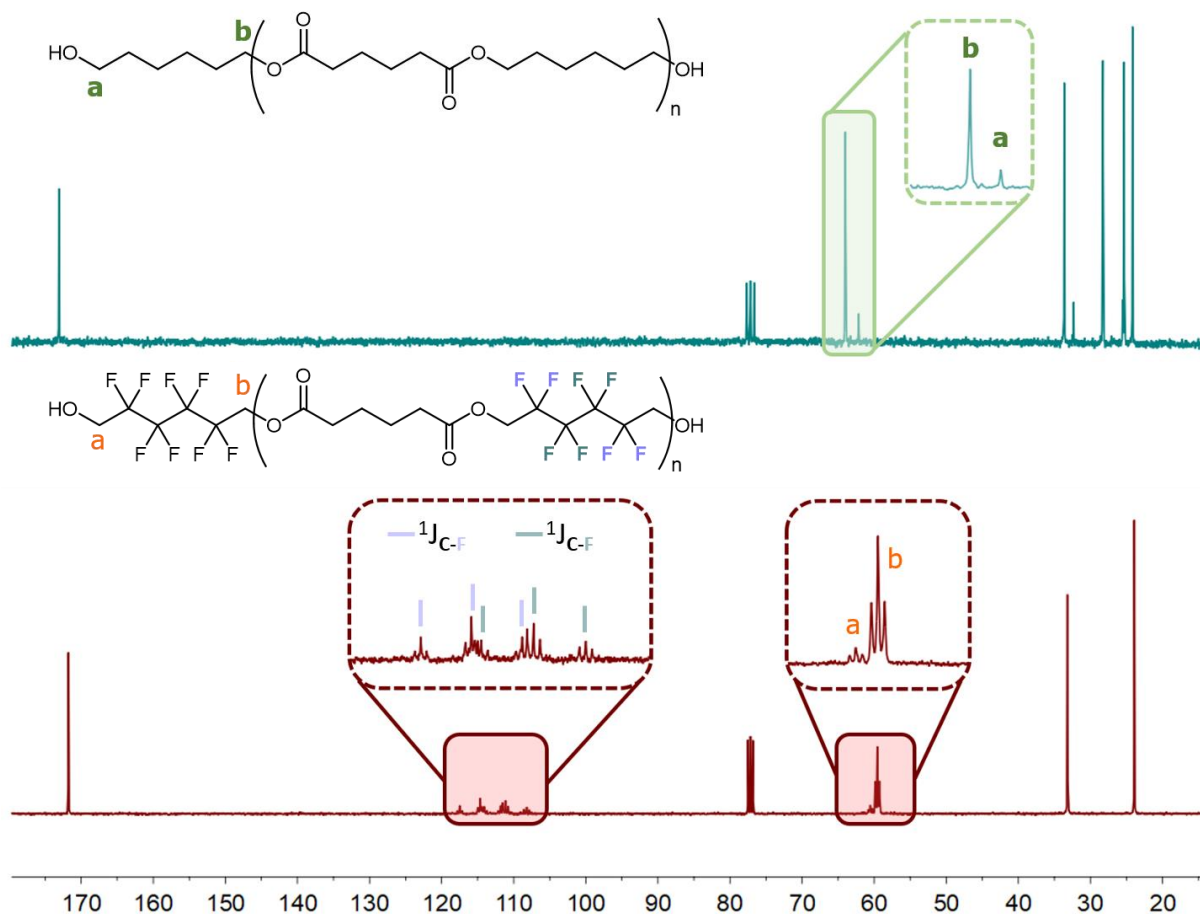


Figure 5.3. $^{13}C\{^1H\}$ NMR spectra of **ADP:HDO** (top, 62.90 MHz) and **ADP:HDO-8F** (bottom, 90.55 MHz). Significant areas are enlarged in dashed line squares. Solvent: $CDCl_3$.

The M_n of these polyols is relatively small, thereby enabling the identification of the terminal methylene ($-CH_2OH$, **a**) and the esterified methylene ($-CH_2O-CO$, **b**), comparable to the 1H NMR spectra observations. The hydroxyl-terminated peak is more shielded when it belongs to the non-fluorinated **HDO** ($-CH_2OH$, δ_c 62.67 ppm) than the esterified methylene ($-CH_2O-CO$, δ_c 64.32 ppm). In comparison, **ADP:HDO-8F** displays the opposite behavior with the internal signal at higher fields than the bonded to an hydroxyl ($-CH_2O-CO$, δ_c 59.56 ppm *vs* $-CH_2OH$, δ_c 60.54 ppm). Moreover, these two signals exhibit multiplicity as the carbons are vicinal to $-CF_2$ group.

5.1.1.1.2. FTIR analysis

The normalized ATR-FTIR spectra of **ADP:HDO** (top) and **ADP:HDO-8F** (bottom) in the range of 4000-600 cm^{-1} are shown in Figure 5.4. The low-intensity band at 3500 cm^{-1} , which is typically related to the hydroxyl stretching, indicates the presence of few terminal groups on the polymer and little to no unreacted diol. Peaks near 2960 cm^{-1} and 2880 cm^{-1} are ascribed to the asymmetric and symmetric stretching of the methylene groups, respectively, in both polyols. In the case of **ADP:HDO-8F**, since the number of CH_2 bonds is smaller than in **ADP:HDO**, the intensity is reduced.

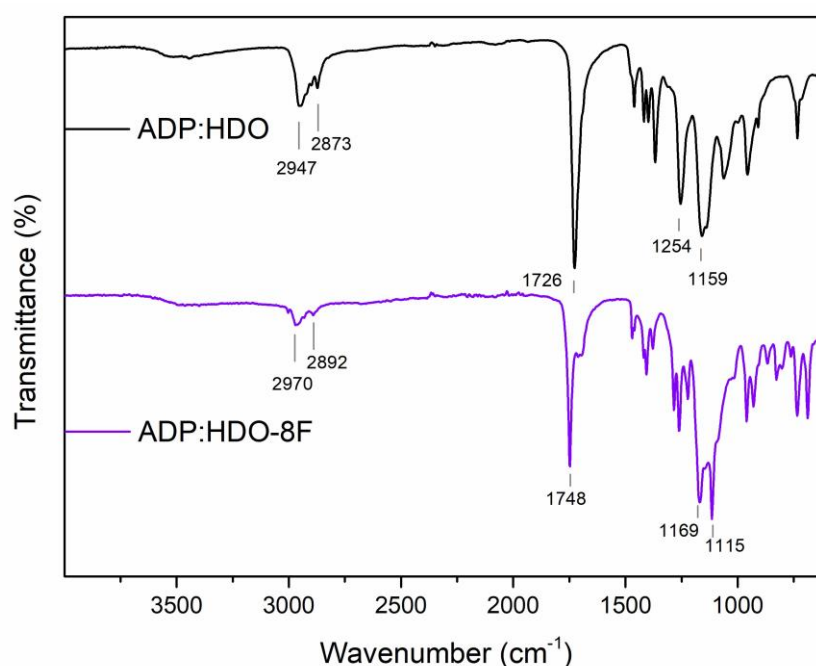


Figure 5.4. Stacked infrared spectra of **ADP:HDO** (top) and **ADP:HDO-8F** (bottom).

As expected for polyesters, one of the strongest bands in the spectra corresponds to the stretching vibration of the $\text{C}=\text{O}$ group of esters. Owing to the inductive effect of fluorine, **ADP:HDO-8F** peak shifts toward higher wavenumbers (1748 cm^{-1}) than its hydrogenated analog (1726 cm^{-1}). Correspondingly, the stretching associated with the $\text{C}-\text{O}$ is also displaced to higher wavenumbers when there is fluorine on the structure (1169 cm^{-1} in **ADP:HDO-8F** against the 1159 cm^{-1} in **ADP:HDO**). The most intense peak on **ADP:HDO-8F** overlaps vibrations that can be attributed to the stretching $\text{C}-\text{O}$ of the $\text{O}-\text{CH}_2$ and $\text{C}-\text{F}$. The fingerprint regions of the two polyesters are significantly different, likely owing to the vibrations arising from the fluorine atoms.

5.1.1.1.2. Thermal Analysis

ADP:HDO and **ADP:HDO-8F** are solids at room temperature and were studied by DSC to study their thermal behavior. T_m , T_c , and their corresponding ΔH° values were determined using a heating rate of 10 °C/min under a N₂ atmosphere. DSCs measurements of both compounds are displayed in Figure 5.5 and the gathered data is listed in Table 5.2, omitting the first heating scan to erase the thermal history of the sample.

The compounds under study do not evidence a change on the baseline in the explored range that could be associated with a T_g . However, both polyesters display melting and crystallization peaks, confirming the semi-crystalline nature of the produced polyesters.

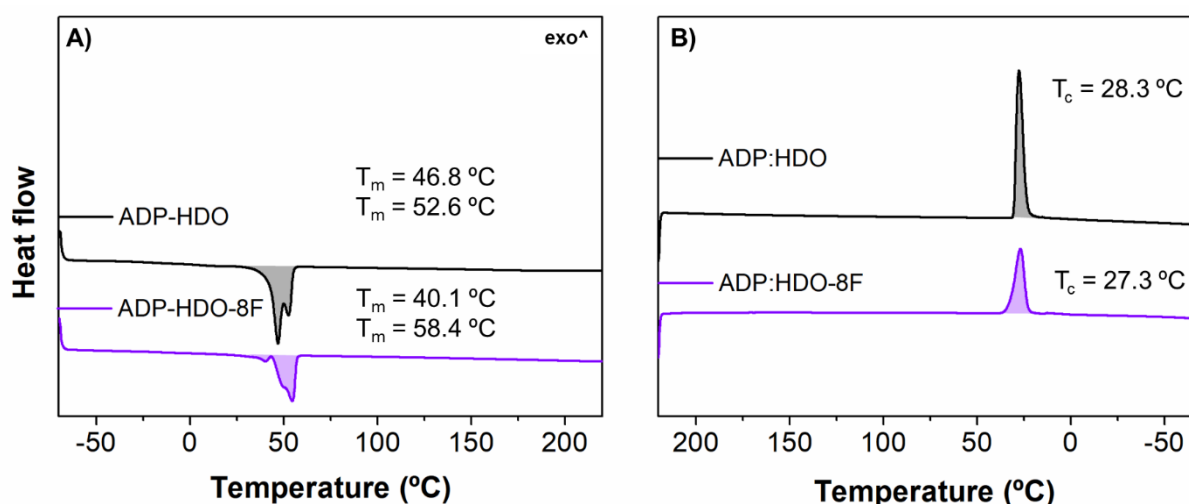


Figure 5.5. **ADP:HDO** and **ADP:HDO-8F** DSC thermograms of A) the second heating process and B) the first cooling process. Shaded areas indicate regions used to determine the corresponding processes.

Table 5.2. DSC data of both synthesized compounds.

	ADP:HDO		ADP:HDO-8F	
	wt.% F	0.0		43.0
T_g (°C) [a]	--		--	
T_m (°C) [a]	46.8	52.6	40.1	58.4
ΔH_m° (J/g) [a][b]	74.5		43.6	
T_c (°C)	28.3		27.3	
ΔH_c° (J/g)	72.1		47.0	

[a] Transitions were captured in the second heating scan at 10 °C/min.

[b] Total enthalpy of the endothermic process.

Focusing on the second melting process (Figure 5.5.A) the overlap of more than one endothermic process spanning from 25 °C to 60 °C was detected. In particular, a clear double

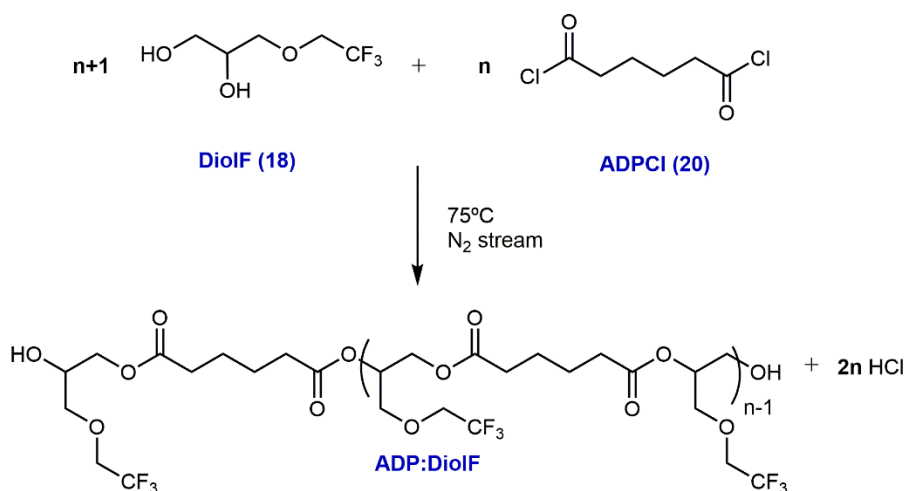
melting is observed in **ADP:HDO**, while in the **ADP:HDO-8F** exists a small shoulder before the broad and more intense endotherm. The presence of multiple peaks suggests crystallite reorganization when the temperature increases. This behavior has been already reported by some other authors for semi-crystalline materials and it is associated with the heating and cooling rate.^{[13][14]} The lowest temperature endotherm corresponds to the melting of the crystallites already formed in the sample from the previous cooling process. As the quantity of amorphous material increases with temperature, it recrystallizes into more perfect crystals, which afterward melt at a higher temperature. The multiples melting peaks of both samples occur at similar temperatures. As the peaks could not be separated, a unique enthalpy value stands for the complete endothermic processes. **ADP:HDO** displayed a melting enthalpy of 74.5 J/g and **ADP:HDO-8F** of 43.6 J/g, indicating a higher number of ordered crystallites in the fluorine-free polyester.

Conversely, a single peak was obtained during the cooling process of both samples (Figure 5.5.B). The two polyesters had crystallize at a similar temperature, but **ADP:HDO-8F** exhibits a lower enthalpy. The higher values of the **ADP:HDO**'s enthalpies with respect to its fluorinated analog suggest a slightly better and most abundant packaging of the chains when no fluorine is present. Although hydrogen and fluorine have a small size, perfluorinated compounds tend to repel other chains. Therefore, the introduction of fluorinated chains into the structure diminished their chain packing, reducing the cohesive forces and leading to the formation of slightly less ordered structures.

5.2. Synthesis of ADP:DiolF

5.2.1. Synthesis of ADP:DiolF by acyl chloride approach (1)

The previously adapted method was attempted for the synthesis of the polyester **ADP:DiolF** with a M_n of 2000 g/mol (Scheme 5.3). The initial tests were carried out under identical conditions as in the previous case: 75 °C, without solvent, and adding the acyl chloride **20** dropwise over **DiolF**. Again, a continuous N₂ stream was used to remove the acid produced in the reaction by the Venturi effect.



Scheme 5.3. Synthesis of **ADP:DiolF** from **ADPCI**.

After 24 hours of reaction, a brown viscous resin was obtained. The analysis of the sample by NMR spectroscopy revealed no signal attributable to the acyl chloride, thereby a complete conversion of the monomer was reached. However, unexpectedly, peaks around 178 ppm appeared on the $^{13}\text{C}\{^1\text{H}\}$ NMR spectrum of the crude (Figure 5.6.A), which were ascribed to $-\text{COOH}$ groups. [16]

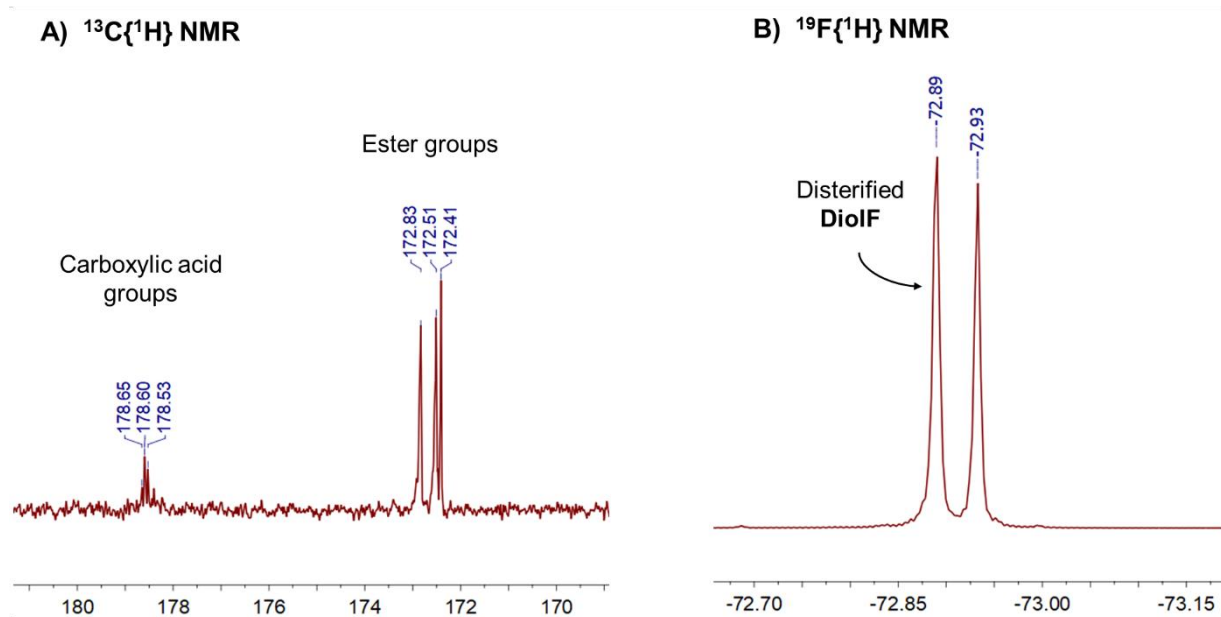
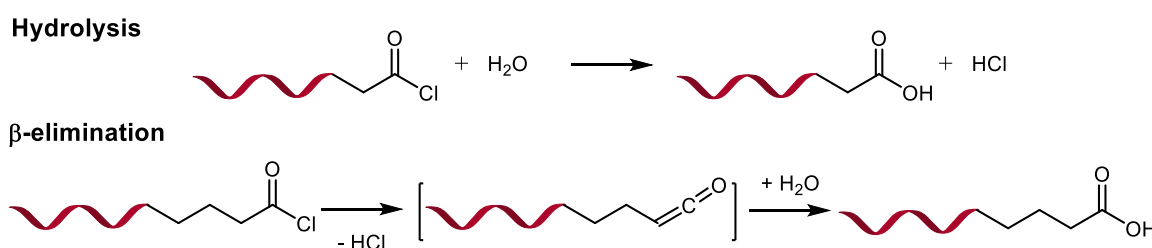


Figure 5.6. Fragmented NMR spectra of the reaction crude after 24 hours at 75 °C. A) Fragmented $^{13}\text{C}\{^1\text{H}\}$ NMR spectrum (100.63 MHz) of the carbonyl region. B) Fragmented $^{19}\text{F}\{^1\text{H}\}$ NMR spectrum (376.5 MHz). Solvent: CDCl_3 .

Moreover, two different peaks were observed in the $^{19}\text{F}\{^1\text{H}\}$ NMR spectrum (Figure 5.6.B). [12] The proximity between both signals indicates a similar chemical environment. No other peaks associated with free **DiolF** or other moieties containing the halogen, like $=\text{CF}_2$ or CHF_2 were

observed in the recorded spectra. The peak more deshielded corresponded to a $-\text{CF}_3$ group of **DiolF** that has been esterified, while the second signal had an undetermined origin.

Commonly, the formation of carboxylic acids from acyl chloride derivatives is produced by its hydrolysis with water or by the β -elimination of HCl from the reagent and the subsequent addition of water to the ketene group (Scheme 5.4). Both reactions may compete with the polymerization, generating undesired byproducts and preventing the straightforward synthesis of the polyester.

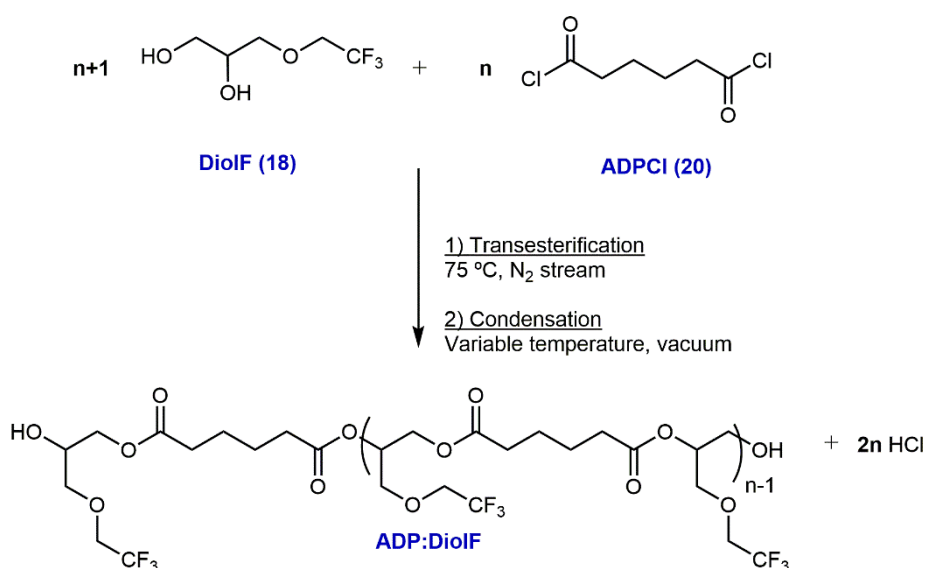


Scheme 5.4. Possible side reactions leading to carboxylic acids.

To avoid these side reactions, monomers were further purified to ensure the absence of water. **ADPCI** was distilled under reduced pressure, and **DiolF** was exhaustively dried by azeotropic distillation with toluene. But the use of these treated reagents led to the same outcome. It seems that somehow, the reaction forms carboxylic-ending oligomers that hinder the direct obtention of the desired polyester M_n by acting as end-capping agents under the tested conditions.

5.2.1.1. Alternative synthesis of ADP:DiolF by acyl chloride approach (2)

ADP:DiolF synthesis was reattempted with some modifications to the previous methodology. The same set-up was employed to carry out the addition of the acyl chloride **20** under identical initial conditions. Subsequently, a posterior condensation process under reduced pressure was assessed to esterify the formed carboxylic acids and increase the M_n (Scheme 5.5). This reaction was carried out at a 6 g scale with a target M_n of 1500 g/mol.



Scheme 5.5. Adapted synthesis of **ADP:DiolF** from **ADPCI** and **DiolF**.

The alternative procedure was monitored by $^{13}\text{C}\{^1\text{H}\}$ NMR analysis to explore the variation in the carboxylic peaks and $^{19}\text{F}\{^1\text{H}\}$ NMR analysis to quantify the progress of two signals. Finally, ^1H NMR spectroscopy was employed to monitor the ratio of the reagents and if some loss by evaporation or thermal degradation existed.

Figure 5.7 illustrates the evolution in the polyester formation in terms of carboxylic acid peaks and variation between the fluorine signals. The carboxylic acid peaks appeared before 12 hours of reaction at 75 °C at atmospheric pressure (**E1**). Curiously, at **E1** only three peaks of esters appeared on the spectrum. Then, to condensate the formed acid, an increase in temperature was assessed. Longer reaction times at higher temperatures under atmospheric pressure were applied (**E2**). After 32 hours of reaction, vacuum was applied to the system as an attempt to displace the formed carboxylic acids by means of water elimination (**E3**), but no significant changes were observed on the carboxylic signals signposting a slow reactivity at 150 °C. Thus, the mixture was subjected to 180 °C under vacuum (**E4**). Complete condensation of the -COOH moieties was achieved after several hours under these conditions. Additional 15 hours at 180 °C and reduced pressure (**E5**) were applied to ensure the complete disappearance of the acid group. Nevertheless, after 52 hours at reduced pressure, the coloration of the crude increased, preventing the conventional AI titrations. Regarding the fluorine spectrum (Figure 5.7.B), the evolution of the signals was depicted, increasing the concentration of the one associated with the diesterified diol (quantified in Table 5.3).

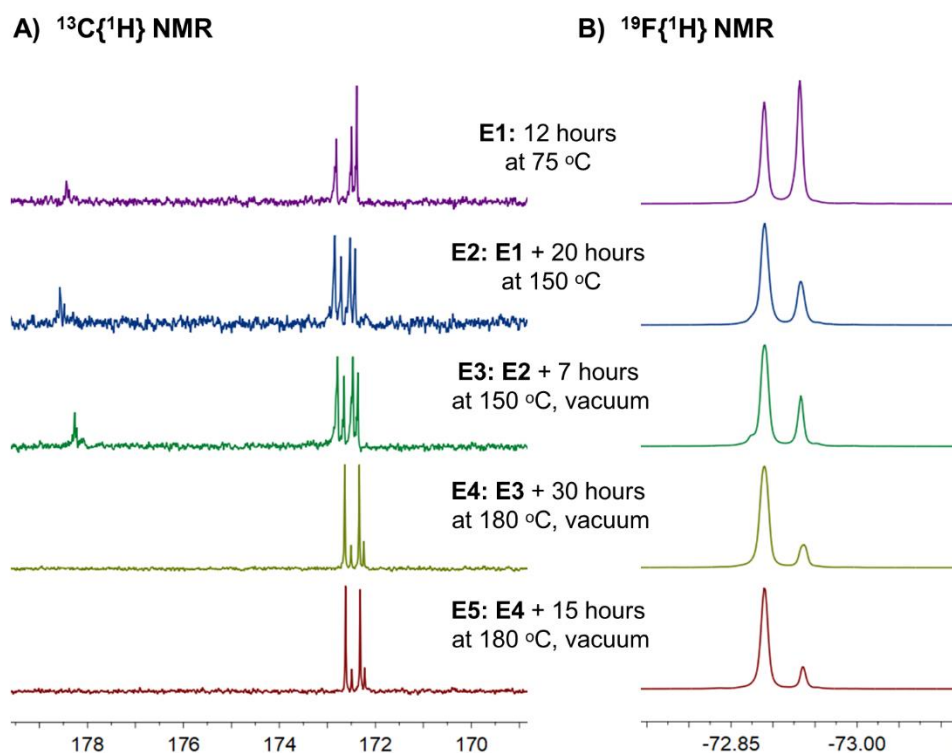


Figure 5.7. Fragmented spectra of the crude evolution with time and temperature. A) $^{13}\text{C}\{^1\text{H}\}$ NMR spectra (100.63 MHz) of the carbonyl region (Peaks around 178.6 ppm correspond to carboxylic acid groups, while peaks located at 172.6 ppm are attributed to ester moieties). B) $^{19}\text{F}\{^1\text{H}\}$ NMR spectra (376.5 MHz) recorded with a delay time of 10 seconds to ensure quantification. (Peak centered at -72.89 ppm is ascribed to the diesterified **DiolF**, whereas the peak at -72.93 had an undetermined origin). Solvent: CDCl_3 .

The ratio among the reagents was quantified by ^1H NMR spectra and is summarized in Table 5.3. Similar values were obtained, proving that no significant quantity of the reagents was lost with the N_2 stream, and only a slight decrease was detected under vacuum, which could be expected. Therefore, as no significant loss of fluorine was detected, the observed variation of the fluorine peaks in Figure 5.7.B, must be an interconversion of the signals, from the undermined CF_3 to the diesterified.

Table 5.3. Evolution of the reaction crude according to the conditions.

Entry	Tested conditions	Ratio DiolF: Diacid ^[a]	Ratio diesterified: undetermined compound ^[b]
E1	12 h at 75 °C. N_2 stream.	1.20	0.93
E2	E1 + 20 at 150 °C. N_2 stream.	1.19	2.36
E3	E2 + 7 hours at 150 °C. Reduced pressure.	1.20	2.60
E4	E3 + 30 hours at 180 °C. Reduced pressure.	1.18	4.60
E5	E4 + 15 hours at 180 °C. Reduced pressure.	1.18	5.29

^[a] Value calculated by dividing the sum of the integration values arising from **DiolF** peaks and the diacid, after normalizing by the number of protons of each component.

^[b] Value obtained by dividing the areas of the peak of the diesterified CF_3 and between the terminal one.

Regarding the ^1H NMR spectra, the formation of a polyester containing **DioIF** after the first 12 hours at 75 °C was observed. No new signals appeared in the spectra as conditions changed, with the only variation being a different proportion of the peaks.

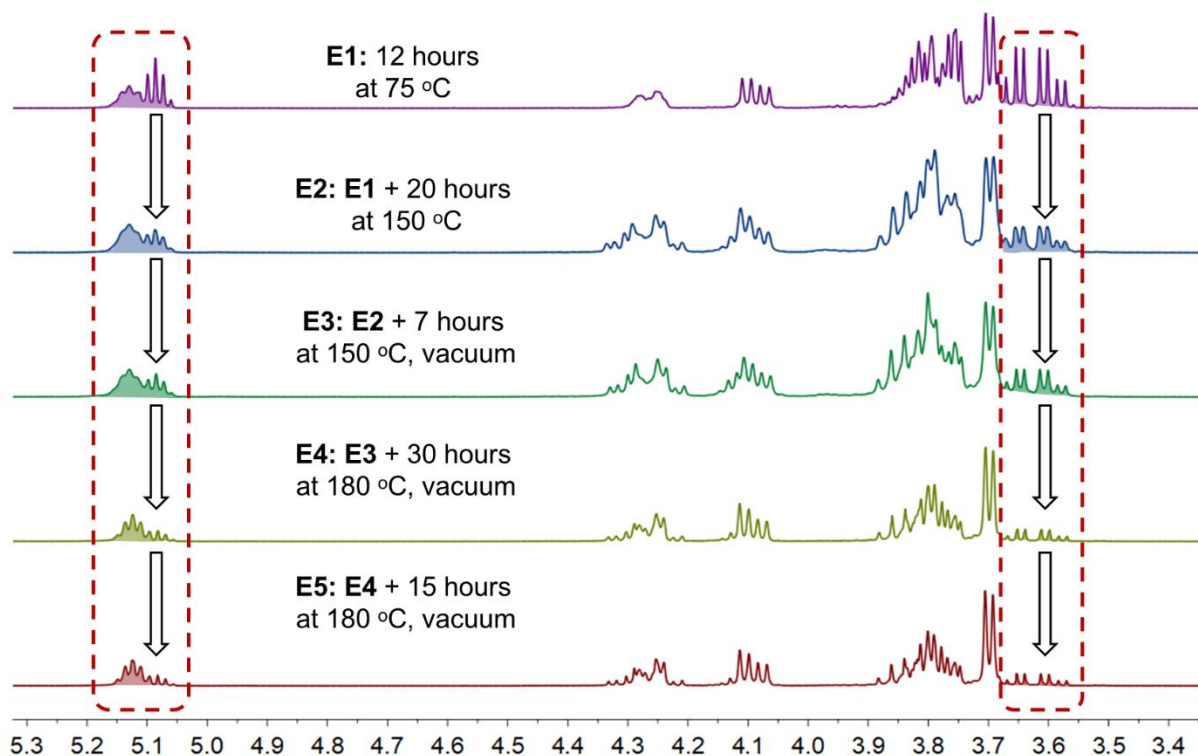
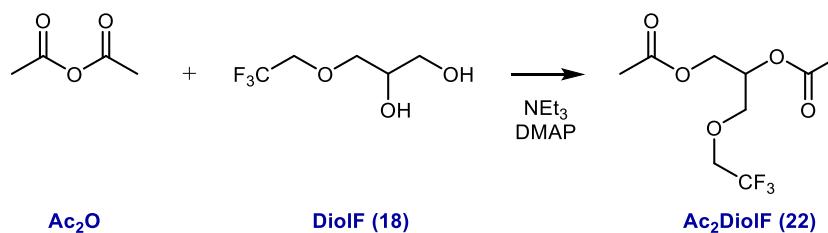


Figure 5.8. Fragmented ^1H NMR spectra (400 MHz) of the reaction crude with time and temperature. All of them were recorded with a delay time of 10 seconds to ensure quantification. Solvent: CDCl_3 .

However, as time increased, two regions of the spectra varied (red squares in Figure 5.8). At earliest stages of the reaction, an apparent quintuplet was observed at 5.10 ppm next to a broad signal at 5.15 ppm, which was attributed to the central methine group of **DioIF** when it is esterified by both hydroxyls. However, as harsher conditions were tested, the quintuplet decreased while the more deshielded signal evolved to a better resolution and a larger integration value. As the ratio between the diol and the diacid fragments remained constant, the signals located at 5.15 ppm and 5.10 ppm seemed to be interconverting. Moreover, the two doublets of doublets located at 3.66 ppm and 3.61 ppm decreased with time. The observed trend in the ^1H NMR spectra (Figure 5.8) agrees with the variations depicted in the ^{19}F $\{^1\text{H}\}$ NMR (Figure 5.7.B). Therefore, the mentioned signals might arise from the same undetermined structure.

Opposite to other linear polymers, the M_n of the system could not be determined by end-group analysis, as signals arising by either of the esterified hydroxyls of **DioIF** could not be detected.

When the reaction mixture was subjected to high temperatures and reduced pressure for even longer periods of time, the spectrum of the crude (Figure 5.9.Top) tends to resemble more to the diesterified compound **Ac₂DioIF (22)**. This compound was synthesized starting with **DioIF** and an excess of acetic anhydride (**Ac₂O**, 4 equivalents), employing 4-*N,N'*-dimethylaminopyridine (DMAP, 5 mol%) as catalyst in a NEt₃ solution at room temperature (Scheme 5.6). **Ac₂DioIF** is a light-yellow liquid at room temperature, which was easily isolated from the reaction mixture by a common liquid-liquid extraction process.



Scheme 5.6. Synthesis of **Ac₂DioIF** from **DioIF** with **Ac₂O**.

Ac₂DioIF presents seven proton peaks in its ¹H NMR spectrum (Figure 5.9.Bottom), some of which originate from the same methylene group. Protons marked as *d* in the spectra are diastereotopic; therefore, they couple with each other and present their own multiplicity. Protons ascribed to *a* are also diastereotopic; however, their chemical shifts are relatively similar and appeared as a doublet of quadruplets or a multiplet on the spectra. Assignment of the rest of the signals is directly indicated in the spectrum. Comparing the spectra of the diacetylated diol and the polymer, existed a slight displacement on the chemical shift owing to the nature of the carboxylic acid derivative, but the rest of the signals are practically identical considering that one is a polymer while the second in a discrete compound. This fact confirms the formation of a polyesters containing the alcohol. The only additional peaks observed in the reaction crude (Figure 5.9.Top) are those denoted with a black circle.

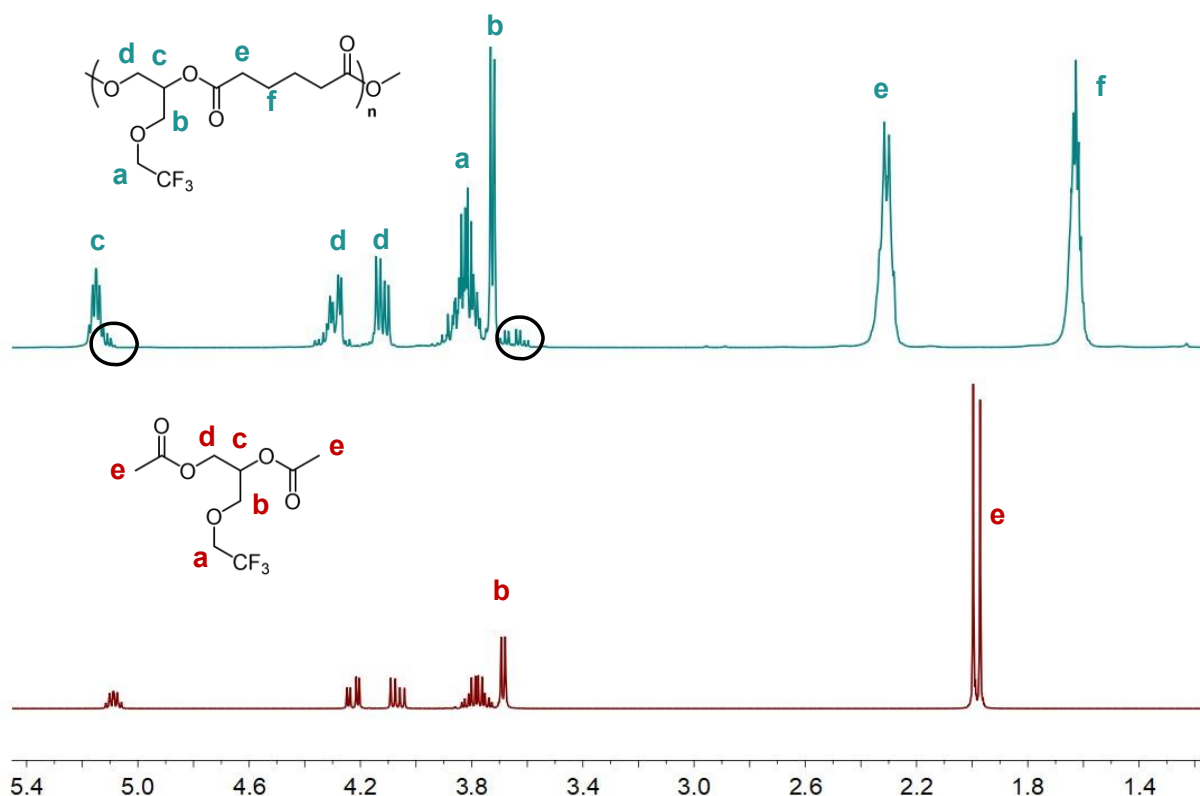
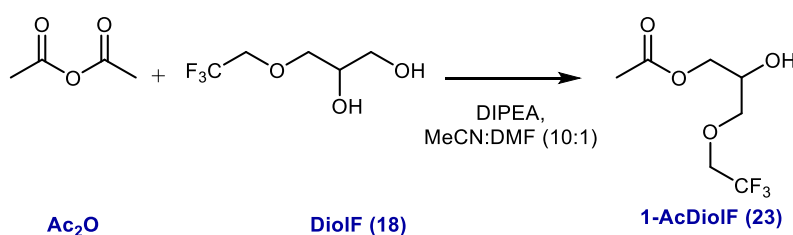


Figure 5.9. ¹H NMR spectra (400 MHz) of the reaction crude (after 8 days at high temperatures and reduced pressure) (top) and the synthesized **Ac₂DiolF** (bottom). Black circles indicated residues of the undetermined signal. Solvent: CDCl₃.

Further tests were explored to ascertain the nature of the unassigned peaks on both ¹H, ¹³C{¹H} and ¹⁹F{¹H} NMR spectra. As the unidentified compound clearly contains fluorine, it needs to be some kind of structure containing **DiolF**. One possible origin of these signals could just be the terminal position of **DiolF**. To verify the presence or absence of terminal diol, **DiolF** was selectively acetylated to obtain the corresponding oligomer **23** (Scheme 5.7).



Scheme 5.7. Selective monoacetylation of **DiolF**.

The reaction is stereospecific to the acylation of the primary alcohol, allowing the study of the ¹H NMR signals arising from a terminal position of **DiolF**.^[17] The reaction is catalyzed by diisopropylethylamine (DIPEA) in a mixture of MeCN and DMF at 40 °C for 18 hours. The major

advantage of this reaction, as well as in the previous synthesis of **Ac₂DioIF**, is that no acyl chloride is employed, which prevents potential by-products arising from this reagent.

The reaction crude comprised mainly the targeted compound **1-AcDioIF**. However, traces of the diesterified diol, **Ac₂DioIF**, and the monoesterified by the secondary hydroxyl (**2-AcDioIF**, **24**) were also observed. A filtration with acid alumina allowed the obtention of the two monoacetylated compounds in a **1-AcDioIF**: **2-AcDioIF** ratio of 86:14 (Figure 5.10).

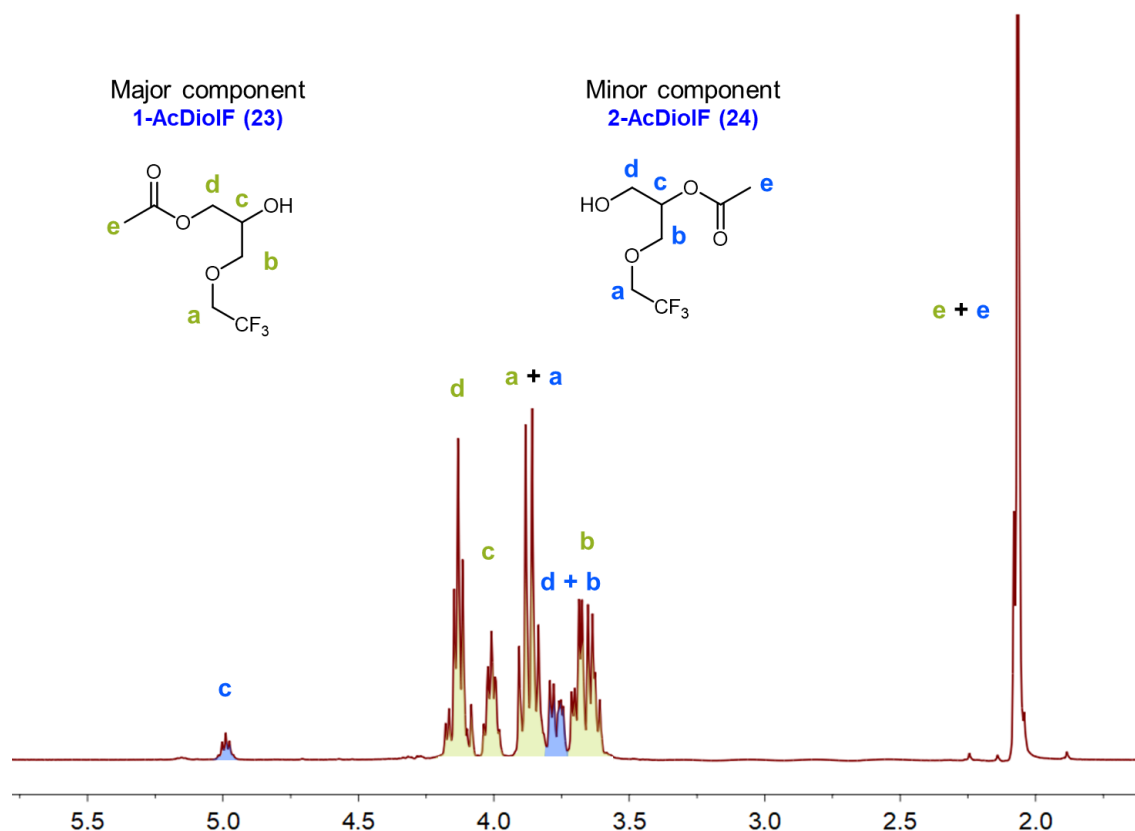


Figure 5.10. ^1H NMR spectrum (360 MHz) of the monoacetylated **DioIF** derivatives. Peaks colored in green corresponded to **1-AcDioIF (23)**, while blue peaks are associated with the acetylated derivative by the secondary hydroxyl. Solvent: CDCl_3 .

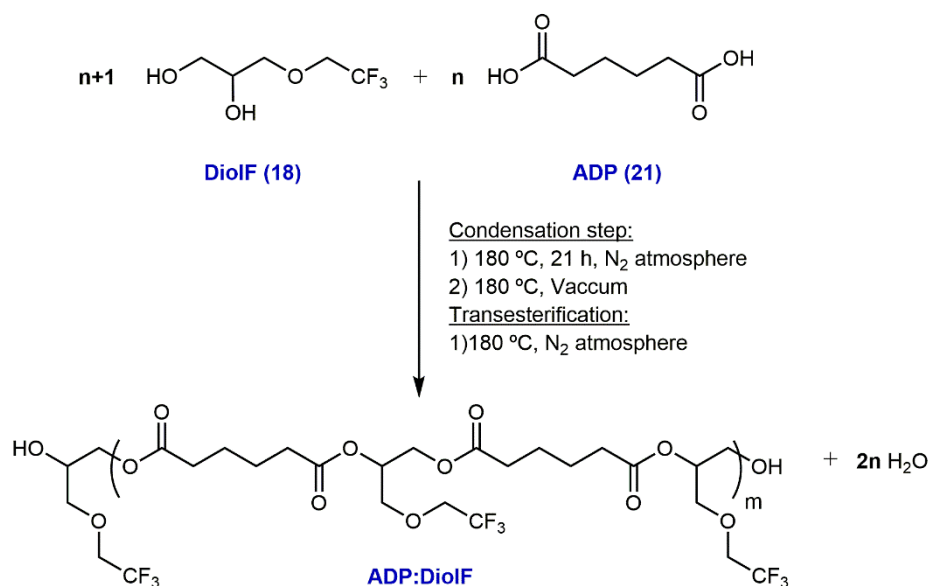
Peaks denoted with the letter **c** in ^1H NMR spectrum correspond to the central methine group of **1-AcDioIF** and **2-AcDioIF**. Although their chemical shifts are similar to that of the unidentified fluorinated compound in the polymer mixture, they do not match with the previously observed spectra. This observation reinforced the structure assignment of the produced polymer. Moreover, this simple experiment allows the confirmation of the absence of terminal **DioIFs** moieties in the acyl chloride approach, indicating that some side reactions take place under the tested conditions.

Therefore, although a polyester containing **DiolF** was obtained, this procedure was only suitable for small-scale reactions. When 100 g of product was attempted, the reaction times largely increased, and the sample became a dark brown resin. Thus, no satisfactory results were obtained in the production of relatively large scales of **ADP:DiolF** by the direct addition of the corresponding monomers. Some undefined side reactions occurred, and carboxylic acid groups and other subproducts were generated in the crude. The solvent-free and base-free reaction of acyl chlorides with linear diols, either with or without fluorine (*i.e.* **BDO** or **HDO-8F**), successfully synthesized polyesters with specific M_n without any further purification process. However, for diols with fluorinated pendant chains and primary and secondary hydroxyls groups (**DiolF** or **DiolSF**), the same reaction resulted in the hydrolysis of the acyl chloride terminations, which hindered the polymer's production.

5.2.1.2. Synthesis of ADP:DiolF by melt-phase polycondensation approach

Discarding the acyl chloride approach, the conventional methodology for melt-phase polycondensation between a dicarboxylic acid and a glycol was essayed. This route involves several potential drawbacks, mainly some loss of the more volatile compounds, and the use of harsh conditions. The loss of volatile monomers requires of the so-called corrections, further additions of pre-dried diol, to displace the reaction equilibrium. Moreover, the reaction must be continuously monitored through AI and OHI titrations, losing 10-12 g of crude per analysis.

The polycondensation reaction traditionally comprises a condensation step, followed by a transesterification phase (Scheme 5.8). In the initial stages of the condensation, the generated water was distilled at 180 °C for 21 hours at atmospheric pressure. Subsequently, 20 ppm of $\text{SnCl}_2 \cdot 2\text{H}_2\text{O}$ was incorporated into the mixture and the reaction progressed at reduced pressure until reaching low values of AI. The second step of the reaction tuned the M_n by transesterifying the polymer chains with hydroxylated monomers. Therefore, more diol was added to the mixture and reacted under an inert atmosphere of N_2 .



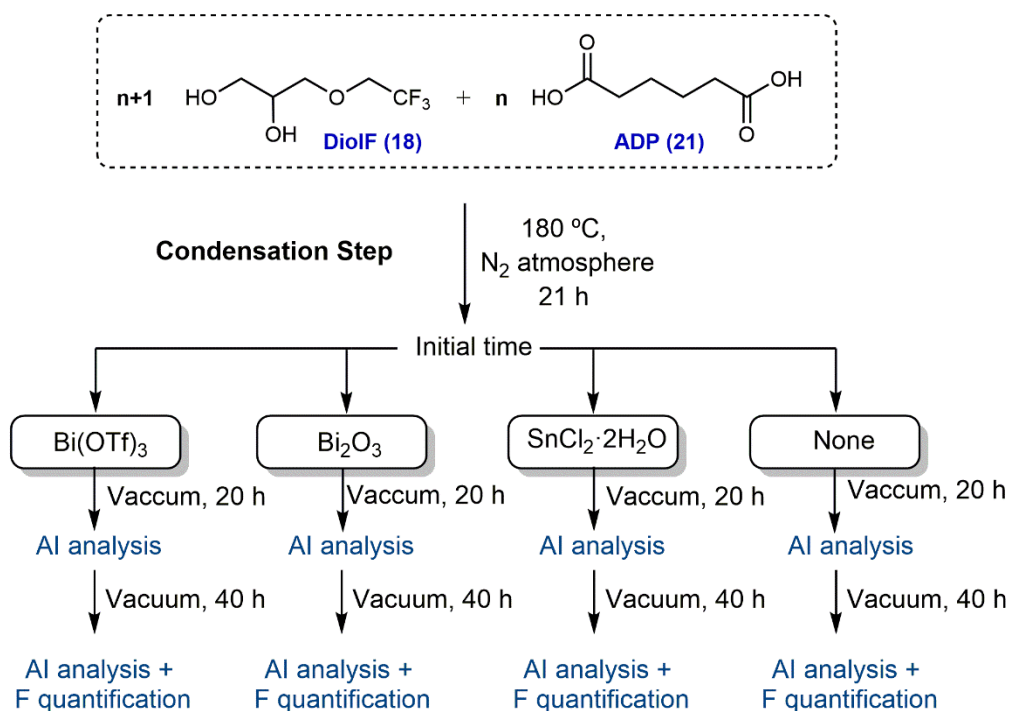
Scheme 5.8. General synthesis of **ADP:DiolF** from compound **18** and **ADP**.

The reaction was monitored by means of AI and IOH titrations to control the condensation degree and the M_n of the sample. Nevertheless, subjecting the mixture to long reaction times generated dark crudes, which interfered with appropriate titration of the sample.

5.2.1.2.1. Catalyst tests

Reducing the reaction time is an important factor to avoid thermal degradation of the polymer and provide good-quality compounds. Aiming for shorter reaction times and a less colored product, various transesterification catalysts were tested. The selected compounds were tin chloride ($\text{SnCl}_2 \cdot 2\text{H}_2\text{O}$), bismuth (III) oxide (Bi_2O_3), and bismuth (III) trifluoromethanesulfonate ($\text{Bi}(\text{OTf})_3$). SnCl_2 is a solid compound with relatively high stability towards moisture and oxygen, which is an interesting feature at industrial scale. Conversely, bismuth catalysts exhibit lower toxicity.

The test consisted of condensing **DiolF** and **ADP** for 21 hours under N_2 atmosphere. Then, from a single crude, four equal samples were separated to study the condensation step at reduced pressure (Scheme 5.9).



Scheme 5.9. Outline of the catalyst study.

The catalytic study was carried out with 45 ppm of catalyst, a concentration higher than commonly used for a polyester synthesis, but which will enable a clearer detection of the changes. Identical reaction conditions were tested in all samples with a StarFish™ equipment. The three metal compounds and a blank sample were evaluated by means of AI at two different times (20 hours and 40 hours). In addition, after completing the time, fluorine was quantified by ¹⁹F{¹H} NMR spectroscopy to ensure no excessive loss under the reaction conditions.

Variations in AI values are shown in Figure 5.11.A. Overall, samples exhibit a decline in the carboxylic acid concentration after 20 hours. Compared with the blank sample at that time, catalyzed samples reduced AI to a larger extent. SnCl₂ was the best catalyst, especially at short times. Bismuth compounds did exhibit catalytic behavior in the first 20 hours under vacuum, but were slower than tin, which can be explained by their lower Lewis acidity.

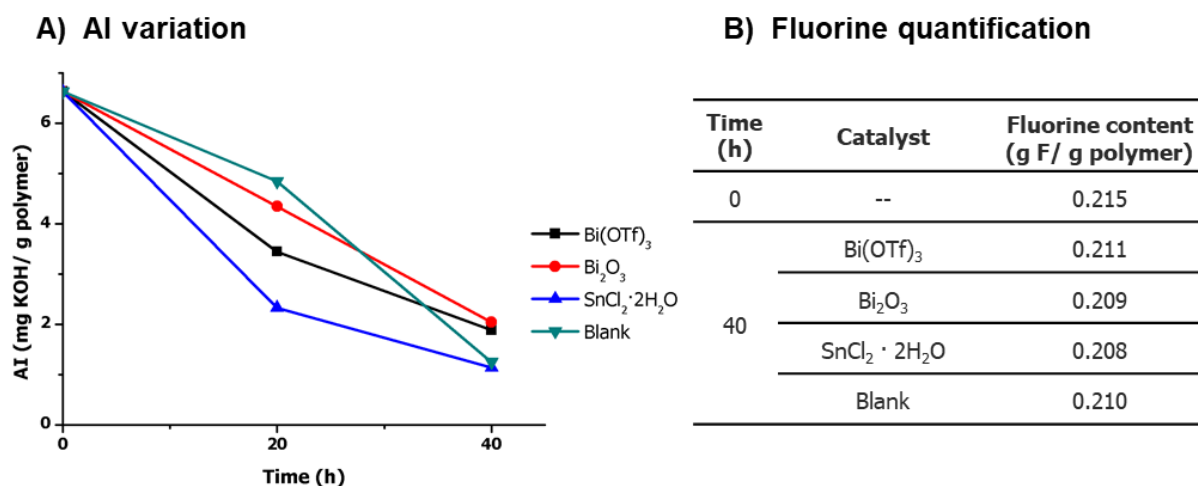


Figure 5.11. A) Evolution of AI with different catalysts. B) Fluorine quantification of the reaction crude by $^{19}\text{F}\{^1\text{H}\}$ NMR spectroscopy using 3-bromobenzotrifluoride as standard.

After 40 hours at reduced pressure, the condensation rate of the catalysts diminished, except for Bi_2O_3 . Bismuth catalysts seem to inhibit the reaction evolution, displaying higher AI values than the blank. However, scarcely better results were obtained employing the tin-based catalyst than in the blank test

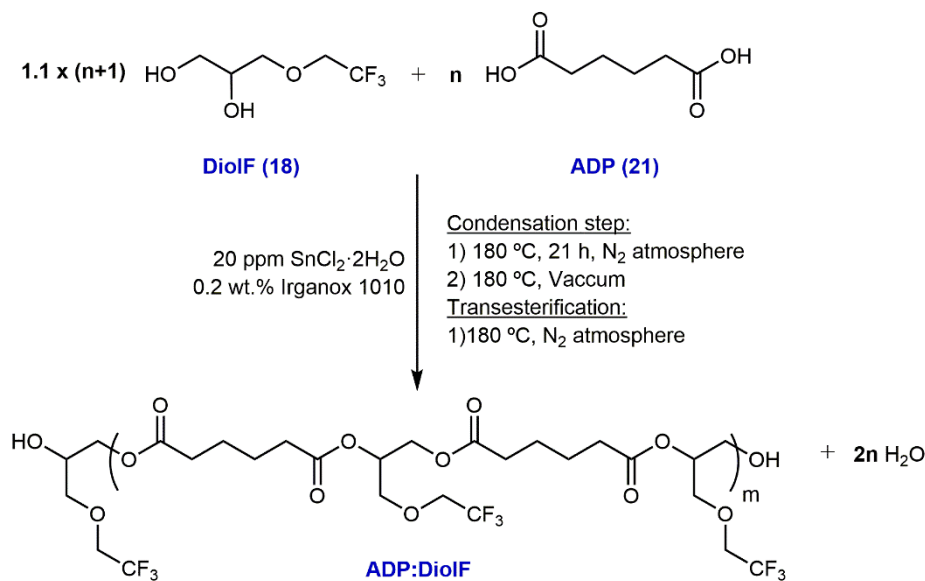
The activity of these compounds may be affected by several factors. Harsh reaction conditions of high temperature and the produced water may deactivate the catalysts. This fact would diminish the reaction rate, but a second catalyst addition could help to decrease the AI faster.

The fluorine content after 40 hours (Figure 5.11.B) was slightly smaller than the initial sample, but it was within a similar range for all the specimens. The decrease was to be expected as reduced pressure was applied to the system.

To summarize, $\text{SnCl}_2 \cdot 2\text{H}_2\text{O}$ displayed the best result at short times. But at larger times, values similar to the uncatalyzed mixture were reached. A second addition of the tin-based catalyst could be necessary if the condensation step reaches stagnation. Moreover, better results might be obtained with diol addition to foster the displacement of the reaction. These results confirmed the suitability of the employed catalyst for the polycondensation reaction.

Targeting a 2000 g/mol **ADP:DiolF**, the reaction between **18** and **21**, with 20 ppm of catalyst in a 400 g scale was carried out (Scheme 5.10). The efficiency of the process was improved by an excess of **DiolF** (10 wt.% respect the stoichiometric ratio) to promote the formation of oligomers at the initial stages of the reaction. Moreover, Irganox 1010, an antioxidant, was

incorporated into the mixture (0.2 wt.%) to prevent degradation of the polymer and reduce its color. This approach resulted in the synthesis of the desired product in approximately 5-6 days.



Scheme 5.10. Modified synthesis of **ADP:DiolF** from compound **18** and **21**.

As expected for linear diols with a pendant chain, the polymer did not crystallize at room temperature, and viscous compounds were obtained. Although the modification in the **ADP:DiolF** synthesis had a lower coloration in comparison with the previous tests, it is more yellowish than traditional aliphatic polyesters.

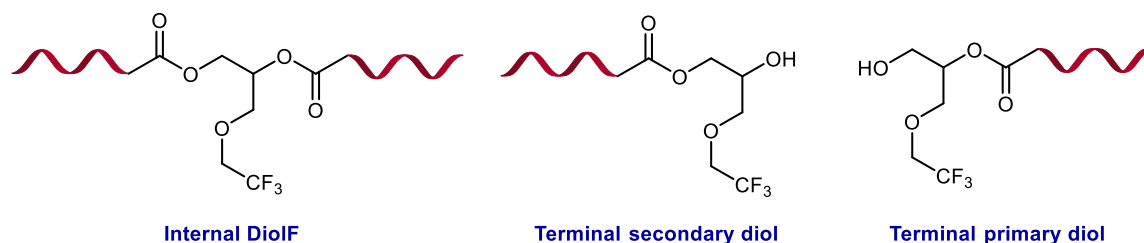
The polyester employed in the synthesis of TPUs (Section 6.3), exhibited the following features. Titration of the samples resulted in a polyester with an AI value of 0.94 mg KOH/g polymer and a M_n of 1990 g/mol after 5 days. Although the concentration of carboxylic acids is higher than the standard values (conventional polyesters reach an AI of 0.5 mg KOH/g polymer in the same conditions), the polyester was accepted to generate TPUs. The fluorine content of this polyester was 21 wt.%, according to the number of diols introduced in the macromolecule.

5.2.1.3. Characterization of ADP:DiolF

5.2.1.3.1. Structural analysis

NMR analysis of **ADP:DiolF** is more complex than other linear aliphatic polymers. One factor that increases the difficulty is the asymmetry of the diol, which generates chemical environments different from common monomers such as **BDO** or **HDO**. The presence of trifluoromethyl groups increases the multiplicity of some signals and modifies the expected chemical shifts. Finally, as was mentioned earlier in the acyl approach, exists three distinct

possibilities to bound **DiolF** to the polyester (Scheme 5.11): diesterified diol (internal), or terminal esterified by the primary alcohol, or by the secondary hydroxyl. All of them will contribute to a mixture of signals according to their content in the mixture. All these aspects lead to complex NMR spectra, which must be studied carefully.



Internal DiolF

Terminal secondary diol

Terminal primary diol

Scheme 5.11. Positions of **DiolF** in the polymer chain.

5.2.1.3.1.1. ^1H NMR analysis

The recorded spectrum of the produced compound is displayed in Figure 5.12. The ^1H NMR of the synthesized compound exhibit the characteristic signals of the adipic fragment at 1.63 ppm and 2.34 ppm.

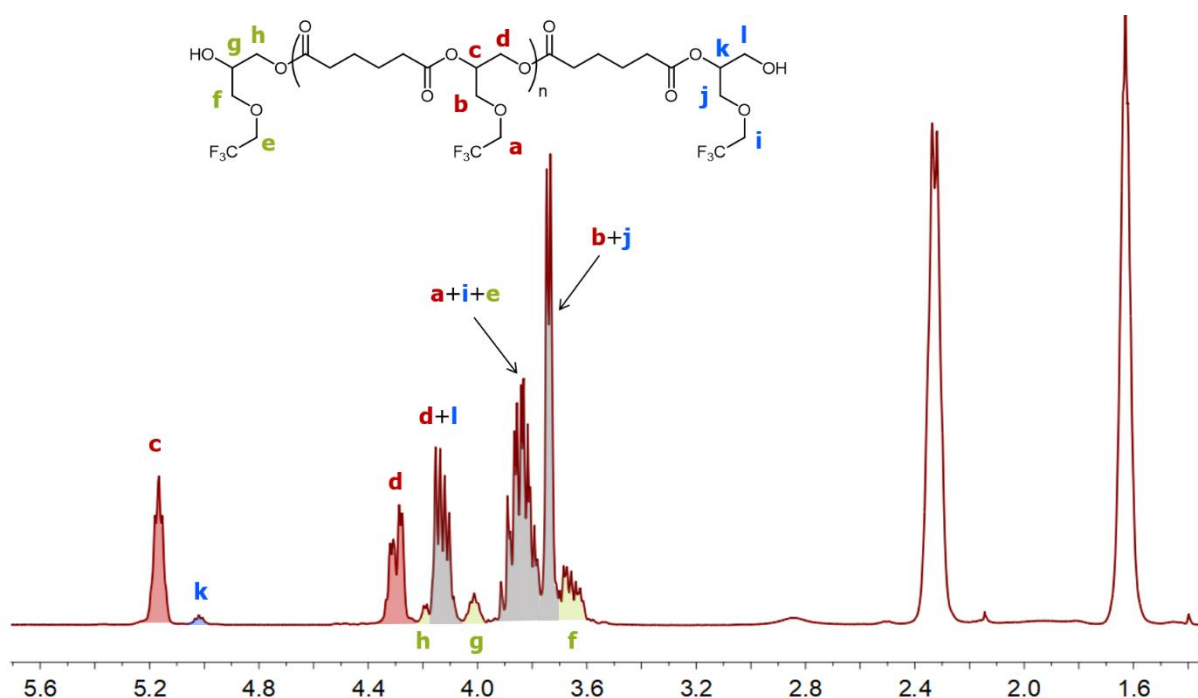


Figure 5.12. ^1H NMR (250 MHz) spectra of **ADP:DiolF** with a delay time of 10 seconds to ensure quantification. Areas colored in red are attributed exclusively to protons of the internal diol. Areas colored in green are assigned to the terminal secondary hydroxyl while areas in grey indicate overlapped signals from different positions. Solvent: CDCl_3 .

The rest of the peaks are ascribed to the diol in its diverse positions in the polymer. The assignment of each hydrogen takes importance to identify those distinctive signals that allow

the calculation of the OHI number. Although most of the protons are overlapped in the same region of the spectra (3.6-4.4 ppm), two multiplets at low field (δ_{H} 5.17 ppm and δ_{H} 5.02 ppm) are easily integrable. They correspond to the methine group of the internal alcohol (-OCH H -CH₂-O, **c**) and terminal primary diol (-OCH H -CH₂-OH, **k**), respectively. However, contrary to **ADP:HDO-8F** or **ADP:HDO**, there is not a single signal corresponding to the terminal alcohol, but two. The terminal secondary diol exhibits the analog system (HOCH H -CH₂-O, **g**) at higher fields (δ_{H} 4.01 ppm), consequence of the shielding of the hydroxyl in comparison with the ester moiety. The ratio between the terminal secondary and primary alcohols for an **ADP:DiolF** with $M_n \approx 2000$ is 4:1, indicating the higher reactivity of the former under the tested conditions.

The identification of these three signals allows the calculation of the OHI number by end-group analysis. The obtained M_n values agree with those obtained by titration. However, the low intensity of the terminal moieties in addition to the overlap of the **g** signal at the first stages of the reaction discourage the use of this technique to quantify the length of the polymer.

5.2.1.3.1.2. $^{13}\text{C}\{^1\text{H}\}$ NMR analysis

The complexity of the synthesized compounds is also observed on the $^{13}\text{C}\{^1\text{H}\}$ NMR spectrum (Figure 5.13), in which exists an elevated number of peaks with different intensities and even multiplicity in those carbons close to fluorine.

At the end of the reaction, no carboxylic signal is displayed on the carbonyl regions between 170 ppm and 180 ppm, signposting the consumption of the monomer. Moreover, the presence of two peaks with similar intensity at 172.9 ppm and 172.6 ppm reflects two chemical environments of the internal ester moieties. The former corresponds to the carbonyl formed with a secondary alcohol (-CH-O CO , **a**), while the latter is consistent with a primary (-CH₂-O CO , **b**). Nevertheless, the visualization of the terminal esters depends on the degree of polymerization. Only at the early stages of the condensation, both peaks are clearly observed, but as the chain length of the polymer grew, the concentration of terminal diols decreases. Owing to the proportion among the secondary and the primary ($\sim 1:4$), only the predominant is observed in polymers with M_n around 2000 g/mol (HO-CH-CH₂-O CO , **c**).

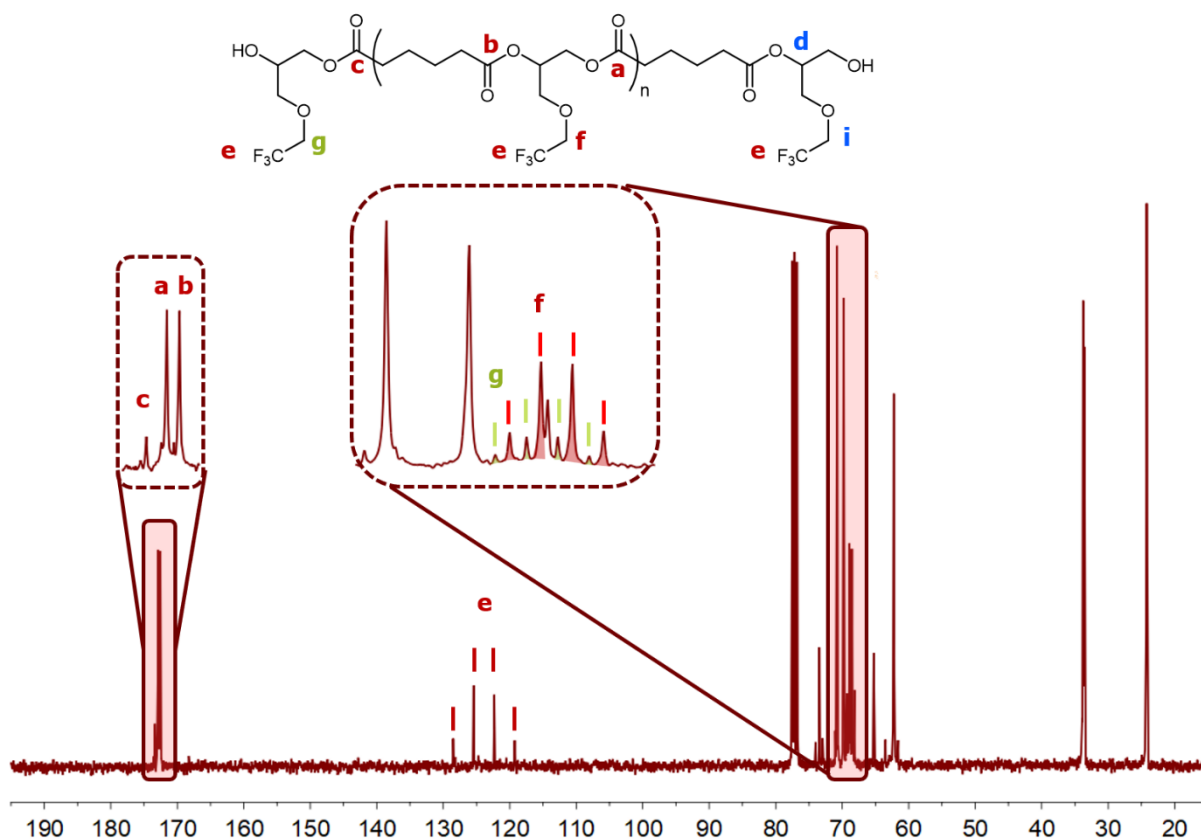


Figure 5.13. $^{13}\text{C}\{^1\text{H}\}$ NMR spectra (90.56 MHz) of **ADP:DiolF**. Enlarged areas are embedded in dashed line squares without considering the scale. Solvent: CDCl_3 .

Resulting from the coupling of the three fluorine with different carbon atoms, quadruplets are depicted in the spectrum. The high electronegativity of fluorine causes the deshielding of the carbon atoms and the corresponding downfield shifts. Trifluoromethyl carbon (**e**) displays a quadruplet with a coupling constant within the common range of $-\text{CF}_3$ moieties ($^1J_{\text{C-F}} = 279.8$ Hz). This fragment is independent of the position of the alcohol in the chain, as only one signal is observed. However, the vicinal methylene is sensitive to the terminal or inner location of **DiolF**, thus displaying different chemical shifts and intensities (Figure 5.13, embedded region). Owing to the elevated number of internal diols, the quadruplet centered at 68.7 ppm exhibit the major intensity ($\text{CF}_3\text{-CH}_2\text{-O-}$, $^2J_{\text{C-F}} = 34.2$ Hz, **f**). As in the carboxylate carbon, only the terminal primary ester is depicted at 69.0 ppm ($\text{CF}_3\text{-CH}_2\text{-O-}$, $^2J_{\text{C-F}} = 34.2$ Hz, **g**) while **i** is not observed under the tested conditions. However, other peaks arising from both terminal diols, are detected with an intensity similar to the one found through the ^1H NMR spectroscopy.

5.2.1.3.1.3. FTIR analysis

The ATR-FTIR spectrum of **ADP:DiolF** is shown in Figure 5.14 in the wavenumber range of 4000-600 cm^{-1} . The low intensity of the hydroxyl stretching vibration signposts the high conversion of the monomers in the polycondensation reaction.

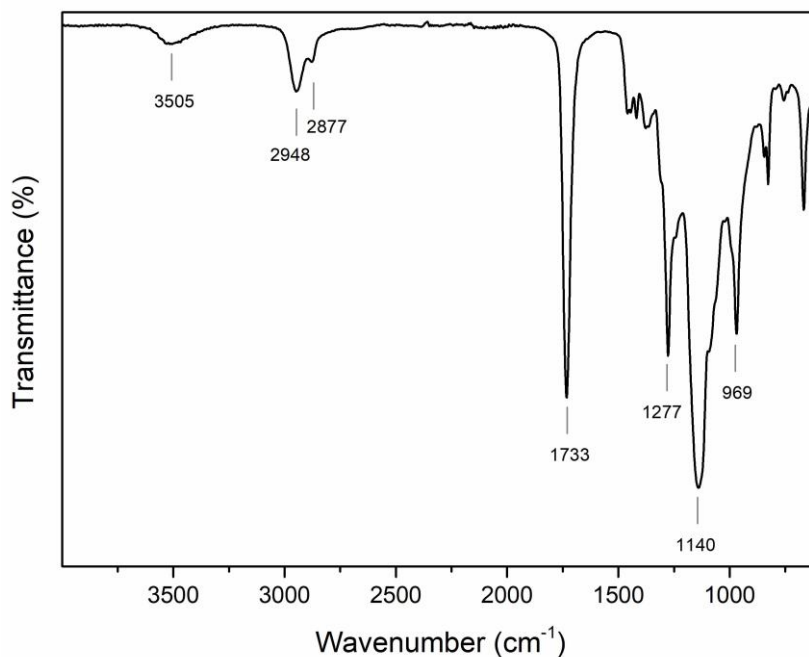


Figure 5.14. Infrared spectrum of **ADP:DiolF**.

The spectrum displays the expected absorptions for a polyester containing a hydrogenated segment like **ADP**. At 2948 cm^{-1} and 2877 cm^{-1} arise the asymmetric and symmetric stretching of the methylene group and at 1733 cm^{-1} , the C=O stretching band of the ester. The inductive effect of **DiolF** causes a shift toward a higher wavenumber compared to the previously synthesized **ADP:HDO** (1726 cm^{-1}). However, the more intense bands of the spectrum overlap the fingerprint region. The 1277 cm^{-1} and 969 cm^{-1} bands are ascribed to the asymmetric and symmetric C-O-C stretching. The vibration centered at 1140 cm^{-1} is attributed to the C-O-C stretching, but the small shoulder that is observed at lower wavenumbers corresponds to the C-F stretching.

5.2.1.3.1.4. Thermal Analysis

ADP:DiolF was analyzed by DSC to unravel the thermal behavior of the sample under a N_2 atmosphere with a heating rate of 10 $^{\circ}\text{C}/\text{min}$ (Figure 5.15 and Table 5.4). Sample was scanned

between -70 °C and 200 °C. The first melting of the sample is omitted and only the second scan is displayed on the following thermogram to avoid the thermal history of the polymer.

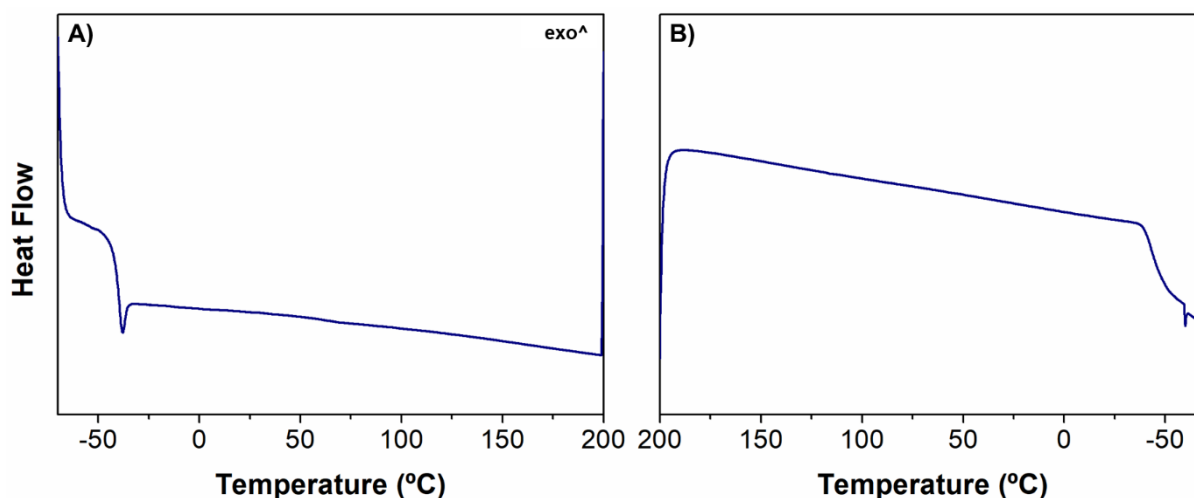


Figure 5.15. DSC thermogram of **ADP:DiolF**. A) the second heating scan and B) the first cooling scan.

Table 5.4. DSC data of **ADP:DiolF**.

ADP:DiolF	
wt. % F	21.0
T_g (°C) ^{[a][b]}	-39.7

^[a] T_g was determined at the inflection point of the shift.

^[b] Transition was captured in the second heating scan at 10 °C/min.

The polyol is a dense liquid at room temperature, so it is expected that no melting nor crystallization processes were observed, signposting the high amorphous stage of the studied polymer. The only observable transition corresponds to the T_g at around -40 °C, but it overlaps with an endotherm hysteresis peak in the second heating scan. This enthalpic relaxation is consequence of the residual strain of the rapid cooling process.

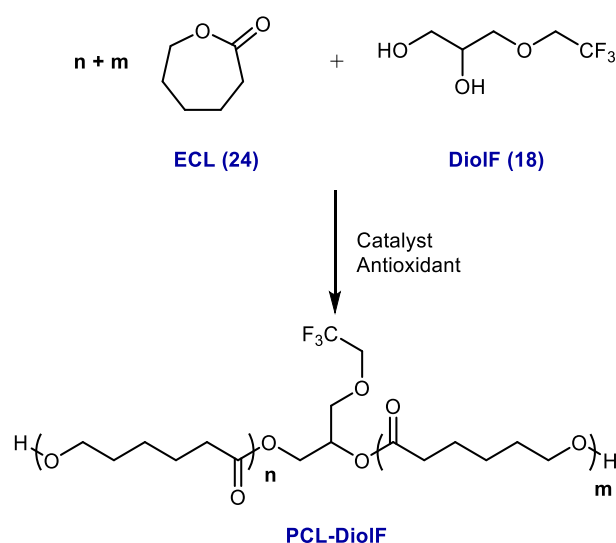
5.3. Synthesis of PCL-DiolF by Ring Opening Polymerization approach

Biodegradable materials have arisen a great interest in the last years towards a greener production and their excellent applications in medical fields.^{[18][19][20]} Because of that, PCLs have been one of the selected polyols to be essayed. In addition, they are comparable with other polyadipates as they are also linear polyesters with similar thermal behavior and semi-crystallinity. Therefore, PCLs and linear polyesters are good candidates to form compatible blends.

Lubrizol is a well-established company in the field of PCL-based TPUs and possesses patented methodologies to produce these polyols. Owing to confidentiality reasons, the detailed process of PCL synthesis cannot be disclosed hereafter.

The purpose of this section is to synthesize **PCL-DioIF**, a PCL initiated with **DioIF 18** through the melt-phase polymerization of **ECL (24)**. In this project, the ROP process is carried out in bulk without solvents involving a tin catalyst. The employed catalyst is sold by common chemical suppliers as a compound easy-to-handle and soluble in organic solvents. It is reported that the catalyst possesses a good activity toward ROP of caprolactones with alcohols.

PCL-DioIF was synthesized by the addition of the required quantity of pre-dried **DioIF** over **24** along with the catalyst and antioxidant (Scheme 5.12). Owing to the polymer nature, only one diol monomer is incorporated into the structure, greatly reducing the fluorine content of the polymer. The aimed M_n was 2000 g/mol, and in this case, the synthesizes were carried out at 1800 g scale. **PCL-DioIF** was easily produced without an additional purification process. However, it exhibits a slightly light-yellow appearance.



Scheme 5.12. General synthesis of **PCL-DioIF**.

For comparative purposes, the non-fluorinated analog of **DioIF** was considered to generate the non-fluorinated equivalent PCL. Its synthesis was attempted, but poor yields were obtained even at a small scale. Buying the monomer was also deemed, but a price of €6700 /kg of product according to Sigma-Aldrich catalog, ruled out its use. Therefore, **PCL-DioIF** features are compared with a commercially available non-fluorinated polymer, **PCL-BDO**.

5.3.1. Characterization of PCL-DiolF and PCL-BDO

Employing the same methodology, **PCL-BDO** of 2000 g/mol (Figure 5.16) was synthesized by Lubrizol with **BDO** as initiator. Both polymers are solids at room temperature but, the fluorinated PCL has a waxy texture.



Figure 5.16. Structure of **PCL-BDO**.

5.3.1.1. Structural analysis

5.3.1.1.1. ^1H NMR analysis

^1H NMR spectra of the two polyols in CDCl_3 are shown in Figure 5.17. As could be expected, the PCL spectra are dominated by peaks assigned to the opened **ECL** fragment owing to being the most repetitive unit in the polymers. The low intensity of the peaks attributed to the initiator is caused by its reduced content in the mixture. Moreover, the diesterified **BDO** is an aliphatic compound with peaks that overlap those of the opened lactone. Therefore, in **PCL-BDO**'s spectrum is not possible to discern the peaks of the initiator from the rest of the polymer (Figure 5.17. top). In contrast, in **PCL-DiolF** spectrum, the signals associated with the initiator can be distinguished from the signals from the opened **ECL** (green squared area in Figure 5.17. bottom). As expected, the multiplicity and chemical shift of the diesterified initiator are equal to those of **Ac₂DiolF**. Signals of the closed **ECL** ring are absent in both spectra, indicating an almost complete monomer conversion.

Correspondingly to the polyester, the polyols' M_n can be calculated by means of end-group analysis (See detail in 9.5.3). According to the integration values of the ^1H NMR spectra, the M_n of **PCL-DiolF** employed in Section 6.2 corresponded to 2215 g/mol, while the M_n of **PCL-BDO** is 2021 g/mol. The content of fluorine estimated for the **PCL-DiolF** sample was 2.9 wt.% of fluorine.

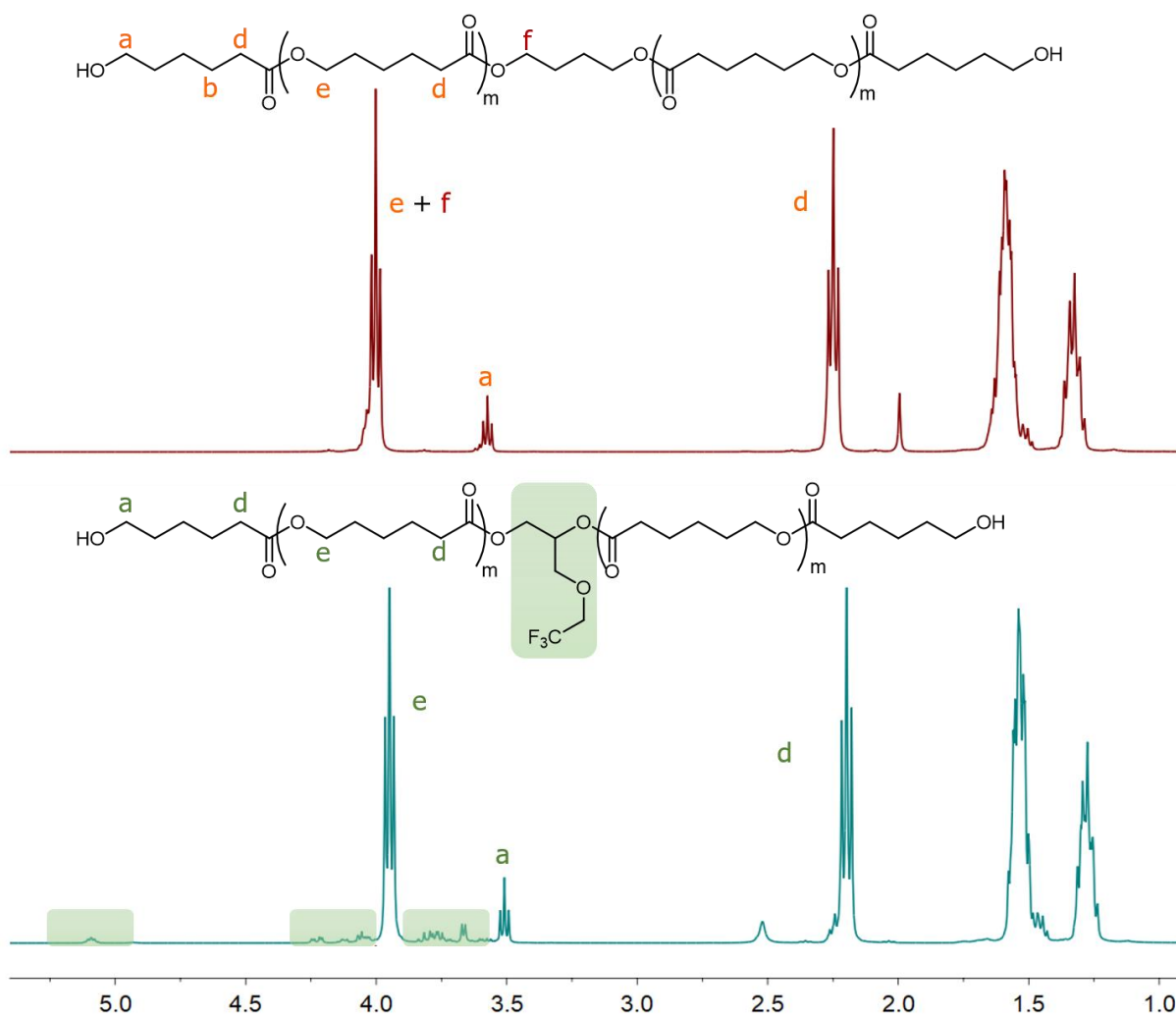


Figure 5.17. ¹H NMR spectra (400 MHz) recorded with a delay time of 10 seconds. Displayed letters correspond to the assignment of the most relevant protons of **PCL-BDO** (top) and **PCL-DioIF** (bottom). Solvent: CDCl₃.

5.3.1.1.2. ¹³C{¹H} NMR analysis

Room temperature ¹³C{¹H} NMR spectra of **PCL-DioIF** and **PCL-BDO** in CDCl₃ are shown in Figure 5.18. No peaks from the **ECL** appeared in any of the spectra, confirming the high conversion of the monomer.

Owing to **DioIF** asymmetry and its fluorinated pendant chain, carbon peaks of the diesterified compound are shifted to lower fields (between 65 and 75 ppm in the bottom spectrum). Conversely, **BDO**, as a linear aliphatic alcohol, displays the corresponding carbon signals nearer to those of the opened lactone at the upfield regions. In particular, the O-CH₂- of **BDO**,

assigned to the letter **e** on the spectra, had very similar chemical shift to the O-CH₂- coming from the opened **ECL** (letter **c** in the spectrum).

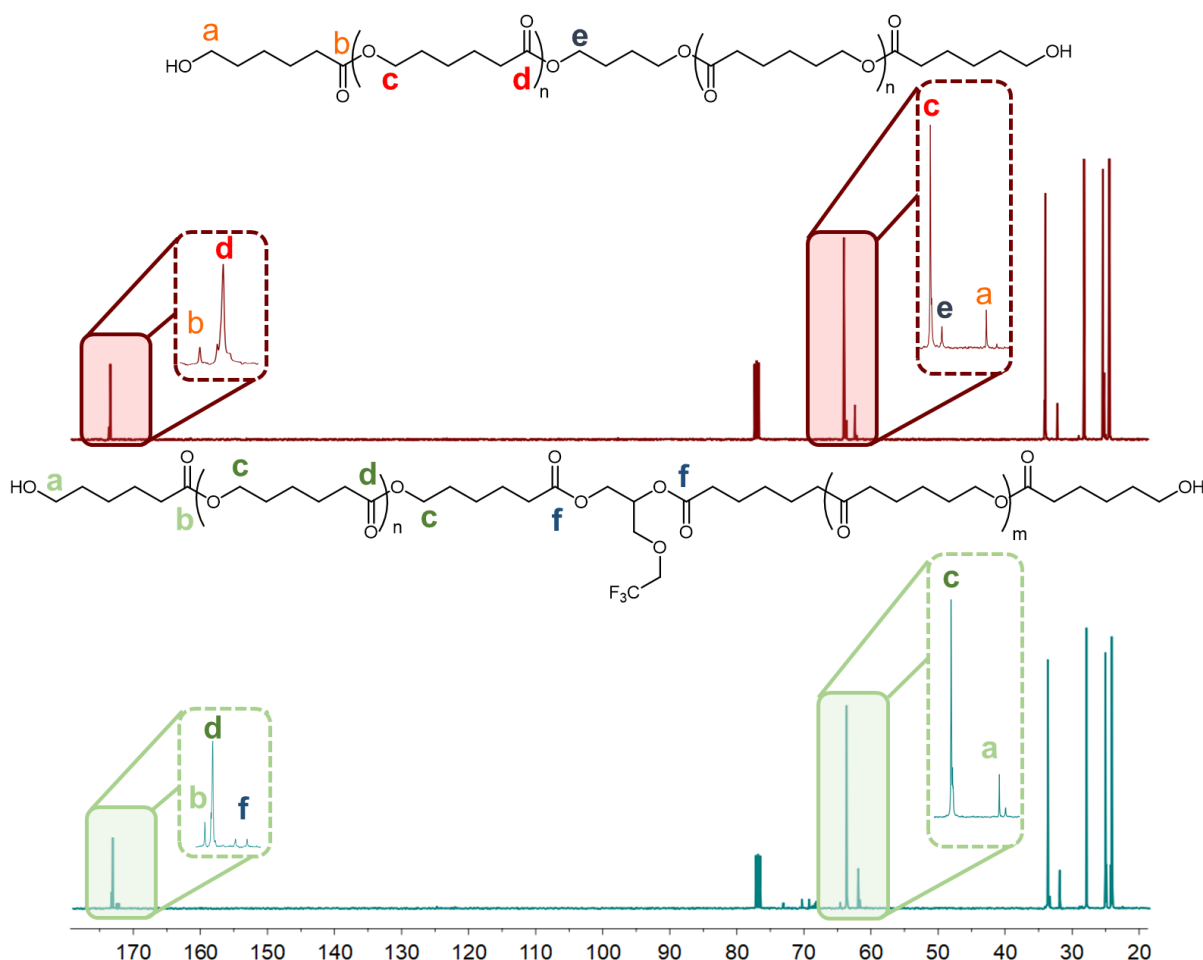


Figure 5.18. ¹³C{¹H} NMR spectra (100.61 MHz) of **PCL-BDO** (top) and **PCL-DioIF** (bottom). Significant areas are enlarged in dashed line squares. Solvent: CDCl₃.

Although ¹³C{¹H} NMR spectroscopy is not a quantitative analysis *per se*, it is sensitive to the concentration of the components, which in this case explains the low intensity of the initiator peaks. Moreover, this reduction of the intensity is also observed in the terminal fragments of the opened **ECL**, in comparison with the inner segment. Likewise as the previous polymers, the carbonyl signals are distinguishable, depending on the position of the moiety on the chain. The carbonyl signal of the terminal lactones (**b**) is slightly more deshielded than the peak ascribed to the internal moiety (**d**). Furthermore, the fluorinated PCL displays two other signals (**f**) in the carbonyl region of **PCL-DioIF** spectrum (Figure 5.18, embedded square), with similar intensity between them. These two peaks arise from the esters produced by the esterification reaction of **DioIF**'s hydroxyls.

5.3.1.1.3. FTIR analysis

Both FTIR spectra of **PCL-DioIF** and **PCL-BDO** are compared in Figure 5.19, exhibiting highly similar results among them, and with other **ECL**-based polymers.^[21] The absorptions bands are proportional to the times that the functional groups befall within the molecule. Therefore, and as a consequence of the low concentration of initiator in contrast to the **ECL**, the bands ascribed to the diols are not discerned in the spectra.

Other significant signals exhibited in the spectra are the two peaks at 2942 cm^{-1} and 2863 cm^{-1} ascribed to the asymmetric and symmetric C-H stretching vibration of the hydrocarbon chains and the strong bands associated with the carbonyl stretching of the esters at 1721 cm^{-1} in both PCLs. Bands in the range between $1600\text{--}600\text{ cm}^{-1}$ are considered as the fingerprint of the compounds. They are attributed to the absorption of the skeletal structure, which is practically identical for both compounds as was expected for polymers with equally repetitive units.

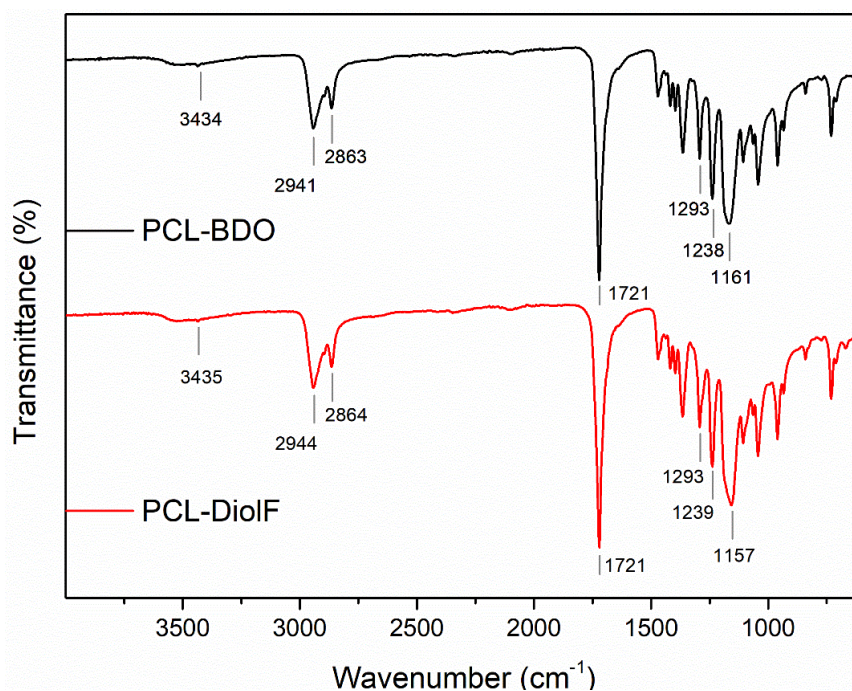


Figure 5.19. Stacked Infrared spectra of **PCL-BDO** (top) and **PCL-DioIF** (bottom).

5.3.1.1.4. Thermal Analysis

Figure 5.20 and Table 5.5 display the DSC data from both PCLs recorded in a range temperature range between -70 to $200\text{ }^{\circ}\text{C}$ with a heating rate of $10\text{ }^{\circ}\text{C}/\text{min}$. Only the second heating scan is illustrated in the following figure, to omit the thermal history of the materials.

The recorded thermograms of the synthesized PCLs exhibit melting and crystallization processes, confirming the formation of semi-crystalline polymers. Although PCLs usually have a T_g around -60 °C, no transition is detected in any of the DSC measurements in the studied temperature range.

Likewise to the behavior of the **ADP:HDO** and **ADP:HDO-8F**, the studied PCLs exhibited a reorganization process while heating the samples, evidenced by the overlapping of the melting peaks in Figure 5.20.A. For **PCL-BDO**, the onset of the melting appeared around 36 °C, while the fluorinated compound had a narrower melting at slightly higher temperatures. Although **PCL-DioIF** seems to have more perfect crystals, the number of those is higher in the fluorine-free PCL as it is depicted by the larger enthalpy value.

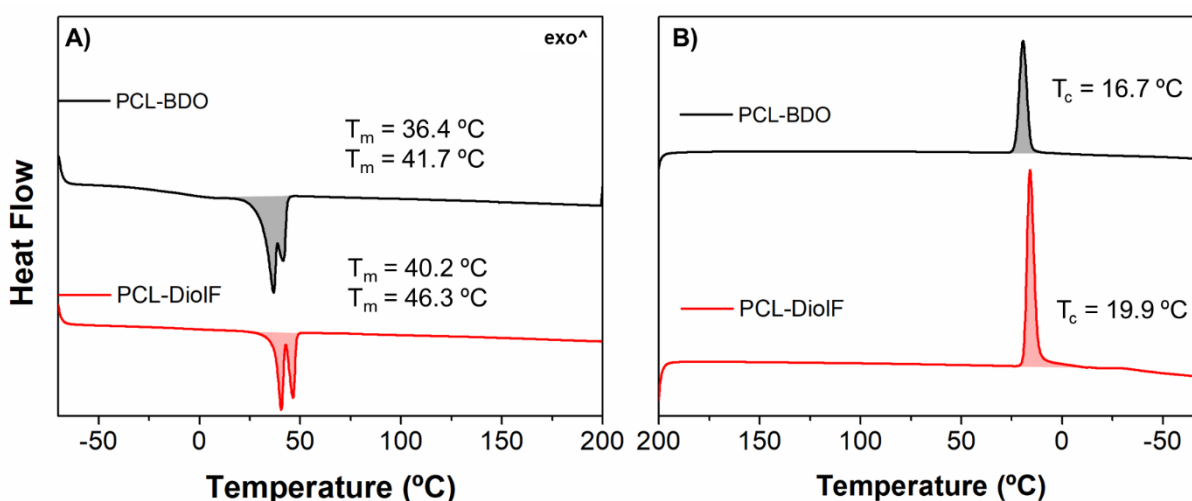


Figure 5.20. DSC thermograms of **PCL-BDO** (black line) and **PCL-DioIF** (red line). A) Second heating process and B) first cooling process. Shaded areas indicate regions used to determine the corresponding processes.

Table 5.5. DSC data of both compounds.

	PCL-BDO	PCL-DioIF
wt. % F	0	2.9
T_g (°C) ^[a]	--	--
T_m (°C) ^[a]	36.4 41.7	40.2 46.3
ΔH_m° (J/g) ^{[a][b]}	87.0	77.6
T_c (°C)	16.7	19.9
ΔH_c° (J/g)	71.1	74.9

^[a] Transitions were captured in the second heating scan at 10 °C/min.

^[b] Total enthalpy of the endothermic process.

Regarding the crystallization (Figure 5.20.B), only one exotherm peak was detected per compound. The T_c and the associated enthalpy are quite similar for both polymers, suggesting a similar degree of order. The resemblance in both values suggests that the initiator did not interfere in the packing, likely by the segregation of the side chain out of the ordered regions of the polymer.

5.4. Summary and conclusive remarks

Three fluorinated polyesters were produced by three different approaches, two of which effectively incorporate **DiolF**. In addition to these fluorinated polymers, their hydrogenated analogs were also studied. The selected ones were **PCL-BDO**, as the standard polycaprolactone with a M_n of 2000 g/mol and **ADP:HDO** to compare with **ADP:HDO-8F**. Concretely, **ADP:HDO** and **ADP:HDO-8F**, contain the same number of monomers in their chains, but since hydrogens are substituted by fluorine, their M_n values differ.

The reaction between an acyl chloride and a fluorinated diol has been assessed by adapting to a solvent- and base-free methodology. Successful results were accomplished in the generation of the target **ADP:HDO-8F** under mild conditions. The synthesized compound (Figure 5.21) has a M_n around 3300 g/mol and a 43 wt.% fluorine in its structure.

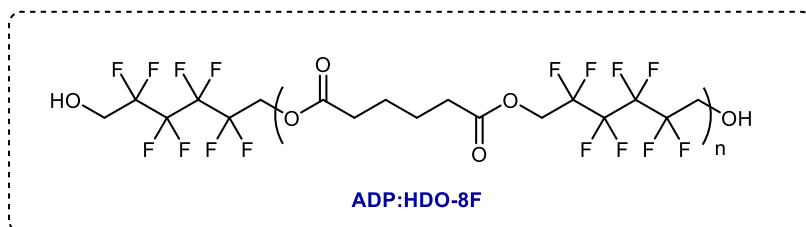


Figure 5.21. Structure of the synthesized **ADP:HDO-8F**.

However, opposite results were obtained for **ADP:DiolF**. Direct reaction of **ADPCI** with the diol under a nitrogen stream was unsuccessful. Some difficulties arose in the reaction between the monomers, which generated carboxylic acids in the mixture and undetermined impurity

Subsequently, the conventional polycondensation reaction was assessed. **ADP** reacted at 180 °C with **DiolF** in the presence of a catalyst and antioxidant. Larger reaction times were required in the polyester synthesis, possibly owing to the lower reactivity of the secondary alcohol. **ADP:DiolF** was obtained with the target M_n (~ 2000 g/mol) and a fluorine content of 21 wt.% (Figure 5.22). This structure possesses a hydrogenated backbone with fluorinated side chains, which generated a remarkably flexible polymer.

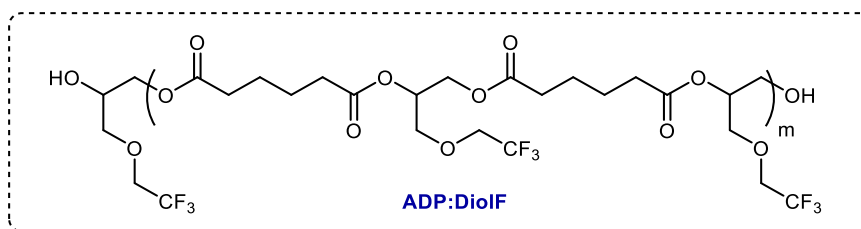


Figure 5.22. Structure of the synthesized **ADP:DiolF**.

Finally, **PCL-DiolF** (Figure 5.23) was also efficiently synthesized following Lubrizol standard methodology, in which **DiolF** was employed as the initiator in the ROP process. The obtained PCL had a M_n of around 2300 g/mol and a fluorine content of 2.9 wt.%. **PCL-DiolF** has the lowest fluorine content among the synthesized polymers as only one fluorinated monomer is incorporated per macromolecule.

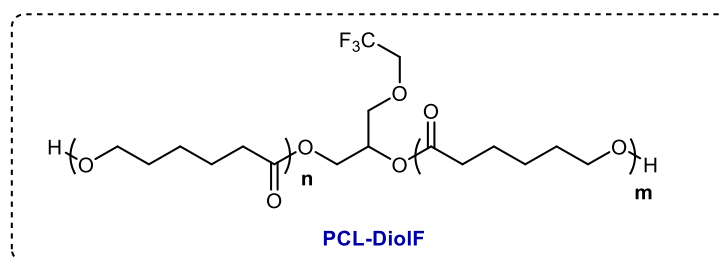


Figure 5.23. Structure of the synthesized **PCL-DiolF**.

Literature

- [1] S. Lingier, R. Szpera, B. Goderis, B. Linclau, F. E. Du Prez, *Polymer (Guildf)*. **2019**, *164*, 134–141.
- [2] T. Hiyama, in *Organofluor. Compd.*, Springer-Verlag Berlin Heidelberg GmbH, **2000**, p. 281.
- [3] F. D. Trischler, J. Hollander, *J. Polym. Sci. Part A-1 Polym. Chem.* **1969**, *7*, 971–975.
- [4] A. E. Mera, R. Griffith, *J. Fluor. Chem.* **1994**, *69*, 151–155.
- [5] S. R. Turner, Y. Liu, in *Polym. Sci. A Compr. Ref.* (Eds.: K. Matyjaszewski, M. Möller), Elsevier B.V., **2012**, pp. 311–331.
- [6] E. N. Peters, in *Appl. Plast. Eng. Handb.* (Ed.: S. Ebnesajjad), Elsevier Inc., **2017**, pp. 3–26.
- [7] R. C. Reis-Nunes, E. Riande, N. C. Chavez, J. Guzmán, *Macromolecules* **1996**, *29*, 7989–7994.
- [8] K. A. Dobina, S.-A. Kamysheva, G. Y. Novikova, I. M. Dolgopol'skii, A. . Marei, T. P. Sarayeva, M. I. Sinaiskaya, *Polym. Sci. U.S.S.R* **1971**, *13*, 1848–1852.
- [9] T. D. Caliskan, I. Luzinov, *J. Polym. Res.* **2020**, *27*, DOI 10.1007/s10965-020-02103-7.
- [10] M. Levi, S. Turri, *J. Polym. Sci. Part A Polym. Chem.* **1998**, *36*, 939–947.
- [11] W. R. Dolbier, in *Guid. to Fluor. NMR Org. Chem.* (Ed.: W.R. Dolbier), John Wiley & Sons Inc., Hoboken, New Jersey, **2016**, pp. 237–272.
- [12] W. R. Dolbier, *Guide to Fluorine NMR for Organic Chemists*, John Wiley & Sons Inc., Honoken, New Jersey, **2009**.
- [13] M. S. Nikolic, J. Djonlagic, *Polym. Degrad. Stab.* **2001**, *74*, 263–270.
- [14] X. Kong, H. Qi, J. M. Curtis, *J. Appl. Polym. Sci.* **2014**, *131*, 4–10.
- [15] S. Gestí, A. Almontassir, M. T. Casas, J. Puiggalí, *Biomacromolecules* **2006**, *7*, 799–808.
- [16] E. Breitmaier, W. Voelter, in *Carbon-13 NMR Spectrosc.*, **1990**, pp. 183–325.
- [17] B. Ren, L. Gan, L. Zhang, N. Yan, H. Dong, *Org. Biomol. Chem.* **2018**, *16*, 5591–5597.
- [18] R. M. Mohamed, K. Yusoh, *Adv. Mater. Res.* **2016**, *1134*, 249–255.
- [19] P. Mandal, R. Shunmugam, *J. Macromol. Sci. Part A* **2020**, *58*, 111–119.
- [20] E. Malikmammadov, T. E. Tanir, A. Kiziltay, V. Hasirci, *J. Biomater. Sci. Polym. Ed.* **2017**, *29*, 863–893.
- [21] K. Phillipson, J. N. Hay, M. J. Jenkins, *Thermochim. Acta* **2014**, *595*, 74–82.
- [22] G. Siegemund, W. Schwertfeger, A. Feiring, B. Smart, F. Behr, H. Vogel, B. McKusick, *Ullmann's Encycl. Ind. Chem.* **2012**, 443–494.

Chapter 6

Fluorinated thermoplastics polyurethanes

This chapter comprises the synthesis of fluorinated TPUs and their respective non-fluorinated analogues. Two different formulations, one based on a polycarbonate (PC) soft segment and another of PCL are assessed. The behavior of these materials is studied by means of thermal, visual, surface and mechanical properties.

6. FLUORINATED TPUs

Perfluorinated polymers are characteristic for their low Surface Free Energy (SFE) values and their chemical, thermal and tribological stability.^{[1][2]} From an industrial perspective, these materials are appealing as they might induce an enhancement of the durability and weatherability of the produced objects. Furthermore, they improve the surface properties by providing outstanding hydrophobicity and oleophobicity.^{[3][4]} Nevertheless, totally perfluorinated chains are usually expensive and difficult to process on their own.

One possible approach to decrease the cost of the produced polymers is to incorporate fluorinated fragments into copolymers to benefit from their advantages. Several authors have reported that the incorporation of the halogen into PUs augmented the anti-adhesion, stain resistance, and weatherability, especially when fluorine atoms are located in side chains.^{[5][6]} The combination of halogenated and hydrogenated compounds with enough SFE difference is proposed to promote the reorganization and the segregation of the fluorinated chains toward the outmost part of the material, consequently minimizing their interfacial energy.^{[7][8][9]} However, the migration of fluorine towards the surface could cause in some systems a reduction of the hardness and some modification of the tribological properties, like friction or wear.^{[10][11]} For that reason, a compromise between the enhancement of the superficial behavior and the variation of the physical properties must be achieved. Moreover, owing to the cost of fluorinated derivatives or monomers, a reduction of their content in the final polymer will be also industrially enticing. Considering all these facts, a decrease in the concentration might foster a reduction in the price without withdrawing the polymer properties. A limited fluorine content on the TPUs might be achieved by two different strategies. Concretely, it could be reached by blending different polymers in the SS of TPUs, being at least one of them fluorinated. The main advantages are the straightforwardness preparation and the possibility to tailor different properties by changing the ratios between the fragments or the molecular

weight of the implicated compounds. The second approach is to design polymers with a low concentration of fluorine in their structure, like PCLs, that only would incorporate the halogen in the initiator.

Ideally, the main objective is to synthesis TPUs with enough fluorine to saturate only the outermost region of the material and thereby, enhancing especially the surface properties, without altering to great extent the bulk properties or increasing the price (Figure 6.1). An improvement of the final properties with small amounts of this element might be economically and practically viable to produce new materials at an industrial scale.

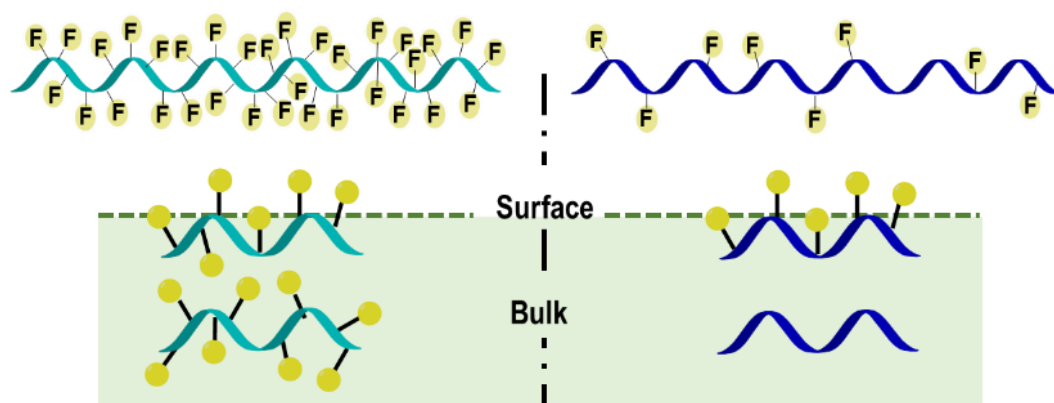


Figure 6.1. Schematic representation of an standard perfluorinated material (left) and the target fluorinated material (right).

6.1. General information

Previous to start with the results and discussion of this chapter, it is worth mentioning again, that the experimental work of this manuscript has been developed in collaboration with Lubrizol. Owing to confidentially reasons, all the elaborated work during this thesis is not detailed hereafter.

Two different formulations with low content of fluorine were carefully evaluated in this section. The building blocks involved in the TPU synthesis are typically one of the key factors to tune the final properties of the materials. Therefore, bearing in mind the desired surface and tribological properties, the employed reagents were carefully selected.

Aromatic diisocyanates are widely used in the TPUs industry, but aliphatic counterparts offer biocompatibility, higher resistance to hydrolysis, and superior ultraviolet and thermal stability.^[12] In addition, the degradation products of their urethanes consist of non-toxic amines, as opposed to aromatic carbamates. In accounts of SFE, compounds containing

methylene moieties decrease to a significant degree the wettability of the material compared to aromatic groups.^[13] As a bonus for certain applications, when aliphatic diisocyanates are used in low % HS, the produced TPUs are prone to be transparent materials. Therefore, the use of aliphatic diisocyanate as **HDI** is preferred to **MDI** or **TDI** in this project.

As a rule of thumb, polyester-based TPUs provide resistance to oils and solvents, and good weatherability and mechanical properties.^{[14][15]} Because of that, previously synthesized polyols (**PCL-DioIF**, **ADP-DioIF**, **ADP:HDO-8F**, and their respective non-fluorinated analogs) were exploited through a single SS formulation or co-polymerized with another polymer as a blend in the SS.

If required, some additives are incorporated in commercial polymers formulation. An additive referred to as *W* was used to prepare some TPUs in this project. Even though fluorinated TPUs did not require it, some of the hydrogenated polymers could not be properly processed without its presence.

Each formulation comprises its own features in terms of % HS, chain extenders, and polyols, which are described in detail in the following lines. TPUs are named according to the following structure: **A-B-n%-W**, where *A* denotes the major component of the SS, *B* the second constituent, if it is a blended system, and *n%* accounts for the total content of fluorine (wt.%). Finally, *W* corresponds to the presence of the additive *W* on the formulation. For further clarification, TPUs are written in blue.

6.1.1. Synthesis

Considering the industrial viewpoint of this research, all TPUs were produced batchwise by one-shot method. The reaction was carried out in bulk as the avoidance of organic solvents is recommendable for the synthesis of potentially biodegradable polymers and in large-scale productions. To ensure a random polymerization, polyols must be completely melted in a homogeneous phase prior to the addition of the remaining reagents. Therefore, once the polyesters were melted, the corresponding amounts of catalyst, chain extenders, and ultimately isocyanate were incorporated while they were mechanically homogenized. The reaction was completed when the mixture whitened and a single phase with a higher viscosity was obtained. The synthesized TPUs were then poured into teflonated molds and cured for several hours in an oven (See Experimental part 10.3.2 for detailed information). Cured TPUs were unmolded and frozen overnight prior to the shredding (Figure 6.2.A). Further, regrinds were injected in

the form of 8 x 8 cm plaques (Figure 6.2.B). Then, the produced materials were conditioned in a controlled environment for at least 24 hours (23 °C and 55 % humidity) to enable the relaxation of any strain that the plaque may possess after the injection.

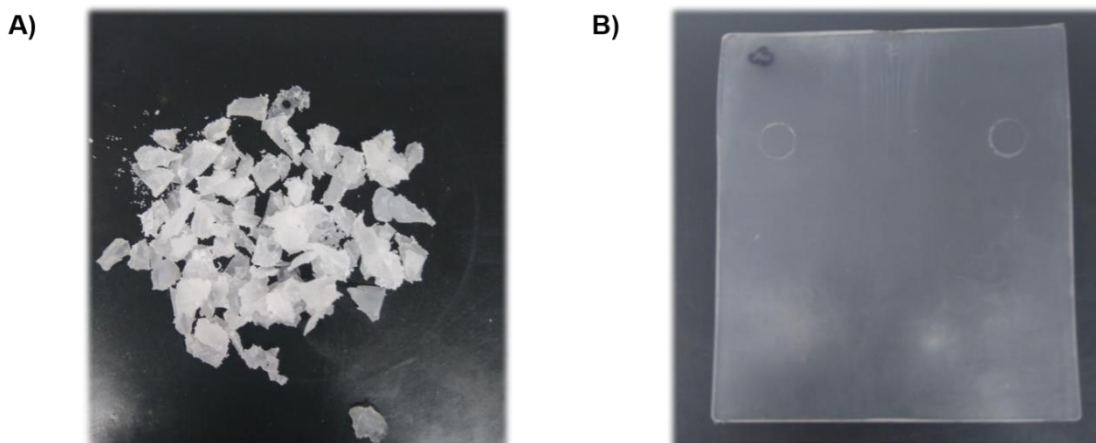


Figure 6.2. Post-synthesis TPU images: A) shredded B) injected plaque.

6.1.2. Characterization

After a brief summary of the synthetic parameters, each compound was initially evaluated with FTIR analysis. When the products were successfully synthesized and the structure was confirmed, an attempt to quantify an extremely subjective factor to the human eye as it is the visual appearance was carried out. TPUs were examined in terms of yellowness index (YI)^[a], transmittance,^[b] and haze.^[c]

The determination of the temperatures in which materials undergo changes is essential to the characterization, processability, and thermal stability of those compounds. Hence, the softening and the melting point of the polymer were obtained through Kofler measurements. However, thermal transitions as the melting, crystallization and glass temperature (T_m , T_c , or T_g , respectively) were gathered by Differential Scanning Calorimetry (DSC) measurements.

The durability of the studied material under certain aggressions might be estimated by the tribological properties. The interaction of the surface of the produced polymers with moving objects was assessed through the abrasion resistance,^[d] and the coefficient of friction (COF)

[a] Measurements carried out according to ASTM E313.^[26]

[b] Measurements carried out according to ASTM D1003.^[27]

[c] Measurements carried out according to ASTM D1003.^[27]

[d] Measurements carried out according to ASTM D5963:15.^[33]

against a counter surface of aluminum.^[e] Moreover, the density^[f] and the hardness^[g] of the synthesized compounds were also displayed.

Ultimately, the performance of these compounds in contact with diverse liquids may mark their possible use as anti-staining materials. To appraise the hydrophobicity, the oleophobicity, and the consequent wettability of those compounds, materials were analyzed with the static water contact angle (WCA) and the SFE.

Altogether, the obtained results determined the feasibility of introducing small percentages of fluorine in TPUs through polyols. Those materials displaying small COF values, high resistance toward wear, and low wettability might be potential candidates for industrial production. Moreover, it is desired for some uses that the materials exhibit transparency and smooth surfaces. Hence, their implementation in automobile pieces or wearable supports, among other applications, will be based on the successful fulfillment of the previous parameters.

^[e] Measurements carried out according to ASTM D1894.^[34]

^[f] Measurements carried out according to ASTM D792.^[31]

^[g] Measurements carried out according to ISO 868:2003.^[32]

6.2. Single-component PCL-based TPU family

The following section focuses on the synthesis and characterization of TPUs comprising a single-component SS. For that purpose, two of the previously described semicrystalline polyols, which might exhibit good tensile stress and excellent UV stability, were examined: the linear **PCL-BDO** and the fluorinated **PCL-DioIF**. The M_n of the last polyol restricts the maximum fluorine concentration that can be reached in the TPU owing to the incorporation of only one mol of **DioIF** per PCL chain. In addition to the other participating reagents, the chemical structure of the employed polyols is displayed in Figure 6.3.

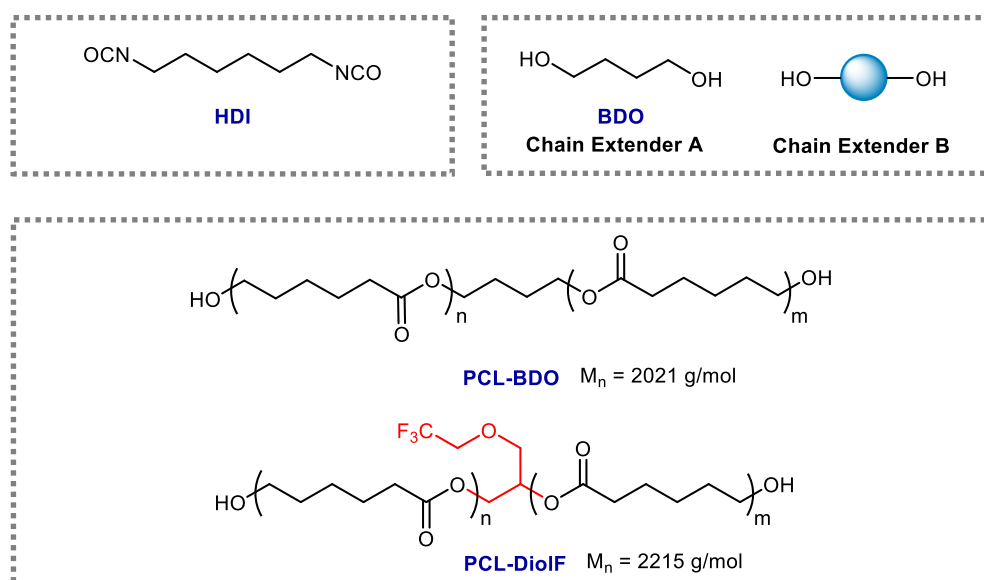


Figure 6.3. Employed reagent for the synthesis of single-component PCL-based TPUs.

One of the main features of all TPUs is the physical crosslink produced by the crystalline HS domains. It is achieved when chains are arranged with regularity, thereby creating intermolecular interactions between the carbamate moieties. However, the presence of side chains in the HS, especially if they are bulky, causes imperfections on the packing, inhibiting the interaction among the chains and thus, reducing the crystallinity of the segment.^[16] As counterpart, they might also enhance characteristics such as flexibility and chain mobility of the SS, fostering the segregation of the low SFE components to the surface. Because of that, in addition to **HDI**, the assessed formulation employed a mixture of chain extenders. The **chain extender A** corresponds to **BDO** while the second **chain extender B** (undisclosed structure owing to confidential reasons) might reduce the packing capacity of the system. Additionally, it has been previously reported that the incorporation of a co-chain extender in

this type of formulation might increase its transparency. Especially in those compounds in which **BDO** is used as a chain extender.^{[17][18]}

Hence, three TPUs were synthesized at a 750 g scale by the one-shot method according to the features listed in Table 6.1. Systems comprising **PCL-BDO** were synthesized as the hydrogenated reference compounds. Concretely, to determine the effect of the additive in the formulation, **PCL-BDO-0%-W** and **PCL-BDO-0%** were produced differing in the incorporation of W. When **PCL-DiolF** was employed as a single polyol, it resulted in **PCL-DiolF-2%**, meaning a final halogen content in the TPU of 2 wt.%.

Table 6.1. Summary of synthesized TPUs with a single-component SS.

	PCL-BDO-0%-W	PCL-BDO-0%	PCL-DiolF-2%
wt.% F	0	0	2
Soft Segment	PCL-BDO	PCL-BDO	PCL-DiolF
Additive W	Yes	No	No
% HS	20.2	20.2	20.3
NCO/OH	1.0	1.0	1.0
Weight (g)	756	750	750
MFI (g/ 10 min) ^[a]	9.5	40.9	28.7

^[a] Tested conditions: 190 °C and 2.16 kg.

Owing to the insolubility of the products in common organic solvents, the M_n of the synthesized compounds could not be determined, neither by GPC nor by NMR spectroscopy. However, the MFI values of the samples were within the appropriate range to be injected.

6.2.1. Infrared analysis

The structure of the synthesized TPUs was confirmed by ATR-FTIR spectroscopy between the wavenumber range of 4000 cm^{-1} and 600 cm^{-1} with shredded fragments. The spectra of TPUs with a single-component SS are shown in Figure 6.4, all of them normalized to the most intense peak.

None of the three TPUs exhibited the characteristic band at 2273 cm^{-1} ascribed to the N=C=O stretching absorption, pointing out the complete consumption of the isocyanate group. In addition, the successful formation of urethanes was confirmed by the weak peak close to 3300 cm^{-1} attributed to the N-H stretching absorption.

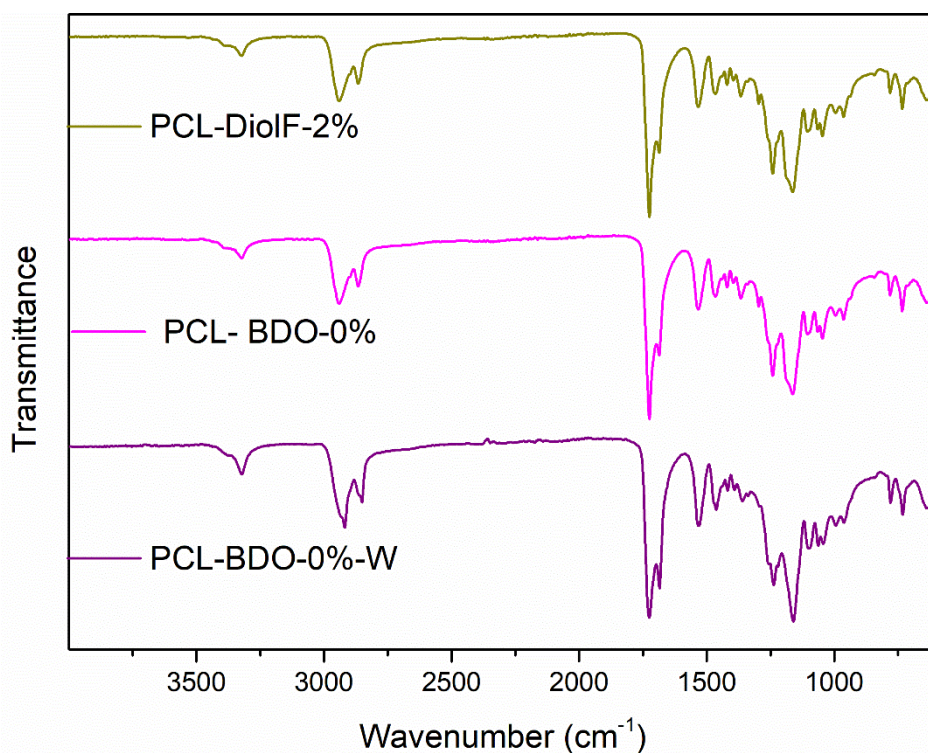


Figure 6.4. Stacked ATR-FTIR spectra of the synthesized PCL-based TPUs with a single-component SS.

The observed absorptions were comparable among the three produced TPUs, signposting a similar polymer structure. Bands located around 2940 and 2865 cm^{-1} were assigned to the asymmetric and symmetric stretching of the CH_2 fragments. The stretching absorption of the $\text{C}=\text{O}$ was depicted at 1723 cm^{-1} and 1685 cm^{-1} . The C-N stretching and N-H in-plane bending absorption of the urethane groups contributed to the peak around 1532 cm^{-1} . The 1463 cm^{-1} peak arose from the methylene in-plane bending vibration. The peak centered at 1240 cm^{-1} overlapped different vibrations associated with C-N stretching, N-H bending, and symmetric CH_2 bending. The strong peak at 1160 cm^{-1} was attributed to the asymmetric C-O-C stretching of the PCL fragment. The absorption peak at 1063 cm^{-1} corresponded to the C-O stretching vibration of the polyol segment. Altogether, results are consistent with other similar PCL-based PUs.^[19] In addition, owing to the small concentration of fluorine in the sample and the frequency at which the CF_3 group or the C-F moiety resonate, no significant peaks were observed at 1350-1100 cm^{-1} or 780-680 cm^{-1} .

The degree of phase segregation between HS and SS in a sample is, by some authors, estimated by examining the acceptor and donor groups involved in hydrogen bonds, starting from the premise that groups partaking in these interactions have their vibration more

restricted and thereby, resonate at lower wavenumbers than free groups. Therefore, they propose FTIR as a practical technique for analyzing the synthesized compounds (Figure 6.5).

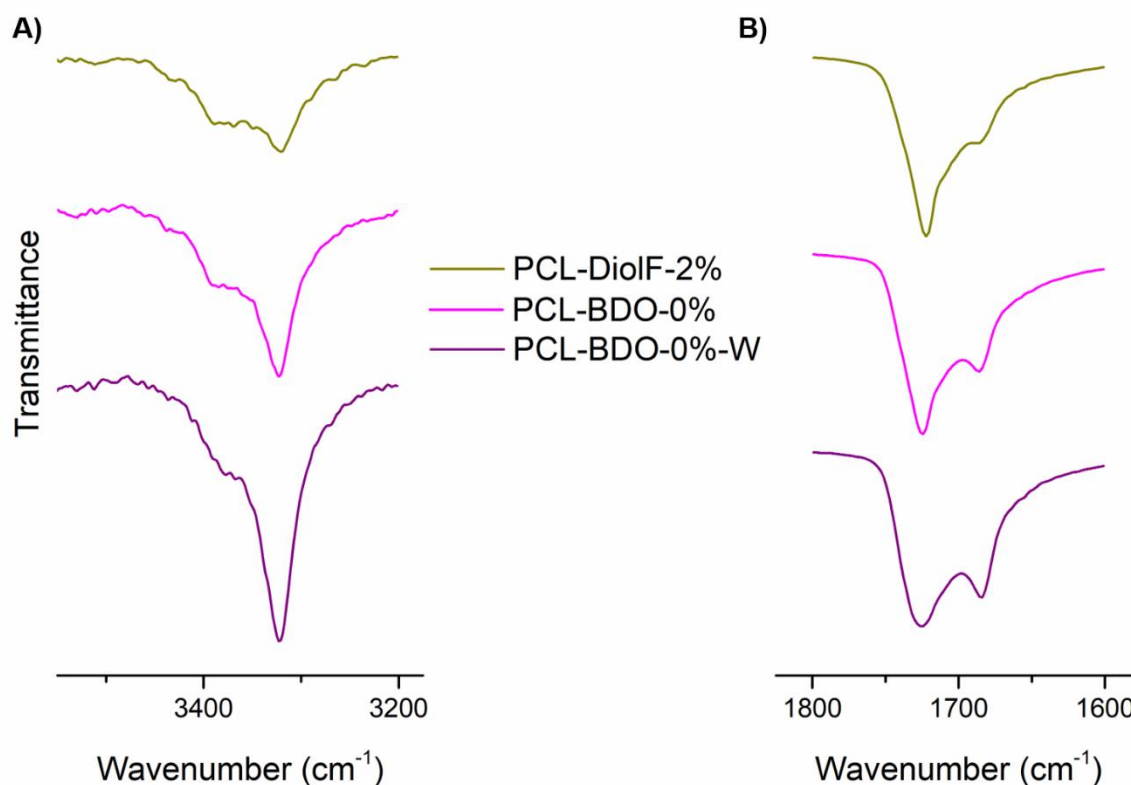


Figure 6.5. Fragmented stacked FTIR spectra of the single-component PCL-based TPUs. A) N-H stretching region ($3550\text{ cm}^{-1} - 3200\text{ cm}^{-1}$). B) C=O stretching region ($1800\text{ cm}^{-1} - 1600\text{ cm}^{-1}$). The plotted intensity of each region is not at the same scale. The transmittance scale was increased in the N-H stretching inset to depict more clearly the region.

The N-H stretching region (Figure 6.5.A, $3550\text{--}3200\text{ cm}^{-1}$) might provide useful information about the hydrogen bonds as urethanes are the only donor group in the samples. In the literature, the peak centered at 3321 cm^{-1} is attributed to the absorption of the N-H linked by hydrogen bonds.^[20] Conversely, the band associated with the non-hydrogen bonded N-H vibration is reported to be centered at $\sim 3445\text{ cm}^{-1}$. Hence, the peak depicted at 3322 cm^{-1} in **PCL-BDO-0%-W** and **PCL-BDO-0%**, and 3320 cm^{-1} in **PCL-DiolF-2%** was attributed to the N-H stretching associated by hydrogen bond (Figure 6.5.A). However, the peak corresponding to free urethane was not observed in the spectra and only a small shoulder appeared on account of the carbonyl's overtone ($\sim 3385\text{--}3380\text{ cm}^{-1}$). Therefore, most of the N-H groups in the TPUs were hydrogen-bonded to a carbonyl, either a urethane or ester group, but no further information could be extracted from this region.

Peaks around the 1700 cm^{-1} region of an FTIR spectrum are attributed to the C=O stretching vibration in the sample. Figure 6.5.B shows the presence of at least two bands overlapping at the same wavelength region. When the three compounds were compared, the ratio of the peaks varied, especially between the benchmark TPUs and **PCL-DiolF-2%**, signposting a different arrangement of the involved groups in the sample. However, there is a considerable controversy in the literature about the assignment of the peaks and how to calculate the degree of hydrogen bonding owing to the coexistence of carbonyl groups. Some authors claimed that the two observed bands are the hydrogen-bonded and free carbonyl group, without giving due consideration to the fact that, on polyester-based TPUs, there are two different types of carbonyl moieties, the carbamate, and the ester.^[21] However, some other authors differentiated the carbonyl stretching from the ester and the urethane and their corresponding hydrogen or non-hydrogen bonded peaks, forcing the deconvolution of the band into four Gaussian distributions to unravel the proportion of each peak.^[22] Usually, the stretching vibration of the ester's carbonyl interacting with a hydrogen donor is centered at 1721 cm^{-1} while the non-interacting moiety vibrates at 1733 cm^{-1} . In the case of the urethane's carbonyls, the hydrogen-bonded absorption is at 1693 cm^{-1} , while the free is at 1709 cm^{-1} .^[23]

From the reported information, additional arguments arise from the established procedure. On the basis that no agreement is reached in the assignation of the bands, and that some authors seem to forget the contribution of esters to the FTIR spectra, concepts as the absorptivity and the concentration of each type of bond are usually omitted on the published papers. Moreover, oppositely to polyether-based TPUs, in which a high degree of hydrogen bonding determines the phase segregation of the HS and SS, in polyester-based systems the hydrogen bond is formed between both the esters of the SS and the urethanes of the HS. Hence, a high number of these interactions might promote the miscibility of the segments, resulting in no straightforward conclusion from the carbonyl region.

6.2.2. Visual behavior

In complex formulations containing numerous components and additives, a recurrent phenomenon is the segregation of some constituents of the mixture to the surface of the material. This process is known as blooming and may modify properties as the visual appearance, the surface behavior, and consequently, the biocompatibility of the material.^[24] It can be observed as an increase in haze and the generation of more matt surfaces. Compounds that produce this effect are mainly non-covalently bounded low- M_w substances, such as

catalysts, residual monomers, or additives.^[25] Hence, their diffusion rate and their residence time on the surface are difficult to define. Additionally, the segregation of these substances can potentially affect the reproducibility of the analyzed parameters.

All TPUs synthesized with the previous formulation exhibited blooming on the plaques, possibly as a result of the diffusion of the free monomers or small **ECL** oligomers. To be able to study the real properties of the prototypes, different approaches to clean the surface were tested. Finally, it was decided to carefully wipe all the samples with a cotton fabric prior to any analyses to remove the exuded substances.

The appearance of the produced plaques is displayed as photographs in Figure 6.6. At naked eye, all compounds are quite transparent and colorless, being **PCL-BDO-0%-W** slightly hazy. Nevertheless, to be able to quantify the visual parameters of the materials, measurements of YI and transparency were carried out (Table 6.2). All analyses were conducted according to the standardized methods with cleaned plaques.



Figure 6.6. Photographs of the injected plaques of the single-component SS TPUs with the UAB logotype underneath.

Table 6.2. Visual properties of PCL-based TPUs with single-component SS.

	PCL-BDO-0%-W	PCL-BDO-0%	PCL-DioIF-2%
wt.% F	0	0	2
Soft Segment	PCL-BDO	PCL-BDO	PCL-DioIF
Additive W	Yes	No	No
Blooming	Yes	Yes	Yes
YI (%) ^[a]	7.72 ± 0.08	7.2 ± 0.2	11.0 ± 0.3
Transmittance (%) ^[b]	83.9 ± 0.8	84.7 ± 0.4	85.4 ± 0.2
Haze (%) ^[b]	57 ± 14	18 ± 4	22 ± 4

^[a] Measurements carried out according to ASTM E313.^[26] Average value of two measurements.

^[b] Measurements carried out according to ASTM D1003.^[27] Average value after six measurements (three points per plaque) at 23 °C.

Injected TPUs plaques exhibited a deviation toward the yellow, displaying **PCL-DioIF-2%** the highest YI's value. It is worth noting that polyol **PCL-DioIF** already evidenced a more significant coloration than the other PCL. Thereby, a YI higher than the rest of TPUs was

expected. Although the obtained values were acceptable, the YI could be reduced by introducing antioxidants and UV stabilizers in the formulation or adjusting the synthesis and injection temperatures.

The degree of crystallinity determines both the transmittance and the haze of a sample. The three TPUs showed similar results in transparency, displaying quite high percentages in transmittance. Conversely, haze presented two different behaviors. Meanwhile, **PCL-BDO-0%** and **PCL-DioIF-2%** exhibited rather similar haze values, both below 30%, **PCL-BDO-0%-W** was a light-diffusing material, which resulted in a cloudy appearance and difficulty to see the object behind the plaque (Figure 6.6). The additive interfered with the light transmission, probably because its refractive index is quite different from the matrix.^[28]

The low haze and high transmittance values suggest that HS and SS are partially miscible, and no crystallites with dimensions similar to the light wavelength were formed. The introduction of fluorine did not alter the transparency of the materials, displaying comparable results. Hence, both **PCL-BDO-0%** and **PCL-DioIF-2%** might be interesting for applications involving transparent materials. However, a residual yellow undertone will remain the color base of the compounds if no additional optimizations are carried out.

6.2.3. Thermal behavior

6.2.3.1. Kofler measurements

All samples were thermally assessed prior to their injection into plaques using Kofler measurements to obtain the approximate values for the injection temperature profiles and evaluate the energy efficiency of the process (Figure 6.7). Considering the industrial point of view, the injection of polymers requires a certain energy, which will be reduced when the difference between the melting point, the temperature at which the material is injected, and the softening point, threshold temperature in which the material could be demolded without deformation, is the smallest. Therefore, the melting and the softening temperatures of the three synthesized TPUs allow an estimation of the energy efficiency to produce them.

Unexpectedly, the softening and melting points of **PCL-BDO-0%-W** were 20 °C and 30 °C higher than **PCL-BDO-0%**. The reason for the appreciable variations in **PCL-BDO-0%-W** temperatures is not straightforward as it may arise either from the difference in TPU's M_n or the additive W. However, TPUs synthesized net, **PCL-BDO-0%** and **PCL-DioIF-2%**,

exhibited similar ranges for their softening and melting. These results suggest that, at least for the injection temperature profile, the substitution of **BDO** by **DioIF** as the initiator in PCL did not produce a significant effect. Nevertheless, the highest efficiency for an injection molding process seems to be obtained in **PCL-BDO-0%**, as the melting and softening points differed by only 12 °C.

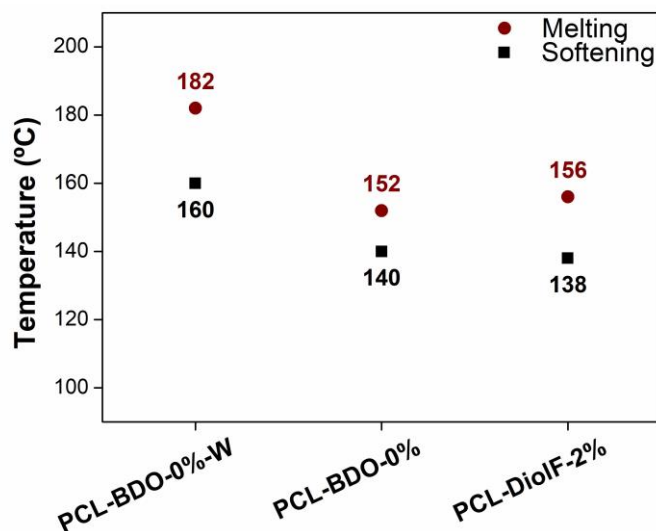


Figure 6.7. Kofler measurements of TPUs with a single-component SS. The uncertainty of the data is ± 2 °C.

6.2.3.2. Differential Scanning Calorimetry

To obtain a more thorough understanding of the thermal properties of the materials, DSC measurements were carried out in the temperature range of -70 °C to 220 °C with a constant heating and cooling rate of 10 °C/min. Results for the three TPUs are illustrated in Figure 6.8 and summarized in detail in Table 6.3. The thermal history of the samples was removed, and only the second heating process is displayed on the reported data.

All three TPUs showed a T_g baseline shift around -53 °C, which is associated with the disruption of the amorphous region of the PCL's SS.^[29] This value is superior to the temperature of the neat polyol owing to the anchoring of the chain ends and the subsequent restriction in mobility.

Two weak endothermic peaks were depicted in all analyzed samples (Figure 6.8.A), but in **PCL-DioIF-2%**, an exotherm peak preceded the two endotherms. The fluorine-containing TPU underwent a cold crystallization process of the SS as temperature increased. Equally to the T_m or the T_c , the cold crystallization temperature (T_{cc}) was determined as the maximum point of the exotherm. This transition was observed at -20.9 °C, indicating that the material

could not reach the maximum crystallization during the cooling process, and the disordered region crystallized from the glassy state upon heating. The existence of this exotherm only on the fluorinated compound points toward the steric hindrance of **DiolF** side chain as a hampering factor for the SS order.

Subsequently, the endotherms displayed in the range of $-10\text{ }^{\circ}\text{C}$ to $50\text{ }^{\circ}\text{C}$ correspond to the melting of the ordered SS while the analogous HS's process occurs at higher temperatures between $64\text{ }^{\circ}\text{C}$ and $150\text{ }^{\circ}\text{C}$. Among the **PCL-BDO** TPUs, similar T_m values were obtained, while the introduction of fluorine decreases in both SS and HS endotherm maximums. Concretely, for the **PCL-DiolF-2%**, the T_m values were approximately $12\text{ }^{\circ}\text{C}$ and $5\text{ }^{\circ}\text{C}$ lower than the respective non-halogenated ones. However, the same behavior is not observed in their enthalpies. In the case of the SS peak, similar to what happens with the temperature, exists a striking decrease of more than 10 J/g on the fluorinated TPU with respect to that of the reference materials. Contrarily, the enthalpies of the HS peak show a slight increase of $2\text{-}4\text{ J/g}$ for **PCL-DiolF-2%**. These data suggest the formation of less ordered SS phases in **PCL-DiolF-2%** while their HS are more abundant, but made out of smaller chain fragments.

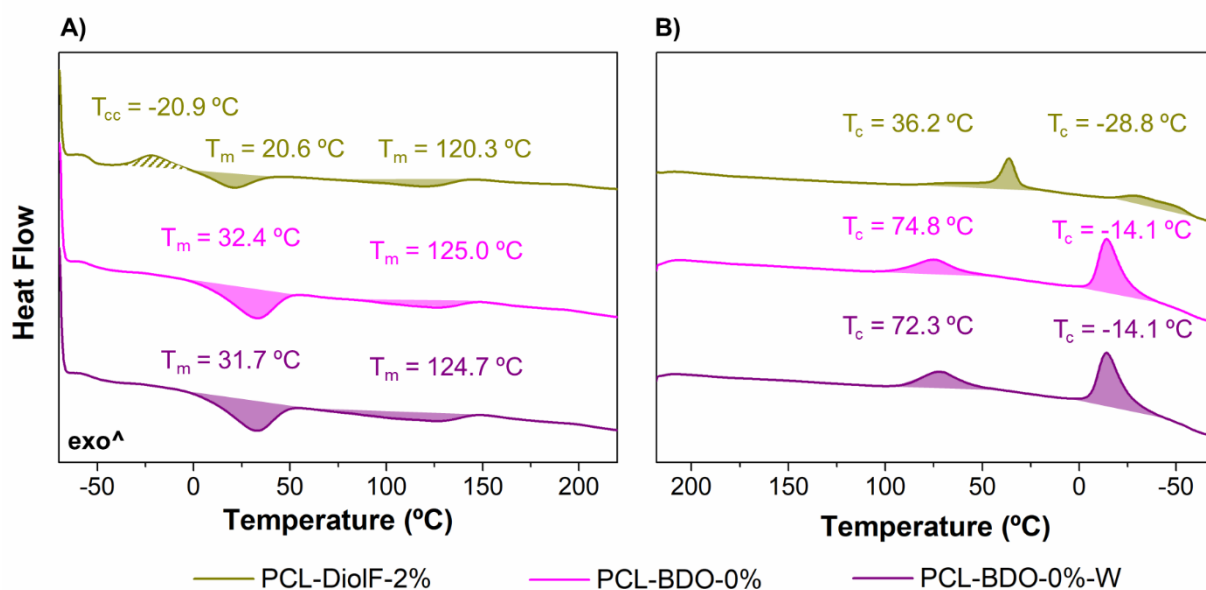


Figure 6.8. DSC thermograms of A) the second heating process and B) the first cooling process. Shaded areas indicate regions used to determine the corresponding processes. The striped areas correspond to the cold crystallization process.

Table 6.3. DSC results of the synthesized TPUs with a single-component SS.

	PCL-BDO-0%-W		PCL-BDO-0%		PCL-DioIF-2%	
wt.% F	0		0		2	
Soft Segment	PCL-BDO		PCL-BDO		PCL-DioIF	
Additive W	Yes		No		No	
T_g (°C) ^{[a][b]}	-53.2		-54.7		-53.0	
T_{cc} (°C) ^[b]	--		--		-20.9	
ΔH_{cc}° (J/g) ^[b]	--		--		5.3	
T_m (°C) ^[b]	31.7	124.7	32.4	125.0	20.6	120.3
ΔH_m° (J/g) ^[b]	20.9	9.5	20.7	7.5	10.1	11.0
T_c (°C)	72.3	-14.1	74.8	14.1	36.2	28.8
ΔH_c° (J/g)	9.2	16.0	10.7	16.8	13.1	2.0

^[a] T_g was recorded at the inflection point of the shift.

^[b] Transitions captured on the second heating scan at 10 °C/min.

Focusing on the cooling process illustrated in Figure 6.8.B, samples based on **PCL-BDO** display two crystallization peaks, a weak exotherm near 73 °C and a narrower one at -14 °C. The former corresponds to the HS crystallization while the endotherm with the lowest temperature belongs to the SS. Although the two peaks are noticed in the cooling process of **PCL-DioIF-2%**, their intensities are the opposite of the reference non-fluorinated polymers. Moreover, the halogenated TPU exhibits a downshift on the T_c values respect the benchmark **PCL-BDO-0%** of 37 °C and 14 °C, following the same trends as their meltings. Likewise also to what happens during their melting, the endothermy of the SS crystallization process is lower for the fluorinated TPU, while that of the HS is higher. This suggests that, under the tested conditions, the crystallization of the **PCL-DioIF** is limited in comparison with that of the non-fluorinated equivalents. As could be expected, the presence of the fluorine chain hinders the SS's crystallization, which is only achieved by cold crystallization when enough energy is provided to the system. The increase in the HS enthalpies could indicate a higher phase segregation of the fluorinated system with regard to the non-fluorinated one, which would lead to the formation of a larger number of HS domains.

The existence of the four transitions (T_{cc} , T_g , T_m , and T_c) confirms that the three TPUs are semi-crystalline polymers with partially ordered segregated phases. Owing to the chemical nature of the polyol which possesses a high number of ester moieties, the three TPUs are prone to exhibit some miscibility between the segments, reducing the ordering of the chains. Moreover, although the structure of **HDI** favors the formation of ordered domains, the mixture co-chain extenders hampers the crystallization of the HS, which leads to low enthalpy values.^[30]

The variation in the melting and crystallization temperatures among the non-halogenated TPUs, **PCL-BDO-0%-W** and **PCL-BDO-0%**, were in the measurement uncertainty (2 °C) range. Therefore, there was no clear evidence that the low concentration of dispersed additive interferes with the packing of the segments. However, the introduction of 2.0 wt.% of fluorine on the TPU disrupts the structure of both HS and SS. The branched chain decreases the crystallinity of **PCL-DioIF-2%**'s SS. The reason behind that behavior is more likely the steric hindrance of the side chain than the presence of fluorine on the compound. This tangling chain might hamper the formation of the appropriate interactions, among the polyester chains. However, the increase in the HS enthalpies of the fluorinated polymer could indicate that the presence of fluorine causes an increase in the phase segregation.

6.2.4. Tribological behavior

The tribological properties of the synthesized TPUs were studied with the injected plaques and are summarized in Figure 6.9 and Figure 6.10. The displayed data was obtained from plaques cleaned with the previously described method and analyzed following the standardized procedures at a controlled and constant temperature (23 °C).^{[31][32][33][34]}

Shore A Hardness and density values are within the standard ranges for formulated TPUs. Among the analyzed samples, **PCL-DioIF-2%** exhibited a slightly higher density than the other two TPUs, indicating that worse packing of the former is overcome by the presence of fluorine (Figure 6.9.A). In terms of hardness (Figure 6.9.B), which might be related to the elastic modulus and the viscoelastic properties of the materials, the smallest resistance to indentation was as well displayed by **PCL-DioIF-2%**.

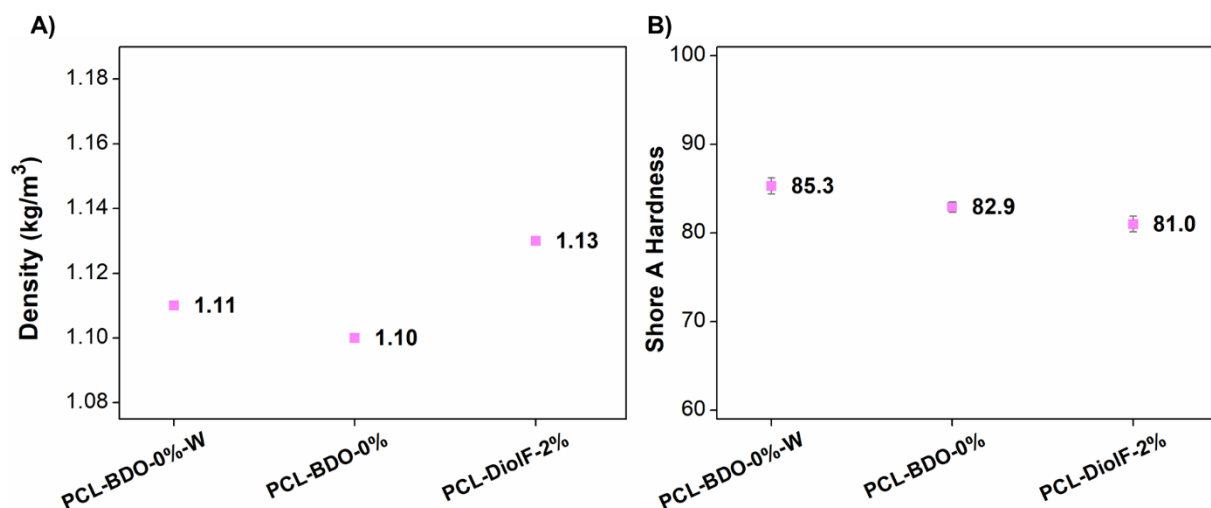


Figure 6.9. Single-component SS TPUs results of A) density (average value of four measurements carried out according to ASTM D792)^[31] and B) Shore A Hardness (average value of ten measurements carried out according to ISO 868).^[32] Bars represent the standard deviation of the results.

Abrasion resistance is defined as the capacity of a material to resist the tear and wear against an abradant usually harder than the tested compound and hereinafter it was quantified as the volume loss in cubic millimeters in standard abrasion conditions. Results of this parameter (Figure 6.10.A) were remarkably similar between the **PCL-BDO-0%-W** and **PCL-BDO-0%**, indicating that the additive did not affect this parameter. However, the **PCL-DiolF-2%**'s volume loss was three-fold that of the non-fluorinated samples, indicating that the introduction of **DiolF** as initiator fostered swifter wear of the material against a hard abradant sheet. This indicates that the introduction of a side chain into the structure decreases the cohesion strength of the material, as could be expected owing to a poorer SS chain packing.

For all TPUs, measurements of coefficient of friction (COF) were carried out with the same load over an aluminum plane. The static (μ_s) and dynamic (μ_d) COF under dry sliding conditions are shown in Figure 6.10.B. Respect the reference compound **PCL-BDO-0%**, the μ_s increases nearly 63 % in **PCL-BDO-0%-W** and 40 % in **PCL-DiolF-2%**. In the case of the μ_d , the increment corresponds to 87 % and 47 %, respectively. However, the rise of the observed standard deviation in **PCL-BDO-0%-W** hindered the drawing of proper conclusions on the materials, as the proper data can be assured. The incorporation of the additive W could increase the heterogeneity of the surface, resulting in a higher standard deviation of the measurement.

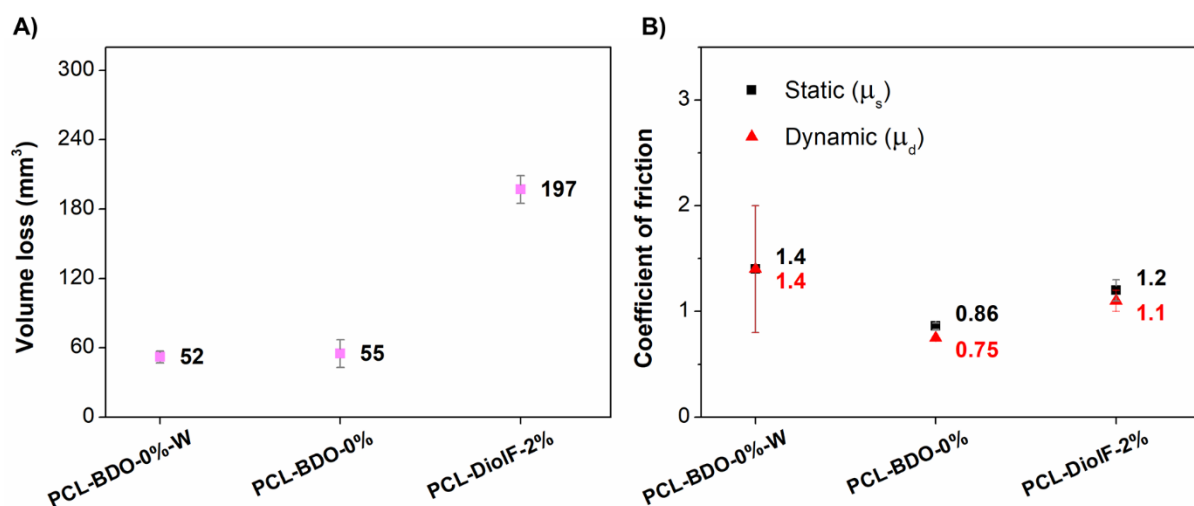


Figure 6.10. Single-component SS TPUs results of A) abrasion resistance (average value of three replicates carried out according to ASTM D5963:15)^[33] and B) friction against an aluminum surface (average value of three cleaned plaques measured carried out according to ASTM D1894).^[34] For comparison purposes, all the analyses were carried out with the same tested conditions (normal load and sliding speed) in the same apparatus. Bars represent the standard deviation of the results.

The introduction of fluorine as side chains was thought to create a lubricant-like outermost layer and thus, decrease the adhesion to an opposite counter face when the surface was enriched in said halogen. Therefore, friction should be reduced by the lower interaction and when a force was applied, the decrease in the shearing of the chains might prevent the overheating and loss of material. However, gathered results suggested that the migration of fluorine to the surface has not been achieved, as no improvement on the friction or the abrasion resistance was obtained. Furthermore, substituting a PCL initiated by a linear alcohol, such as **BDO**, by one initiated by **DioIF** caused the decrease of the cohesion within the material.^[35] The tail allocated within the material impedes a correct chain packing, which causes an easier tear out of the polymer chains in contact with the abradant and higher resistance against an aluminum surface as the polymer chains do not slide smoothly.

6.2.5. Surface behavior: Wettability

Ultimately, the behavior of the TPUs with different liquids was evaluated to unravel their wettability, hydrophobicity, and oleophobicity. For that purpose, analysis of the static water contact (WCA) and the subsequent Surface Free Energy (SFE) were carried out after the removal of the blooming. The final measurement results are summarized in Figure 6.11. Plaques were injected in the same mold with the same rugosity profile; thus, all the systems were considered comparable for the analyses. Based on the assumption that plaques were

chemically inert, rigid, and non-porous, the physical and chemical defects were neglected in the study.

Results revealed two distinct behaviors between water and polymers. **PCL-BDO-0%-W** lies on the edge of hydrophobicity with a 92° WCA. In contrast, **PCL-BDO-0%** and **PCL-DioIF-2%** measurements exposed a hydrophilic surface, both compounds displaying WCA values below 90°. Hence, the additive W reduced the interaction between the surface of the material and the liquid. The absence of any improvement in WCA of the fluorinated polymer stresses the lack of fluorine enrichment of the surface as its behavior mirrors that of **PCL-BDO-0%**.

Commonly, materials that exhibit hydrophobic and oleophobic behavior are associated with low SFE. In this research, the SFE was calculated based on Owens, Wendt, Rabel, and Kaelble (OWRK) model,^{[36][37]} which considers both polar and non-polar interactions between the solid material and various liquids with distinct polarities. Instead of carrying out this estimation with two solvents, the analysis was based on three liquids (water, ethylene glycol, and DMF). None of the tested solvents dissolved, swelled, or altered the appearance of the surface of the plaques.

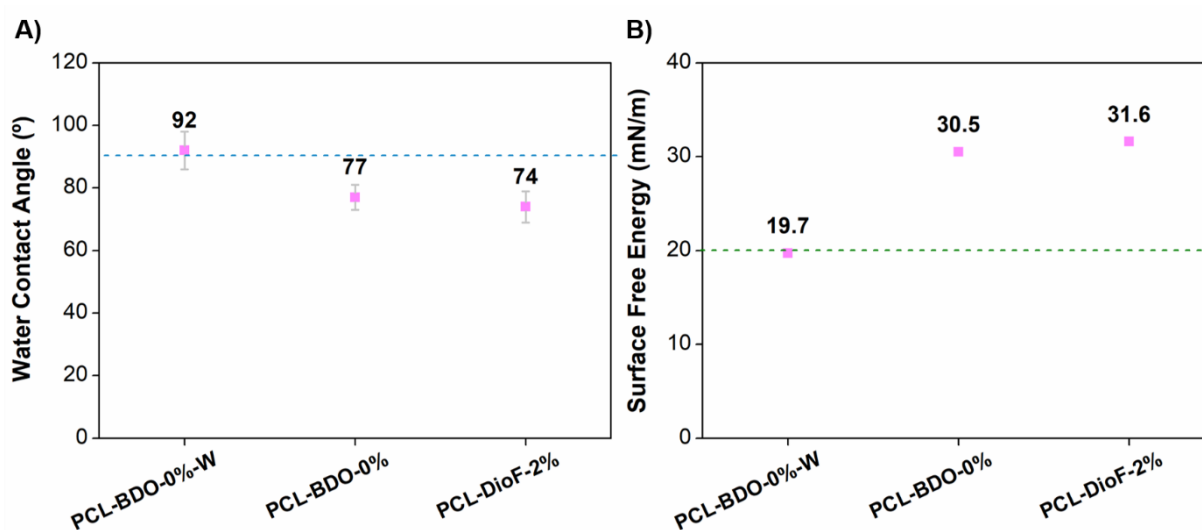


Figure 6.11. Results of the three single-component SS TPUs in A) WCA (16 measurements on two cleaned plaques)) and B) SFE (eight measurements on two cleaned plaques with water, ethylene glycol, and DMF). The blue dashed line indicates the 90° threshold in WCA and the green dashed line denotes the benchmark of PTFE's SFE. Bars represent the standard deviation of the results.

As far as SFE is concerned, **PCL-BDO-0%** and **PCL-DioIF-2%**, exhibited values superior to 30 mN/m. Altogether, the assessed formulation displayed lower SFE results than other hydrophobic polymers such as polyethylene (35.7 mN/m) and poly(ethylene terephthalate)

(44.6 mN/m)^[38] but, they were far from the PTFE value (20.0 mN/m).^[38] Contrarily, the effect of the additive was clearly observed in this analysis. The SFE value of **PCL-BDO-0%-W** after wiping the TPU surface reached 19.7 mN/m. This low figure implied that liquids would wet this polymer to a lesser extent than those TPUs synthesized without the additive.

In systems as complex as TPUs, where polar and apolar segments co-exist, it is interesting to determine the contribution of each component to the SFE. Just as a benchmark, the dispersive and polar components of PTFE correspond to 18.4 mN/m and 1.6 mN/m (92% and 8% of the total SFE, respectively), and for polydimethylsiloxane (PDMS), the reported values are 19.0 mN/m and 0.8 mN/m (96 % and 4%).^[38] Although both parameters contribute to the total SFE, and thus they shall be minimized, the most relevant to consider in the produced TPUs is the polar component, owing to the high number of carbonyl groups. The principal component in all the SFE estimations of the three studied TPUs (Figure 6.12) corresponded to the dispersive, ranging from 14 mN/m to 19.9 mN/m, whereas the polar oscillated between 5.7 mN/m and 11.9 mN/m.

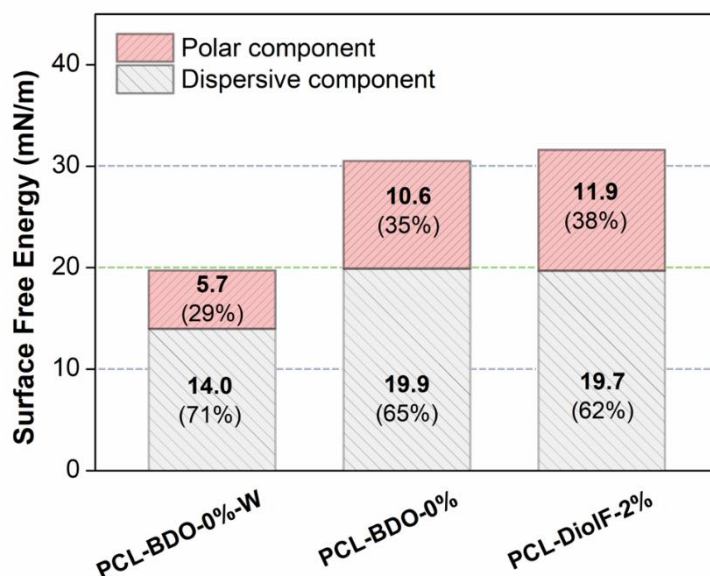


Figure 6.12. SFE decomposed in values and percentage of dispersive and polar components measured in the cleaned surfaces. The green dashed line represents the PTFE's SFE value.

PCL-BDO-0%-W reached an SFE value close to that of PTFE, although the distribution between the components was quite different from the perfluorinated polymer. The introduction of additive *W* not only decreased the exposure of the polar groups and the corresponding decline on the SFE value, but also, reduced the dispersive contribution. Hence, this additive provided both hydrophobicity and oleophobicity properties to the surface. Although good

results seemed to be achievable by introducing this additive to the formulation, its durability is not yet certain as it is not chemically bound to the polymer matrix.

The polar and dispersive components of **PCL-BDO-0%** and **PCL-DioIF-2** displayed comparable values, with the latter being the predominant in both TPUs. The polar groups on the surface are accessible, thereby fostering interactions with polar liquids. Therefore, solvents such as water or short alcohols would spread over these two materials to a greater extent than on **PCL-BDO-0%-W**.

In short, the attempts to develop a TPU containing a low fluorine content to maintain the mechanical properties of the polymer while enabling the segregation of fluorine toward the surface have not been successful. The introduction of **PCL-DioIF** as polyol seems to interfere with the TPU packing and thus, affects the thermal and tribological stability of the material. The surface properties were similar to those of the reference compound, which implies that trifluoromethyl groups were not concentrated at the outmost region of the material. It is unclear if fluorine is homogeneously distributed within the bulk or on the contrary, if just the addition of 2 wt.% of the halogen was not enough to cause a change on the surface.

Therefore, **PCL-DioIF-2%** did not fulfill the expectation. Its high interaction with water and oils discourages its application in anti-staining materials. Moreover, the exhibited increase in friction and wear might decrease the durability of the produced objects.

6.3. Blended PCL-based TPU family

The gathered data of the single-component SS TPUs suggested a uniform distribution of the halogen in the polymer matrix. To evaluate if one mol of **DiolF** per polyol is insufficient to uncoil the chains and saturate the outmost layer of the polymer, an alternative approach was sought. The apparent lack of positive results has led us to assess if a notable increase in the fluorine content might promote its enrichment into the surface and the subsequent enhancement of hydrophobicity, oleophobicity, and friction.

Owing to the chemical nature of the **PCL-DiolF**, the fluorine concentration could only be increased by shortening the **PCL** chain length, which may lead to a decline in the mechanical and thermal properties of the material.^{[39][40]} Therefore the blend of two polyols in the SS was assessed by combining **PCL-BDO** with various quantities of the fluorinated **ADP:DiolF** to modulate the halogen content. This polyether provides a higher local concentration of the halogen as each **ADP:DiolF** chain contributes with about 22 mols of fluorine, instead of the 3 mol procured through **PCL-DiolF**.

The selected diisocyanate remained **HDI**, while the mixture of co-chain extenders **A** and **B** continued to be used. The combination of the three reagents and the low HS content in the formulation had already proven to hamper the formation of large-size crystalline domains, producing transparent materials. For a more comprehensive overview of the chemical structures of the employed reagents see Figure 6.13.

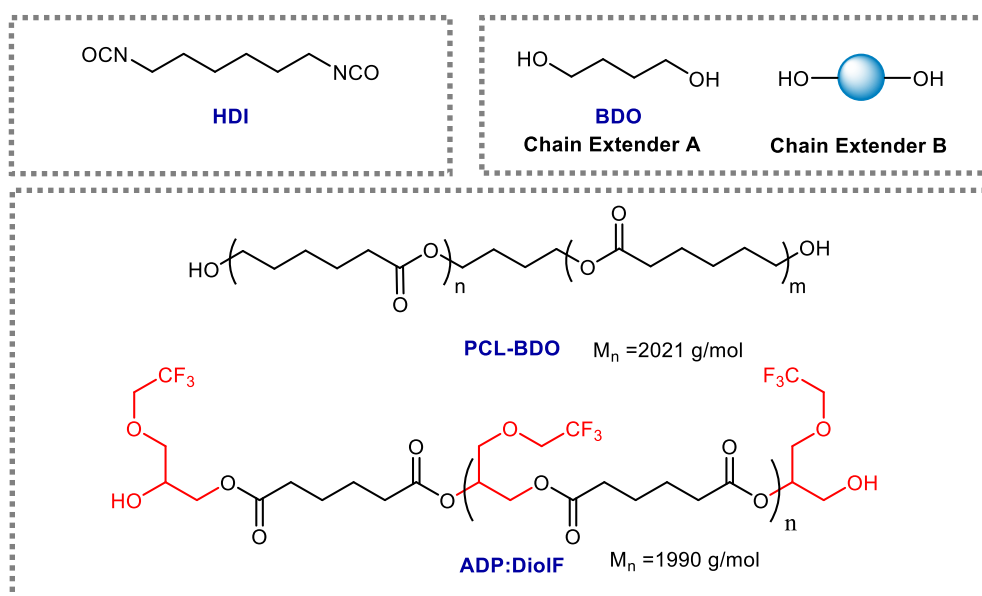


Figure 6.13. Structure of the employed monomers for the synthesis of blended PCL-based TPUs.

To gauge the role of fluorine, three relatively low halogen concentrations have been tested, starting with a similar quantity of halogen to the **PCL-DioIF-2%**. Therefore, **PCL-ADP:DioIF-1.9%**, which contained 1.9 wt.% of fluorine, **PCL-ADP:DioIF-3.7%** and **PCL-ADP:DioIF-7.0%** were synthesized with 3.7 wt.% and 7.0 wt.% of halogen, respectively. The three TPUs comprised blended SS and were compared to **PCL-BDO-0%** as reference material.

The three polymers were produced following the same procedure and formulation as the previous compounds, but at a 500 g scale. The TPUs were devised by replacing mols of **PCL-BDO** by mols of **ADP:DioIF** until reaching the target fluorine content. An outline of the synthetic parameters is exposed in Table. 6.4.

Table 6.4. Summary of synthesized TPUs with a blended SS.

	PCL-BDO-0%	PCL-ADP:DioIF-1.9%	PCL-ADP:DioIF-3.7%	PCL-ADP:DioIF-7.0%
wt.% F	0	1.9	3.7	7.0
Soft Segment	PCL-BDO	PCL BDO + ADP:DioIF	PCL BDO+ ADP:DioIF	PCL-BDO + ADP:DioIF
Additive W	No	No	No	No
% HS	20.2	20.3	20.3	20.3
NCO/OH	1.0	1.01	1.015	1.015
Weight (g)	750	500	500	500
MFI (g/ 10 min) ^[a]	40.9	30.1	52.1	6.4

^[a] Tested conditions: 190 °C and 2.16 kg.

Prior to the injection, the compounds were analyzed by MFI. All the synthesized TPUs exhibited values in the appropriate range to flow through the injection screw and were correctly unmolded.

6.3.1. Infrared analysis

The ATR-FTIR spectra of the fluorinated TPUs, in addition to the reference **PCL-BDO-0%**, are displayed in Figure 6.14. To confirm their structure according to their characteristic functional groups, all spectra were recorded in the range from 4000 cm⁻¹ to 600 cm⁻¹ and normalized to the most intense band. The synthesis of the TPUs was confirmed by the absence of any peaks at 2277 cm⁻¹ arising from the characteristic N=C=O stretching vibration of the **HDI** and the presence of the N-H stretching absorption at 3320 cm⁻¹. Hence, the reaction between the isocyanate groups and the hydroxyl moieties of the reagents was completed.

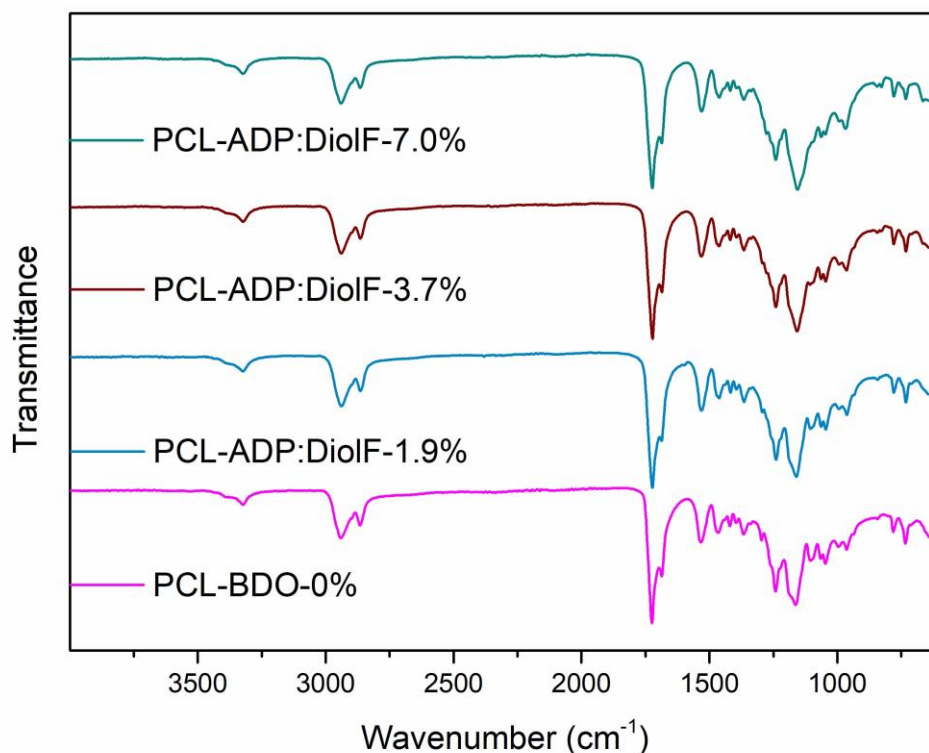


Figure 6.14. Stacked FTIR spectra of the synthesized PCL-based TPUs with blended SS (**PCL-BDO** + **ADP:DiolF**) and single-component PCL TPU.

The position and intensity of the main absorptions were practically identical for all four compounds. The assignment of the bands is similar to the single-component TPUs. The peaks appearing at 2940 cm^{-1} and 2865 cm^{-1} were allocated to the asymmetric and symmetric stretching vibration of CH_2 group. The bending vibration of the N-H group was observed at 1530 cm^{-1} overlapped with the stretching vibration of the C-N of the urethane. Lowering the wavenumber, the most relevant peaks were 1240 cm^{-1} , 1160 cm^{-1} , and 1063 cm^{-1} , which were attributable to the symmetric bending of the CH_2 group, the asymmetric stretching of the C-O-C moiety of the ester groups, and the stretching of C-O. No identifiable peaks associated with the C-F bond were detected.

The presence of hydrogen donor groups (N-H of carbamates) and hydrogen acceptor moieties (C=O of urethanes and esters) results in complex systems with a large number of hydrogen bonds. Focusing on the amine stretching region ($3500\text{--}3200\text{ cm}^{-1}$), there was a weak band of the stretching vibration of the N-H arising from the urethane (Figure 6.15.A). The position of the main band (3320 cm^{-1}) and the lack of absorption at higher wavenumber ($3450\text{--}3550\text{ cm}^{-1}$) proclaimed that most amine groups were interacting with other acceptor groups.

The width and intensity of the bands were alike, suggesting that the urethane moieties behaved similarly in all the synthesized compounds.

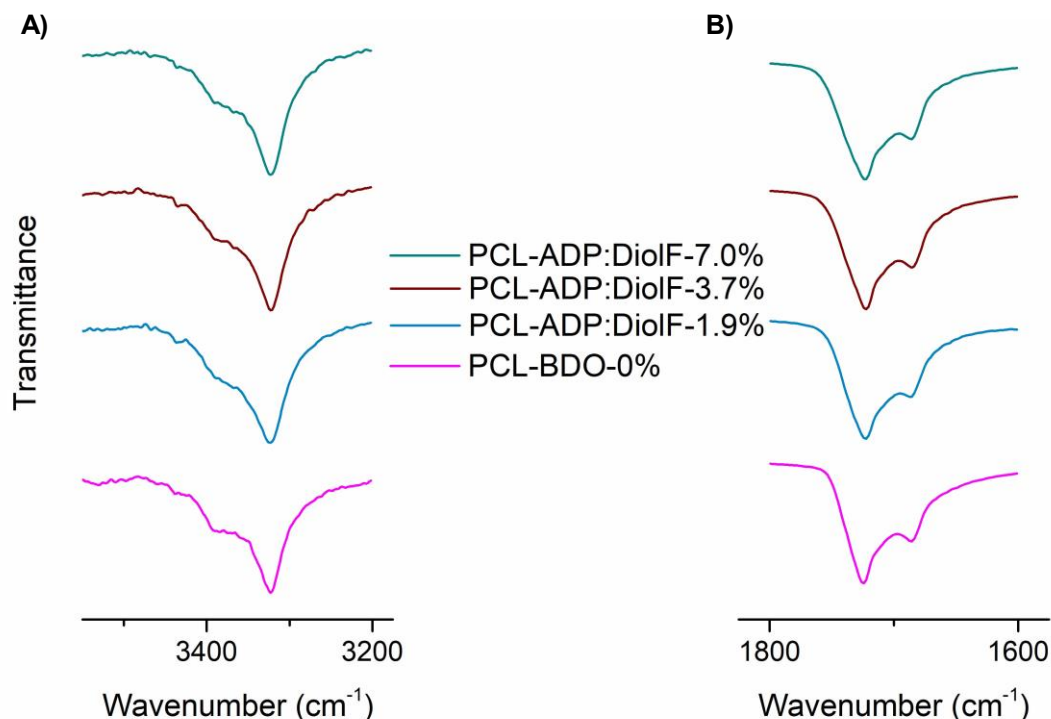


Figure 6.15. Fragmented stacked FTIR spectra of the blended PCL-based TPUs. A) N-H stretching region ($3550\text{ cm}^{-1} - 3200\text{ cm}^{-1}$). B) C=O stretching region ($1800\text{ cm}^{-1} - 1600\text{ cm}^{-1}$). The plotted intensity of each region is not at the same scale. The transmittance scale was increased in the N-H stretching inset to depict more clearly the region.

In Figure 6.15.B can be observed that the carbonyl region did not show different profiles in terms of intensity, breadth, or number of bands when the content of fluorinated polyester increases. Furthermore, the peak width indicates the overlapping of more than two signals. Likewise in the N-H region, the urethane and ester might be interacting similarly in all the compounds. Nevertheless, no further information can be extracted for these intricate systems, in which more than three types of carbonyls might resonate in this area.

6.3.2. Visual properties

Correspondingly to PCL-based TPUs, all the samples exhibited blooming after a few weeks of being injected, requiring the removal of the exuded substance prior to analysis. The visual appearance of the produced plaques is shown in Figure 6.16, where a significant coloration was produced when the fluorine content rise. Although the logotype could be seen, the blend of two polyols increases the cloudiness.

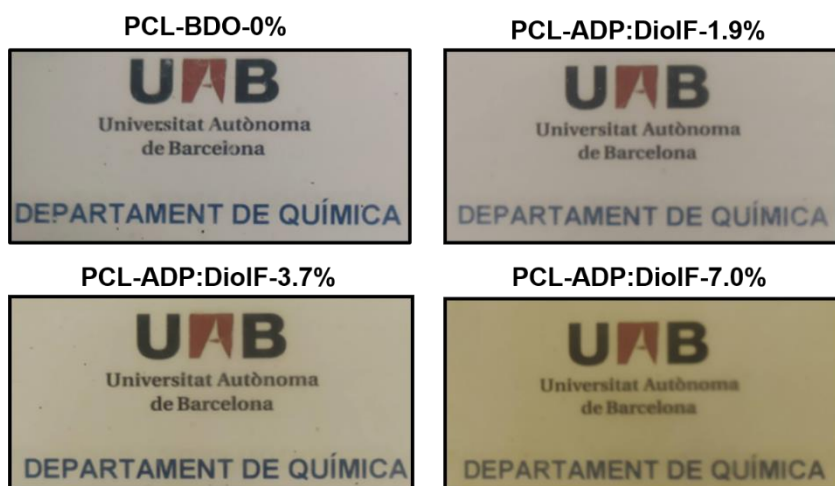


Figure 6.16. Photographs of the injected plaques with the UAB logo underneath.

The quantification of the visual features of the materials is outlined in Table 6.5. YI, transmittance, and haze were measured according to the standard procedures.^{[26][27]}

Table 6.5. Visual properties of blended SS TPUs.

	PCL-BDO-0%	PCL-ADP:DiolF-1.9%	PCL-ADP:DiolF-3.7%	PCL-ADP:DiolF-7.0%
wt.% F	0	1.9	3.7	7.0
Soft Segment	PCL-BDO	PCL BDO+ADP:DiolF	PCL BDO+ADP:DiolF	PCL BDO+ADP:DiolF
Additive W	No	No	No	No
Blooming	Yes	Yes	Yes	Yes
YI (%) ^[a]	7.2 ± 0.2	14.0 ± 0.6	17.7 ± 0.6	30 ± 2
Transmittance (%) ^[b]	84.7 ± 0.4	80 ± 3	82.4 ± 0.7	77 ± 3
Haze (%) ^[b]	18 ± 4	41 ± 14	35 ± 7	31 ± 13

^[a] Measurements carried out according to ASTM E313.^[26] Clean plaques.

^[b] Measurements carried out according to ASTM D1003.^[27] Average value after 6 measurements (three points per plaque) in surfaces that have been wiped with cotton.

The significant rise of positive YI values signposts the departure of the white shade of the plaques toward the yellow. The major deviation was measured with the highest content of **ADP:DiolF**, reaching about fourfold the value of the reference **PCL-BDO-0%**. The color of the previously synthesized polyol was darker than other commercially available polyesters, such as **PCL-BDO** or **ADP:BDO**. Hence, as the **ADP:DiolF** concentration grew, the pigmentation was expected.

Under identical conditions, the transparency of the plaques was explored through transmittance and haze. The blended TPUs exhibit an elevated percentage of transmittance albeit slightly lower than **PCL-BDO-0%**. For the haze, all fluorine-containing compounds display values

higher than 30 %. Therefore, they are light-diffusing materials, leading to the view of blurry images through them.

The high values of transmittance reflected notable compatibility between the two components of the TPU and a large degree of disorder in the structure. However, some short-order assembly was possibly formed by the semi-crystalline **PCL-BDO** or the **HDI:BDO** moieties causing an increase in the haze.

6.3.3. Thermal behavior

6.3.3.1. Kofler measurements

The softening and melting points measured in a Kofler bench are shown in Figure 6.17. The TPU with the smallest concentration of fluorine, **PCL-ADP:DiolF-1.9%** showed results equivalent to the reference material in terms of the melting point. However, there was a decrease in the softening point from 140 °C in **PCL-BDO-0%** to 130 °C of the blended TPU. When the concentration of fluorine increased to 3.7 wt.%, both studied temperatures decreased almost 10 °C respect **PCL-ADP:DiolF-1.9%**. Conversely, **PCL-ADP:DiolF-7.0%** displayed the highest softening and melting points, increasing 20 °C and 36 °C more than the reported non-fluorinated reference.

The fact that **PCL-BDO-0%** and **PCL-ADP:DiolF-1.9%** had similar melting points suggests that despite the doping, both compounds possess alike structures. However, the TPUs with higher fluorine content showed distinct behaviors, which cannot be explained merely with this analysis. While **PCL-ADP:DiolF-3.7%** displays a decrease on both parameters, **PCL-ADP:DiolF-7.0%** was the compound with the highest thermal stability. Regardless, the most favorable compounds to be injected are **PCL-ADP:DiolF-1.9%** and **PCL-ADP:DiolF-3.7%**. Both of them display the smallest difference between the softening and the melting points; thereby, their processability is the least energy-consuming. However, their low temperatures could hamper some of their potential applications.

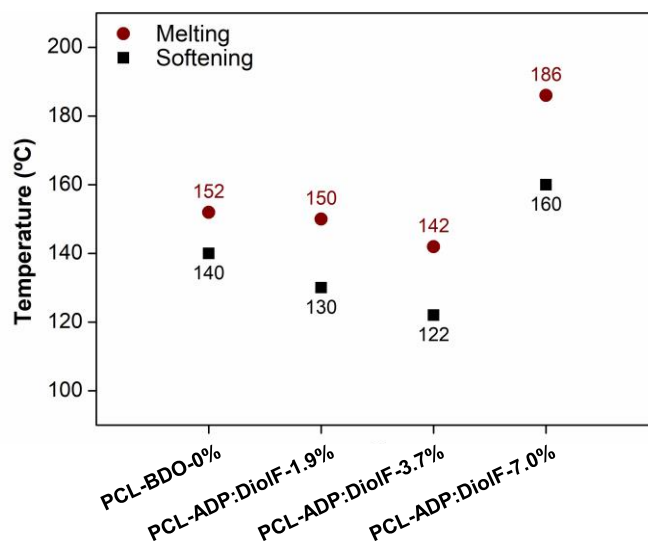


Figure 6.17. Kofler measurements of TPUs with blended-PCL-SS and its reference. The uncertainty of the measurement is ± 2 °C.

6.3.3.2. Differential Scanning Calorimetry

A complete thermal characterization of the studied materials was carried out by DSC analysis, using the same triple-cycle method as in the previous section. The obtained results are highlighted in Figure 6.18 and Table 6.6, omitting the data from the first heating process to remove the thermal history of the samples.

The blend of two polyols allows the study of different fluorine concentrations on a similar matrix, but it is worth bearing in mind that the formulation maintains the number of mols of polyol constant. Thus, as the **ADP:DiolF** concentration increased, the number of **PCL-BDO** chains was reduced. **PCL-ADP:DiolF-3.7%** contains a 22.1 wt.% of **ADP:DiolF** in the SS and **PCL-ADP:DiolF-7.0%** a 41.5 wt.%. Therefore, the structure of the samples is modified from a predominantly PCL-based SS to a highly fluorinated polyester enriched SS. The use of semi-crystalline **PCL-BDO** as the major component of the blend provides partial crystallinity of the SS, as depicted in the single-component PCL-based TPUs. Conversely, as **ADP:DiolF** is an amorphous material under the tested conditions (See Section 5.2.3.2), it does not show either melting or crystallization peaks. Thus, the first-order transitions produced could only arise from the PCL segment. However, as illustrated in the following thermograms (Figure 6.18), not all compounds underwent the same thermal changes. **PCL-BDO-0%**, **PCL-ADP:DiolF-1.9%**, and **PCL-ADP:DiolF-3.7%** presented two melting and two crystallization exotherms probably arising from the SS and HS domains. In contrast, **PCL-ADP:DiolF-7.0%** only exhibited a melting peak and a crystallization peak.

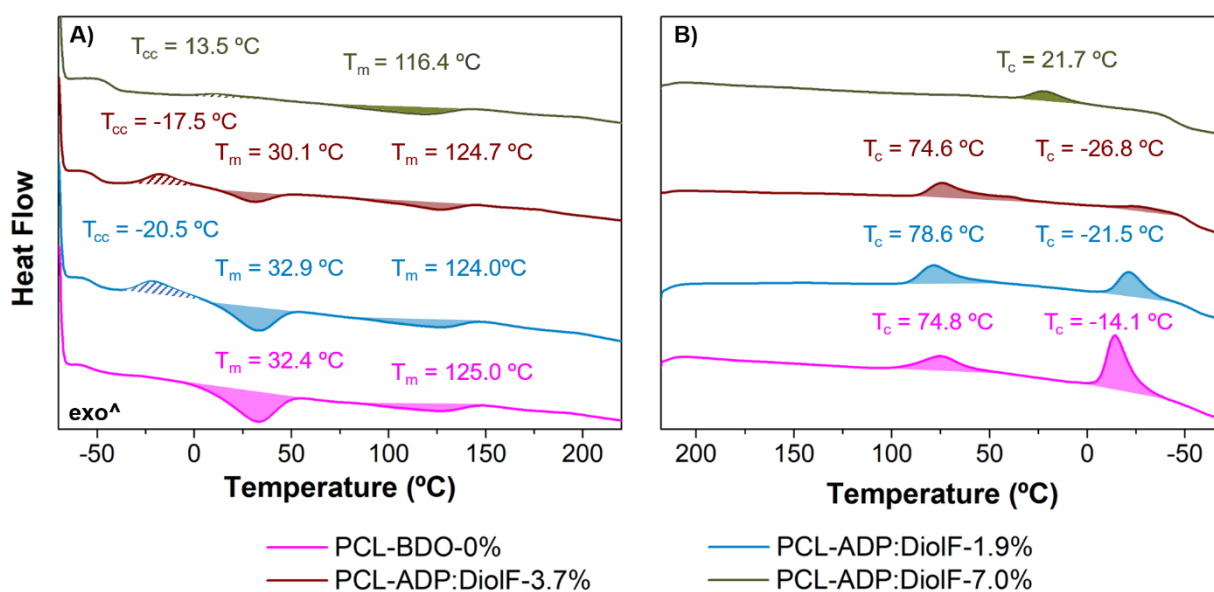


Figure 6.18. DSC thermograms of A) the second heating process and B) the first cooling process. Shaded areas indicate regions used to determine the corresponding processes. The striped areas correspond to the cold crystallization process.

Table 6.6. DSC results of the synthesized TPUs with a blended SS.

	PCL-BDO-0%		PCL-ADP:DiolF-1.9%		PCL-ADP:DiolF-3.7%		PCL-ADP:DiolF-7.0%	
wt.% F	0.0		1.9		3.7		7.0	
Soft Segment	PCL-BDO		PCL-BDO + ADP:DiolF		PCL-BDO + ADP:DiolF		PCL-BDO + ADP:DiolF	
Additive W	No		No		No		No	
T_g ($^{\circ}\text{C}$) ^{[a][b]}	-54.7		-52.0		-50.5		-43.2	
T_{cc} ($^{\circ}\text{C}$) ^[b]	--		-20.5		-17.5		13.5	
ΔH_{cc}° (J/g) ^[b]	--		8.3		7.2		4.4	
T_m ($^{\circ}\text{C}$) ^[b]	32.4	125.0	32.9	124.0	30.1	124.7	116.4	
ΔH_m° (J/g) ^[b]	20.9	9.5	15.1	10.9	7.8	7.6	9.9	
T_c ($^{\circ}\text{C}$)	74.8	-14.1	78.6	-21.5	74.6	-26.8	21.7	
ΔH_c° (J/g)	10.7	16.6	16.6	10.0	11.2	1.3	5.8	

^[a] T_g was recorded at the inflection point of the shift.

^[b] Transitions captured on the second heating scan at 10 $^{\circ}\text{C}/\text{min}$.

The observed baseline shift in the region between -52 $^{\circ}\text{C}$ and -43 $^{\circ}\text{C}$ (Figure 6.18.A) corresponds to the transition from the glassy to the rubbery state of the amorphous SS. Traditionally, T_g is employed as a gauge of the SS purity and the subsequent degree of phase segregation. An increase in the mixing between HS and SS is reflected in a raise on the T_g compared to the value of the neat compound.^[41] In the case of the studied compounds, the T_g increases with the fluorine content in the polymer. Although normally it will be related with

better miscibility of the SS and HS, in these cases, the disruption of **PCL-BDO** domain is not only caused by HS fragments but probably also by the branched **ADP:DiolF**. The random coiling and interpenetration of **ADP:DiolF** chains within the **PCL-BDO** might promote the packing distortion and the entangling of the chains, which might act as a crosslinking point that unable the rotational movement of the polymer in the amorphous regions.^{[42][43]}

Focusing on the heating process (Figure 6.18.A), the three fluorinated TPUs display a cold-crystallization peak and one or two melting peaks. The exotherm is attributable to the rearrangement of **PCL-BDO** as it gains energy upon heating. The cold crystallization process has only been depicted on samples containing **DiolF**, so it is plausible that introducing a fluorinated branched diol in the SS hampers the alignment of the **PCL-BDO** chains while cooling. While the associated T_{cc} increases with the fluorine content, the process enthalpies become smaller owing to the reduction in the number of **PCL-BDO** chains in the TPU. Although the T_m of **PCL-ADP:DiolF-1.9%** and **PCL-ADP:DiolF-3.7%** SS were comparable to those of **PCL-BDO-0%**, the increase in fluorinated polyester concentration caused the decrease of the melting endotherm depicted around 30°C until its complete disappearance on **PCL-ADP:DiolF-7.0%**. The replacement of **PCL-BDO** chains by **ADP:DiolF** resulted in the formation of fewer and smaller ordered domains of SS. This fact was depicted with the decrease of the enthalpy associated with the first endotherm as the fluorine content increases. Regarding the second melting peak, which belongs to the HS, similar enthalpies and T_m were obtained on **PCL-BDO-0%**, **PCL-ADP:DiolF-1.9%**, and **PCL-ADP:DiolF-3.7%**, suggesting a similar structure of the hard domains. However, when moving to **PCL-ADP:DiolF-7.0%** a stark decrease on HS T_m of 8 °C is observed, which evidences a change in the domain structure. This downshift in T_m might suggest the formation of smaller HS domains, which could be brought upon by a hindrance of chain mobility by the branched diol.

Figure 6.18.B reveals the thermal processes that the samples undergo when cooled at a constant rate. In particular, the compound with the lowest halogen content follows the same behavior as the reference material regarding the number of crystallization peaks. However, when fluorine concentration increased, the peaks were less evident. The formation of the ordered HS domains is attributed to the highest temperature exotherm ($T_c \approx 75$ °C), while the alignment of the SS chains is observed at negative temperatures. Only slight differences are depicted in the T_c and the enthalpy associated with the HS crystallization between the reference material, **PCL-ADP:DiolF-1.9%** and **PCL-ADP:DiolF-3.7%**, indicating, just as in the case of the melting transitions, the formation of similar HS domains. In contrast, a single exotherm

is detected in **PCL-ADP:DiolF-7.0%**, probably corresponding to the formation of HS domains. The low value of its T_c signposts the creation of smaller ordered regions in the TPU.

Figure 6.18.B emphasizes the noticeable decrease in SS crystallization with the concentration of fluorine, both in terms of temperature and enthalpy. The rise of the **ADP:DiolF** content up to 3.7 wt.% of fluorine causes a decrease of 12 °C in the SS T_c , as well as a reduction of 15 J/g in the enthalpy associated with the process. Moreover, **PCL-ADP:DiolF-7.0%** does not display the second exotherm ascribed to the SS.

Overall, the produced TPUs form partially ordered structures, in which it was possible to differentiate the common thermal transitions of semi-crystalline materials. However, the low values of enthalpies signpost the formation of few ordered regions with large size distributions. Considering all the information, fluorine does not seem to promote better phase segregation. Oppositely, the fact of co-polymerizing a second component on the SS decreases the order in the system, owing to the reduction of the semi-crystalline PCL. Moreover, when the concentration of polyester reaches a certain value, not only the SS is affected, but also the formation of HS is disrupted. The branches of the polyester produce irregularities in the systems, resulting in the formation of smaller HS crystallites with lower melting temperatures. Because of that, **PCL-ADP:DiolF-7.0%** exhibits a pretty amorphous system. The lack of crystalline fragments arising from the SS denotes the high compatibility of **ADP:DiolF** with **PCL-BDO** and as consequence, the distribution of the fluorinated component within the bulk.

6.3.4. Tribological behavior

The effect of different fluorine concentrations on the durability of the produced TPUs was assessed through their tribological properties, which are summarized in Figure 6.19 and Figure 6.20. The hardness, density, friction in dry sliding conditions against an aluminum surface, and abrasion resistance were measured with injected plaques under the same stipulations as those on single-component SS TPUs.

Regarding density (Figure 6.19.A), TPUs exhibit a linear increment on this parameter proportional to the fluorinated polyester concentration. The blending of a second polyester in the SS influenced the structure of the polymer, modifying the efficiency of the packing. Although the produced TPUs presented higher values than the reference **PCL-BDO-0%**, their densities are within the common range for this class of polymers. All of them can be considered

as equivalent in terms of hardness (Figure 6.19.B), possibly by the similar composition and percentage of HS.

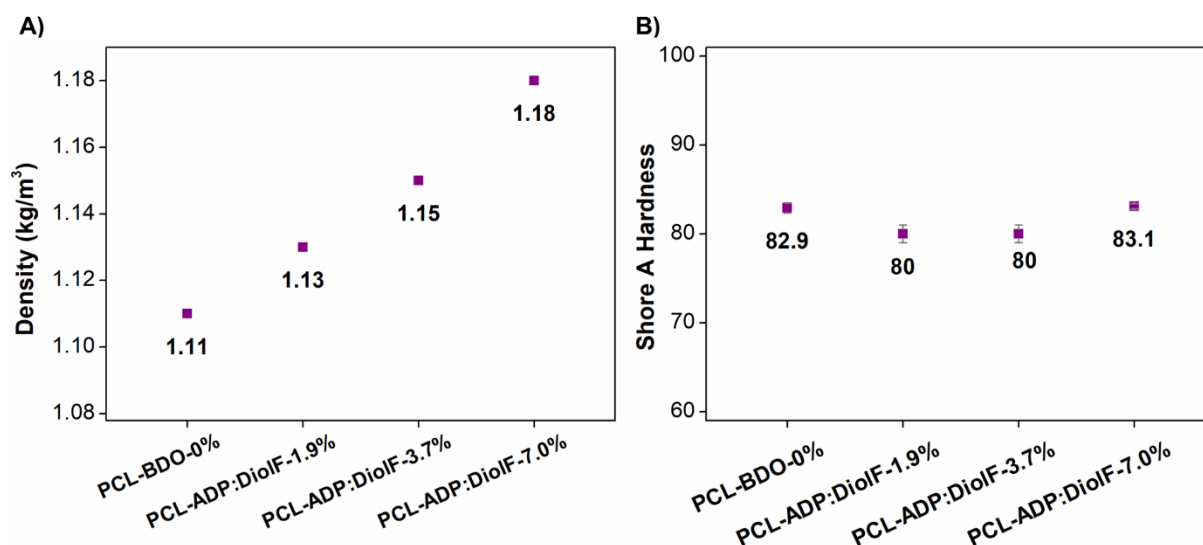


Figure 6.19. Blended-SS TPUs results of A) density (average value of four measurements carried out according to ASTM D792)^[31] and B) Shore A Hardness (average value of ten measurements carried out according to ISO 868).^[32] Bars represent the standard deviation of the results.

The abrasion of the studied systems displays a noteworthy increase with the addition of the polyester as co-polyol (Figure 6.20.A). **PCL-ADP:DiolF-1.9%** is less resistant than the non-fluorinated TPU. The obtained value corresponds to a 125% increase in wear with respect to the reference sample. In turn, **PCL-ADP:DiolF-3.7%** shows an increase of over 262%, while **PCL-ADP:DiolF-7.0%** exhibits a volume loss of 382%. The introduction of large quantities of the branched polyester disrupts the cohesion and promotes a higher loss of material.

In the case of the friction analysis (Figure 6.20.B), the COF values decrease initially with a 1.9 wt.% of fluorine and then, increases with the halogen content. **PCL-ADP:DiolF-1.9%**, exhibits potentially interesting properties as it showed better results than the non-fluorinated reference. Specifically, the obtained μ_s and μ_d exhibits a reduction of 30 % and 33 %, respectively, relative to the **PCL-BDO-0%** values. However, the behavior is not followed by the other compounds. **PCL-ADP:DiolF-3.7%** displays more than a two-fold growth in comparison with **PCL-ADP:DiolF-1.9%** in both coefficients. Furthermore, **PCL-ADP:DiolF-7.0%** presents a resistance toward motion nearly five times higher than the TPU with the lowest fluorine content (**PCL-ADP:DiolF-1.9%**).

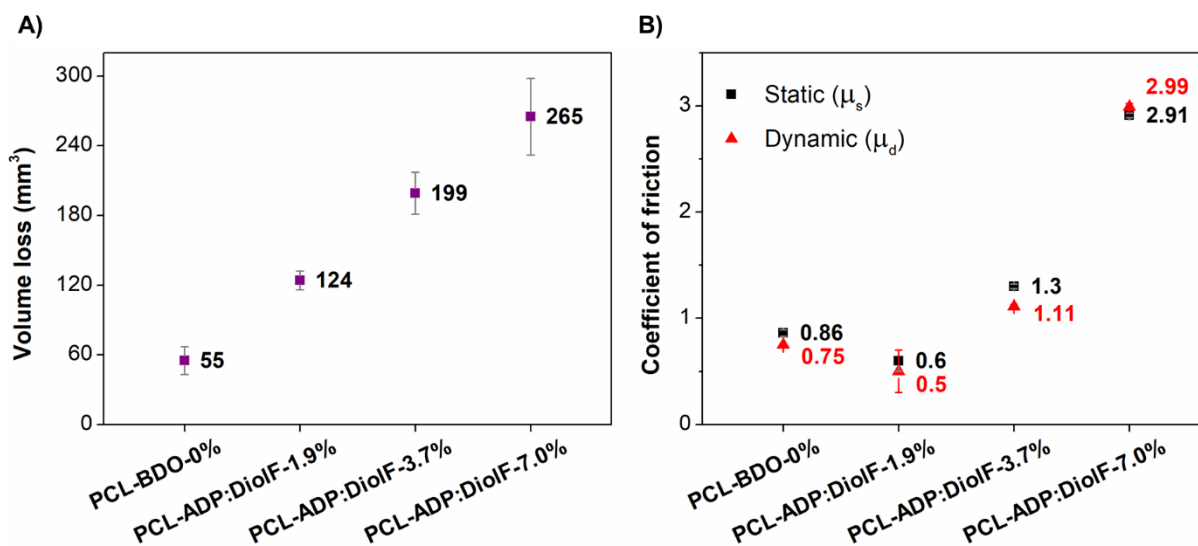


Figure 6.20. Blended-SS TPUs results of A) abrasion resistance (average value of three replicates carried out according to ASTM D5963:15.^[33]) and B) friction against an aluminum surface (average value of three plaques measured carried out according to ASTM D1894.^[34]). For comparison purposes, all the analyses were carried out with the same tested conditions (normal load and sliding speed) in the same apparatus. Bars represent the standard deviation of the results.

Initially, it was postulated that the fluorinated polyester would segregate to the surface of the TPU, enriching the outermost region of the compound, thereby reducing the friction against an aluminum plane. However, these results suggest that fluorine does not preferentially migrate to the surface, but rather it stays dispersed through the materials.

ADP:DiolF, similarly to **PCL-DiolF**, exhibits a larger molar volume than the completely linear **PCL-BDO**, as a consequence of the dangling trifluoroethyl chain. Bearing in mind the structure of the blended polyols, the branched polyester might act as an entanglement point obstructing chain mobility and/or forcing their separation by behaving like a plasticizer. Therefore, the higher the concentration of **ADP:DiolF**, the greater the disruption to the structure. The combination of lower cohesive forces, the steric hindrance of the branch, and the produced heat against an abradant surface might cause the high tearing of the outermost region of the polymer. Therefore, friction and abrasion resistance of the evaluated materials seem to be more sensitive to the blend of a branched polyester in the SS than to the presence of fluorine itself.

6.3.5. Surface behavior: Wettability

The behavior of fluids on the surface of the synthesized compounds was studied using WCA and SFE, and the results of these measurements are illustrated in Figure 6.21. Owing to the

existence of blooming in all the TPU plaques, all the surfaces were wiped with a cotton piece prior to the analysis.

Concerning WCA (Figure 6.21.A), there is no difference among the synthesized TPUs, as all of them show a contact angle around 77° . Since none of the analyzed polymers overcome the threshold of 90° , they are classified as hydrophilic materials, similarly to the previously studied TPUs. This fact supports that fluorine is homogeneously dispersed through the material and had not preferentially migrated to the outermost region and enriched the surface.

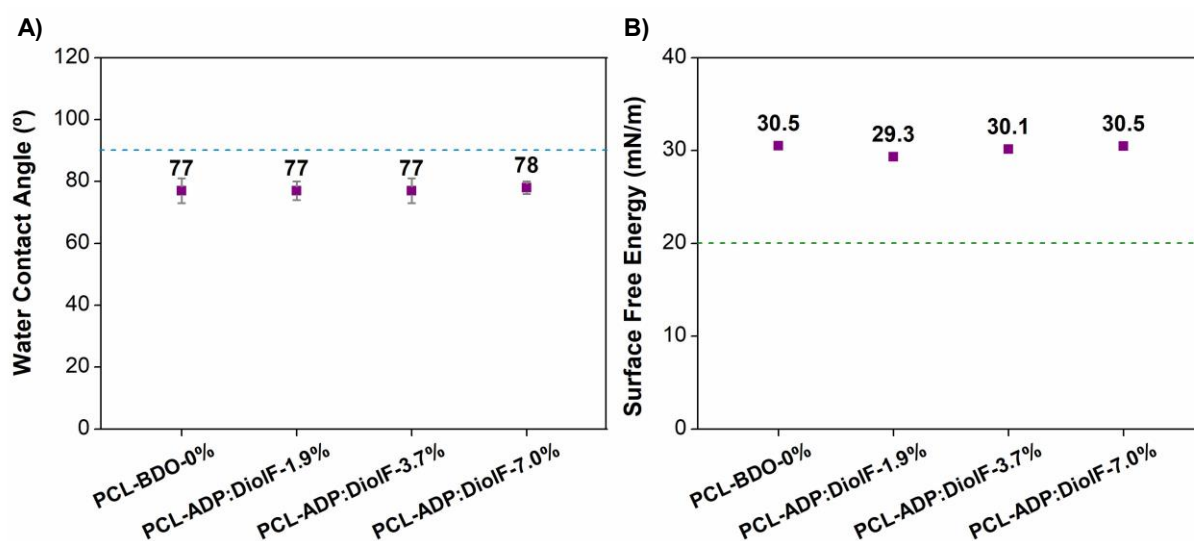


Figure 6.21. Results of the blended-SS TPUs in A) WCA analysis (16 measurements on two cleaned plaques) and B) SFE (eight measurements on two cleaned plaques with water, ethylene glycol, and DMF). The blue dashed line indicates the 90° threshold in WCA and the green dashed line denotes the benchmark of PTFE's SFE. Bars represent the standard deviation of the results.

Moreover, the four compounds display a similar value of the total SFE among other hydrophilic polymers with values around 30 mN/m (Figure 6.21.B). Therefore, no hydrophobic behavior was achieved with the tested compounds. Although none of the analyzed TPUs reached the PTFE (20 mN/m) or the polydimethylsiloxane value (PDMS, 19.8 mN/m),^[38] they showed a decrease from the common value of 40 mN/m of SFE in TPUs.^{[44][45]} Probably the use of the hydrophobic PCL in combination with a low HS percentage produces a lower polarity than other commercial TPUs.

To discern a possible pattern on the surface behavior, values of the polar and dispersive components of the SFE are represented in Figure 6.22. The predominant component in all the synthesized TPUs is the dispersive, being over 60% in all the as-injected plaques. The obtained values are far from the 8% of polar component and the 92 % of the dispersive component in

PTFE. The similarity of all the results reaffirms the lack of migration of the halogen toward the surface of the material as no variation on the SFE is observed with the increase in fluorine.

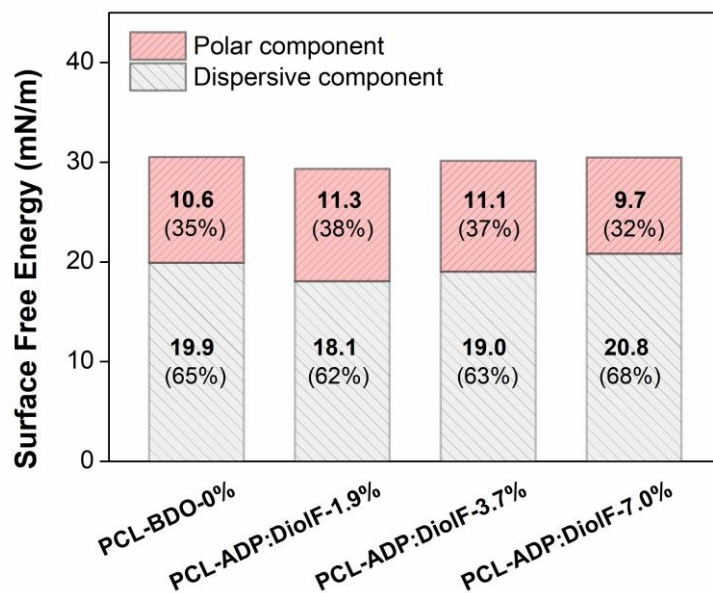


Figure 6.22. SFE decomposed in values and percentage of dispersive and polar components measured in cleaned surfaces. The green dashed line represents the PTFE's SFE value.

Based on the above, it seems that the introduction of a polyester alters the structure of the system and the corresponding properties, but the presence of fluorine was not the motive. Just as **PCL-DiolF** could not enhance the surface properties, different contents of fluorine added by substituting **PCL-BDO** mols for **ADP:DiolF** did not enhance the surface properties either. The obtained values signposted that no migration had taken place and fluorine remained homogeneously distributed in the TPUs.

Although some variations on the studied properties were observed, they are a more likely consequence of the branched structure of **ADP:DiolF** than of the role of fluorine. Parameters as transparency, WCA, and SFE of the produced polymers were very similar regardless of the polyester concentration. However, other features as thermal transitions, abrasion resistance, and friction, which are indeed more structure defined, were highly affected by the blended content. The branched structure of **ADP:DiolF** and its increment in the formulation reduced the crystallization capability of the semi-crystalline **PCL-BDO** chains and therefore, modified greatly the thermal and tribological properties of the compounds.

6.4. PC-based family

Two different fluorinated polyesters, **ADP:DiolF**, with different molar ratios to the PCL providing different halogen contents, and **PCL-DiolF**, were assessed with unsuccessful results. Although several authors claim that the introduction of fluorine in side chains provides higher mobility to the system and an enhancement of the surface properties,^{[16][46]} such outcomes were not obtained in our systems. The gathered results brought on the possibility that the tested formulation was not appropriate for the study owing to the high compatibility of components or the entanglement of the side chains, which hindered the segregation. Therefore, another formulation with different polyols and a low fluorine concentration was considered to unravel their effect on the analyzed properties. To remove the influence of the dangling chains on the segregation of the halogen, linear compounds containing fluorine in the backbone were assayed.

To simplify the studied structure, the synthesized TPUs only consisted of an HS constructed around a single diisocyanate, **HDI**, and one chain extender, **BDO**. Their content on the final polymers was maintained low (~6-7 wt.%) to form fewer physical crosslinked points and not constrain the potential migration of the fluorinated structures to the surface. Moreover, other the co-chain extender **B** was removed to foster to some extent the segregation. The chemical structure of the reagents involved in this set of TPUs is illustrated in Figure 6.23.

This new formulation was based on a SS of poly(hexamethylene) carbonate diol (**Eternacoll**[®]), hereinafter referred to as **PC**. Polycarbonates are known for their attractive properties as their high transparency under visible light and their excellent weatherability, consequence of the hydrolytic stability of the carbonate's group, and high oxidation resistance.^[47] Moreover, they are widely employed in blends owing to their good compatibility with other polymers like acrylonitrile-butadiene-styrene (ABS) or poly(ethylene terephthalate) (PET).^[48] Therefore, they are employed in films, adhesives, and coatings with acrylate derivatives.^{[49][50]} Moreover, PC-based TPUs are usually reported as biocompatible and exhibit good mechanical and optical properties. Contrary to the PCL-based TPUs which contained the fluorine in the dangling chain, this formulation explored the effect of blending linear fluorinated compounds in a TPU matrix. To this end, the two already synthesized **ADP:HDO** and **ADP:HDO-8F** were selected as the linear polyesters to co-polymerize with **PC**. Moreover, to gauge the ester compatibility in the formulation, a blend with a perfluorinated polyether (**FLK**) with similar M_n to the other polyols

was also evaluated. Owing to confidential reasons, the precise structure of the polyether and the synthetic details had not been disclosed in this thesis manuscript.

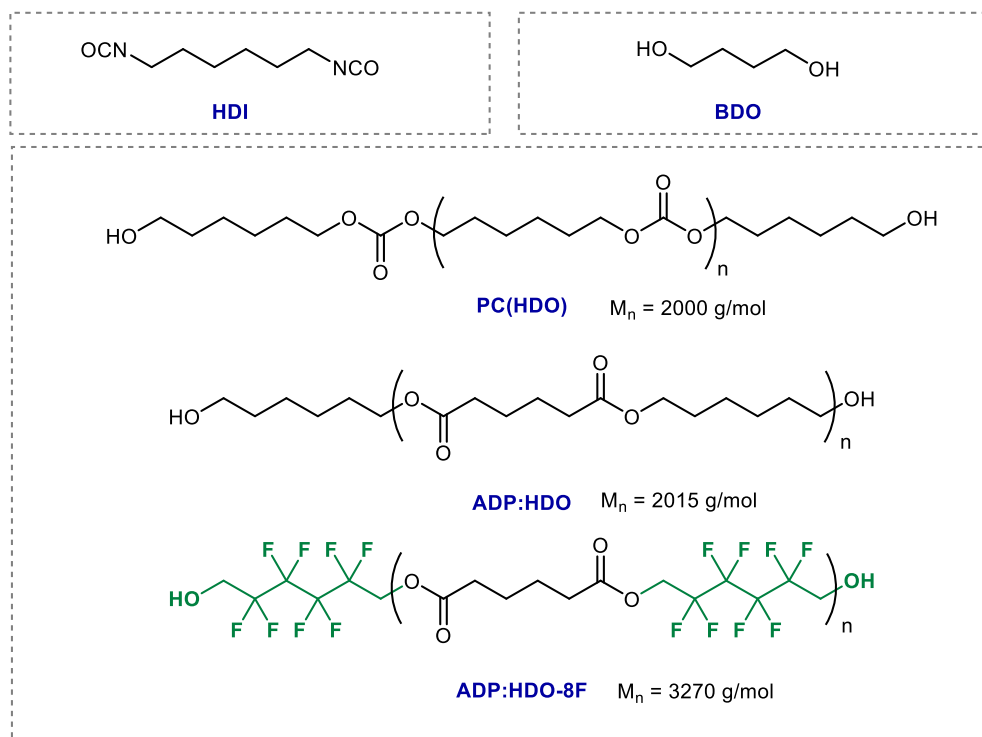


Figure 6.23. Employed reagent for the synthesis of the PC-based TPUs

The PC-based formulation was tested with four different TPUs (Table 6.7). The effect of introducing a fluorinated chain (**ADP:HDO-8F** or **FLK**) was carefully compared with two non-fluorinated references, **PC-0%-W**, comprising a single-component SS, and **PC-ADP:HDO-0%-W**, a blended SS of **PC** and **ADP:HDO**. Regarding halogenated TPUs, **PC-ADP:HDO8F-3%** represented the isostructural fluorinated equivalent of **PC-ADP:HDO-0%-W**, which blended **PC** with **ADP:HDO-8F** instead of **ADP:HDO**. Both polyesters were designed to contain the identical number of monomers in each structure and merely differed in the replacement of the hydrogen by fluorine. This modification results in an elevated local concentration of fluorine in certain areas, while the rest of the polymer consists of the traditional hydrogenated regions. **PC-ADP:HDO-0%** was synthesized replacing the number of mols of **ADP:HDO-8F** by **ADP:HDO**. Conversely, **PC-FLK-3%** was synthesized substituting the required number of mols of **PC** to reach the target fluorine content in the TPU.

Only minor amounts of the second polyol were incorporated into the SS in all the blended systems. In particular, **PC-ADP:HDO-0%-W** contained 4.5 wt.% of polyester in the TPU,

PC-ADP:HDO8F-3% incorporated 7.0 wt.% of the fluorinated polymer, and finally, **PC-FLK-3%** included 5.2 wt.% of the polyether.

When it was required the additive W was incorporated to the mixture. The employed additive was the same as in the previously studied **PCL-BDO-0%-W**. Therefore, their effect on the TPUs should only be considered in the wettability of the materials.

Table 6.7. Summary of synthesized TPUs.

	PC-0%-W	PC-ADP:HDO-0%-W	PC-ADP:HDO8F-3%	PC-FLK-3%
wt.% F	0	0	3	3
Soft Segment	PC(HDO)	PC(HDO) + ADP:HDO	PC(HDO) + ADP:HDO-8F	PC(HDO) + Perfluoropolyether
Additive W	Yes	Yes	No	No
% HS	6.5	6.7	6.8	6.0
NCO/OH	1.0	1.0	1.0	1.0
Weight (g)	750	732	750	750
MFI (g/10 min) ^[a]	24.2	286.9	7.1	5.4

^[a] Tested conditions: 190 °C and 2.16 kg.

It is worth mentioning that PC-based TPUs were only used as proof-of-concept compounds. The elevated price of the fluorinated polyols, especially **ADP:HDO-8F**, deters their use for industrial applications if only a moderate enhancement is obtained. However, **PC-ADP:HDO8F-3%** could shed light on the effect of incorporating fluorine within a linear polyester. **PC-FLK-3%** was tested for comparison purposes owing to its ether moieties, which might display weaker interactions with carbamates and carbonates and lead to higher phase segregations.

Neither GPC analysis nor ¹H-NMR spectroscopy could be used to determine the molecular mass distribution, the polydispersity, or the TPUs' structure in solution owing to the insolubility of the polymers in common organic solvents. Hence, MFI measurements were used to establish the flowability of the materials.

6.4.1. Infrared analysis

FTIR spectra of the samples were recorded to confirm the chemical structure of the produced TPUs according to their characteristic peaks and the isocyanate conversion. Figure 6.24 shows the spectra of the polymers between the 4000 cm⁻¹ and 600 cm⁻¹ normalized to the most intense band. As described in previous sections of this project, the absence of free isocyanate peaks centered at 2273 cm⁻¹ ascribed to the N=C=O stretching, and the existence of the band

attributed to the N-H stretching of the carbamate at 3321 cm^{-1} indicated the final conversion of the isocyanate group into urethanes. The low HS content was observed by the weak intensity of the last-mentioned vibration in comparison with the rest of the bands on the spectra.

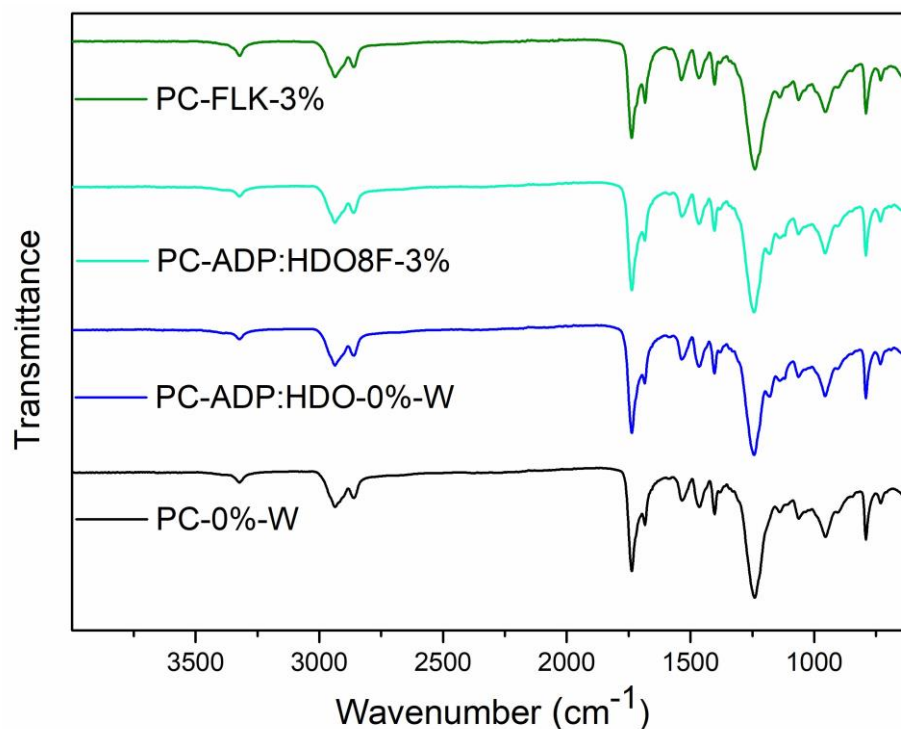


Figure 6.24. Stacked FTIR spectra of the synthesized PC-based TPUs.

On the other hand, the main peaks of the spectra agree with data reported in the literature.^{[51][52][53]} No significant variations were observed in the spectra of the blended compounds in comparison with **PC-0%-W**. Most of the peaks were centered in the same wavenumber, only varying up to 3 cm^{-1} between samples. The main difference between the PCL-based system and the ones reported here arises from the carbonate moieties. The O-C=O asymmetric stretching absorption of carbonates and esters at 1240 cm^{-1} is observed as the most intense peak of each spectrum. In the least energetic region of the spectra, two peaks stood out at 1063 cm^{-1} and 790 cm^{-1} . They were ascribed to O-C-O symmetric stretching and the O-CO-O out-of-plane bending of the carbonate, respectively.

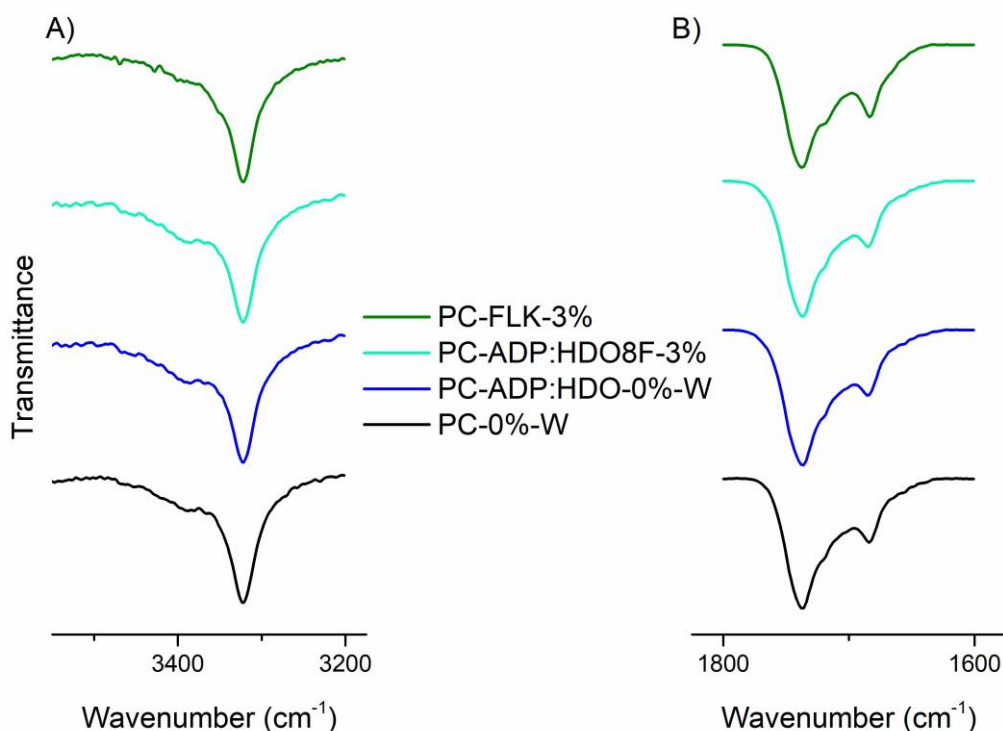


Figure 6.25. Fragmented stacked FTIR spectra of the synthesized PC-based TPUs. A) N-H stretching region ($3550\text{ cm}^{-1} - 3200\text{ cm}^{-1}$). B) C=O stretching region ($1800\text{ cm}^{-1} - 1600\text{ cm}^{-1}$). The transmittance scale was not equal for both wavelength ranges as the amine inset was increased to depict more clearly the region.

A more thorough examination of the N-H stretching region (3500 cm^{-1} to 3200 cm^{-1} , Figure 6.25A) disclosed a peak centered around 3322 cm^{-1} , commonly ascribed to the urethane moiety interacting by hydrogen bonding. However, no peak was not observed in the spectra at $\sim 3445\text{ cm}^{-1}$. This absence indicates that most of the N-H moieties are interacting with accepting groups of esters, carbonates, or urethanes.

As aforementioned, PC-based or polyester-based TPUs exhibit a carbonyl region (1800 cm^{-1} - 1600 cm^{-1}) complex to assign (Figure 6.25.B). In these systems, three types of carbonyls (esters, carbonates, and urethanes) cohabit at similar wavenumber. Although all the samples exhibit a similar profile in this region, a shoulder can be observed around 1718 cm^{-1} , especially in **PC-FLK-3%**.

6.4.2. Visual properties

The aspect of the obtained polymers differs from that of the previously studied PCL-based TPUs. As displayed in Figure 6.26, the introduction of a second polyol in the SS leads to a decrease in the transparency in **PC-ADP:HDO-0%-W**, while the two fluorinated polyols

resulted in opaque TPUs. Therefore, TPUs containing the halogen atoms seem to be more incompatible with the matrix and cause the formation of non-transparent materials which impede the visualization of objects underneath the plaques.

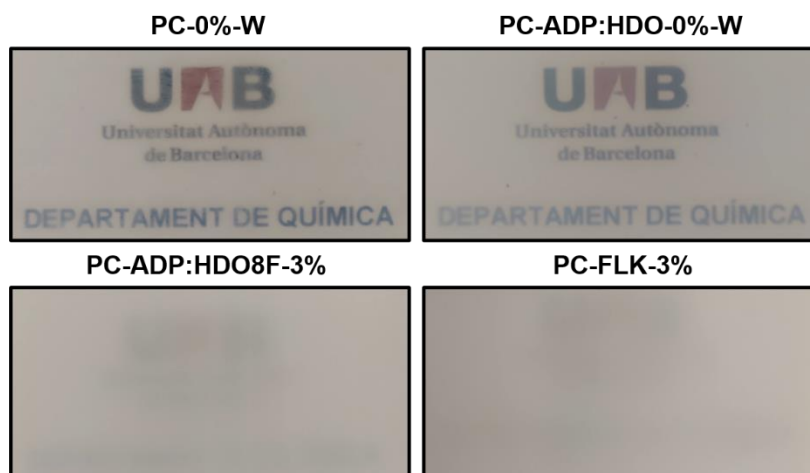


Figure 6.26. Photographs of the PC-based TPU injected plaques with the UAB logotype underneath.

Blooming was only observed in the two fluorine-free TPU plaques. While in the PCL-based TPUs the blooming arose from small oligomers of the **ECL** and the additives of the formulation, in the PC-based TPUs, the exuded substances were mainly polycarbonate oligomers as revealed by NMR analysis of the exuded material.

To quantify the visual appearance of the materials, the YI, transmittance, and haze were measured after cleaning the plaques surfaces. The results of the materials under consideration are detailed in Table 6.8. The YI measurements of the plaques exhibited little deviation from the white. Data were in the acceptable range for TPU prototypes without the addition of stabilizers that would inhibit degradation processes caused by UV radiations or temperature.

Blending two components in the SS reduced the percentage of light transmitted passing through the material compared to the reference. The addition of **ADP:HDO** polyester to the **PC** SS decreased the transparency, but this behavior was more strongly spotted with the fluorinated polyols. For **PC-ADP:HDO8F-3%** and **PC-FLK-3%** the transmittance of the cleaned samples was reduced around 30% and 55% respect **PC-0%-W**, while **PC-ADP:HDO-0%-W** exhibited only a 13% decline. The decrease in transmittance reflected the increase in opacity visually observed. This suggests a higher incompatibility of the HS and SS fostering the formation of crystallites of larger dimensions and consequently, a higher degree of light scattering. Owing to the low transmittance values, the haze was not considered in the fluorinated samples.

Table 6.8. Visual properties of PC-based TPUs.

	PC-0%-W	PC-ADP:HDO-0%-W	PC-ADP:HDO8F-3%	PC-FLK-3%
wt.% F	0	0	3	3
Soft Segment	PC(HDO)	PC(HDO) + ADP:HDO	PC(HDO) + ADP:HDO-8F	PC(HDO) +Perfluoroether
Additive W	Yes	Yes	No	No
Blooming	Yes	Yes	No	No
YI (%) ^[a]	6.4 ± 0.4	-0.20 ± 0.04	4.1 ± 0.2	0.75 ± 0.03
Transmittance (%) ^[b]	83.7 ± 0.6	72.5 ± 0.3	59 ± 6	38 ± 1
Haze (%) ^[b]	88 ± 7	73 ± 4	--	--

^[a] Measurements carried out according to ASTM E313.^[26] Average value of two measurements.

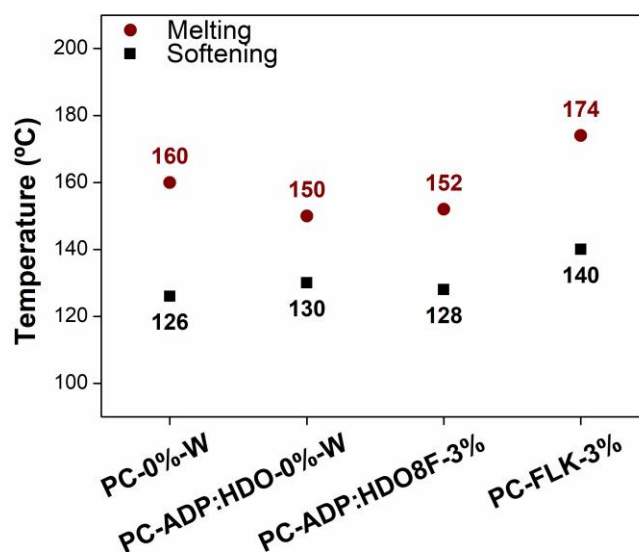
^[b] Measurements carried out according to ASTM D1003.^[27] Average value of six measurements (three points per plaque) in clean plaques.

To sum up, the blending of two components caused a significant impact on the transparency of the polymers, reducing both their see-through capabilities. Hence, the use of these blended TPUs in applications that require high transparency, such as glasses or masks, was discouraged.

6.4.3. Thermal behavior

6.4.3.1. Kofler measurements

Kofler results are exposed in Figure 6.27, showing both the softening and the melting points of the studied TPUs.

**Figure 6.27.** Kofler measurement of PC-TPUs.

The softening temperature, for the TPUs incorporating ester moieties to the matrix, was quite similar. However, the introduction of a fluorinated polyether increases the stability of the

compound by 14 °C. Blending a **PC** with a polyester, regardless of being **ADP:HDO** or **ADP:HDO-8F**, caused a decrease of nearly 10 °C on the melting point of the TPUs compared to **PC-0%-W**. In contrast, higher results are achieved with **PC-FLK-3%**, in almost 14 °C, pointing again to higher thermal stability.

In terms of processability, the smallest difference between the two studied parameters was for the polyesters-based TPUs, being 20 °C and 24 °C for **PC-ADP:HDO-0%-W** and **PC-ADP:HDO8F-3%**, respectively. Both compounds were the most favorable to be processed in terms of involved energy.

6.4.3.2. Differential Scanning Calorimetry

DSC measurements complement the previous thermal results by continuously monitoring the change in heat flow at a constant heating and cooling rate. Figure 6.28 represents the obtained thermograms and Table 6.9 summarizes the results of the PC-based TPUs with measurements under a triple-cycle method. Again, to establish accurately the information of the melting process, only the second heating curve has been considered as it does not contain the thermal history of the sample.

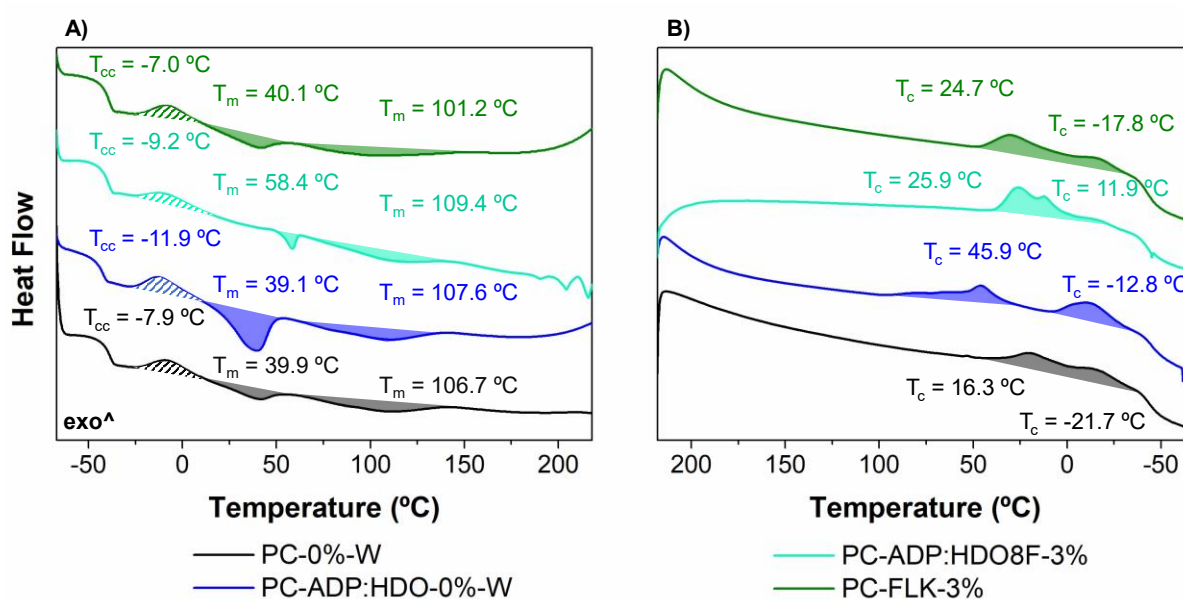


Figure 6.28. DSC thermograms of A) the second heating process and B) the first cooling process. Shaded areas indicate regions used to determine the corresponding processes. Stripped areas correspond to the cold crystallization process.

Table 6.9. DSC results of the PC-based TPUs.

	PC-0%-W		PC-ADP:HDO-0%-W		PC-ADP:HDO8F-3%		PC-FLK-3%	
wt. % F	0		0		3		3	
Soft Segment	PC(HDO)		PC(HDO) + ADP:HDO		PC(HDO) + ADP:HDO-8F		PC(HDO) + Perfluoroether	
Additive W	Yes		Yes		No		No	
T_g (°C) ^[a] ^[b]	-38.7		-42.4		-39.5		-39.2	
T_{cc} (°C) ^[b]	-7.9		-11.9		-9.2		-7.0	
ΔH_{cc}° (J/g) ^[b]	3.4		5.3		2.1		3.8	
T_m (°C) ^[b]	39.9	106.7	39.1	107.6	58.4	109.4	40.1	101.2
ΔH_m° (J/g) ^[b]	3.2	5.8	9.3	8.3	1.95	3.8	2.5	5.2
T_c (°C) ^[c]	16.3	-21.7	45.9	-12.8	25.9	11.9	24.7	-17.8
ΔH_c° (J/g)	24.4		8.6	5.8	12.2		10.8	

^[a] T_g was recorded at the inflection point of the shift.

^[b] Transitions recorded in the second heating scan at 10 °C/min.

^[c] Overlapped peaks were deconvoluted to estimate T_c .

Unlike **ADP:DiolF**, which was an amorphous polymer, the polyesters **ADP:HDO** and **ADP:HDO-8F** blended with **PC** are semi-crystalline compounds, as it was already described in the previous chapter (see Chapter 5.1). However, the quantity of polyester required to reach the target content of fluorine in these TPUs was relatively low. **PC-ADP:HDO-0%-W** contains only 4.5 wt.% of **ADP:HDO**, while **PC-ADP:HDO8F-3%** incorporates 7.5 wt.% of **ADP:HDO-8F**. Conversely, the employed polyether did not evidence crystallization or melting processes. Hence, the transitions detected in the studied TPUs might not only arise from the amorphous or ordered regions of the **PC** or the HS, but also to a lesser extent, from the blended components.

The four synthesized compounds display a prominent T_g between -38 °C and -43 °C, denoting the existence of a significant fraction of amorphous **PC** domains. Contrarily, no T_g at a higher temperature (up to 220 °C) was observed in the thermogram, whether it was from the HS or the second polyol.

Examining the heating scan in Figure 6.28.A, all the samples display cold crystallization in the range between -7 °C and -12 °C, indicating the need for thermal energy to rearrange the SS. All the compounds exhibit low ΔH_{cc}° values, being the highest **PC-ADP:HDO-0%-W**. Moreover, each sample exhibits at least two melting endotherms, one related to the SS and another associated with the HS. Peaks centered around 40 °C arise from the former fragment and only in the case of **PC-ADP:HDO8F-3%**, the maximum of the endotherm is located around 58 °C, indicating a different crystallization structure of the SS. This discrepancy is even

more striking when looking at the SS ΔH_m° . On **PC-ADP:HDO-0%-W**, the addition of the polyester increases to a great strength the crystallization of the SS, as the heat of the process increases threefold compared to the reference **PC-0%-W**. However when the fluorinated polyester **PC-ADP:HDO8F-3%** is added, not only the T_m shifted to higher temperatures, but also the heat of the process is greatly reduced more than tenfold compared to the non-fluorinated polyester. This points out that the presence of fluorine in the polyester backbone disrupts the chain packing of the material. However, when fluorine is introduced as polyether, little to no change is observed in the SS ΔH_m° , signposting the poor compatibility between the polyether and the polycarbonate that leads to low mixing, and thus, no interferences in the structure occur.

In the case of the T_m arising from the HS, the difference between **PC-0%-W**, **PC-ADP:HDO-0%-W**, and **PC-ADP:HDO8F-3%** is minimal, having the latter the highest temperature. Although the incorporation of polyether in the structure did not modify the T_m of the SS, it caused a slight decrease in the melting endotherm of the HS. The T_m , which corresponds to the maximum of the endotherm, was similar to all the studied compounds, but the breadth of the melting peak changed, implying a large size distribution of the structured regions. Despite the different widths, the HS ΔH_m° of the different compounds were quite similar amongst them, with **PC-ADP:HDO-0%-W** showing the bigger deviation. Just as in the SS, the non-fluorinated polyester showed the highest HS crystallinities, which decrease once fluorine was incorporated in the polyester structure, while the incorporation of the polyether resulted in almost no change. This confirms that the addition of fluorine in the polyester inhibits chain packing and disrupts the structure while the polyether's addition leads to a segregated material with little to no interaction between the polyether and the rest of the compounds in the structure

The same behavior can be observed in the crystallization thermogram (Figure 6.28.B). Although all the samples displayed two peaks, only on **PC-ADP:HDO-0%-W** two well-defined exotherms were detected, as the crystallization of the HS shifted to higher temperatures, evidencing a higher crystallinity than the rest of TPUs. Just as before, the addition of fluorine as polyester decreased the crystallinity of the TPU while the addition in form of polyether lead to no major structural changes.

6.4.4. Tribological behavior

Density and hardness measurements of the plaques are outlined in Figure 6.29. Despite the disparities in chemical composition, only subtle differences were obtained in the evaluated TPUs. **PC-ADP:HDO8F-3%** and **PC-FLK-3%** exhibited the largest density values (Figure 6.29.A). Regarding the sample hardness (Figure 6.29.B), the gathered data do not differ significantly from one another, and values are within the standard range for prototypes with similar formulations.

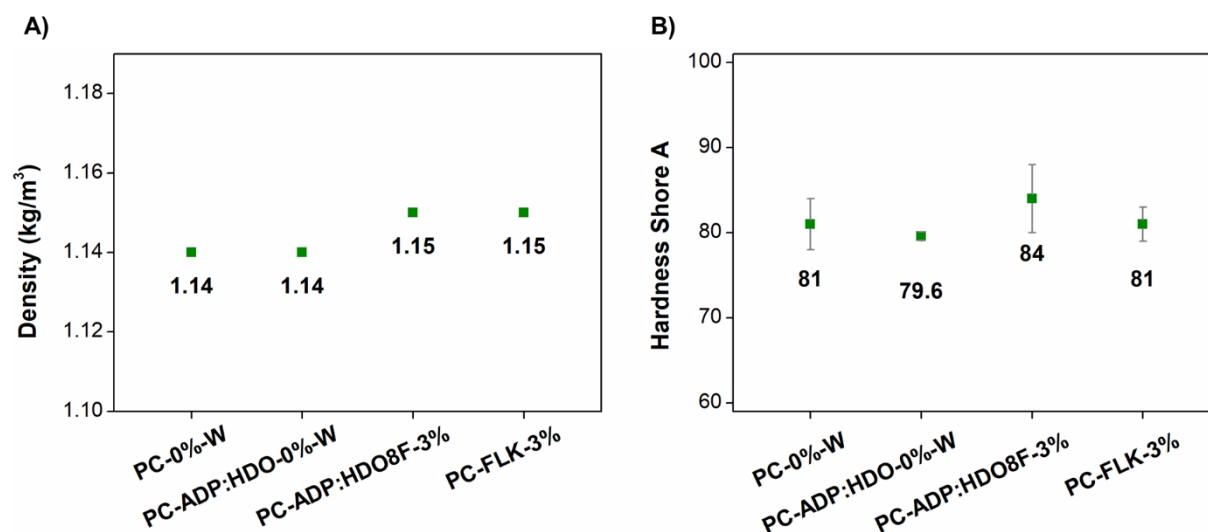


Figure 6.29. PC-based TPUs results of A) density (average value of four measurements carried out according to ASTM D792^[31] and B) Shore A Hardness (average value of ten measurements carried out according to ISO 868).^[32] Bars represent the standard deviation of the results.

Results of the TPU abrasions are depicted in Figure 6.30.A. Under the same tested conditions, PC-based TPUs exhibited an excellent abrasion resistance, which was even lower than the previously obtained in PCL-based systems. Interestingly, despite the low content of **ADP:HDO** polyester in the **PC-ADP:HDO-0%-W** (4.5 wt.%), a significant decrease of around 44% in the wear of the material was observed regarding the benchmark **PC-0%-W**. Conversely, blending the **PC** with the fluorinated **ADP:HDO-8F**, isostructural with the aliphatic, led to an increased abrasion of almost 66%. This could be correlated with the better crystallinity and thus, chain packing, observed by DSC measurements of the non-fluorinated **PC-ADP:HDO-0%-W** with respect to the fluorinated one. Amongst the studied compounds, **PC-FLK-3%** was the least resisting against abrasion, rising the volume loss up to 132% more than the benchmark **PC-0%-W**.

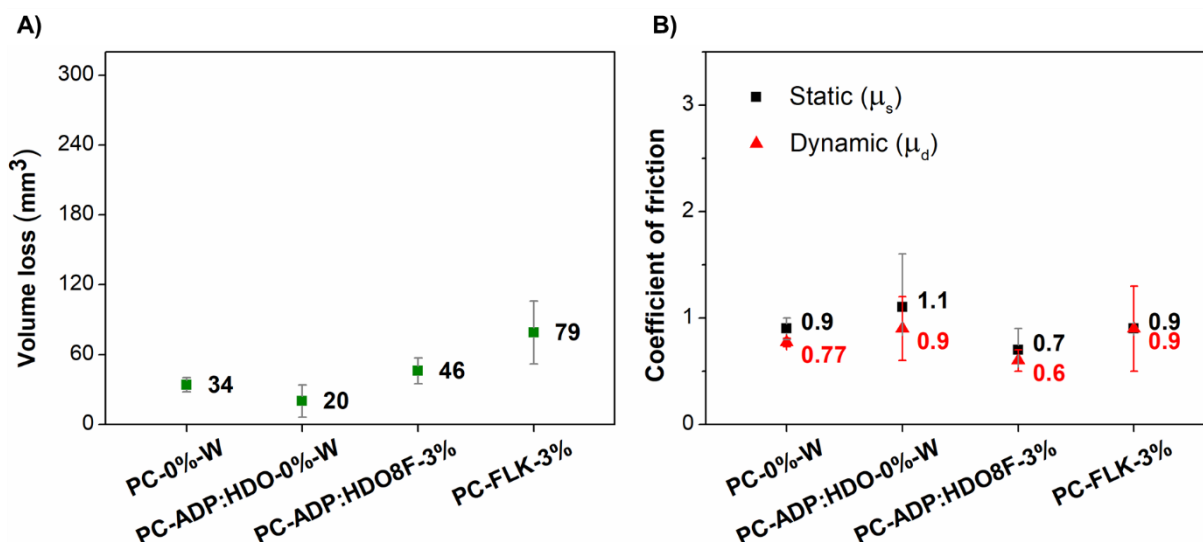


Figure 6.30. PC-based TPUs results of A) abrasion resistance (average value of three replicates carried out according to ASTM D5963:15)^[33] and B) friction against an aluminum surface (average value of three cleaned plaques measured carried out according to ASTM D1894).^[34] For comparison purposes, all the analyses were carried out with the same tested conditions (normal load and sliding speed) in the same apparatus. Bars represent the standard deviation of the results.

The friction of the TPUs studied under equal conditions of load and against an aluminum plane exhibited μ_s and μ_d values around the unity (Figure 6.30.B). The reference TPU, **PC-0%-W**, displayed low COF values, showing a similar opposition to motion than previous PCL-based TPUs ($\mu_s = 0.86$ and $\mu_d = 0.75$). In the case of PC-based TPUs, contrasting trends were observed in COF measurements. The blend with the non-fluorinated polyester, **PC-ADP:HDO-0%-W**, showed a 22% and 17% increase in the resistance to starting moving and sliding, respectively. Equivalently, **PC-FLK-3%** evidenced an increase of μ_d of 17% with respect to the **PC-0%-W**, while the μ_s did not vary. However, **PC-ADP:HDO8F-3%** exhibited positive results, reaching the lowest COF values among the four compounds. The addition of 3 wt.% of fluorine to the TPU formulation resulted in a decline of 29% in the μ_s and 28% in the μ_d .

However, it must be recalled, that **PC-0%-W** and **PC-ADP:HDO-0%-W**, contain the additive W. It was previously observed in the PCL-based formulation that its use caused an increase in the COF values and their standard deviation.

The analysis of these four materials revealed that both the blending of the second component and the presence of the fluorine compound in the mixture affect the tribological behavior of the samples. Blending a linear aliphatic polyester in the SS improved the abrasion resistance, but increased the friction. In contrast, the blend with the fluorinated polyester decreased the

COF values, but increased the tear of the material. Finally, the TPU containing the fluorinated polyether in the SS, **PC-FLK-3%**, exhibited the highest abrasion and one of the highest resistances toward motion.

Different data in the literature shows that perfluorinated polymers reduce friction of the material, by acting as an internal/ intrinsic lubricant, fostering the sliding of the chains. However, the reduction of the friction will be only reached if fluorinated chains successfully enrich the outermost region of the material with the halogen atoms. COF values suggest that only **PC-ADP:HDO8F-3%-W** might exhibit this event. On the contrary, **PC-ADP:HDO-0%-W** and **PC-FLK-3%** appear to have a more heterogeneous surface and therefore, displayed similar or higher resistance to motion than **PC-0%-W**.

Concerning the wear, when **PC-ADP:HDO-0%-W** was compared with **PC-0%-W**, there was an increase in the abrasion resistance possibly because the employed polyester is harder than the **PC**. It could be speculated that the polyester behaves as a filler, similarly to CaCO_3 or silica particles, which are known to increase abrasion resistance. In contrast, the fluorinated polyols were softer and as they incorporated the halogen, fewer interactions occur within the chains. The reduction of cohesive forces fosters a higher degree of wear. Moreover, polyethers are compounds with lower polarity than polyester polyols, which might be translated into weaker interaction with the carbonates and urethanes moieties, which might also cause an easier tear of the material.

6.4.5. Surface behavior: Wettability

Wettability of liquids on TPUs was evaluated by the static WCA and the SFE measurements of the material after removing the exuded compounds. Results obtained from both parameters are listed in Figure 6.31. As in the TPUs described above, measurements were carried out under the assumption of smooth, even, and chemically homogenous surfaces.

The reference TPU, **PC-0%-W**, manifested a hydrophilic behavior when its plaques were measured, notwithstanding that their results were slightly higher than those of the PCL-based formulation ($\text{WCA} \approx 77^\circ$). TPUs with polyesters as the co-polymerized SS do not reach the threshold value and thus, they are also classified as hydrophilic compounds. **PC-FLK-3%** was the only compound that overpassed the 90° WCA, becoming the sole TPU that could be classified as hydrophobic under the tested conditions.

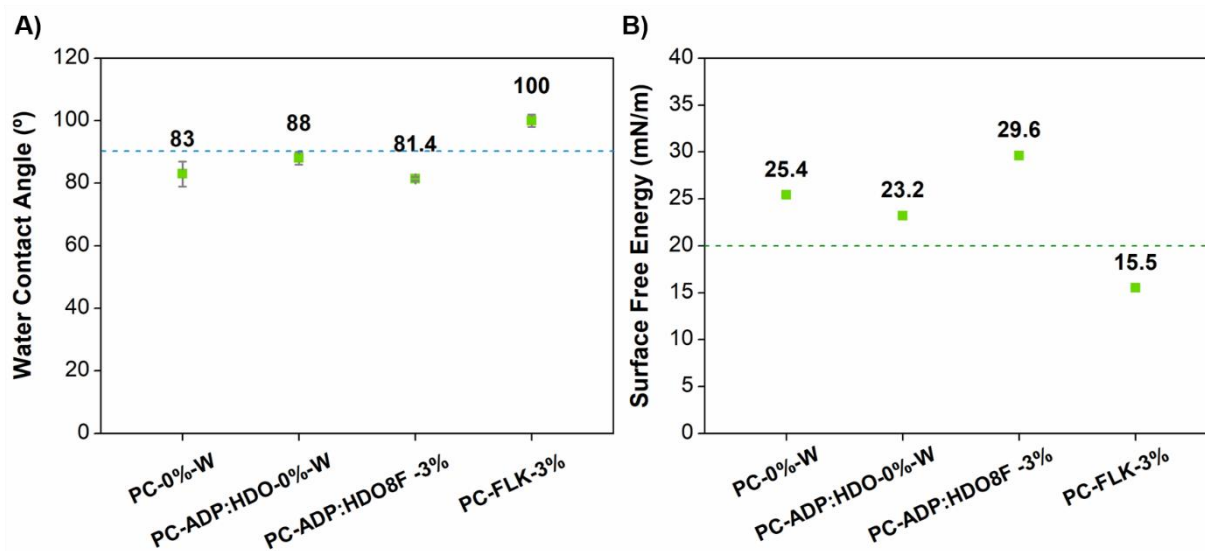


Figure 6.31. Results of PC-based TPUs in A) WCA (16 measurements on two cleaned plaques) and B) SFE (eight measurements on two cleaned plaques with water, ethylene glycol, and DMF). The blue dashed line indicates the 90° threshold in WCA and the green dashed line denotes the benchmark of PTFE's SFE. Bars represent the standard deviation of the results.

In terms of SFE, the produced TPUs displayed lower values than other previously reported TPUs, probably owing to the decrease in the HS content. **PC-ADP:HDO-0%-W** was the compound with the lowest SFE among the polyester/polycarbonate blend with about 23 mN/m in as-casted plaques. However, it was worth recalling that the fluorine-free TPUs were produced with the additive W, which in the PCL-based TPUs decreased to a great extent the SFE values. Therefore, it might be the reason for the lower SFE values of **PC-0%-W** and **PC-ADP:HDO-0%-W** in comparison with **PC-ADP:HDO8F-3%**. However, the relatively high SFE value of **PC-ADP:HDO8F-3%** suggests that the addition of **ADP:HDO-8F** does not enhance the TPU capability to repel liquids. Possibly, the 3 wt.% of fluorine is distributed along the material and does not segregate to the surface. This is even more noticeable when analyzing the dispersive and polar components of SFE (Figure 6.32). PC-based TPUs displayed polar components ranging from 5.5 to 9.2 mN/m, which corresponded to values lower than in the previous PCL-based TPUs (~10.7 mN/m). However, **PC-ADP:HDO8F-3%** does not show a stark change in the distribution of the polar and dispersive contributions, which could be expected if some fluorine migration was observed. In the case of blending a fluorinated polyether with **PC**, **PC-FLK-3%** reached even better results than the reference PTFE or PDMS (20 mN/m and 19.8 mN/m, respectively),^[38] denoting a lower interaction between the sample with the tested liquids. This result suggested that the segregation of the halogen to the interface was achieved, producing the desired decrease in the wettability of the material.

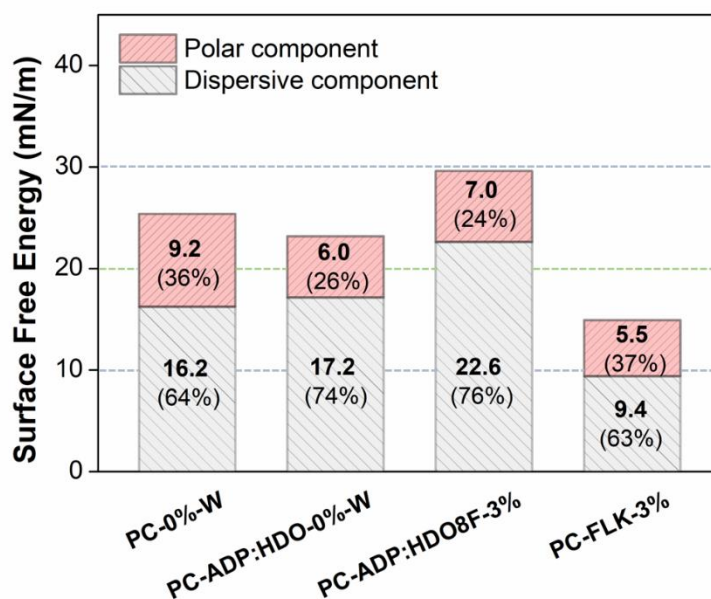


Figure 6.32. SFE decomposed in values and percentage of dispersive and polar components measured in cleaned surfaces. The green dashed line represents the PTFE's SFE value.

The PC-based formulation presented better results in terms of tribological and surface properties than those based on PCL-based TPUs (SFE \approx 30 mN/m), but they did not reach the reference values of PTFE when a polyester was blended. However, an enhancement of the WCA and SFE was reached with the partially perfluorinated polyether blend. Owing to the weaker cohesive interaction of the polyether with the matrix it could segregate to the surface, whereas the polyester strongly interacts with the other components of the TPUs, and under the processing conditions, did not segregate. The carbonyl group of the polyester will strongly interact with the carbonyl groups of the HS and of the SS promoting the compatibility and miscibility of the segments, with the corresponding restriction of movement. In contrast, the polyether produced lower and fewer interactions with the SS and HS, facilitating its migration to its surface.

From the gathered results, it seems that the limiting factor for the migration of the fluorinated segments was the high compatibility of the esters groups with the TPU matrix. Most of the studied parameters were measured with injected plaques at 23 °C, a temperature below the T_m of the SS ($T_m \approx$ 32 °C for PCL-based TPUs and $T_m \approx$ 40°C for PC-based TPUs according to the DSC analysis). At these conditions, the material still exhibited a high degree of crystallinity in both the SS and HS. Therefore, the mobility of the system was restricted which inhibited the rearrangement of the chains.

One last attempt was tried out with a non-chemically bounded perfluorinated additive to assess if the lack of mobility of the system might be the reason for the low migration of the halogen moieties to the surface. Thus, the reference TPU, **PC-0%-W**, was employed as the base formulation into which the additive (a fine PTFE powder) was added up to reach a concentration of 3 wt.% of fluorine in the final polymer. Once the material was injected, plaques displayed opacity (transmittance 55.2%), signposting a certain incompatibility of the additive with the TPU matrix. However, the measured friction and wettability displayed values of $\mu_s = 1.28 \pm 0.09$, $\mu_s = 1.2 \pm 0.1$, $WCA = 80 \pm 3^\circ$ and $SFE = 26.6 \pm 0.9$ mN/m, respectively. None of the studied parameters exhibited improvement from the benchmark polymer **PC-0%-W**.

6.5. Aging and annealing effect on TPU properties

Fluorinated chains disrupted the packing of the polymeric matrix and modified the thermal and mechanical properties of the materials. However, as described earlier, no relevant changes were observed in the surface properties, because fluorine moieties did not reach the interface of the compound. The lack of segregation towards the surface could be caused by the processing of the material. The rapid quenching during injection molding usually results in the departure of the equilibrium state, low crystallinity, and the inability to diffuse and rearrange the chains. Conversely, in the literature, in most of the cases reporting an enhancement of the surface properties by fluorine migration the TPUs were synthesized by the pre-polymer approach in solution which is a not scalable process.^{[54][55]} Even for those polymers produced from the melt, the analyzed films or plaques were formed by slow evaporation of the employed solvent.^{[56][46]} Hence, it allows a lengthier time to segregate the fluorinated fragments of the polymer chains to the outermost region of the materials and generate TPUs with low SFE. Dissolving the polymer in an organic solvent facilitates the reorganization of the backbone owing to the lack of the physical restriction of the chains. Moreover, commonly used organic solvents (DMF, DMAc, NMP, THF...) are polar and have relatively high boiling points, which require a certain temperature or vacuum for their evaporation process. When films were produced under these conditions, the temperature of the polymer was above the T_g and even the T_m of some of their segments, allowing the chains to rotate. The additional thermal energy of the system overpassed the interactions formed between the chains and fosters the migration of fluorine owing to its low surface energy.

Consequently, it was evaluated if subjecting TPUs to a certain temperature for a specific period, referred commonly as annealing, could promote the migration toward the surface of the fluorinated moieties of the polyols, trying to emulate similar mobility conditions as those in solution casting. In the case of the semi-crystalline polymers in a non-thermodynamic equilibrium, heating them at temperatures below their T_m might cause the rearrangement of the chains and the formation of a lower free energy system.^{[57][8]} Furthermore, the displacement toward the outermost region of the fluorinated moieties might allow the rearrangement of the chains in the bulk, obtaining a higher degree of micro-separation of the phases within the polymer and the recovery to some extent of the thermal and mechanical properties of the non-fluorinated analogs.

Thus, a preliminary annealing test was assessed with **PCL-DiolF-2%** as the studied TPU. This compound had a low fluorine content and exhibited similar results to its benchmark **PCL-BDO-0%**. The selected temperature for annealing was 80 °C. This corresponds to a temperature higher than the T_g and the SS T_m of the material, which might allow a higher degree of mobility to the fluorinated chains.

To determine the effect of the annealing, the TPU was resynthesized with the same formulation (see details in Table 6.10) and injected as was done previously. Thereafter, half of the obtained plaques were thermally treated at 80 °C for 24 hours and then, conditioned at 23 °C and 55% humidity. Contrary, the other half were stored from the outset under the same controlled environment. Following the stipulated period, plaques were maintained under the mentioned conditions and analyzed at 48 hours, 7 days, and 30 days after being injected.

Table 6.10. Summary of synthesized TPUs.

	PCL-DiolF-2%
wt.% F	2.0
Soft Segment	PCL-DiolF
Additive W	No
% HS	20.3
NCO/OH	1.0
Weight (g)	675
MFI (g/ 10 min) ^[a]	71.1

^[a] Tested conditions: 190 °C and 2.16 kg.

Among the diverse test previously carried out, the prime focus was the visual, tribological, and surface properties of the compound. The former would provide information about the generated blooming, whereas the latter would explore the wettability of materials treated differently.

6.5.1. Visual properties

Among the different visual parameters that may be evaluated, gloss and transparency are two of the most relevant, both of which depend on the roughness of the surfaces and the crystallinity of the system under study. Thermal treatments typically increase the order of the semi-crystalline polymers, which consequently might promote the formation of more translucent and/or opaque materials. Therefore, an analysis of the above-mentioned features over time might be helpful to acquire a preliminary estimation of the TPU morphological changes after the annealing.

The segregation of low molecular weight substances toward the surface does not only affect the aesthetic of the produced object but might also produce a risk in the consumer safety, as they might be released from the TPU to the environment and condense in other materials. Therefore, strong regulations have been approved to limit the quantities of volatile organic compounds (VOC) or semi-organic volatile compounds (SVOC) that can be released, especially for indoor applications. For that purpose, two different parameters are commonly controlled in produced polymers: the concentration of VOCs on a sample and the FOG value, which determines the capability of a plastic to volatilize substances that then are condensed on other surfaces, like the windshield of vehicles.^[58] In the case of the VOC, the released compounds are determined by GC analysis while the most standard methods to establish the FOG, are gravimetric, haze meter, and reflectometer. However, prior to the quantification of these parameters and the consequent optimization to reduce them, the release of the volatile compounds over time must be monitored. The first assessment corresponds to the evolution of blooming in thermally treating or non-treating TPUs, as these exuded substances might be the easiest to be released in form of VOC and/or FOG.

In the studied case, blooming was visually observed in non-treated **PCL-DiolF-2%** plaques, even after only 48 hours of being injected. However, the annealed plaques did not exhibit this phenomenon during the hole evaluated time (30 days). But further along, exuded substances did moderately appear on the samples.

To assess the effect of thermal treatment and to quantify the evolution of the blooming, the shine of the surface was measured by the specular gloss of the plaques after 48 hours, 7 days, and 30 days of injection. Results of the 60° Gloss over the month after being injected without removing the blooming of the plaques are illustrated in Figure 6.33.A. Both annealed and non-treated samples displayed low luster at short times. Nevertheless, the gloss value of annealed **PCL-DiolF-2%** exhibited a significant increase, reaching a semigloss appearance after 30 days. Conversely, the non-treated **PCL-DiolF-2%** plaques remained more matt and with lower gloss values after the same studied time.

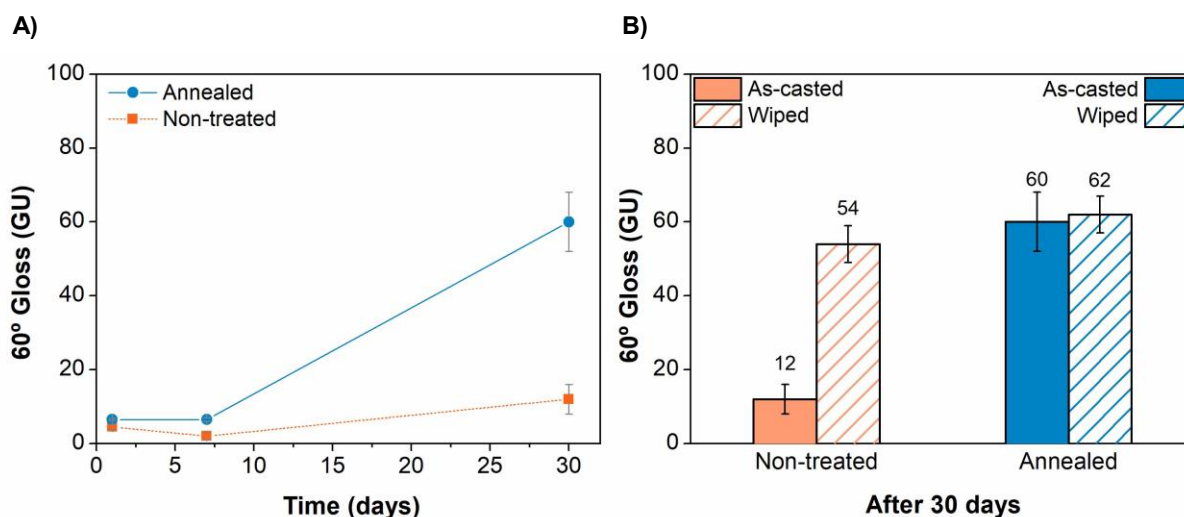


Figure 6.33. A) Evolution over time of 60° Gloss of the thermally treated and not treated as-casted plaques of **PCL-DiolF-2%**. B) 60° Gloss after 30 days of annealed and non-treated **PCL-DiolF-2%** plaques as-casted and after wiping the surface. Solid columns correspond to measurements to the as-casted plaques while sparse columns to wiped surfaces. Bars represent the standard deviation of the results.

Although the non-treated **PCL-DiolF-2%** displayed the lowest gloss value (Figure 6.33) its inherent luster was masked by the exuded substances, which modified the gloss from 12 GU to 54 GU after removing the blooming. In the case of the annealed samples, they displayed a higher shine than the non-treated ones, and wiping the surface of those plaques practically did not vary the measured parameters. Altogether, annealed and non-annealed samples reached similar gloss values after wiping, indicating that the tested compounds have an alike finishing, and the exuded substances were responsible for the material's unconventional matte appearance. As far as gloss is concerned, the thermal treatment did not affect the outermost region of the plaques. However, it looks like the annealing decreased the amount of blooming observed on the sample, which might be explained by the evaporation of the bloomed compounds at the temperatures reached during annealing.

In terms of transparency, the transmittance and the haze of thermally treated and non-treated samples are outlined in Figure 6.34. Analogously to the gloss test, both parameters were monitored along time without altering the external region of the plaques and subsequently, after 30 days, results were compared with those of the wiped surfaces. **PCL-DiolF-2%** exhibited high transmittance percentages (Figure 6.34.A), displaying no significant differences between untreated and annealed samples. However, there was an increment in the heterogeneity of the non-treated surface observed by the higher standard deviation of the results, probably due to the exuded substances. Once the blooming was removed, similar

values were obtained for both types of samples (Figure 6.34.B). In the case of the annealed plaques, no variation was observed between as-casted and wiped, denoting less blooming at the material.

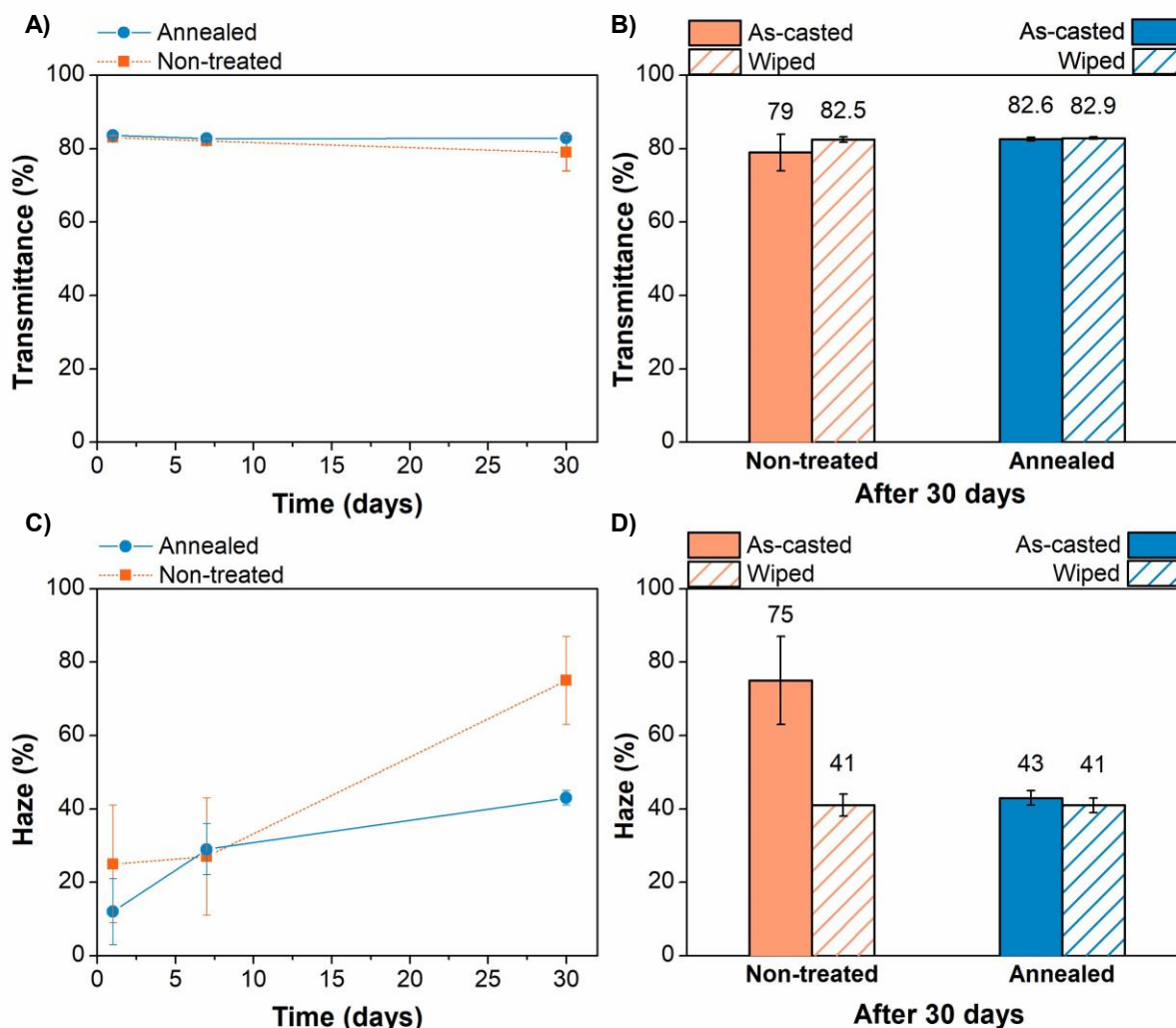


Figure 6.34. Transparency results of thermally treated and non-thermally treated **PCL-DiolF-2%** according to ASTM D1003.^[27] A) Evolution over time of transmittance. B) Transmittance after 30 days of as-casted and wiped plaques. C) Evolution over time of haze. D) Haze after 30 days of as-casted and wiped plaques. Solid columns correspond to measurements to the as-casted plaques while sparse columns to wiped surfaces. Bars represent the standard deviation of the results.

As for the haze of this compound (Figure 6.34.C), in both treated and non-treated TPUs, there was a progressive increase with time. However, the material became cloudier in the non-treated samples after 30 days. Moreover, this significant increase was coupled with an increment to the standard deviation of the measurement, denoting a more heterogeneous surface. Conversely, the annealed samples displayed lower haze values, although they also became light-diffusing materials (haze > 30 %). Just as in the case of the gloss, after wiping the surface

one month later of being injected the annealed and the non-treated samples displayed similar values (Figure 6.34.D). Both materials exhibited cloudiness. As with transmittance, the observed variation between the as-casted non-treated samples was caused by the presence of the exuded substances, as the plaques exhibited a decline on the haze of almost 54 % when this blooming was removed.

Regarding the foregoing, the annealing treatment did not alter the visual properties of the materials, but it affected the blooming. The presence of the exuded substances in the non-annealed plaques masked the real data, which was uncovered after the removal process. This behavior suggests that the applied temperature for the annealing had promoted the diffusion, and the released of these low molecular weight compounds from the matrix to the media, probably becoming VOCs. It is possible that as a consequence of the low vapor pressure of the bloomed substances, they were displaced toward the gas phase, which substantially decreased the remaining amount on the solid. Contrarily, the non-treated samples bloomed more progressively and the segregated substances remained on the surface. Therefore, by subjecting the TPU to a certain temperature the emissions of volatile compounds increase, suggesting high worrying values of VOC and/or FOG for this polymer. Therefore, additional treatments must be sought to quantify and reduce the produced bloomed substances before the potential commercialization of the product.

6.5.2. Surface behavior: Wettability

For the assessment of the wettability of the materials after thermal treatment, the produced TPUs samples were studied by WCA and SFE measurements over time. After 30 days, plaques were cleaned with a cotton cloth and measured again. Obtained results of these analyses are summarized in Figure 6.35 and Figure 6.36.

The WCA value of the annealed samples was superior to the non-treated plaques at all tested times, practically reaching the threshold of the hydrophobicity (Figure 6.35.A). The WCA of the non-treated samples displayed a slight rise with time. However, when as-casted plaques were compared with the wiped ones (Figure 6.35.B), the WCA decreased from 84° to 75°, which is similar to the previously reported value (Section 6.2.5). This fact indicates that the observed blooming masked the true hydrophilic behavior of the surface sample. In contrast, WCA values of the annealed samples remained within the limit of a hydrophobic surface (WCA > 90°) and no significant variation was determined between as-casted and wiped plaques.

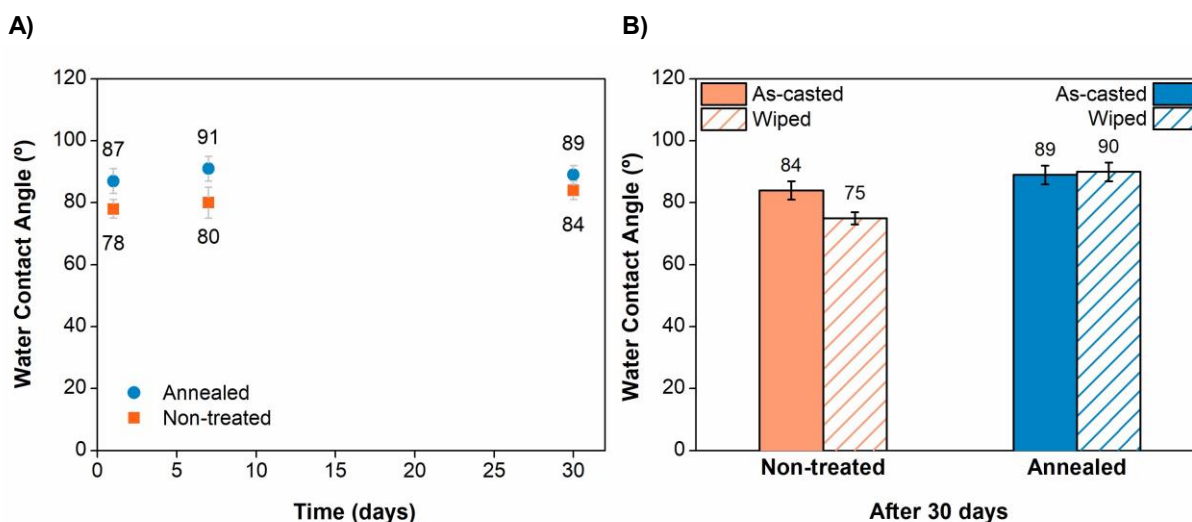


Figure 6.35. WCA results of A) as-casted annealed and non-treated **PCL-DiolF-2%** plaques along time and B) annealed and non-treated **PCL-DiolF-2%** plaques after 30 days. Bars represent the standard deviation of the results.

PCL-DiolF-2% displayed an increase of 15° in the WCA measurement by subjecting the plaques to 80°C for 24 hours. The preliminary annealing test resulted in an enhance in the surface hydrophobicity, probably by enriching the outermost region of the material with fluorine.

To confirm this trend, the SFE was equally determined over time (Figure 6.36.A), and results of as-molded and wiped plaques after a month are compared in Figure 6.36.B. In all measurements, the annealed samples displayed lower values than those of the non-treated plaques (Figure 6.36.A). Although the as-casted exhibited SFE inferior to other TPUs, the achieved results were far from the desired. Conversely, the annealed sample reached values similar to those reported by PTFE. The removal of the blooming, likewise as in the other explored parameters, seems to affect only the non-treated surfaces (Figure 6.36.B). While the annealed plaques exhibited a similar result after wiping the surface, once the exuded substances were removed from the non-treated plaques, the SFE increased. Therefore, treated plaques were less wettable than the previously studied TPUs which might possess the potential to be further developed.

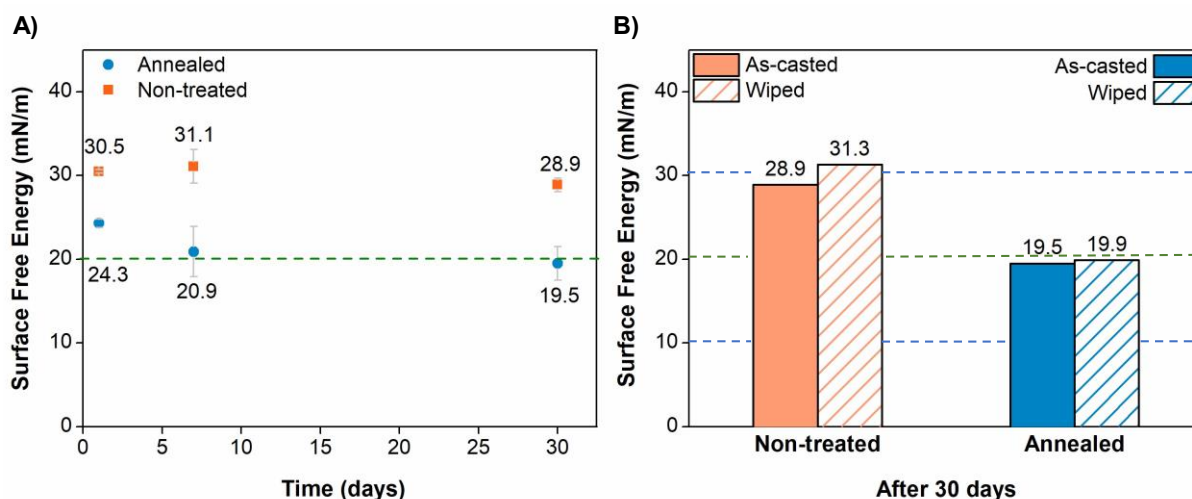


Figure 6.36. SFE results of A) as-casted annealed and non-treated **PCL-DioIF-2%** plaques along time and B) annealed and non-treated **PCL-DioIF-2%** plaques after 30 days. Bars represent the standard deviation of the results.

Concerning the wettability of the sample, an evident enhancement was obtained by annealing the material. SFE was reduced by 36 % from the wiped non-treated surfaces to the annealed plaques, pinpointing the presence of trifluoromethyl groups at the surface of the material. The side chain of **DioIF** seemed to migrate and increase the concentration of the halogen atom at the air/solid interface of the material, creating a more hydrophobic and less wettable surface. Therefore, interactions between liquids and the studied TPU surface were reduced after an annealing process.

6.6. Summary and concluding remarks

Two different TPU formulations with two SS matrices (polycaprolactones and polycarbonates) and different fluorine concentrations were tested and compared with the corresponding non-fluorinated benchmarks to produce hydrophobic materials with the potential to be anti-staining materials or be incorporated into wearable products. Although good results were obtained for the visual appearance and some of the tribological properties, the thermal and surface properties were inadequate.

The introduction of the fluorinated single-component in TPU using **PCL-DioIF** did produce the disruption of the packing of the sample and the reduction of the crystallinity of the system, compared with its fluorine-free analog. Furthermore, the incorporation of **DioIF** caused an increase in the wear and the COF values. However, no improvement on the WCA and SFE was

obtained by the incorporation of this fluorinated PCL, proving a lack of migration of fluorine to the surface.

Trying to increase the concentration of fluorine with different quantities of **ADP:DiolF** with the aim of saturating the outermost region of the material was also fruitless. The fluorinated **ADP:DiolF** remained distributed within the bulk of the material causing the reduction of the cohesive forces among the polymer chains by the branched side of **DiolF**. The rise of fluorine on the TPUs decreased the crystallinity of the systems producing larger wear and higher friction than the benchmark compound. No variations in WCA and SFE were observed in either of the tested TPUs.

A second formulation based on **PC** was assessed, with similar results. Although the change of formulation improved some of the studied properties, they did not overpass nor reach similar results to the benchmark PTFE. The blend of a polyester, **ADP:HDO** or **ADP:HDO-8F**, in the SS did not lead to satisfactory results either. However, the polyether blend **PC-FLK-3%** improves some of the studied parameters, especially in the wettability field, indicating that the high polarity of the polyester increases its miscibility in the TPU matrix which in turn, hampers the production of fluorine-enriched surfaces.

Finally, a post-treatment was evaluated to discern if the production method was incompatible with the desired properties. Subjecting a TPU to an annealing process did enhance to some extent the hydrophobicity of the studied system. Therefore, it seems that the major inconvenience was the quick quenching of the melted TPUs, which limits the rearrangement of the chains and inhibits the migration of fluorine to the surface of the material. From an industrial point of view, the requirement of treating each sample after being injected at a certain temperature is perhaps unfeasible for so little improvement.

6.7. Final conclusions about fluorinated TPUs

The proposed strategy to produce TPUs at low cost with a low concentration of fluorine through the incorporation of polyesters was not efficient, being the high compatibility of the segments and the rapid injection molding of the material the limiting factors. Nevertheless, the developed **DiolF** could be employed in other roles within the polymeric field. Its effect as chain extender or co-chain extender in amorphous TPUs has not been tested and could endow interesting behaviors. Furthermore, its polymerization in polyester or polyethers could generate low molecular weight compounds appealing as compatibilizers.

Literature

- [1] S. .- Gangal, P. D. Brothers, *Encycl. Polym. Sci. Technol.* **2010**, 1–15.
- [2] G. J. Puts, P. Crouse, B. M. Ameduri, *Chem. Rev.* **2019**, *119*, 1763–1805.
- [3] R. Dams, K. Hintzer, in *Fluorinated Polym. Vol. 2 Appl.* (Eds.: B. Ameduri, H. Sawada), The Royal Society Of Chemistry, **2017**, pp. 1–31.
- [4] S. Ebnesajjad, P. R. Khaladkar, in *Fluoropolymer Appl. Chem. Process. Ind.* (Eds.: S. Ebnesajjad, P.R. Khaladkar), William Andrew Publishing, **2018**, pp. 1–6.
- [5] H. M. McNair, J. M. Miller, in *Basic Gas Chromatography* (Eds.: H.M. McNair, J.M. Miller), John Wiley & Sons Inc., Honoken, New Jersey, **2018**, pp. 14–28.
- [6] T. Ho, A. A. Malik, K. J. Wynne, T. J. McCarthy, K. H. Z. Zhuang, K. Baum, R. V. Honeychuck, in *Step-Growth Polym. High-Performance* (Eds.: J.L. Hedrick, J.W. Labadie), **1996**, pp. 362–376.
- [7] D. W. Grainger, C. W. Stewart, in *Fluorinated Surfaces, Coatings, Film.* (Eds.: D.W. Grainger, C.W. Stewart), American Chemical Society, Washington, D.C., **2001**, pp. 1–14.
- [8] W. Ma, B. Ameduri, A. Takahara, *ACS Omega* **2020**, *5*, 8169–8180.
- [9] C. Tonelli, G. Ajroldi, *J. Appl. Polym. Sci.* **2003**, *87*, 2279–2294.
- [10] X. Jiao, Z. Feng, Q. Jiao, L. Xu, C. Li, B. Guo, C. Feng, Y. Zhao, *ACS Omega* **2021**, *6*, 4719–4725.
- [11] Y. S. Kim, J. S. Lee, Q. Ji, J. E. McGrath, *Polymer (Guildf).* **2002**, *43*, 7161–7170.
- [12] S. Chatani, R. J. Sheridan, M. Podgo, C. N. Bowman, *Chem. Mater.* **2013**, *25*, 3897–3901.
- [13] W. A. Zisman, in *Contact Angle, Wettability Adhes.* (Ed.: F.M. Fowkes), American Chemical Society, Washington, D.C., **1964**, pp. 1–51.
- [14] A. Fradet, M. Tessier, in *Synth. Methods Step-Growth Polym.* (Eds.: M.E. Rogers, T.E. Long), John Wiley & Sons Inc., Hoboken, New Jersey, **2003**, pp. 17–134.
- [15] Q. Zhang, M. Song, Y. Xu, W. Wang, *Prog. Polym. Sci.* **2021**, *120*, 101430.
- [16] W. Yu, M. Du, D. Zhang, Y. Lin, Q. Zheng, *Macromolecules* **2013**, *46*, 7341–7351.
- [17] J. M. Cox, M. F. Lerma, Francisco, Sonnenschein, *Low Haze Thermoplastic Polyurethane Using Mixture of Chain Extenders Including 1,3- and 1,4-Cyclohexanedimethanol*, **2012**, US 8242228 B2.
- [18] R. M. Bernabe, M. P. Barenys, J. S. Serna, *Thermoplastic Polyurethane Composition*, **2017**, WO 2017/116798 A1.
- [19] A. Güney, C. Gardiner, A. McCormack, J. Malda, D. W. Grijpma, *Bioengineering* **2018**, *5*, 1–14.
- [20] Y. I. Tien, K. H. Wei, *Polymer (Guildf).* **2001**, *42*, 3213–3221.
- [21] K. Kwiatkowski, M. Nachman, *Polymers (Basel).* **2017**, *9*, 1–13.
- [22] F. Sen Yen, J. L. Hong, *Macromolecules* **1997**, *30*, 7927–7938.
- [23] W. Liu, Y. Zhao, R. Wang, F. Luo, J. Li, J. Li, H. Tan, *Chinese J. Polym. Sci.* **2018**, *36*, 514–520.
- [24] M. Nouman, J. Saunier, E. Jubeli, N. Yagoubi, *Polym. Degrad. Stab.* **2017**, *143*, 239–

- 252.
- [25] J. T. Koberstein, *Encycl. Polym. Sci. Technol.* **2006**, 1–26.
- [26] *ASTM E313-05. Standard Practice for Calculating Yellowness and Whiteness Indices from Instrumentally Measured Color Coordinates*, West Conshohocken, PA, **2005**.
- [27] *ASTM D1003-00. Standard Test Method for Haze and Luminous Transmittance of Transparent Plastics*, West Conshohocken, PA, **2000**.
- [28] W. Wildner, D. Drummer, *Int. Sch. Res. Not.* **2014**, 2014, 1–5.
- [29] V. Kupka, L. Vojtova, Z. Fohlerova, J. Jancar, *express Polym. Lett.* **2016**, 10, 479–492.
- [30] Z. S. Petrovic, *Polym. Rev.* **2008**, 48, 109–155.
- [31] *ASTM D792-07. Standard Test Methods for Density and Specific Gravity (Relative Density) of Plastics*, **n.d.**
- [32] M. properties Technical Committee ISO/TC 61, Plastics, Subcommittee SC 3, *ISO 868. Plastics and Ebonite. Determination of Indentation Hardness by Means of a Durometer (Shore Hardness)*, **2003**.
- [33] ASTM International, *ASTM D5963: Standard Test Method for Rubber Property—Abrasion Resistance*, **2015**.
- [34] *ASTM D1894-00. Standard Test Method for Static and Kinetic Coefficients of Friction of Plastic Film and Sheeting*, West Conshohocken, PA, **2011**.
- [35] L. Maisonneuve, T. Lebarbé, E. Grau, H. Cramail, *Polym. Chem.* **2013**, 4, 5472–5517.
- [36] D. . Owens, R. . Wendt, *J. Appl. Polym. Sci.* **1969**, 13, 1741–1747.
- [37] D. H. Kaelble, *J. Adhes.* **1970**, 2, 66–81.
- [38] D. W. Van Krevelen, K. Te Nijenhuis, in *Prop. Polym.*, Elsevier B.V., Amsterdam, The Netherlands, **2009**, pp. 229–244.
- [39] H. Janik, M. Sienkiewicz, J. Kucinska-Lipka, in *Handb. Thermoset Plast.* (Eds.: H. Dodiuk, H. Goodman, Sidney), Elsevier, **2014**, pp. 253–295.
- [40] D. M. González-García, Á. Marcos-Fernández, L. M. Rodríguez-Lorenzo, R. Jiménez-Gallegos, N. Vargas-Becerril, L. Téllez-Jurado, *Polymers (Basel)*. **2018**, 10, 991–1006.
- [41] T. R. Hesketh, J. W. . Van Bogart, S. . Cooper, *Polym. Eng. Sci.* **1980**, 20, 190–197.
- [42] J. D. Menczel, L. Judovits, R. B. Prime, H. E. Bair, M. Reading, S. Swier, in *Therm. Anal. Polym. Fundam. Appl.* (Eds.: J.D. Menczel, R.B. Prime), John Wiley & Sons Inc., Honoken, New Jersey, **2009**, pp. 7–239.
- [43] B. D. Ahn, S. H. Kim, Y. H. Kim, J. S. Yang, *J. Appl. Polym. Sci.* **2001**, 82, 2808–2826.
- [44] P. Król, B. Król, *Colloid Polym. Sci.* **2012**, 290, 879–893.
- [45] P. Król, B. Król, K. Pielichowska, S. Pikus, *Colloid Polym. Sci.* **2011**, 289, 1757–1767.
- [46] H. Tan, X. Xie, J. Li, Y. Zhong, Q. Fu, *Polymer (Guildf)*. **2004**, 45, 1495–1502.
- [47] K. L. Kull, R. W. Bass, G. Craft, T. Julien, E. Marangon, C. Marrouat, J. P. Harmon, *Eur. Polym. J.* **2015**, 71, 510–522.
- [48] G. Abts, T. Eckel, R. Wehrmann, *Ullmann's Encycl. Ind. Chem.* **2014**, 1–18.
- [49] Y. Yuan, J. Li, Y. Dong, H. Miao, *J. Coatings Technol. Res.* **2020**, 17, 777–783.
- [50] J. Liu, B. Wang, Y. Yuan, R. Liu, Z. Li, X. Liu, *J. Coatings Technol. Res.* **2017**, 14, 233–241.
- [51] M. Rogulska, A. Kultys, S. Pikus, *J. Therm. Anal. Calorim.* **2017**, 127, 2325–2339.
- [52] G. Jintang, Z. Meihua, T. Yan, B. Wang, *J. Mater. Sci.* **2007**, 42, 5508–5515.
- [53] R. Zhu, X. Wang, J. Yang, Y. Wang, Z. Zhang, Y. Hou, Y. Li, *Appl. Sci.* **2017**, 7, 1–15.
- [54] C.-L. Wu, S.-H. Chiu, H.-T. Lee, M.-C. Suen, *Polym. Adv. Technol.* **2016**, 27, 665–676.
- [55] T. B. Nguyen, A. Martel, R. Dhal, G. Dujardin, *Synlett* **2009**, Supporting informaiton.
- [56] O. Smirnova, A. Glazkov, A. Yarosh, A. Sakharov, *Molecules* **2016**, 21, 1–10.
- [57] E. W. Fischer, *Pure Appl. Chem.* **1972**, 31, 113–132.
- [58] International Organization for Standardization, *ISO 6452:2000. Rubber- or Plastic-Coated Fabrics -- Determinations of Fogging Characteristics of Trim Materials in the Interior of Automobiles.*, **2000**.

Chapter 7

Objectives

Part II

Chapter 7 describes the general objectives of the second project developed in collaboration with Lubrizol Advanced Materials Spain S.L. in the studied of TPUs films.

7. Objectives II

The second project of this thesis is closely related to the industrial production of amorphous film TPUs. This research is in collaboration with an on-going global study of Lubrizol Advanced Materials Spain S.L to produce in continuous a material already synthesized batch-wise in other facilities of the company.

The main target was to identify and study some of the chemical features of the synthetic process to generate the target TPU with high reproducibility and excellent quality. Hereafter, the following variables have been explored:

- Variability of the raw materials (**ECL** monomer and **H₁₂MDI**).
- Control of the M_n of the synthesized PCL and its thermal stability.
- Control of the components of the polyol mixtures.
- Chemical comparison between TPU produced in batch and in continuous.
- Control of the catalyst loading.
- Speciation of the antioxidant in polymeric mixtures.
- Detection and identification of imperfections on the produced films.

Chapter 8

Part II. Process control

Chapter 8 summarizes some of the studied parameter to control the process and quality of a new TPU-based film. Variables as the raw materials, the involved polymers, the stability of the mixture and the produced polymer are some of the factors under consideration.

8. Process control

The second part of this doctoral thesis was focused on the study and development of several control parameters for the synthesis of an aliphatic TPU-based film designed as a protective material for enhancing the service life and appearance of the valuable objects it covers. For this reason, the extruded films must exhibit excellent abrasion, impact, and erosion resistance. TPUs are known for their high wear resistance caused by their high-energy absorption and elastic deformation without tearing. Moreover, their mass production at a reasonable cost is one of their greatest advantages for their selection as polymers.

The multinational company Lubrizol synthesizes the target TPU and commercializes it as pellets. Afterward, it is up to the client to extrude the material under the recommended parameters. The production is carried out completely in Montmeló factory, from the formation of the PCL to the polyol mixture, the TPU synthesis, and the pelletization. The synthesis of the polyester is executed batchwise, while the TPU is formed on a multi-tonne scale in a reactive twin-screw extruder.

The studied aliphatic TPU was successfully synthesized with the desired batchwise quality in other company facilities. However, when this polymer was aimed to be commercialized at a large scale (multiples tonnes), the production had to be adapted to a continuous process, targeting first-class quality materials with high reproducibility among the fabrications. Another requirement is that the resulting TPU must exhibit a defect-free surface with excellent optical properties such as high degree of transmittance, clarity, and gloss. However, initial results in the continuous process led to materials with variable quality between the productions. The extruded films were not as flawless as in the batchwise production and displayed visual defects that distorted the appearance of the sheet. Large-scale processes such as reactive extrusion, injection molding, or calendaring require the material to withstand elevated temperatures (above its T_g , or T_m) and high shear to produce fast flowability along the screws, molds, or channels. These harsh conditions might degrade the compound, vary the M_n , and modify

certain material properties, like its transparency or its mechanical and electrical performance.^[1] The observed imperfections, which were considered as gels, might originate from the synthetic process, or during the posterior extrusion of the film.

The source of gel formation is complex and highly dependent on the raw materials, the synthetic processes, the blends, or the presence of any contaminants. In addition, humidity, polymer stabilization packages, catalyst residues, and dispersion of inorganic additives may be other factors that may increase the number of imperfections.^{[2][3][4]} Although these defects are commonly detected in linear polyethylene (PE), they may be present in any material used to produce films. Usually, their existence causes the decline of their mechanical properties, weakening the material, and ultimately leading to the film rupture. In the literature, several types of gels from diverse origins have been reported, but the most observed are:

- Oxidized gels. They are generated through an oxidative process, usually in the stagnant regions of the screw. They can appear as crosslinked areas, or even in the worst-case scenario, carbon degradation, with the subsequent variation of the polymer color.^[5] Their presence can be mitigated by employing long residence times screw under an inert atmosphere. Furthermore, the use of fluoropolymers additives might help to reduce friction.^[6]
- Highly-entangled gels. They represent areas where the polymer M_w is higher than the rest and cannot be dispersed during the extrusion process. Predominantly, these defects will not display a different color from the matrix. They might be reduced by applying shear forces while extruding the material to disentangle the chains.
- Unmelted gels. This type of defect originates from a portion of the polymer, which does not melt and exits the die as a solid fragment owing to lack of stress or high extrusion rates during the processing.
- Agglomerates. They typically arise from fillers or additives (*e.g.*, silica, talc anti-blocking agents, colorants...) incorporated into the formulation, and with low matrix compatibility. For such imperfections, special attention must be paid to the solubility and compatibility with the formulation.
- Contaminants. They may come in at different points of the process from materials such as fibers, lint, inorganic salts, organic or metallic particles, or silicone rubbers, among others.^[7] Moreover, some cross-contamination of other polymers or reagents should equally be considered.

To be able to reach the specified TPU quality, the number of detected gels had to be reduced. To this end, Lubrizol implemented a global statistical study designed as a Design of Experiments (DoE) analysis to explore correlations between multiple variables of the production and quality of the patented product. This section of the thesis focuses on some of the explored chemical features of the process, such as the raw materials, the variability between the synthesized PCLs, the TPU properties, and the characterization of the extruded films (purple variables in Figure 8.1). Factors like temperature profiles, shear, reagent stoichiometry, or addition order, among others, were also assessed by Lubrizol.

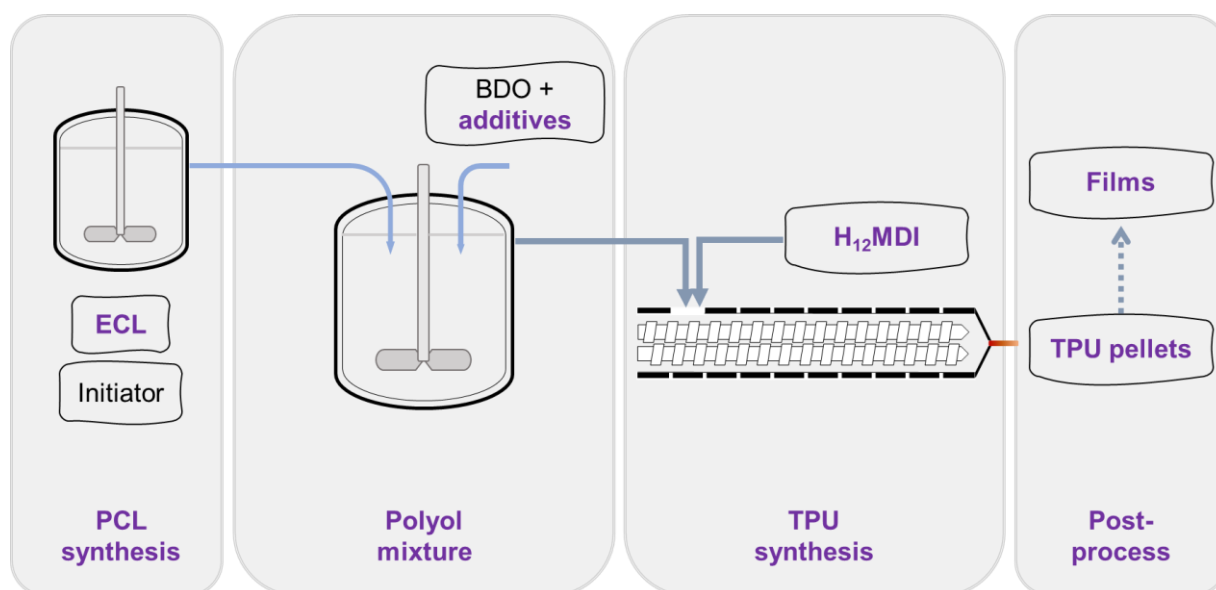


Figure 8.1. Overview of the synthetic process and the studied parameters (in purple).

8.1. System description

The target TPU is a low crystalline material with a Shore A hardness of around 80-90. It is based on a low- M_n PCL as SS, a cycloaliphatic diisocyanate, and a common chain extender (see Figure 8.2 for detailed structures). Moreover, to enhance the processability and stability of the product, some stabilizers, antioxidants, and additives were incorporated. The produced TPU is under patent; therefore, the exact composition and distribution of the chemicals likewise as some specific aspects of the process must be sought elsewhere.

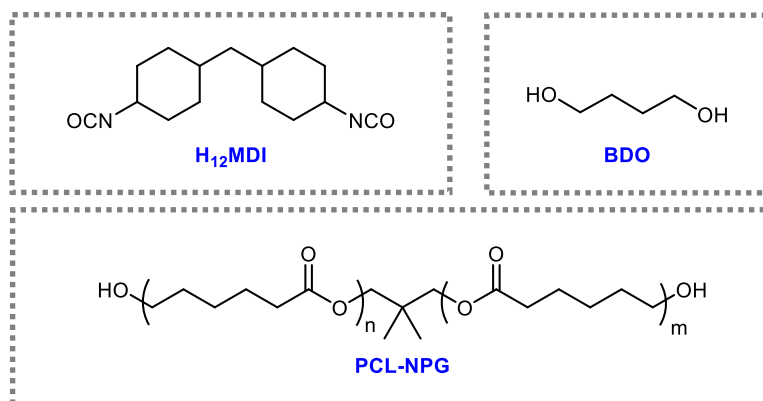


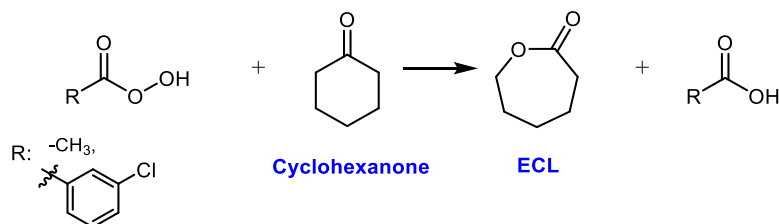
Figure 8.2. Chemical structure of the employed components.

This project has its origin in the adaptation of a batchwise synthesis to an automatic, continuous, scaled-up production of the same material. Batch-fed processes are technologically simpler as less equipment is usually required. Concretely, for the synthesis of the studied TPU, the reaction takes place in a tank at a fixed low temperature for a certain period of time. Nevertheless, the main disadvantages are related to the scale, the difficulty to control the heat transfer, and the homogenization once the viscosity of the mixture increases, resulting in materials with high heterogeneous M_n . Subsequently, the produced polymer must be cured and extruded through high-shear mesh to narrow the TPU polydispersity, which decreased the synthesis yield. All these processes resulted in only being able to produce TPUs on a sub-tonnes scale.

Conversely, in the continuous process developed in Montmelò facilities, the synthesis is carried out in a reactive extrusion screw, which allows the automatic incorporation of the involved reagents at different temperatures and stages of the production line. Therefore, more controlled conditions (atmosphere, temperature, residence time...) can be established, producing polymers with lower polydispersity and higher yields. Although it also requires the curing of the pellets, the temperature and the times are shorter than in the batchwise process.

This continuous synthesis allows commercial-scale production with high efficiency and elevated yield. Notwithstanding, to produce appropriately the desired material, some modifications were necessary. Several synthetic parameters, as the ratio of reagents, temperatures, and stabilities of the mixtures were considered and altered if required.

ϵ -caprolactone (ECL) is the basic reagent of PCL synthesis. Traditionally, ECL has been synthesized by a Baeyer-Villiger oxidation of cyclohexanone by a peroxydicarboxylic acid, like peracetic acid or *m*-chloroperbenzoic acid (Scheme 8.1).^[8]



Scheme 8.1. General synthesis reaction to form **ECL**.

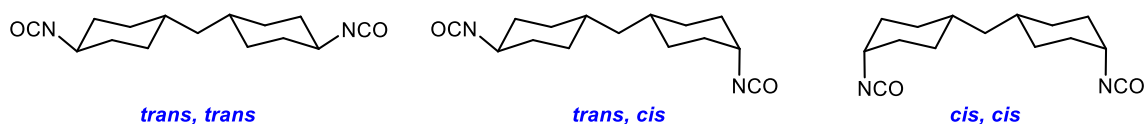
However, the employed oxidants are potentially unsafe materials owing to being shock-sensitive, highly irritant, and explosive under some conditions. Therefore, their use is currently discouraged, and other oxidants and catalysts are employed to obtain the desired product.^{[9][10]} The principal producers have adapted the synthetic method to their own process.^{[11][12][13]} Historically, Lubrizol's PCLs were manufactured from **ECL** supplied by two companies, A and B (due to a confidential agreement, the name of the suppliers was not disclosed).

The employed diisocyanate for the TPU production is the cycloaliphatic **4,4'-dicyclohexylmethane diisocyanate (H₁₂MDI)**, which is also referred to as hydrogenated **MDI**. Owing to the excellent hydrolysis resistance and good mechanical properties of its TPUs, it is frequently consumed in coatings.^{[14][15][16]} This cycloaliphatic compound exhibits lower reactivity toward alcohols and amines than other commonly used diisocyanates like **HDI** and **MDI**. Compared with the former, the isocyanate of **H₁₂MDI** is bound to a secondary carbon, while **HDI** is in a primary and more reactive position.^[17] Regarding **MDI**, the aromaticity of the latter increases the susceptibility to nucleophilic substitution.

Although **H₁₂MDI** is a widely employed substance, little attention has been paid to the study of its composition or its structure. It is commercialized as a liquid mixture of three geometric isomers **4,4'-trans**, **trans**-, **4,4'-trans**, **cis**-, and **4,4'-cis**, **cis**- and four constitutional **2,4'-isomers** (Figure 8.3). The terminology *cis* or *trans* is labeled with respect to the

methylene group in between the two cyclohexyl rings and refers to the so-called axial and equatorial position of the isocyanate. It is noteworthy that a proportion superior to 25 % of the **4,4'-trans, trans**-isomer at temperatures around 25 °C might generate heterogeneities on the mixture as a consequence of its precipitation.^{[18][19]} Hence, the distribution of the isomers must be extremely controlled.

4,4'- diisocyanate isomers



2,4'- diisocyanate isomers

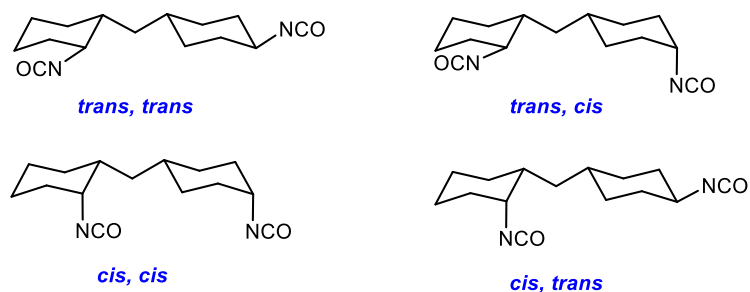
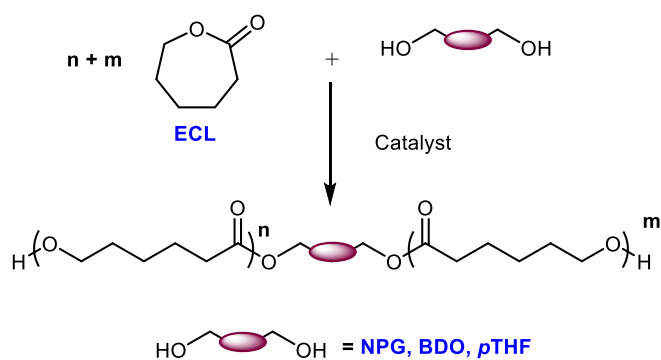


Figure 8.3. Structure of the isomers contained in the commercial mixture of **H₁₂MDI**.

The first step in the TPU production corresponds to the synthesis of the PCL *via* **ECL**'s ROP, benefiting from the release of the monomer ring strains. The reaction is conducted at a relatively high temperature and in some instances, a hydroxylated compound is required as initiator (Scheme 8.2).

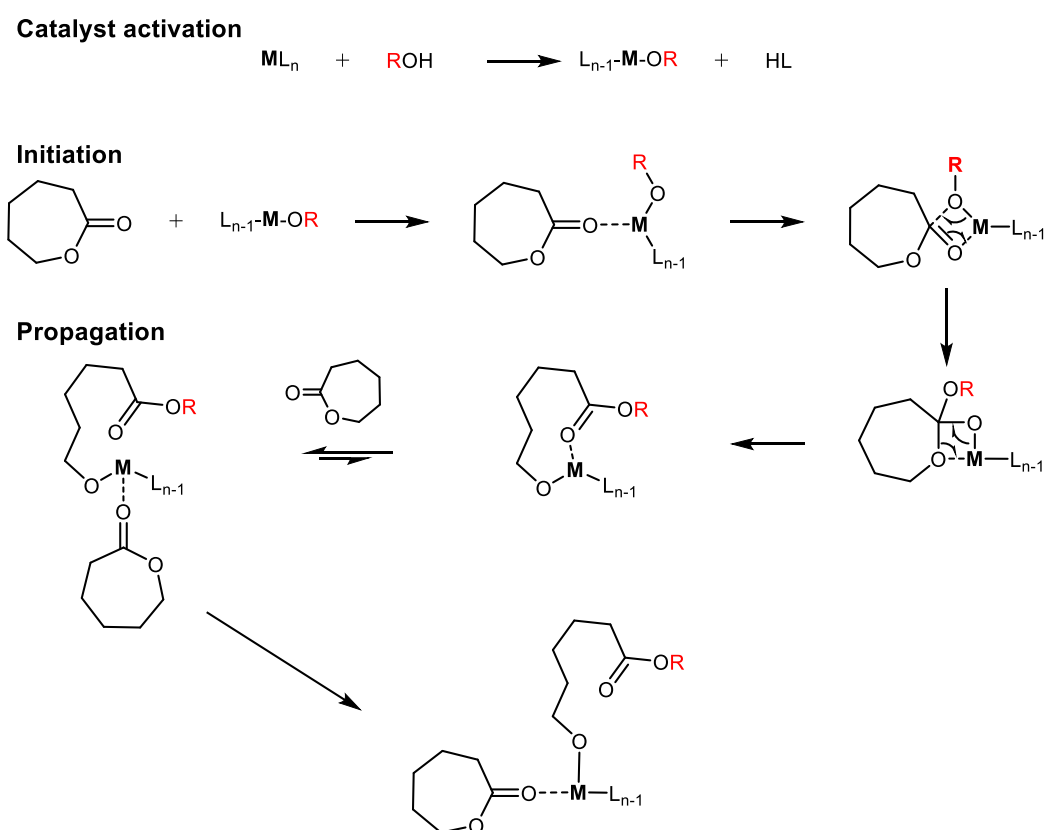


Scheme 8.2. Overview of a **PCL** synthesis.

The reaction is catalyzed by a metal complex (ML_n) through a coordination-insertion mechanism. The metal complex may comprise several types of ligands, such as trifluoromethanesulfonate^{[20][21]} or borohydride,^{[22][23]} but the most commonly used in the

industry are carboxylates.^{[24][25][26]} Finally, in industrial production, additives and/or antioxidants are added to enhance the stability and durability of the produced materials.

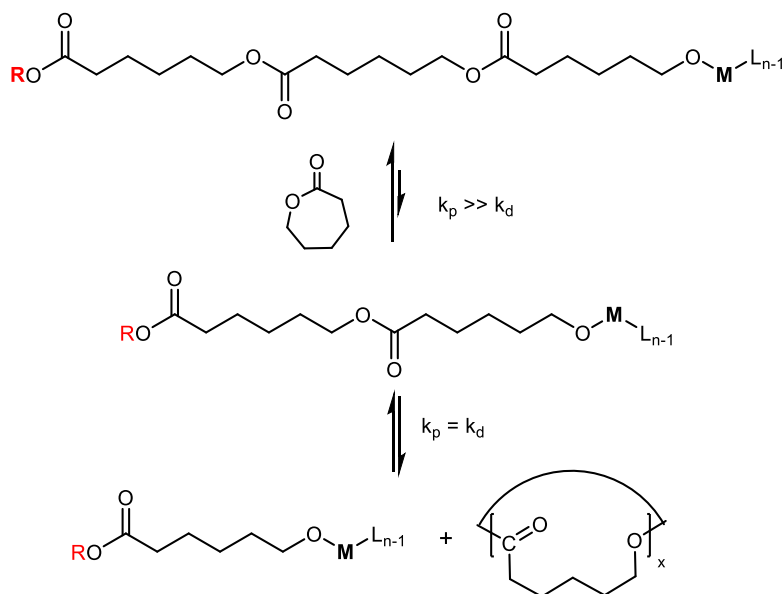
The mechanism of the reaction is a process co-initiated by a nucleophile, normally an alcohol and the catalyst. The activation of the metallic compound takes place by exchanging one of the ligands by an alcohol present in the media. Then, in the initiation step, the cyclic monomer coordinates to the metal through the polarization of the carbonyl, and subsequently, the alkoxide carries out a nucleophilic attack over the carbonyl, cleaving the *O*-acyl bond and ring-opening the monomer. Ultimately, the carbonyl is decoordinated, and a new **ECL** enters the catalytic cycle (Scheme 8.3).^[27] Finally, the hydrolysis of the active metal alkoxide produces a hydroxyl end on the polymer and deactivates the catalyst.



Scheme 8.3. Proposed mechanism for the catalyzed ROP of **ECL**. Adapted from ^{[28][29]}.

Despite the formation of the linear PCL, other side reactions might occur. The propagation stage comprises a reversible step in which not only the desired linear chains are produced (k_p), but also conformationally stable cyclic compounds are formed by transesterifications in the depolymerization process (k_d) (Scheme 8.4).^{[30][31][32]} Concretely, the back biting, either to form the monomer or the dimer, is a competing reaction with the linear polymerization, especially

as times go on. The rate of each reaction is the fact that determines the concentration of both types of products in the mixture.

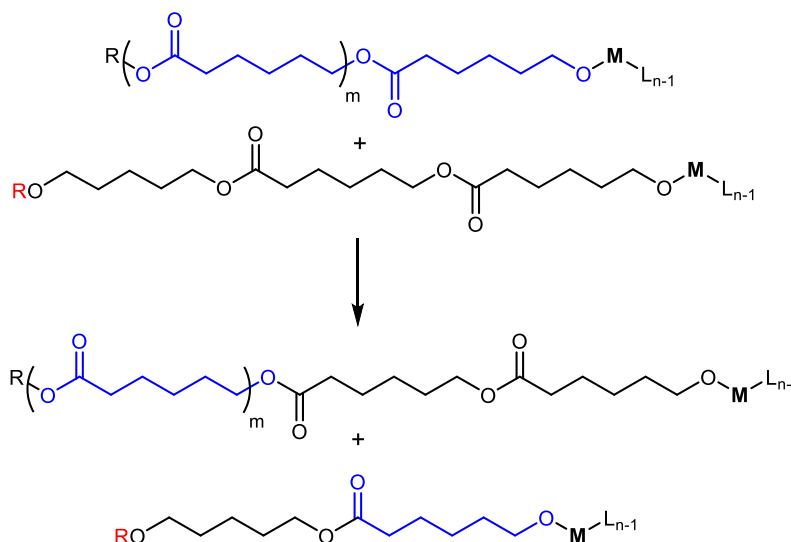


Scheme 8.4. Overview of the cycle formation.

The formation of cycles is commonly fostered at high temperatures and high polymerization degree, as a gain of entropy occurs with the cyclization.^[33] Previous studies by our research group revealed that the formation of the cyclic monomer from the linear PCL quickly reaches an equilibrium state, signposting that the back-biting process is thermodynamically controlled. It was observed that the lower the temperature at the later stages of the reaction, the smaller the monomer concentration that could be reached.^[34] Conversely, the kinetic product of the cyclization is defined as a compound formed by at least one new σ -bond, stable during the polymerization and that does not participate in it afterward.^[35] This fact was confirmed in a previous evaluation, where the dimer showed a constant concentration once produced, which may indicate that the **ECL dimer** is the kinetic cyclization controlled product.^[36] The lack of reactivity in the polymerization can be explained by the low ring strain of the larger cyclic compounds in which the activation energy associated with its formation is reported to be similar to its ring-opening.^[37] Thus, its concentration is independent of the time and the temperature.

Although some articles of the literature reported cycles up to 7 monomeric units,^[37] the size of the cycles depends on the polymerization degree of the polyol. The larger the M_n of the PCL, the larger they might be formed. The relatively small degree of polymerization of the studied PCLs decreases the probability of forming big macrocycles.

In addition to the back-biting reaction described as intramolecular transesterification, intermolecular transfer might also occur (Scheme 8.5). This second side reaction involves chain scission that rearranges the M_n distribution of the mixture.



Scheme 8.5. Intermolecular transesterification.

Both inter- and intramolecular side reactions depend on the temperature, the catalyst, and the involved reagents.^{[29][38][39]} Although they occur during the polymerization, they especially exhibit a significant effect in the post-synthetic process, leading to an increase in the polymer polydispersity.

Industrial processes are carried out at a large scale and involve, apart from high quantities of raw material, large facilities. Aiming an easier transport and accessibility of the involved chemicals, whenever possible, reagents are desired to be liquid. Owing to that, PCLs are not solidified, but maintained melted at a relatively low temperature. Prior to the reaction with the isocyanates, PCLs are mixed with the selected chain extender and the compatible additives and/or stabilizers, creating what is known as the polyol mixture. This mixing process ensures a constant ratio between the reagents. However, the multi-tonne scale requires high volumes of polyol mixture, which are consumed at different times during the TPU production. Although the temperature of the mixture is set to be inferior to that of the polymerization, some side reactions might arise and cause variability in the produced compound. Therefore, the composition and stability of said mixture must be carefully considered.

Finally, after the reactive extrusion reaction where the TPUs are formed, the extrudate is processed into spherical pellets. The formation of the granulates is followed by cooling down

the material submerging it in a water bath. Subsequently, the produced material is separated from the liquid and dried in an oven.

Although gels cannot be observed on the pellets, once the sample is extruded, imperfections on the film appear. These defects differ from the rest of the material owing to a refractive index different from that of the matrix. Even in some cases, their size was big enough to be detected by the naked eye as small white spots in the films. To quantify the produced gels, a quality-control methodology based on an Optical Control System (OCS) was implemented in Lubrizol's facilities. The equipment coupled an extrusion system with a precision camera to detect imperfections of the produced material. Through a standardized procedure, it counts the number of gels per unit of area and categorizes them according to their dimension into macrogels or microgels. However, their composition and origin could not be identified through the already developed protocols and further exploration of the different steps of the process is required.

After a detailed overview of the process, some of the parameters that have been studied in collaboration with Lubrizol to standardize the quality of the produced material will be described in the following section. The quality and the composition of some of the raw materials were sought. Subsequently, the characterization of the PCLs, polyol mixtures, and TPUs were assessed to gain knowledge of the products and detect abnormalities affecting the production. In addition, the role of some additives was also examined. Finally, films containing gels were analyzed to shed light on their formation and composition.

The data reported in this thesis falls within the DOE analysis, aiming the determination of correlations between the studied parameters, the product, and its quality.

8.2. Raw material analysis.

Targeting the avoidance of unexpected outcomes such as unusual reaction's exotherm, or abnormal performances in the produced materials, a study of the essential chemicals was pursued. The following section aims to report the analyses and methodologies developed to ensure the reproducibility of the employed chemicals among different batches and suppliers. Amongst the numerous compounds engaged in the TPU synthesis, particular attention was directed to **ECL** and the cycloaliphatic **H₁₂MDI**.

Some of the created methods were intentionally designed to be implemented in Lubrizol's facilities, so the use of techniques as NMR spectroscopy may be limited there. Mainly, GC was selected as the routine technique for the systematic control of the raw materials, as it typically requires simple preparation, short analysis time and easy access to the equipment.

8.2.1. ϵ -caprolactone monomer

To identify any abnormality that might modify the polymerization reactivity and assess the interchangeability when purchasing **ECL** from Company A and B, 3 different samples from each supplier were compared through GC analysis, ICP-MS quantification, and NMR spectroscopy. The variability between the two companies was evaluated by the presence of **ECL dimer**, stabilizers, additives, or metal traces, in addition to **cyclohexanone's** remanents. Those substances are possible products that may originate from the **ECL** synthesis and might interfere in the posterior production of polymers.

¹H NMR and ¹³C{¹H} NMR spectra of the samples were recorded in CDCl₃ to determine the presence of possible contaminations or traces of organic substances. Owing to the nature of the compound under study, the deuterated solvent was filtered through basic alumina to remove any traces of HCl (the common degradation product of the solvent) and avoid the ring-opening of the monomer.

The studied compound consists of a seven-membered ring reported to be preferentially in a chair-like conformation in solution.^[40] Owing to the closeness to the ester group, both α and ϵ protons are deshielded, and their ¹H NMR signals are observed as crown-like peaks at 2.5 ppm and 4.1 ppm, respectively (Figure 8.4). Finally, two additional multiplets were detected at 1.6 ppm and 1.7 ppm. The former overlaps the signal of γ and δ methylene, whereas the latter is derived from the β -CH₂ group.

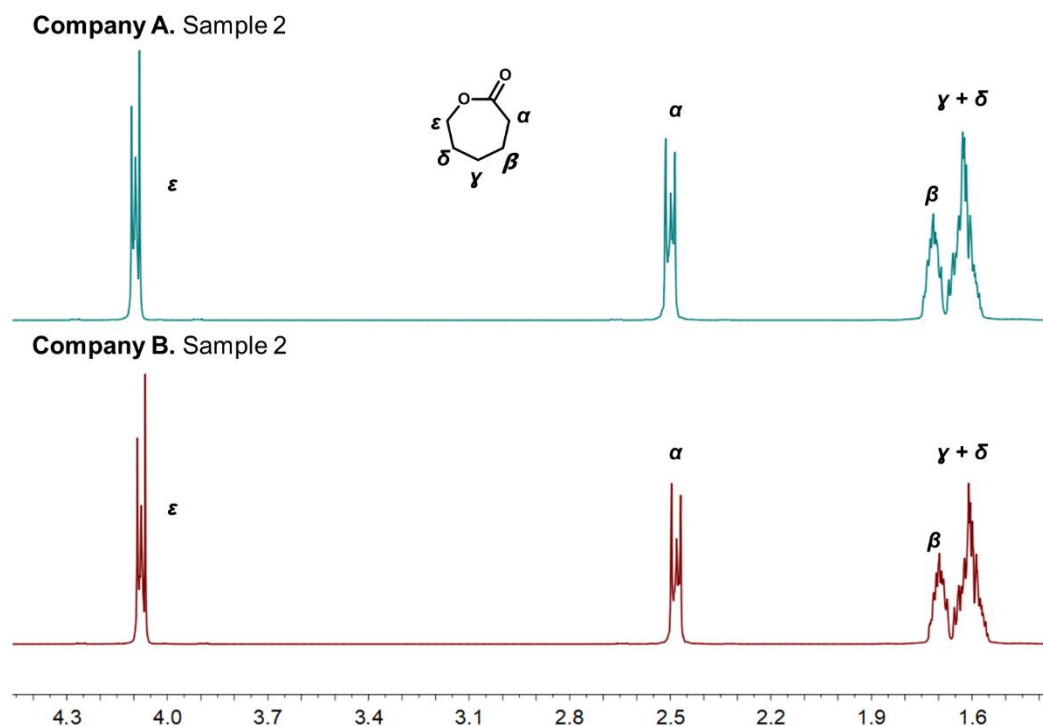


Figure 8.4. Example of ^1H NMR spectra (400 MHz) of two studied **ECL** samples of company A (top) and Company B (bottom). Solvent: CDCl_3 filtered through basic alumina.

In terms of disparities, no differences were observed in the samples analyzed by NMR spectroscopy (Figure 8.4). Byproducts of the synthesis like **cyclohexanone** or some organic peroxocarboxylic acids were not detected. Not **6-hydroxyhexanoic acid**, the opened **ECL** ring, nor the dimer were noted in the recorded spectra. The $^{13}\text{C}\{^1\text{H}\}$ NMR spectra of the analyzed samples (See Annex A.7) did not shed light on other byproducts. From a spectroscopic point of view, there were no differences between the two reviewed companies, being the six studied compounds of high purity.

Aiming for a quality-control technique that can be implemented at Lubrizol's facility, GC analysis was employed to ensure the absence of byproducts. Two different chromatographic methodologies were assessed, one with a low-temperature profile to detect low volatile compounds such as the **ECL dimer**, and another comprising more elevated temperatures to study high boiling point additives or stabilizers (See methods in measuring procedures 9.19). The former approach was already optimized in our research group, validating the retention time of **ECL** monomer and **dimer** under conditions that neither foster further formation of cycles nor produce ring-opening in the instrument.^[36]

The six samples were dissolved in CH_2Cl_2 and analyzed using the described methods. The resulting chromatographs did not present additional peaks of additives or stabilizers. Moreover, **cyclohexanone** was sought on the spectra, but it was not detected in any of the samples.

Finally, different variations of the reactivity of the process, which might produce an increase in the ROP rate, a temperature rise, or the appearance of undesired reactions, might be catalyzed by metal traces that were unperceived by the previous techniques. Semi-quantitative analyses by ICP-MS were carried out on all the samples, paying special attention to those elements commonly known by their catalytic behavior, like Ti, Sn, Al, P, or Mn, among others. An overview of the tested elements is detailed in Table 8.1.

Table 8.1. Summary of the ICP-MS results of the analyzed **ECL** samples with the corresponding detection limit.^[a]

Sample	Element					
	Ti ($\mu\text{g/g}$)	Sn ($\mu\text{g/g}$)	Al ($\mu\text{g/g}$)	P ($\mu\text{g/g}$)	Mn ($\mu\text{g/g}$)	
Company A	1	< 0.5	< 0.5	< 25	< 25	< 0.5
	2	1	< 0.5	< 25	< 25	< 0.5
	3	< 0.5	< 0.5	< 25	< 25	< 0.5
Company B	1	< 0.5	< 0.5	< 25	< 25	< 0.5
	2	< 0.5	< 0.5	< 25	< 25	< 0.5
	3	< 0.5	< 0.5	< 25	< 25	< 0.5

^[a] Samples were digested in an acid mixture (HNO_3 , HCl, and HF) prior to the analysis.

Most of the samples were metal-free over the detection limit of the technique. Only Sample 2 from Company A (Table 8.1) revealed small quantities of titanium. The origin of 1 ppm of Ti could not be exactly determined but, as it was not detected in either of the other samples of the same company, these traces likely arose from contamination in the transport or the storage of this specific batch of **ECL**. Just as a comparison, the employed catalyst for the **ECL** polymerization consists of almost 3 ppm of Sn. Thus, 1 ppm of Ti in the form of an active catalyst might compete or interfere with the reaction. Although it seems unlikely that this quantity could affect the reactivity of the samples in a significant manner, polymers produced from this lot had to be considered with caution and monitored whether an abnormality emerged.

Based on the obtained results, **ECL** supplied by the two companies did not contain any impurity from the synthetic process. All the previous analyses led to the conclusion that **ECL** samples did present neither significant differences between suppliers nor batches. Both companies

provided the compounds with similar features in terms of purity, and their products could be processed interchangeably.

8.2.1.1. Polycaprolactone synthesis

Although no disparities were found in the analyzed samples, when the catalyst was incorporated into **ECL** from Company B for the synthesis of a PCL, an abnormal exotherm was detected. Hence, to test potential different reactivities, two **PCL-BDO**s were synthesized in Lubrizol's facilities, one per supplier. Posteriorly, each was condensed in an **H₁₂MDI**-based TPU. Both types of polymers were produced batchwise according to the common laboratory-scale procedures.

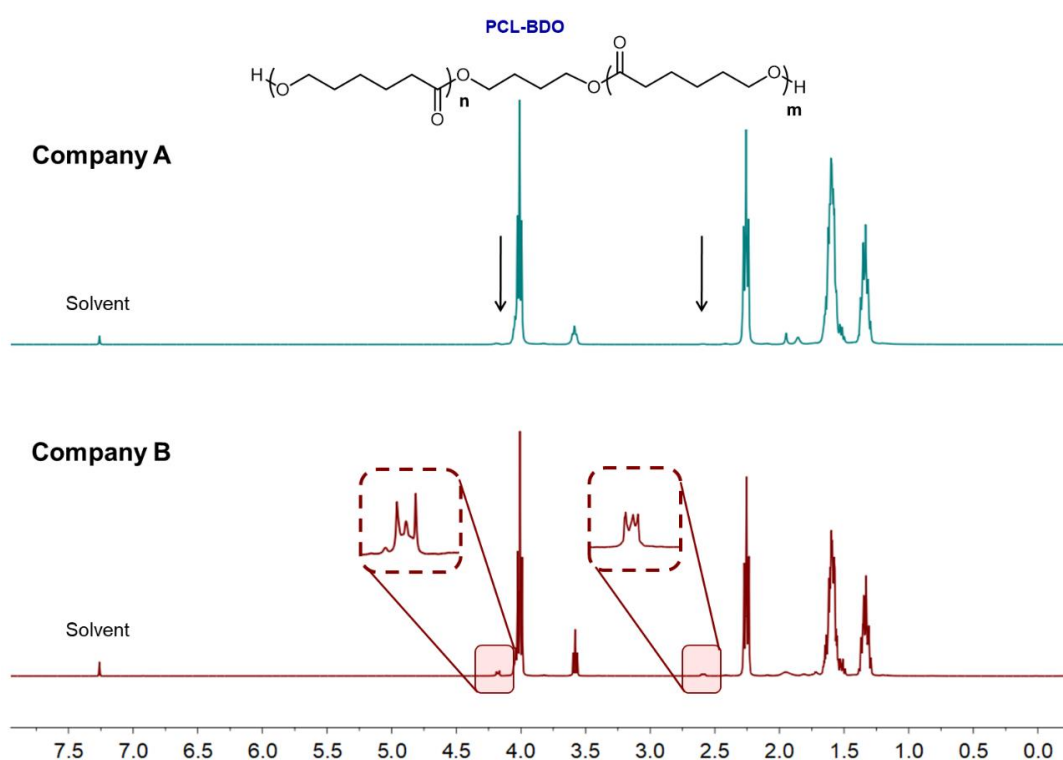


Figure 8.5. ^1H NMR spectra (400 MHz) of **PCL-BDO** samples synthesized from **ECL** supplied by Company A (top) and Company B (bottom). Spectra recorded with a 10 second delay time to ensure quantification. Solvent: CDCl_3 .

^1H NMR spectra of the synthesized polyols displayed the expected signals ascribed to a PCL polymer (Figure 8.5), but no other substantial component was observed. No peaks arising from **6-hydroxyhexanoic acid** were detected in neither of the spectra. As for the minor components, **PCL-BDO** of Company B exhibited two characteristic signals at 4.18 ppm and 2.59 ppm (embedded squares in Figure 8.5) in a proportion higher than in Company A. Considering the crown-like profile and the chemical shifts, these two peaks were attributed to the **ECL** monomer. The **ECL dimer** could not be identified in the spectra owing to the overlap

of their signals with those of the PCL. Since the unreacted **ECL** cannot be differentiated from the one generated by the back-biting reaction, its presence may be the result of a lower degree of polymerization, or conversely, an elevated rate of depolymerization.

Owing to the low concentration of **ECL** observed in the ^1H NMR spectra, its quantification was reinforced by GC analysis on both PCLs. The chromatographic conditions employed for the detection of the **dimer** in the previous raw material inspection were employed to determine the concentration of the monomer and other formed cycles.^[36] Table 8.2 summarized the quantifications carried out to these two samples. The obtained M_n values were relatively close to the target value ($M_n \approx 2000$ g/mol). But among them, **PCL-BDO** from Company B displayed a lower degree of polymerization, which was translated into a system with a lower viscosity.

Table 8.2. Main features of **PCL-BDO** samples.

PCL from	AI (mg KOH/ g polymer)	M_n (g/mol) ^[a]	ECL (%) by ^1H NMR ^[b]	ECL (%) by GC ^[c]	ECL dimer (%) by GC ^[c]
Company A	0.2	1983 17	0.35	0.308 ± 0.006	0.38 ± 0.03
Company B	0.5	1916	1.54	1.61 ± 0.05	0.229 ± 0.006

^[a] Measured by ^1H NMR end-group analysis. Spectra were recorded in CDCl_3 with a delay time of 10 seconds to ensure quantification.

^[b] Percentage obtained by ratio between the α -methylene groups of ECL and PCL in the ^1H NMR spectrum.

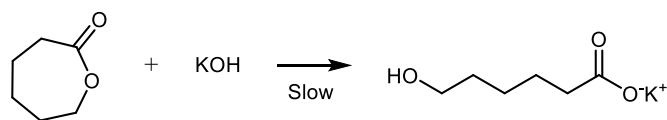
^[c] Samples freshly dissolved in CH_2Cl_2 . Quantification was carried out with *n*-decane as the internal standard. Value after \pm corresponded to the standard deviation from the replicates.

The uneven concentration of the monomer in both PCLs was confirmed by GC analysis, as well as the NMR results. The monomer quantity was five-folds higher in the PCL synthesized with Company B's **ECL**. Moreover, the presence of **ECL dimer** was detected in the samples, reaching similar values in both polymer mixtures. It is expected that the concentration of **ECL dimer** remains constant after the early stages of the reaction, while the formation of **ECL** varies until reaching equilibrium. Owing to this piece of information, it is challenging to ascertain whether the difference in the monomer concentration arose from an undetected abnormal reactivity or by the two polymers being in distinct equilibrium stages.

The AIs measured by titration exhibited large values, especially compared with the maximum recommended for this ROP process is 0.2 mg KOH/ g PCL (corresponding to 0.06 mg H_2O / g PCL or 3.6 μmol of H_2O /g polymer). Between the two evaluated PCLs, Company B displayed a higher value of 0.5 mg KOH/g PCL. Some potential explanations for the increase the AI were considered hereafter.

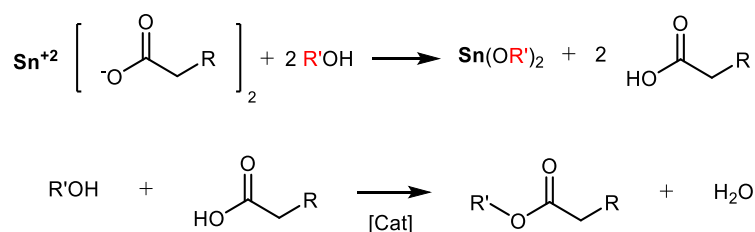
Whether or not the unreacted monomers could cause an increase in the AI values under the titration conditions was previously examined in our research group. It was concluded that

although **ECL** undergoes alkaline hydrolysis (Scheme 8.6), the reaction rate is slower than that of the acid-base titration. Hence, there is not a direct correlation between the increased concentration of **ECL** monomer and the AI measurement.^[36]



Scheme 8.6. Basic hydrolysis of **ECL**.

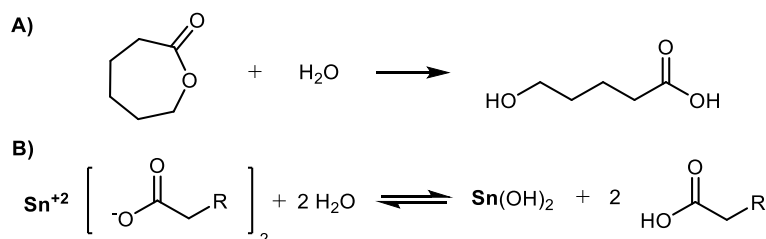
Kricheldorf *et al.* reported that tin(II) carboxylate catalysts are activated by the coordination of a hydroxyl group and the simultaneous release of a carboxylic acid fragment, which in turn might be esterified by any hydroxyl group in the media (Scheme 8.7).^[41] Then, this reaction produces a molecule of water per each new ester, which in turn could hydrolyze a polymer chain or a monomer. However, for this PCL, the maximum value of IA that could emerge from the catalyst, considering all the carboxylates were in form of acid or caused the hydrolysis of an ester group, is negligible (<0.01 mg KOH/g PCL). Consequently, the obtained AI values are neither explained by the selected catalyst.



Scheme 8.7. Catalyst activation and posterior transesterification of the acid residue.

However, under the polymerization temperatures, traces of water can open the monomer or hydrolyze polymer chains, producing carboxylic groups (Scheme 8.8.A). These acid moieties are less reactive than **ECL** for the polymerization reaction, and thereby, harsher conditions and longer times are required to incorporate them into the polymeric chains. The raw material is certified with a maximum water content of 0.03 wt.% and PCLs samples are routinely analyzed after the polymerization, displaying values lower than 0.02 wt.% of H₂O. However, if these percentages are converted to AI, they correspond to 0.9 mg KOH/g PCL and 0.6 mg KOH/g PCL, respectively, which are values superior to the recommended. Moreover, in addition to hydrolyzing the monomer, water could also deactivate the catalyst by forming their less reactive hydroxides (Scheme 8.8.B), which would also explain the lower degree of polymerization. Consequently, the difference in the water content of each batch of monomer, even under the certification standards, might cause elevated and different AI values. This experimental factor

was not considered during the PCL synthesis and in hindsight could explain the variability of AI in the samples.



Scheme 8.8. Roles of water with the A) **ECL** monomer and B) the catalyst.

In addition, two TPUs were synthesized with the previous PCLs, **H₁₂MDI**, **BDO**, and a tin-free catalyst (MX_n). Samples analyzed by NMR spectroscopy displayed low-resolution signals owing to the high M_n of the polymer and the different conformations of the structure (Figure 8.6). Despite that, no significant differences were obtained between the two products. **ECL** is not consumed in the condensation reaction with isocyanates, therefore, the higher content of monomer observed in **PCL-BDO** from Company B remained in the TPU produced with this PCL (red squares in the bottom spectra **of Figure 8.6**).

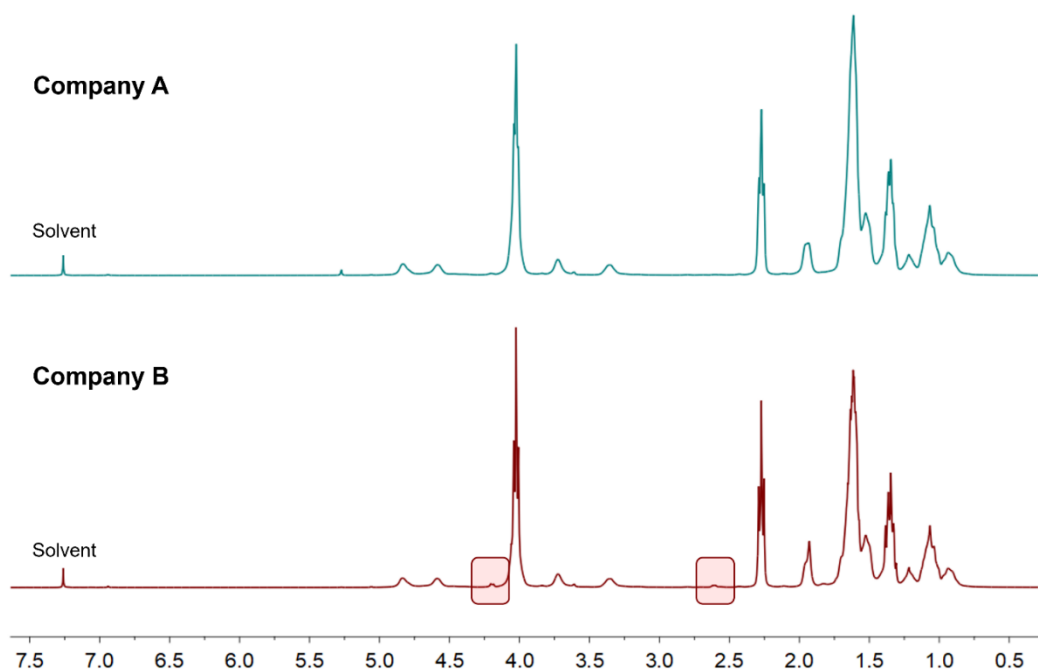


Figure 8.6. ¹H NMR spectra (400 MHz) of TPUs synthesized from **ECL** supplied by Company A (top) and Company B (bottom). Spectra recorded with a 10 second delay time to ensure quantification. Solvent: CDCl₃.

The concentration of metals was also quantified by ICP-MS to detect any abnormality that could explain different reactivities. Values reported in Table 8.3 displayed reproducible and comparable results between the two tested polymers, which dismiss the hypothesis of side

reaction as a consequence of different metal content. Tin was introduced as the catalyst for the PCL synthesis and its obtained values matched the theoretical ones. In the case of MX_n , the results were consistent and close to the theoretical value. Hence, the metal content was not a distinguishable factor explaining the potentially different reactivities. The presence of titanium in the studied TPUs was unexpected, likely arising from some contamination on the tank.

Table 8.3. ICP-MS results of the synthesized TPUs from **ECL** of different suppliers.^[a]

TPU from	Sn ($\mu\text{g/g}$) ^[b]	M ($\mu\text{g/g}$) ^[c]	Ti ($\mu\text{g/g}$) ^[d]
Company A	2	18	4
Company B	2	18	4

^[a] Samples were digested in an acid mixture (HNO_3 , HCl and HF) prior to the analysis.

^[b] Sn detention limit $\approx 0.5 \mu\text{g/g}$.

^[c] M detention limit $\approx 0.5 \mu\text{g/g}$.

^[d] Ti detention limit $\approx 0.5 \mu\text{g/g}$.

In closing, several aspects of the PCLs produced from Company A and Company B were explored, obtaining slightly different results in M_n , AI, and **ECL**'s concentration. Both PCLs successfully generated TPUs in accordance with laboratory standard conditions. The identified discrepancies may arise from the experimental factors, and further replicates should be required to detect any trend. Variables such as water content or the state of the catalyst have been not examined, and they may play a significant role in the reactivity of the different **ECL**'s suppliers or batches.

8.2.1.2. PCL reactivity

The PCL production is industrially monitored through the exothermy of the polymerization reaction according to certain already optimized temperature profiles. However, to assess whether the presence of carboxylic acids affects the catalyzed process, a simple preliminary test was carried out. The role of the acid was explored simulating a 175 g-scale **PCL-BDO** synthesis, using previously dried **BDO** and doubling the acid content in the **ECL** as **6-hydroxyhexanoic acid**. The ROP is a slightly exothermic reaction, so, if the reaction evolves normally, an increase in the mixture's temperature is expected.

The acid content of the used **ECL** batch was evaluated with the AI of the sample. It was measured by the standard titration methodology, resulting in 0.14 mg KOH/ g **ECL**. Considering that all the acid groups proceed from the monomer ring-opening, the required water content was $5 \cdot 10^{-3} \%$ or 0.05 mg $\text{H}_2\text{O/g}$ **ECL**, which values lower than the certified specification of the material. Therefore, the batch was proper for PCL synthesis.

The tested procedure involved heating the monomer to 155 °C, and once that constant temperature was reached, the initiator, the catalyst, and when required the opened monomer, were added to the vessel. This moment was considered the initial time for all the samples (t_0). The recovery of the mixture's temperature was measured as a function of time as the reactor was externally heated at 165 °C. The temperature profile of the reaction in which **6-hydroxyhexanoic acid** was added was compared to an additional experiment that did not include the opened monomer. The obtained results from the four experiments are plotted in Figure 8.7.

The addition of **BDO** and catalyst at t_0 , decreased the temperature of the mixture, which was easily recovered afterward by the exothermy of the system at the early stages of the reaction. The presence of acid evidenced a decrease in the produced heat, as samples containing this additive did not show the same recovery. The temperature of the two samples slowly rose when heating, but there was not an abrupt change. The presence of acid seemed to affect the reaction by reducing the produced heat.

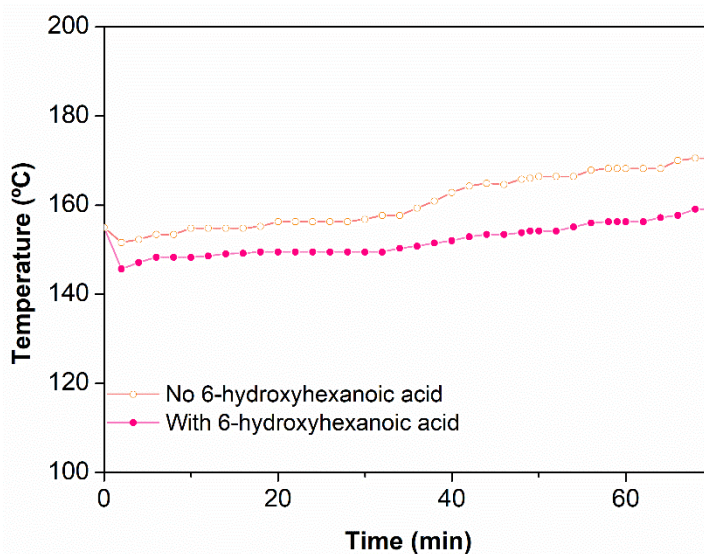


Figure 8.7. Variation of the temperature along time.

Moreover, the effect of the temperature was also observed in the ^1H NMR spectra of the samples externally heated at 165 °C for 70 minutes. The calculated average-number value of polymerization degree (\bar{X}_n) was 2.1 when no **6-hydroxyhexanoic acid** was included (Figure 8.8.A) and 1.2 for the reaction with acid (Figure 8.8.B), indicating that at a relatively early stage of the reaction, longer polymer chains are reached in the reference reaction. These results pointed to the inhibition of the polymerization by the presence of acid in the mixture.

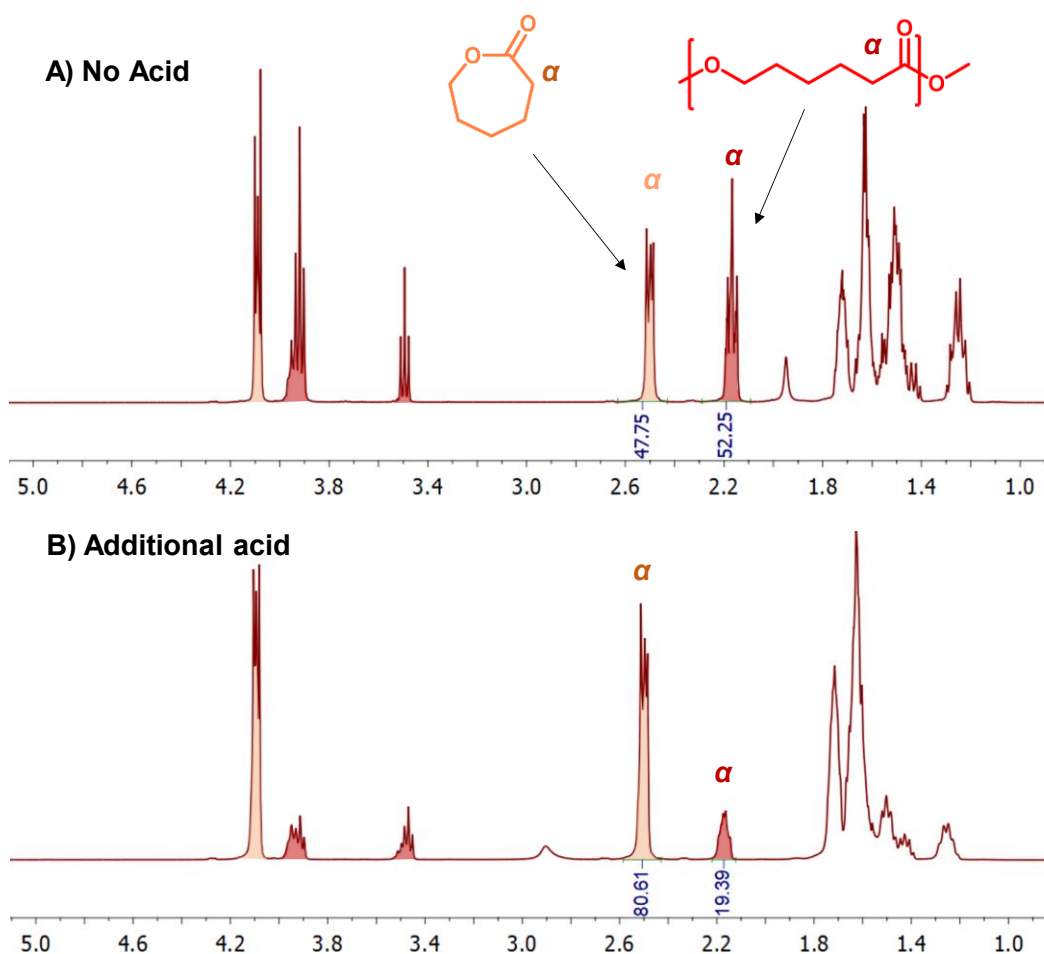


Figure 8.8. ^1H NMR spectra (400 MHz) of the reaction crude after heating at 165 °C for 70 minutes. A) Reference reaction crude without acid B) Reaction mixture containing **6-hydroxyhexanoic acid**. Solvent: CDCl_3 .

The **6-hydroxyhexanoic acid** stems from the hydrolysis of the monomer, so the presence of water seems to be of great significance in the polymerization. As mentioned earlier, water might have two effects on the system. First, it could deactivate the catalyst by forming a hydroxy stannous compound, or it could also cause the monomer ring-opening and the subsequent rate decrease. However, to quantify the impact of the water content in a more precise manner, further experiments under highly controlled conditions must be performed.

8.2.2. 4,4'-dicyclohexylmethane diisocyanate

Continuing with the study of the raw materials for the TPU film production, **H₁₂MDI** was explored. The concentration of 4,4'-isomer in the sample and the distribution of its isomers were the main goals for the developed technique. These results allow the assessment of the variability of the batches, the suppliers, or the raw materials at different stages of the

production. Values reported in the product specifications, specifically those in the isomer distribution, have a wide range, so the study of the mixture might pinpoint the acceptable percentages and swiftly determine any disparity.

8.2.2.1. Method development

Initial tests were carried out by NMR spectroscopy to quantify the sample as-provided. Even though this technique allows the estimation of the 4,4'-isomer distribution in **H₁₂MDI** samples and the determination of contaminations, the required equipment is not available in Lubrizol's facilities. Thereby, it could not be used as the routine technique for the analysis of these compounds, and a GC methodology was also designed. According to the information provided by the supplier, the quantification was carried out assuming that the structural isomer 2,2'-diisocyanate was not present in the sample.

A reported characterization of the commercial mixture determined the concentration of the three major compounds (**4,4'-isomers**) through a quantitative $^{13}\text{C}\{^1\text{H}\}$ NMR spectrum.^[42] They reported that the isocyanate carbon signal centered at 122.5 ppm, 122.3 ppm, and 122.0 ppm corresponded to the **4,4'-trans, trans-, 4,4'-trans, cis-, and 4,4'-cis, cis-** isomers, respectively. However, when Sample 1 was analyzed by quantitative $^{13}\text{C}\{^1\text{H}\}$ NMR spectroscopy to assess the previously reported information, incongruent results were obtained (Figure 8.9). In contraposition to the published assignation, the integration values did not resemble the distribution provided by the supplier nor the obtained by other techniques. Therefore, it is proposed that the peaks of the isocyanates (embedded region A in Figure 8.9) correspond to the **4-trans-** (122.4 ppm) and **4-cis-** (122.2 ppm), without differentiating whether they belong to the **trans, trans-**, the **trans, cis-**, or the **cis, cis-isomer**. The low-intensity peak at 121.9 ppm was assigned to the isocyanate located at the **2-cis**, while the **2-trans** is not observed likely by its low abundance in the sample (< 2%). A similar distribution was depicted in Figure 8.9.B for the tertiary carbon bounded to the isocyanate (51.4 - 59.4 ppm), where the peaks from the same three isomers were displayed in addition to **2-trans** (59.4 ppm).

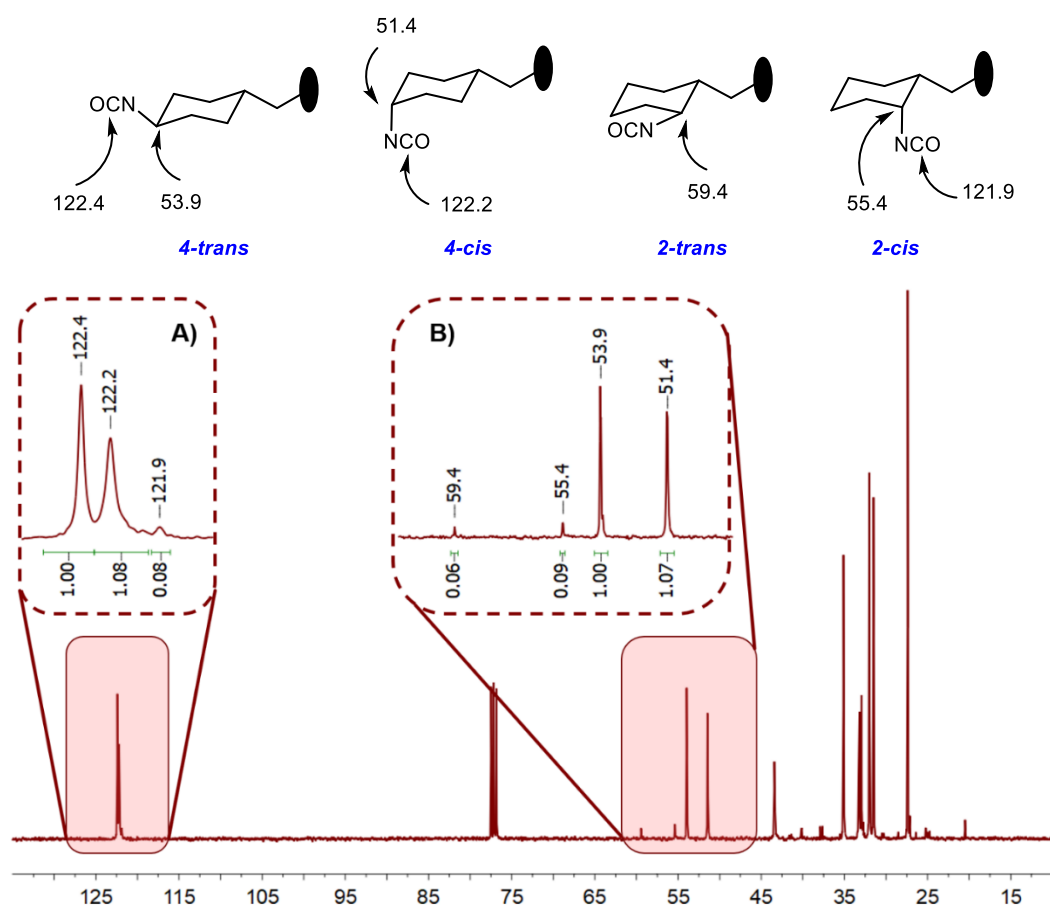


Figure 8.9. Quantitative $^{13}\text{C}\{^1\text{H}\}$ NMR (100.6 MHz) spectrum of Sample 1 of **H₁₂MDI** recorded with a delay time of 20 seconds. Solvent: CDCl_3 .

Alternatively, the ^1H NMR spectrum of a pure mixture of **H₁₂MDI** provides insight into the composition of the sample, as can be depicted in Figure 8.10. The axial and equatorial orientation of the cyclohexyl hydrogens, the numerous signals of the two rings, in addition to the multiple conformations of the products, generate a complex spectrum to elucidate.

The main distinctive area that could be used for quantification is enlarged in Figure 8.10, which is assigned to the geminal hydrogen of the isocyanate. However, from this region of the spectrum only the ratio between the **4,4'-isomer** and the **2,4'-isomer** could be determined, but not the isomer distribution among the 4,4'-compounds. The studied signals are named according to the position of the isocyanate relative to the central methylene group, so the observed hydrogen peaks are the ones located in the opposite position. As an example, the peak labeled **4-cis** ($\delta = 3.80$ ppm) denoted the hydrogen in the *trans* position to the central methylene. The triplets attributed to the methylene bounding both rings ($\delta = 1.00$ - 1.20 ppm) might have allowed the quantification of the isomer distribution, but they overlap with signals from the cyclohexyl group.

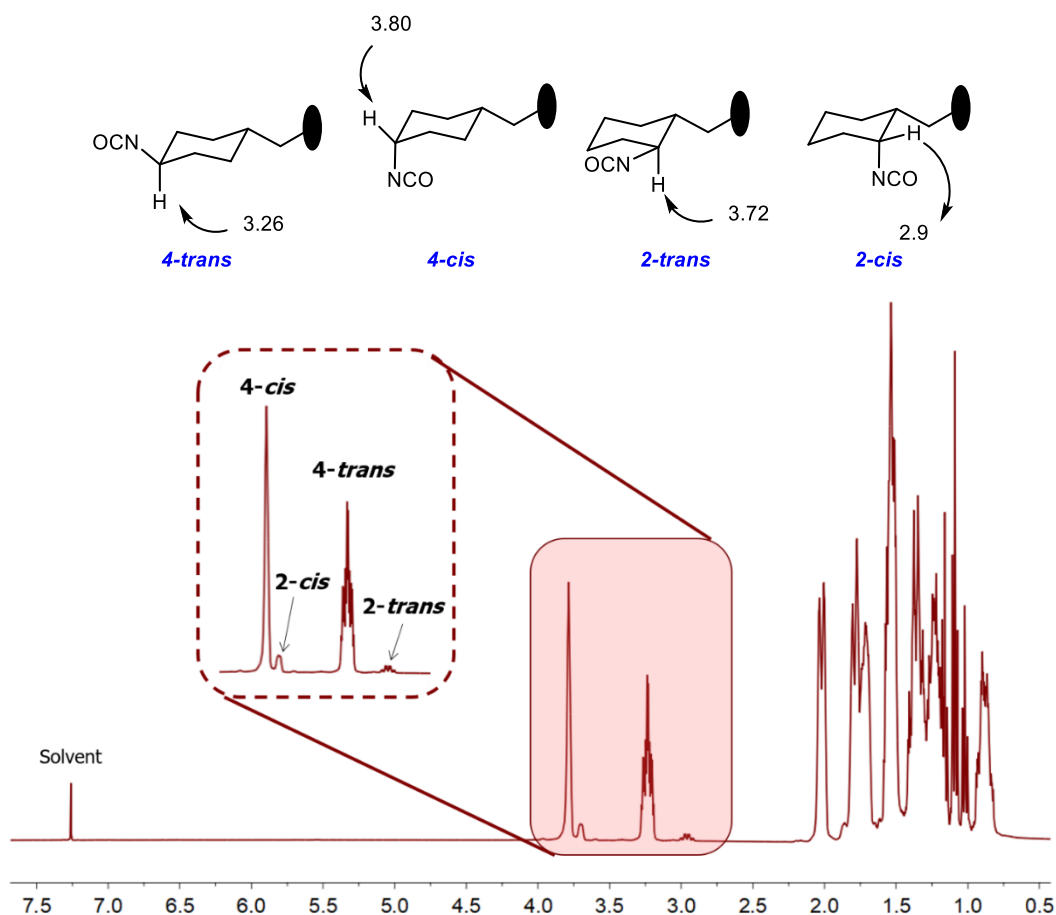


Figure 8.10. Schematic representation of the observed hydrogens. Tags in blue indicate the name of the isocyanate isomer. ^1H NMR (400 MHz) spectrum of Sample 1 of **H₁₂MDI** recorded with a delay time of 10 seconds to ensure the quantification. Solvent: CDCl_3 .

Six different samples were analyzed employing ^1H NMR spectroscopy, some of them directly provided by the supplier and others collected from different steps of the production process. Employing the integration values of the labeled peaks, the quantification was carried as detailed in 9.22.1. The estimated results are displayed in Table 8.4. Obtained values of the **2,4'**- and **4,4'**- isomer distribution agree with results provided by the supplier (12.5 % **2,4'**-isomer), except in Sample 5. Moreover, it was possible to identify some impurities on the provided samples, likely arising from cross-contamination with **MDI** on the transporting pipes or storage tanks.

Although NMR spectroscopy was sought to determine the isomer distribution in the commercial sample, only the relation between the constitutional **2,4'**-isomer and **4,4'**-isomer could be extracted. However, the stereoisomers quantification could not determine neither by ^1H NMR or the $^{13}\text{C}\{^1\text{H}\}$ spectra, as no characteristic and individual signal from each of the isomers was displayed.

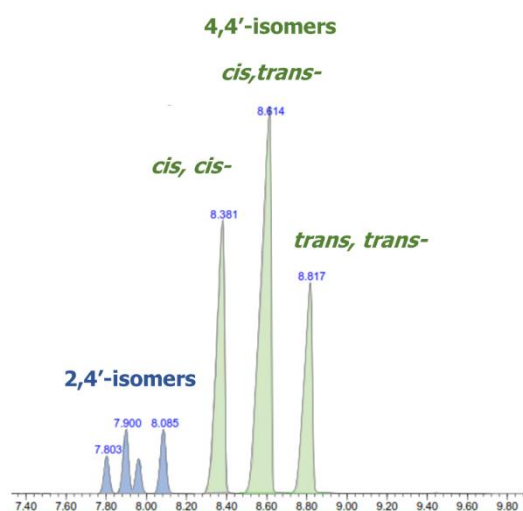
Table 8.4. Content of **2,4'-isomers** and **4,4'-isomers** obtained by ^1H NMR spectroscopy.^{[a][b]}

	2,4'-isomers (%)	4,4'-isomers (%)	Contamination
Sample 1	12.5 ± 0.2	87.5 ± 0.2	--
Sample 2	12.7 ± 0.3	87.3 ± 0.3	--
Sample 3	12.3 ± 0.2	87.7 ± 0.2	MDI, ~10 %
Sample 4	12.9 ± 0.2	87.1 ± 0.2	MDI, ~ 0.4 %
Sample 5	14.0 ± 0.4	86.0 ± 0.4	--
Sample 6	12.6 ± 0.9	87.4 ± 0.9	--

^[a] Spectra recorded in CDCl_3 with a delay time of 10 seconds to ensure quantification.

^[b] Values calculated from at least two replicates.

Considering the above, a GC method was developed to evaluate the **H₁₂MDI** mixture (See details in 9.22.2). The obtained chromatograms were like image in Figure 8.11, in which four minor components at low retention times are associated with the **2,4'-isomer** (blue peaks), while the three most intense are related to the **4,4'-isomer** (green peaks). Among these last, the peak assignment was based on the supplier information and corresponded, increasing the retention time, to the **4,4'-cis, cis-**, **4,4'-trans, cis-** and **4,4'-trans, trans-**, respectively. No additional peaks were detected in the chromatogram, confirming the lack of the **2,2'-isomer** in the mixture.

**Figure 8.11.** GC chromatogram of a pure mixture of **H₁₂MDI**.

The areas under the peaks of the GC chromatogram were directly associated with the composition of the isomers without the use of internal standards owing to the similar structure of the studied compounds. For clarification of the reported results, the sum of the integration values of the 4 minor constituents (blue peaks in Figure 8.11) provides the concentration of the **2,4'-isomers** on the sample. If no additional peaks appeared, the rest until 100 correspond

to the **4,4'-isomers** (green peaks in **Figure 8.11**). Suppliers commonly reported the proportion of **4,4'-isomers** normalizing the three major peaks to 100 and determining the percentage for each.

Some of the previous samples, plus an additional one, were analyzed by GC and the values are reported in Table 8.5. Samples exhibiting contaminations were omitted from the report figures owing to the overlap of the peaks with the impurity.

Table 8.5. GC results of the **H₁₂MDI** mixtures.^[a]

	2,4'-isomers (%)	4,4'-isomers (%)	4,4'-cis, cis- (%)^[b]	4,4'-trans, cis- (%)^[b]	4,4'-trans, trans- (%)^[b]
Supplier specifications	12.5	87.5	25-32	47-52	17-24
Sample 1	12.6	87.4	27.3	49.6	23.1
Sample 2	12.6	87.4	27.8	50.0	21.8
Sample 5	12.8	87.2	27.8	50.2	22.0
Sample 6	13.0	87.0	28.0	50.2	21.8
Sample 7	12.6	87.4	27.5	49.8	22.7

^[a] Samples dissolved in CH₂Cl₂. The standard deviation of the results <0.1 %.

^[b] Distribution of 4,4'-isomers normalized to 100 %.

The obtained percentages of **2,4'-isomers** and **4,4'-isomers** agreed with the previously reported by ¹H NMR spectroscopy, validating the results of both analyses. The ratio among the **4,4'-isomers** was within the specifications provided by the suppliers displaying mean values of 27.7 ± 0.3 %, 50.0 ± 0.3 %, and 22.3 ± 0.6 % for the **4,4'-cis, cis-**, **4,4'-trans, cis-**, and **4,4'-trans, trans-**, respectively.

The GC analysis proved to be a suitable technique to assess the composition of the **H₁₂MDI** samples, providing a more specific composition than the one reported by the suppliers. Moreover, it consisted of a quick and simple methodology that could be easily implemented in Lubrizol's facilities for routine analysis of the raw materials.

8.2.2.2. *Supplier validations*

Similarly to the **ECL** case, two additional suppliers were evaluated to assess the potential purchase of the cycloaliphatic diisocyanate depending on market availability. Samples from both companies were examined by ¹H NMR and GC to determine the concentration of the **4,4'-isomer**, the distribution of the three compounds, and any potential contaminants.

¹H NMR spectra of the provided samples did not exhibit any impurity nor significant differences amongst them. Moreover, the isomer quantification carried out by NMR spectroscopy and GC

agreed once again, displaying a minor concentration of the **2,4'-isomer** (Table 8.6). The difference between both companies was around 0.3 %, which could be considered within the experimental variations. However, these two new companies exhibited a slight enrichment of the **4,4'-isomer** compared to the initial supplier.

Table 8.6. Content of 2,4'-isomer and 4,4'-isomers of **H₁₂MDI** mixture of two new suppliers.

	2,4'-isomers (%)		4,4'-isomers (%)	
	¹H NMR^[a]	GC^[b]	¹H NMR^[a]	GC^[b]
Initial supplier^[c]	12.8	12.7	87.2	87.3
Company C	10.9	11.0	89.1	89.0
Company D	11.2	11.2	88.8	88.8

^[a] ¹H NMR spectra were recorded with a 10 second delay time to ensure quantification. Solvent: CDCl₃

^[b] Samples dissolved in CH₂Cl₂.

^[c] Average values from the previously analyzed samples.

In terms of isomeric distribution (Table 8.7), Company C and D exhibited similar results of the three stereoisomers percentages. Although results are within the initial supplier specifications, there was a slight increase in the percentage of the **4,4'-trans, trans-** in the Company D mixture.

Table 8.7. Isomer distribution obtained by GC of the **H₁₂MDI** mixtures reported over 100 %.^[a]

	4,4'-cis, cis- (%)	4,4'-trans, cis- (%)	4,4'-trans, trans- (%)
Initial supplier^{b]}	27.7	50.0	22.3
Company C	27.8	49.7	22.5
Company D	27.0	49.9	23.1

^[a] Samples dissolved in CH₂Cl₂. The standard deviation of the results was <0.1 %.

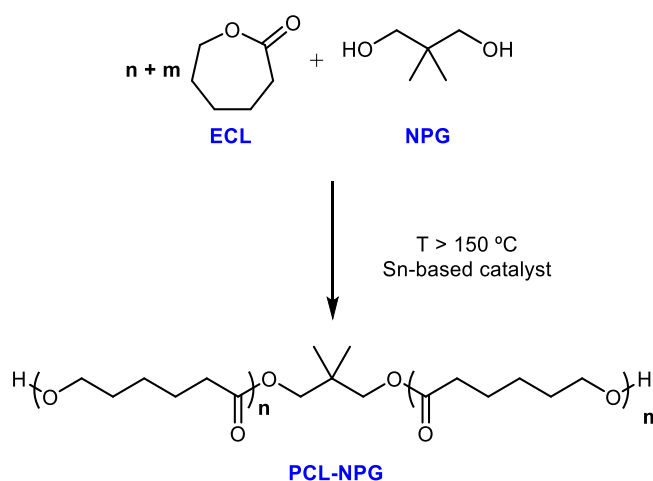
^[b] Average values from the previously analyzed samples.

Company C and D could be interchangeable, but concerning the initially employed company, there were some small disparities like the lower content of 2,4'-isomer. The effect of this small change should be studied in TPU productions.

8.3. PCL analysis

8.3.1. PCL-NPG analysis

For the synthesis of the target TPUs, a **PCL-NPG** with low- M_n and synthesized from the ROP of **ECL** with neopentyl glycol (**NPG**) was employed (Scheme 8.9.) The use of a diol as an initiator enables the synthesis of a dihydroxyl-terminated polymer with two potentially different statistical distributions of caprolactone fragments (m and n) around the initiator.



Scheme 8.9. PCL-NPG synthesis.

The initiator can be situated in three positions within the chains (Figure 8.12). **NPG** is referred to as *internal* when the alcohol is esterified by both ends. Conversely, when only one of the alcohols is bonded to a caprolactone segment and thereby, the chain only grew by one end, **NPG** is called *terminal*. Finally, if **NPG** does not react with any other monomer, it is considered *free*. The **NPG** distribution in **PCL** samples was previously explored by our research group concluding that it was possible to differentiate them by ^1H NMR spectroscopy owing to the different chemical environments of the methyl groups. These peaks and all the others emerging from the caprolactone segment are assigned in Figure 8.13.

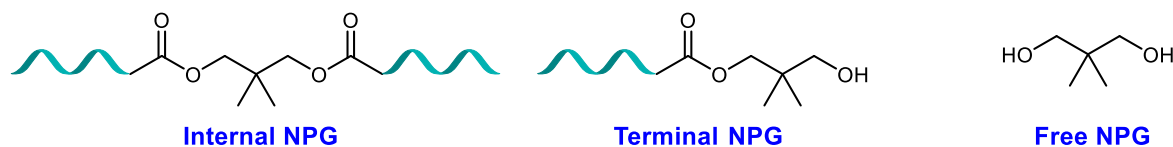


Figure 8.12. Schematic representation of the positions of **NPG** in PCL's sample.

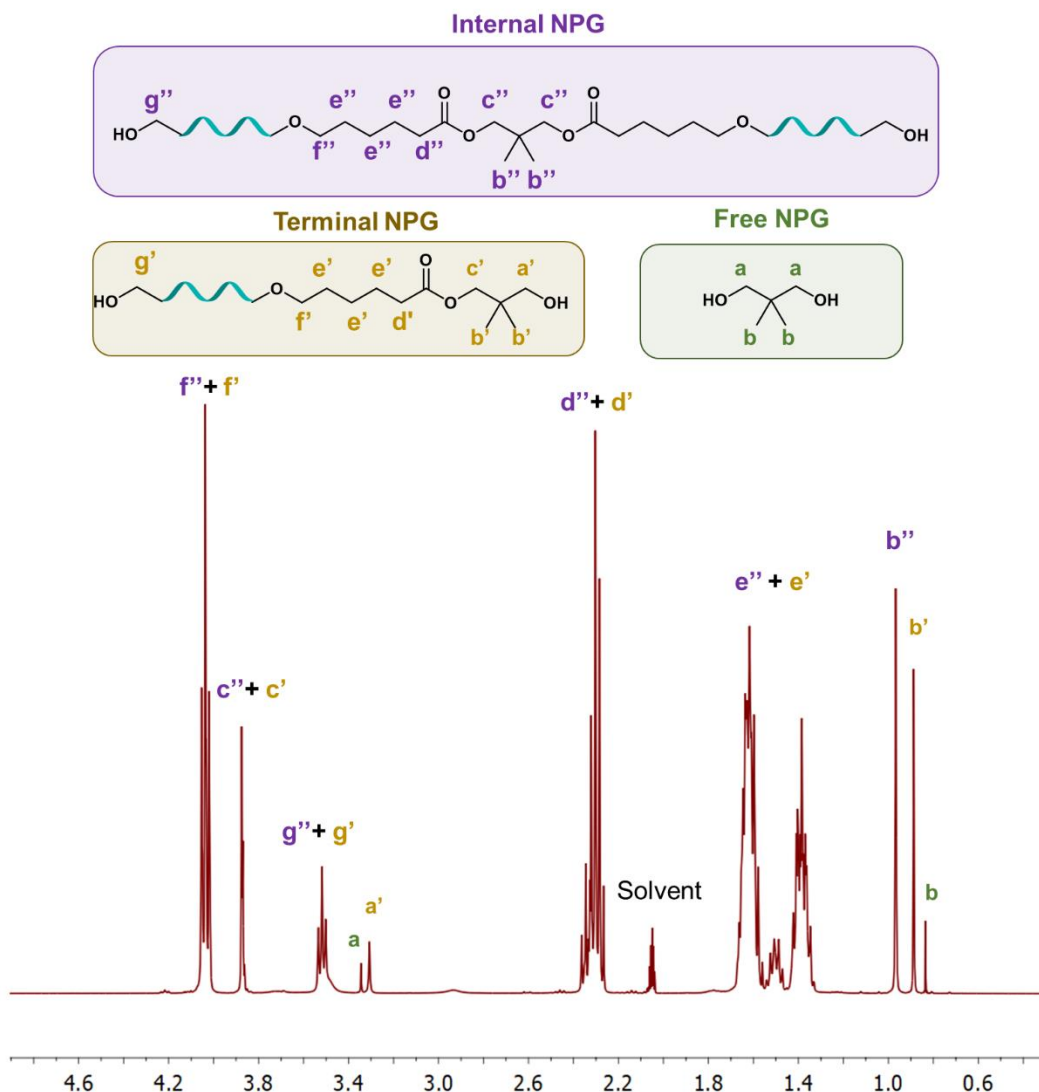


Figure 8.13. Example of a ^1H NMR (400 MHz) spectrum of **PCL-NPG**. Samples were recorded with a 10 second delay to ensure quantification. Solvent: Acetone- d_6 .

During this thesis, several **PCL-NPG** were assessed regarding their M_n and **NPG** distribution, as these might affect the reproducibility and final properties of the material. Most of them were produced at multi-tonnes scale, under similar conditions, and employing an Sn-based catalyst. All the studied PCLs were synthesized in Lubrizol targeting the same M_n and maintaining constant the ratio among **ECL** and initiator, regardless of the scale in which the production was carried out. Nevertheless, the distribution of **NPG** in the polymer is very sensitive to the synthetic conditions, and slight variations in the reaction temperature, the catalyst state, reagent purity, or atmosphere might cause changes in the proportions.

In addition to the **NPG** distribution, the ^1H NMR spectrum allowed the estimation of the M_n of the PCL. However, as the samples are employed as-synthesized, the polymer mixture contains

unreacted **NPG**, which decreased the overall M_n of the mixture. Considering the integration values of the involved reagents, it was possible to quantify both the M_n of the mixture and the M_n of the PCL (See in detail 9.23).

Although most of the **PCL-NPG** were adequate for producing TPUs, some difficulties emerge from a polymer. **PCL-1** exhibited problems during the condensation reaction, being unable to generate the desired TPU. In contrast, **PCL-2**, which was synthesized with the same method, and **PCL-3**, produced at a larger scale, did not manifest similar issues. Therefore, to find out an explanation for the unusual reactivity, the composition (Table 8.8) and the thermal stability (Figure 8.14) of the three **PCL-NPG** were explored.

In terms of the mixture's M_n , the three samples displayed similar values of around the theoretical value (for confidential reason the exact value cannot be disclosed and will be referred as M_t . Values obtained experimentally will be denoted as M_t plus or minus the difference from the theoretical). However, when only the PCL polymer was considered, a deviation from the target value was observed, especially for those with higher free **NPG** content. The main difference between the problematic sample and the rest is on the quantity of free **NPG**, exhibiting **PCL-2** and **PCL-3** a substantially higher percentage of free **NPG** than **PCL-1**, the problematic sample.

Table 8.8. Results of the studied **PCL-NPG**.^[a]

PCL	Production scale	M_n mixture (g/mol) ^[b]	M_n PCL (g/mol) ^[b]	NPG distribution (%)		
				Internal	Terminal	Free
1	Kg	$M_t + 24$	$M_t + 36$	73.9	24.8	1.3
2	Kg	$M_t + 20$	$M_t + 70$	60.5	34.3	5.2
3	Tn	$M_t - 4$	$M_t + 54$	58.2	35.6	6.2

^[a] Samples dissolved in acetone-*d*₆. Spectra recorded with a delay time of 10 seconds to ensure quantification.

^[b] Measured by ¹H NMR end-group analysis.

The variation of the free initiator content does not directly affect the amount of isocyanate used in the condensation reaction, as NCO/OH ratio remains unchanged. However, variations in the quantity of free **NPG**, which will act as a chain extender, will modify the content and nature of the HS, and if there is a significant change, the expected properties of the produced TPU.

The contribution of the free **NPG** from **PCL-1** and **PCL-3** to the TPU crude corresponds to a 0.07 wt.% and 0.31 wt.% respectively. Overall, the observed variations were relatively small, but they might affect the posterior TPU production. The lack of **NPG** will decrease the amount

HS, but at the same time, it will be more close-packed. This variation is likely to affect the flowability of the produced compound. In contrast, a content of **NPG** substantially superior to the optimized value might decrease the crystallinity of the material. In productions controlled by the MFI of the generated material, this lack of order might imply the incorporation of an additional amount of diisocyanate to increase the apparent low M_n . Therefore, since the increase in the MFI value is not due to the unbalanced reaction stoichiometry, but low crystallinity, the extra **H₁₂MDI** might result in some type of chemical crosslink. Therefore, depending on the **NPG** content, two different behaviors in the TPU production might be observed. A value higher than the optimized might result in a highly reticulated structures, while a lower value might increase the expected crystallinity and destabilize the production. The latter option may be the reason behind the issues to related to **PCL-1**, as **PCL-2** and **PCL-3** exhibited a more similar **NPG** content to the adjusted system.

The lack of thermal stability of a compound in the reaction conditions could also modify the condensation parameters or the extrusion of the produced materials. High degrees of degradation at early condensation stages might lead to difficulties in the production, the alteration of the final properties of the material, or changes in the film's appearance in the form of black spots or discoloration. Because of that, the stability of the previous three samples under thermal stress was explored through TGA analysis upon a linear temperature increment. Especial attention was paid to the temperature at which the PCL mixture gets in contact with the other reagents of the TPU condensation to ascertain that all the studied PCLs can be safely processed. PCLs were subjected to a low heat rate of 10 °C/min under two different conditions: an inert atmosphere (Argon) and an oxidative atmosphere (21% O₂ + 89 % N₂) to study their decomposition. In TGA analysis, the first transitions to be observed will be those arising from the evaporation of the volatile compounds present in the mixture. Afterward, the cleavage of the bonds that form volatile compounds may be detected in order of the weakest to the stronger interaction.

The obtained TGA thermograms are illustrated in Figure 8.14. Moreover, temperatures at which the 2%, 5%, and 25% weight loss takes place ($T_{2\%}$, $T_{5\%}$, and $T_{25\%}$, respectively) are summarized in Table 8.9.

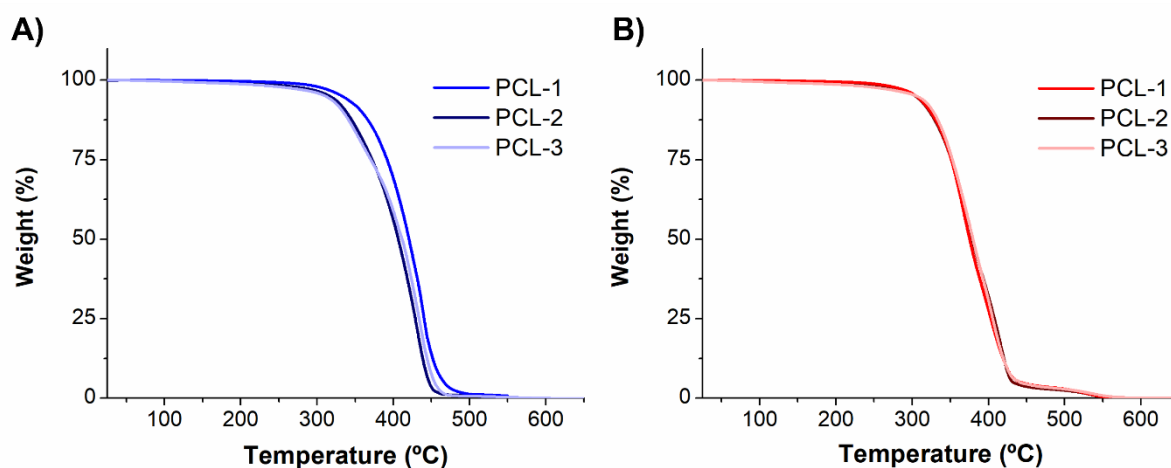


Figure 8.14. Thermogram profiles of the **PCL-NPG** samples. Analysis carried out under A) inert atmosphere and B) oxidative atmosphere.

Both thermograms displayed an apparent single-stage weight loss reaching 0% around 550 °C, although under oxidative conditions existed the decomposition of the formed char. As it could be expected, samples heated under an inert atmosphere exhibited higher thermal stability than under an oxidative one.^[43] At temperatures lower than 150 °C, both atmospheres show a very small weight loss corresponding to the extremely low water content absorbed in the polymer mixture. Under an oxidative atmosphere, the degradation onsets ($T_{2\%}$) started between 246 °C and 278 °C, whereas inert conditions exhibited higher temperatures in the range between 263 °C and 300 °C. The differences in the onset temperatures seemed to emerge from the volatilization of a higher content of free **NPG** and probably the terminal **NPG**. Once the initiator in these two forms was volatilized, all three **PCLs** exhibited similar temperature profiles.

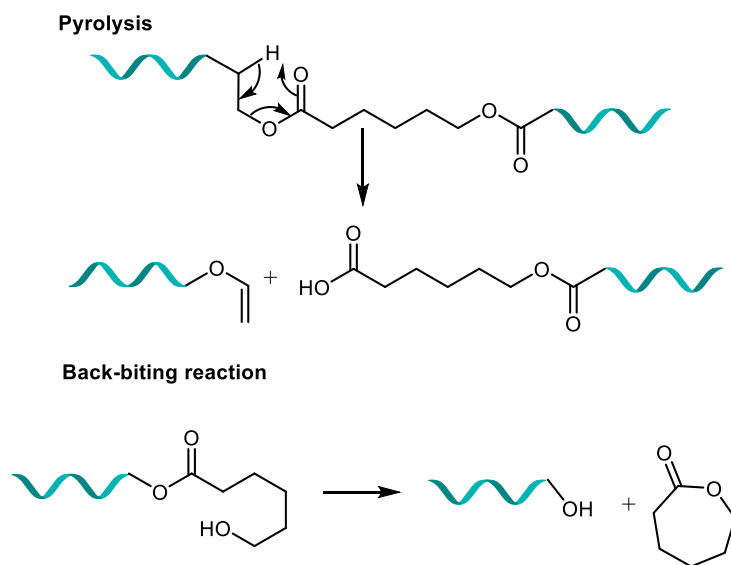
Table 8.9. Detailed TGA temperatures of the studied **PCL-NPG** under both atmospheres.^[a]

	Inert atmosphere			Oxidative atmosphere		
	PCL-1	PCL-2	PCL-3	PCL-1	PCL-2	PCL-3
$T_{2\%}(\text{°C})$	300	263	263	278	264	246
$T_{5\%}(\text{°C})$	333	312	311	310	304	311
$T_{25\%}(\text{°C})$	392	367	370	356	351	358

^[a] Heating rate: 10 °C/min

The DTG curves revealed overlapped degradation processes (see Annex A.9). The existence of more than one event agrees with the reported sequential two-steps degradation mechanism for PCLs, in which chains pyrolysis and unzipping depolymerization (also referred to back-biting) occur (Scheme 8.10). Commonly, water, carbon dioxide, alkenes, small organic carboxylic

acids, and **ECL** are released under thermal stress.^[43] These processes lead to unresolved DGT curves with maximum decomposition temperatures quite similar for all the tested compounds.



Scheme 8.10. Decomposition mechanisms of PCLs.

The formation of **ECL** requires the presence of hydroxyl ends. Therefore, it is to be expected that the studied PCLs, that possess a low M_n , exhibited a higher mass loss through the back-biting reaction than others with higher length.^[44] The dependency between thermal stability and elevated OHI value is of particular significance at the early stages of the TPU condensation, in which the temperature rises but the hydroxyls have not completely reacted with the isocyanate. At temperatures close to the moment of mixing with **H₁₂MDI**, none of the PCLs displayed a significant degree of degradations (mass loss lower than 5%), signposting a proper processing temperature. However, if mixing times increase, the formation of volatile **ECL** will be favored, which could lead to other productions issues.

In regard to the thermal stability, the three PCLs seemed suitable for the TPU synthesis under standard conditions. The observed M_n and **NPG** distribution differences did not affect the overall stability of the evaluated system, especially at higher temperatures when the small fragments of the initiator were evaporated. No difference could be identified as the reason behind the different reactivity of the compounds.

Eighteen extra **PCLs** produced batchwise at a large-scale were analyzed in terms of M_n of the mixture (**PCL-NPG** + free **NPG**), M_n of the PCLs, and **NPG** distribution (Table 8.10). None of them exhibited processing difficulties once they were synthesized, except for the aforementioned **PCL-1**. A small statistic evaluation of the obtained values was carried with the

21 samples to determine parameters as the mean and the standard deviation and to visualize the dispersion of the samples and the presence of outliers.

The average M_n value of the mixture and the PCL was around $M_t + 29$ g/mol and $M_t + 71$ g/mol, respectively, within a dispersion of around 2%. Moreover, the average value of the initiator distribution was 62 ± 5 mol % of internal **NPG**, 34 ± 4 mol% of terminal **NPG**, and 4 ± 2 mol% of free **NPG**.

Table 8.10. Data from the analyzed **PCL-NPG**.^[a] Box in purple indicate outliers.

PCL	M_n mixture (g/mol) ^[b]	M_n PCL (g/mol) ^[c]	NPG distribution (% mol)		
			Internal	Terminal	Free
1 ^[d]	$M_t + 24$	$M_t + 36$	73.9	24.8	1.3
2 ^[d]	$M_t + 20$	$M_t + 70$	60.5	34.3	5.2
3 ^[d]	$M_t - 4$	$M_t + 54$	58.2	35.6	6.2
4	$M_t + 36$	$M_t + 77$	61.7	34.1	4.2
5	$M_t - 17$	$M_t + 36$	60.6	33.7	5.7
6	$M_t + 52$	$M_t + 95$	61.1	34.6	4.3
7	$M_t + 58$	$M_t + 65$	65.4	33.9	0.7
8	$M_t + 53$	$M_t + 79$	69.0	28.3	2.7
9	$M_t + 1$	$M_t + 59$	56.1	37.8	6.1
10	$M_t + 28$	$M_t + 76$	62.2	32.9	4.9
11	$M_t + 33$	$M_t + 98$	55.0	38.5	6.5
12	$M_t + 47$	$M_t + 85$	65.6	30.5	3.9
13	$M_t + 49$	$M_t + 98$	58.8	36.3	4.9
14	$M_t + 28$	$M_t + 72$	60.7	34.8	4.5
15	$M_t + 40$	$M_t + 85$	59.9	35.5	4.6
16	$M_t + 12$	$M_t + 48$	63.7	32.5	3.8
17	$M_t + 8$	$M_t + 69$	53.4	40.3	6.3
18	$M_t + 20$	$M_t + 59$	64.8	31.1	4.1
19	$M_t + 58$	$M_t + 1$	62.2	33.5	4.3
20	$M_t + 33$	$M_t + 56$	70.4	27.2	2.3
21	$M_n + 27$	$M_n + 73$	62.2	33.1	4.7

^[a] Samples dissolved in acetone- d_6 . Spectra were recorded with a 10 second delay time to ensure quantification.

^[b] Measured by ^1H NMR end-group analysis.

^[c] Measured by ^1H NMR end-group analysis considering only the **NPG** causing polymerization.

^[d] Samples already presented in Table 8.8.

Data has been represented through box plots to generate a visual representation of the obtained values (Figure 8.15). The presented box is referred to as the interquartile box and contains 50 % of the provided data divided into quartiles. The lack of symmetry in the

interquartile box reaffirmed that the values did not follow a normal distribution. Moreover, Turkey-style whiskers that extent to 1.5 times the interquartile range, are represented.

Samples displaying values beyond the whiskers are considered numerically distant from the rest and are referred to as outliers. The limits for each parameter correspond to $[(M_t - 80) - (M_t + 88)]$ g/mol for mixture M_n , $[(M_t + 20) - (M_t + 121)]$ g/mol for PCL M_n , $[52.6 - 72.2]$ % for Internal **NPG**, $[28.4 - 40.0]$ % for terminal **NPG** and $[2.0 - 7.2]$ % for free **NPG**. Regarding the mixture M_n and PCL M_n , all the 21 samples were within the interquartile range (Figure 8.15.A). However, different behavior was observed for the **NPG** distribution. In internal **NPG** only **TPU-1** was situated outside the whiskers (Figure 8.15.B). Meanwhile, terminal **NPG** exhibited four outliers and free **NPG**, two. Specific samples that were assignee as outliers are highlighted in purple in Table 8.10.

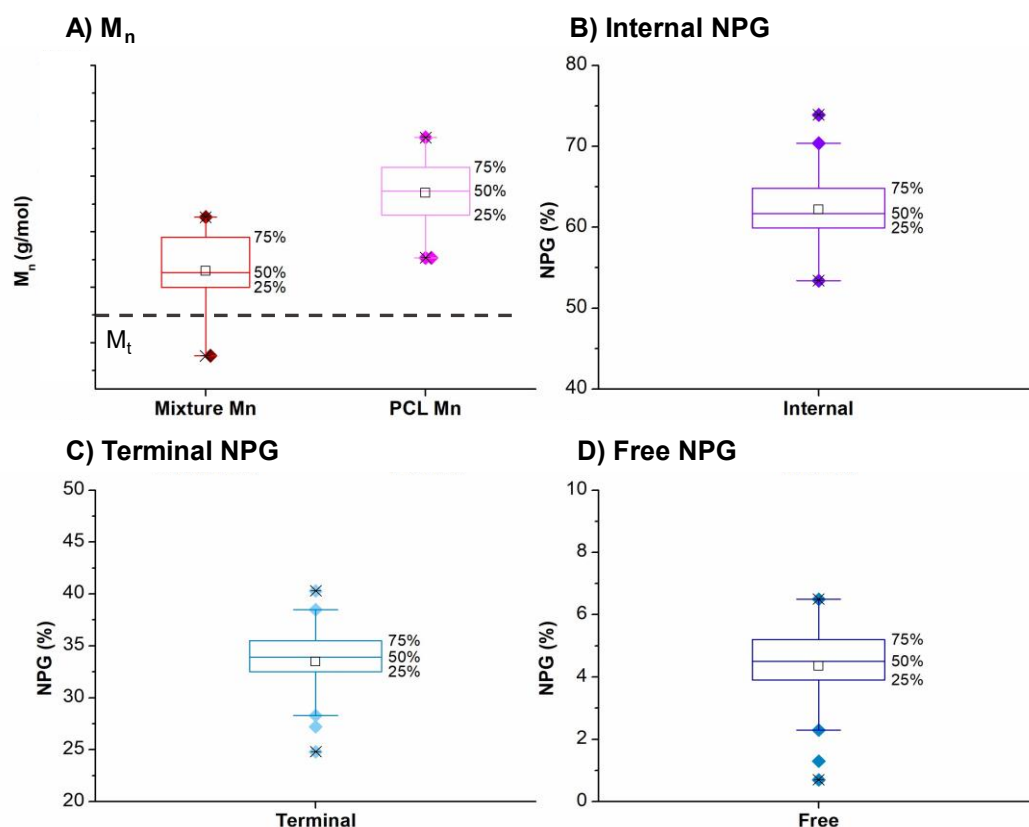


Figure 8.15. Box plot of the A) M_n of the mixture and the PCL, and the proportion of B) internal **NPG**, C) terminal **NPG**, and D) free **NPG**. Black dashed line in A indicates the M_t value. Black crosses indicated the maximum and minimum values of a variable. Diamonds represented samples at the limit of the interquartile range or beyond.

Altogether, the comparison between a problematic PCL and others produced at different scales concluded that the main difference between the samples was the **NPG** distribution within the

mixture. Thermal stability of the systems seemed suitable for the production of TPUs, although short mixing times are required to avoid the formation of volatiles. The only PCL that exhibited a problem to condensate and form TPU was the only sample that displayed distant values for the three **NPG** variables. Although more data would be required to draw proper conclusions, it seems that samples outside the provided intervals might be susceptible to abnormal outcomes.

8.3.2. Polyol analysis

The employed polyol mixture comprises a specific proportion of **BDO**, the chain extender, **PCL-NPG** of $M_n \approx M_t$ g/mol, a UV stabilizer, and an antioxidant. For confidential reasons the detailed structure of the additives and the reagent ratios will not be disclosed hereafter. The mixture is prepared in advance of the TPU production and stored at a certain temperature. Although the temperature used is lower than that at which backbiting and transesterifications side reactions have a significant impact, some alterations on the PCL structure may occur.^[38]

As mentioned earlier, this thesis participated in a more global study of a TPU production. Regarding the polyol mixture, a control procedure was designed to evaluate these potential changes by ^1H NMR spectroscopy (Figure 8.16). The evolution of some polyol mixtures was assessed to ensure the ratios of the reagents and the absence of significant contaminants.

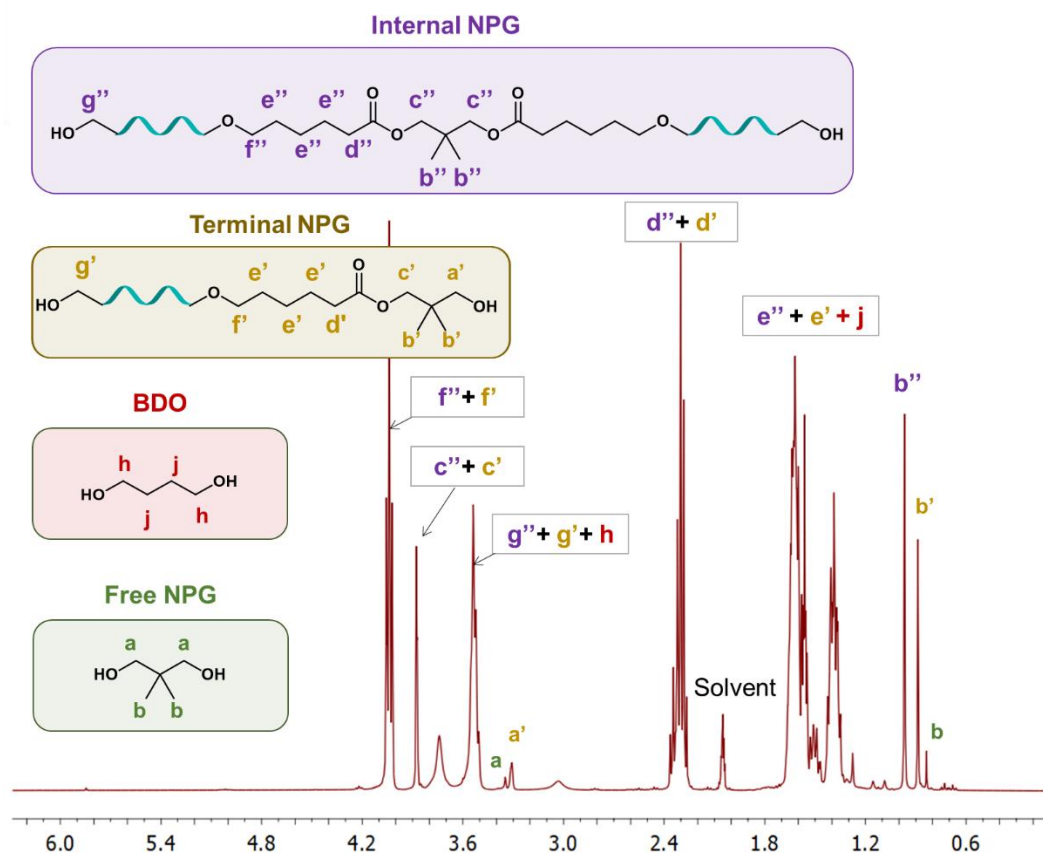


Figure 8.16. Example of a ^1H NMR (400 MHz) spectrum of a polyol mixture. Samples were recorded with a 10 second delay to ensure quantification. Solvent: Acetone- d_6 .

The percentage of chain extender, polyester, and free **NPG** in the mixture was quantified considering the integration of each peak and applying some mathematical expressions (see

details in 9.23). Results are displayed in Table 8.11. To be able to detect variations, the results of the polyol mixture are always compared to the original PCL.

Table 8.11. ^1H NMR results of the polyol mixtures.^[a]

Sample	BDO (wt.%)	NPG distribution (% mol)			Contamination
		Internal	Terminal	Free	
PCL-2 ($M_t + 20$ g/mol)	--	60.5	34.3	5.2	
Polyol mixture 1	15.7	61.2	34.8	4.0	ρTHF , 6.6 wt. %
Polyol mixture 2	16.1	60.6	34.6	4.8	
Polyol mixture 3	15.8	60.5	35.4	4.1	ρTHF , 8.3 wt. %
Polyol mixture 4	16.4	60.4	35.1	4.6	ρTHF , 1.8 wt. %
Polyol mixture 5	16.0	60.8	35.1	4.1	
Polyol mixture 6	16.0	60.7	34.8	4.6	
PCL-8 ($M_t + 53$ g/mol)	--	69.0	28.3	2.7	
Polyol mixture 7	18.0	67.5	29.1	3.4	
Polyol mixture 8	17.8	67.7	29.1	3.2	
Polyol mixture 9	18.0	67.7	29.1	3.2	
Polyol mixture 10	16.2	65.6	30.4	4.0	
PCL-10 ($M_t + 28$ g/mol)	--	62.2	32.9	4.9	
Polyol mixture 12	16.2	63.1	32.9	4.0	
Polyol mixture 13	16.2	62.2	33.4	4.4	

^[a] NMR spectra recorded in acetone- d_6 for at least 1400 scans.

The analyzed polyol mixtures are samples collected at different times and productions. From the 13 samples, three of them show a contamination arising from polytetrahydrofun (ρTHF). In general, the amount of **BDO** in the polyol mixture was slightly superior to the theoretical formulation (15.6 wt.%), which might cause difficulties to adjust the stoichiometry of the condensation reaction. Finally, regarding the **NPG** distribution, mixing the PCL with the other constituent causes a redistribution of the ratios, almost reaching an equilibrium around a 4 % of free **NPG**.

Polyol mixture 7, 8 and 9, were a special case in which the same sample was studied along time. During the studied time, the amount of **BDO** remains constant, but compared with the theoretical value, it exhibited a superior percentage.

Overall, the previous results must be taken with precaution as most of the analysis were carried out several months after the production. Despite being storage at room temperature, the samples might have to evolve.

8.4. TPU analysis

8.4.1. Comparison batchwise vs. continuous production

One of the adjustments implemented in the continuous process was the employed catalyst. Sn-based compounds are being removed from the industry to fulfill with the regulatory rules and reduce the environmental problems that might arise from them. The Sn-based complex used in the batchwise process was replaced by a MX_n catalyst for the in the continuous process. To confirm that the concerned compounds had the same chemical and physical features, two TPUs synthesized in continuous, each of them with a different catalyst for the condensation with the diisocyanate, were compared to a polymer generated batchwise (**TPU-1**). **TPU-2** was produced with the Sn-based catalyst while **TPU-3** employed the tin-free catalyst MX_n . Moreover, as both of the continuously produced polymers are synthesized from the same PCL, the quantity of catalyst used in the ROP was equal for both polymers. Samples were analyzed in terms of NMR spectroscopy, metal traces, and thermal stability. Beyond that, Lubrizol's personnel carried out a more extensive characterization (DSC, FTIR, MFI analysis...).

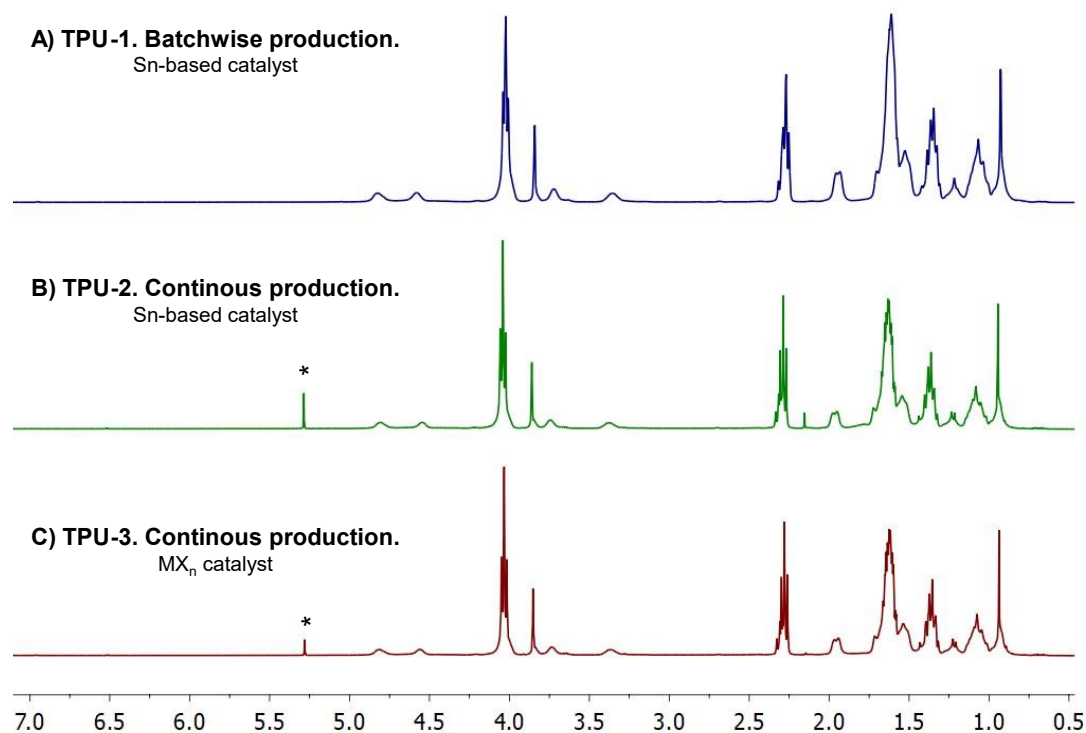


Figure 8.17. ^1H NMR (400 MHz) spectra of A) TPU produced batchwise catalyst, B) TPU produced in continuous with a Sn-catalyst and C) TPU produced in continuous with MX_n catalyst. Spectra recorded with a 10 second delay to ensure quantification. Asterisk denoted the presence of CH_2Cl_2 from the analysis solvent. Solvent: CDCl_3 .

From the spectroscopic standpoint, no differences were detected between the analyzed TPUs (Figure 8.17). Analogous to the TPUs generated from **PCL-BDO** in a previous section, the observed signals displayed a low resolution owing to the high polymer M_n and the different isomeric conformations. However, it was possible to observe the absence of the peaks ascribed to terminal and free **NPG** ($\delta_H < 1.0$ ppm), signposting the complete reaction of these fragments with the isocyanates. Regarding ratios, all three compounds followed the theoretical formulation, indicating that the adaptation to the continuous process was successfully carried out.

Pellets from batchwise and continuous processes were semi-quantitatively analyzed by ICP-MS to detect and identify different chemical elements in the matrix (Table 8.12). The elements detected by ICP-MS were phosphorus, from one of the employed antioxidants, and tin and M, from the metal catalysts. Concerning the analyzed amount of additive, it was significantly lower than expected, indicating that the antioxidant was not appropriately introduced in the system.

Table 8.12. Semi-quantitative ICP-MS analysis of pellets from different production processes. Values in parenthesis indicate the theoretical values for each element.^[a]

Sample	Process	Production Scale	P ($\mu\text{g/g}$) ^[b]	Sn ($\mu\text{g/g}$) ^[b]	M ($\mu\text{g/g}$) ^[b]
TPU-1	Batch	Kg	75 (106)	17 (17)	--
TPU-2	Continuous	Kg	72 (106)	28 (32)	--
TPU-3	Continuous	Kg	68 (106)	6 (3)	26 (25)

^[a] Samples were digested in an acid mixture (HNO_3 , HCl , and HF) prior to the analysis.

^[b] Detection limit P: 25 $\mu\text{g/g}$.

^[c] Detection limit Sn: 0.5 $\mu\text{g/g}$.

^[d] Detection limit M: 0.5 $\mu\text{g/g}$.

The concentration of both metal centers was intentionally different to compensate for their distinct catalytic activity. Moreover, the concentration of metals was optimized for a continuous process and required higher loadings than in batchwise production. The target values exclusively for the continuous condensation reaction were 25 ppm of M and 29 ppm of Sn. However, the data reported in Table 8.12 for **TPU-2** were inconsistent with the theoretical formulation. Conversely, **TPU-1** and **TPU-3** catalyst loadings were similar to the expected, pointing toward a precise addition. This lack of reproducibility in catalyst loading should be explored further to ascertain any issues on the pipelines or in the weighting of the catalyst.

In the case of the samples produced in continuous, the total theoretical value for tin in **TPU-2** and **TPU-3** should be 31.7 ppm and 3 ppm, respectively. Both **TPU-2** and **TPU-3** were produced from the same PCL, thereby the existence of 6 ppm of tin in **TPU-3** can be correlated with an equal quantity in **TPU-2**. Consequently, an approximate content of 22 ppm of tin

emerges exclusively from **TPU-2** condensation catalyst. It seems that a lower catalyst content was incorporated into the mixture at the condensation step.

In a common PCL synthesis in Lubrizol's facilities, when the exothermy of the reaction is lower than the desired profile, the catalyst loading is increased. This procedure could explain the increase in the observed tin loading. Although the PCL catalysts degrade when in contact with air, or moisture, all the TPU production processes are carried out sequentially in the same plant and under an inert atmosphere. As such, the catalyst may remain active and participate in the condensation of the TPU.^[45] This factor should be carefully considered when some difficulties adjusting the production parameters befalls, as the system could be more active than expected.

Ultimately, the thermal stability of the three TPUs was compared through TGA analysis to determine any disparities between the different synthetic processes and catalysts. Therefore, thermograms obtained by subjecting the samples to thermal stress of 10 °C/min under oxidizing and inert conditions are displayed in Figure 8.18.

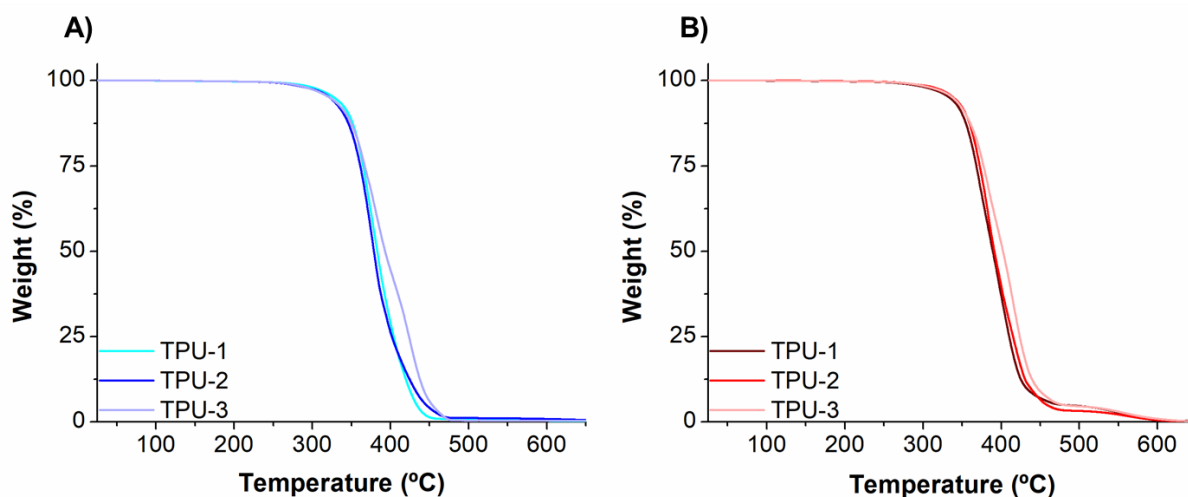
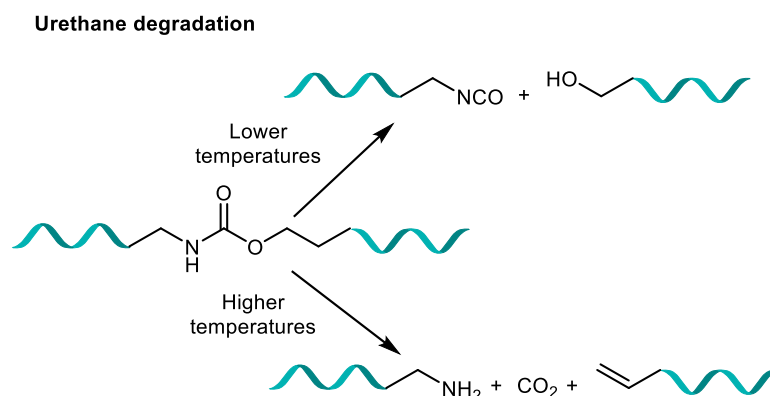


Figure 8.18. Thermogram profiles of the **TPU** samples. Analysis carried out under A) inert atmosphere and B) oxidative atmosphere.

The profile of both conditions was rather similar, with the weight loss starting at around 300 °C. The main difference between both atmospheres was the ultimate degradation of the carbon matter at temperatures higher than 500 °C under an oxygen-rich atmosphere. All samples exhibited an apparent single slope, but the DGT curves revealed the typical multi-step degradation of TPUs. Generally, the first process involves the cleavage of the carbamate moiety formed among the isocyanate and the chain extender. Initially, dissociates into isocyanate and glycol, and later, it produces amines, CO₂, and alkenes (Scheme 8.11).^[46] Afterward, the remains of the polyester degrade into smaller segments, likely following the previously

mentioned pyrolysis mechanism for the PCL (Scheme 8.10). These processes overlap in a temperature range between 300 °C and 500 °C.



Scheme 8.11. Thermal degradation process of TPUs adapted from [47].

Table 8.13 lists the temperature at which 2%, 5%, 25%, and 50% weight loss occurred. The elevated temperature of the degradation onset points to a low concentration of volatiles in the samples. At 5% weight loss, the degradation temperature is in the range of 322-328 °C under an inert atmosphere and 334-339 °C under air. The observed range is narrow, highlighting the similarities of the initial degradation steps. Only in the late stages, weight loss over 40%, the TPU catalyzed by a MX_n complex shows slightly higher stability. Since the structure of the involved reagents and the ratio between them were equal by ^1H NMR spectroscopy, the distinct behavior may emerge from the catalyst. The higher acidity of tin as Lewis acid might polarize the carbonyl of the carbamate and ester to a greater extent, fostering an easier bond cleavage and decreasing the stability of the compound.

Table 8.13. Detailed TGA of studied TPUs under both conditions.^[a]

	Inert atmosphere			Oxidative atmosphere		
	TPU-1	TPU-2	TPU-3	TPU-1	TPU-2	TPU-3
T_{2%}(°C)	300	292	292	304	309	309
T_{5%}(°C)	328	322	322	334	339	338
T_{25%}(°C)	365	361	367	368	377	377
T_{50%}(°C)	383	379	393	389	391	402

^[a] Heating rate = 10 °C/min.

Ultimately, the thermal stability at the maximum temperature of the condensation reaction and the injection post-process is important to avoid the formation of specks or defects in the produced material. Under the maximum working temperatures in the reactive screw, the produced compounds did practically not show weight loss. Although the extrusion conditions of pressure, temperature and shear cannot be replicated in the TGA, it can be concluded that

the temperature during the process is adequate, and no relevant degradation will occur during the production.

Given the spectroscopic information, the metal content, and the thermal stability, materials produced batchwise or in continuous can be considered as equal. Other techniques performed in Lubrizol (FTIR, DSC, GPC...) agree with these observations. However, the comparison among the catalyst sheds light on the differences between the theoretical values of metal content of the formulation and the ones produced in continuous. Moreover, materials generated from the M-based catalyst exhibit a slight enhancement in thermal stability.

8.4.2. Analysis of the TPU pellets

Several batches of TPUs produced in a continuous process were analyzed by ICP-MS to assess the correct incorporation of some of the additives and catalyst in the polycondensation mixture. The metals employed in the TPU synthesis and expected to be measured are M arising from the MX_n catalyst for the condensation reaction and tin emerging from the PCL. Moreover, one of the employed additives contain phosphorus. To quantify the concentration of these three elements and detect any potential cross-contamination, a semi-quantitative ICP-MS analysis was carried out. Measurement results from different lots of pellets produced in a multi-tonne scale are detailed in **Table 8.14**. The theoretical values for each element are also reported in the first entry of the following table.

Analogous to the previous ICP-MS results, phosphorus, tin, and M remain the detected elements in the analyzed pellets. The values reported from the antioxidant were consistent with what was previously observed, in which there is a relatively broad range of phosphorus content. In all cases, it is below the theoretical value (106 ppm). A punctual exception was detected in **TPU-7** in which no traces of the studied element were detected.

Concerning the elements emerging from the catalyst, tin matches the expected values for a PCL synthesis (3 ppm of ROP catalyst). Only **TPU-9** and **TPU-10** required an additional catalyst loading for producing the low- M_n polymer, but it could be considered within the normal parameters for this polymerization. Moreover, **TPU-6** and **TPU-8** exhibit higher concentrations of tin and practically absence of M, suggesting TPU condensations catalyzed with the Sn-based compound, opposite to the standard methodology.

Table 8.14. Summary of the semiquantitative ICP-MS results.^[a]

Sample	P ($\mu\text{g/g}$) ^[b]	Sn ($\mu\text{g/g}$) ^[c]	M ($\mu\text{g/g}$) ^[d]
Theoretical value	106	3	43
TPU-4	55	3	49
TPU-5	55	3	50
TPU-6^[e]	85	25	2
TPU-7	--	3	28
TPU-8	95	28	--
TPU-9	94	4	27
TPU-10	94	4	56
TPU-11	77	3	47
TPU-12	80	3	46
TPU-13	73	3	46
TPU-14	60	3	46
TPU-15	77	3	46

^[a] Samples were digested in an acid mixture (HNO_3 , HCl , and HF) prior to the analysis.

^[b] Detection limit P: 25 $\mu\text{g/g}$.

^[c] Detection limit Sn: 0.5 $\mu\text{g/g}$.

^[d] Detection limit M: 0.5 $\mu\text{g/g}$.

^[e] Sample containing 1 $\mu\text{g/g}$ of lead

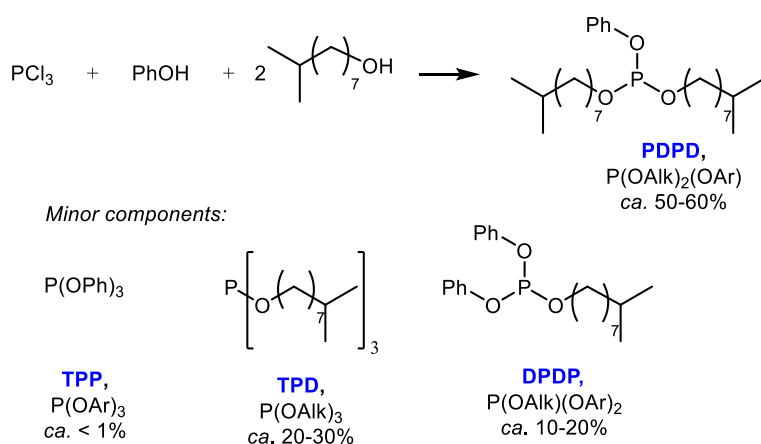
Finally, the M concentration reports significant differences. From **TPU-7** to **TPU-9**, different concentrations of the studied element were determined, likely due to catalyst loading studies. Besides these compounds, the concentration values were in between 46 and 56 ppm of M, which could be converted to 159-195 ppm of pure MX_n catalyst, signaling slightly over-catalyzed processes, but more importantly, with high variability in the produced lots. The employed catalyst is commonly purchased as a solution of the metal complex in a glycol with an elevated viscosity, which could difficult the appropriate incorporation in the TPU production.

8.5. Effect of antioxidants.

As aforementioned in the Introduction, several compounds can be used as polymer stabilizers. Among them, the role of the antioxidant on the TPU production takes significant importance during the synthetic process and the posterior shelf-life. Therefore, the composition and stability of said compounds should be considered prior to their implementation in an industrial process. Two phosphorus-based compounds, **PDDP** and **Irgafos 126**, were explored for their use as secondary antioxidants in the synthesis of the TPU films. They are reported to inhibit the propagation of radicals, reducing the thermal oxidation during the production, and in the long term, decreasing the coloration of the polymer. The composition of both phosphorus-based compounds and their speciation were evaluated in different matrixes.

8.5.1. Phenyl diisodecyl phosphite (PDDP)

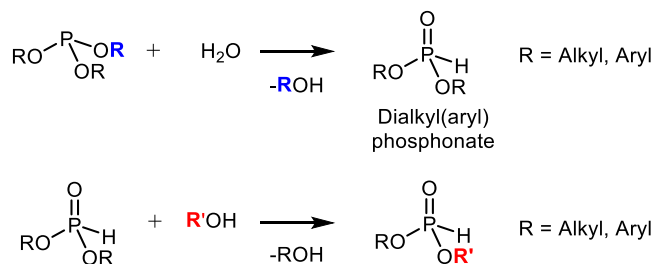
The name **PDDP** corresponds to phenyl diisodecyl phosphite (**PDDP**). However, it is commercialized as a mixture of four phosphites. The synthetic route for this phosphite involves the reaction of phosphorus trichloride with phenol and isodecanol in a 1:1:2 molar ratio, usually in the presence of a base, or temperature (Scheme 8.12). Hence, the compound that gives the name to the product is only *ca.* 50-60 % of the total phosphorus content in the sample. The main reason for its use apart from its low price, is that the other phosphites might also behave as antioxidants, flame retardants, or lubricants, and therefore the mixture of said compounds provides a synergetic effect on the final polymer's properties.



Scheme 8.12. General synthesis of **PDDP** and the subproducts on the commercialized mixture.

The specific distribution of the phosphites was assessed through $^{31}\text{P}\{^1\text{H}\}$ NMR spectroscopy by dissolving the mixture in CDCl_3 . However, analyzing the sample as-provided led to the observation of hydrolyzed products, which increased over time. The expected degradation

products are dialkyl(aryl) phosphonates, resulting from the hydrolysis of the trialkyl(aryl) phosphite in the presence of water (**Scheme 8.13**).^[48] Moreover, in the presence of hydroxyl groups, such as chain extenders or free initiator, transesterification of the phosphonate might take place, resulting in multiple new compounds in the polyol mixture.



Scheme 8.13. General hydrolysis reaction of phosphite.

Therefore, and owing to the high reactivity of the compounds, all the analyses were carried out with deuterated solvent filtered through basic alumina to avoid their degradation (Figure 8.19). Phosphites can be easily distinguished from the degradation products as they show up in a different region of the $^{31}\text{P}\{^1\text{H}\}$ NMR spectrum (from 145 to 125 ppm, *vs* -20 to 20 ppm, respectively).

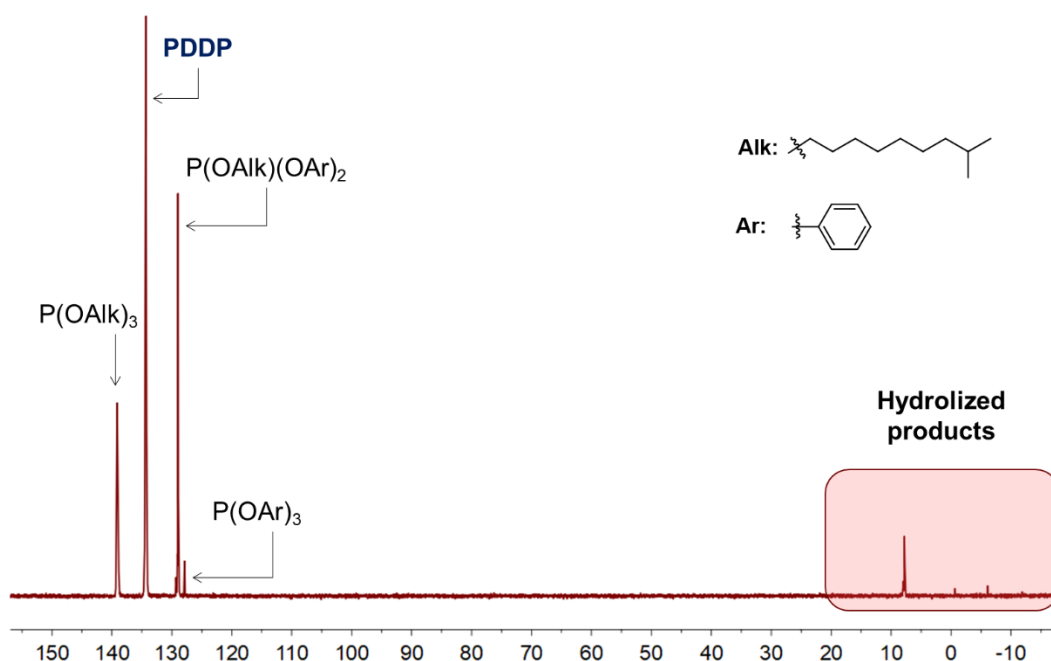


Figure 8.19. $^{31}\text{P}\{^1\text{H}\}$ NMR spectrum (162.0 MHz) of a **PDDP** sample recorded with a delay time of 10 seconds. Solvent: CDCl_3 previously filtered through basic alumina.

The integration value of each peak provides the molar fraction of the analyzed compounds and allows the estimation of the purity of the sample. The four phosphites comprised at least 95.5 % mol of the sample, being the rest hydrolyzed products. The relative ratio of the four

non-hydrolyzed compounds is detailed in Table 8.15, confirming that **PDDP** was the main component of the mixture.

To correlate the measured data with the one provided by the supplier, the signal of the four phosphite was normalized to 100% and the content of each compound was calculated. Results displayed in Table 8.15 are an approximation as the hydrolyzed products were not identified and thereby, the exact M_n of the mixture could not be quantified. Albeit roughly, the percentages in weight of the phosphites are within the values reported by the supplier.

Table 8.15. Phosphite speciation in the provided mixture.^[a]

Compound	Chemical shift (ppm)	Phosphorus distribution (% mol) ^[b]	Supplier specifications (wt.%)	Mixture distribution (wt. %) ^[c]
TDP , P(OAlk) ₃	139.9	24.9	20-30	29.6
PDDP , P(OAlk) ₂ (OAr)	135.1	51.7	50-60	53.6
DPDP , P(OAlk)(OAr) ₂	129.7	18.0	10-20	16.0
TPP , P(OAr) ₃	128.6	0.9	< 1	0.8
Degraded products	-15 to 15	4.5		--

^[a] Sample dissolved in CDCl₃ filtered through basic alumina. ³¹P{¹H} NMR spectrum was recorded with 10 seconds delay to ensure quantification.

^[b] Proportion of each phosphorous compound normalizing to 100 all the ³¹P{¹H} signals.

^[c] Omitting the degraded products.

Due to the sensitive nature of the antioxidant mixture, a great proportion of degradation products might be obtained if they were not treated carefully either during the production, the mixing, or the storage. This fact might play a significant role in polymer shelf-life as it is assumed that the antioxidant property arises only from the phosphites and their degradation products do not preserve these properties.

8.5.1.1. Antioxidant in the polyol mixture and TPU

TPUs are polymers with a lower concentration of radicals than other types of resins such as polyolefins, so they are less sensitive to thermoxidation degradation. Hence, the action of phosphites is not restricted to decomposing hydroxyperoxides formed during the production, but also to promoting color stabilization in long term. It might be arguable said that the higher the phosphite content in the final product, the longer the service life.

When the polyol mixture is prepared, it includes the **PCL-NPG**, **BDO**, and some additives, one of them, the antioxidant **PDDP**. This mixture is formed before the TPU production and is stored at an optimized temperature until the completion of the reaction. The medium must be almost neutral and the amount of water should be extremely low, as their presence would affect the

condensation reaction. The maximum water content in the **PCL** is 0.2 wt.%, which corresponds to $5 \cdot 10^{-3}$ mol of water/100 g of TPU, while an AI of 0.2 mg KOH/g PCL correlates to $0.18 \cdot 10^{-3}$ mols of acid/100 g of TPU. Although such low concentrations might not directly affect the TPU formation, they are tenfold higher than the antioxidant content. Even if just a fraction of the water and acid content reacts with the antioxidant, the hydrolysis of the antioxidant might reach a high degree even before the condensation starts. Moreover, the temperature at which the polyol mixture is stored might foster antioxidant degradation.

Six polyol mixtures prepared with either **PCL-2**, or **PCL-8**, and the same quantity of **PDDP** were evaluated by NMR spectroscopy to determine the state of the additives in the sample. Although the **PCLs** are equal for the first four polyol mixture, the rest of the components, such as **BDO**, and additives could come from different batches with different water content. Moreover, the studied polyol mixtures containing **PDDP** were stored for at least 4 months before the NMR analysis was carried out, and the conditions of sampling and storage were unknown.

Results of the NMR spectra were summarized in **Table 8.16**. The speciation of **PDDP** after the mixing of all the constituents changed significantly. All the analyzed samples presented a high percentage of hydrolysis, with at least 42 % of the active phosphite degraded. **Polyol mixture 6** comprises an outlier, as no phosphorus signal was depicted in the spectrum.

Table 8.16. $^{31}\text{P}\{^1\text{H}\}$ NMR results of the polyol analysis.^[a]

PCL	Polyol mixture	Phosphite (% mol)^[b]
2	1^[c]	32
	2	58
	5	7
	6	~ 0 ^[d]
8	7	57

^[a] $^{31}\text{P}\{^1\text{H}\}$ NMR spectra recorded in acetone- d_6 for at least 1400 scans.

^[b] Sum of the four phosphite species (% mol) respect the total amount of phosphorus in the sample.

^[c] Sample containing polyether contamination.

^[d] No phosphorus signal was observed.

These results show a high degree of degradation of the antioxidant in the polyol mixture, even stored at room temperature. Therefore, it seems that introducing **PDDP** into the polyol mixture may decrease the effectiveness of the antioxidant properties in the material.

Likewise, TPU pellets were analyzed to assess the evolution of **PDDP** during the synthesis. Employing two of the previously evaluated polyols, two TPUs were produced and analyzed to

quantify the antioxidant degradation in the production process. The difference between the two samples, the polyol mixture, and the TPU, should provide the degree of degradation during the condensation reaction. Owing to the low phosphorus concentration in the sample and the low solubility of these TPUs, even in the best solvent found (CDCl₃/Pyridine), the signal/noise ratio on the ³¹P{¹H} NMR spectra was low. The obtained results are summarized in Table 8.17.

The speciation of the antioxidant was somewhat unexpected since, even if the TPU condensation process did not increase the degradation, the percentage of phosphite should remain at least similar to the polyol mixture. Nevertheless, the phosphite content after the TPU synthesis was higher, implying a further degradation in the polyol mixture. This fact raises some doubts about the stability of the antioxidants in the polyol mixture.

Table 8.17. Results of **PDDP** speciation in the polyol and the subsequent TPU.

PCL	Polyol mixture	Phosphite (% mol)^[a]	TPU	Phosphite (% mol)^[b]
2	1^[c]	32	TPU-16	84
	2	58	TPU-17	65

^[a] ³¹P{¹H} NMR spectra recorded in acetone-*d*₆ for at least 1400 scans

^[b] Samples dissolved in CDCl₃ /pyridine at room temperature for eight hours. ³¹P{¹H} NMR spectra were recorded with 27300 scans.

^[c] Sample containing polyether contamination.

The analysis of the polyol mixture was not carried out with freshly formulated mixtures, but with samples stored for at least four months. Samples of the polyol mixture at the moment of the TPU production were not available to be measured. It should be remembered that the polyol mixture is prepared before the condensation reaction and remains in the tank at a fixed temperature for variable times, which might foster hydrolysis. Moreover, the mixture continues to have a relative viscosity even stored at room temperature, conferring mobility to the components of the mixture, and potentially allowing further reactivity of the considered antioxidants. Therefore, bearing in mind the unknown conditions of sampling and/or storage and considering that the analysis was performed several months after the preparation of the polyol mixture, values in Table 8.17 reflect the different evolution of the antioxidant in these two types of samples. The observed variation implies that the mixture of **PCL**, **BDO**, and additives might somehow promote the hydrolysis of the antioxidant over time, while once the mixture is condensate in the form of TPU, the degradation rate of the phosphites is significantly slower.

To increase the amount of phosphite in the final TPUs, some small modifications of the synthetic process were evaluated (Table 8.18). The previously discussed **TPU-16** and **TPU-17** were the

reference materials prepared in continuous and incorporating the antioxidant into the polyol mixture. To assess if there was any issue with the continuous process, materials synthesized from **PDDP** mixed in the polyol mixture but produced batchwise (**TPU-18** to **TPU-21**) were considered. Furthermore, and given the relative reactivity of the antioxidant in the mixture, it was explored its introduction at the early stages of the TPU condensation reaction (**TPU-22** to **TPU-23**) or at the end (**TPU-25**).

Batch samples exhibited a degree of hydrolysis between 30-40 % mol, similar to the continuous process of blending the antioxidant in the polyol mixture. Conversely, a slight increase in the phosphite concentration was noted when **PDDP** was added during the condensation reaction, reaching only 20-25 % mol of additive degradation. The latter approaches in which **PDDP** was not directly mixed with **PCL-NPG** and **BDO** provided better results in terms of phosphite in the final material.

Table 8.18. Antioxidant speciation in TPUs with different **PDDP** additions.

Sample	Process	Addition of phosphite	Phosphite (% mol) ^[a]
TPU-16	Continuous process	Polyol	84
TPU-17	Continuous process	Polyol	65
TPU-18	Batch process	Polyol	63
TPU-19	Batch process	Polyol	71
TPU-20	Batch process	Polyol	60
TPU-21	Batch process	Polyol	71
TPU-22	Continuous process	Initial stage of the condensation	77
TPU-23	Continuous process	Initial stage of the condensation	75
TPU-24	Continuous process	Initial stage of the condensation	80
TPU-25	Continuous process	Final stage of the condensation	80

^[a] Samples dissolved in CDCl₃ /pyridine at room temperature for eight hours. ³¹P{¹H} NMR spectra were recorded with 27300 scans.

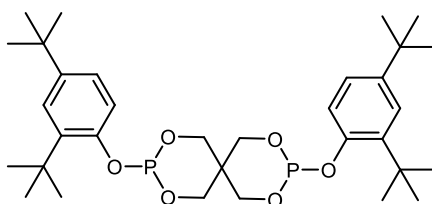
In summary, the polyol mixture is clearly capable of hydrolyzing **PDDP**, being the most likely origin the water and the acid content of the mixture. By introducing the antioxidant at the later stages of the production without combining it with the polyol mixture, its degradation is reduced.

8.5.2. IRGAFOS 126

Aiming to improve the stability and durability of the produced TPUs, the substitution of **PDDP** by another antioxidant, **Irgafos 126**, was studied by the R+D department of Lubrizol (Scheme 8.14). However, these TPUs displayed lower viscosities than the **PDDP** benchmarks,

exhibiting longer condensation times, or in some cases, the impossibility to successfully produce the polymer. To understand these disparities, different conditions were studied by Size Exclusion chromatography (SEC) and NMR spectroscopy, focusing on the polyol mixture and the structure of the antioxidant.

Contrary to the previously employed additive, **Irgafos 126** is a diphosphite commercialized as a single product with at least a 95 wt.% purity (according to the supplier). This high purity was confirmed by $^{31}\text{P}\{^1\text{H}\}$ NMR spectroscopy. However, equally to **PDDP**, hydrolysis or eventually oxidation to P(V) compounds were observed in the spectrum if the solvent contained traces of acid or water. Moreover, it was qualitatively observed that the degradation processes were substantially swifter than the previous compound.



Scheme 8.14. Structure of **Irgafos 126**.

The evolution of a polyol mixture was studied to determine the abnormalities behind the decrease in viscosity over time. The concentration of “active” **Irgafos 126** in the samples was quite low in all the cases, displaying a high degree of degradation in the polyol mixture.

Table 8.19. Summary of the $^{31}\text{P}\{^1\text{H}\}$ NMR results.^{[a][b]}

Polyol mixture	Sample	Irgafos 126 (% mol) ^[c]
7	Polyol + additive (t)	38
8	Polyol + additive ($t + 24$ h)	34
9	Polyol + additive ($t + 28$ h)	34

^[a] ^1H NMR spectra recorded in acetone- d_6 and 10 seconds delay time to ensure quantification.

^[b] **PCL-NPG** features: $M_t + 50$ g/mol; Internal **NPG** = 69.0 %; Terminal **NPG** = 28.3 %; Free **NPG** = 2.7 %.

^[c] $^{31}\text{P}\{^1\text{H}\}$ NMR spectra recorded in CDCl_3 for at least 1400 scans.

SEC was used to assess the evolution of the M_n and the polydispersity of the polyol mixtures (Figure 8.20). As a benchmark, a freshly prepared polyol mixture with the same **PCL-NPG** and lacking additives was also analyzed. To mimic the already evaluated samples, the polyol mixture was heated at the tank’s temperature during a period of time (t).

SEC chromatograms displayed a multimodal molecular weight distribution, which was to be expected in a mixture of **BDO** and **PCL-NPG**. The peak observed at higher elution volumes (20.3 ml) corresponded to **BDO** and thereby, it was absent in the pure PCL sample. The

remaining peaks arose from the PCL and their transformations. SEC results of the PCL did show that most polymer chains were distributed in a common gaussian peak centered at 17.8 ml. However, even as-synthesized, a small fraction of chains possessed smaller M_n (elution time 19.3 ml). As time went on, the intensity of this last peak increased, signposting a rise in the cleavage of the polymer chains to form smaller fragments. Moreover, in samples containing **Irgafos 126** an additional peak emerged at a lower elution volume (12.0 ml). This peak suggests that some kind of crosslink of several polymer chains took place.

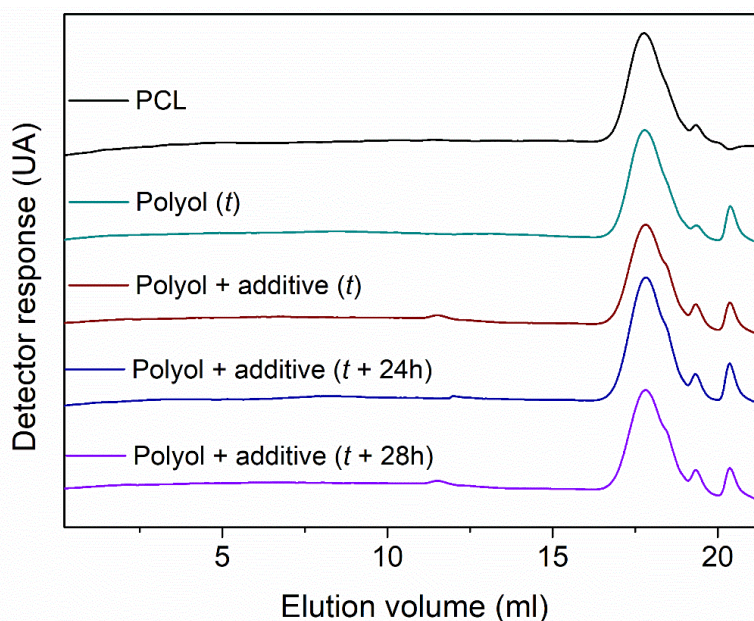


Figure 8.20. SEC chromatograms of tested samples dissolved in THF.

Table 8.20. Summary of the SEC results of the tested samples.^{[a][b]}

Sample	Elution volume (ml)	M_n (g/mol) ^[c]	M_w (g/mol) ^[c]	D
PCL (t_0)	17.8	$M_n + 470$	$M_n + 1350$	1.6
Polyol (t_0)	17.8	$M_n + 440$	$M_n + 1300$	1.6
Polyol + additive (t_0)	17.8	$M_n + 330$	$M_n + 1240$	1.7
Polyol + additive ($t_0 + 24$ h)	17.8	$M_n + 350$	$M_n + 1240$	1.7
Polyol + additive ($t_0 + 28$ h)	17.8	$M_n + 290$	$M_n + 1220$	1.7

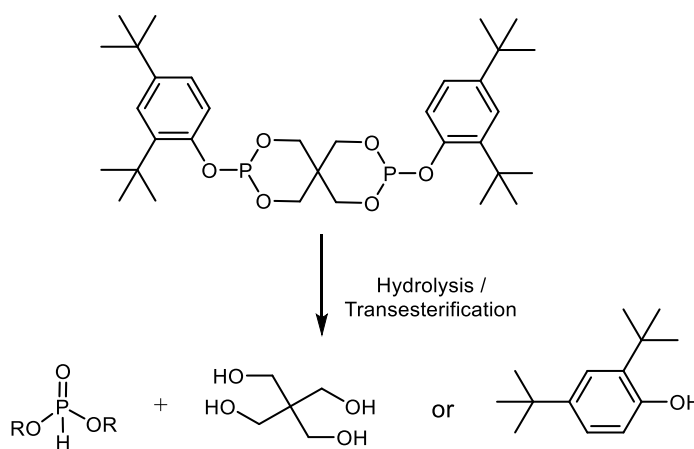
^[a] Sample dissolved in THF.

^[b] **BDO** M_n corresponded to 119 g/mol.

^[c] SEC analysis calibrated with polystyrene standards.

The measured values are quantitatively summarized in Table 8.20, considering as whole the PCL section of the SEC plot (from 17 to 20 ml), and not each specific peak. The blend of the chain extender and the PCL decreased the M_n as could be expected when the mixture was subjected to temperature. However, this variation was much smaller when no additive was added, indicating that the antioxidant was promoting the cleavage of some ester moieties of the PCL.

The decrease in the M_n of the PCL and the formation of longer chains might be explained by the nature of the antioxidant. In the presence of water or alcohols in the mixture, the antioxidant might hydrolyze or transesterify and release pentaerythritol or substituted phenols to the medium (Scheme 8.15). These alcohols can further react with polyester chains, creating crosslinked star-like structures with higher M_n than the initial PCL, or in the case of the phenol end-capped chains. To achieve this crosslink, some PCL fragments must be cleaved, leading to a decrease in the homogeneity of the sample and the corresponding decrease in viscosity. Moreover, the phosphonate could also act as a crosslinker point, increasing the heterogeneity of the chain lengths.



Scheme 8.15. Potential products of hydrolysis and/or transesterification of **Irgafos 126**.

The technical datasheet of the product was extensively inspected. It mentioned the compatibility with TPUs, but polyesters were not mentioned. The product was not completely recommended for their use in polyester-based TPUs as some of the degradation products could promote partial hydrolysis of the polyester.^[49]

Altogether, the alternative of using **Irgafos 126** instead of **PDDP**, at least by introducing it in the polyol mixture does not seem appropriate. The degree of hydrolysis of the former was similar to the standard antioxidant, but some side effects like the decrease of the viscosity and the overall M_n of the sample were observed.

8.6. Films analysis

One of the main targets of this project was the identification of gels on the extruded TPU films and the reduction of their number. Defining the nature of the observed gels was the first step to being able to control, lessen or even eliminate them. Several materials from different lots, synthetic methods, and post-processes were examined to detect the origin of the specks.

From the observations carried out on the material, the nature of the detected gels was not oxidized gels, as no variation of the color was detected. Moreover, it was studied that the TPU withstand the working temperatures and the process was optimized for avoiding this type of imperfection. Therefore, the spotted gels might arise from fragments of unmelted domains of the polymer either owing to a superior crystallinity, a high degree of entanglement, or by some external contaminants or additives.

8.6.1. ICP-MS measurements

The preliminary attempts carried out to characterize the composition of the material collided with the nature of the produced material. The extruded polymers were so thin ($<500\ \mu\text{m}$), and the defects had such a low concentration that hinder the analysis by conventional techniques. Semi-quantitative analysis of the samples reported the same results as with the pellets. The two metal catalysts were appropriately detected, and in most of the cases also phosphors. But other elements such as sodium or silicon could not be detected over the detection limit (Si in films $< 250\ \text{ppm}$ and Na $< 50\ \text{ppm}$). However, its concentration seems to be below the detection limits of the ICP-MS for both pellets and films.

8.6.2. X-ray photoelectron spectroscopy

Subsequently, X-ray photoelectron spectroscopy (XPS) was explored to analyze the surface of a film produced in continuous. Figure 8.21 shows the obtained results, in which carbon, nitrogen, and oxygen were detected with binding energy values centered around 285 eV, 399 eV, and 532 eV, respectively. Moreover, the presence of two low-intensity peaks at 101 eV and 151 eV indicated a low concentration of silicon. It was not observed in the pellet owing to the low concentration and the dispersed only on the surface of the particle. However, when the material was extruded, it was distributed and could be detected by XPS. No other compounds could be detected with confidence. The beam dimensions were bigger than the studied gels,

which prevent the focalization in certain regions of the material to discern if the composition of the gel was different from that of the matrix.

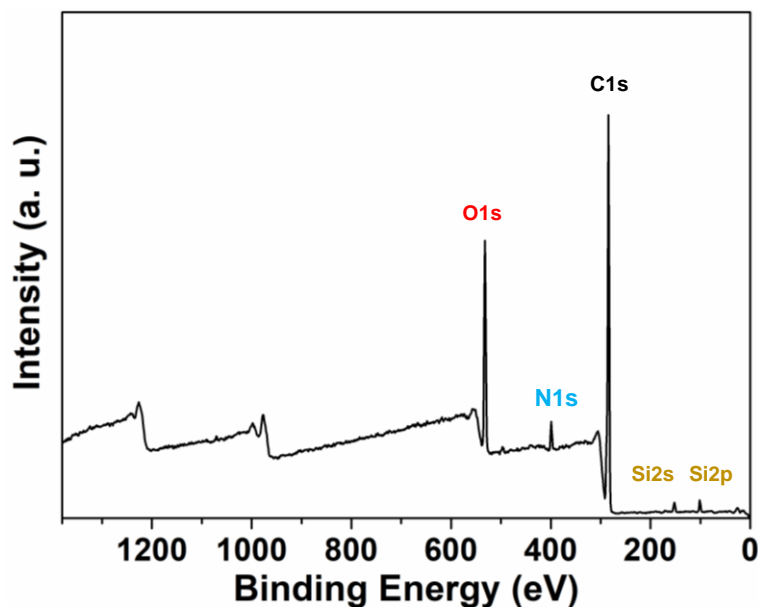


Figure 8.21. XPS survey scans of a film.

The produced material exhibits a low conductivity, so when the polymeric film was subjected to the X-ray beam, it resulted in a charged surface which generated artifacts on the produced results such as shifts regarding the reported values and broadness of some of the signals.^{[50][51]} Henceforth, quantification of the detected elements could not be properly carried out.

8.6.3. Scanning Electron Microscopy

Further studies for trying to elucidate the nature of the observed gels by Scanning Electron Microscopy (SEM) were carried out on the films. Ideal samples to be examined by electronic microscopy are those with flat or polished surfaces, not beam-sensitive, with homogeneous composition over the interacting volume, and that remain unaltered over the analysis. However, sheets studied in this section are far from an ideal specimen, as was concluded with the XPS measurements. Typically, the high energy of the incident beam over a non-conductive sample might cause the degradation of the surface. As result, the loss of some amount of matter, especially from the lighter elements is frequent, while the heavier remains on the sample.^[52] Therefore, to explore the presence of the specks that might modify the refractive index of the produced materials and avoid a swift degradation, the films were metalized with a Pd/Au mixture to improve the conductivity of the sample and decrease the charging of the surface.

Areas containing defects identified at the naked eye, or sheets with a substantial number of imperfections detected by OCS were selected for analysis. Among them, grains formed by elements with higher electronic density than carbon, oxygen and nitrogen were observed (Figure 8.22). The detected particles were not homogeneously distributed throughout the material and seemed to be localized in depressed areas of the surface. Although the analyzed spots did not contain particles with dimensions close to the gels detected by the OCS as macrogels ($< 200 \mu\text{m}$), the crystallization or aggregation of crystallites on the surface of the material or near it might cause changes in the local refractive index and the appearance of visual flaws. Besides, the arrangement of several particles resembles the formation of spherulites (Right side of Figure 8.22.B). That fact in combination with the higher electronic density of the spots suggested that they originated from inorganic elements with an elevated tendency to crystallize like some common salts.

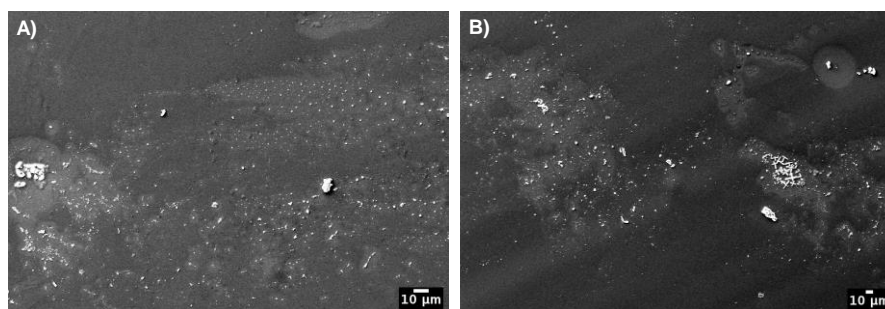


Figure 8.22. SEM micrograph of a film produced in continuous. Magnification: 500 kX.

The chemical composition of the observed particles was explored through an EDX analyzer coupled to the SEM instrument. The incident electron beam causes the release of different X-ray radiations which is specific for each element. The chemical information of the studied films was visualized in various forms as illustrated in Figure 8.23, where a spectrum of a single point was obtained, or by mapping the analyzed area (Figure 8.24).

The preliminary analysis exposed a considerable number of inorganic elements on the observed specks, being chlorine, calcium, sodium, potassium, and silicon the predominant detected compounds. Owing to the testing conditions, it was impossible to differentiate between bromine and aluminum, as another major constituent of the flaws. The employed technique does not allow the obtaining of the chemical formula, but it is plausible the proposal of particles arising from salts like NaCl, KCl, CaCO_3 . Therefore, their identification confirmed the presence of

inorganic salts that when crystallized, might have a sufficiently different refractive index to be detected by the OCS. Most of the detected elements had an undetermined origin.

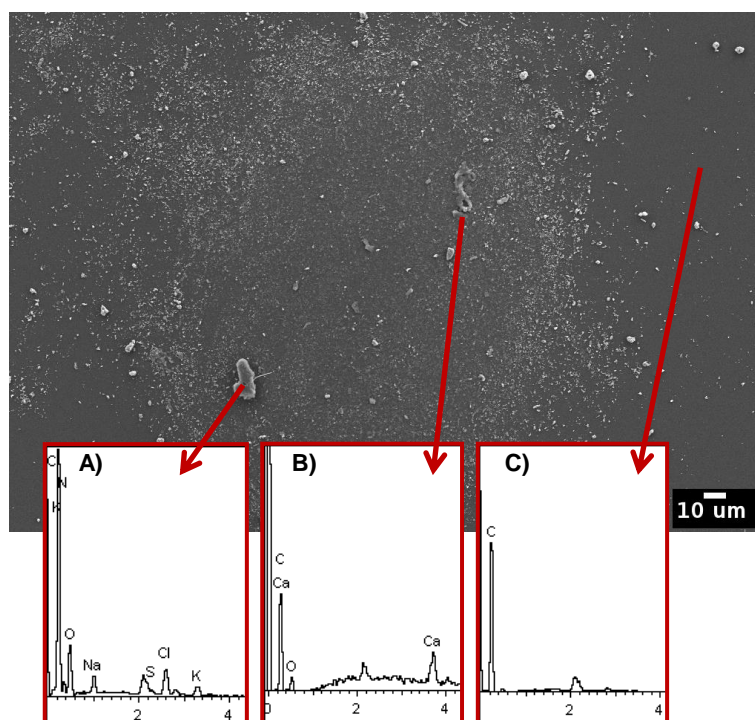


Figure 8.23. SEM micrograph with three EDX spectra of different regions of the sheet. A and B correspond to EDX analysis of two particles of high dimensions and C to an uncluttered area as a benchmark. Magnification: 850 kX.

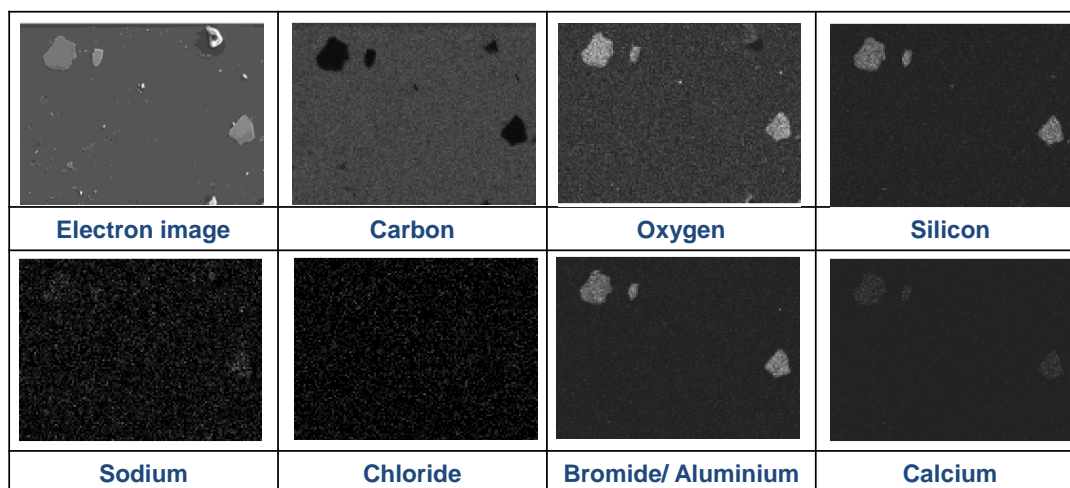


Figure 8.24. EDX mapping analysis of a small region of a sheet. The brighter the area, the higher the element content.

Conversely, other samples with a smaller number of gels were also examined by SEM (Figure 8.25). Those sheets exhibited surfaces cleaner and with fewer flaws. Moreover, the amount of bright speck emerging from inorganic elements was reduced. In those spots with inorganic elements, the principal components were similar to the previous material. Moreover,

some organic gels were observed for the first time. Hence, it seems that the presence of salts increased to a great extent the gel content detected by OCS. Thereby, reducing the ionic compounds would not eradicate the presence of gels in the samples but could enhance the quality of the material.

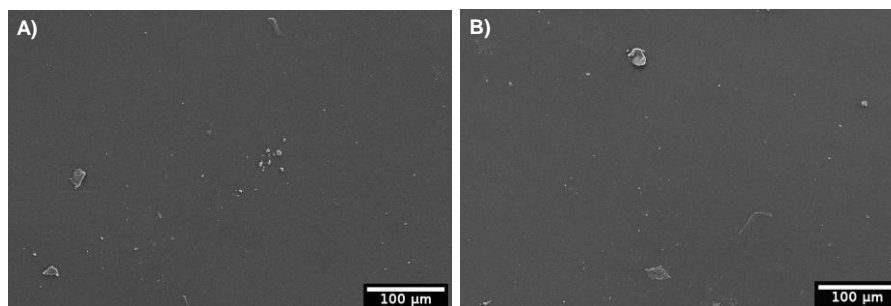


Figure 8.25. SEM micrographs of low gel content film. Magnification: 500 kX.

After considering several aspects of the synthetic process as the salt's origin, the composition of the cooling water employed in the pelletization step was explored. Its components were routinely analyzed, resulting in water with a high content of carbonates and common inorganic salts. Moreover, some antifoam agents and bleach were added in extremely low percentages to avoid bacterial growth and foam. Although some elements were added to enhance the stability of the liquid and therefore it could not be considered as common water, henceforward it will be referred to as tap water.

To delve into if the inorganic content of the cooling bath influenced the number of gels, two TPUs were synthesized according to the standard procedure, but one of them was treated with deionized water in the refrigerating step instead of the referred tap water. If the inorganic salts did not originate from the ordinary bath, both films must exhibit similar type and concentration of gels. However, if the contents of the cooling bath were responsible for the imperfections, the sheet cooled with tap water should show a more elevated number of gels.

Previous experiments did shed light on the fact of cross-contamination in the extrusion process. It was observed that a substantial content of salts and anti-tacking agent remained in the extruder and were randomly distributed on the following extruded material. Therefore, it is arduous to ensure the complete elimination of salt residues of the tanks, pipes, or equipment, although all of them were rinsed before the synthesis, and polyethylene was employed to clean the extruder.

To determine the quality of the material, the studied films were previously analyzed by OCS, and the number of gels was quantified. Results presented in Table 8.21 exhibit similar values

of the microgels (<200 μm), but a substantial decrease in the concentration of macrogels (> 200 μm) was detected when moving from tap to deionized water. Furthermore, a comparison of both samples at the naked eye displayed a lower number of defects in the films produced after a cooling bath with deionized water, suggesting that visual imperfections may be mainly those with bigger dimensions.

Table 8.21. OCS results measured at Lubrizol's facilities.

Sample	Scale	OCS quantification (counts/m ²)	
		Microgels	Macrogels
Tap water	Kg	≈ 198 000	≈ 5540
Deionized water	Kg	≈ 211 000	≈ 2660

The SEM analyses of the two extruded films exhibited different phenomena as can be seen in Figure 8.26. The two left micrographs display particles throughout the surface, drawing a "Milky Way" illusion. However, Figure 8.26.C and Figure 8.26.D, associated with two regions of the sheets cooled down with deionized water, were cleaner and with more reduced content of inorganic granules.

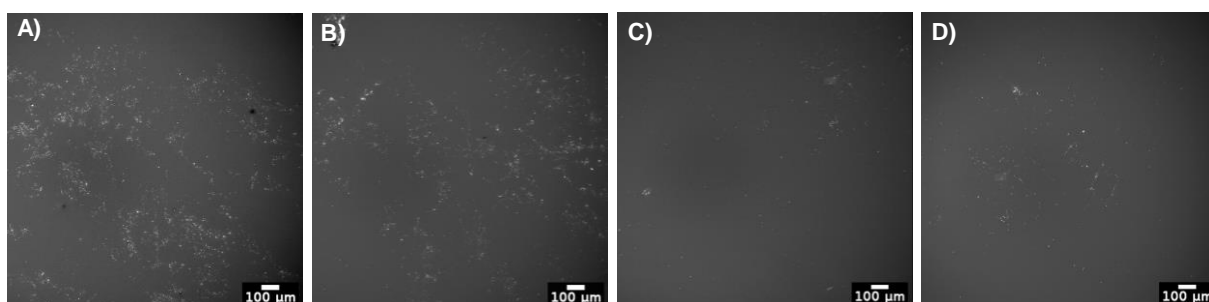


Figure 8.26. SEM micrographs at low magnification of films produced with tap water (A and B) and deionized water (C and D). Films metalized with Au/Pd. Magnification: 120 kX.

In general, the material cooled down in deionized water displayed surfaces with a lower concentration of particles. They exhibited relatively small size and heterogeneous shapes. Focusing on areas with defects (Figure 8.27), the analysis of the sheets at higher magnifications revealed a tendency of the particles to be located close to each other in the space. The major axis of the ellipses drawn in Figure 8.27.B, Figure 8.27.C, and Figure 8.27.D were around 40-50 μm , which might be detected by OCS. The main component of those particles was calcium, but to less extend also X-ray lines from sodium, chloride, or potassium were identified. Generally, salts containing calcium are less soluble than those comprising sodium or chloride. Thereby, they could remain deposited in pipes and reactors easily and are more difficult to eliminate. Moreover, the green square region of Figure 8.27.D was enlarged in Figure 8.27.E

and revealed air ruptures of the material, likely due to the extrusion process, containing primarily silicon and oxygen. Finally, some gels with organic origin were detected at higher magnifications (Figure 8.27.F, blue circles). Nevertheless, it was not possible to determine if they correspond to unmelted or to highly-entangled polymers. It seems that once the number of salts decreases or they concentrate in certain areas, other phenomena could be easily detected.

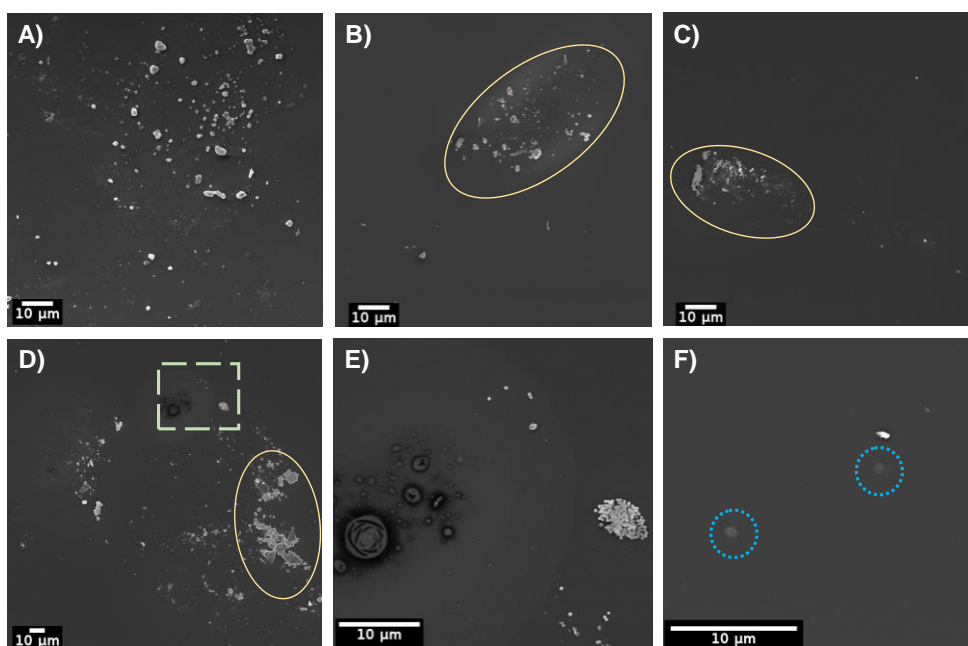


Figure 8.27. SEM micrographs of areas containing imperfections of a film cooled down with deionized water. Images A, B, and C were recorded with the same magnification (2000 kX). Image D was recorded at 1000 X. The region within the green square of D was enlarged in Image E (magnification 5000 kX). F) was recorded with 8000 kX.

Conversely, films obtained from a material cooled down with tap water, displayed particles of small size and were more homogeneously distributed in the space (Figure 8.28). The dimensions of the salts remain comparatively small ($< 5 \mu\text{m}$), but there was a high heterogeneity, reaching in some cases up to $20 \mu\text{m}$.

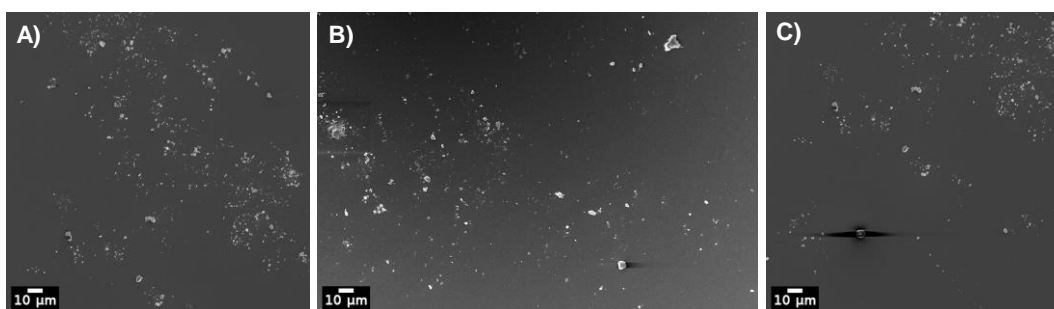


Figure 8.28. SEM micrographs of areas containing imperfections of a film cooled down with tap water. Magnification 1000 kX.

The composition of the spotted particles was slightly different from the previously studied film. Materials treated with tap water contained calcium, sodium, chloride, and potassium in a significant number of particles. Moreover, other elements as magnesium, aluminum, or bromide (likely the latter, but could not be identified with confidence) were detected in some of the brightest spots.

SEM analysis of the films revealed that most of the observed imperfections arose from inorganics salts and to a lesser scale some organic grains. The chemical composition of these salts agreed with elements found in relatively elevated concentrations in water. Therefore, it seems that processing the material with tap water favored the adhesion of the ions dissolved in the liquid to the polymer. Once water was evaporated and the TPU was processed, those ions crystallized/solidified in the form of diverse particles. Owing to the limited size of most of the specks, they may not be the reason for the macrogels when considered individually. However, the aggregation of multiple small particles in a region of the material might change the local refractive index, observed as an imperfection by the naked eye. Factors as the concentration of ions in the water, which is refilled to compensate its evaporation, thus increasing the salt concentration, as well as the time that the pellets remained in the bath, or the extrusion conditions may affect the number and size of the measured defects and cause variability between the batches.

The reduction of the concentration of those ionic compounds in deionized water led to cleaner films with the particles only gathered in some areas. Moreover, the assembly of the specks in limited regions allows the identification of other imperfections that before were disguised and that might come from the polymer itself. Although the use of deionized water did not eradicate the presence of defects on the produced films, it decreased its number and enhanced the quality of the material. Therefore, it was proposed the substitution of tap water by deionized water in the cooling process. Some organic gels continued to be observed on the films, thereby

further investigation must be carried out, but the quality of the films remained far superior to prior to the cooling water change. It is plausible that other forms of gels could not be observed by the employed technique, especially if they have the same composition as the rest of the polymer and do not alter significantly the surface morphology.

8.6.4. Small-angle X-Ray Scattering

Finally, to detect if the organic gels arise from differences in the crystallinity of the TPU phases, the two last samples (produced in continuous and cool down in tap and deionized water) and a film produced batchwise were analyzed by Small-angle X-ray Scattering (SAXS) at ALBA synchrotron facilities. The same films analyzed by SEM were the ones employed to carry out SAXS experiments, but with an aging of approximately a year. Films were produced with a height in the range of 100 to 300 μm and exhibit a completely transparent appearance, suggesting crystallites of small dimensions which do not interact with the visible light. Therefore, to study the nanostructure of the produced materials, SAXS was employed. It allows the analysis of small, ordered structures, such as the HS domains, by their difference in electron density within the matrix. The use of different models allows the determination of the size and spacing between HS domains.

The gathered SAXS data of the three studied samples is shown in Figure 8.29. A single-scattering peak was observed, which indicates the formation of a segregated system with crystallites.

In order to extract information from the scattering curves, a spherical form factor was selected coupled to two different structure factors. Firstly using the Percus-Yevick model^[53], the HS domain radius (R) and its *hard-sphere interaction radius* (R_h) were analyzed. This R_h is referred to as the radius of the less ordered HS or SS domains around the HS that has its chain movement constricted by its covalent bonds to the HS. The three samples displayed ordered particles with a radius between 1.5-2 nm and a R_h radius of around 3.1-3.4 nm. The narrow distribution of the obtained values indicated the high structural similarity between the samples. Then, the distances between HS domains were obtained through the Zernike-Prins model.^[54] All the samples exhibited a quite similar value, indicating that the interdomain spacing (d) between HS domains was within the experimental variations and independent of the producing method. The sample synthesized in batch displayed $d=5.5 \pm 2.7$ nm, while film process with deionized water and with tap water exhibited $d= 5.3 \pm 3.2$ nm and $d= 5.6 \pm 2.6$ nm,

respectively. These results point to TPUs with fairly similar HS domain morphologies with small segments distributed similarly around the SS matrix.

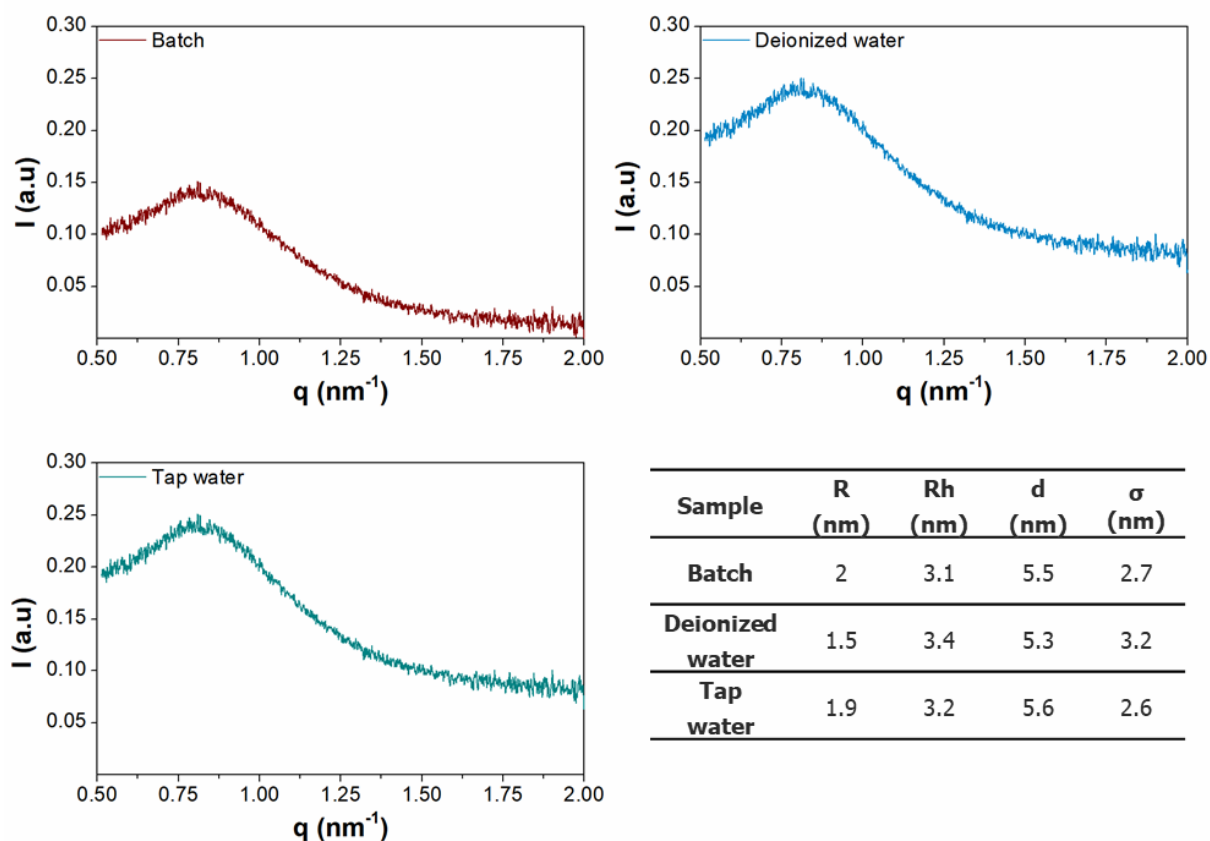


Figure 8.29. SAXS profiles for three extruded films. The embedded table displays the obtained results where R is the radius of the ordered particle, R_h corresponds to the radius of the ordered HS domain plus the surrounding ordered SS referred to as *hard-sphere interaction radius*, d is the interdomain distance between the ordered particles and σ is the standard deviation between the intercrystalline domains of the measured distances.^[55]

From the obtained SAXS results, there was no apparent difference in phase morphology between the samples. The organic gels do not seem to derive from a difference in the polymer's crystallinity of the HS. However, to fully determine this, a complete mapping of a film with a high quantity of organic gels should be performed to observe any differences in crystallinity between the gels and the bulk material.

8.6.5. Summary and concluding remarks

The most remarkable ideas developed in this chapter are divided into the studied factor that might affect the quality of the products:

-Raw Materials

Chemical features, as purity, metal content, and isomer distribution of several supplied batches of the two main raw materials were analyzed, and there was no reason to expect different reactivity.

ECL did not contain traces of metals, dimers, or synthetic precursors. However, the concentration of water in the monomer and the subsequently ring-opened acid inhibited to some extent the synthesis of PCLs.

As for **H₁₂MDI**, a GC method was implemented to quantify the **2,4-** and the **4,4- isomers** and their isomer contributions.

To conclude, the DOE analysis stated that these two parameters did not influence the formation of gels.

-Polyesters Analysis

Different side reactions were proposed for a polyol mixture, which could be reflected in changes in the M_n distribution and polydispersivity of the sample. Despite attempts, the identification of the amount of **BDO** that could cause transesterification in polymer chains was not reached. However, it was possible to determine whether the generated polyol mixture possessed the theoretical quantity of chain extender and when required, the existence, identification, and quantification of some contaminations.

-TPU Analysis

Several TPUs were analyzed by NMR and semi-quantitative ICP-MS confirming the expected proportion of the reagents, but usually observing over-catalyzed processes. However, no relevant difference could be determined on the samples. A material produced batchwise was compared with two other TPUs produced in a continuous process with two different catalysts. From the spectroscopic standpoint, the three TPUs were very similar. However, the TGA analysis showed a slight difference at relatively high temperatures. The sample produced with Mi-based catalyst did exhibit higher thermal stability.

In addition, the role and composition of two additives in both the polyol and the TPU were studied. The nature of the antioxidant played a crucial role in their posterior chemical behavior in the polyol mixture. When **PDDP** was employed, the speciation of these additives was very variable and it was remarked the importance of the sampling, as the polyol mixture remained active even at room temperature along time. Results with higher confidence were obtained in the TPU as the system appeared not to change over time as much as the previous. It was concluded that if a certain quantity of the antioxidant must be in the active form after the production, it should not be incorporated into the polyol mixture, but in posterior stages in the condensation reaction. However, when **Irgafos 126** was assessed, a broadness on the polydispersivity of the polyol mixture was observed. In addition to the common transesterification side reaction of the PCL with **BDO** in the media, the antioxidant might act as an ester itself and release a tetraol or a sterically hindered phenol to the mixture, which in turn formed a small concentration of dendrimer-like structures or end-capped polymers.

Considering all the previous factors and correlating them with Lubrizol's results, no clear relationship was found between the formation of gels and the slight difference in the raw materials, the PCL, or the TPU production.

-Film analysis

Finally, the surface of the produced films was characterized by several techniques. XPS was unable to determine other elements apart from carbon, oxygen, nitrogen, and a low concentration of silicon. Analyses with SEM displayed sheets with an elevated concentration of salts, principally composed of sodium, chloride, calcium, potassium, silicon, and probably bromide. Tests of samples treated with deionized water in the cooling step displayed a lower number of gels and inorganic particles more localized. It appeared that a reduction of the defects was consequence of the decrease of salts. However, a reduced number of organic defects, usually of small size, were detected, but their assignation as unmelted or highly entangled could not be determined. It is possible that the employed technique did not provide complete information on the sample, and other types of gels were undetected. SAXS measurements revealed that the phase segregation of the tested samples was similar.

To conclude, further studies were carried out by Lubrizol to increase the knowledge about the produced material, determine primary variables, and develop protocols to improve the production and quality of the TPU.

Literature

- [1] C. Capone, L. Di Landro, F. Inzoli, M. Penco, L. Sartore, *Polym. Engi* **2007**, *47*, 1813–1819.
- [2] M. A. Spalding, E. I. Garcia-Meitin, S. L. Kodjie, G. A. Campbell, T. W. Womer, *J. Plast. Film Sheeting* **2018**, *34*, 300–323.
- [3] Qenos Technical Guides, *Film Extrusion and Conversion -Technical Guides*, **2010**.
- [4] G. A. Campbell, M. A. Spalding, in *Anal. Troubl. Single-Screw Extruders*, Hanser Publications, Cincinnati, **2013**, pp. 477–540.
- [5] M. A. Spalding, Q. Gou, X. Sun, Q. Shi, *J. Plast. Film Sheeting* **2018**, *34*, 381–392.
- [6] L. Van Den Bossche, O. Georjon, T. Donders, K. Focquet, G. Dewitte, J. Briers, *Die Build-up During Polyolefin Processing : A Matter of Polymer Desing and Fluoropolymer-Based Processing Additives·D*, **1997**.
- [7] R. M. Holsworth, in *Polym. Charact. Spectrosc. Chromatogr. Phys. Instrum. Methods* (Ed.: C.D. Craver), American Chemical Society, Washington, D.C., **1983**.
- [8] A. Baeyer, V. Villiger, *Berichte der Dtsch. Chem. Gesellschaft* **1899**, *32*, 3625–3633.
- [9] M. C. Rocca, G. Carr, A. B. Lambert, D. J. Macquarrie, J. H. Clark, *US 6,531,615 B2. Process for the Oxidation of Cyclohexanone to E-Caprolactone*, **2003**.
- [10] V. A. Kuznetsov, M. G. Pervova, Y. G. Yatluk, *Russ. J. Appl. Chem.* **2013**, *86*, 176–181.
- [11] R. Pinkos, G.-D. Tebben, D. Breuninger, T. Sirch, C. Bauduin, M. G. Guardia, T. Krug, *US 8,217,186 B2. Process for Preparing Epsilon-Caprolactone*, **2012**.
- [12] O. Abillard, D. Breuninger, E. Kretzchmar, R. Pinkos, *US 2012 / 0059174 A1. Process for Preparin Epsilon-Caprolactone and 1,6-Hexanediol*, **2012**.
- [13] E. Ohara, K. Kawazumi, *US 6,936,724 B2. Process for Producing Epsilon-Caprolactone*, **2005**.
- [14] S. A. Yesudass, S. Mohanty, S. K. Nayak, C. C. Rath, *Eur. Polym. J.* **2017**, *96*, 304–315.
- [15] Y.-K. Cho, S.-H. Hwang, *Polym. Bull.* **2018**, *75*, 5795–5807.
- [16] A. Ali, Y. Xiao, L. Song, J. Hu, Q. Rao, M. Shoaib, B. U. Amin, X. Zhan, Q. Zhang, *Colloids Surfaces A Physicochem. Eng. Asp.* **2021**, *625*, 126946.
- [17] C. Six, F. Richter, in *Ullmann's Encycl. Ind. Chem.*, **2003**, pp. 63–82.
- [18] S. D. Seneker, L. Born, H. G. Schmelzer, C. D. Eisenbach, K. Fischer, *Colloid Polym. Sci.* **1992**, *270*, 543–548.
- [19] S. D. Seneker, S. A. Kane, *US005455374A. Liquification of Trans,Trans-4-4'-Diisocyanate Dicyclohexylmethane by Partially Reaction the Isocyanate Groups Woth Blocking Agents*, **1995**.
- [20] M. Möller, R. Kange, J. L. Hedrick, *J. Polym. Sci. Part A Polym. Chem.* **2000**, *38*, 2067–2074.
- [21] N. Nomura, A. Taira, A. Nakase, T. Tomioka, M. Okada, *Tetrahedron* **2007**, *63*, 8478–8484.
- [22] S. Fadlallah, M. Terrier, C. Jones, P. Roussel, F. Bonnet, M. Visseaux, *Organometallics*

- 2016**, *35*, 456–461.
- [23] I. Palard, M. Schappacher, A. Soum, S. M. Guillaume, *Polym. Int.* **2006**, *55*, 1132–1137.
- [24] E. J. Campbell, S. K. Czaplewski, B. M. Kobilka, J. T. Wertz, *Flame Retardant Polycaprolactone*, **2019**, US 2019 / 0249086 A1.
- [25] M. Labet, W. Thielemans, *Chem. Soc. Rev.* **2009**, *38*, 3484–3504.
- [26] C. J. Evans, in *Chem. Tin*, **1998**, pp. 442–479.
- [27] A. Kowalski, A. Duda, S. Penczek, *Macromol. Rapid Commun.* **1998**, *19*, 567–572.
- [28] I. Nifant'ev, P. Ivchenko, *Molecules* **2019**, *24*, 1–50.
- [29] A. Arbaoui, C. Redshaw, *Polym. Chem.* **2010**, *1*, 801–826.
- [30] H. Jacobson, W. H. Stockmayer, *J. Chem. Phys.* **1950**, *18*, 1600–1606.
- [31] A. Schindler, Y. M. Hibionada, C. G. Pitt, *J. Polym. Sci. A1*. **1982**, *20*, 319–326.
- [32] J. Baran, A. Duda, A. Kowalski, R. Szymanski, S. Penczek, *Macromol. Symp.* **1997**, *123*, 93–101.
- [33] H. R. Kricheldorf, S. M. Weidner, J. Falkenhagen, *Polym. Chem.* **2021**, *12*, 4989–5118.
- [34] A. Duda, A. Kowalski, J. Libiszowski, S. Penczek, *Macromol. Symp.* **2005**, *184*, 71–83.
- [35] H. R. Kricheldorf, N. Lomadze, *Polym. Sci. Ser. C* **2009**, *51*, 133–147.
- [36] M. de las M. Cordón Acedo, *Estudi Sobre Poliuretans Termoplàstics i Els Seus Monomers. Síntesis de Triarilfosfines Carboxíliques i Sulfonades.*, **2021**.
- [37] S. Sosnowski, S. Slomkowski, S. Penczek, L. Reibel, *Die Makromol. Chemie* **1983**, *184*, 2159–2171.
- [38] H. R. Kricheldorf, M. Berl, N. Scharnagl, *Macromolecules* **1988**, *21*, 286–293.
- [39] S. Penczek, A. Duda, R. Szymanski, J. Baran, J. Libiszowski, A. Kowalski, in *Ion. Polym. Relat. Process.* (Eds.: J.E. Puskas, A. Michel, S. Barghi), Springer Science + Business Media Dordrecht, **1999**, pp. 283–299.
- [40] C. Alemán, O. Betran, J. Casanovas, K. N. Houk, H. K. Hall Jr, *J. Org. Chem.* **2009**, *74*, 6237–6244.
- [41] H. R. Kricheldorf, I. Kreiser-Saunders, A. Stricker, *Macromolecules* **2000**, *33*, 702–709.
- [42] A. Saralegi, A. Etxeberria, B. Fernández-D'Arilas, I. Mondragon, A. Eceiza, M. A. Corcuera, *Polym. Bull.* **2013**, *70*, 2193–2210.
- [43] O. Persenaire, M. Alexandre, P. Degée, P. Dubois, *Biomacromolecules* **2001**, *2*, 288–294.
- [44] M. Unger, C. Vogel, H. W. Siesler, *Appl. Spectrosc.* **2010**, *64*, 805–809.
- [45] Y. Schellekens, B. Van Trimpont, P. Goelen, K. Binnemans, *Green Chem.* **2014**, *16*, 4401–4407.
- [46] S. Petrovic, Zoran, Z. Zavargo, J. H. Flynn, W. J. Macknight, *J. Appl. Polym. Sci.* **1994**, *51*, 1087–1095.
- [47] M. L. Matuszak, K. C. Frisch, *J. Polym. Sci. Polym. Chem. Ed.* **1973**, *11*, 637–648.
- [48] F. H. Westheimer, S. Huang, F. Covitz, *J. Am. Chem. Soc.* **1988**, *110*, 181–185.
- [49] B. Heins, C. Saron, *Mater. Res.* **2012**, *15*, 467–472.
- [50] G. Greczynski, L. Hultman, *Prog. Mater. Sci.* **2020**, *107*, 100591.
- [51] G. Greczynski, L. Hultman, *Angew. Chemie - Int. Ed.* **2020**, *59*, 5002–5006.
- [52] J. I. Goldstein, D. E. Newbury, P. Echlin, D. C. Joy, C. E. Lyman, E. Lifshin, L. Sawyer, J. R. Michael, in *Scanning Electron Microsc. X-Ray Microanal.*, Springer Science + Business, New York, **2003**, pp. 453–536.
- [53] K. Percus, Jerome, J. Yevick, George, *Phys. Review* **1958**, *110*, 1–13.
- [54] F. Zernike, J. A. Prins, *Zeitschrift für Phys. A Hadron. Nucl.* **1927**, *141*, 184–194.
- [55] I. Krakovsky, Z. Bubeníková, *Polymer (Guildf)*. **1997**, *38*, 3637–3643.

Chapter 9

Measuring procedures

Chapter 9 details the procedures carried out to measure and characterize the studied samples, from the starting monomers, to the final TPU properties.

9. Measuring procedures

9.1. Fluorine quantification

Fluorine is quantified by $^{19}\text{F}\{^1\text{H}\}$ NMR spectroscopy with an internal standard carefully selected according to its solubility in the analysis solvent. The general procedure comprises weighing the internal standard (KPF_6 or 3-bromobenzotrifluoride) and the sample under consideration on an analytical balance (accuracy of ± 0.1 mg). The mixture is dissolved in 0.3 mL of the corresponding deuterated solvent and then, quantitatively transferred to an NMR tube. Residues are dragged with two additional fractions of the deuterated solvent (0.1 mL each).

All ^{19}F spectra are obtained in the range between 25 to -175 ppm (fluorobenzene as reference δ_{F} : -113.15 ppm) and centered at $\delta_{\text{F}} = -75$ ppm. Each sample is recorded with at least 16 scans. A delay time of 10 seconds is implemented to ensure complete T1 relaxation and the corresponding quantification of the signal area. The spectra are recorded decoupling the proton frequency to prevent the multiplicity arising from the neighboring hydrogen atoms and each signal must be detected as a distinct, well-separated, and non-overlapping peak. Moreover, the concentration of the internal standard is adjusted to produce signals with similar integration values to the studied compound.

From the achieved spectrum, the fluorine content (wt.%) and the purity (%) of the fluorinated compound can be calculated with Equation 9.1 and Equation 9.2, respectively.

$$\text{Fluorine content [wt. \%]} = \frac{\text{Int}(\text{compound})}{\text{Int}(\text{standard})} \cdot \frac{M_{\text{F}}}{M_{\text{w}(\text{standard})}} \cdot \frac{W_{(\text{standard})}}{W_{(\text{mixture})}} \cdot N_{\text{F}(\text{standard})} \cdot 100$$

Equation 9.1.

$$\text{Purity [\%]} = \frac{\text{Int}(\text{compound})}{\text{Int}(\text{standard})} \cdot \frac{N_{\text{F}(\text{standard})}}{N_{\text{F}(\text{compound})}} \cdot \frac{M_{\text{w}(\text{compound})}}{M_{\text{w}(\text{standard})}} \cdot \frac{W_{(\text{standard})}}{W_{(\text{mixture})}} \cdot 100$$

Equation 9.2.

where $\text{Int}(\text{compound})$ and $\text{Int}(\text{standard})$ represent the integration value of the peaks arising from the studied sample and the standard. M_{F} is the atomic weight of fluorine (19.0 g/mol) and $M_{\text{w}(\text{standard})}$ and $M_{\text{w}(\text{compound})}$ are the molecular weight in g/mol of the standard and the compound

under study. $W_{(mixture)}$ and $W_{(standard)}$ correspond to the weight in grams of the studied mixture and the standard. Lastly, $N_{F(standard)}$ and $N_{F(compound)}$ are the number of fluorine atoms in the standard and the fluorinated compound.

More than one fluorinated substance can be analyzed in the same sample with this method, assuming that there is no overlap in their $^{19}\text{F}\{^1\text{H}\}$ NMR signals, that samples are soluble enough in the selected NMR solvent, and that there are no reactions between the samples and the internal standard.

9.2. Acidity index

The Acidity Index (AI) determination consists of a volumetric titration with a standardized basic solution. Specifically, a quantity of polymer (2 to 4 g) is accurately weighed in a 250 mL Erlenmeyer flask and dissolved in 60 mL of THF. The mixture is heated until an utterly transparent solution is achieved, denoting the complete dissolution of the polymer in the organic solvent. Moreover, two blanks are produced with two additional Erlenmeyer flasks with 60 ml of THF and heated for the same time as the samples. Each experiment is titrated with a standardized solution of KOH in MeOH:Acetone (1:1) (*ca.* 0.025 M) and two drops of phenolphthalein solution (0.2 wt.% in MeOH) until the appearance of a light pink coloration in the mixture.

The AI is calculated as described in Equation 9.3 with the volume of KOH solution required to reach the equivalent point in the sample titration (V_{sample} , mL) and in the blank (V_{blank} , mL). C_{KOH} corresponds to the exact concentration of the titrating solution, $M_{w(KOH)}$ represents the molecular weight of KOH (56.1 g/mol) and $w_{polymer}$ is the weight of the titrated polymer in grams. The reported AI is the mean value of at least three replicates.

$$AI \left[\frac{\text{mg KOH}}{\text{g polymer}} \right] = (V_{sample} - V_{blank}) \cdot \frac{C_{KOH} \cdot M_{w(KOH)}}{w_{polymer}} \quad \text{Equation 9.3}$$

9.3. Hydroxyl Index

The Hydroxyl Index (OHI) determination involves a back-titration of an acetylated polymer with an alkaline solution. A known quantity of a polymer of less than 3 g is weighed in a 250 mL Erlenmeyer flask. Next, 2 mL of 1-methylimidazole and 10 mL of acetylating solution (40 mL acetic anhydride in 0.5 L of THF) are accurately added to the flask with two-mark volumetric pipettes. The mixture is dissolved in 70 ml of THF and refluxed until a completely transparent solution is obtained, and then heated for another additional 15 minutes. Subsequently, the

heating is turned off and 10 mL of deionized H₂O is incorporated to hydrolyze the remaining acetic anhydride. The resulting mixture is left to react for 10 minutes before carrying out the volumetric analysis. Two blanks are prepared simultaneously following the same procedure without polymer. Both the blanks and the samples are titrated with a standardized solution of KOH (*ca.* 0.75 M) in MeOH, employing a drop of a phenolphthalein solution (0.2 wt.% in MeOH) as indicator until the appearance of a light pink hue.

The experimental OHI value (OHI_e) is calculated according to Equation 9.4, where V_{blank} and V_{sample} are the required volume to reach the equivalent point on the titration of the blank and the sample in milliliters. C_{KOH} and $M_{w(KOH)}$ correspond to concentration (mol/L) and the molecular weight of KOH (56.1 g/mol). Lastly $w_{polymer}$ is the weighted polymer in grams. In these experiments, the carboxylic groups remaining on the polymer are also titrated, thereby they must be corrected through the AI value. The reported value of OHI is the mean value of three replicates.

$$OHI \left[\frac{\text{mg KOH}}{\text{g polymer}} \right] = (V_{blank} - V_{sample}) \cdot \frac{C_{KOH} \cdot M_{w(KOH)}}{w_{(polymer)}} + AI \quad \text{Equation 9.4}$$

9.4. Polyester M_n determination by titration

The number average molecular weight (M_n) of difunctional polymers, and that are not crosslinked, can be estimated from the values obtained by titration. In the case of polyesters and polycaprolactones used in this thesis, most of the chains end in hydroxyl groups, but in some cases, a fraction of the polymer chains also terminates in a carboxylic acid group. While the former is considered with the OHI value, the latter is related to the AI. Therefore, the employed relation between the OHI, AI, and the M_n is described in Equation 9.5.

$$M_n \text{ [g/mol]} = M_{w(KOH)} \cdot \frac{1000 \text{ mg KOH}}{1 \text{ g KOH}} \cdot \frac{1}{(OHI + AI)} \cdot \frac{2 \text{ mol KOH}}{1 \text{ mol polymer}} = \frac{112200}{OHI + AI} \quad \text{Equation 9.5}$$

where $M_{w(KOH)}$, OHI and AI correspond to the previously described parameters, and the functionality of the polyol is considered by the two equivalents of KOH per mol of polymer.

9.5. Polyol M_n determination by ¹H NMR spectroscopy

An alternative method to determine the M_n of a polymer comprises the analysis by ¹H NMR spectroscopy in solution. The analysis of the samples is based on the end-group analysis in which the ratio between terminal fragments and inner/internal fragments is determined. This

value provides the number of repetitive units in the polymer, and consequently the M_n of the polymer. Although the preparation of the samples is quite similar for all the studied polymers, each type requires its own characteristic signals to determine M_n . Ideally, those signals employed in the analysis are distinctive and non-overlapping.

Routinely, samples are dissolved in the appropriate solvent, usually $CDCl_3$ or acetone- d_6 (ca. 0.2-0.3 g polymer/0.8 mL solvent) and rapidly analyzed in the corresponding spectrophotometer at 298 K to avoid possible hydrolysis. If required in the case of $CDCl_3$, the solvent is filtered through basic alumina or $MgSO_4$ to remove any traces of HCl or water. If broad signals overlap the main peaks, a couple of drops of deuterated water are added to eliminate the interchangeable protons of the hydroxyl groups. To ensure the quantification, spectra are recorded with a delay time of 10 seconds.

9.5.1. Determination of the M_n of linear aliphatic polyesters

The estimation of the M_n for linear aliphatic polyesters by the end-group analysis requires the estimation of the IOH of the mixture, which considers those chains ended in hydroxyl groups. It is determined through the number of monomeric units in the polymer (n). This value obtained by the integration values of the methylene groups attached to an hydroxyl, thereby being **a**, the terminal residue ($Int(a)$), and **b** the ω -methylene bounded to the ester ($Int(b)$) of the 1H NMR spectrum (Figure 9.1) according to Equation 9.6.

$$n = \frac{Int(b)}{Int(a)} \quad \text{Equation 9.6}$$

Subsequently, the IOH value of the mixture is calculated with Equation 9.7.

$$IOH \left[\frac{mg \text{ KOH}}{g \text{ polymer}} \right] = \frac{112200}{n \cdot M_{w(acid \ derivative)} + (n + 1)M_{w(diols)} - 2 \cdot n \cdot M_{w(released \ subproduct)}} \quad \text{Equation 9.7}$$

where $M_{w(acid \ derivative)}$, refers to the molecular weight of the dicarboxylic acid or the diacyl chloride compound employed in the polymerization, $M_{w(diols)}$ to the molecular weight of the employed glycol and finally, $M_{w(released \ subcompound)}$ represents the molecular weight of H_2O in a traditional condensation or HCl in the acyl approach

The M_n of the mixture must reflect both hydroxylated- and carboxylic acid-terminated chains. Therefore, it is calculated with **Equation 9.5** with the OHI obtained with the 1H NMR spectrum and the AI achieved by titration.

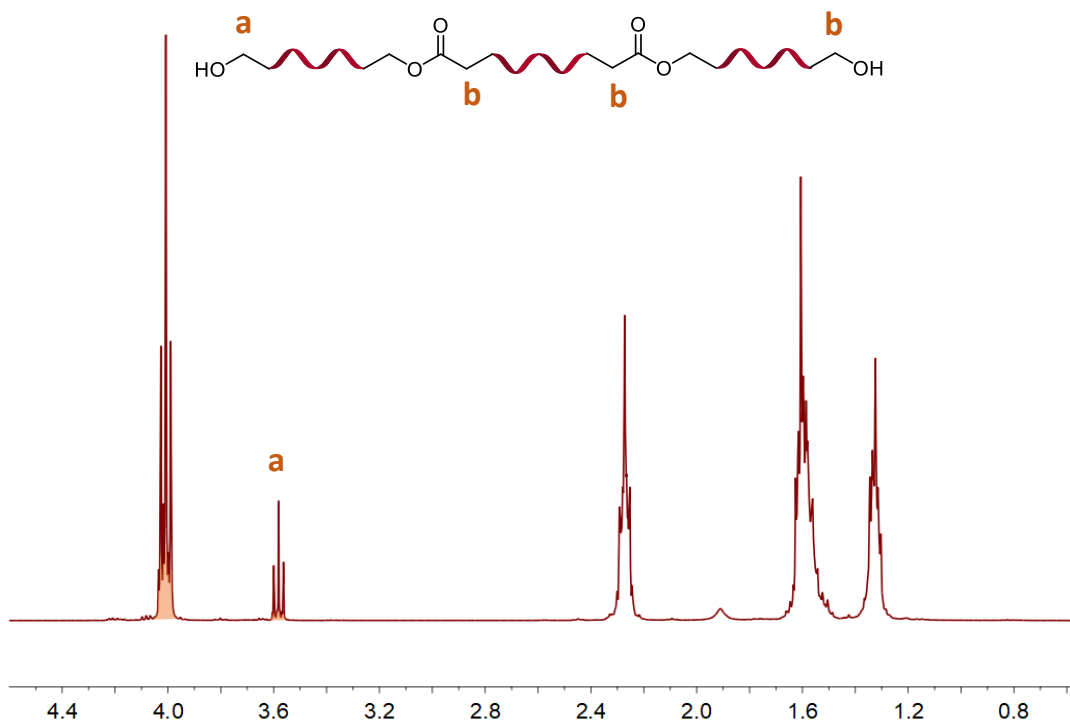


Figure 9.1. Example of ^1H NMR spectrum (400 MHz) of an aliphatic polyester. Colored peaks denoted signals employed in the n calculation. Solvent: CDCl_3 .

9.5.2. Determination of the M_n of ADP:DiolF

The nature of the employed diol with a primary and a secondary alcohol results in distinctive signals in the ^1H NMR spectrum for the diesterified glycol, or the monoesterified by either one or the other alcohol (Figure 9.2). In particular, the signal arising from the methine group of **DiolF** has different chemical shifts depending on the oxygen bound to an ester.

Hence, taking profit of the different chemical environments of the central methine and following the prior premise of calculating n as a relation of the internal fragment respect the external, n is estimated with the following expression (Equation 9.8). **ADP:DiolF** possesses two terminals alcohols per each internal **DiolF** moieties. Therefore, to obtain the appropriate value of n the integration values of the external hydroxyls must be normalized to the number of hydrogens involved in the peak by dividing by two.

$$n = \frac{\text{Int}(c)}{\frac{\text{Int}(g) + \text{Int}(k)}{2}} \quad \text{Equation 9.8.}$$

The OHI value of the mixture is calculated according to Equation 9.7, employing this time the molecular weight of the compounds involved in the synthesis: **ADP**, **DiolF**, and H_2O as the

released product. Ultimately, the associated M_n is calculated in the same manner as in Equation 9.5, considering both the OHI value just obtained and the AI by titration.

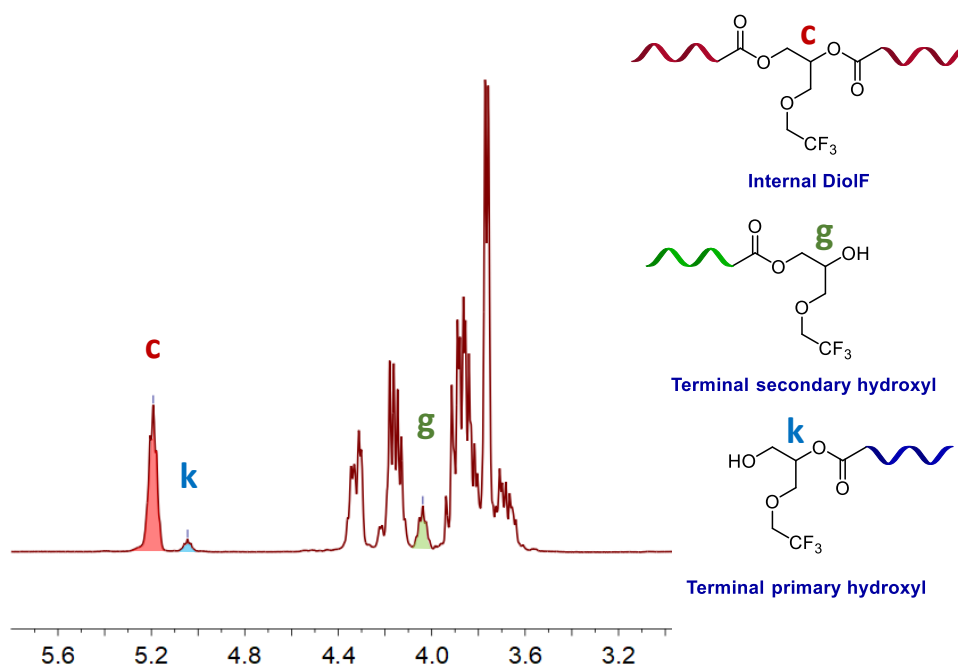


Figure 9.2. Fragmented ^1H NMR spectrum (360 MHz) of **ADP:DiolF**. Colored areas correspond to the integration values used to estimate n . Solvent: CDCl_3 .

9.5.3. Determination of M_n of PCL

For this type of polymer, n is considered as the number of **ECL** units in the chain and it is obtained by the relation of the number of internal **ECL** fragments respect the external fragment in the ^1H NMR spectrum.

In contraposition of the polyester analysis, the signal arising from the inner $-\text{CH}_2\text{OCO}$ (**e**) arising from the lactone overlaps with the initiator (**f**). Therefore, for a PCL, the n is calculated as described in the modified Equation 9.9. Peaks at 2.25 ppm in the spectrum of Figure 9.3 corresponds to all lactone fragments, regardless of the position on the chain. Therefore, the appropriate expression for the PCLs corresponds to the relation between the integration value of $-\text{CH}_2\text{CO}$ ($\text{Int}(d)$) with the terminal hydroxymethylene signal ($\text{Int}(a)$), since $\text{Int}(a) = \text{Int}(f)$

$$n = 2 \cdot \frac{\text{Int}(d)}{\text{Int}(a)} \quad \text{Equation 9.9}$$

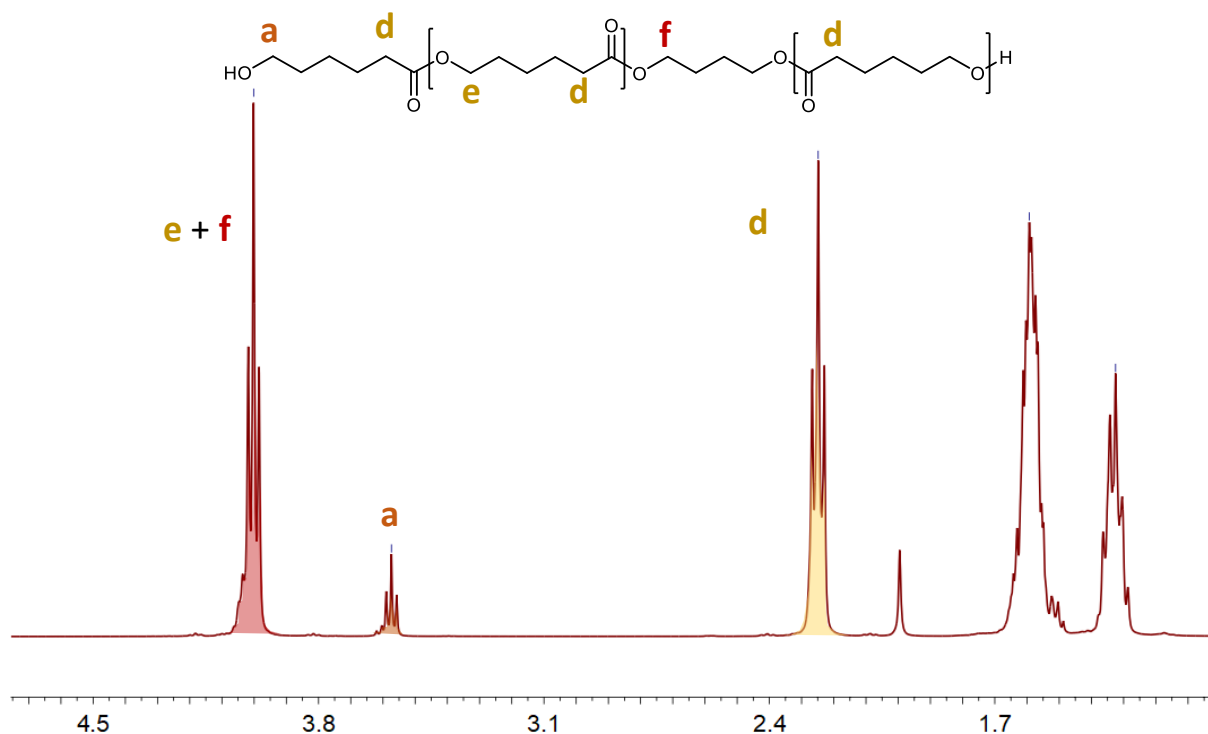


Figure 9.3. Example of a ^1H NMR spectrum (400 MHz) of **PCL-BDO**. Solvent: CDCl_3 .

For this type of polymers, the M_n is determined by the quantification of the number of **ECL** units (n) in the polymer plus the initiator as shown in Equation 9.10.

$$M_{n(\text{mixture})} [\text{g/mol}] = n \cdot M_w(\text{ECL}) + M_w(\text{initiator}) \quad \text{Equation 9.10}$$

where $M_w(\text{ECL})$ and $M_w(\text{initiator})$ are the molecular weight of the **ECL** and that of the diol used as initiator.

9.6. Melt Flow Index

The Melt Flow Index (MFI) determination is carried out with previously dried shredded polymers or pellets. Since the humidity of the samples might modify the results, before the analysis, approximately 6 g of sample is placed in a vial and dried at 80 °C for 2 hours in an oven under vacuum. To preserve these conditions, vials are taken out the oven, hermetically sealed, and cooled down to room temperature.

Prior to the analysis, the barrel of the Melt Indexer must be stabilized at the tested temperature for at least 15 minutes. Subsequently, the already weighed sample is introduced into the equipment as fast as possible. The polymer remains inside the apparatus for 6 minutes at the select temperature and then, the piston applies the selected weight for 10 minutes. The amount

of material that flows through a standardized die during this time corresponds to the MFI value of the sample (g polymer/10 minutes).

Frequently employed weights are 2.16, 21.6, and 5.0 Kg. Temperature is usually modified from 120 °C to 220 °C according to the requirements. However, these parameters depend on the type of material and the tested method. Furthermore, to avoid sources of error, all surfaces in direct contact with the polymer must be carefully polished prior to use.^[1]

9.7. Kofler

Kofler measurements are carried by gently placing small, shredded fragments along the metal surface of the bench. Before using it, the apparatus must be turned on for at least 30 minutes to completely stabilize the temperature. Subsequently, the hot bench is calibrated with various organic standards with known melting temperatures. Small amounts of the reference substances are placed on the bench from the cold end to the hot side and the point where the standard starts to melt is employed to calibrate the bar according to the known melting temperature. Routinely, this process is replicated with at least two compounds with different melting temperatures. Then the sample is dispersed along the bench and both the melting and the softening point are determined after 15 minutes. The softening corresponds to the temperature at which the material begins to adhere to the bench. The melting relates to the temperature at which the sample is liquid. To ensure the results, the melting point of the sample should be between the melting temperatures of the standards used to calibrate the bench.

9.8. Differential Scanning calorimetry

DSC experiments have been carried out with small pieces of shredded polymer in sealed aluminum pans, which comprise a crucible and a lid. 6 to 10 mg of the sample is weighted in the crucible and then a perforated lid is placed on top. The rim of both components is cold weld in a press to produce the required assembly to analyze the sample.

Measurement conditions can be adapted, but comparable results are only obtained by examining samples with an identical method. A triple method scan is extensively employed in this thesis. It consists of cooling to -70 °C and maintaining that temperature for 3 minutes. Then, the first scan heats the material to 220 °C at a rate of 10 °C/minute. Next, it is cooled down to -70 °C again and then reheated it until reaches 220 °C with the same thermal rate.

Melting data of samples analyzed by this method correspond to the second scan unless otherwise stated.

Reported T_m is determined at the maximum point of the melting peak. In the same way the crystallization temperature (T_{cryst}) corresponds to the maximum point of its curve. However, semi-crystalline materials usually show broad peaks, and hence, the melting temperature, temperature in which the process starts, is also frequently displayed. The crystallization enthalpy (ΔH_{cryst}) correlates to the normalized area under the curve, and it is typically provided by the instrument software. T_g , when can be observed, shows a variation (*i.e.* a smooth step) in the baseline and it is ascertained at the inflexion of the step. In some particular cases, it is possible to observe an exothermic peak during the heating process. It corresponds to the cold crystallization (T_{cc}) which is established at to the inflection point of the displayed peak.

9.9. Hardness tests

Shore A Hardness tests are carried out in accordance with ISO 868:2003^[2] in a temperature and humidity-controlled room at 23 °C and 55% humidity. The measurements require injected TPUs with a minimum thickness of 6 mm. To attain the proper dimensions, three plaques are piled together and located under the steel road. To determine Shore A Hardness, tested samples are placed on a firm surface, and the indenter is pressed into the material with a pressure of 8.064 N. The reported result is obtained as the mean value of 10 measurements taken across the surface.

9.10. Density

Density (kg/m^3) has been determined at 23 °C according to the procedure described in ASTM D792.^[3] It requires a modified balance, comprising a hanging support with a small platform and a metal basket submerged in liquid (**Figure 9.3**).

The measurement process requires a rectangular fragment of polymer sheet (about 0.5 x 1 cm), which is placed on the platform and weighed (accuracy ± 1 mg). Subsequently, the sample is transferred to the metal basket, immersed in the liquid, and weighed again.

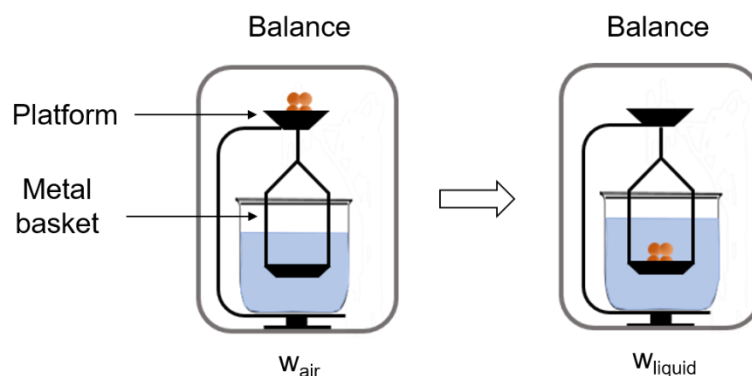


Figure 9.4. Schematic representation of the immersion method.

The density is calculated by the instrument itself according to the following expression (Equation 9.11), where $\rho_{polymer}$ and ρ_{liquid} are the density of the polymer and the liquid, respectively. W_{air} and W_{liquid} correspond to the weight of the sample at air and submerged in the liquid. The reported specific density is obtained as the mean value of three replicates per polymer at 23 °C.

$$\rho_{polymer} [g/cm^3] = \rho_{liquid} \cdot \frac{W_{air}}{W_{air} - W_{liquid}} \quad \text{Equation 9.11}$$

9.11. Friction

Among the different parameters of friction, this thesis employs the coefficient of friction, COF, to explore the resistance of the surface of a material toward motion. COF measurements comply with ASTM D1894^[4] maintaining a constant 23 °C of temperature and 55% of humidity. Experiments are based on a stationary and horizontal aluminum plane and a sled that is pulled parallel by the instrument (Figure 9.5). Moreover, friction measurement depends on the material surface to a considerable extent. Therefore, all sheets are produced in the same injection machine and mold.

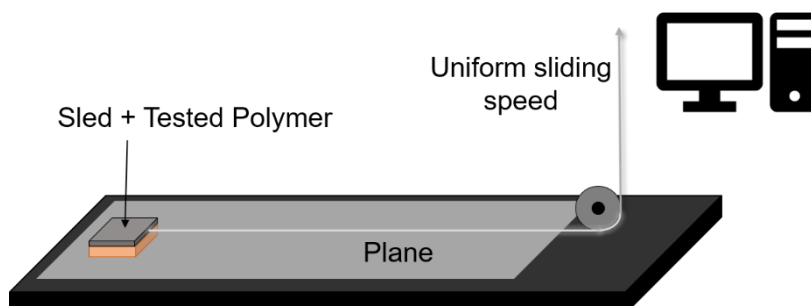


Figure 9.5. Graphic representation of COF measurements.

Prior to the friction evaluation, polymer sheets are carefully cut to the same dimension as the sled and attached to it with double-faced tape. Furthermore, the plane is wiped with ethanol (96%) and allowed to dry to remove any possible dust, fingerprints, or remnants of the samples previously studied. This cleaning process is carried out just before each measurement to ensure the results. Subsequently, the sled is connected to the traction device by a filament. This fiber is placed on the pulley and gently stretched until it is slightly taut on the other extreme of the plane. Valid results are obtained when the tested specimens have run through the plane and the software provides their COF values. The static coefficient of friction (μ_s) is obtained at the point of maximum force without movement. Contrary, the dynamic coefficient of friction (μ_d) is estimated once the two materials are in motion. Three sheets are used to determine both the μ_s and μ_d , and the displayed COF values represent the average of the three replicates.

9.12. Abrasion resistance

Abrasion resistance measurements are carried out according to the procedure described in ASTM D5963:15.^[5] The pieces required for the test are obtained by die-cutting injected TPU plaques in a cylindrical shape and then adhering them to a resistant and hard polymer. Ultimately, they are preserved for 24 hours under a weight to ensure the assembly.

To have comparable conditions, the abrasive sheet has to be acclimated by passing a standard reference rubber through the drum before the analysis. The abrasive sheet is at adequate conditions when causes a weight loss of 180 mg to 220 mg on the standard reference rubber. The process is repeated as many times as required to achieve these values.

The polymer samples under study are weighed in a balance (accuracy ± 0.1 mg) and placed on the drum holder. The pieces are subjected to a total abrasion path of 40 m with a steady speed of 40 rpm and a constant load of 10 N. Samples that bear the abrasion distance and remain on the support after the analysis are considered as valid tests. Abraded specimens are carefully disassembled from the holder and weighed again to determine the difference in weight. The volume loss (ΔV , mm^3) is assessed according to Equation 9.12

$$\Delta V [\text{mm}^3] = \frac{(w_i - w_f)_{\text{polymer}}}{\rho} \cdot \frac{K}{(w_i - w_f)_{\text{standard}}} \quad \text{Equation 9.12}$$

where w_i and w_f correspond to the weight in mg before and after the displacement against the abradant of the tested polymer or the standard. Moreover, ρ (g/cm^3) is the density of the material being tested, and K represents a constant of the abrasive sheet with a value of 200

mg. The ratio between K and $(W_i - W_f)_{standard}$ is determined for each analysis to normalize the effect of the abrasive sheet.

9.13. Yellowness Index

The yellowness index (YI) measurements have been performed in accordance with ASTM E313.^[6] Both shredded polymer and plaques can be used to determine YI. However, comparable results are obtained with samples in the same state and similar thickness.

Plaques are directly situated in the center of the port on the spectrophotometer and are shielded by a black opaque cover to prevent interference from ambient light. Then, YI is recorded. Two or three replicated per polymer type are measured and the reported result is the average value. Likewise, shredded TPUs are placed on a transparent glass cup to contain the solid and protected with a black cover. The same procedure is carried out to analyze this material.

9.14. Transmittance and Haze

Both transmittance and haze have been measured in a single Haze-gard according to ASTM D1003.^[7] Measurements are carried out with plaques that must be as even as possible. If the sample exhibits some deformation, it might cause the deflection of the incident light and the misread of the results. Therefore, these areas must be circumvented during the analysis. In addition, to avoid differences in absorbance or scattering, samples must have similar thicknesses.

Before use, the lamp of the instrument must be stabilized for several minutes. To obtain transmittance and haze results, a plaque is located on the haze port where the measurement takes place. Four different spots in each plaque are measured, and the transmittance and haze values are determined as the average of two or three plaques. Samples with blooming are wiped with a cotton cloth before the analysis.

9.15. Gloss

Gloss measurements have been carried out with injected plaques and do not require any preparation of the sample. However, samples with blooming are wiped with a cotton cloth to remove it from the material's surface when required. The analysis is carried out by placing the plaque above a white surface and beneath the glossmeter. The instrument is configured to

provide the gloss of three angles (20°, 60°, and 85°). Gloss values for each angle are reported as the average of at least three readings for each TPU.

9.16. Contact angle

The contact angle (CA) measurement is based on the Sessile Drop Method and it is carried out with injected TPU sheets. The CA of three different solvents (deionized water, ethylene glycol, and DMF) is explored by the same method. Prior to the analysis, the blooming of the sample is removed with a cotton cloth when required.

The measuring procedure consists of placing a rectangular strip of the studied material on the goniometer holder to ensure the flatness of the surface, and it is located between a light source and a camera (Figure 9.6).

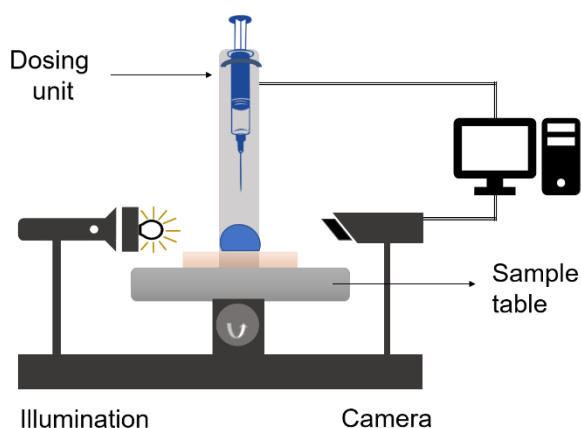


Figure 9.6. Schematic representation of goniometer.

A plastic syringe suspends a controlled dose (2 μl) at the end of the needle. To transfer the drop to the tested surface, the holder is moved upward until the liquid and the material come into contact. Next, the holder is gently moved downward to separate the fluid from the needle. After a few seconds, an image of the drop and the surface is recorded, and the baseline is determined. The goniometer's software uses the Young-Laplace fitting to adjust the profile of the drop and obtain the CAs of both sides of the deposited liquid. This process is repeated six times along the sheet, and at least two plaques are measured per polymer.

9.17. Surface free energy

The Surface Free Energy (SFE) of a solid is calculated using the already measured CA and applying Owens, Wendt, Rabel and Kaëlble (OWRK) model, which is based on Equation 2.11.^{[8][9]} This model requires the use of at least two solvents, preferentially one polar

and another non-polar. However, to achieve more reliable values, three solvents (water, ethylene glycol, and DMF) are used.

$$\frac{\gamma_{LA}(1 + \cos \theta)}{2 \cdot (\gamma_{LA}^d)^{1/2}} = (\gamma_{SA}^p)^{1/2} \cdot \left(\frac{\gamma_{LA}^p}{\gamma_{LA}^d} \right)^{1/2} + (\gamma_{SA}^d)^{1/2} \quad \text{Equation 2.11}$$

where γ_{LA} and γ_{SA} represent the surface tension of the liquid and the solid SFE, respectively, and the superscripts p and d correspond to the dispersive and polar components of each energy.

The mean values of the measured CAs and the already tabulated dispersive and polar parameters of the solvents (Table 9.1) are plotted as $\frac{\gamma_{LA}(1 + \cos \theta)}{2 \cdot (\gamma_{LA}^d)^{1/2}}$ vs $\left(\frac{\gamma_{LA}^p}{\gamma_{LA}^d} \right)^{1/2}$, to create a regression line (Figure 9.7).

Table 9.1. Reported data of the liquids used for determining SFE.

Liquid	Reported by	Surface tension (mN/m)		
		Complete	Dispersive part	Polar part
Water	Busscher <i>et al.</i> ^[10]	72.10	19.90	52.20
<i>N,N</i> -Dimethylformamide	Fowkes ^[11]	37.30	32.42	4.88
Ethylene glycol	Erbil ^[12]	48.00	29.00	19.00

The intercept point of the axis and the slope correspond to the square root of γ_{SA}^p and γ_{SA}^d and the total SFE is calculated as the sum of the two values. This process is usually carried out automatically by the goniometer's software with the tabulated values for each solvent.

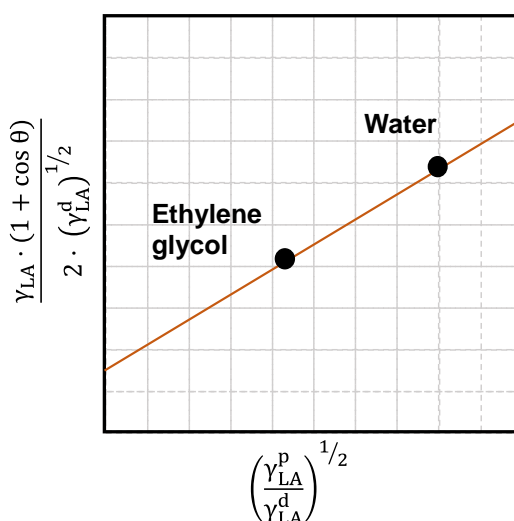


Figure 9.7. Regression line to obtain the dispersive and polar components of SFE.

9.18. Inductively coupled plasma mass spectrometry

Samples have been treated as described hereafter by the technicians of *Servei d'Anàlisi Químic* (SAQ) of UAB. In a microwave oven, *ca.* 0.5 g of each sample is digested in a concentrated solution of HNO₃, HCl, and HF. Next, they are diluted with a solution of HNO₃ 1%(v/v) and then, injected into the equipment. A semi-quantitative estimation is obtained from the molar response *vs* atomic weight curve. Any instrumental interferences are corrected with the blank samples, that have been treated in an identical manner.

9.19. Analysis ECL samples by Gas Chromatography

Samples are prepared by dissolving a small amount of the provided compound (*ca.* 0.05 mL-0.15 mL) in CH₂Cl₂ (1 mL) directly in the GC vial. **ECL** solutions are promptly analyzed to prevent alterations in the mixture. The following methods are used for the sample evaluation.

-Method I: Low temperature method.

Injector Temperature: 150 °C.

Detector Temperature: 200 °C.

Initial Temperature: 150 °C. Isotherm 30 minutes.

Method II: High temperature method.

Injector Temperature: 250 °C.

Detector Temperature: 280 °C.

Initial Temperature: 100 °C. 3 min hold.

Gradient: 30 °C/ min until 280 °C. 5 min hold.

The obtained results are qualitative, since no standard is employed to determine the exact concentration of the sample.

9.20. Determination of ECL monomer and dimer in a PCL by Gas Chromatography

The quantification of **ECL** monomer and dimer in a PCL sample is carried out by weighting *ca.* 0.1 g of PCL and 0.008 g of *n*-decane, as internal standard directly in the GC vial and dissolving the mixture in CH₂Cl₂. Samples freshly prepared are analyzed with the low-temperature method (**Method I**) described previously (9.19. Analysis ECL samples by Gas Chromatography). The quantification was related to a previously performed calibration in the employed GC equipment.

-Calibration line for ECL monomer-

$$\frac{\text{Area ECL peak}}{\text{Area } n\text{-decane peak}} = 0.5865 \cdot \frac{w_{\text{ECL}}}{w_{n\text{-decane}}} + 0.0011$$

$$\text{ECL [wt. \%]} = \frac{w_{\text{ECL}}}{w_{\text{PCL}}} \cdot 100$$

-Calibration line for ECL dimer:

$$\frac{\text{Area ECL dimer peak}}{\text{Area } n\text{-decane peak}} = 0.6404 \cdot \frac{w_{\text{ECL dimer}}}{w_{n\text{-decane}}} + 0.0181$$

$$\text{ECL dimer [wt. \%]} = \frac{w_{\text{ECL dimer}}}{w_{\text{PCL}}} \cdot 100$$

where $w_{n\text{-decane}}$ and w_{PCL} are the weight in grams of the internal standard and the PCL mixture, respectively. The area of the peaks of the standard and the **ECL** monomer and dimer are obtained by the GC spectrum.

9.21. Determination of ECL monomer in a PCL by ^1H NMR spectroscopy

The estimation of the quantity of monomer contained in a PCL sample by ^1H NMR spectroscopy considers the relation between the proton signals arising from the α -methylene of **ECL** monomer and the one arising from the PCL, which are centered at δ 2.6 ppm and δ 2.3 ppm, respectively (Figure 9.8). However, the second signal only considers the **ECL** fragments comprised on a PCL, and not the M_n of the polymer chain because the initiator contribution is missing. Therefore, the associated correction corresponds to Equation 9.13.

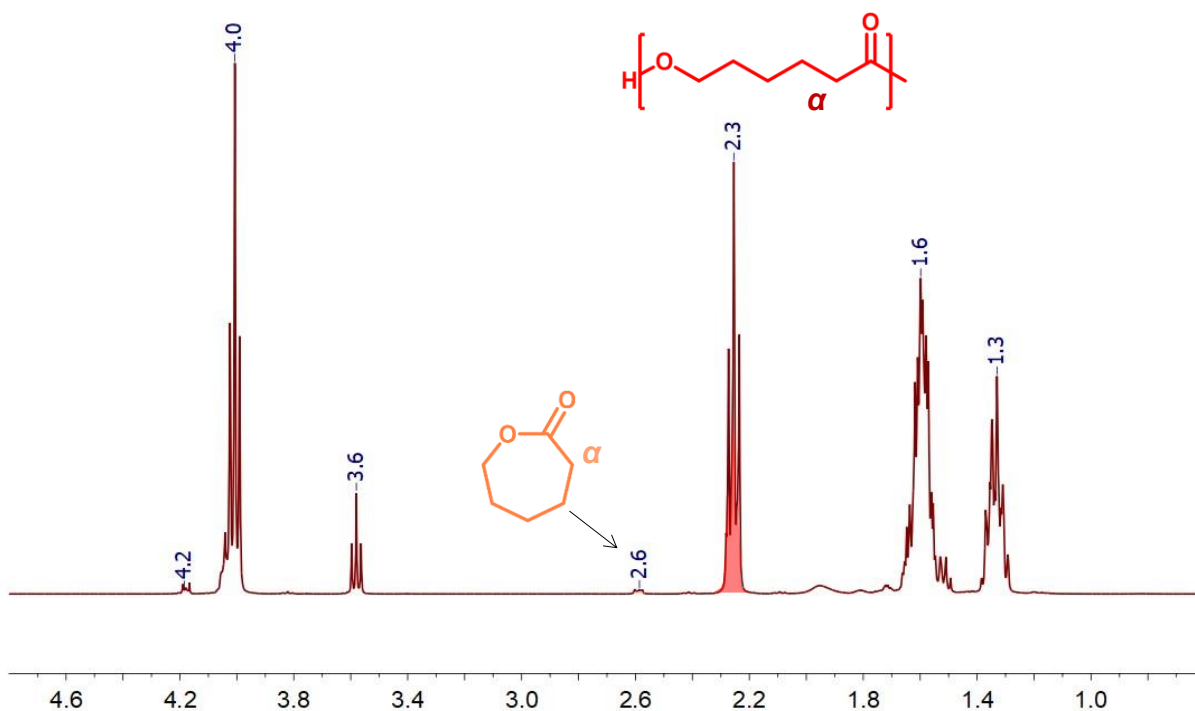


Figure 9.8. Example of a ¹H NMR spectrum (400 MHz) of **PCL-BDO** recorded with 10 second delay time. Solvent: CDCl₃.

$$\text{ECL [\%]} = \frac{\text{Int}(\alpha \text{ ECL})}{\text{Int}(\alpha \text{ PCL})} \cdot M_{w(\text{ECL})} \cdot \frac{n}{M_{n(\text{PCL})}} \cdot 100 \quad \text{Equation 9.13}$$

where $\text{Int}(\alpha\text{-ECL})$ and $\text{Int}(\alpha\text{-PCL})$ represent the integration values of the two mentioned peaks in the ¹H NMR spectrum, the $M_{w(\text{ECL})}$ is the molecular weight of the **ECL** monomer (114.14 g/mol), n is the number of **ECL** units in the PCL and $M_{n(\text{PCL})}$ is the calculated molecular weight of the polymer (g/mol).

9.22. Isomer distribution in H₁₂MDI samples

The analysis of **H₁₂MDI** by either ¹H NMR spectroscopy or Gas Chromatography (GC) requires a previous homogenization of the sample by heating the sample at 35 °C for a few minutes to ensure a complete transparent mixture.

9.22.1. Distribution determination by ¹H NMR spectroscopy

To study the sample by means of ¹H NMR spectroscopy, *ca.* 0.01-0.02 mL of the mixture is dissolved in 0.5 mL of CDCl₃. To avoid degradation of the product, the deuterated solvent is previously dried with basic alumina. A spectrum of the freshly prepared samples is recorded rapidly in the range between -0.5 and 15 ppm, and with a delay time of 10 seconds to ensure the relaxation of the nuclei. The quantification of the **2,4'-isomers** and **4,4'-isomer** of

H₁₂MDI is calculated with the integration values of the colored areas of the ¹H NMR spectrum (Figure 9.9) according to Equation 9.14 and Equation 9.15.

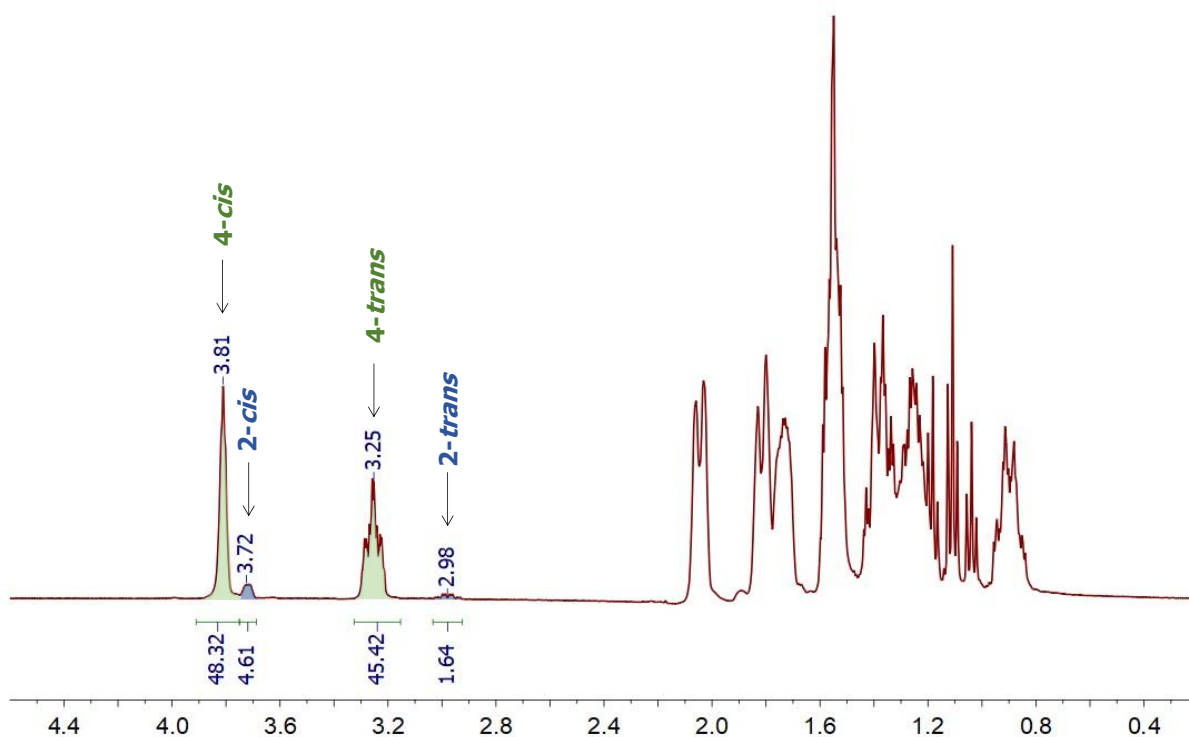


Figure 9.9. Example of ¹H NMR spectrum (400 MHz) of **H₁₂MDI** sample recorded with 10 second delay time. Solvent: CDCl₃.

$$2,4\text{-isomer [\%]} = \frac{2 \cdot [\text{Int}(2\text{-cis}) + \text{Int}(2\text{-trans})]}{\text{Int}(2\text{-cis}) + \text{Int}(2\text{-trans}) + \text{Int}(4\text{-cis}) + \text{Int}(4\text{-trans})} \cdot 100 \quad \text{Equation 9.14}$$

$$4,4'\text{-isomer [\%]} = \frac{\text{Int}(4\text{-cis}) + \text{Int}(4\text{-trans}) - [\text{Int}(2\text{-cis}) + \text{Int}(2\text{-trans})]}{\text{Int}(2\text{-cis}) + \text{Int}(2\text{-trans}) + \text{Int}(4\text{-cis}) + \text{Int}(4\text{-trans})} \cdot 100 \quad \text{Equation 9.15}$$

9.22.2. Distribution determination by Gas Chromatography

After homogenizing the samples, 0.02 mL of the mixture is transferred to a gas vial and dissolved in CH₂Cl₂. The vial was rapidly closed and analyzed.

- *2,4'-isomer and 4,4'-isomer quantification*

The area of all the peaks associated with the diisocyanate was normalized to 100. The sum of the peak areas of the 4 small constituents provided the quantity of 2,4'-isomer on the sample. If no additional peaks appeared on the sample, the rest until 100 corresponded to the 4,4'-isomer.

- *4,4'-isomer distribution*

4,4'-isomers were quantified by normalizing the three major peaks to 100 and determining the percentage of each. This allowed the comparison of the values with the ones reported by the suppliers.

9.23. PCL-NPG analysis

The determination of the **NPG** distribution and the M_n of the mixture and PCL through ^1H NMR spectroscopy is achieved by dissolving 5-10 mg of the mixture in acetone- d_6 . The dissolution of the polymer in CDCl_3 allows the determination of the M_n of the sample, but not the determination of the **NPG** distribution owing to the overlap of the methyl signals. To ensure the relaxation of all the nuclei, the spectra had to be recorded with a significant delay time (10 seconds). The quantification of the two parameters is estimated with the integration values associated with the different positions of **NPG** in the mixture and the polymerized **ECL** fragments in a ^1H NMR spectrum (see Figure 9.10).

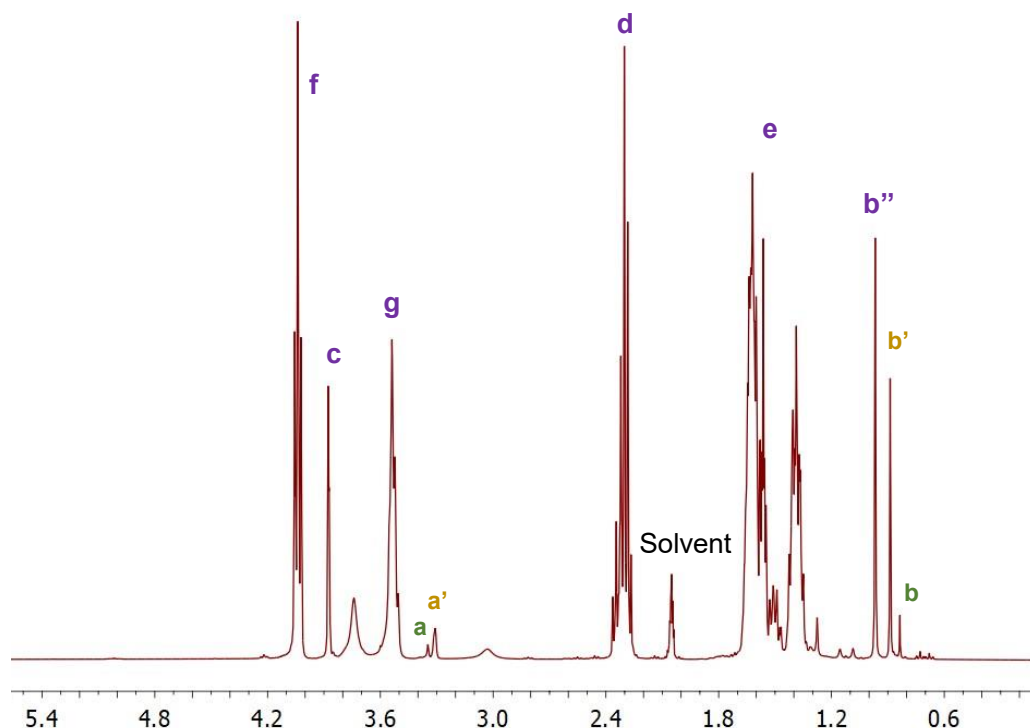


Figure 9.10. Example of a ^1H NMR spectrum (400 MHz) of a **PCL-NPG**. Solvent: Acetone- d_6 .

Regarding the estimation of the M_n , it required the obtaining of the number of repetitive **ECL** units in the polymers (n). The experimental average n value was determined with the number of mols of **NPG** (Equation 9.16) and **ECL**. The monomer had different signals in the spectrum

which enable the calculation, thereby for this last parameter, an average of the related peaks was used (the number of mols of **ECL** is the average of Equation 9.17, Equation 9.18, and Equation 9.19). All the integration values are normalized to the number of hydrogen atoms causing the signal.

$$NPG [mols] = \frac{\sum Int (b'' + b' + b)}{6} \quad \text{Equation 9.16}$$

$$(1) \quad ECL [mols] = \frac{Int(e)}{6} \quad \text{Equation 9.17}$$

$$(2) \quad ECL [mols] = \frac{Int(d)}{2} \quad \text{Equation 9.18}$$

$$(3) \quad ECL [mols] = \frac{Int(f) + Int(c)}{2} \quad \text{Equation 9.19}$$

The relation between both monomers provided the n value (Equation 9.20).

$$n = \frac{\text{average ECL}}{NPG} \quad \text{Equation 9.20}$$

The M_n of the mixture is calculated similarly to other PCL previously studied, by substituting the n value in the following expression (Equation 9.10), where $M_{w(ECL)}$ and $M_{w(initiator)}$ correspond to the molecular weight of **ECL** and **NPG**, respectively.

$$M_n (\text{mixture}) [g / mol] = n \cdot M_w (ECL) + M_w (\text{initiator}) \quad \text{Equation 9.10}$$

The analyzed mixture contains both **PCL-NPG** and the free initiator. Therefore, to calculate exclusively the M_n of the **PCL-NPG**, only the mols of **NPG** involved in the polymerization must be considered. Those are obtained following Equation 9.21.

$$NPG [mol] = \frac{Int(Internal\ NPG(b''))}{6} + \frac{Int(Terminal\ NPG(b'))}{6} \quad \text{Equation 9.21}$$

The M_n is obtained by substituting the newly calculated NPG mols in Equation 9.20 and subsequently applying Equation 9.10

9.24. Polyol mixture

The quantification of the constituents of the polyol mixture had to go hand by hand with the determination of the mols of **NPG** and PCL carried out in the PCL analysis. A similar process is carried out to prepare the sample for the 1H NMR analysis. Around 5-10 mg of the mixture is

dissolved in 0.5 mL of acetone- d_6 and the spectrum is rapidly recorded with a 10 second delay time.

Considering a ^1H NMR spectrum as the one displayed in Figure 8.16, the number of mols of **NPG** and **ECL** are calculated as in the **PCL-NPG** analysis with Equation 9.16, Equation 9.18, and Equation 9.19. The **ECL** mols are quantified as the average value of the two last expressions. **BDO** hydrogens overlap with signals arising from the polymer. Therefore, the corresponding integration value arising from the chain extender is obtained by subtracting the contribution of the polymer (Equation 9.22) to the area of the overlapped area (Equation 9.23). Equation 9.22 quantified the mols of methylene groups attached to a hydroxyl arising from the polymer. As one PCL termination is obtained per each esterified alcohol of the initiator, the PCL contribution is considered as follow:

$$PCL\ CH_2OH\ [mol] = \frac{2 \cdot Int(b'')}{6} + \frac{Int(b')}{6} \quad \text{Equation 9.22}$$

$$BDO\ [mol] = \frac{Int(g) - PCL\ CH_2OH}{4} \quad \text{Equation 9.23}$$

It could also be obtained from the internal methylene signals of the **ECL** located at δ 2.5 ppm (Equation 9.24)

$$BDO\ [mol] = \frac{Int(e) - PCL\ CH_2}{4} = \frac{Int(e) - \frac{2 \cdot Int(d)}{6}}{4} \quad \text{Equation 9.24}$$

The number of mols of **BDO** was obtained as the average of the calculated values of Equation 9.23 and Equation 9.24. Knowing the molecular weight of **NPG**, **ECL**, and **BDO**, the number of mols are translated to weight and the weight percentage of each species is calculated.

9.25. Speciation of the antioxidants in polymeric samples

9.25.1. PDDP Content

Samples were dissolved in the appropriate deuterated solvent. For the polyol mixture, samples are dissolved in acetone- d_6 and directly analyzed. However, two pellets are dissolved in filtered CDCl_3 (1 mL) with pyridine to increase the solubility and stirred for at least 8 hours until obtained a transparent solution. The $^{31}\text{P}\{^1\text{H}\}$ NMR spectrum of each polyol mixture was recorded for at least 1400 scans, while the TPUs samples were obtained after 27300 scans.

To evaluate the phosphite hydrolysis, all the phosphorous signals are integrated and normalized to 100. The sum of the areas of the four phosphites provides the % of mol of phosphites preserved as the antioxidant over the total number of mols of phosphorous, being the remaining phosphorus products derived from the hydrolysis of the phosphites.

9.25.2. Irgafos Content

The estimation of the antioxidant in the polyol mixture is conducted through $^{31}\text{P}\{^1\text{H}\}$ NMR spectra of the samples in CDCl_3 filtered through basic alumina and recorded for at least 1400 scans. The quantification of the studied compound contemplates the fact that the antioxidant is a diphosphite, thereby contains two phosphorus atoms per mol of compound. Therefore, the sum of all the integration values of the phosphorous signals is normalized to 100 and, the content of "active" antioxidant is obtained as half of the area of the studied compounds (δ_p : 117.15 ppm relative to H_3PO_4)

9.26. Scanning Electron Microscopy and Energy-dispersive X-ray spectroscopy

Analyzed films are cut in small squares (*ca.* 0.5 x 0.5 cm) and adhered to a double-sided conductive carbon tape over a metallic stub. Owing to the low conductivity of the sample, they are coated by a thin film of Ag/Pt in a sputter coater (2 minutes under a current of 15 mA in a vacuum of $2 \cdot 10^{-1}$ mbar).

Samples are loaded on the SEM according to the operating procedure of Microscopy facilities. The angle of the EDS detector is about 30° from the surface and the working distance is about 4 mm, but the actual values vary depending on the sample. Analyses have been carried out at low accelerating voltages to prevent the degradation of the samples but providing enough signal to carry out an X-ray spectroscopy (EDX) mapping. According to the observed surface, EDX of different points, some with irregularities and other blanks, or mapping of a concrete region of the sample are carried out.

9.27. Small-Angle X-ray scattering

Samples are cut in *ca.* 0.5 x 0.5 cm squares and the thickness of each individual specimen is measured with a digital measuring caliper. Then, samples are adhered to the holder with a double-faced tape. Samples are exposed to an X-ray beam of synchrotron radiation under a vacuum atmosphere.

Once the background is subtracted from the obtained data, a 1D pattern can be obtained by representing the scattering vector (q) in the X-axis and the intensity (I) in the Y-axis (Figure 9.11). Parameters like R , R_H , d and σ are obtained by fitting Perkus-Yevick and Zernike-Prins models (which were previously described in Section 2.21) to the experimental data with the solver tool of Excel.

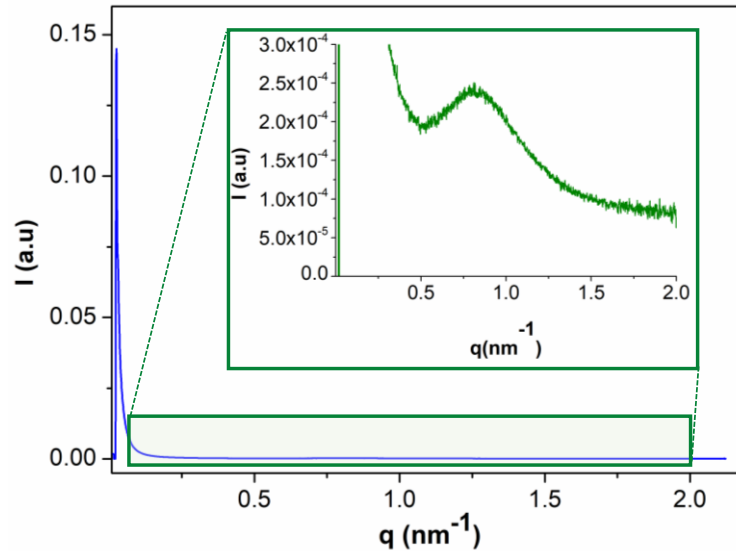


Figure 9.11. Example of a 1D SAXS pattern for a TPU film.

Literature

- [1] A. V. Shenoy, D. R. Saini, *Adv. Polym. Technol.* **1986**, *6*, 1–58.
- [2] M. properties Technical Committee ISO/TC 61, Plastics, Subcommittee SC 3, *ISO 868. Plastics and Ebonite. Determination of Indentation Hardness by Means of a Durometer (Shore Hardness)*, **2003**.
- [3] *ASTM D792-07. Standard Test Methods for Density and Specific Gravity (Relative Density) of Plastics*, **n.d.**
- [4] *ASTM D1894-00. Standard Test Method for Static and Kinetic Coefficients of Friction of Plastic Film and Sheeting*, West Conshohocken, PA, **2011**.
- [5] ASTM International, *ASTM D5963: Standard Test Method for Rubber Property—Abrasion Resistance*, **2015**.
- [6] *ASTM E313-05. Standard Practice for Calculating Yellowness and Whiteness Indices from Instrumentally Measured Color Coordinates*, West Conshohocken, PA, **2005**.
- [7] *ASTM D1003-00. Standard Test Method for Haze and Luminous Transmittance of Transparent Plastics*, West Conshohocken, PA, **2000**.
- [8] D. . Owens, R. . Wendt, *J. Appl. Polym. Sci.* **1969**, *13*, 1741–1747.
- [9] D. H. Kaelble, *J. Adhes.* **1970**, *2*, 66–81.
- [10] H. J. Busscher, A. W. J. van Pelt, P. de Boer, H. P. de Jong, J. Arends, *Colloids and Surfaces* **1984**, *9*, 319–331.
- [11] F. M. Fowkes, in *Surf. Interfacial Asp. Biomed. Polym. Vol. 1. Surf. Chem. Phys.* (Ed.: J.D. Andrade), Plenum Press, New York, **1985**, pp. 337–372.
- [12] H. Y. Erbil, *Langmuir* **1994**, *10*, 2006–2009.

Chapter 10

Experimental Part

Chapter 10 summarizes the employed instrumentation used for carried out the two projects and synthetic procedures in detail to produce monomers, polyols and TPUs.

10. Experimental part

10.1. Chemicals

General reagents and solvents were purchased from the common commercial supplier, such as Sigma-Aldrich, Cymmit, or Scharlab.

Reagents involved in the second part of the thesis (**ECL**, **H₁₂MDI**, **PCL-BDO**, **PCL-NPG**, **polyol mixtures**, **additives**, **catalysts**, and **TPUs**) were provided by Lubrizol Advanced Materials Spain, S.L.

Chemicals were used without further purification unless otherwise mentioned, like the ones detailed here:

- Triethylamine was purified by distillation and stored with activated molecular sieves.
- Acetonitrile was distilled over CaH₂.
- CH₂Cl₂ was dried with activated molecular sieves.
- Deuterated solvents:
 - CDCl₃ and Acetone-*d*₆ were dried with activated molecular sieves and neutralized with activated basic alumina when required.
 - DMSO-*d*₆ was dried with activated molecular sieves overnight.
- Anhydrous alcohols were used when required. The elimination of water was carried out using different standard procedures:
 - Fluorinated Diols (**HDO-8F**, **DiolF**, and **DiolSF**) were dried with azeotropic distillation with toluene or ether before their use.
 - 1,4-butanediol (**BDO**) was distilled over CaH₂.
- Adipoyl chloride was purified through an atmospheric distillation.

10.2. Instrumentation

▪ **Nuclear Magnetic Resonance (NMR) spectroscopy** was carried at *Servei de Ressonància Magnètica Nuclear* (SeRMN) at the UAB on three different spectrometers:

- Bruker Avance 250 MHz (250.16 MHz for ^1H , 62.90 MHz for ^{13}C , 235.2 MHz for ^{19}F)
- Bruker Avance DPX 360 (360.13 MHz for ^1H and 90.56 MHz for ^{13}C)
- Bruker Avance III 400 (400.13 MHz for ^1H , 100.61 MHz for ^{13}C , 376.50 MHz for ^{19}F , 161.98 MHz for ^{31}P)

^1H and $^{13}\text{C}\{^1\text{H}\}$ chemical shifts are referenced relatively to the signal of the residual undeuterated solvent according to the literature.^[1] Chemical shifts are reported in the δ scale and coupling constants (J) are expressed in Hertz (Hz). $^{31}\text{P}\{^1\text{H}\}$ chemical shifts are relative to the external standard 85% H_3PO_4 (0.0 ppm). ^{19}F experiments are referenced to fluorobenzene (-113.15 ppm with respect to CFCl_3), or 2,2,2-trifluoroethanol (-77.16 ppm with respected CFCl_3).

All the NMR experiments were performed at 298 K, but the relaxation delay was increased up to 10 or 20 seconds to have an accurate determination of the integration values in the mentioned cases.

▪ **Inductively Coupled Plasma-Mass Spectrometry (ICP-MS)** measurements were carried out on an Agilent Inductively Coupled Plasma Mass Spectrometer, model 7500ce. Samples were previously digested in a microwave Milestone, Ultrawave model.

▪ **Gas chromatography (GC)** experiments were carried out in an Agilent Technologies 6850 equipped with an FID detector, an Agilent 7683B Series Injector, and an Agilent HP5 column (30 m long, 0.32 mm internal diameter, and 0.25 μm film thickness) at the Organic Chemistry Unit at UAB. The stationary phase comprises 5% of diphenylpolysiloxane and 95% dimethylpolysiloxane.

▪ **Attenuated Total Reflectance Fourier transform Infrared spectroscopy (ATR-FTIR)** was recorded in a Bruker IT Tensor 27 spectrometer equipped with an ATR Specac Golden Gate single reflexion diamond ATR system. All the spectra were recorded using 16 scans at 4 cm^{-1} resolution in a range of 4000 to 600 cm^{-1} at the *Servei d'Anàlisi Química* (SAQ) of the UAB.

▪ **Melt Flow Index (MFI)** values were obtained out in a Göttfert Melt Indexer-3 calibrated with samples of polystyrene at Lubrizol Advanced Materials Spain S.L.

- **Kofler** was measured in Kofler Bench Wagner&Mundz Heizbank type WME with a temperature ranging between 50 and 260 °C calibrated with three samples with a known and narrow melting point at Lubrizol Advanced Materials Spain S.L.
- **Differential Scanning Calorimetry (DSC)** analyses were recorded in a Mettler Toledo DSC 3+ apparatus employing platinum crucibles at Lubrizol Advanced Materials Spain S.L.
- **Thermogravimetric analysis (TGA)** experiments were carried out on a TGA7 Pekin Elmer at Physics Department, in the Material Science and Metallurgic Engineering Section at UAB.
- **Yellow Index (YI)** values were obtained in a Hunterlab ColorFlex® CX1584 spectrophotometer at Lubrizol Advanced Materials Spain S.L. It has a directional annular 45° illumination and 0° measuring.
- **Transmittance and Haze** tests were performed in a Haze-gard plus BYK at Lubrizol Advanced Materials Spain S.L.
- **Gloss** was measured at 60°, with a Gloss Meter PicoGloss Model 503 of Erichsen at Lubrizol Advanced Materials Spain S.L.
- **Shore Hardness** measurements were performed with a Zwick-Roell Shore Hardness Tester 3130/3131 at Lubrizol Advanced Materials Spain S.L.
- **Density** was determined in a balance Mettler Toledo model XSR105 at Lubrizol Advanced Materials Spain S.L.
- **Coefficient of friction (COF)** were determined with a dynamometer Zwick/Roell Z010 at Lubrizol Advanced Materials Spain S.L.
- **Abrasion resistance** was measured in a Rotary drum (Ats Faar S.P.A) at Lubrizol Advanced Materials Spain S.L.
- **Static Water Contact Angle (WCA)** measurements were performed in a Contact Angle System OCA Data Physics at Lubrizol Advanced Materials Spain S.L.
- **Surface Free Energy (SFE)** results were obtained through the approximations of Owens, Wendt, Rabel, and Kaelble model^{[2][3]} already implemented in the WCA instrument software.
- **Size Exclusion Chromatography (SEC)** experiments were carried out on Agilent Technologies 1260 Infinity II GPC/SEC hardware, coupled with a UV and Refractive index detector at the Organic Chemistry Unit at UAB.
- **X-ray photoelectron spectroscopy (XPS)** measurement was carried out in a Phoibos 150 analyzer (SPECS GmbH, Berlin, Germany) with a monochromatic aluminum K_α X-

ray source (1486.74 eV) under ultra-high vacuum conditions at Institut Català de Nanociència i Nanotecnologia (ICN2) at the UAB campus.

- **Scanning Electron Microscopy (SEM)** analyses were carried out using a Merlin Zeiss Microscope coupled with a dual Oxford Instrument X-Max Energy-dispersive X-Ray (EDS) detector and backscattered electron (BSE) detectors at *Servei de Microscopia* of the UAB. The acceleration voltage of the electron beam was adapted to the sample but was between 2.00 kV and 10.0 kV. The elements present in a sample were identified automatically by the microscope software and denied or confirmed manually by comparison with the tabulated lines of each element, matching the *L* and *M* peaks of each element. Before the analysis, samples were coated with a thin layer of Pd/Au using a sputter coater with a current of 15 mA for 2 minutes.

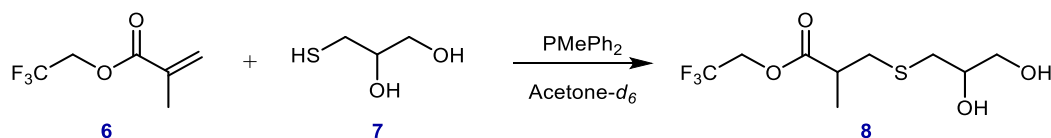
- **Small-Angle X-ray Scattering (SAXS)** measurements experiments were conducted at the NCD-SWEET beamline (BL11) at ALBA Synchrotron facilities in Barcelona. Data were collected using X-ray energy of 12.40 keV and a Pilatus 1M detector from Dectris (981 x 1043 pixels, 172 x 172 μm^2 each) mounted orthogonal to the beam path at a distance of 6.677 m from the sample. Silver behenate (AgBH) was used as a calibration standard.

10.3. Detailed procedures. Part I. Fluorinated Polyurethanes

10.3.1. Monomer synthesis

2,2,2-trifluoroethyl 3-((2,3-dihydroxypropyl)thio)-2-methylpropanoate (**8**)

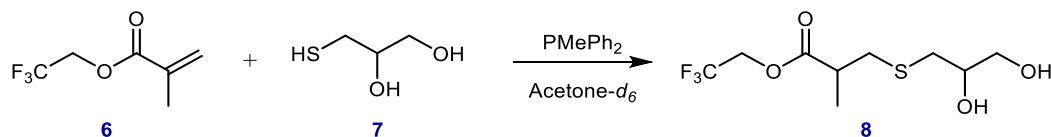
Synthesis with methyldiphenylphosphine (PMePh₂)



NMR tube scale

The synthesis of diol **8** was attempted adapting the methodology reported in the literature.^[4] Under N₂ atmosphere, 35.0 μL of 2,2,2-trifluoroethyl methacrylate (0.246 mmol), 32.0 μL of α-thioglycerol (0.370 mmol) and 2.3 μL of methyldiphenylphosphine (PMePh₂, 0.012 mmol, 5 mol%) were charged in an NMR tube and dissolved in 0.5 mL of acetone-*d*₆. The reaction was monitored by ¹H NMR spectroscopy, but the target product was not obtained. After 140 minutes, 41% of the starting reagent had released the trifluoroethyl moiety.

Synthesis with dimethylphenylphosphine (PMe₂Ph)



NMR tube scale

Synthesis of compound **8** was carried following the same procedure as with PMe₂Ph.^[4] Under N₂ atmosphere, 35.0 μL of 2,2,2-trifluoroethyl methacrylate (0.246 mmol), 32.0 μL of α-thioglycerol (0.370 mmol) and 1.75 μL of dimethylphenylphosphine (PMe₂Ph, 0.012 mmol, 5 mol%) were charged in an NMR tube and dissolved in 0.5 mL of acetone-*d*₆. The reaction was monitored by ¹H NMR spectroscopy at room temperature. After 50 min, the reaction was considered completed as no olefinic hydrogens remained in the sample, but traces of released trifluoroethanol were observed. ¹⁹F{¹H} NMR spectrum allowed the quantification of the species: 91% of target diol **8** and 9% of 2,2,2-trifluoroethanol. No traces of 2,2,2-trifluoroethyl methacrylate **6** were detected in the spectra.

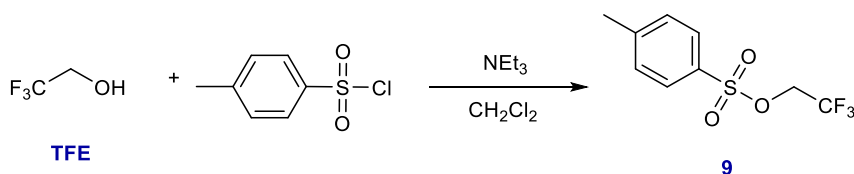
Scale-up reaction

Degassed 2,2,2-trifluoroethyl methacrylate **6** and α -thioglycerol **7** in the corresponding stoichiometry (ratios described in Table 4.2) were charged on a Schlenk flask under a N₂ atmosphere and dissolved in the corresponding volume of degassed acetone. The solution was then cooled down to 0 °C in an ice bath and dimethylphenylphosphine (PMe₂Ph, 5 or 1 mol%, according to the corresponding entry) was added with a micropipette surrounded by an inert atmosphere. After 30 minutes at 0 °C, the reaction crude was allowed to warm up to room temperature and let react. Reaction evolution was monitored by ¹H and ¹⁹{¹H} NMR spectroscopy with the disappearance of the olefinic peaks of the reagent. When no olefinic peaks were detected, the reaction mixture was quenched with air to oxidize phosphine. Subsequently, distilled water was incorporated into the mixture, but the formation of two phases was not observed. Subsequently, the solvent was evaporated under reduced pressure to obtain a pallid yellowish transparent liquid as a mixture of products. Experiments with a ratio of 1.0:1.5 of **6**:**7**, resulted in a mixture of the target compound **8** and **7**. However stoichiometric ratio generated products arising from the transesterification of **6**.

¹H NMR of the mixture (400 MHz, CDCl₃) δ_{H} : 4.51 (m, 2.0 H), 3.75 (m, 3.1 H), 3.58 (m, 1.5 H), 2.86 (m, 2.33 H), 2.65 (m, 4.50 H), 1.30 (d, J= 6.7 Hz, 3.00 H).

¹³C{¹H} NMR of the mixture (100.6 MHz, CDCl₃) δ_{C} : 125.90 (q, J= 276.2 Hz), 71.07, 65.27, 36.23, 34.77 (q, J = 32.8 Hz).

¹⁹F{¹H} NMR of the mixture (378.48 MHz, CDCl₃) δ_{F} : -74.02

2,2,2-trifluoroethyl 4-methylbenzenesulfonate (9)

2,2,2-trifluoroethyl 4-methylbenzenesulfonate (**9**) was synthesized following the published procedure with minor adjustments.^[5] In a 500 mL Schlenk flask, 2,2,2-trifluoroethanol (6.47 g, 64.7 mmol) was dissolved in 100 mL of CH₂Cl₂. Then the solution was cooled down in an ice bath and triethylamine (51.00 g, 504.0 mmol) was added dropwise. Subsequently, a solution of 4-toluenesulfonyl chloride (32.03 g in 100 mL of CH₂Cl₂, 168.0 mmol) was added dropwise over the basic mixture. The crude was let warm up until room temperature and stirred for 3 hours. The reaction was quenched by adding 150 mL of distilled water and left stirring

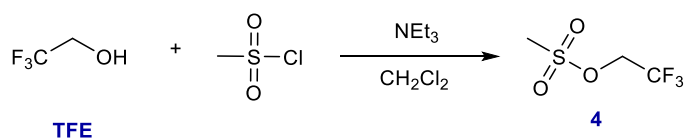
overnight. When the stirring was stopped, the two formed phases were separated. Then, the organic layer was washed with 1.2 M HCl_(aq) solution (100 mL x3), with a saturated NaHCO₃ solution (100 mL x2), and subsequently with distilled water (100 mL x2). Finally, the organic layer was dried over MgSO₄, filtered, and the solvent was evaporated until the appearance of a solid. If required, the round bottom flask was introduced in an ice bath to force the solidification of the product. A slightly yellow solid **6** was obtained. (15.48 g. Yield: 99.80%)

¹H NMR (400 MHz, CDCl₃) δ 7.82 (d, *J* = 8.4 Hz, 2H), 7.39 (d, *J* = 8.3 Hz, 2H), 4.35 (q, *J* = 7.9 Hz, 2H), 2.47 (s, 3H).

¹³C{¹H} NMR (100 MHz, CDCl₃) δ 146.16, 131.77, 130.24, 128.08, 122.01 (q, *J* = 277.6 Hz), 64.63 (q, *J* = 38.0 Hz), 21.60.

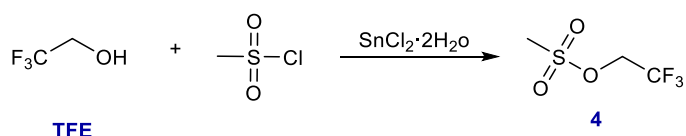
¹⁹F{¹H} NMR (235.39 MHz, CDCl₃) δ -73.80

2,2,2-trifluoroethyl methanesulfonate (**4**)



Typical procedure

In a 500 mL Schlenck flask, 28.05 g of 2,2,2-trifluoroethanol (0.28 mol) was cooled down to 0 °C and diluted with 80 mL of dried CH₂Cl₂. Then, 60 mL of dried triethylamine (43.62 g, 0.43 mol) was added dropwise through a pressure-equalizing funnel, observing the generation of a whitish steam. Finally, 26 mL of methanesulfonyl chloride (38.48 g, 0.34 mol) was added over the crude. At the end of the addition, an orangish suspension with a yellow salt was formed. Reaction crude was let warm up until room temperature and left stirring for 3.5 hours. The mixture was quenched by cooling it down in an ice bath and slowly incorporating 60 mL of HCl_(aq) (2.5 M) until the formation of two reddish phases. Both phases were stirred for one hour at room temperature and then, the organic layer was separated, washed with saturated NaHCO₃ (90 mL), brine (90 mL), and distilled water (100 mL). Then, it was dried over MgSO₄, filtered and the solvent was removed with a rotary evaporator. Lastly, the obtained red liquid was distilled under reduced pressure resulting in 39.06 g (78% yield) of 2,2,2-trifluoroethyl methanesulfonate (**4**) as a colorless liquid. (boiling point of 55 °C at 4 mmHg)

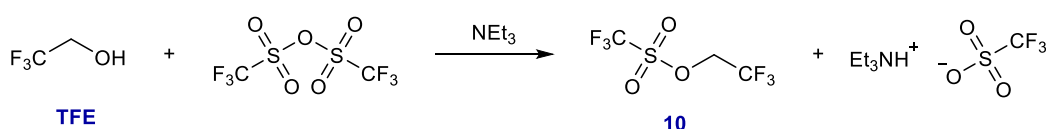
Alternative proposal

A 100 mL two-neck round bottom flask with 19.68 g of 2,2,2-trifluoroethanol (0.197 mol) was cooled down in an ice bath. Then, 1.109 g of $\text{SnCl}_2 \cdot 2\text{H}_2\text{O}$ ($4.91 \cdot 10^{-3}$ mol, 2.5 mol%) was added over the alcohol and stirred until the formation of a white suspension. Next, 24.38 g of methanesulfonyl chloride (0.213 mol) was added dropwise through a pressure-equalizing funnel. The round bottom flask was coupled with a condenser and a T-joint connected to a N_2 stream by one side and a trap full of a saturated solution of $\text{NaOH}_{(\text{aq})}$ by the other. Then, the reaction crude was heated to reflux temperature and monitored through $^{19}\text{F}\{^1\text{H}\}$ NMR spectroscopy. When complete conversion was observed, the mixture was distilled at reduced pressure. 28.39 g (81% yield) of 2,2,2-trifluoroethyl methanesulfonate (**4**) was obtained after 5 days as a colorless liquid (boiling point of 50 °C at 3.5 mmHg).

^1H NMR (250.16 MHz, CDCl_3) δ 4.52 (q, $J = 8.0$ Hz, 2H), 3.13 (s, 3H)

$^{13}\text{C}\{^1\text{H}\}$ NMR (62.90 MHz, CDCl_3) δ 122.14 (q, $J = 277.8$ Hz), 64.17 (q, $J = 38.1$ Hz), 38.41

$^{19}\text{F}\{^1\text{H}\}$ NMR (235.39 MHz, CDCl_3) δ -74.03

2,2,2-trifluoroethyl trifluoromethylsulfonate (10)

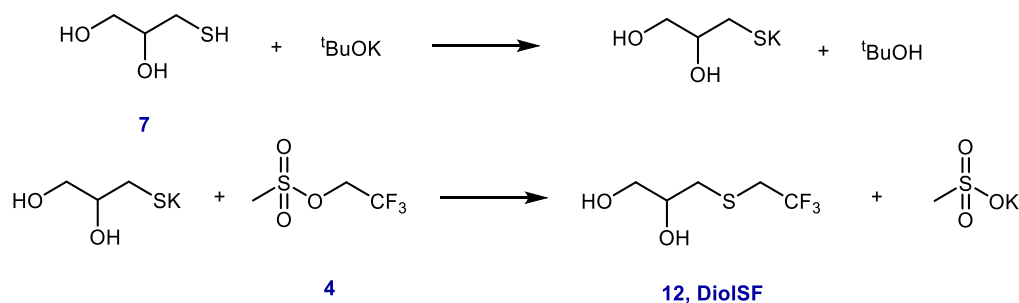
15.0 g of 1,1,1-trifluoromethanesulfonic anhydride (53.2 mmol) and 5.38 g of 2,2,2-trifluoroethanol (53.2 mmol) were charged on a 50 mL round bottom flask and cooled down in a salt/ice bath at a temperature of -20 °C. Then, 5.38 g of dried triethylamine (53.2 mmol) was added dropwise through a pressure-equalizing funnel. At that point, the reaction crude was allowed to warm up until room temperature and was stirred for 4 hours. Subsequently, a distillation setup was coupled to the round bottom flask and distillation at atmospheric pressure was carried out to afford 9.38 g (76% yield) of 2,2,2-trifluoroethyl trifluoromethylsulfonate (**8**) as a colorless liquid (boiling point 91 °C).

^1H NMR (400.13 MHz, CDCl_3) δ 4.70 (q, $J = 7.4$ Hz, 2H)

$^{13}\text{C}\{^1\text{H}\}$ NMR (62.90 MHz, CDCl_3) δ 121.2 (q, $J = 277.5$ Hz), 120.9 (q, $J = 277.5$ Hz), 68.77 (q, $J = 39.7$ Hz)

$^{19}\text{F}\{^1\text{H}\}$ NMR (276.5 MHz, CDCl_3) δ -73.94, 74.25

3-[(2,2,2-trifluoroethyl)thio]-1,2-propanediol (**12**)



39.12 g $t\text{BuOK}$ (98%, 0.342 mol) was charged 250 mL round bottom flask and placed in an ice bath. Then, 37.04 g of α -thioglycerol (0.342 mol) was slowly incorporated while vigorously stirring the mixture. A viscous solid appeared at the bottom of the flask with a transparent supernatant liquid. Subsequently, $t\text{BuOH}$ were evaporated under reduced pressure, and when the viscosity of the crude increased, fractions of toluene (20 mL x3) were added until the formation of a dry white fine powder. If required, the mixture was heated up to 40 °C to accelerate the evaporation.

Optimization study

A 50 mL two neck round bottom flask coupled with a condenser was charged with the corresponding quantity of the obtained salt (1.15 g or 1.73 g, according to the entry in Table 4.4), which was dissolved with the corresponding volume of anhydrous DMF or MeCN. Then, 1.40 g of 2,2,2-trifluoroethyl methanesulfonate (7.9 mmol) was added and the mixture was heated to 80 °C. If required, 0.11 g of tetrabutylammonium chloride (0.4 mmol, 5 mol%) was also incorporated. Through the reaction, a dough is generated which had to be dispersed in some of the reactions. After 48 hours, samples were quantitatively transferred out of the round bottom flask with the help of an additional volume (10-15 mL) of the employed solvent. The yield of the reaction was quantified using $^{19}\text{F}\{^1\text{H}\}$ NMR spectroscopy with 10 seconds delay time.

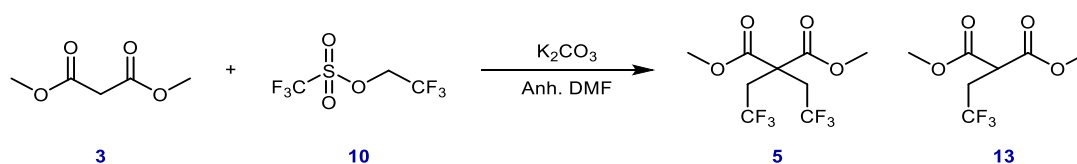
Large scale

In a 500 mL Schlenck flask, 30.79 g of the obtained potassium 2,3-dihydroxypropane-1-thiolate (0.210 mol) was dissolved in 300 mL MeCN. Subsequently, 25.00 g of 2,2,2-trifluoroethyl methanesulfonate (0.140 mol) was slowly added through a pressure-equalizing funnel. Once the addition was completed, the reaction crude was stirred for 20 hours at reflux temperature. The reaction was monitored by $^{19}\text{F}\{^1\text{H}\}$ NMR spectroscopy until the disappearance of the mesylate **4** signal. At that point, the solvent was removed under reduced pressure and the crude was extracted with ether (25 mL x4), which in turn was dried over MgSO_4 and evaporated at reduced pressure. An orange-yellowish liquid was obtained. Produced was purified by reduced pressure distillation. 16.48 g of colorless and transparent liquid were collected. If the analysis reveal the presence of acetate, the product was purified again with a liquid-liquid extraction. The sample was dissolved in 75 mL of Et_2O , and washed with distilled water (75 mL x2). The organic phase was dried with MgSO_4 , filtered and the solvent was removed under reduced pressure.

^1H NMR (400 MHz, CDCl_3) δ 3.90-3.81 (m, 1.00 H), 3.72 (dd, J = 11.4, 3.3 Hz 1.00 H), 3.56 (dd, J = 11.4, 6.5 Hz, 1.00 H), 3.16 (q, J = 9.9 Hz, 2.00 H), 2.80 (dd, J = 13.7, 4.8 Hz, 1.00 H), 2.74 (dd, J = 13.7, 7.8 Hz, 1.00 H).

$^{13}\text{C}\{^1\text{H}\}$ NMR (100.6 MHz, CDCl_3) δ 125.90 (q, J = 276.2 Hz), 71.07, 65.27, 36,23, 34.77 (q, J = 32.8 Hz).

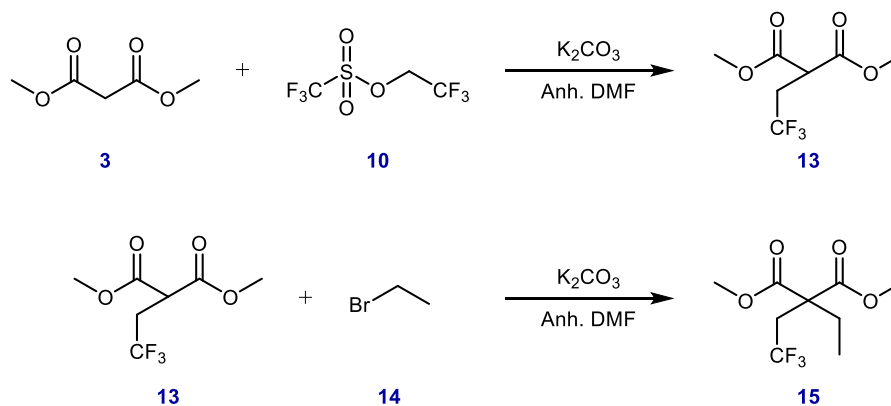
$^{19}\text{F}\{^1\text{H}\}$ NMR (378.48 MHz, CDCl_3) δ -66.54

Dimethyl 2,2-bis(2,2,2-trifluoroethyl) malonate (5)

0.65 g of K_2CO_3 (4.7 mmol) was added to a 5 mL Schlenk flask, dispersed in 1 mL of anhydrous DMF, and the suspension was degassed. Then, with a micropipette, 216 μL of dimethyl malonate (0.25 g, 1.2 mmol) and 627 μL of 2,2,2-trifluoroethyl trifluoromethylsulfonate (1.01 g, 4.4 mmol) were incorporated into the flask and allowed to react at room temperature. The reaction was monitored by GC by taking small aliquots and filtering them through zeolite to remove the generated salt. After the 12 days, the reaction crude exhibited 21 % of the

monoalkylated product dimethyl 2-(2,2,2-trifluoroethyl) malonate **13** and 79 % of the target product dimethyl 2,2-bis(2,2,2-trifluoroethyl) malonate **5**.

Dimethyl 2-ethyl-2-(2,2,2-trifluoroethyl) malonate (**15**)

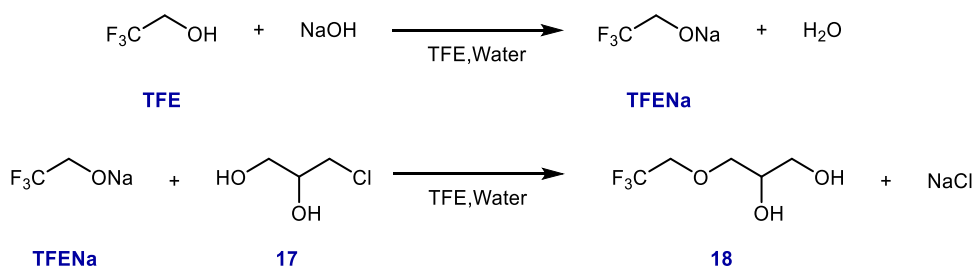


In a 10 mL Schlenk flask, 1.72 g of K_2CO_3 (12.45 mmol), 0.49 mL of dimethyl malonate (0.56 g, 4.27 mmol) were dissolved in 2.5 mL of anhydrous DMF. The system was degassed and later, connected a N_2 atmosphere. The mixture was stirred for 30 minutes, and then 0.66 mL 2,2,2-trifluoroethyl trifluoromethylsulfonate (1.06 g, 4.58 mol) resulting in orange suspension. Small aliquots of the crude filtered through zeolite were used to monitor the reaction evolution by GC. When the ratio among the reagents was constant, the Schlenk flask was introduced in an ice bath and 0.34 mL of ethyl bromide (0.50 g, 4.58 mmol) was slowly incorporated into the mixture. Then, the reaction was thermostatted to 25 °C and after 24 hours, the crude reached a constant ratio between the products according to GC analysis. The reaction crude was dissolved in 5 mL of Et_2O and was neutralized with 5 mL of 6M $\text{HCl}_{(\text{aq})}$ solution. The organic phase was then washed with 6 mL of brine and 6 mL of distilled water. Subsequently, it was dried with MgSO_4 and the solvent was removed under reduced pressure.

^1H NMR of the mixture (400 MHz, CDCl_3) δ 3.78 (s, 0.94H), 3.74 (s, 5.06H), 3.29 (t, $J = 7.6$ Hz, 0.12H), 3.02 (q, $J = 10.3$ Hz, 0.40H), 2.85 (q, $J = 11.0$ Hz, 1.52H), 2.10 (q, $J = 7.5$ Hz, 1.50H), 1.93 (quint, $J = 7.5$ Hz, 0.29H), 0.95 (t, $J = 7.4$ Hz, 0.36H), 0.84 (t, $J = 7.5$ Hz, 2.22H)

$^{13}\text{C}\{^1\text{H}\}$ NMR of the mixture (100.6 MHz, CDCl_3) δ 170.25, 170.03, 168.14, 167.37, 124.46 (q, $J = 281.0$ Hz), 55.04, 53.86, 53.10, 52.54, 35.40 (q, $J = 28.9$ Hz), 24.94, 22.45, 11.95, 8.54

$^{19}\text{F}\{^1\text{H}\}$ NMR of the mixture (378.48 MHz, CDCl_3) δ -61.48 (signal associated to **5**, 22.1 F), -61.55 (signal associated to **13**, 77.9 F)

3-(3,3,3-trifluoroethoxy)-1,2-propanediol (18, DiolF)*Scale-up reaction*

In a 10 L mechanically stirred reactor vessel, 3769 g of 2,2,2-trifluoroethanol (37.67 mol) and 1060 g of water (58.89 mol) were added, and then, it was coupled with a 250 mL pressure-equalizing funnel. 1378 g of NaOH (34.36 mol) were dissolved in the same amount of water (solution 50 wt.% NaOH_(aq)) and incorporated dropwise to the alcohol, monitoring the mixture temperature and maintaining it under 45 °C to avoid evaporation of the reactant. After completing the addition, a suspension was formed and, was let cool down to 35 °C. At this temperature, 952.3 g of 3-chloro-1,2-propanediol **17** (8.62 mol) was added dropwise to the mixture controlling again that the temperature remains below 45 °C. When the diol addition was finished, the reaction mixture was stirred for 90 minutes. The reaction was quenched by neutralizing the formed sodium trifluoroethoxide with concentrated HCl. A maximum of 2550 mL could be employed, but the exact quantity depends on the carbonation of the salt. The acid was slowly incorporated maintaining the temperature under 50 °C until the reaction mixture reached pH 3. Then, the stirring was stopped, and the reaction mixture separated in two phases, being the bottom one enriched in the fluorinated species. Therefore, the inferior one was transferred to a 2 L reactor and 2,2,2-trifluoroethanol first ($T_{\text{boiling}} \approx 83$ °C), and afterward, water, were distilled at atmospheric pressure. Lastly, around 700 g of PPG ($M_n \approx 400$ g/mol) was introduced into the reactor and a reduced pressure distillation was carried out to recover product **18** ($T_{\text{boiling}}(\mathbf{18}) \approx 120$ °C, $P \approx 1$ mbar). 974 g of product **18** was collected as a transparent liquid with a final yield of 65%.

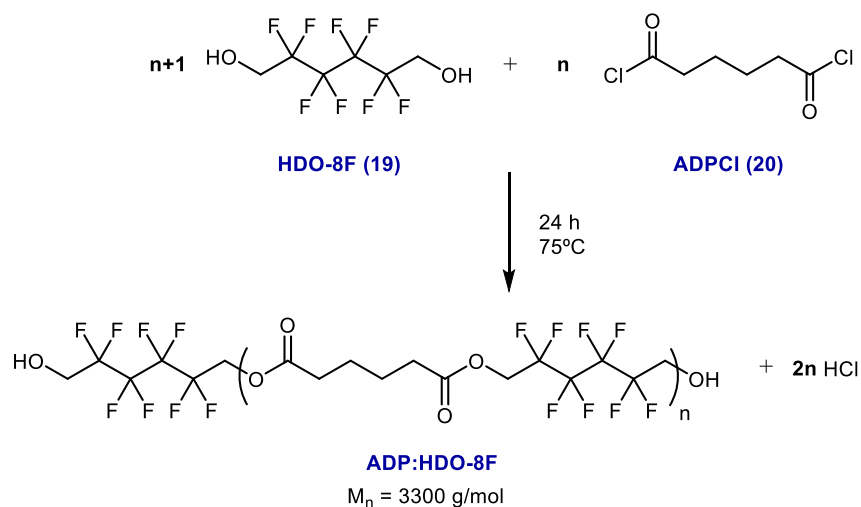
¹H NMR (400 MHz, CDCl₃) δ 3.38 (dd, $J = 17.4, 8.6$ Hz, 3H), 3.25 – 3.06 (m, 4H), 2.99 (s, 2H).

¹³C{¹H} NMR (100.6 MHz, CDCl₃) δ 124.01 (q, $J = 279.5$ Hz), 73.76, 70.92, 68.76 (q, $J = 34.1$ Hz), 63.46

¹⁹F{¹H} NMR (378.48 MHz, CDCl₃) δ -74.68

10.3.2. Polyol Synthesis

Polyadipate of 2,2,3,3,4,4,5,5-octafluorohexane-1,6-diol (ADP:HDO-8F)



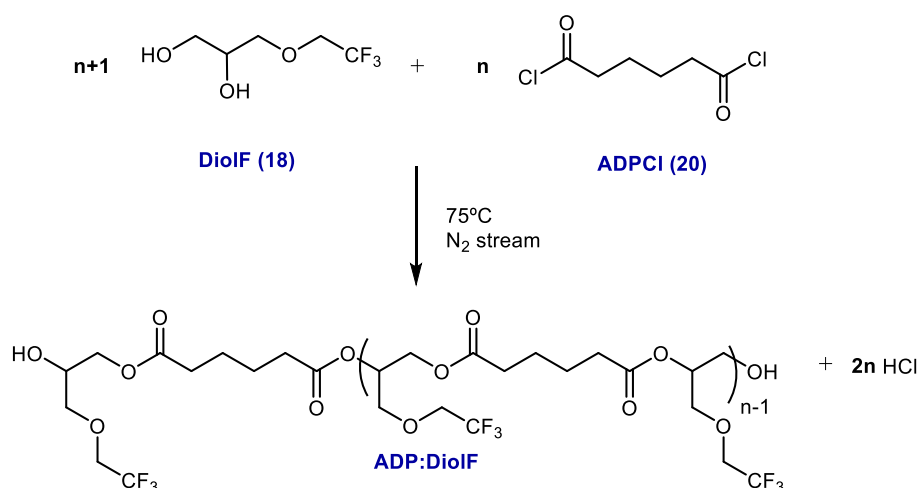
In a 1 L mechanically stirred reactor, 222.69 g of dried 2,2,3,3,4,4,5,5-octafluorohexane-1,6-diol (0.850 mol) was degassed, and heat until 60 °C. Through a pressure-equalizing funnel, 138.78 g of freshly distilled adipoyl chloride (0.758 mol) was slowly added over the diol while the reactor had a continuous flow of N₂ connected to a trap with a saturated solution of KOH_(aq). The mixture was allowed to react at 75 °C, stirred at 150 rpm for 24 hours. Then, the crude was cooled down to room temperature until the appearance of a white solid.

¹H NMR (360.13 MHz, CDCl₃) δ 4.56 (t, *J*= 13.5 Hz, 4.00 H), 4.04 (t, *J*= 14.1 Hz, 0.50 H), 2.43 (s, 4.00 H), 2.69 (s, 4.00 H).

¹³C{¹H} NMR (90.55 MHz, CDCl₃) δ 171.76, 114.65 (tt, *J*= 258.4, 30.8 Hz), 111.15 (tt, *J*=266.5, 32.0 Hz), 60.54 (t, *J*= 25.7 Hz), 59.56 (t, *J*= 26.8 Hz), 33.20, 23.92.

¹⁹F{¹H} NMR (373. MHz, CDCl₃) δ -119.89(s, 14.33 F), -122.70(s, 2.00 F), -123.85(s, 12.31 F), -124.08(s, 3.90 F)

Polyadipate of DiolF (ADP:DiolF) by Acyl approach



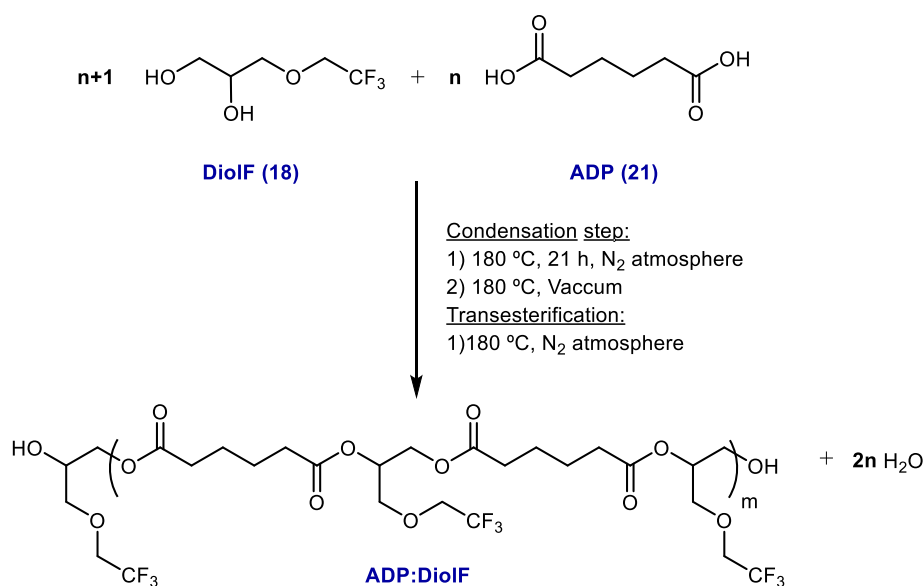
4.114 g of dried DiolF (23.6 mmol) were weighted on a 25 mL two-neck round bottom flask coupled with a condenser and a T-Shape joint. It is connected to a N_2 flow and an exterior trap full of a saturated solution of $\text{NaOH}_{(\text{aq})}$. The system is cooled down in an ice bath and 3.741 g of adipoyl chloride (20.4 mmol) were added dropwise to control the release of HCl. Once the addition ended, the crude was allowed to react at room temperature for 30 min and then, it was warmed up to 75 °C for 18 h. The reaction yielded the polymer together with the undefined impurity.

^1H NMR of the mixture (400 MHz, CDCl_3) δ 5.11 (m, 8H), 4.28 (m, 4H), 4.10 (dd, $J = 12.0$, 6.0 Hz, 4H), 3.80 (m, 26H), 3.71 (d, $J = 5.1$ Hz, 7H), 3.67 (dd, $J = 11.8$, 5.3 Hz, 1H), 3.60 (dd, $J = 11.7$, 5.4 Hz, 1H), 2.30 (s, 28H), 1.62 (s, 28H).

$^{13}\text{C}\{^1\text{H}\}$ NMR of the mixture (100 MHz, CDCl_3) δ 178.44, 172.81, 172.52, 172.39, 123.84 (q, $J=279.5$ Hz), 123.79 (q, $J=279.5$ Hz), 71.11, 70.71, 70.62, 69.74, 68.73 (q, $J = 68.7$ Hz), 68.62 (q, $J = 68.6$ Hz), 62.17, 42.14, 33.65, 33.47, 24.16, 24.09, 24.05.

$^{19}\text{F}\{^1\text{H}\}$ NMR of the mixture (376.50 MHz, CDCl_3) δ -74.19, -74.23

Polyadipate of DiolF (ADP:DiolF) by conventional esterification approach



The polyester was synthesized in a 500 mL mechanically stirred reactor with a metallic heating mantle connected to a PID controller to monitor the reaction temperature. The reactor has connected during all the process a distillation set up, with the column full of Raigshing to increase the efficiency of the separation. 187.64 g of adipic acid (1.28 mol), 284.23 g of DiolF (1.63 mol), and the corresponding weight of the antioxidant (0.2 wt.%) were added to the reactor and degassed under reduced pressure for 10 minutes. Then, the reaction mixture was heated up to 180 °C under N₂ atmosphere, and water was distilled off. At the melt state, high stirring was applied to the system. After 21 hours, 8 mg of SnCl₂·2H₂O (20 ppm) was incorporated into the mixture and let react for a couple of hours prior to applying vacuum to the system via the end of the distillation set up for 20 hours. The mixture was monitored with AI titrations until values lower than 1 mg KOH/g polymer were achieved. If the determined value was superior, the required correction with dried DiolF was carried out, letting react the mixture at atmospheric pressure for two hours after the addition, and then applying vacuum again until the next control. Once the AI reached the target value, the reaction was monitored by the OHI to determine the M_n. The subsequent corrections were carried out at atmospheric pressure until achieving the target value. The resulting brown viscous crude was then cooled down to 120 °C and transferred to an HPDE container.

^1H NMR (360.13 MHz, $d_1 = 10\text{s}$, CDCl_3) δ 5.17 (m, 55H), 5.02 (m, 3H), 4.30 (dd, $J = 11.7$, 3.9 Hz, 55H), 4.13 (dd, $J = 11.9$, 5.9 Hz, 81H), 4.02 (m, 13H), 3.84 (m, 150H), 3.74 (d, $J = 4.9$ Hz, 117H), 3.65 (m, 36H), 2.32 (s, 258H), 1.62 (s, 256H)

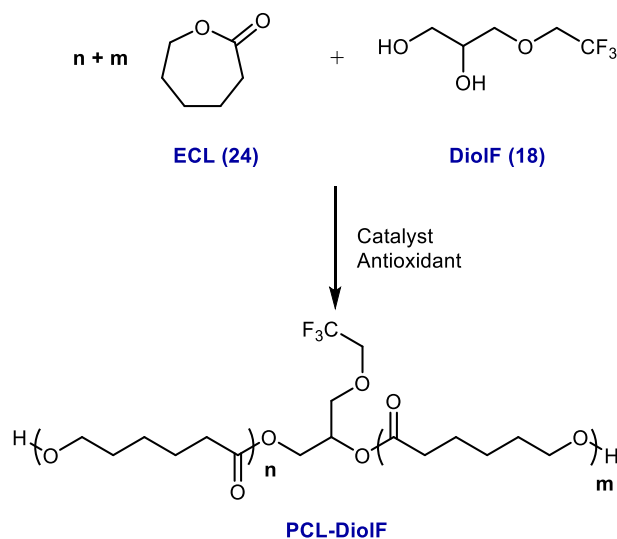
$^{13}\text{C}\{^1\text{H}\}$ NMR (90.55 MHz, CDCl_3) δ 173.38, 172.87, 172.56, 123.88 (q, $J = 279.7$ Hz), 74.00, 73.45, 72.95, 71.04, 70.78, 69.78, 68.90 (q, $J = 34.2$ Hz), 68.83, 68.72 (q, $J = 34.2$ Hz), 65.24, 63.50, 62.23, 61.60, 33.77, 33.75, 33.58, 33.56, 24.20

$^{19}\text{F}\{^1\text{H}\}$ NMR (376.50 MHz, CDCl_3) δ - 74.19 ppm

Catalyst tests

In a 500 mL mechanically stirred reactor with a metallic heating mantel connected to a PID controller to control the temperature, 117.33 g of adipic acid (0.803 mol) and 164.74 g of **DiOLF** (0.946 mol) were charged and degassed. The distillation setup was coupled and the mixture was heated to 180 °C under a N_2 atmosphere. After 21 hours, the mixture was cold down to 80 °C and four 100 mL round bottom flasks were charged with 50.00 g of the mixture each. Then, 45 ppm of the corresponding catalyst ($\text{SnCl}_2 \cdot 2\text{H}_2\text{O}$, $\text{Bi}(\text{OTf})_3$ and Bi_2O_3) were incorporated into the round bottom flask, which were then coupled with a microdistillation setup. The reaction crudes were heated at 180 °C at reduced pressure. After 20 hours, the required quantity of product to carry out the AI was extracted, and the system was subjected to additional 20 hours under the reduced pressure. After the total amount of 40 hours, AI was repeated. Finally, a quantification of the fluorine content on the samples was carried out by NMR spectroscopy with 3-bromobenzotrifluoride as standard.

Polycaprolactone initiated by DiolF (PCL-DiolF)



The reaction was carried out following standard procedures for the Ring-opening polymerization. Owing to confidential reasons, the detailed procedure is not disclosed hereafter.

$^1\text{H NMR}$ (400 MHz, $d_1=10\text{s}$, CDCl_3) δ 5.09 (p, $J = 5.1$ Hz, 6H), 4.23 (dd, $J = 11.9, 4.1$ Hz, 7H), 4.12 (m, 5H), 3.95 (t, $J = 6.6$ Hz, 354H), 3.76 (m, 17H) 3.67 (d, $J = 5.1$ Hz, 17H), 3.51 (t, $J = 6.5$ Hz, 41H), 2.20 (t, $J = 7.5$ Hz, 393H), 1.54 (m, 792H), 1.28 (dt, $J = 15.2, 7.5$ Hz, 398H).

$^{13}\text{C}\{^1\text{H}\}$ NMR (100.6 MHz, CDCl_3) δ 173.59, 173.39, 172.79, 172.49, 123.60 (q, $J = 279.6$ Hz), 73.39, 70.63, 69.55, 68.62 (q, $J = 34.3$ Hz), 64.93, 63.98, 62.24, 34.10, 33.97, 33.84, 33.65, 32.18, 28.20, 25.39, 25.30 24.59, 24.43, 24.31, 24.28.

$^{19}\text{F}\{^1\text{H}\}$ NMR (376.5 MHz, $d_1 = 10\text{s}$, CDCl_3) δ -74.25, -74.31, -74.33

Polycaprolactone initiated by BDO (PCL-BDO)

PCL-BDO was synthesized following the same procedure as PCL-DiolF substituting the initiator. A more detailed synthesis must be sought somewhere else.

$^1\text{H NMR}$ (400 MHz, $d_1=10\text{s}$, CDCl_3) δ 4.00 (t, $J = 6.7$ Hz, 8.48 H), 3.57 (t, $J = 6.5$ Hz, 1H), 2.25 (t, $J = 7.5$ Hz, 8.48 H), 1.58 (m, 17.96 H), 1.32 (m, 8.49 H).

$^{13}\text{C}\{^1\text{H}\}$ NMR (100.6 MHz, CDCl_3) δ 173.74, 173.54, 64.13, 63.79, 62.49, 34.23, 34.11, 32.32, 28.34, 25.52, 25.32, 24.70, 24.57.

10.3.3. TPU synthesis

TPUs formulations were adapted for each mixture maintaining constant the hard segment percentage. Products were targeted for hardness of 80-90 Shore A.

The synthesis of these polymers was carried out in a 2 L capacity Teflon-covered saucepan under mechanical stirring on a hot plate. The required amount of polyol (single component or mixture of components) was melted achieving a homogenous mixture. Then, the corresponding additives were added, and the mixture was heated to the established temperature. At that point, the chain extender/s and the catalyst solution were incorporated into the mixture. The catalyst solution is prepared at 1 wt.% of catalyst in the major component of the polyol. Prior to the last addition, the stirring was increased and the diisocyanate was added to the mixture, which started to become thicker. When the reaction was completed, the material was poured into teflonated molds and cured for 3 hours. To manufacture the materials, they were frozen for 24 hours and grinded to obtain chips. Each material was injected with the appropriate profile to generate sheets of 8x8 cm.

Owing to the low vapor pressure of the employed diisocyanate and the related toxicity by inhalation, the synthetic procedure was carried out with extreme care in fume hoods and with personal protective equipment such as a full-face mask, goggles, gloves, and isocyanate detectors in the surrounding area.

10.4. Detailed procedures. Part II. Process control

10.4.1. PCL reactivity

167.1 g of ECL was charged in a 250 mL three-neck round bottom flask coupled with a Dimroth condenser under a N₂ atmosphere and a thermometer introduced in the mixture. The system was introduced in an aluminum reaction block and heated up to the target temperature (165 °C or 180 °C). Once the internal temperature of the monomer reached the desired value, it was maintained for 5 minutes and then, the other reagents were incorporated into the vessel. For those experiments containing 6-hydroxyhexanoic acid, 50 mg of the opened monomer, 0.25 g of a solution stock of the catalyst in BDO (0.7 wt.%), and 7.63 g of 1,4-butanediol were added. In the reference experiments, only the catalyst and the initiator were introduced. Once the reagents were homogenized the temperature of the mixture was controlled every 5 minutes.

Literature

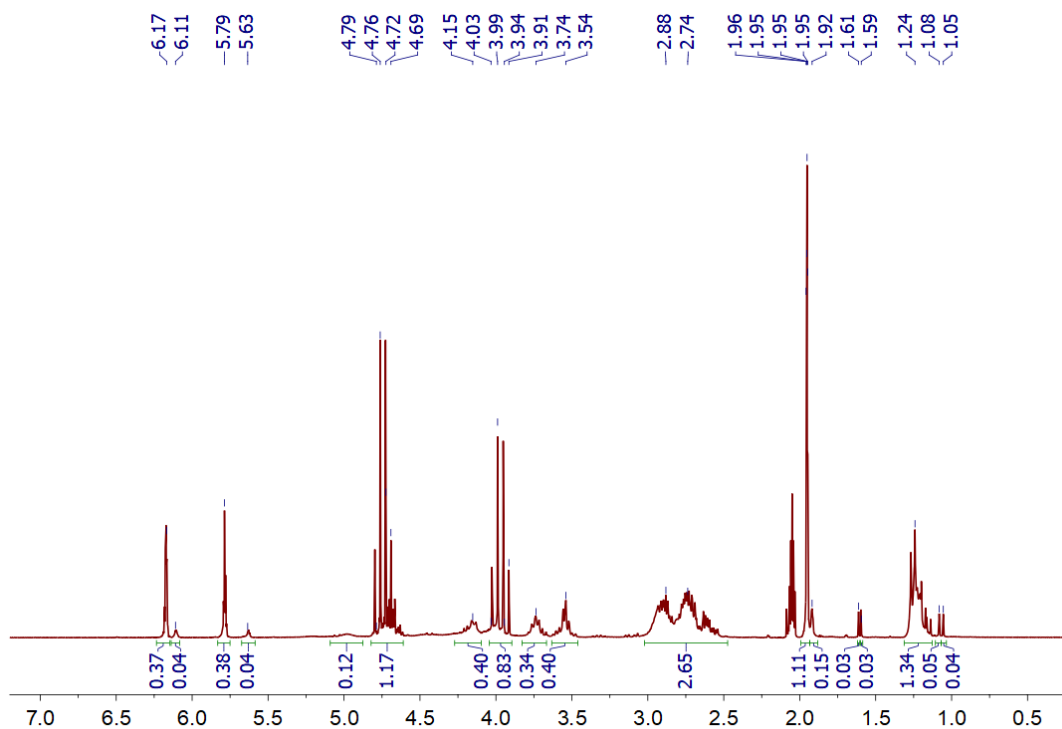
- [1] G. R. Fulmer, A. J. M. Miller, N. H. Sherden, H. E. Gottlieb, A. Nudelman, B. M. Stoltz, J. E. Bercaw, K. I. Goldberg, *Organometallics* **2010**, *29*, 2176–2179.
- [2] D. . Owens, R. . Wendt, *J. Appl. Polym. Sci.* **1969**, *13*, 1741–1747.
- [3] D. H. Kaelble, *J. Adhes.* **1970**, *2*, 66–81.
- [4] G. Z. Li, R. K. Randev, A. H. Soeriyadi, G. Rees, C. Boyer, Z. Tong, T. P. Davis, C. R. Becer, D. M. Haddleton, *Polym. Chem.* **2010**, *1*, 1196–1204.
- [5] N. N. Su, Y. Li, S. J. Yu, X. Zhang, X. H. Liu, W. G. Zhao, *Res. Chem. Intermed.* **2013**, *39*, 759–766.
- [6] B. Ren, L. Gan, L. Zhang, N. Yan, H. Dong, *Org. Biomol. Chem.* **2018**, *16*, 5591–5597.
- [7] A. Kavros, T. N. Huckerby, S. Rimmer, *J. Mater. Chem.* **1999**, *9*, 1071–1076.

Annex

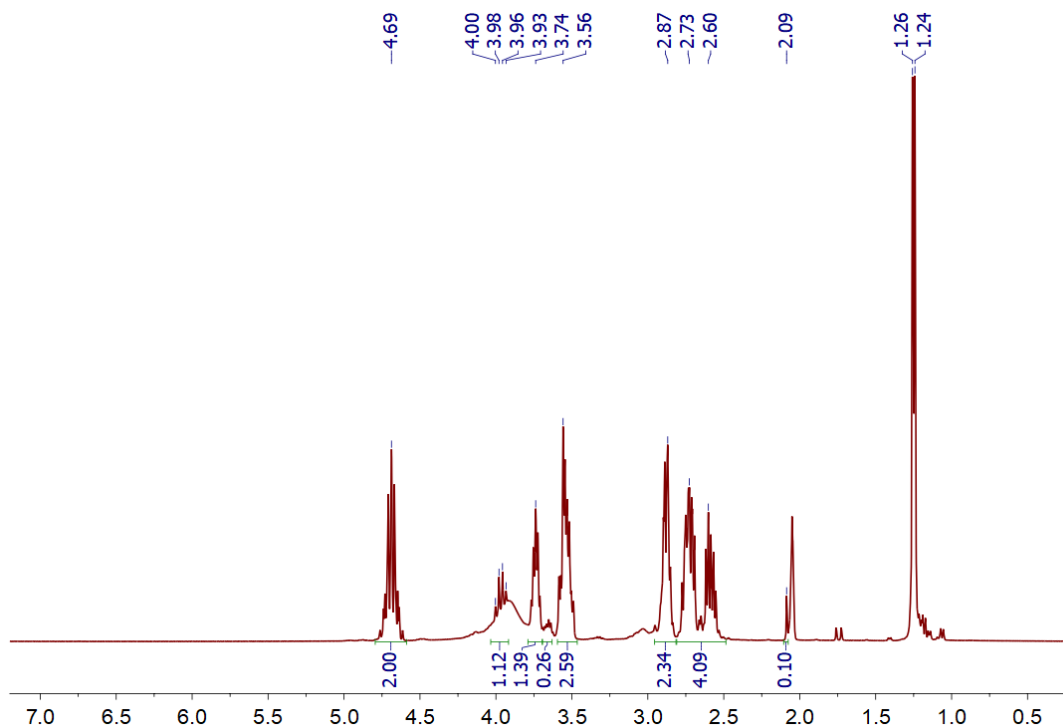
A. Annex

A.1. 2,2,2-trifluoroethyl 3-((2,3-dihydroxypropyl)thio)-2-methylpropanoate (8)

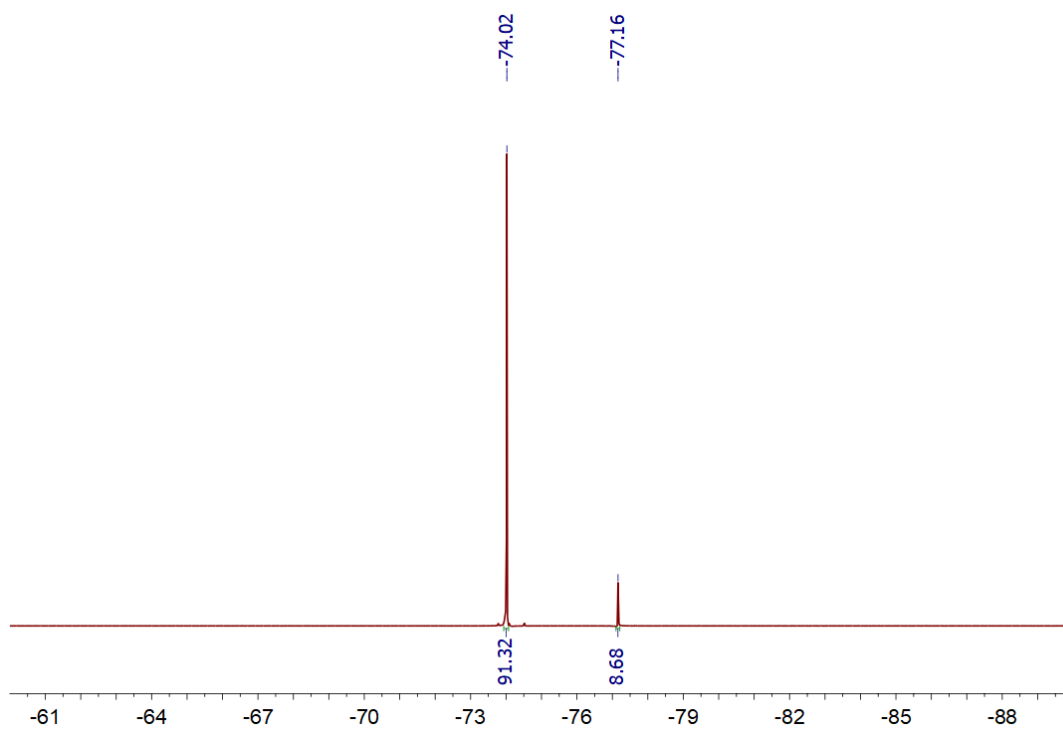
^1H NMR spectrum (250 MHz) of the reaction crude of the Thio-ene Michael addition between 2,2,2-trifluoromethyl metacrylate (**2**) and α -thioglycol (**7**) at NMR tube scale and catalyzed with PMePh_2 . Solvent: Acetone- d_6 .



^1H NMR spectrum (400 MHz) of the reaction crude of the Thio-ene Michael addition between 2,2,2-trifluoromethyl metacrylate (**2**) and α -thioglycol (**7**) at NMR tube scale and catalyzed with PMe_2Ph . Solvent: Acetone- d_6 .

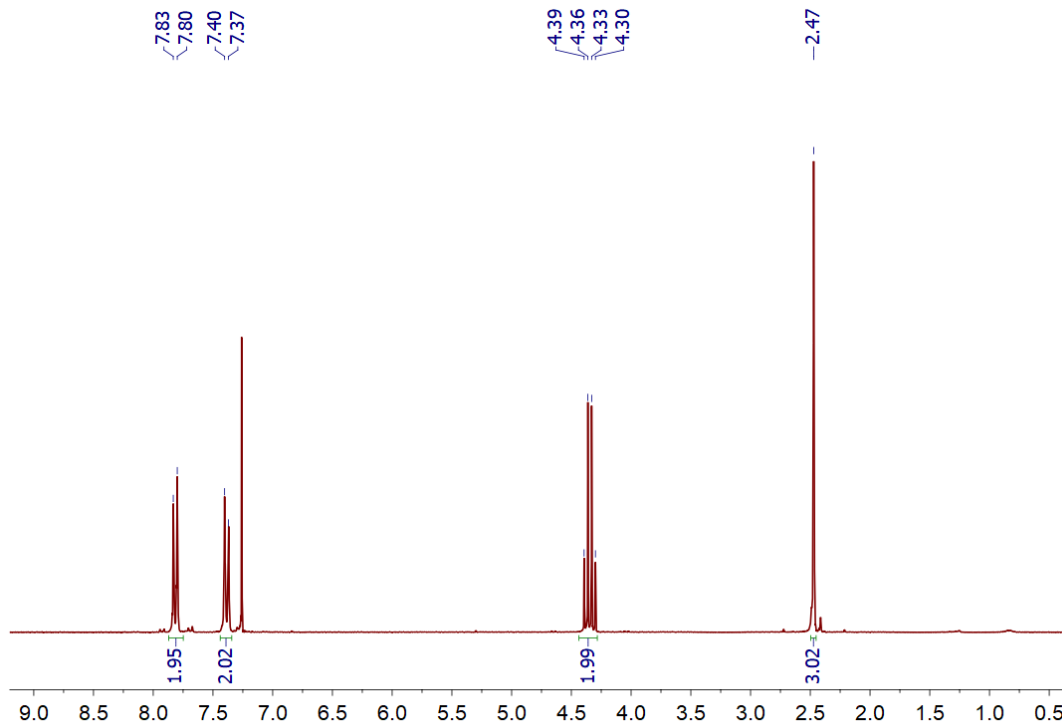


$^{19}\text{F}\{^1\text{H}\}$ NMR spectrum (376.5 MHz) of the reaction crude of the Thio-ene Michael addition between 2,2,2-trifluoromethyl metacrylate (**2**) and α -thioglycol (**7**) at NMR tube scale and catalyzed with PMe_2Ph . Solvent: Acetone- d_6 .

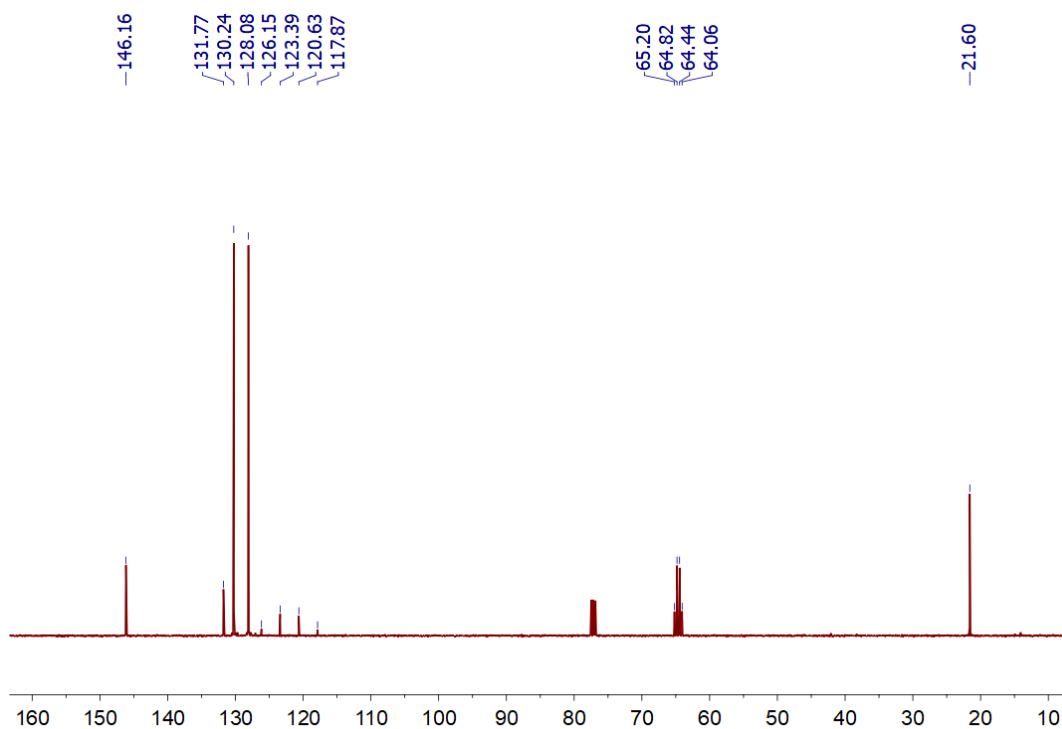


A.2. 2,2,2-trifluoroethyl 4-methylbenzenesulfonate (9)

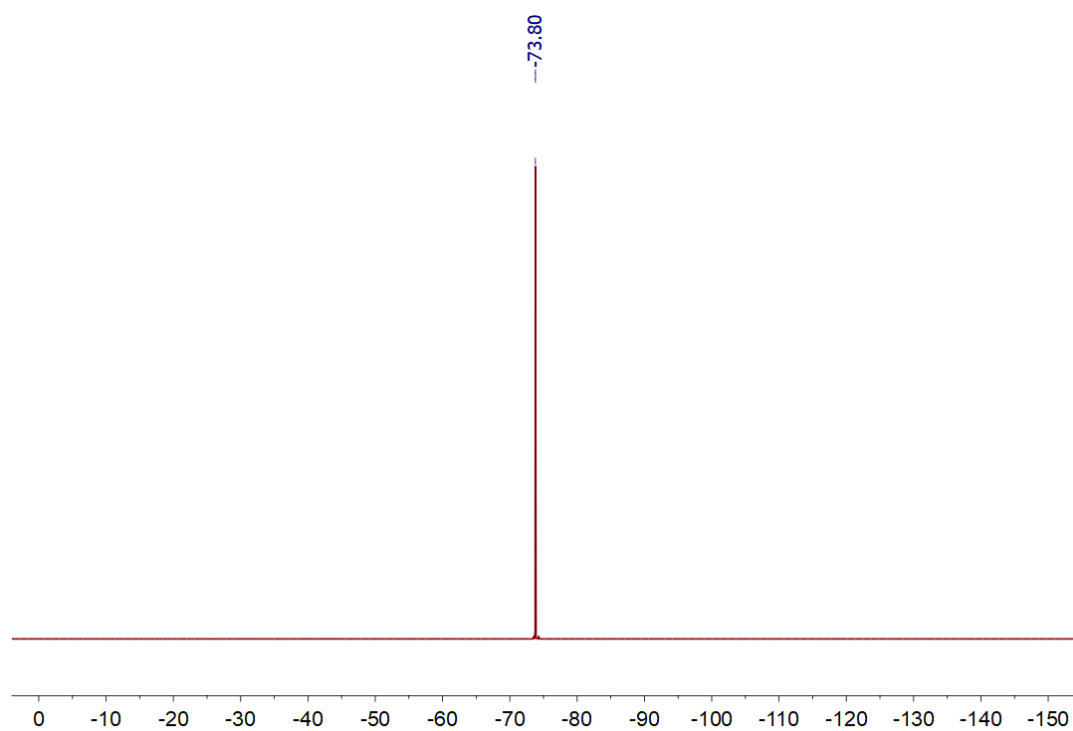
^1H NMR spectrum (400 MHz) of 2,2,2-trifluoroethyl 4-methylbenzenesulfonate (**9**). Solvent: CDCl_3 .



$^{13}\text{C}\{^1\text{H}\}$ NMR spectrum (100.6 MHz) of 2,2,2-trifluoroethyl 4-methylbenzenesulfonate (**9**). Solvent: CDCl_3 .

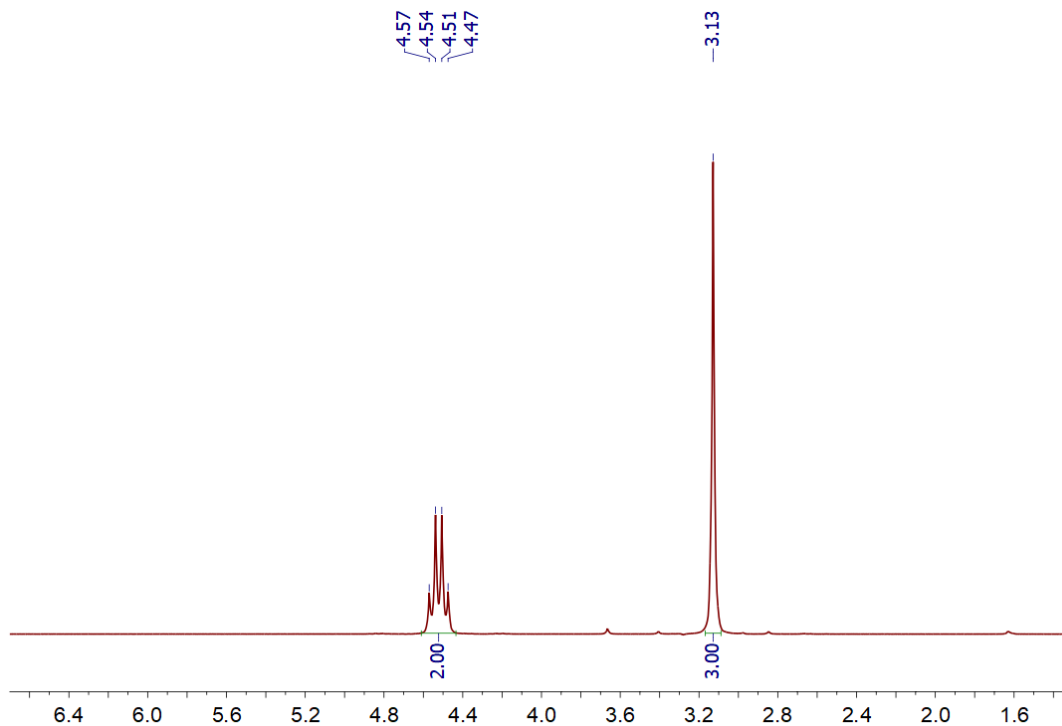


$^{19}\text{F}\{^1\text{H}\}$ NMR spectrum (376.5 MHz) of 2,2,2-trifluoroethyl 4-methylbenzenesulfonate (**9**). Solvent: CDCl_3 .

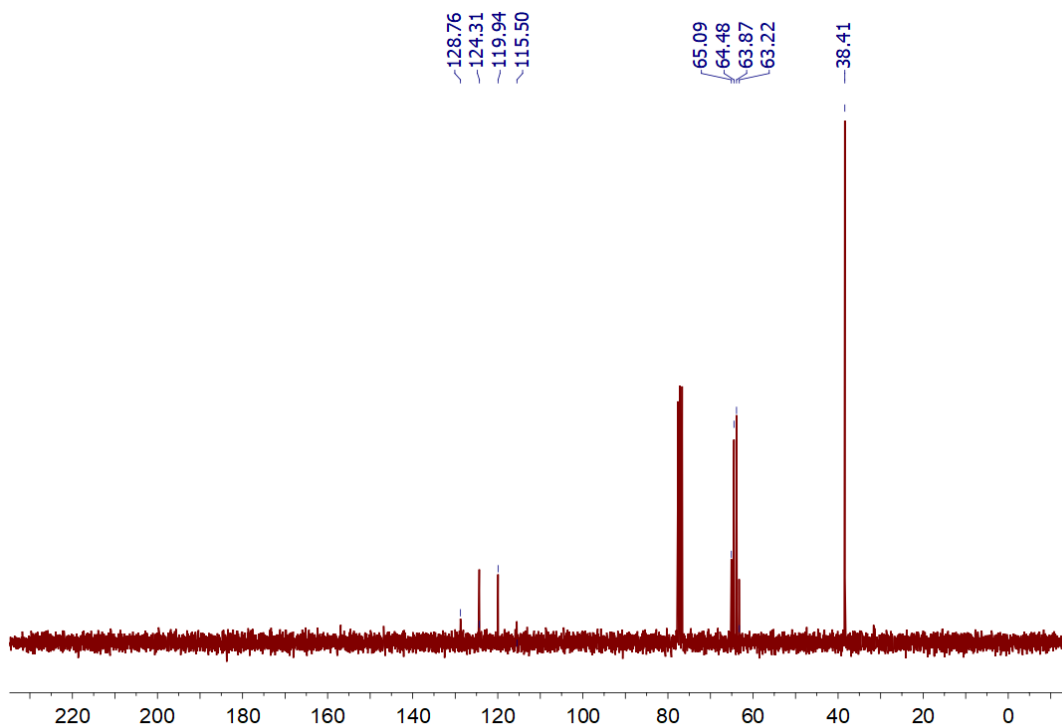


2,2,2-trifluoroethyl methanesulfonate (**4**)

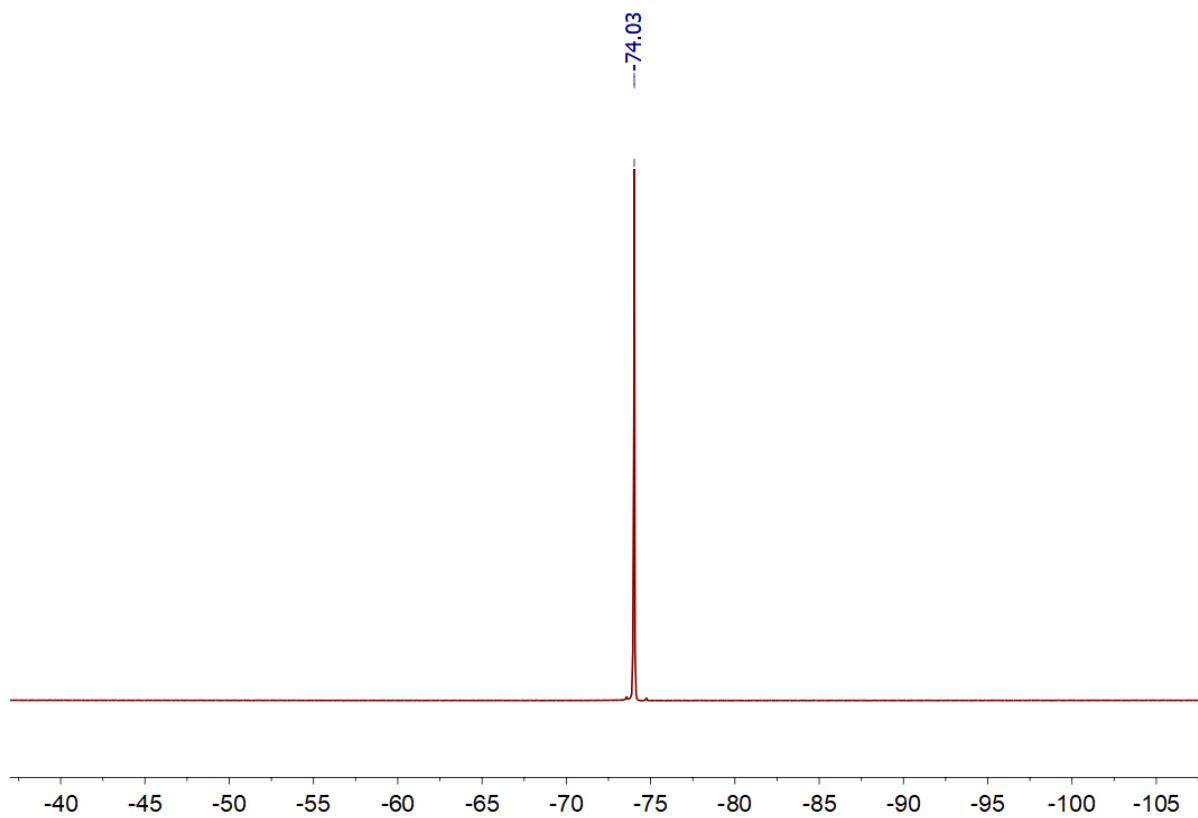
^1H NMR spectrum (250.2 MHz) of 2,2,2-trifluoroethyl methanesulfonate (**4**). Solvent: CDCl_3 .



$^{13}\text{C}\{^1\text{H}\}$ NMR spectrum (62.9 MHz) of 2,2,2-trifluoroethyl methanesulfonate (**4**). Solvent: CDCl_3 .

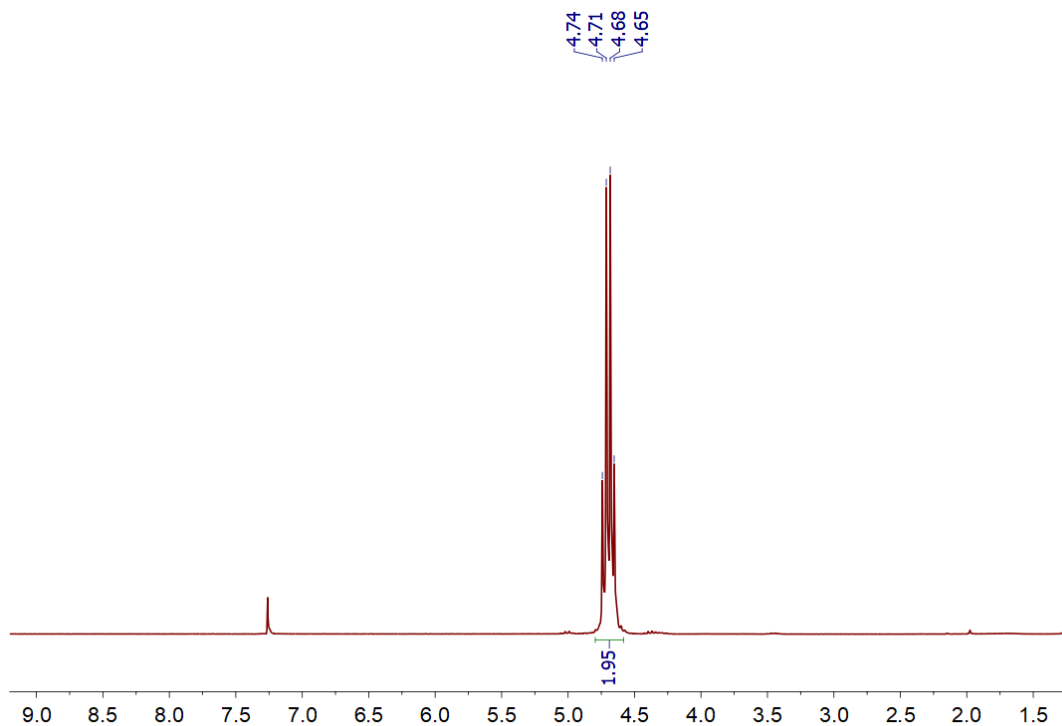


$^{19}\text{F}\{^1\text{H}\}$ NMR spectrum (235.2MHz) of 2,2,2-trifluoroethyl methanesulfonate (**4**). Solvent: CDCl_3 .

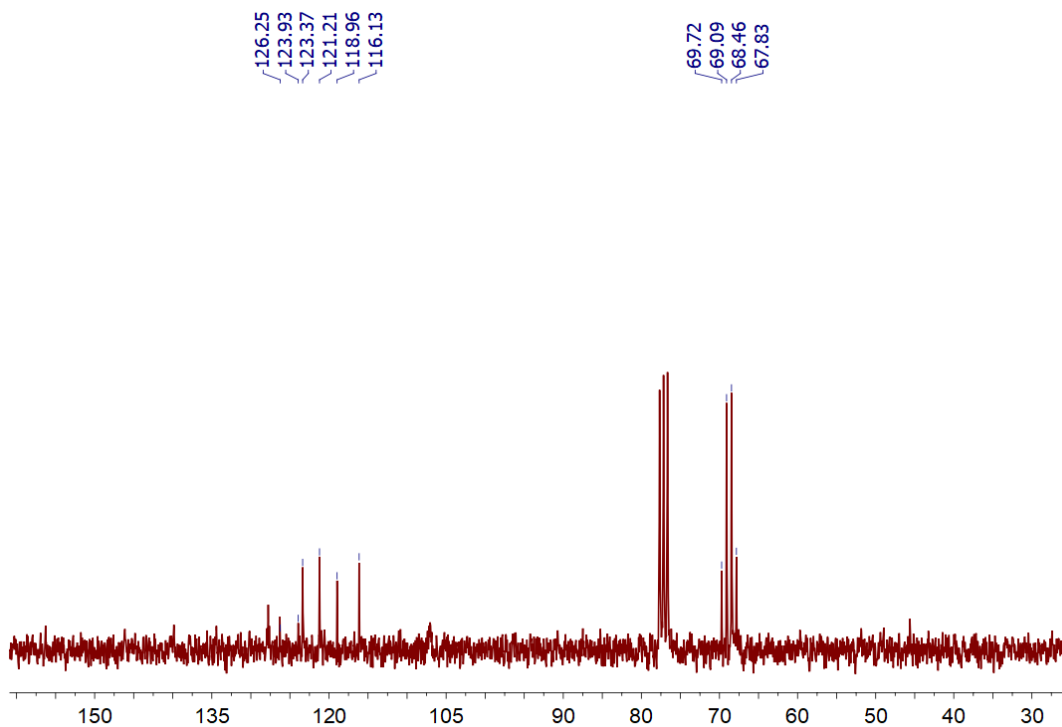


A.3. 2,2,2-trifluoroethyl trifluoromethylsulfonate (**10**)

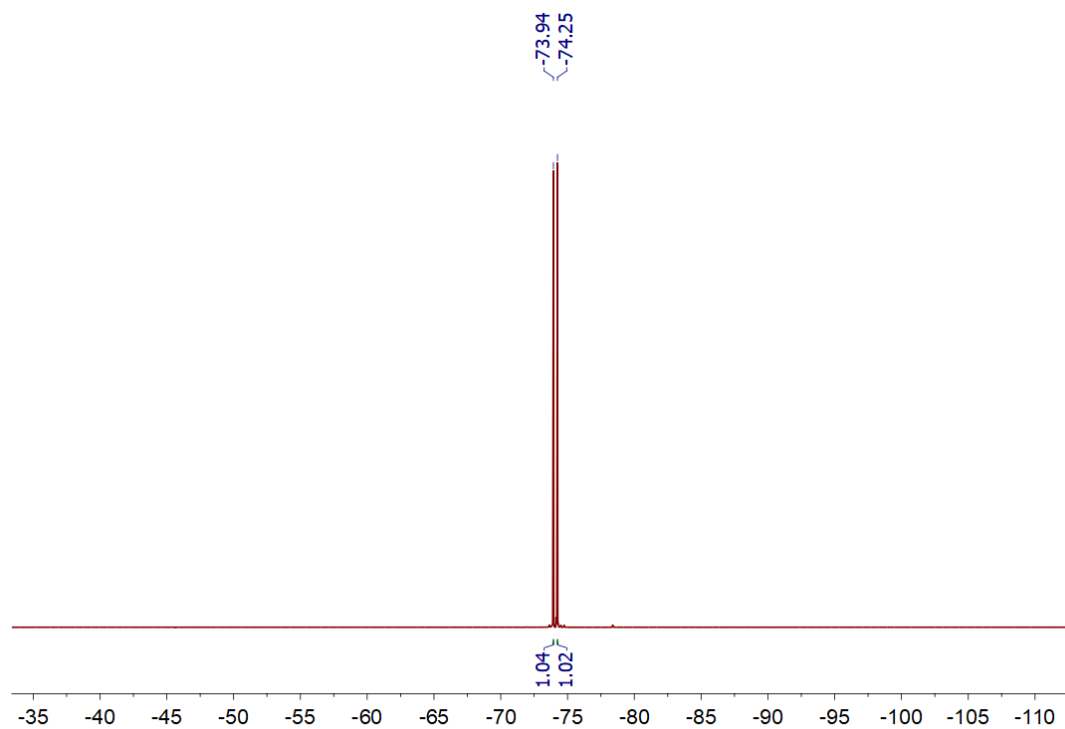
^1H NMR spectrum (400.1 MHz) of 2,2,2-trifluoroethyl trifluoromethylsulfonate (**10**). Solvent: CDCl_3 .



$^{13}\text{C}\{^1\text{H}\}$ NMR spectrum (62.9 MHz) of 2,2,2-trifluoroethyl trifluoromethylsulfonate (**10**). Solvent: CDCl_3 .

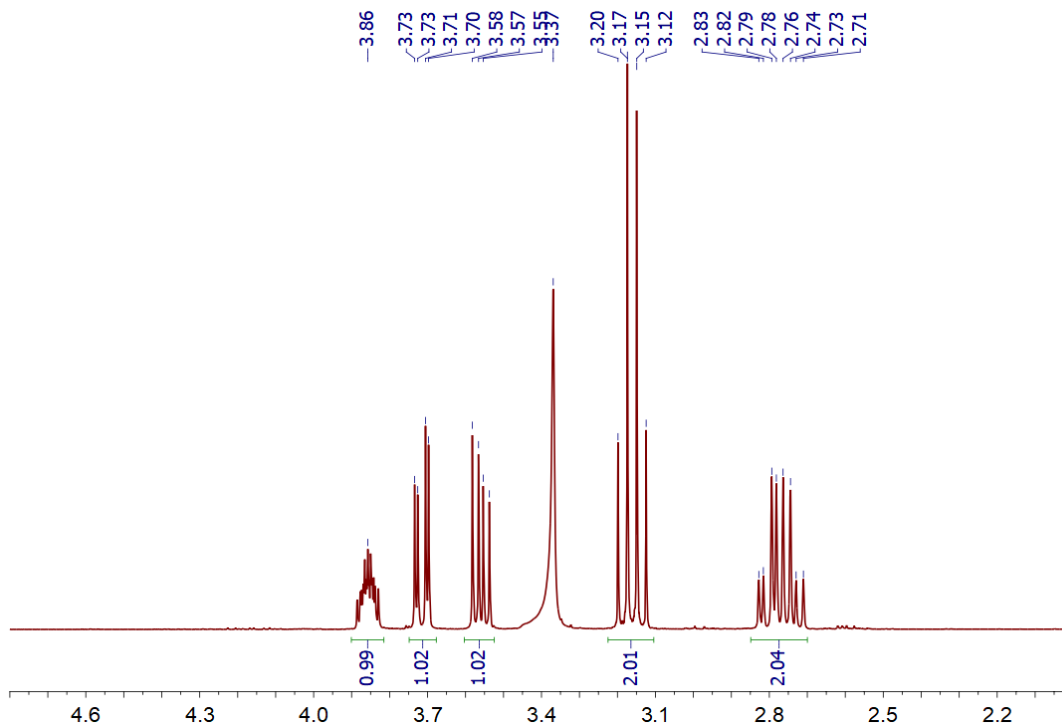


$^{19}\text{F}\{^1\text{H}\}$ NMR spectrum (376.5 MHz) of 2,2,2-trifluoroethyl methanesulfonate (**4**). Solvent: CDCl_3 .



A.4. 3-[(2,2,2-trifluoroethyl)thio]-1,2-propanethiol (**12**)

^1H NMR spectrum (400.1 MHz) of 3-[(2,2,2-trifluoroethyl)thio]-1,2-propanethiol (**12**, **DiolSF**).
Solvent: CDCl_3 .



$^{13}\text{C}\{^1\text{H}\}$ NMR spectrum (100.6 MHz) of 3-[(2,2,2-trifluoroethyl)thio]-1,2-propanethiol (**12**, **DiolSF**).
Solvent: CDCl_3 .

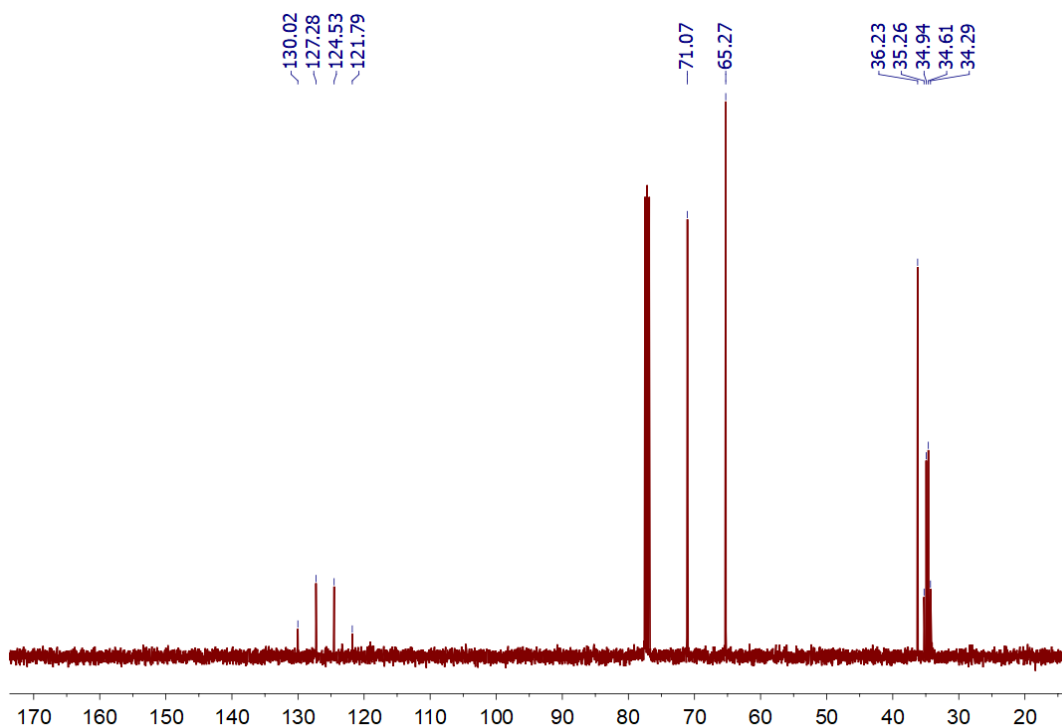
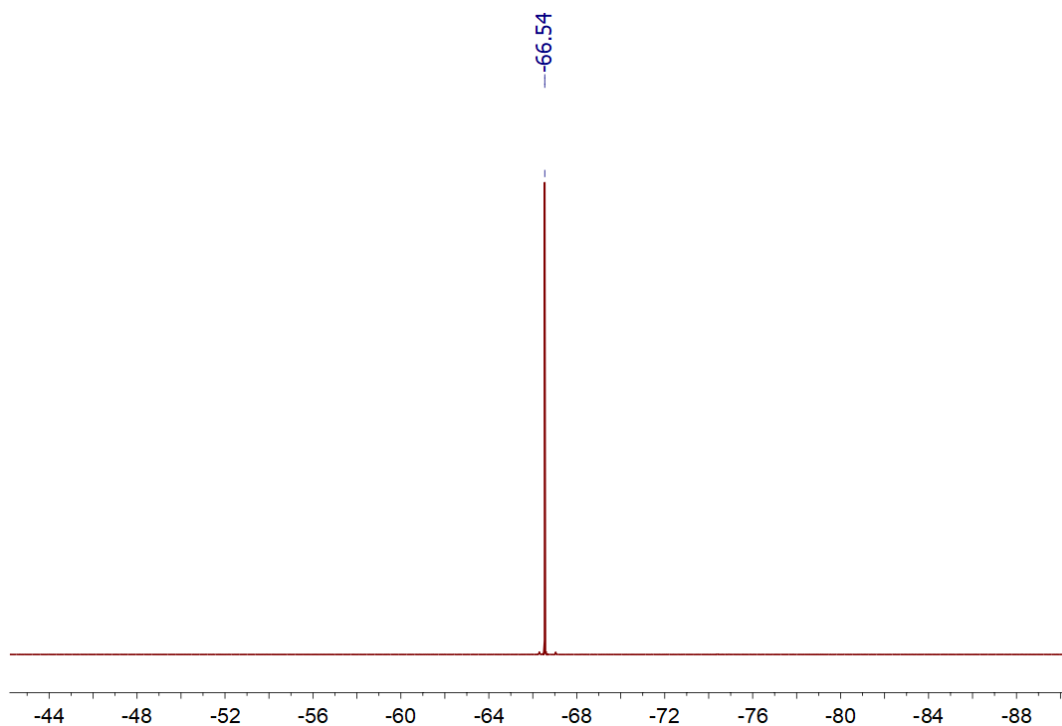
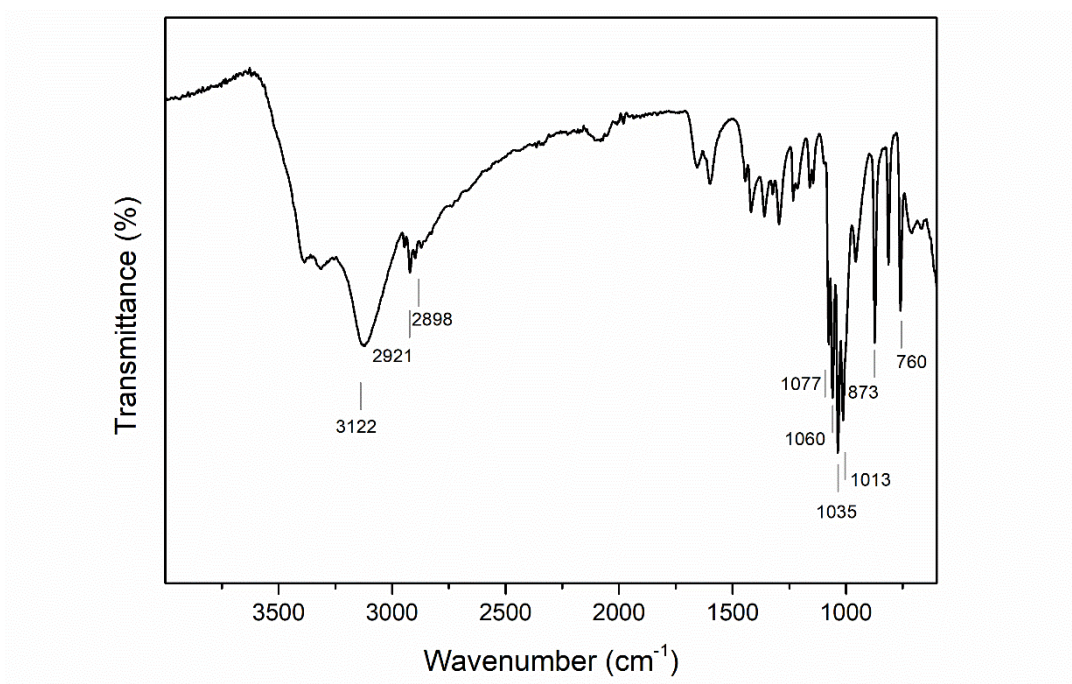


Figure A.1. $^{19}\text{F}\{^1\text{H}\}$ NMR spectrum (376.5 MHz) of 3-[(2,2,2-trifluoroethyl)thio]-1,2-propanethiol (**12**, **DiolSF**). Solvent: CDCl_3 .

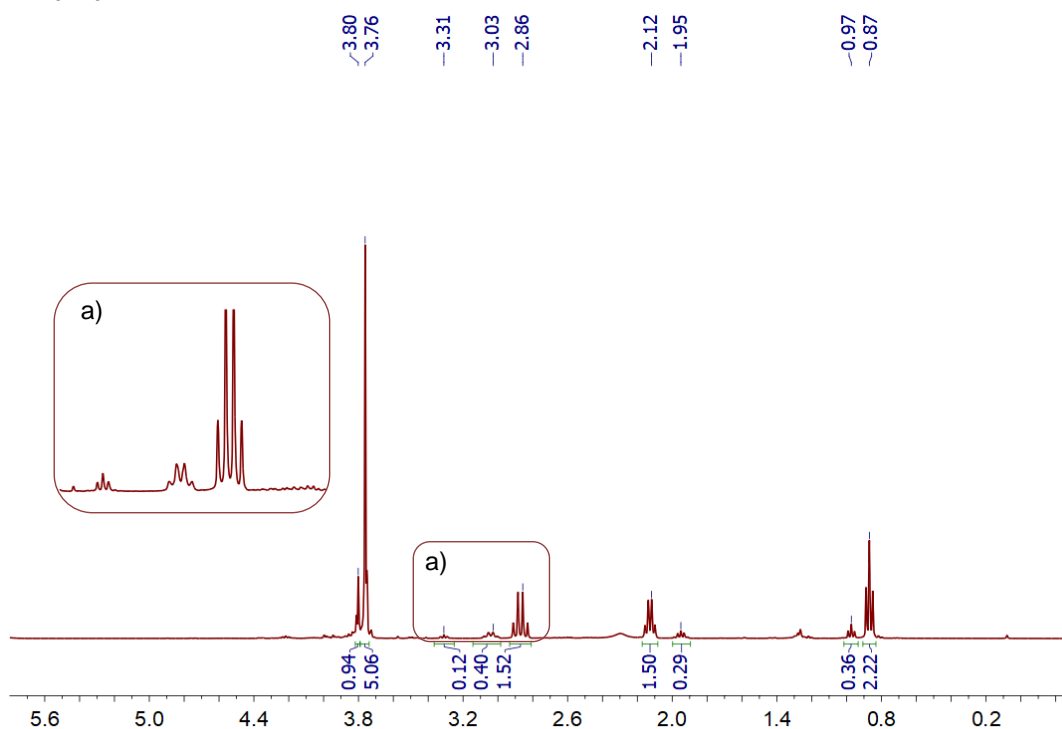


FTIR spectrum of **DiolSF**

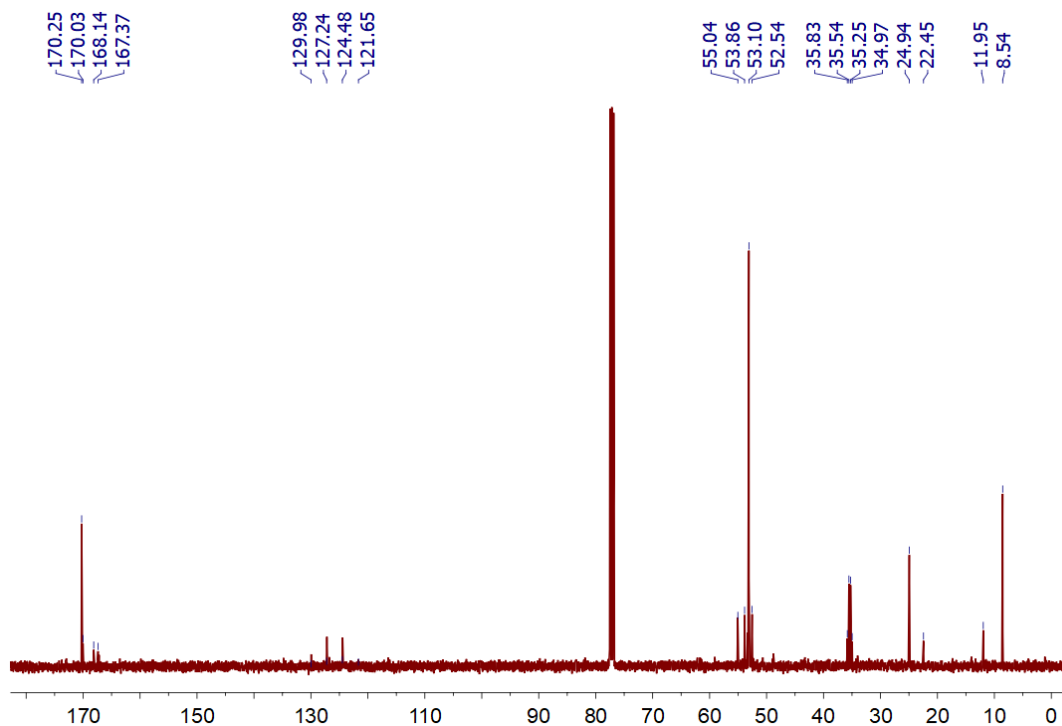


A.5. Dimethyl 2-ethyl-2-(2,2,2-trifluoroethyl) malonate (**15**)

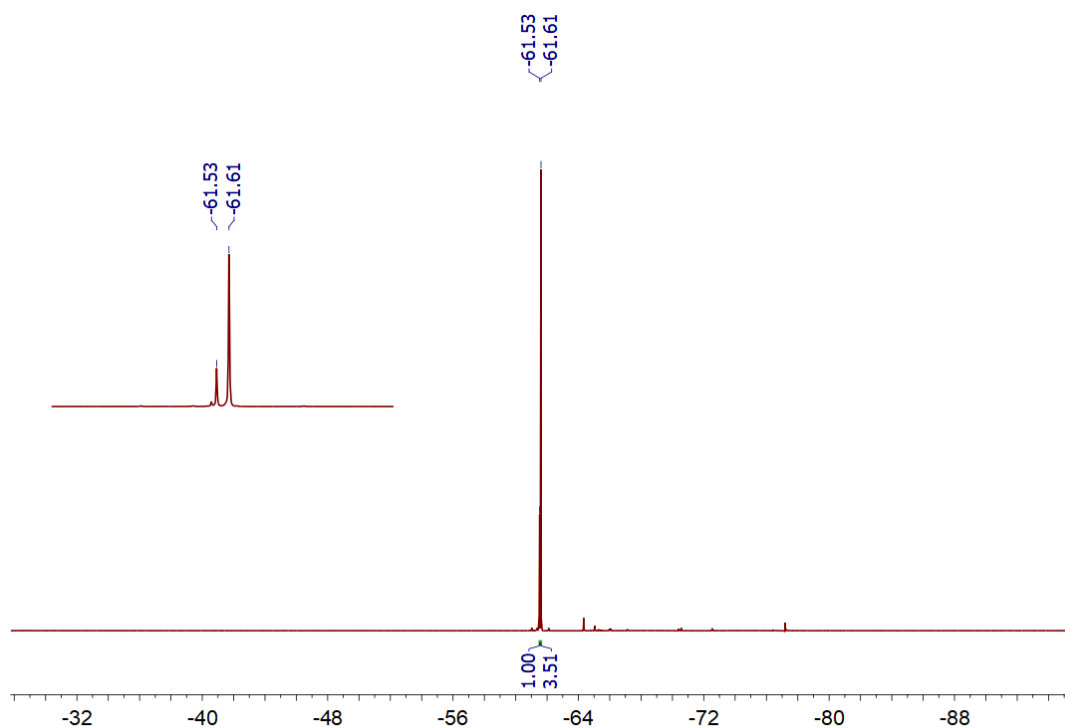
^1H NMR spectrum (400.1 MHz) of the extracted mixture of dimethyl 2-ethyl-2-(2,2,2-trifluoroethyl) malonate (**15**). Solvent: CDCl_3 .



$^{13}\text{C}\{^1\text{H}\}$ NMR spectrum (100.6 MHz) of the extracted mixture of dimethyl 2-ethyl-2-(2,2,2-trifluoroethyl) malonate (**15**). Solvent: CDCl_3 .

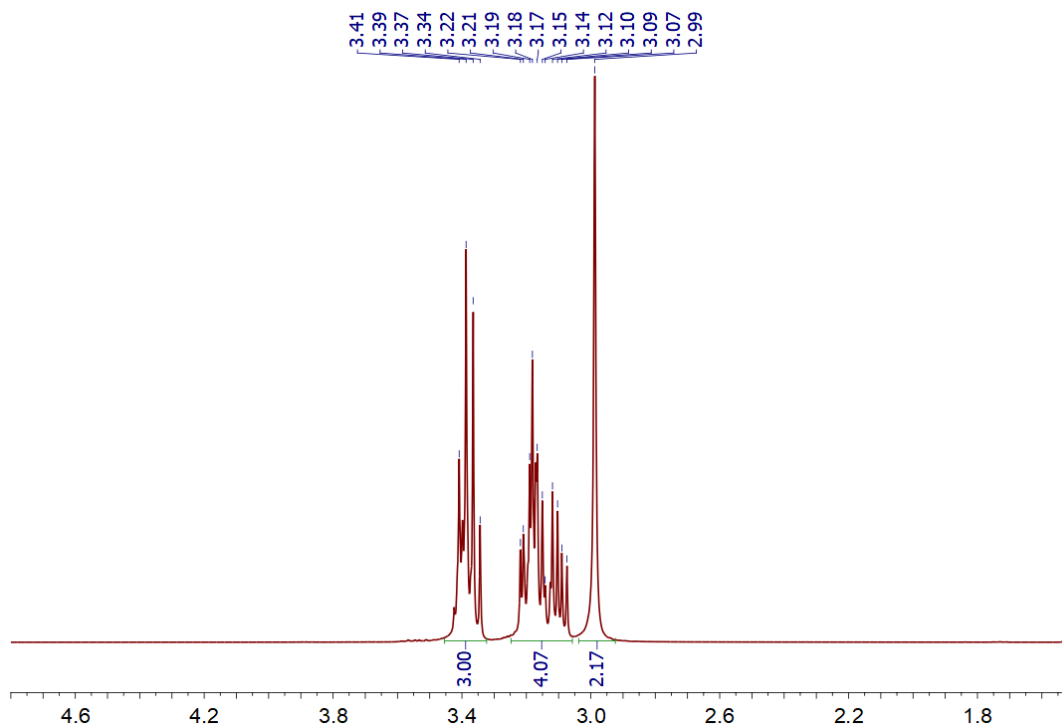


$^{19}\text{F}\{^1\text{H}\}$ NMR spectrum (376.5 MHz) of the extracted mixture of dimethyl 2-ethyl-2-(2,2,2-trifluoroethyl) malonate (**15**). Solvent: CDCl_3 .

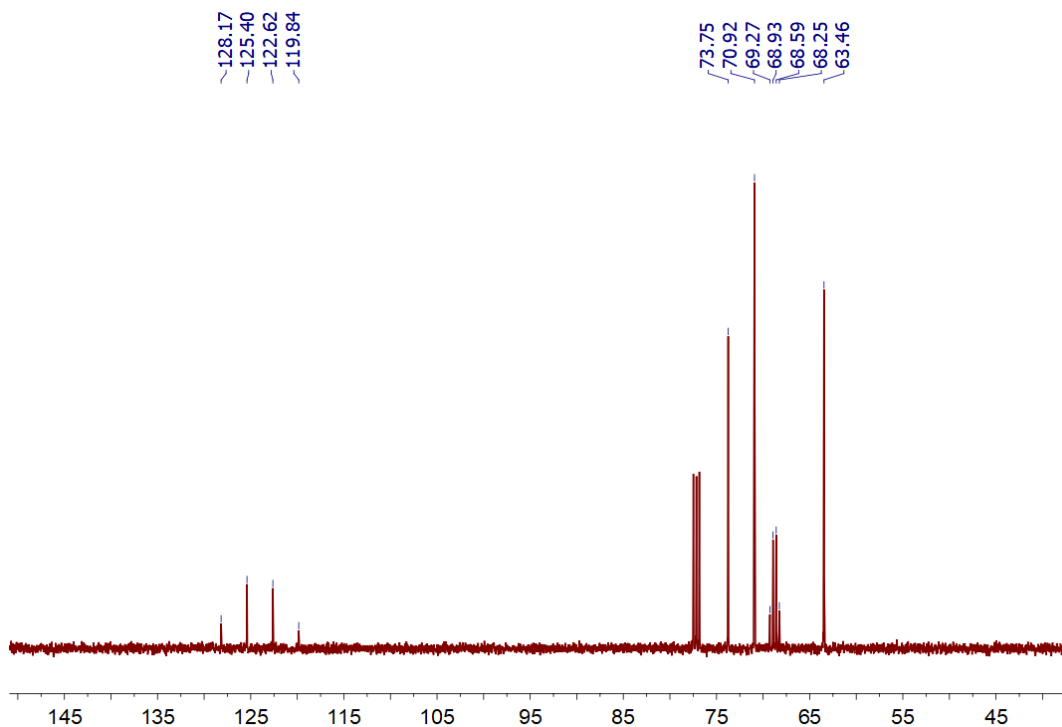


A.6. 3-(3,3,3-trifluoroethoxy)-1,2-propanediol (**18**, **DioIF**)

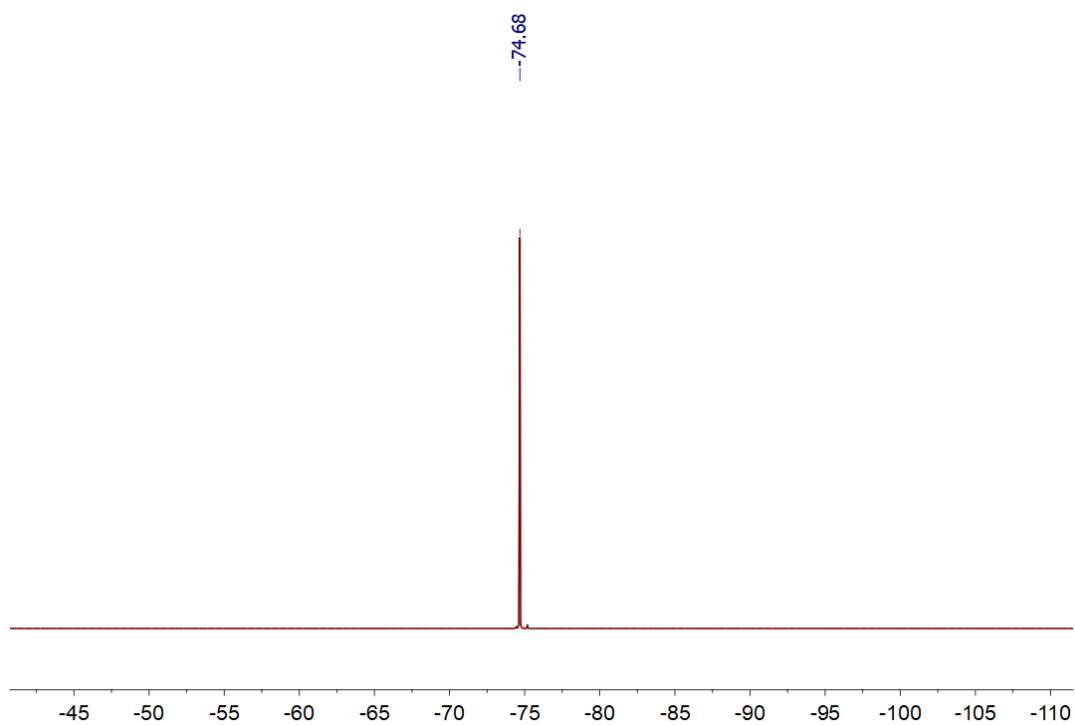
^1H NMR spectrum (400.1 MHz) of 3-(3,3,3-trifluoroethoxy)-1,2-propanediol (**18**, **DioIF**). Solvent: CDCl_3 .



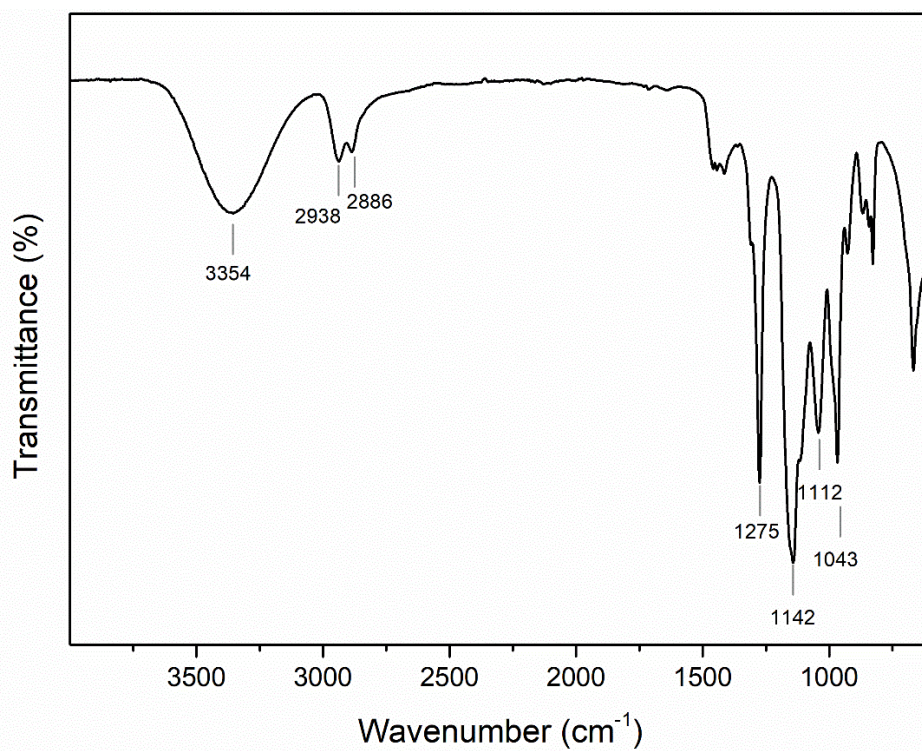
$^{13}\text{C}\{^1\text{H}\}$ NMR spectrum (100.6 MHz) 3-(3,3,3-trifluoroethoxy)-1,2-propanediol (**18**, **DioIF**). Solvent: CDCl_3 .



$^{19}\text{F}\{^1\text{H}\}$ NMR spectrum (376.5 MHz) 2,2,2-trifluoroethyl malonate (**15**). Solvent: CDCl_3 .



FTIR spectrum of **DioIF**.



A.7. ϵ -caprolactone (ECL)

Figure A.2. ^1H NMR spectra of **ECL** from Company A. Sample 1 and 2 was recorded at 400 MHz and Sample C at 360 MHz. Solvent: CDCl_3 .

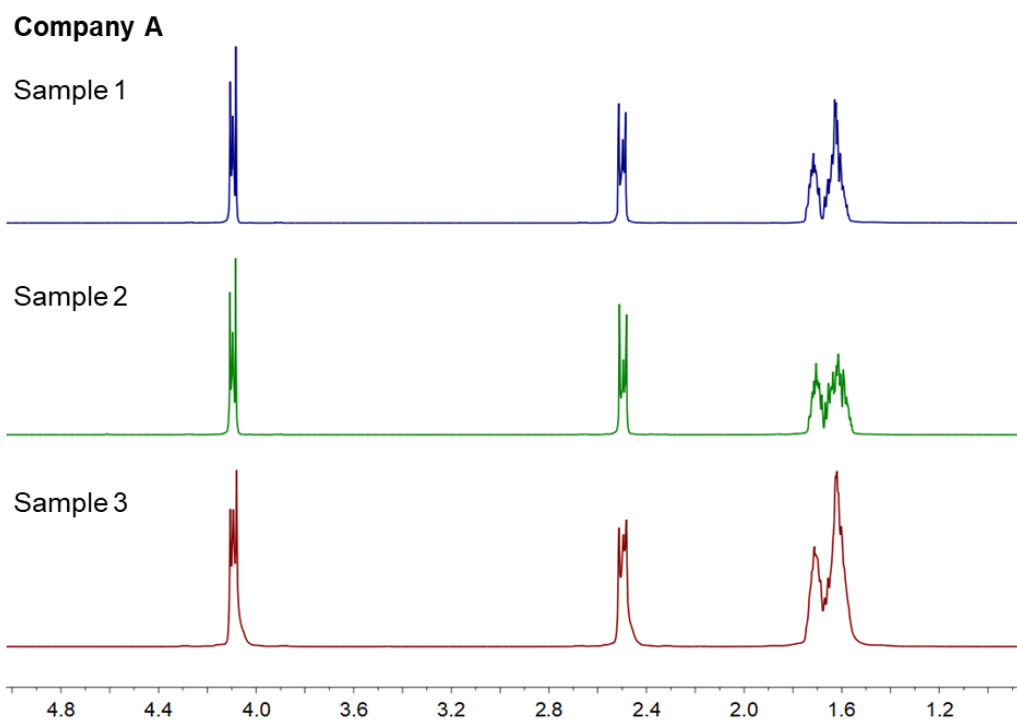
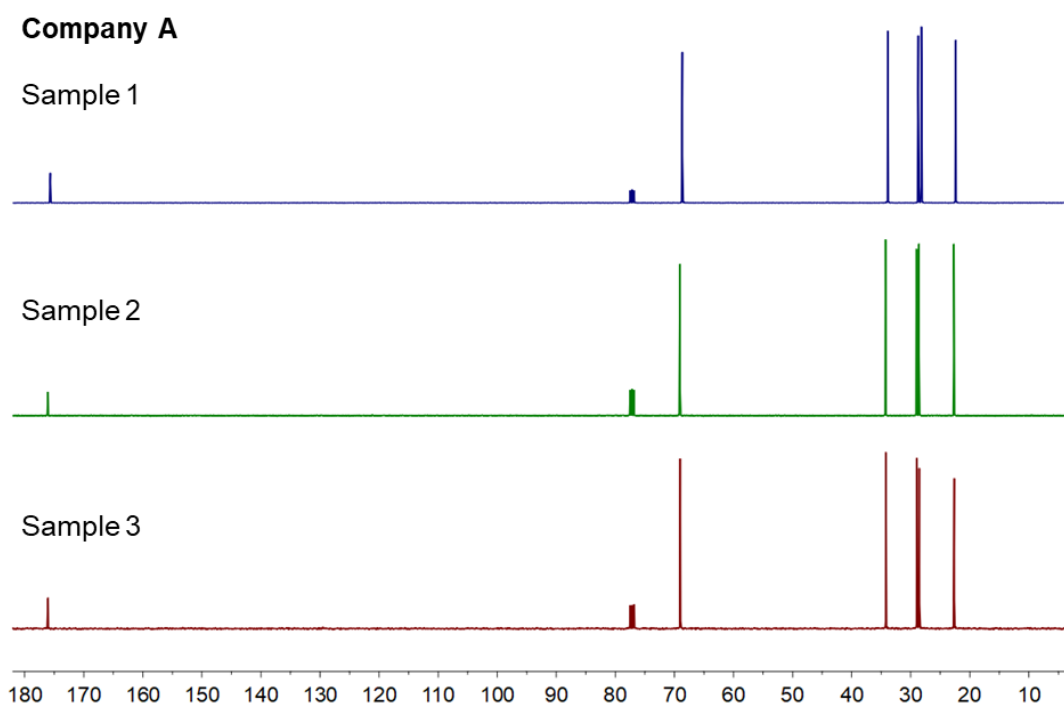


Figure A.3. $^{13}\text{C}\{^1\text{H}\}$ NMR spectra of **ECL** from Company A. Sample 1 and 2 was recorded at 100.6 MHz and Sample C at 90.6 MHz. Solvent: CDCl_3 .



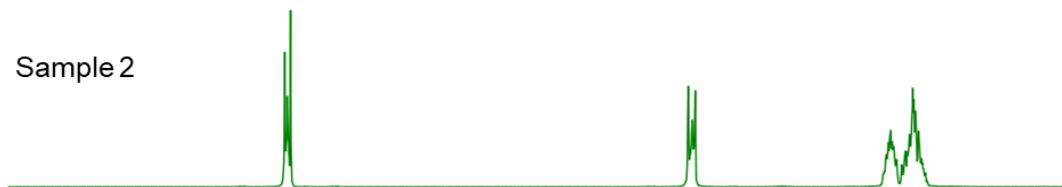
^1H NMR spectra (400 MHz) of **ECL** from Company B. Solvent: CDCl_3 .

Company B

Sample 1



Sample 2



Sample 3

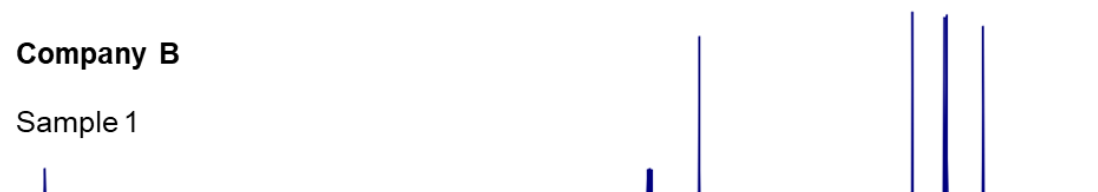


4.8 4.4 4.0 3.6 3.2 2.8 2.4 2.0 1.6 1.2

$^{13}\text{C}\{^1\text{H}\}$ NMR spectra (100.6 MHz) of **ECL** from Company A. Solvent: CDCl_3 .

Company B

Sample 1



Sample 2

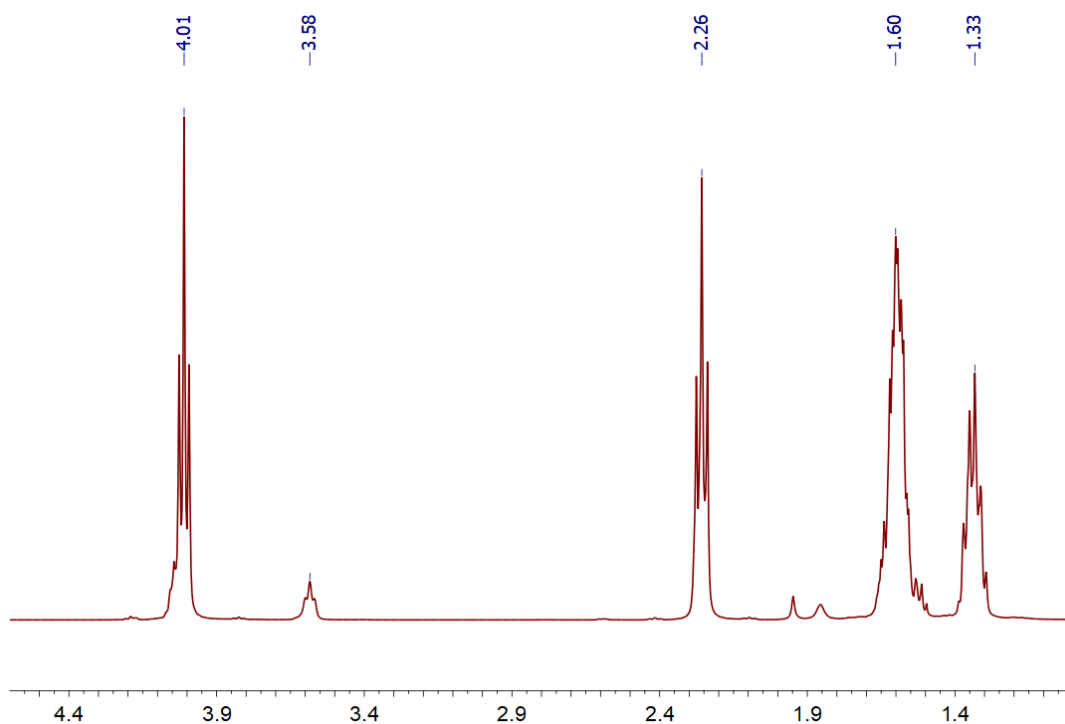


Sample 3



180 170 160 150 140 130 120 110 100 90 80 70 60 50 40 30 20 10

^1H NMR spectra (400 MHz) of **PCL-BDO** from Company A's **ECL** recorded with a 10 second time delay to ensure quantification. Solvent: CDCl_3 .



$^{13}\text{C}\{^1\text{H}\}$ NMR spectra (100.6 MHz) of **PCL-BDO** from Company A's **ECL**. Solvent: CDCl_3 .

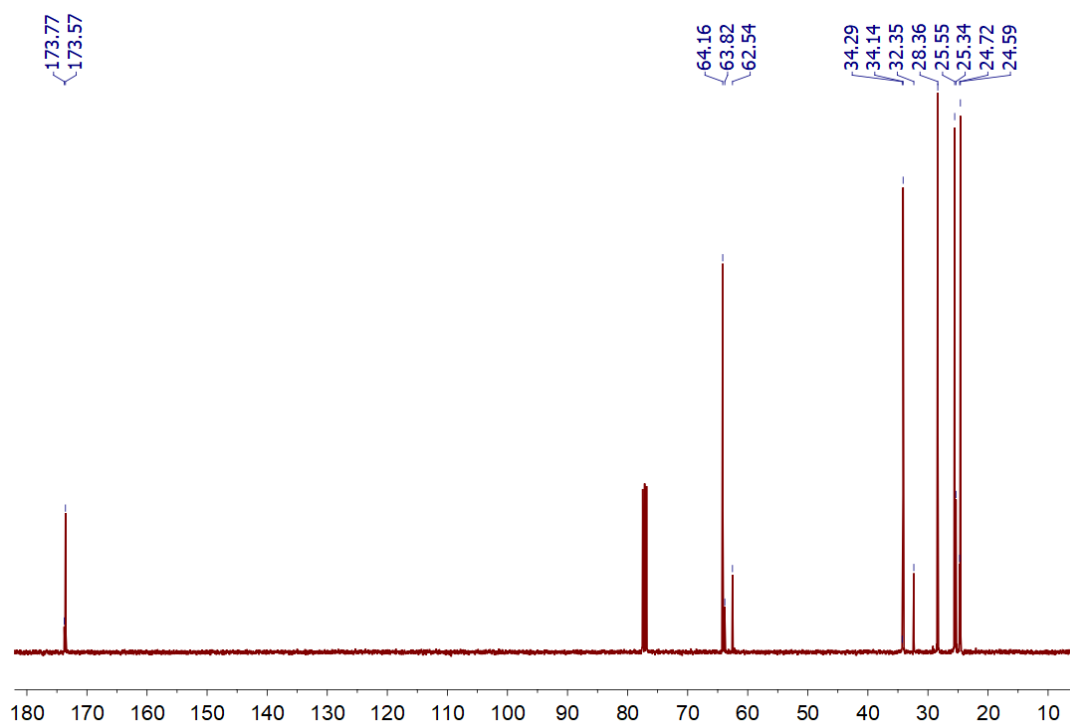
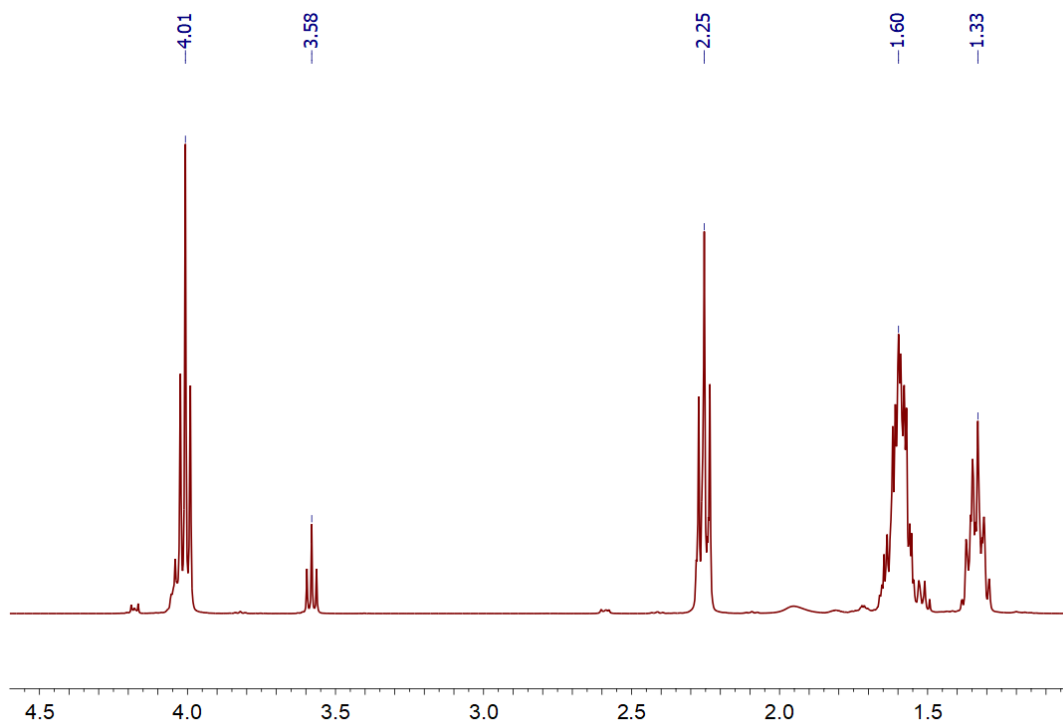
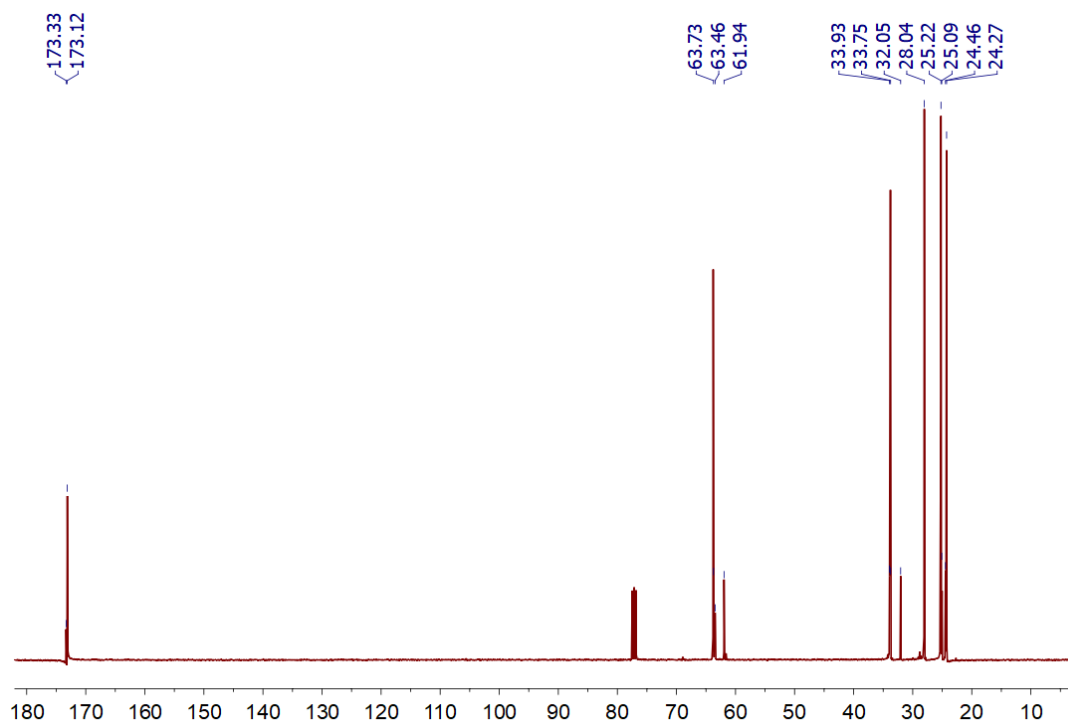


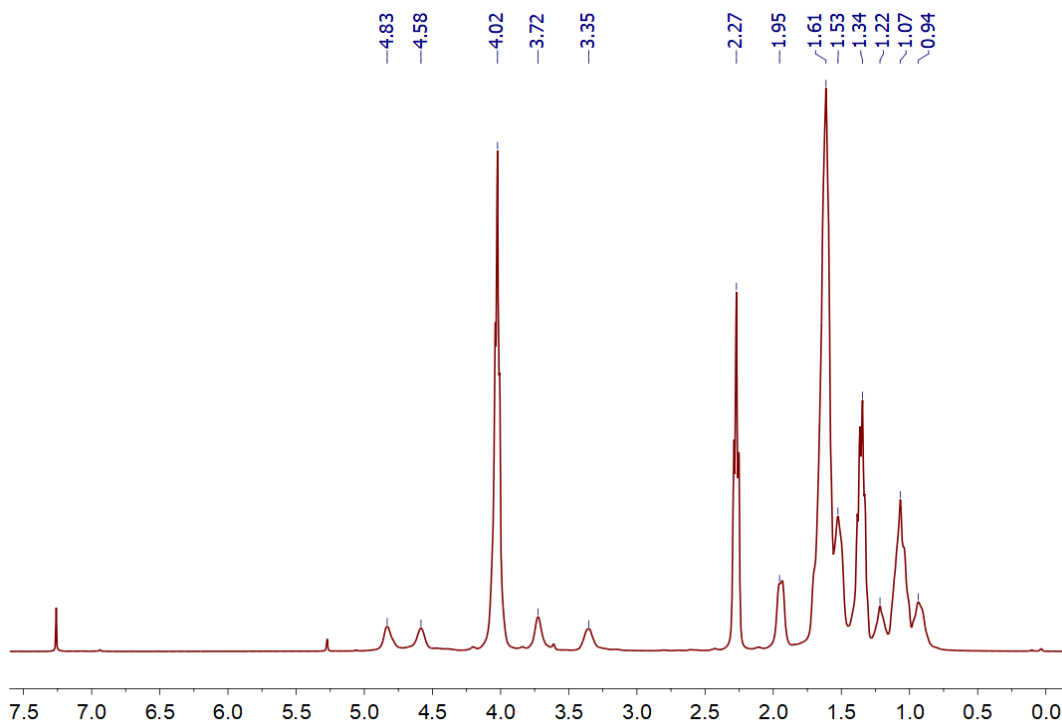
Figure A.4. ^1H NMR spectra (400 MHz) of **PCL-BDO** from Company B's **ECL** recorded with a 10 second time delay to ensure quantification. Solvent: CDCl_3 .



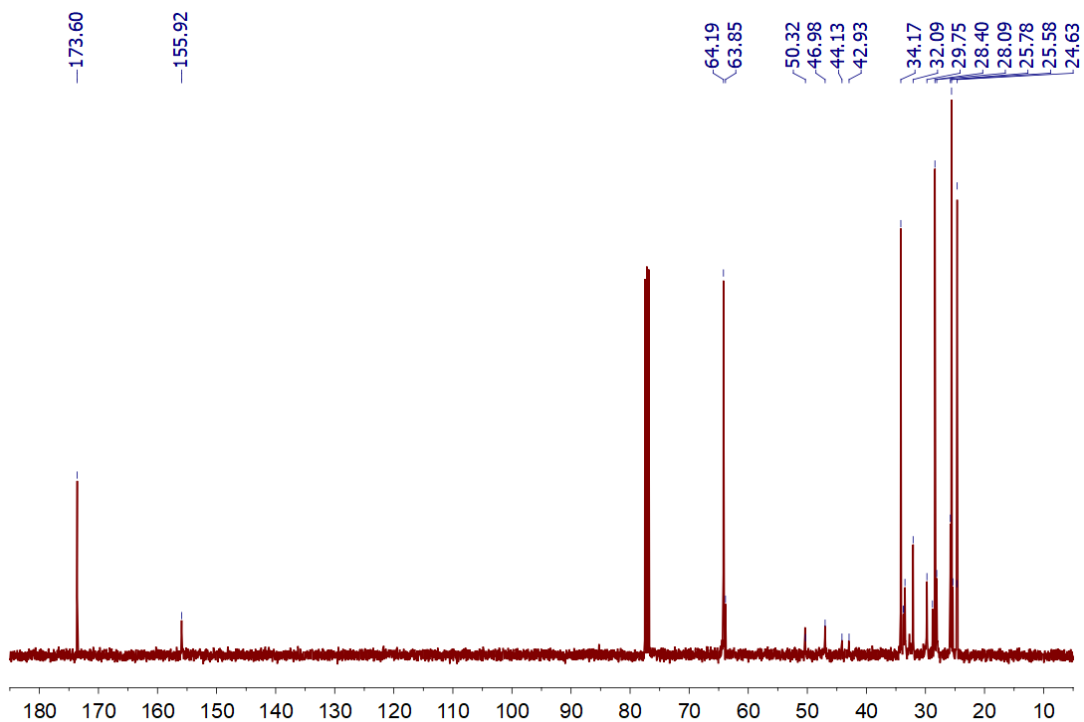
$^{13}\text{C}\{^1\text{H}\}$ NMR spectra (100.6 MHz) of **PCL-BDO** from Company B's **ECL**. Solvent: CDCl_3 .



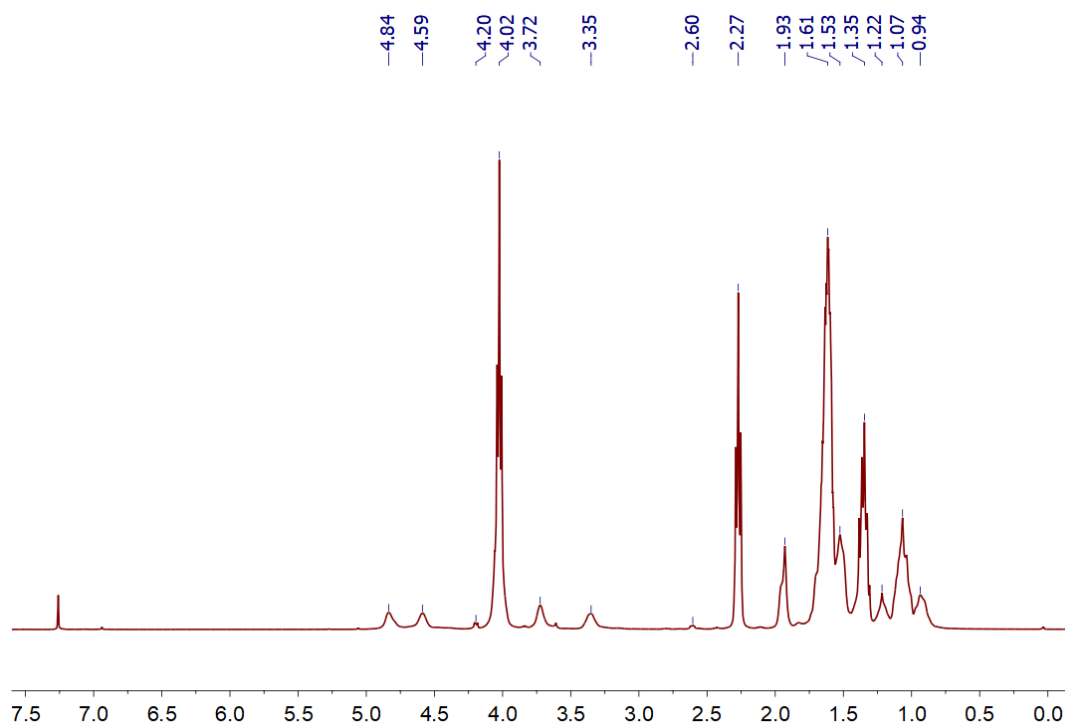
^1H NMR spectra (400 MHz) of **TPU** from Company A's **ECL** recorded with a 10 second time delay to ensure quantification. Solvent: CDCl_3 .



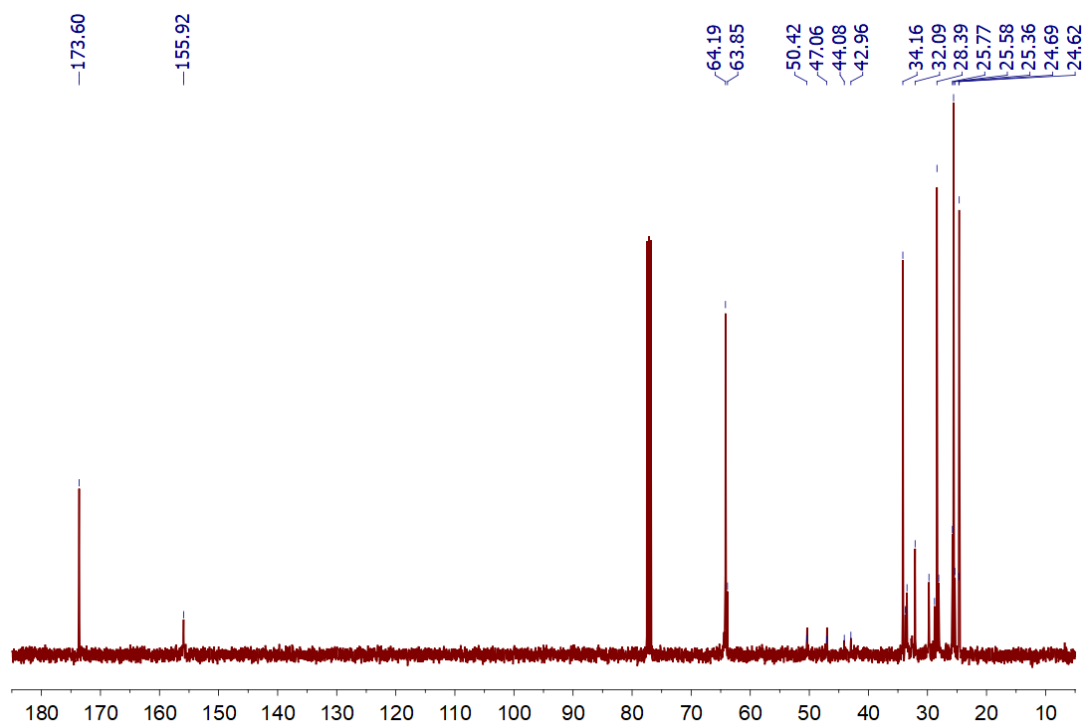
$^{13}\text{C}\{^1\text{H}\}$ NMR spectra (100.6 MHz) of **TPU** from Company A's **ECL**. Solvent: CDCl_3 .



^1H NMR spectra (400 MHz) of **TPU** from Company B's **ECL** recorded with a 10 second time delay to ensure quantification. Solvent: CDCl_3 .

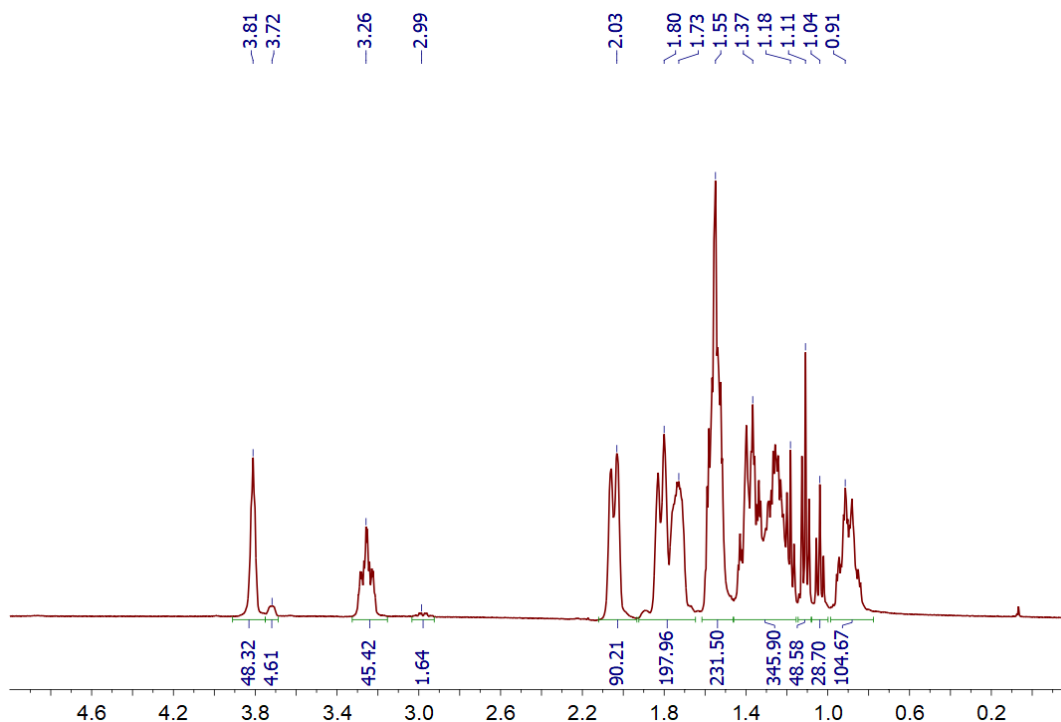


$^{13}\text{C}\{^1\text{H}\}$ NMR spectra (100.6 MHz) of **TPU** from Company B's **ECL**. Solvent: CDCl_3 .

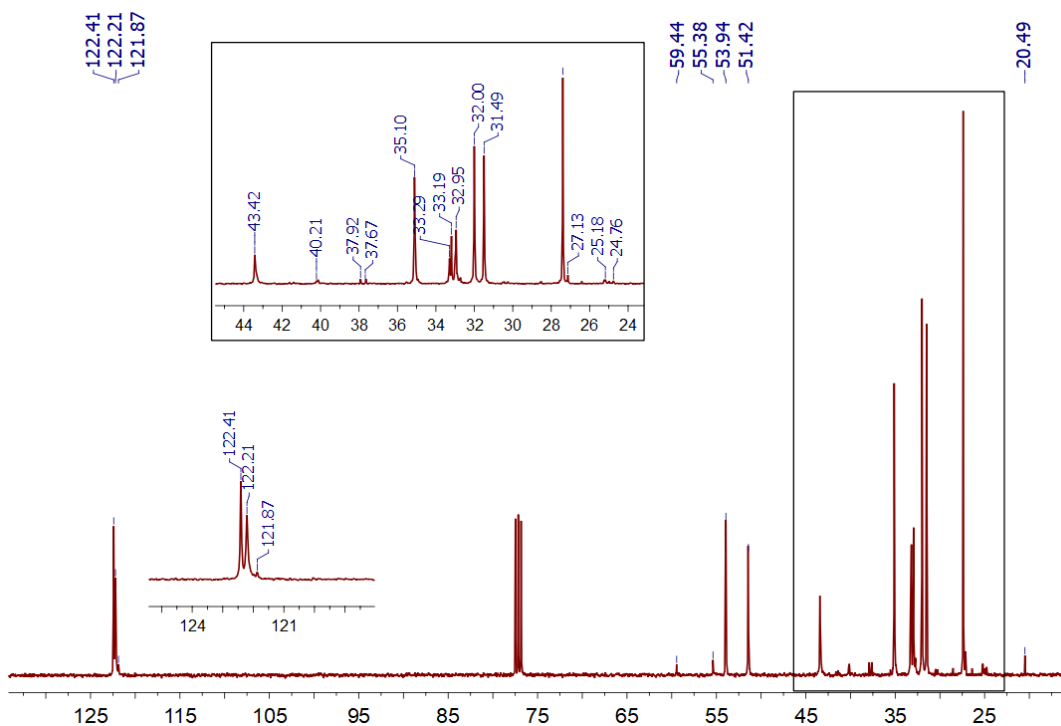


A.8. 4,4'-diisocyanate dicyclohexylmethane (H₁₂MDI)

¹H NMR spectrum (400 MHz) of **H₁₂MDI Sample 1** recorded with a delay time of 10 seconds to ensure the quantification. Solvent: CDCl₃.

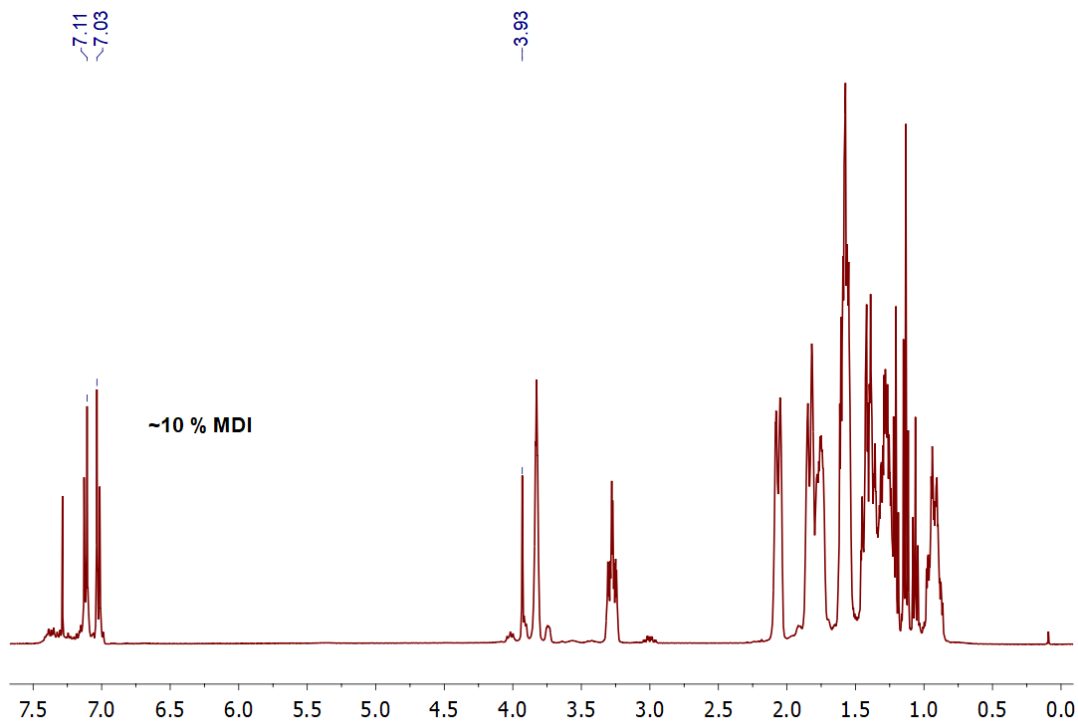


Quantitative ¹³C{¹H} NMR spectrum (100 MHz) of **H₁₂MDI Sample 3** recorded with a delay time of 20 seconds to ensure the quantification. Solvent: CDCl₃.

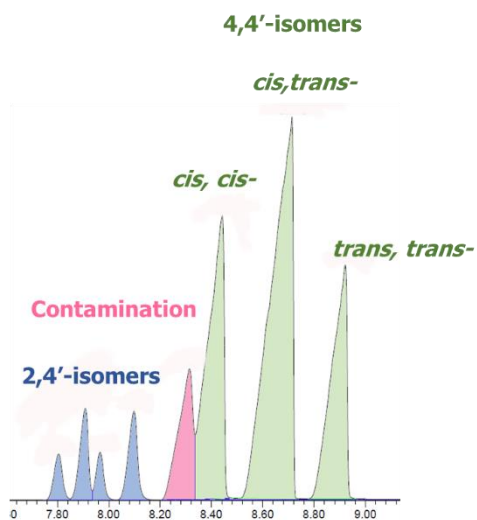


Sample 3.

^1H NMR spectrum (400 MHz) of **H₁₂MDI Sample 3** recorded with a delay time of 10 seconds to ensure the quantification. Peaks denoted with the chemical shift correspond to the **MDI** contamination. Solvent: CDCl_3 .

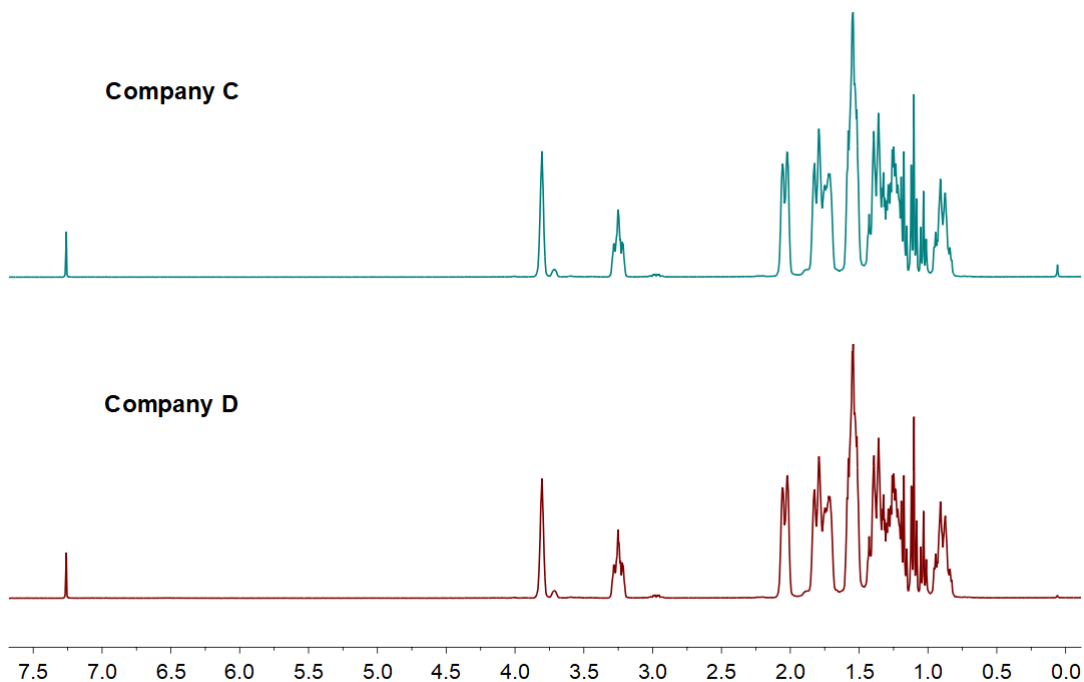


GC chromatogram of **Sample 3** of **H₁₂MDI**.

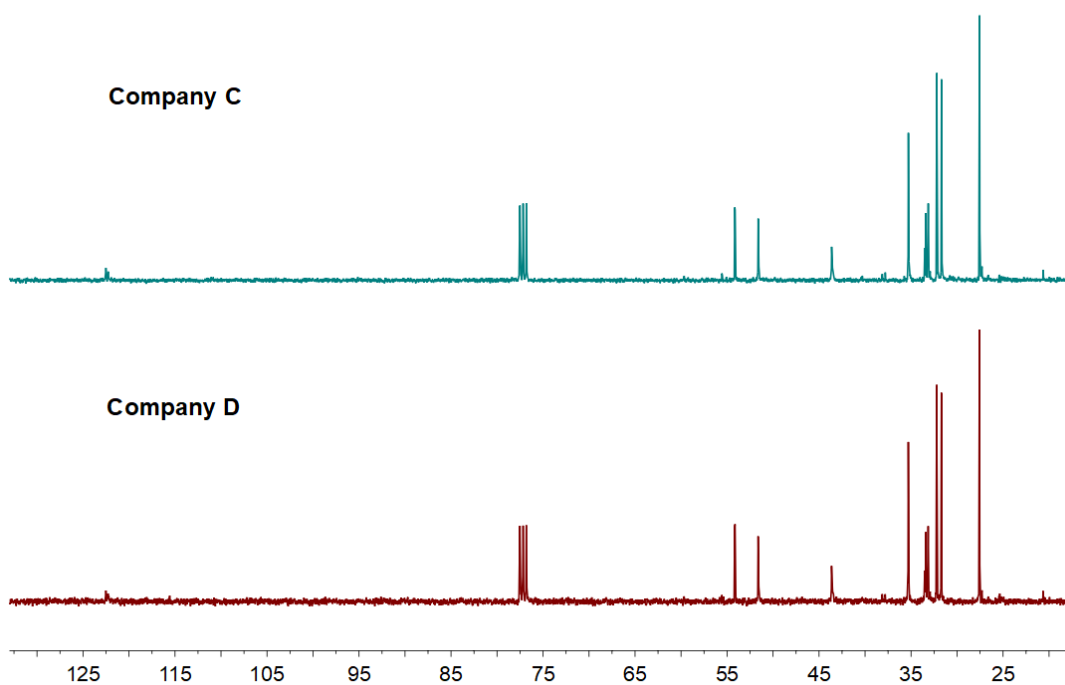


Supplier validation

^1H NMR spectra (400 MHz) of **H₁₂MDI mixture** of Company C (top) and Company D (bottom), recorded with a delay time of 10 seconds to ensure the quantification. Solvent: CDCl_3 .

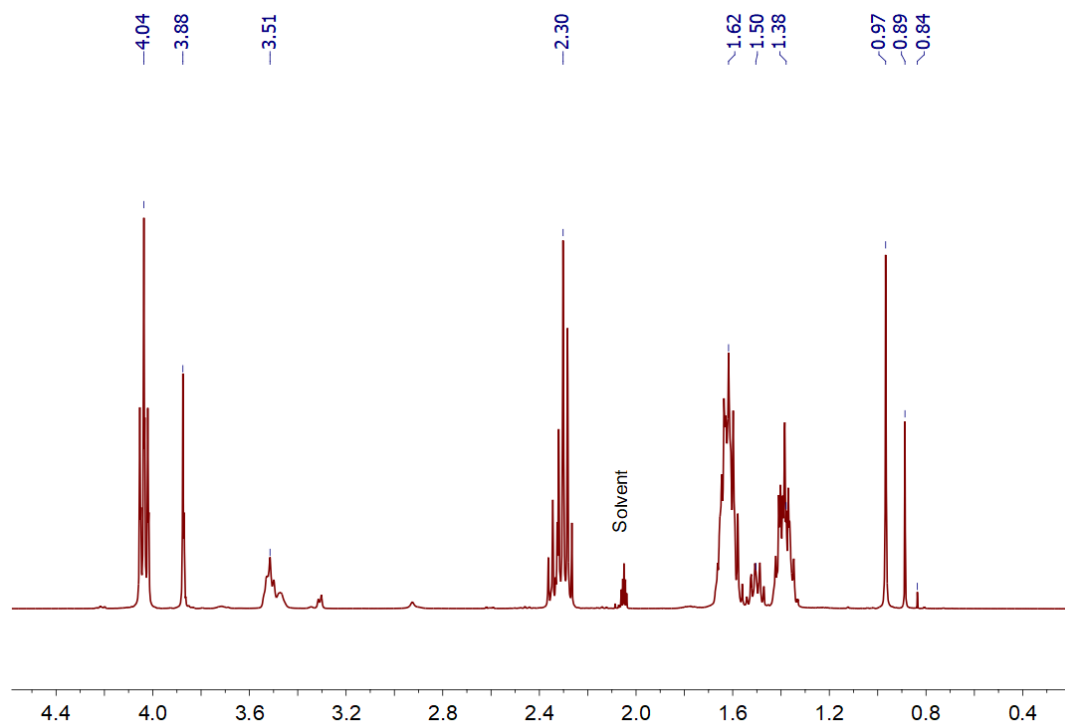


$^{13}\text{C}\{^1\text{H}\}$ NMR spectrum (100 MHz) of **H₁₂MDI mixture** of Company C (top) and Company D (bottom). Solvent: CDCl_3 .

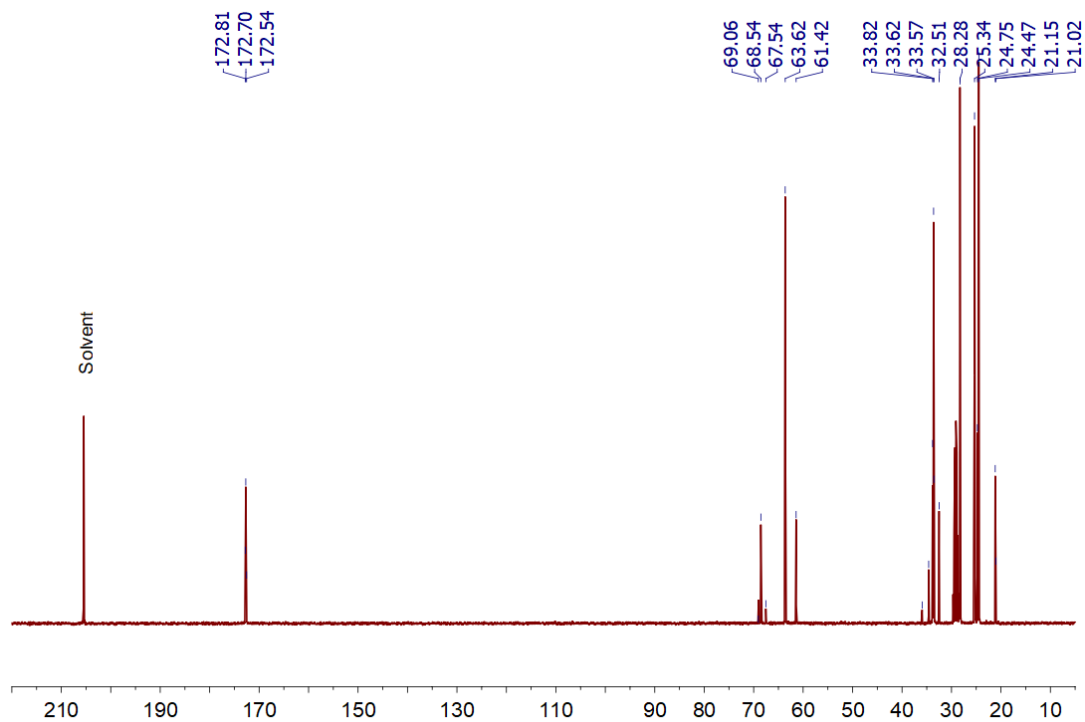


A.9. Polycaprolactone initiated by neopentyl glycol (PCL-NPG)

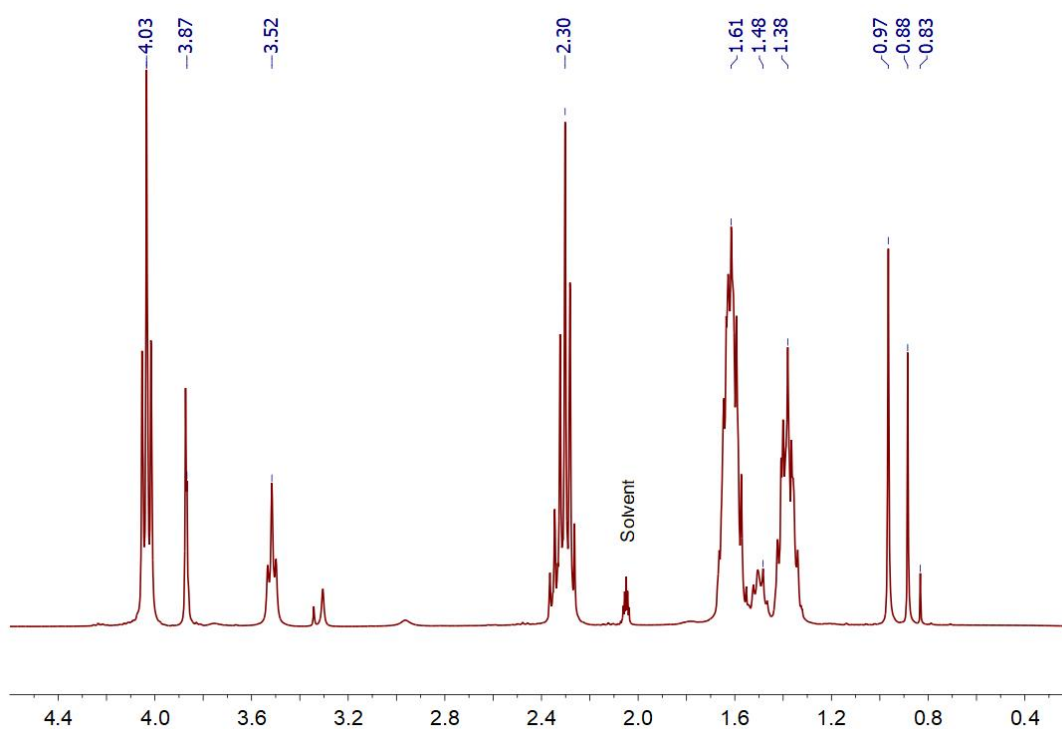
^1H NMR spectrum (400 MHz) of **PCL-1**. Solvent: Acetone- d_6 .



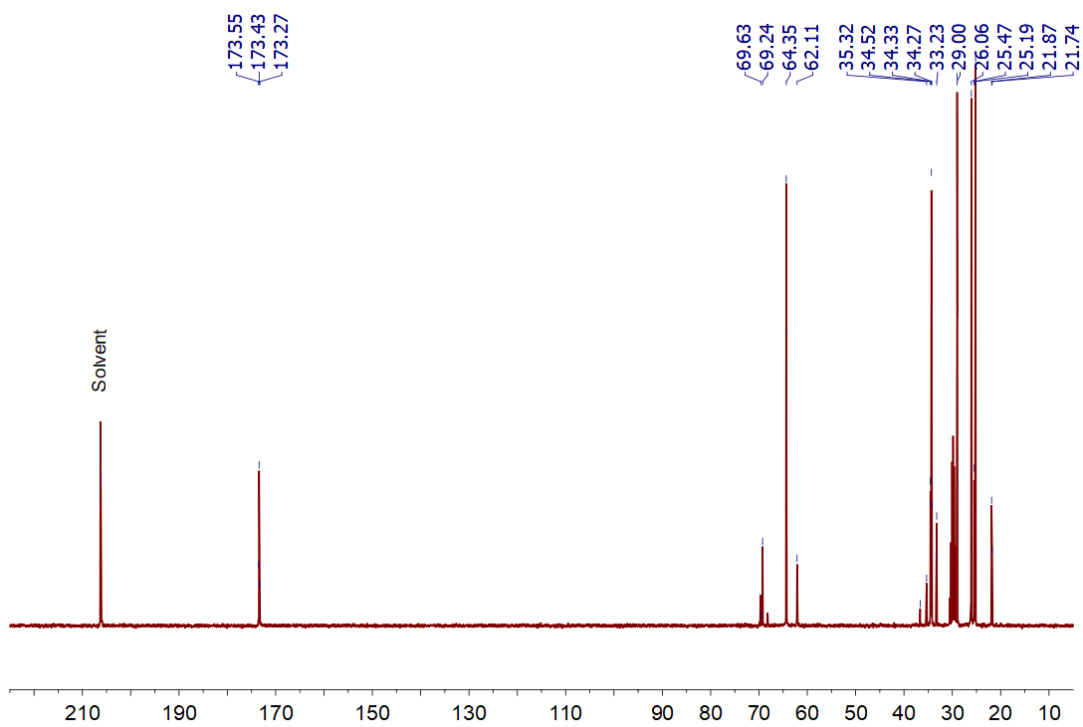
$^{13}\text{C}\{^1\text{H}\}$ NMR spectrum (100.6 MHz) of **PCL-1**. Solvent: Acetone- d_6 .



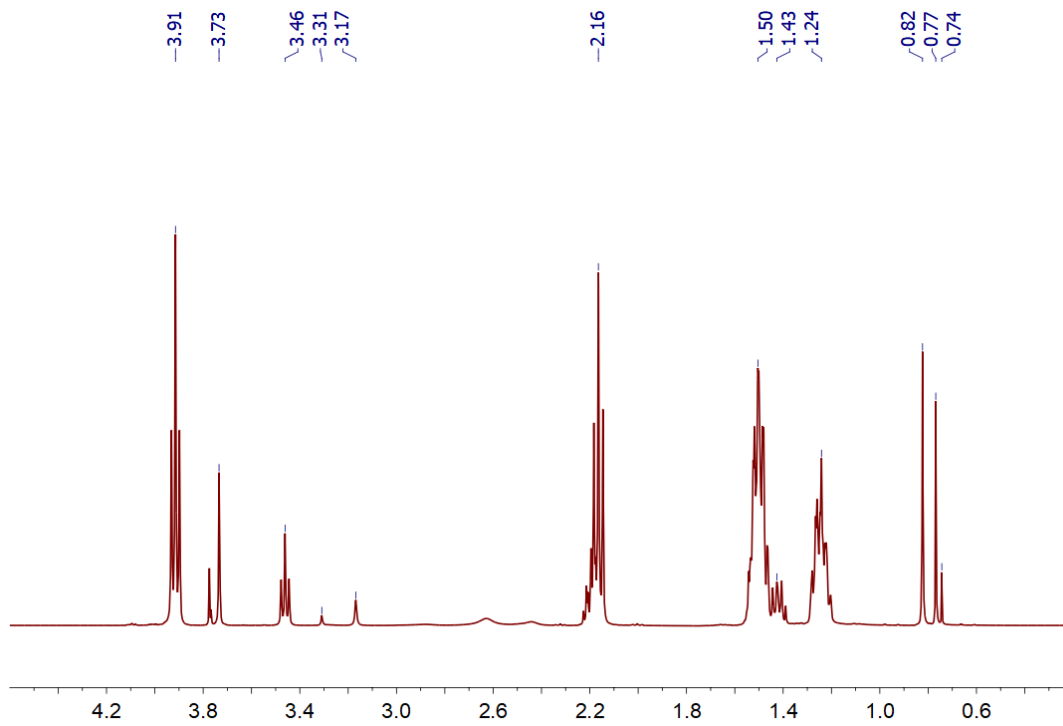
^1H NMR spectrum (400 MHz) of **PCL-2**. Solvent: Acetone- d_6 .



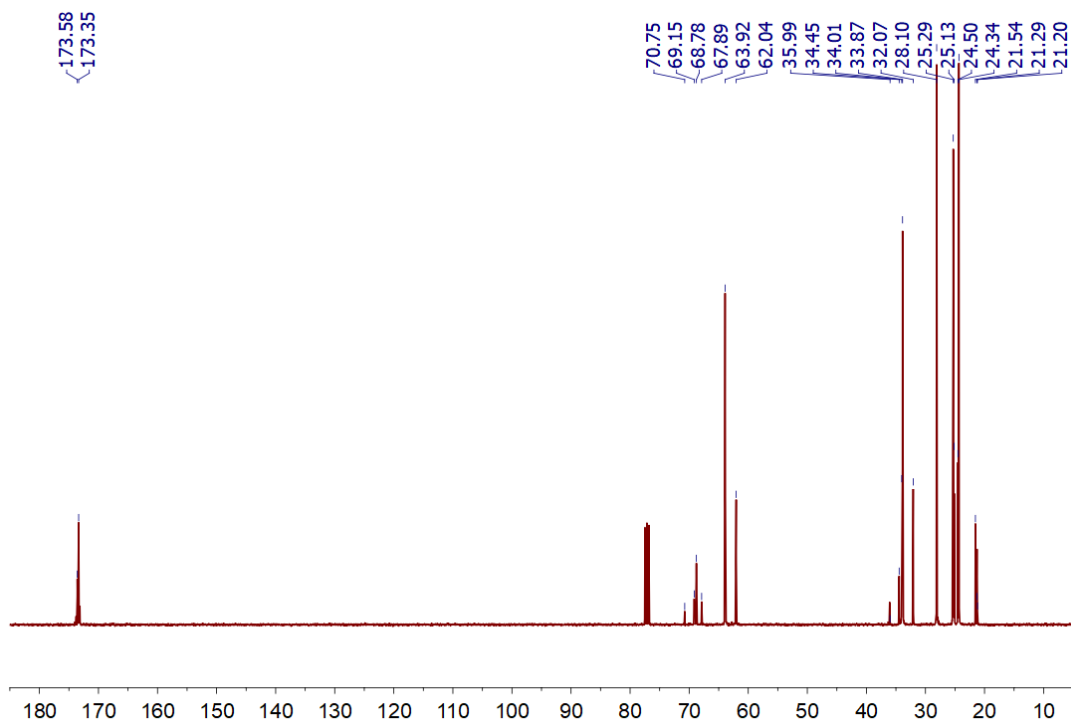
$^{13}\text{C}\{^1\text{H}\}$ NMR spectrum (100.6 MHz) of **PCL-2**. Solvent: Acetone- d_6 .



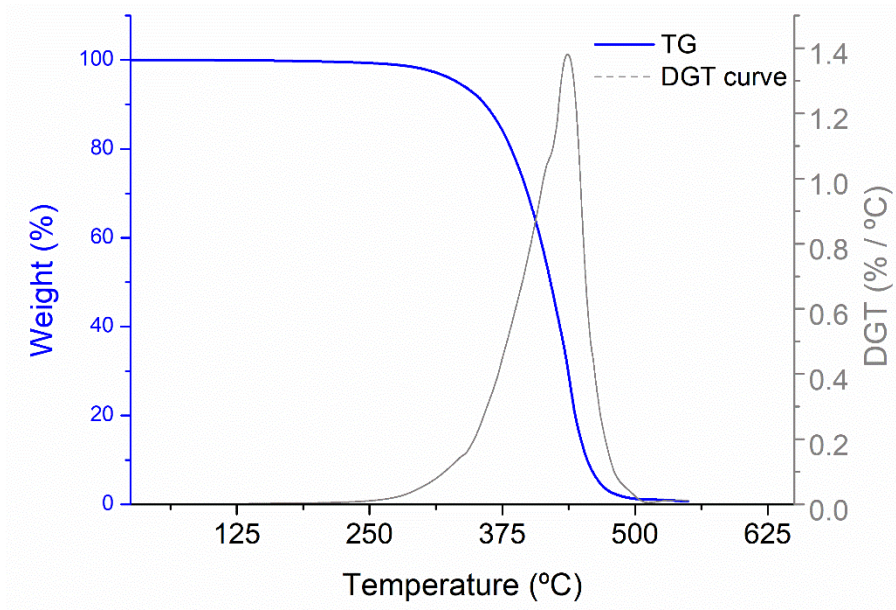
^1H NMR spectra (400 MHz) **PCL-3**. Solvent: CDCl_3 .



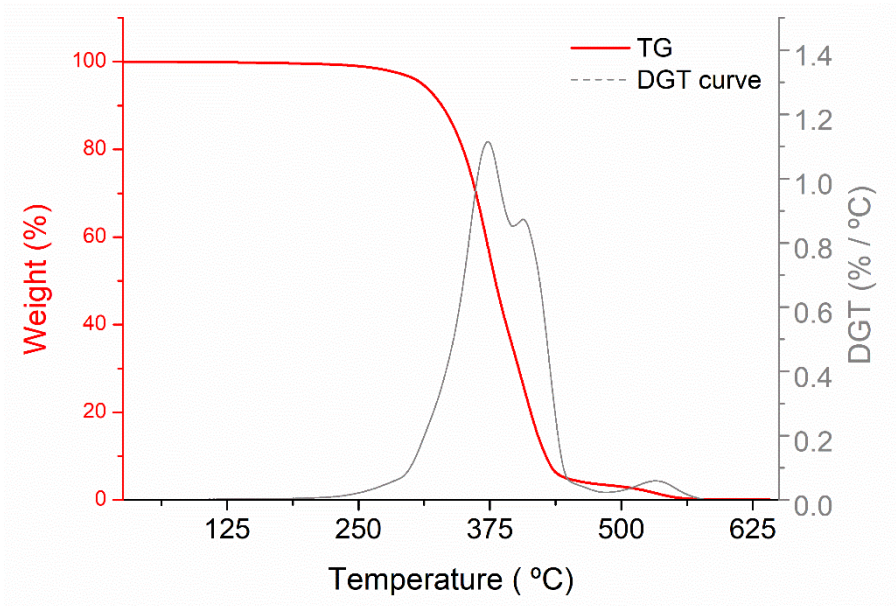
$^{13}\text{C}\{^1\text{H}\}$ NMR spectrum (100 MHz) of **PCL-3**. Solvent: CDCl_3 .



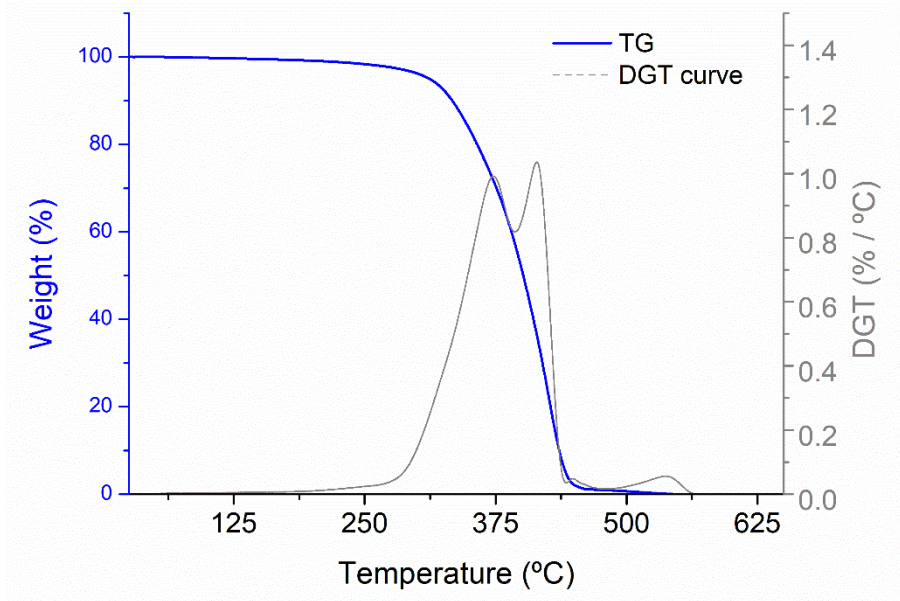
Thermogram profile of **PCL-1** and the corresponding DGT curve under inert atmosphere.



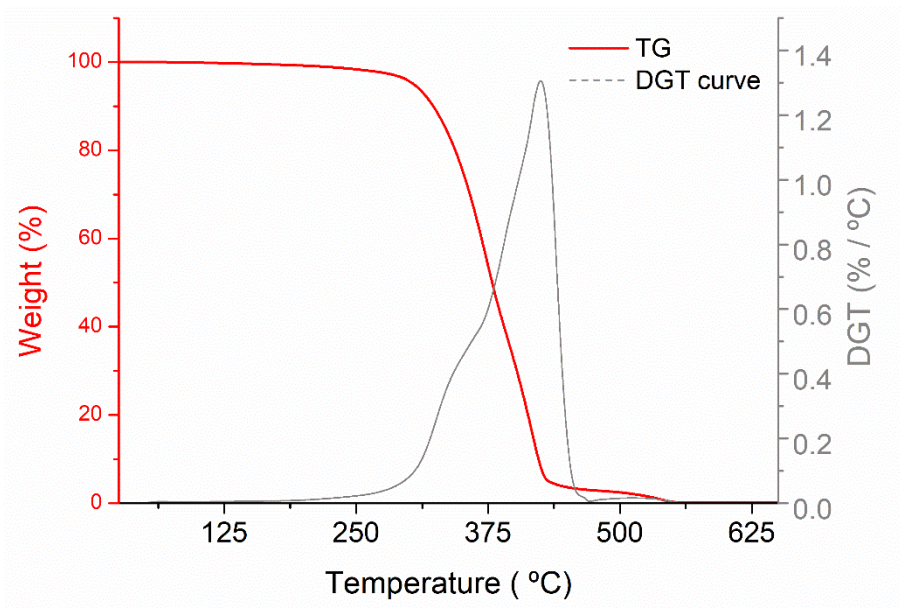
Thermogram profile of the **PCL-1** and the corresponding DGT curve under oxidative atmosphere.



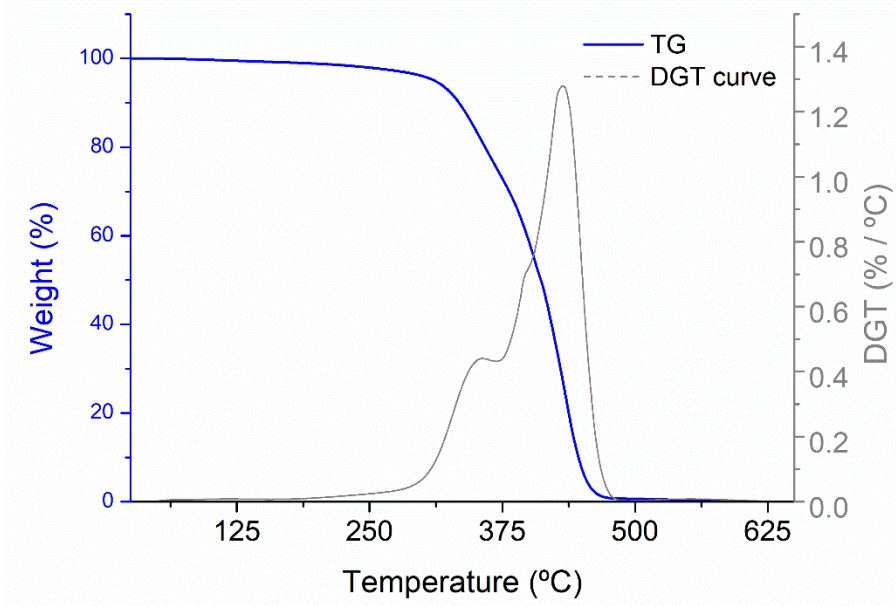
Thermogram profile of **PCL-2** and the corresponding DGT curve under inert atmosphere.



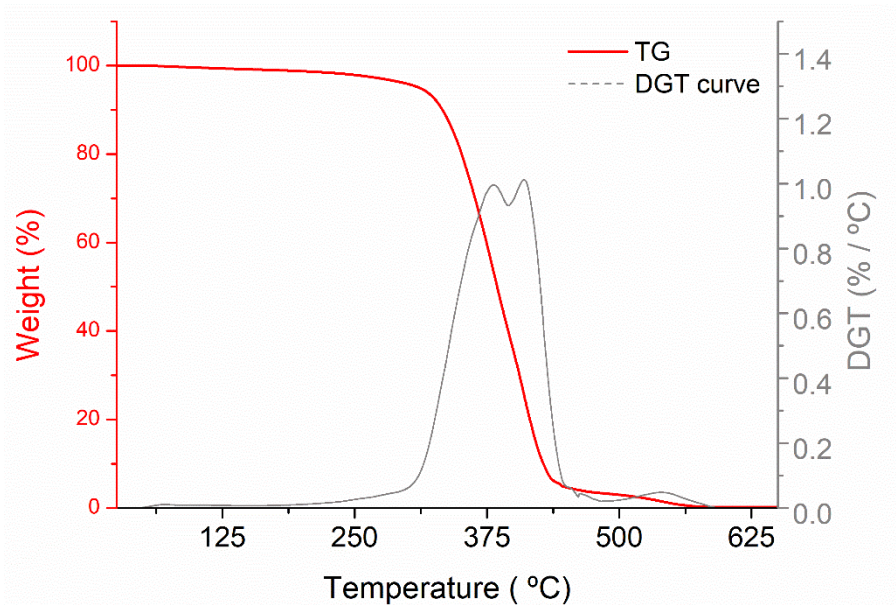
Thermogram profile of the **PCL-2** and the corresponding DGT curve under oxidative atmosphere.



Thermogram profile of **PCL-3** and the corresponding DGT curve under inert atmosphere.

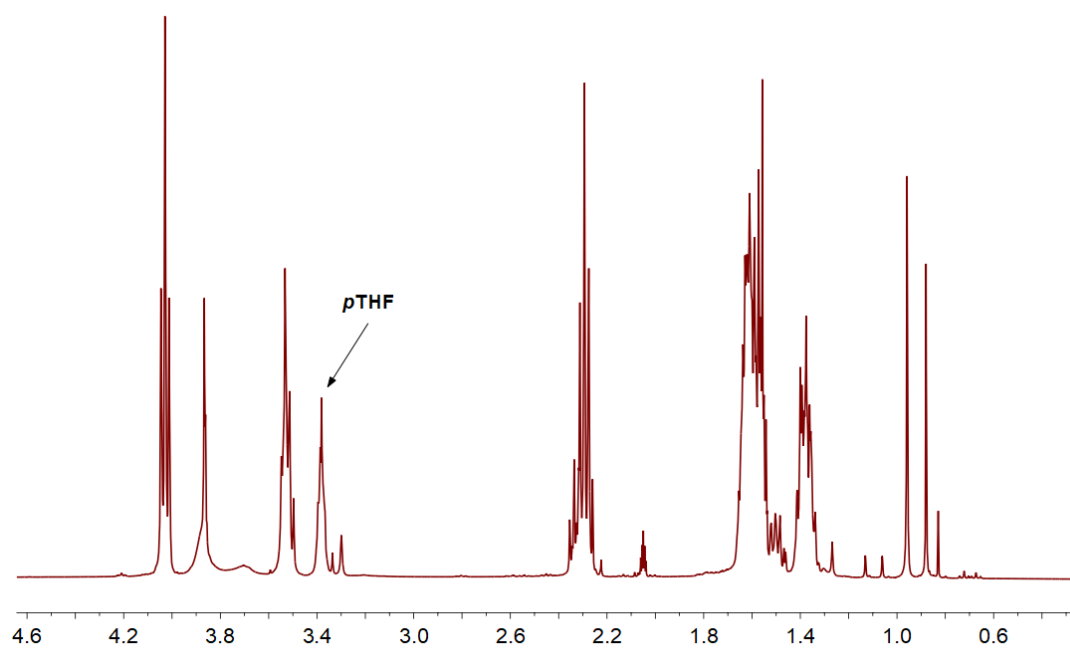


Thermogram profile of the **PCL-3** and the corresponding DGT curve under oxidative atmosphere.



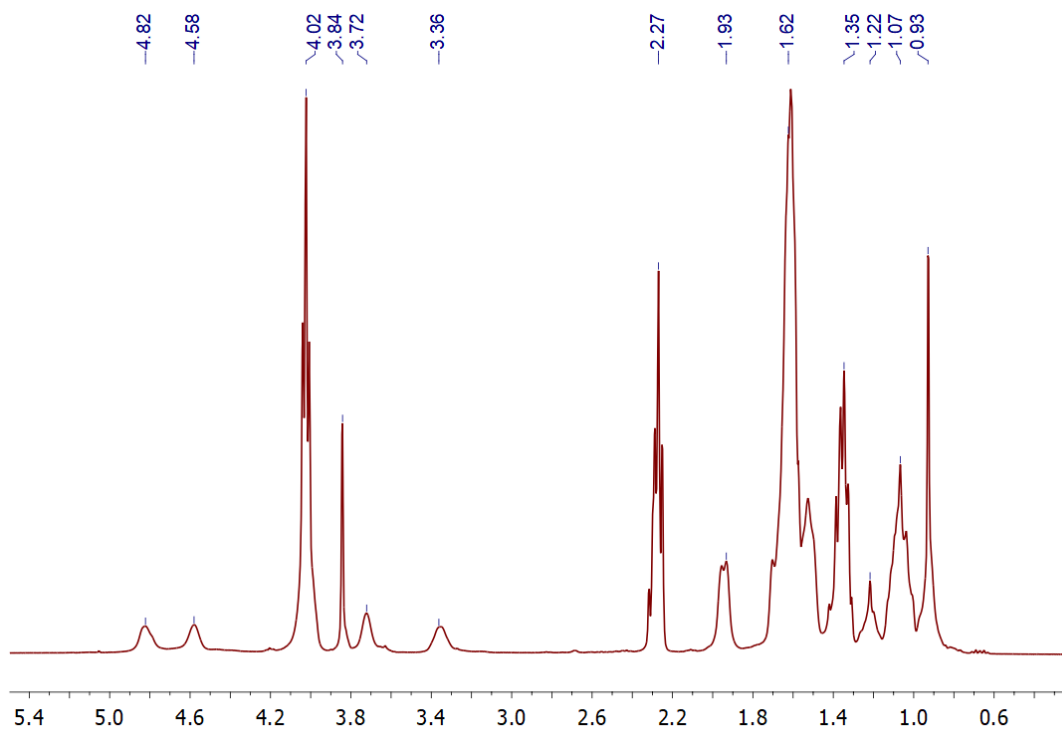
A.10. Polyol mixture

^1H NMR (400 MHz) spectrum the contaminated sample **Polyol mixture 3**. Solvent: Acetone- d_6 .

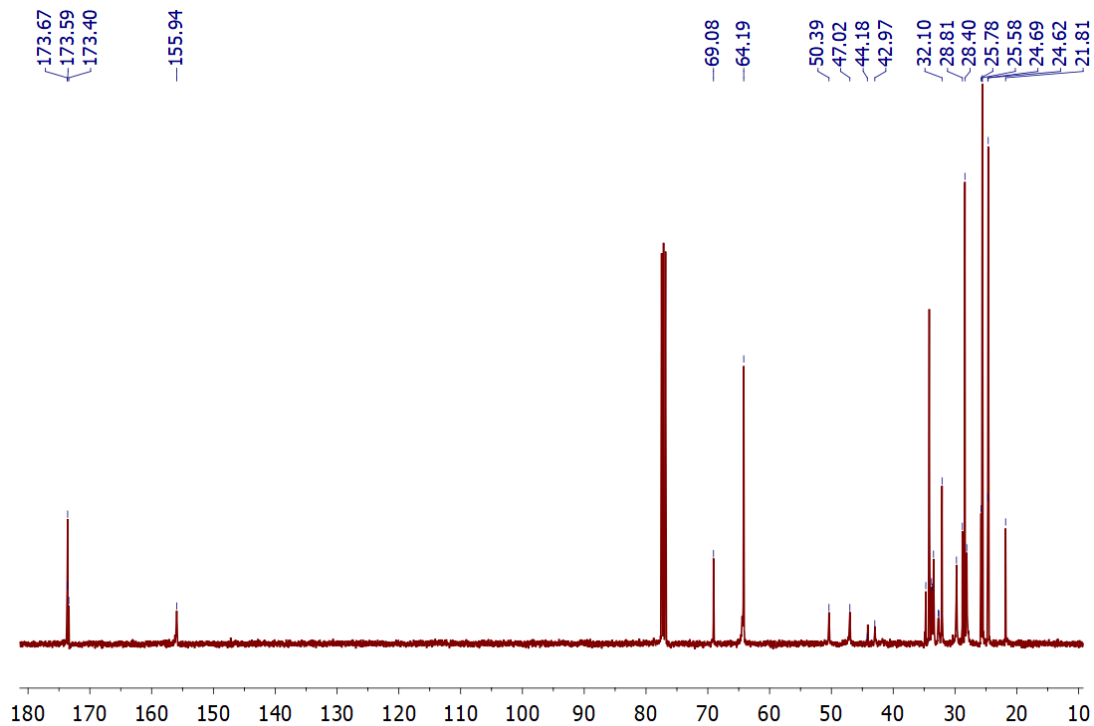


A.11. TPU for films

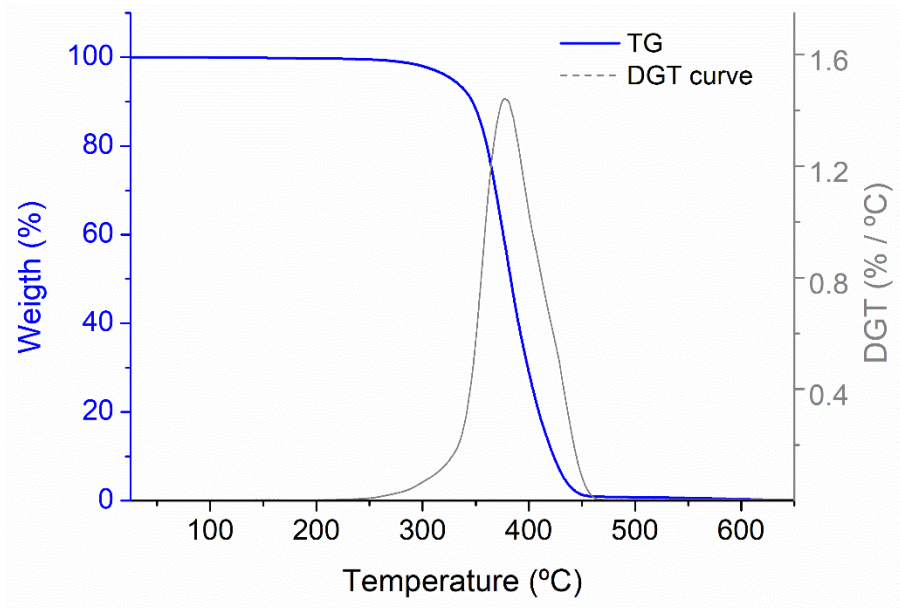
^1H NMR (400 MHz) spectrum of **TPU-1** produced batchwise. Solvent: CDCl_3 .



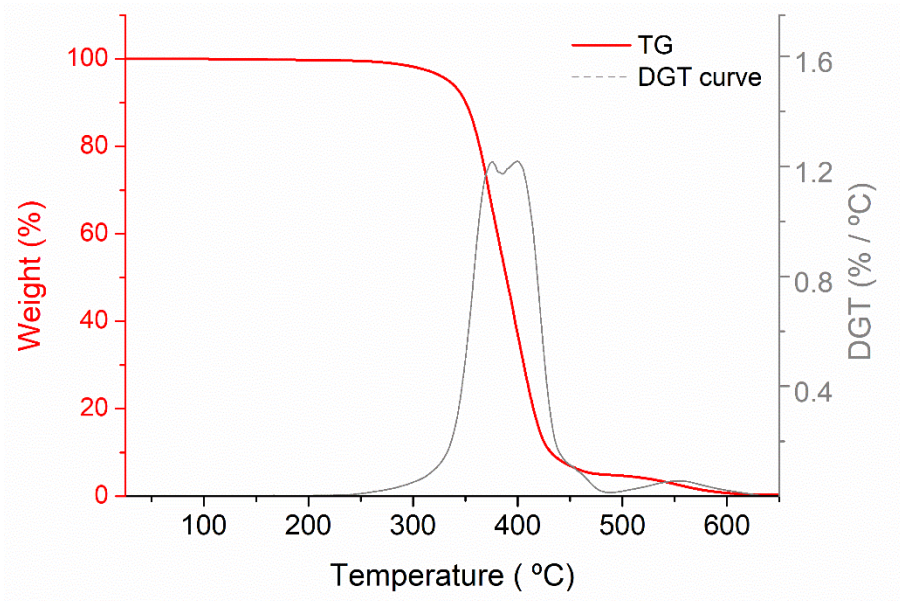
$^{13}\text{C}\{^1\text{H}\}$ NMR (100.6 MHz) spectrum of **TPU-1** produced batchwise. Solvent: CDCl_3 .



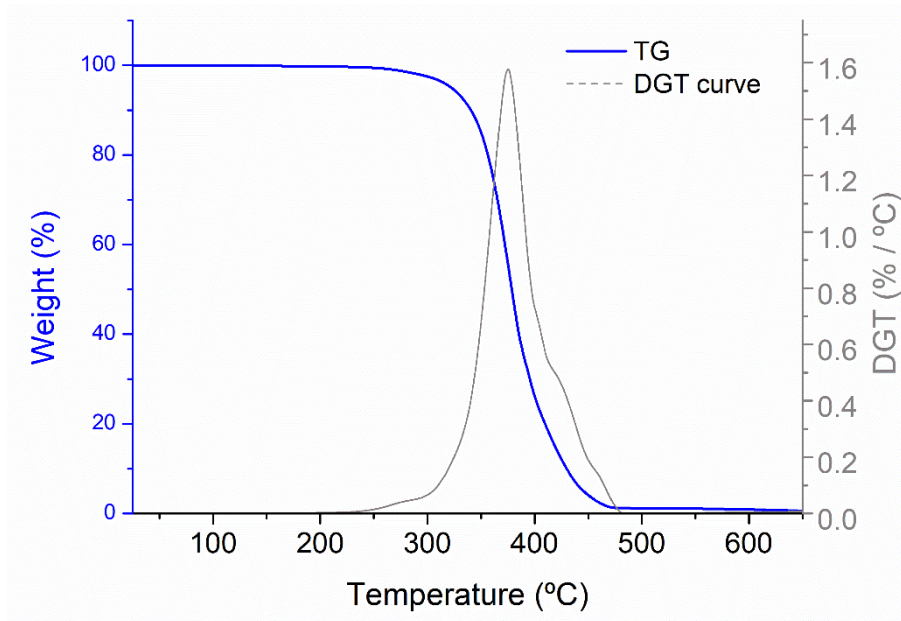
• Thermogram profile of **TPU-1** and the corresponding DGT curve under inert atmosphere.



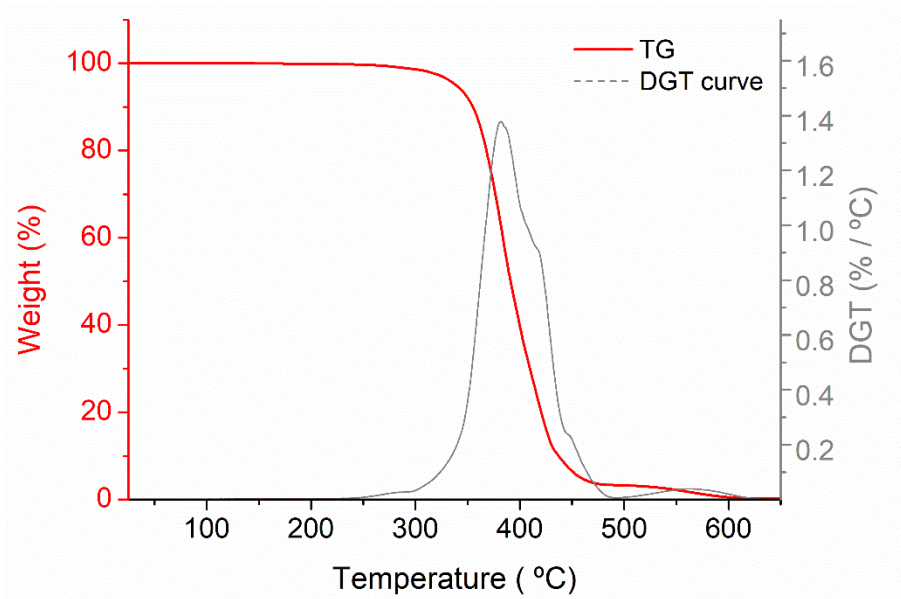
Thermogram profile of **TPU-1** and the corresponding DGT curve under oxidative atmosphere.



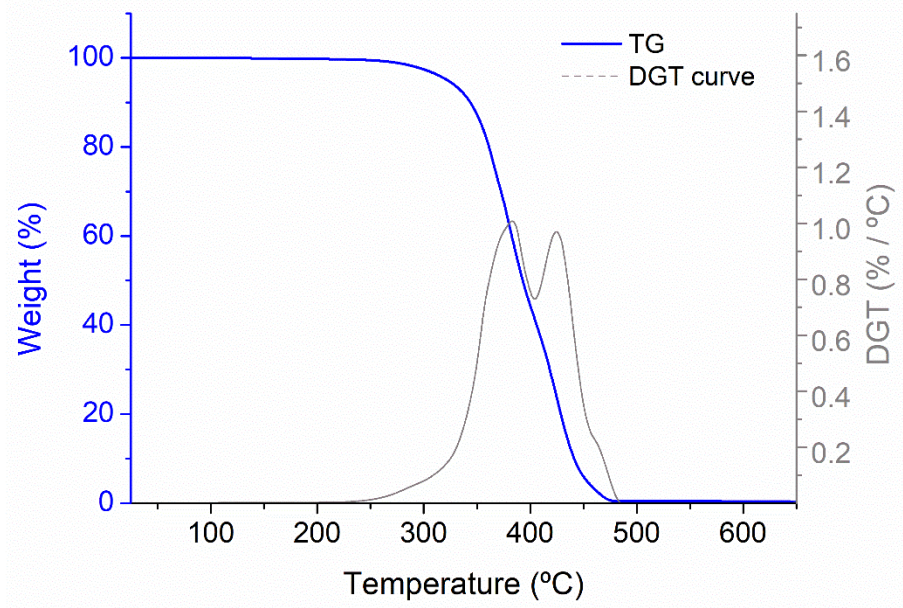
Thermogram profile of **TPU-2** and the corresponding DGT curve under inert atmosphere.



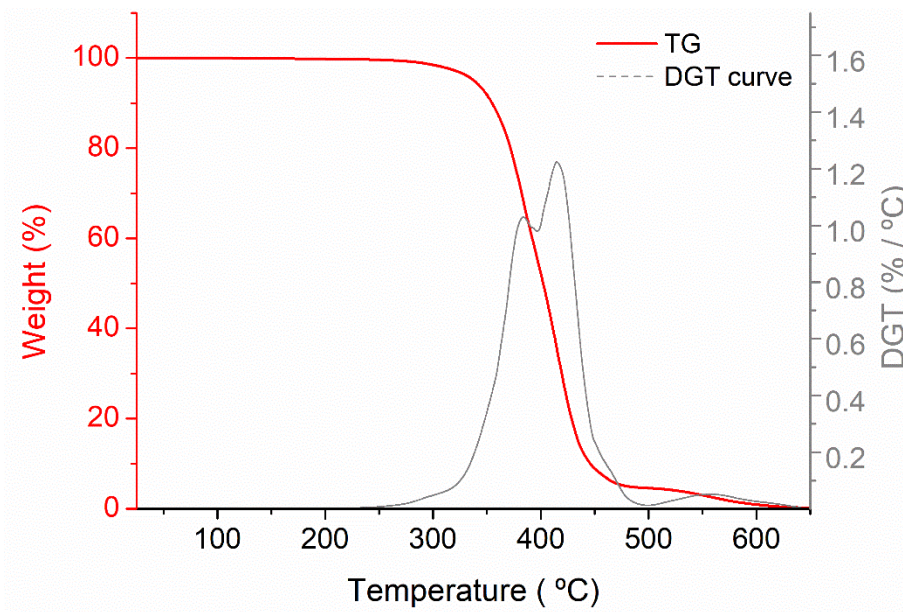
Thermogram profile of **TPU-2** and the corresponding DGT curve under oxidative atmosphere.



Thermogram profile of **TPU-3** and the corresponding DGT curve under inert atmosphere.

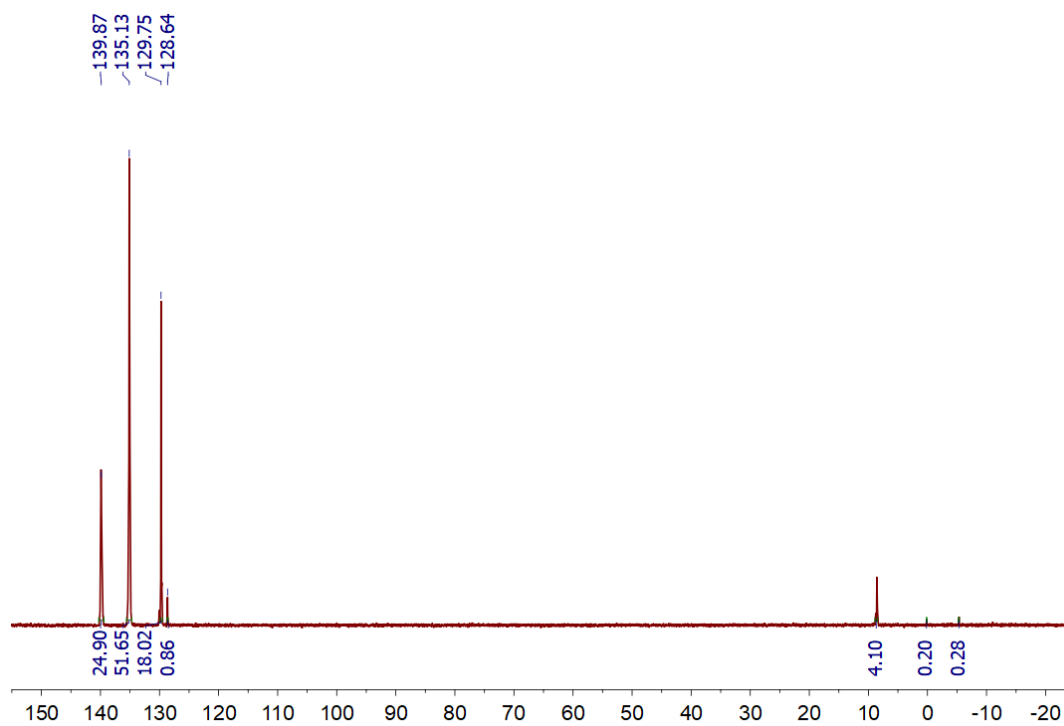


Thermogram profile of **TPU-3** and the corresponding DGT curve under inert atmosphere.

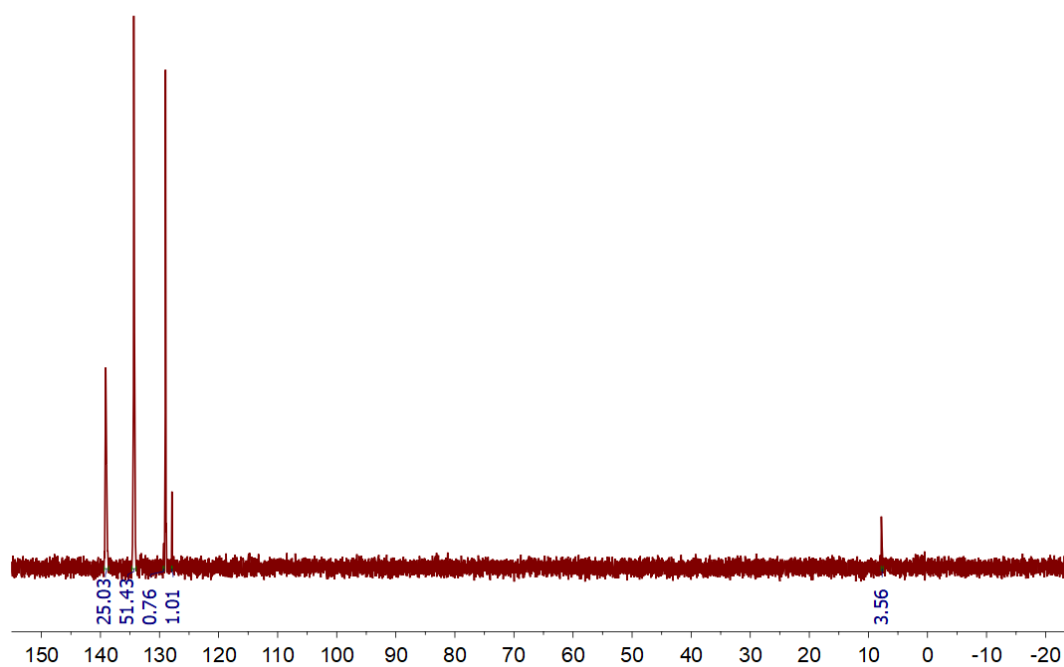


A.12. (PDDP)

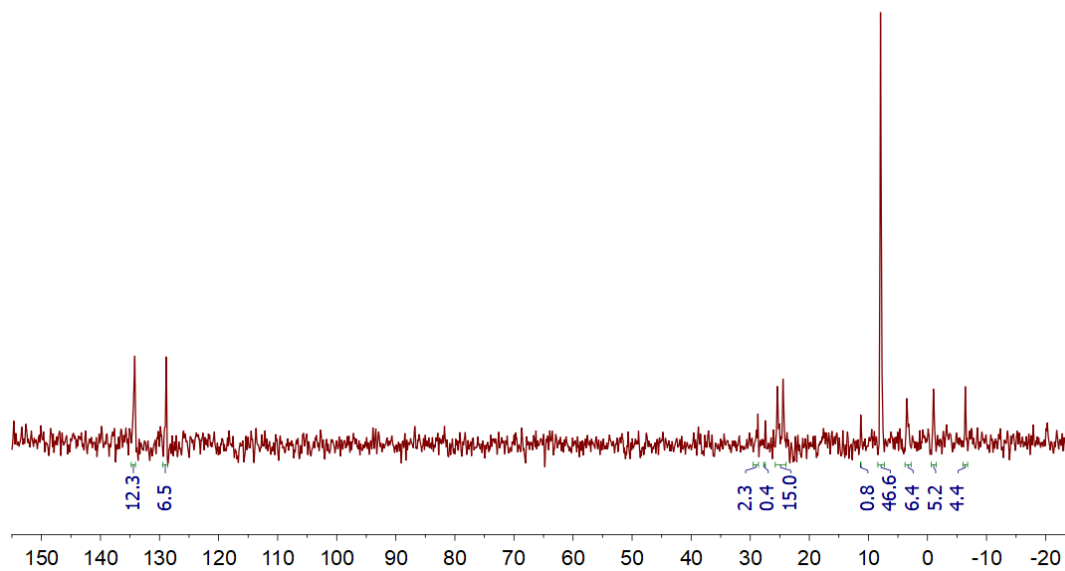
$^{31}\text{P}\{^1\text{H}\}$ NMR spectra of **PDDP**. Solvent: CDCl_3 filtered through basic alumina. 150 scans.



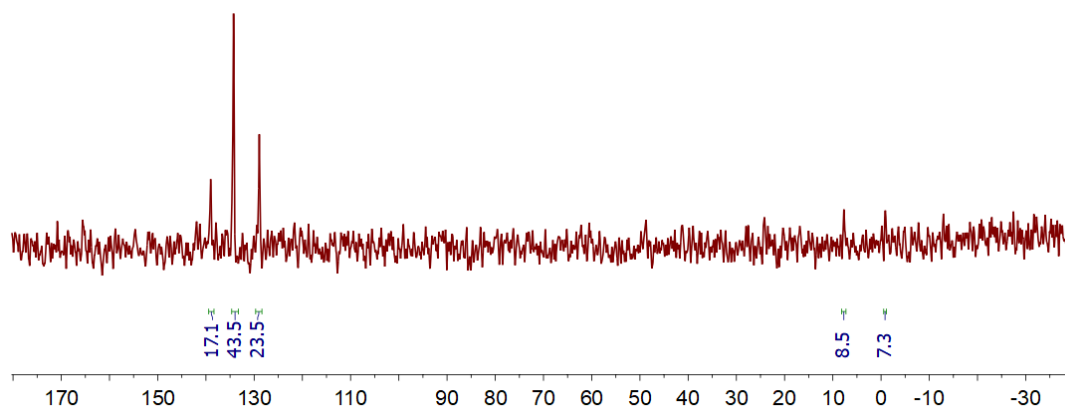
$^{31}\text{P}\{^1\text{H}\}$ NMR spectra of **PDDP**. Solvent: CDCl_3 + Pyridine



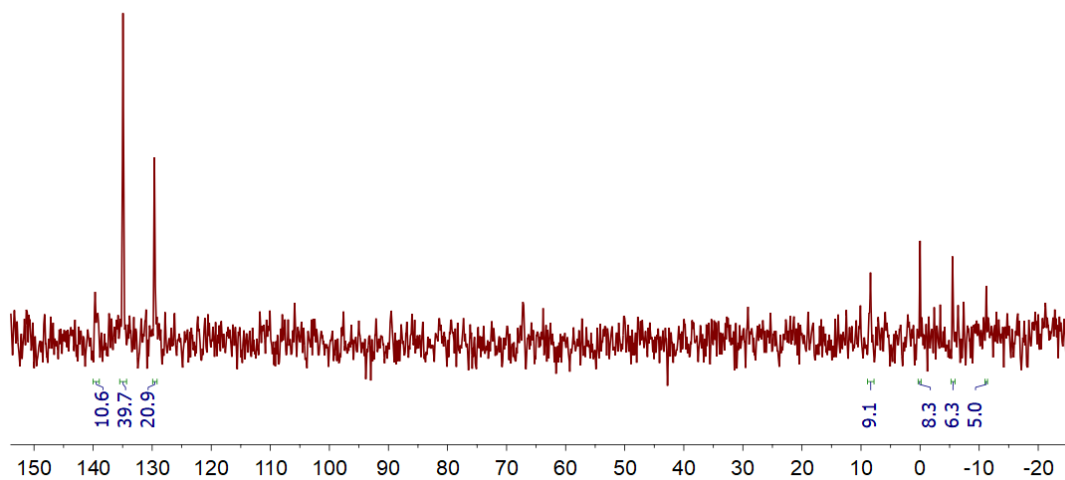
$^{31}\text{P}\{^1\text{H}\}$ NMR spectra of **Polyol 1**. Solvent: CDCl_3



$^{31}\text{P}\{^1\text{H}\}$ NMR spectra of **TPU-16**. Solvent: CDCl_3 + Pyridine

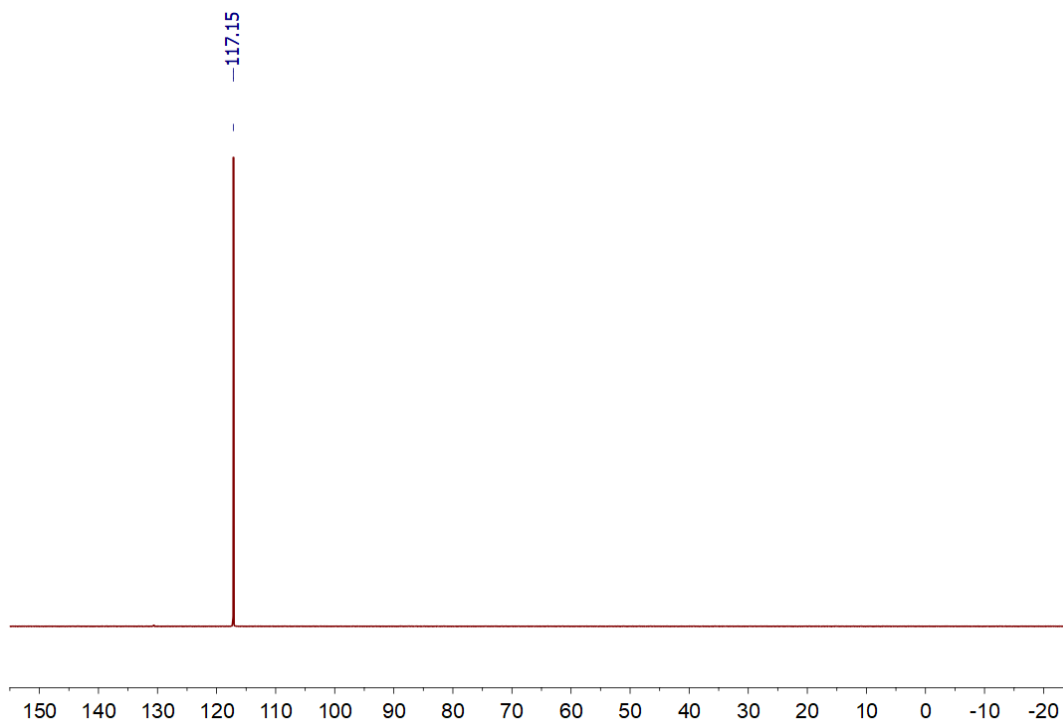


Example of a $^{31}\text{P}\{^1\text{H}\}$ NMR spectrum of **PDDP** in a TPU (**TPU-19**). Solvent: CDCl_3 + Pyridine. 27200 scans.

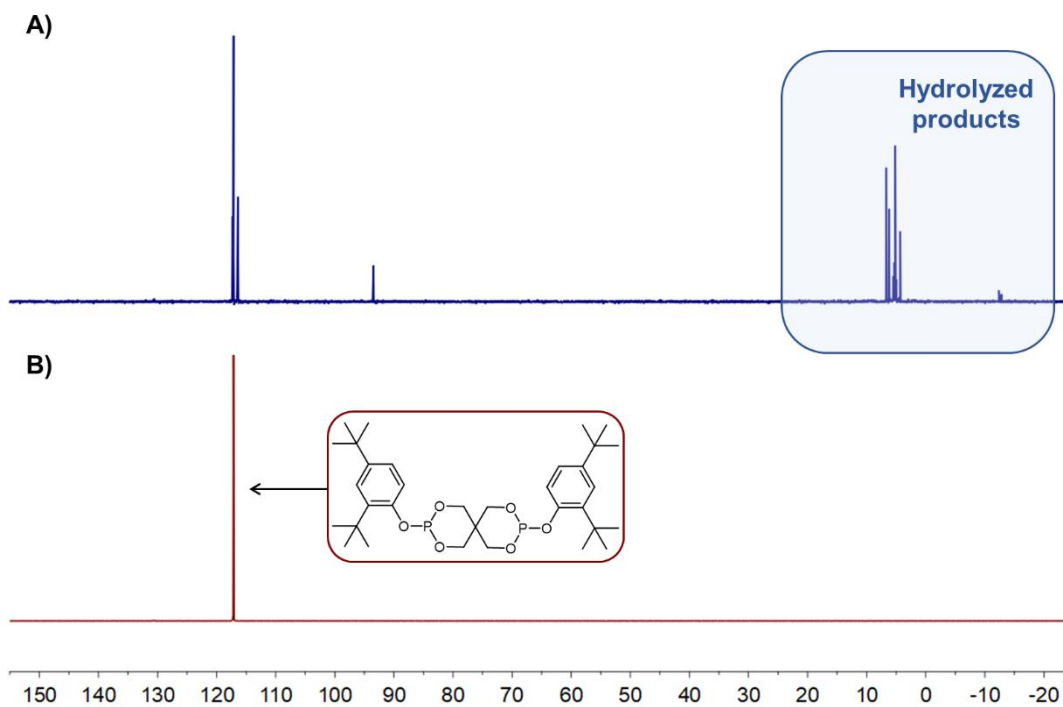


A.13. Irgafos

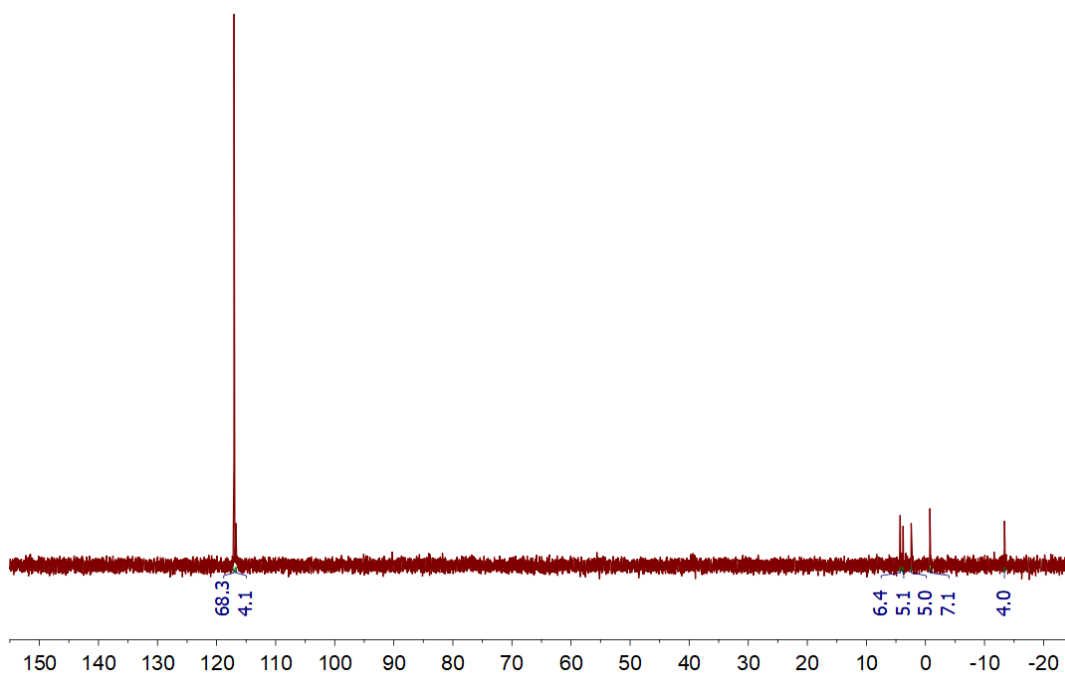
$^{31}\text{P}\{^1\text{H}\}$ NMR spectra of **Irgafos 126**. Solvent: CDCl_3 filtered through basic alumina.



Comparison of $^{31}\text{P}\{^1\text{H}\}$ NMR spectra of **Irgafos 126** analyzed in A) common CDCl_3 and B) in CDCl_3 filtered with basic alumina.



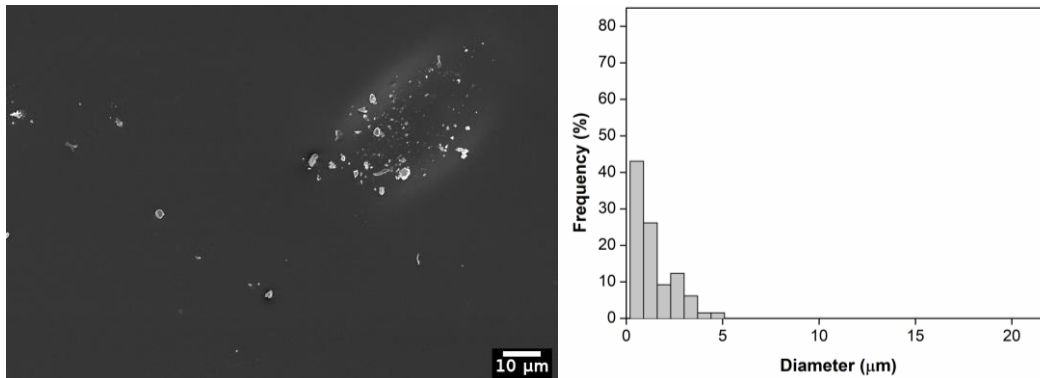
$^{31}\text{P}\{^1\text{H}\}$ NMR spectra of **Polyol mixture 9 [Polyol + additive (t₀ + 28h)]**. Solvent: CDCl_3 . 1600 scans.



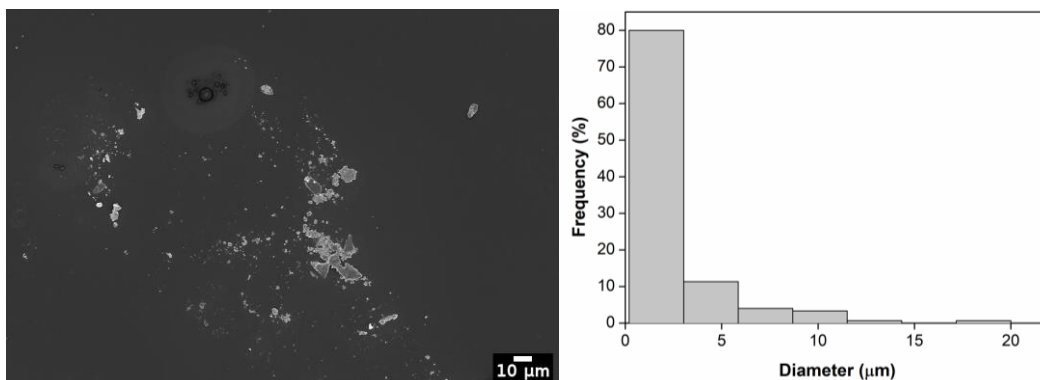
A.14. Analysis by Scanning Electron Microscopy

- Films cooled with deionized water

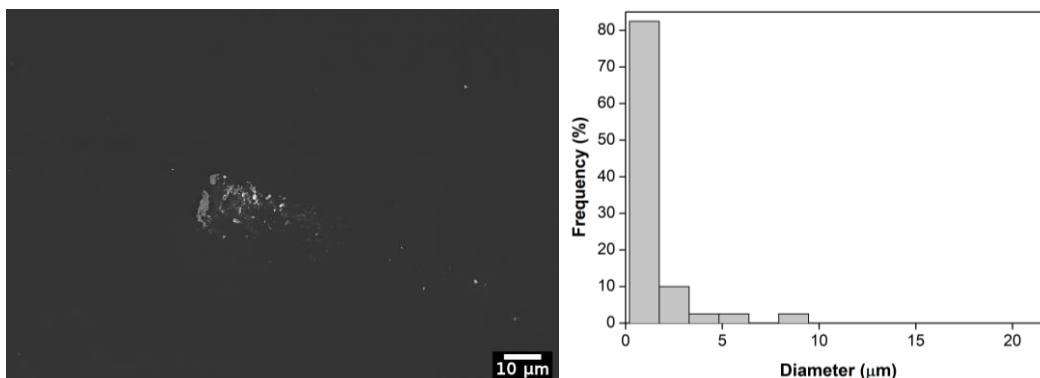
SEM micrograph of a film in contact with deionized water (magnification 2000 KX) and the corresponding histogram (n=65).



SEM micrograph of a film in contact with deionized water (magnification 2000 KX) and the corresponding histogram (n=150).

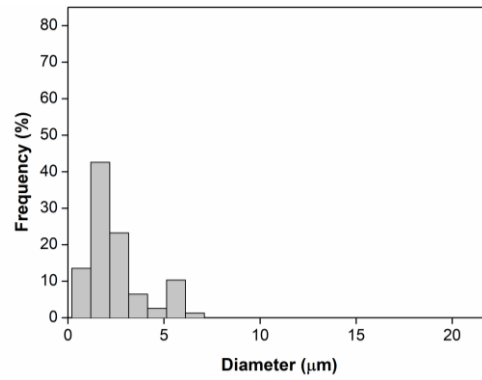
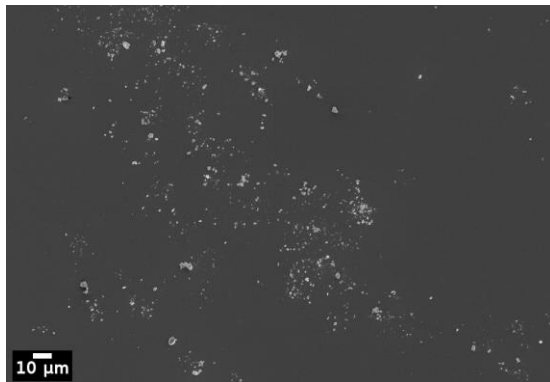


SEM micrograph of a film in contact with deionized water (magnification 2000 KX) and the corresponding histogram (n=40).



-
-
- Films cooled with tap water

SEM micrograph of a film in contact with deionized water (Magnification 1000KX) and the corresponding histogram (n=155).



SEM micrograph of a film in contact with deionized water (Magnification 1000KX) and the corresponding histogram (n=200).

